STABILISING AIRFLOWS IN CHILLED CEILING / DISPLACEMENT VENTILATION ENVIRONMENTS

LATIF IMRAN JALIL

This thesis is submitted to De Montfort University in partial fulfilment of the requirement for the degree of Doctor of Philosophy

November 2005

Department of Product and Spatial Design, De Montfort University, Leicester, UK

Abstract

A significant amount of work has taken place to investigate the performance of chilled ceilings and displacement ventilation systems operated together so as to achieve the appropriate cooling capacities while at the same time enhancing the sensation of thermal comfort. However, Taki etal (1996) have shown that combination of a chilled ceiling with a displacement ventilation system can cause destruction of the displacement flow pattern. In some circumstances this is caused by inversion, or downward cool air currents, which leads to a poorer environment and a failure to realise the enhanced comfort and air quality that these systems are individually claimed to bring. This thesis has investigated a new technique for achieving stable conditions for displacement airflow. The technique used here was the attachment of a honeycomb slat system to the chilled ceiling, thereby suppressing downward cool natural convection. Such investigations were carried out using both computational and experimental study for a range of typical office environment conditions. The vertical temperature profiles of the room air were compared with those from the conventional arrangement and confirmed that such a technique can minimise the downward cool air currents and that the

displacement flow pattern can be preserved in the presence of the chilled ceiling. The outcome of the study is the provision of general advice for designers as regards the combination of radiant cooling/displacement ventilation systems. This has led to a total change in the manner of combination of such systems with the aim of enhancing satisfaction of the occupants, whilst continuing the international trend towards low energy cooling technologies.

Acknowledgements

Firstly I would like thank Allah, Most Gracious, Most Merciful, and Charhardah masumin for giving me the strength to complete this research.

I would also like to thank my Supervisor Dr AH Taki not only for his scientific enlightening contributions but also for his moral support in awaking in me the desire and inspired me into completing the research. Without the continuing support and guidance of Dr AH Taki this thesis could not have been completed.

I would also like to thank Prof DL Loveday and Dr Harry Slat for also contributing in the research.

I would like to thank the materials test facilities at Oxford Brooks university Oxford, England.

I would also like thank my family for help in coating the cardboard with aluminium foil in the manufacturing stage of the honeycomb slats, also for the support they provided me, my

wife, my two daughters Laraybbatoul, Mowaddat-batoul and most importantly my parents. With out their prayers, encouragement, sacrifice and continued support I would not have had the chance to study for this degree. I dedicate these five years of hard work to my parents and my late grandmother.

I Dedicate this Thesis to

My Parents and my late Grandmother

Whom I can never compensate for their guidance, sacrifice and hard work in bringing me up and supporting me at times of need.

In the name of Allah,

Most Gracious, Most Merciful.

Read: In the name of thy Lord Who createth,

Createth man from a clot.

Read: And thy Lord is the Most Bounteous

Who teacheth by the pen,

Teacheth man that which he knew not

Quran 96: 1-6

SMALL MINDS DISCUSS PEOPLE

AVERAGE MINDS DISCUSS EVENTS

GREAT MINDS DISCUSS IDEAS

CONTENTS

ABSTRACT.....ii

ACKNOWLEDGEMENTS.....iv

CONTENTS.....ix

LIST OF FIGURES.....xv

LIST OF TABLES.....xxxi

NOMENCLATURE.....xxxiii

CHAPTER ONE: Introduction

1.0 Introduction.....1

1.1 Overview.....1

1.2 Scientific / technological relevance.....3

1.3 Research objectives.....9

1.4 Structure of the thesis.....13

CHAPTER TWO: Literature review

2.0 Literature review.....15

2.1 Introduction.....15

2.2 Displacement ventilation.....15

2.3 Limitations of displacement ventilation.....17

2.4 Advantages of displacement ventilation.....18

2.5 The chilled ceiling system.....21

2.6 The potential advantages of chilled ceiling panel cooling system 27

2.7 Combined chilled ceiling and displacement ventilation system.....28

2.8 Summary:.....45

CHAPTER THREE:
Computational Fluid Dynamics (CFD)

3.0 Computational Fluid Dynamics (CFD).....47

3.1 What is Computational Fluid Dynamics (CFD).....47

3.2 How does CFD make predictions?.....48

3.2.1 Solver 48

3.2.2 Finite difference method.....50

3.2.3 Finite volume method.....51

3.2.4 Finite element method.....51

3.3.5 The spectral method 52

3.4 Can CFD be trusted?.....54

3.5 CFD code used for the simulations.....55

3.5.1. Eddy viscosity.....56

3.5.2. K-e model.....56

3.6 Validating the CFD code (SABRE-One.....57

3.7 Comparison between the two different CFD models Eddy viscosity and K-epsilon.....77

3.8 Summary.....87

CHAPTER FOUR:
Honeycomb slats and heat transfer

4.0 Honeycomb slats and heat transfer.....89

4.1 Principle of heat transfer.....89

4.1.1 Conduction.....88

4.1.2 Convection.....90

4.1.3 Radiation.....91

4.1.3.1 Emittance 92

4.1.3.2 Reflectance.....93

4.2 Introduction to Rayleigh number.....94

4.3 Honeycomb slats.....97

4.3.1 Natural convection heat transfer.....100

4.3.2 Radiant heat transfer.....104

4.3.3 Overall heat transfer coefficient 105

4.4 Development of CFD simulation regarding slats 115

4.5 K-epsilon versus Eddy viscosity model.....127

4.6 Summary.....139

CHAPTER FIVE:
Optimum configuration of the honeycomb slats

5.0 Optimum configuration of the honeycomb slats.....141

5.1 CFD simulation to achieve optimum configuration of the honeycomb slats.....141

5.2 CFD Simulations in relationship to Rayleigh numbers 155

5.3 Optimum configuration of the honeycomb slats for manufacturing the Honeycomb Slats.....168

CHAPTER SIX:
Manufacturing and installation of honeycomb slats

6.0 Manufacturing and installation of honeycomb slats.....170

6.1 Manufacturing of honeycomb slats.....170

6.2 Experimental results.....179

6.2 The manufacturing process of the honeycomb.....186

CHAPTER SEVEN:
Experimental method

7.0 Experimental method 206

7.1 The experimental facility 206

7.2 Air temperature measurements 210

7.2.1 Air Velocity measurements.....210

7.2.2 Mean radiant temperature 211

7.2.3 Relative humidity 211

7.3 Experimental procedure and test conditions.....218

7.4 Summary.....223

CHAPTER EIGHT:
Experimental results

8.0 Experimental results 225

8.1 Introduction.....225

8.2 Test Conditions 226

8.2.1. The displacement ventilation test cases.....228

8.3 Summary of the result for displacement ventilation.....232

8.4 The displacement ventilation and chilled ceiling test cases.....233

8.4.1 Effect of ceiling temperature.....234

8.4.2 Effect of air changes per hours (ACH).....239

8.5 The displacement ventilation and chilled ceiling tests with honeycomb / slats attached to the ceiling.....243

8.5.1 Effect of change in ACH.....251

8.5.2 Effect of ACH of 6.....259

8.5.3 Effect of ACH of 8.....263

8.6 Discussion of results.....265

CHAPTER NINE:
Verification of laboratory results using CFD

9.0 Verification of laboratory results using CFD.....269

9.1 CFD simulations for verification of laboratory results.....269

9.2 Summary.....280

CHAPTER TEN:
Conclusions and recommendations

10.0 Conclusions and recommendations.....281

10.1 Conclusions.....281

10.2 Further recommendations.....286

References 287

Appendix A.....306

Appendix B.....340

List of Figures

Figures 1.1: Combined slat-clad chilled ceiling and displacement ventilation .....page 6

Figure 1.2: Honeycomb slat with aluminium Foil coating.....Page 6
Figure 1.3: Honeycomb slats attached to the ceiling.....page 7

Figure 2.1: Air from different convection sources settle at different levels in the room ref (Skistad).....page 18

Figure 2.2: Showing the diagrammatic presentation of Kruhne findings that the combined DV&CC system can disturb the displacement airflow pattern .....page 45

Figure 3.1: Finite difference method.....page 50

Figure 3.2: Finite volume method.....Page 51

Figure 3.3: Finite element method.....page 52

Figure 3.4: Showing the comparison of results between CFD used by Cook (1997) and Sabre-One CFD model. We can be seen that the code has predicted the same height of the stratified boundary layer and similar temperature..... page 59

Figure 3.5: Showing the results between the Flovent Code used by Alamdari (1998), and the Sabre-One CFD code. The results show the same temperature profile .....page 60

Figure 3.6: Graph showing the comparison between the results of Taki et al (1996) and the predictions of the CFD code. When various heat loads of 25-37-52-and 62W/m^2 were imposed on the dummies .....page 61

Figure 3.7: Air temperature versus height for a range of ceiling surface temperature at a heat load of 60W/m^2 and supply air temperature is 19°C .....page 62

.
Figure 3.8: Shows the diagrammatic presentation of Figure 3.9.....page 64

Figure 3.9: Showing that due to the chilled ceiling cold air is driven downwards along the walls transporting the mixed air in

to the fresh area zone and disturbs the displacement air flow pattern..... page 64

Figure 3.10: Showing CFD simulation where air flow motion in the room, also it can be seen that the walls have a lower temperature than the room air temperature ..... page 65

Figure 3.11: Graph results showing that wall air temperature is lower than the room air temperature when air temperature was taken at different distance from the walls .....page 65

Figure 3.12: CFD simulation agreeing with skistad that air velocity along the floor increases with distances from the supply unit until it reaches its maximum .....page 67

Figure 3.13: Graph showing the height of the stratified boundary layer, when heat load of 25W/m2 is impose at different heights.....page 70

Figure 3.14: Showing the temperature profile when heat load of 25W/m^2 is imposed at floor height. The results indicates that the air temperature difference between the supply temperature and the ankle height is 78% of the total temperature difference.....page 71

Figure 3.15: Showing the temperature profile when heat load of 25W/m^2 is imposed at height of 1.4m above the flow. The results show the temperature difference between the supply temperature and the ankle height is 26% of the total temperature difference..... ..... page 71

Figure 3.16: The graph represents the velocity at floor level for the same conditions as seen in figure 3.4.....page 72

Figure 3.17: CFD simulations showing the temperature contour profile when heat load of 25W/m^2 was imposed on four stations at floor height level. No heat plume can be seen above the four heat stations.....page 73

Figure 3.18 CFD simulations showing the temperature contour profile when heat load of 25W/m^2 was imposed on four stations at floor height level. No heat plume can be seen above the four heat stations.....page 73

Figure 3.19: Showing the temperature contour profile when heat load of 25W/m^2 was imposed on four stations at a height of 0.6m above floor height. The height of the plume can be seen .....page 74

Figure 3.20: Showing the temperature contour profile at the centre of the room away from the heat loads station, when heat load of 25W/m^2 was imposed on four stations at a height of 0.6m above floor height .....page 74

Figure 3.21: Showing the temperature contour profile when heat load of 25W/m^2 was imposed on four stations at a height of 1m above floor height. The height of the plume can be seen.....page 75

Figure 3.22: Showing a cross section view of the above figure 3.21. Four heat loads and their air temperature plume are seen.....page 75

Figure 2.23: Showing the temperature contour profile when heat load of 25W/m^2 was imposed on four stations at a height of 1.4 meters above floor height.....page 76

Figure 3.24: Showing a cross section view of the above figure 3.24 .....page 76

Figure 3.25: Showing the results of Heat load of 62W/m^2 imposed on 7 heat stations..... page 78

Figure 3.26: Showing the results of Heat load of 40W/m^2 imposed on 7 heat stations).....page 79

Figure 3.27: Showing the effects of different size Diffuser on the room air temperature profile obtained by CFD simulations for 40 W/m^2 heat loads impose on seven heat stations having inlet air supply temperature of 19°C..... page 82

Figure 3.28: Showing the results of room air temperature for the test conditions having a inlet diffuser size of 0.9m x 0.6m using the K-epsilon model. .....page 83

Figure 3.29: Showing the results of room air temperature for the test conditions having a inlet diffuser size of 0.9m x 0.6m using the K-epsilon model.....page 83

Figure 3.30: Showing the results of room air temperature for the test conditions having a inlet diffuser size of 0.9m x 0.6m using the Eddy Viscosity model.....page 84

Figure 3.31: Showing the results of room air temperature for the test conditions having a inlet diffuser size of 0.9m x 0.6m using the Eddy Viscosity model.....page 84

Figure 3.32: Graph showing that the results obtained using Eddy viscosity model had good agreement with Taki etal (1996) laboratory results.....Page 86

Figure 4.1: Convection current cells diagram shows the Cells in the two-dimensional view..... page 96

Figure 4.2: Showing Convection cells circulating in opposite directions. Indicating that the Heat transfer will be by convection. .....Page 96

Figure 4.3: The stability plot for a horizontal layer of fluid heated from below.....page 101

Figure 4.4: Plot showing critical temperature difference below which convection current are suppressed.....page 103

Figure 4.5: Ref: slats104 CFD simulation results for 2 horizontal parallel plates (0.5m height, 4m length ,1m width 2D model) Shows 3 circles of convection current, (temp different set at 26-16 (10 ^{o}C).....page 116

Figure 4.6: CFD simulation showing temperature Contours of convection current of simulation shown in the figure 4.5 .....page 116

Figure 4.7: CFD simulation showing velocity Contours of convection current of simulation shown in the figure 4.5 .....page 116

Figure 4.8: CFD simulation showing Temperature contour suggesting no convection current present.....page 117

Figure 4.9: CFD simulation showing no convection current present.....page 117

Figure 4.10: CFD simulation showing airflow consisting of four circular convection current cells.....page 117

Figure 4.11: CFD simulation showing airflow with four circular convection current cells, in line contours.....page 118

Figure 4.12: CFD simulation showing airflow with four circular convection current cells, in line contours.....Page 119

Figure 4.13: CFD simulation showing a section of one of the convection current in line contour for velocity.....page 119

Figure 4.14: CFD simulation showing air four circular convection current cells, in line contours for velocity.....page 120

Figure 4.15: CFD simulation showing one complete convection current cell (ref slats114) .....page 122

Figure 4:16: CFD simulation showing temperature contour of one complete convection current cell (Ref slats114)....page 123

Figure 4.17: CFD simulation Showing Velocity contour of one complete convection current cell (ref slats114).....page 123

Figure 4.18: CFD simulation showing 4 complete circular convection cells suggesting heat transfer by convection (for ref slats106) .....page 126

Figure 4.19: CFD simulation showing Velocity contours Showing Four (4) complete circular convection cells (ref slats106).....page 126

Figure 4.20: CFD simulation showing the results for case slats 123 in 2D k-epsilon model, 4mx0.25x1m results show convection where for the same boundary condition in Eddy viscosity model show no convection current.....page 128

Figure 4.21: CFD simulation showing simulation results for case Ref slats123: the results are showing the temperature line contour profile.....page 128

Figure 4.22: CFD simulation showing case Ref slats127 which is in 2D k-epsilon model, showing convection current for Rayleigh numbers above 1708.....page 131

Figure 4.23: CFD simulation showing convection current present when change in temperature is introduced.....page 132

Figure 4.24: CFD simulation showing temperature line contours for the case nwslat15, (a temperature line contour representation of the air temperature flow seen in figure 4.26).....page 133

Figure 4.25: CFD simulation showing: Velocity contours for the case nwslat15, (a velocity line contour representation of the air temperature flow seen in figure 4.26).....page 134

Figure 5.1: Showing convection current being suppressed when slats are inserted between two horizontal parallel plates. .....page 142

Figure 5.2: showing temperature contours showing convection current suppressed when slats are inserted between two horizontal parallel plates.....page 142

Figure 5.3: shows the diagrammatic of depth width ratio (d/w) for the Honeycomb slat. The top solid surface represent the chilled ceiling and the opening at the bottom represents the porous environment.....page 145

Figure 5.4: CFD simulation results for depth width ratio of One .....page 149

Figure 5.5: CFD simulation showing that the convection current is present between the honeycomb slats for depth width ratio of six..... page 150

Figure 5.6: CFD simulation showing that convection current is present between the Honeycomb slat for depth width ratio of eight (8).....page 151

Figure 5.7: CFD simulation showing that at depth width ratio of ten (10).....page 152

Figure 5.8: CFD simulation showing the stages of convection current being suppressed between the Honeycomb slats for various Depth Width ratio.....page 153

Figure 5.9: Graph showing the relationship between the Average Air temperature and its Corresponding Rayleigh Number.....page 157

Figure 5.10: Graph showing the relationship between the temperature difference between the Chilled ceiling temperature and the room air temperature.....page 158

Figure 5.11: Graph showing the effects of different Depth Width ratio have on the Convection air flow for Rayleigh Number of 3 million.....page 159

Figure 5.12: Graph Showing the effect different Depth Width ratio has on the Convection air flow for Rayleigh Number of Four (4) million. .....page 161

Figure 5.13: Graph showing the effects different Depth Width ratio have on the Convection air flow for Rayleigh Number of 5 million.....page 162

Figure 5.14: Graph showing the effects different Depth Width ratio have on the Convection air flow for Rayleigh Number of 6 million.....page 163

Figure 5.15: Graph showing the effects different Depth Width ratio has on the Convection air flow for Rayleigh Number of 7 million.....page 164

Figure 5.16: Graph showing the effects different Depth Width ratio have on the Convection air flow for Rayleigh Number of 8 million.....page 165

Figure 5.17: Graph showing the effects different Depth Width ratio have on the Convection air flow for Rayleigh Number of 9 million.....page 166

Figure 5.18: Graph showing the effects different Depth Width ratio have on the Convection air flow for different Rayleigh Numbers ranging form 3 million to 9 million.....page 167

Figure 6.1: Cardboard coated with Humbrol metal coat (polished) sent for testing. .....page 174

Figure 6.2: Cardboard coated with aluminium Foil sent for testing.....page 174

Figure 6.3: Cardboard coated with aluminium paint sent for testing. .....page 175

Figure 6.4: Plain uncoated cardboard sent for testing..page 175

Figure 6.5: Cardboard coated with Silver aluminium Applied Finish.....page 176

Figure 6.6: Samples sent for testing.....page 176

Figure 6.7: Testing equipment at Oxford Brooks university.....page 177

Figure 6.8: Testing equipment at Oxford Brooks university. .....Page 177

Figure 6.9: Testing equipment at Oxford Brooks university. .....page 178

Figure 6.10: Testing equipment at Oxford Brooks university.....page 178

Figure 6.11: Results for the total near-normal hemispherical infrared spectral reflectance of Humbrol metal Coat (polished) sample.....Page 179

Figure 6.12: Results for the total near-normal hemispherical infrared spectral reflectance of Firlex aluminium paint sample.....page 180

Figure 6.13: Results for the total near-normal hemispherical infrared spectral reflectance of Silver aluminium applied finish sample.....page 180

Figure 6.14: Results for the total near-normal hemispherical infrared spectral reflectance of aluminium foil sample.....page 181

Figure 6.15: Results for the total near-normal hemispherical infrared spectral reflectance of uncoated cardboard sample.....page 181

Figure 6.16: Results for the total near-normal hemispherical spectral reflectance of Humbrol metal coat (polished) sample.....page 182

Figure 6.17: Results for the total near-normal hemispherical spectral reflectance of Firlex aluminium paint sample.....page 182

Figure 6.18: Results for the total near-normal hemispherical spectral reflectance of Silver aluminium applied finish sample.....page 183

Figure 6.19: Results for the total near-normal hemispherical spectral reflectance of aluminium foil sample.....page 183

Figure 6.20: Results for the total near-normal hemispherical spectral reflectance of uncoated cardboard sample.....page 184

Figure 6.21: Honeycomb slats mould.....Page 186

Figure 6.22: Honeycomb slats design to correct dimensions on timber.....page 186

Figure 6.23: Machine cutting the honeycomb to correct size.....page 187

Figure 6.24: Machine cutting the honeycomb to correct size.....page 187

Figure 6.25: Machine cutting honeycomb slats..... Page 188

Figure 6.26: Honeycomb slat cutting mould.....page 188

Figure 6.27: Honeycomb slats with the mould..... page 189

Figure 6.28: Cutting the aluminium foil tape to correct size for coating the cardboard.....page 189

Figure 6.29: Cutting the aluminium foil tape to correct size for coating the cardboard.....Page 190

Figure 6.30: Pealing the aluminium foil tape.....page 190

Figure 6.31: Coating the cardboard with aluminium foil tape.....page 191

Figure 6.32: Coating the cardboard with aluminium foil tape.....page 191

Figure 6.33: Coating the top of the cardboard.....page 192

Figure 6.34: Coating the cardboard with the second aluminium foil.....page 192

Figure 6.35: Coating the cardboard with the third aluminium foil tape.....page 193

Figure 6.36: Uncoated and coated card board.....page 193

Figure 6.37: Coated and uncoated cardboard.....Page 194

Figure 6.38: Cutting the coated cardboard to the correct size for fixing.....page 194

Figure 6.39: Showing uncoated cardboard, coated cardboard, cut to correct size honeycomb slat sheet.....page 195

Figure 6.40: Making the small model of the honeycomb slat model.....page 195

Figure 6.41: Fixing the honeycomb slats sheet.....page 196

Figure 6.42: Fixing the honeycomb slats sheet..... .....page 196

Figure 6.43: Fixing the honeycomb slats sheet..... page 197

Figure 6.44: Complete section of the honeycomb slats to be attached to the chilled ceiling.....page 197

Figure 6.45: Measuring the honeycomb slat section to the correct size.....page 198

Figure 6.46: Measuring the honeycomb slat section to the correct size.....page 198

Figure 6.47: Measuring the honeycomb slat section to the correct size.....page 199

Figure 6.48: Measuring the honeycomb slat section to the correct size..... .....Page 199

Figure 6.49: Honeycomb slats, before attaching to the chilled ceiling..... Page 200

Figure 6.50: Honeycomb slats fixed to the ceiling around the inlet diffuser..... page 200

Figure 6.51: Honeycomb slats being attached to the ceiling .....Page 201

Figure 6.52: Honeycomb slats attached to the ceiling .....page 201

Figure 6.53: Honeycomb slats attached to the ceiling.....Page 202

Figure6.54: Honeycomb slats attached to the ceiling...page 202

Figure 6.55: Honeycomb slats attached to the ceiling with air temperature measurement equipment attached to the stall ..... page 203

Figure 6.56: Showing air temperature measuring sensors inserted between the honeycomb slats and the chilled ceiling.....Page 203

Figure 6.57: Showing the end of the honeycomb slat with light reflecting on it.....page 204

Figure 6.58: Showing the bird eye view of the honeycomb slats.....page 204

Figure 7.1: Schematic diagram of the room being modelled .....page 212

Figure 7.2: Showing the test chamber in the laboratory.....page 213

Figure 7.3: Air heating unit, supplying the inlet air to the test chamber.. .....page 213

Figure 7.4: Displacement ventilation supply air inlet with a temperature sensor monitoring the room air inlet temperature..... Page 214

Figure 7.5: Extract air vent, used to extract the room air flow.....page 214

Figure 7.6: Chilled ceiling panel being installed in the test chamber..... page 215

Figure 7.7: Chilled ceiling panel showing pipe work, without the external metal panel.....page 215

Figure 7.8: Heat sources (dummies) used for the experiments... .....page 216

Figure 7.9: Heat source dummies placed on the table, with light representing heat load..... page 216

Figure 7.10: Showing type "T" copper constantan thermocouples, mounted on vertical stand at various heights, to allow measurements of the vertical room air temperature. Also the Honeycomb slat attached to the ceiling are seen.....Page 217

Figure 7.11: Showing type "T" copper constantan thermocouples, mounted on vertical stand to measure air temperature near the ceiling and between the Honeycomb slats which are attached to the ceiling... .....page 217

Figure 7.12: Graph showing results that the same test conditions can be repeated and obtain similar results ..... page 220

Figure 7.13 Showing the test chamber dimensions with the relevant equipment..... Page 222

Figure 8.1: Graph showing the results for test case .....page 228

Figure 8.2: Showing the results for test case 2.....page 229

Figure 8.3: Showing the results for test case 3..... page 230

Figure 8.4: Showing the results for test case 4.....page 231

Figure 8.5: Shows the experimental test results for test case 5.....page 235

Figure 8.6: Shows the experimental test results for test case 6..... page 236

Figure 8.7: Shows the experimental test results for test case 7 .....page 237

Figure 8.8: Shows the experimental test results for test case 8.....page 238

Figure 8.9: Showing the air temperature profile in the room for test case 9. ....page 240

Figure 8.10: Showing the air temperature profile in the room for test case 10..... .....page 241

Figure 8.11: Showing the air temperature profile in the room for test case 11..... Page 242

Figure 8.12: Showing the air temperature profile in the room for test case 12.....page 245

Figure 8.13: Showing the air temperature profile in the room for test case 12..... page 246

Figure 8.14: Showing the air temperature profile in the room for For test case 12 with comparison between ceiling temperatures for with without the honeycomb slats attached to the ceiling for the ceiling temperature of 18°... .....page 247

Figure 8.15: Showing the air temperature profile in the room for test case 12 with comparison between ceiling temperatures for with without the honeycomb slats attached to the ceiling for the ceiling temperature of 16°C..... .....page 248

Figure 8.16: Showing the air temperature profile in the room for test case 12 with comparison between ceiling temperatures for with without the honeycomb slats attached to the ceiling for the ceiling temperature of 14°C..... page 249

Figure 8.17: Showing the air temperature profile in the room for test case 12 with comparison between ceiling temperatures for with without the honeycomb slats attached to the ceiling for the ceiling temperature of 12°C..... page 250

Figure 8.18: Representing the air temperature profile for ach of 4 without the attachment of honeycomb slats attached to the ceiling..... .....Page 251

Figure 8.19: Showing the air temperature profile when Honeycomb slats are attached to the ceiling for ach of 4.....page 252

Figure 8.20: Showing the results of air temperature profile for figures 8.18 and 8.19..... page 253

Figure 8.21: Showing the air temperature profile with and without honeycomb slats attached to the ceiling.....page 254

Figure 8.22: Showing the air temperature profile with and without honeycomb slats attached to the ceiling for ceiling temperature of 18°C..... .....page 255

Figure 8.23: Showing the air temperature profile with and without honeycomb slats attached to the ceiling for ceiling temperature of 16°C.. .....page 256

Figure 8.24: Showing the air temperature profile with and without honeycomb slats attached to the ceiling for ceiling temperature of 14°C..... page 257

Figure 8.25: Showing the air temperature profile with and without honeycomb slats attached to the ceiling for ceiling temperature of 12°C.....page 258

Figure 8.28: Showing the air temperature profile when honeycomb slats are attached to the ceiling for ach of 6..... .....page 259

Figure 8.30: Showing the air temperature profile with and without honeycomb slats attached to the ceiling for ceiling temperature of 18°C..... page 260

Figure 8.31: Showing the air temperature profile with and without honeycomb slats attached to the ceiling for ceiling temperature of 16°C..... .page 261

Figure 8.32: Showing the air temperature profile with and without honeycomb slats attached to the ceiling for ceiling temperature of 14°C... .....page 262

Figure 8.33: Showing the air temperature profile when honeycomb slats are attached to the ceiling for ach of 8 .....Page 263

Figure 8.34: Showing the air temperature profile for the test conditions where with and without honeycomb slats attached to the ceiling for ceiling temperature of 14°C and 16°C.. .....page 264

Figure 9.1: Showing airflow vectors above two the heat source without honeycomb slats, convection current cells can be seen..... page 273

Figure 9.2: Showing airflow vectors above two heat sources with honeycomb slats attached to ceiling.. .....page 273

Figure 9.3: Showing airflow vectors in the room and above a heat source without honeycomb slats, convection current cells can be seen.....page 274

Figure 9.4: Showing airflow vectors above two the heat sources with honeycomb slats attached to ceiling... ....page 274

Figure 9.5: Showing airflow vectors in the room and above 3 heat sources without honeycomb slats, convection current cells can be seen..... .....page 275

Figure 9.6: Showing airflow vectors above 3 the heat sources with honeycomb slats attached to ceiling the convection currents have been suppressed.....Page 275

Figure 9.7: CFD simulation with honeycomb slats attached and the effects the honeycomb slats have on the heat plume and airflow..... page 276

Figure 9.8: CFD simulations showing the airflow near the ceiling and near the honeycomb slats..... Page 276

Figure 9.9: Showing airflow vectors, airflow line contours above two the heat source without honeycomb slats, convection current cells can be seen..... page 277

Figure 9.10: Showing airflow vectors, airflow line contours above two the heat source with honeycomb slats, convection current cells have be suppressed..... page 277

Figure: 9.11: Airflow temperature contours in the room above 3 heat sources without honeycomb slats attached to the ceiling.....page 278

Figure 9.12: Airflow temperature contours in the room above 3 heat sources with honeycomb slats attached to the ceiling..... page 278

Figure 9.13: Airflow temperature contours in the room above two heat sources without honeycomb slats attached to the ceiling..... Page 279

Figure 9.14: Airflow temperature contours in the room above two heat sources with honeycomb slats attached to the ceiling..... page 279

List of Tables

2.1 Showing the outline of review of work carried out by various researcher on the combined displacement ventilation / chilled ceiling system.....Page 31-42

3.1: Showing the temperature at ankle height (0.1m above the floor) for the same boundary conditions but for different CFD models..... ...page 80

4.1: The Emittance of various surfaces is listed in the table .....page 93

4.2: Magnitude of the Heat transfer coefficient for the Four cases.....page 107

Table 4.3: showing the comparison of the results for the same boundary conditions for 2D and 3D Modelling .....page 122

4.4: showing the effects that are seen when horizontal parallel plate length is changed .....page 125

4.5: The change in temperature difference can influence the airflow between the two parallel plates ..... page 135

4.6: The change in the length of the two horizontal parallel plates can influence the airflow between the two plates.....page 136

4.7: Showing that the increase in the length of the two horizontal parallel plates can influence the convection current between the two plates .....Page 137

Table: 5.1 show the relationship between the depth width ratio and the drop in air velocity in the honeycomb slats in percentage.....page 147

Table 6.1: Showing the Emittance of the five samples. (Table presentation of the ten graphs (figures 6.11 to 6.20))..... ..... page 184

Table 8.1: List of test conditions carried out without chilled ceiling attached to the ceiling .....page 227

Table 8.2: Showing the list of test conditions.....page 234

Table 8.3: Shows the test conditions that were carried out to investigate the effect of air change per hour for various ceiling temperatures.....Page 239

Table 8.4: Shows the test conditions that were carried out to investigate the effects of Honeycomb slat attached to ceiling..... Page 244

NOMENCLATURE

SYMBOL	DEFINITION
a	(see equation 4.2)
ACH	Air Changes Per Hour
d	Depth of the honeycomb slat (m)
d/w	Depth width ratio (dimensionless)
g	Acceleration due to gravity ($9.81 m/s^2$)
ha	Convective heat transfer coefficient (W/m^2K)
ka	Thermal conductivity (W/mK)
L	Distance between two horizontal parallel plates (m) (see equation 4.1)
Pr	Prandlt number (dimensionless)
Ra	Rayleigh number (dimensionless)
T_1, T_2	Surface temperatures of surface 1 and 2 (K)
V	kinematic viscosity (m^2/s)
w	width of the honeycomb slat (m)
β	coefficient of volume expansion (1/K)

Chapter One

1.0 Introduction

1.1. Overview

A significant fraction of the total energy consumption in industrialised countries is used for the provision of thermally comfortable, healthy, habitable indoor spaces. In an attempt to limit the adoption of energy-intensive systems, such as air-conditioning, a significant amount of work has taken place to investigate the performance of chilled ceilings and displacement ventilation systems operated either separately or together. These require less energy than conventional mixed flow air-conditioning; in addition, displacement ventilation systems have the potential to provide an indoor environment of good air quality as a result of their full fresh air displacement flow. However, existing thermal comfort criteria presented in International Standard ISO 7730 (1994) limit their cooling capacity. As a result, displacement ventilation systems are often combined with a chilled ceiling system so as to achieve the appropriate cooling capacities while at the same time enhancing the sensation of thermal comfort. However, Taki et al 1996, 1997), has shown that combination of a chilled ceiling with a

displacement ventilation system can cause destruction of the displacement flow pattern in some circumstances, resulting in mixing caused by downward cold currents of air. This is caused by inversion, which leads to a poorer environment in terms of air quality and a failure to realise the enhanced comfort and air quality that these systems are individually claimed to bring. Chilled ceilings and displacement ventilation systems can be successfully operated together only if the downward cold air currents are significantly minimised, thereby stabilising the room airflow.

The aim of this thesis is to investigate computationally and experimentally a new technique for achieving stable conditions for displacement airflow, thereby ensuring that the combined arrangement can work together effectively, whilst maintaining an aesthetically-pleasant interior. The technique proposed here is attachment of a 'slat'-type system to the chilled ceiling, thereby suppressing downward cold natural convection. The outcome of the study will be the provision of general advice for designers as regards the combination of radiant cooling/displacement ventilation systems with the aim of producing thermally stable, comfortable, healthy, and good air quality spaces to the

enhanced satisfaction of the occupants. In addition, the work will enhance knowledge related to the international trend towards low energy cooling technologies.

1.2. Scientific/technological relevance

The performance of a test room employing a combined chilled ceiling and displacement ventilation system has been characterised, including flow visualisation, in previous EPSRC-funded work (Taki et al 1996, 1997). The results showed that, in the conventional chilled ceiling/displacement ventilation combination, destruction of the displacement flow pattern can occur at lower ceiling temperatures (14-16°C); at higher ceiling temperatures (18-21°C), the height of the stratified boundary layer between displacement and mixed flow zones can be reduced to below the occupants' breathing level. These effects are caused by downward cold air currents, due to the fact that the surface temperature of the ceiling is always lower than that of the floor, and the air density decreases in the direction of the gravitational force. This condition is unstable, and free convection currents must exist (when Rayleigh number is greater than 1708; the buoyant force overcomes the fluid resistance and initiates

natural convection currents) in the form of a circulation pattern; this is known as 'inversion' which destroy the displacement flow pattern. The above results are confirmed by Fitzner (1996), when he suggested that the airflow pattern turned into mixed flow when 50% of the cooling load was cooled by the ceiling. Furthermore, he concluded that the vertical profiles of contamination are severely affected by a chilled ceiling, since the relatively low degree of contamination in the supply air layer grows linearly with the cooling capacity of the ceiling. Alamdari and Eagles (1996) also showed that the combination of a chilled ceiling with a displacement ventilation system could potentially have a detrimental effect upon displacement flow. Elimination of these cold convection currents will prevent destruction of the displacement flow, and will allow radiant cooling/displacement ventilation systems, to operate together. It has been already shown that such a combination can offer good thermal comfort (Loveday et al 1998, 2001). Advantages can thus be taken of this, as well as the low energy potential offered by such systems. In this thesis, the use of a 'slat'-type system attached to the chilled ceiling (Figure 1.1) for suppressing the natural convection of cold air will be investigated for preserving displacement flow. Such a convection suppression system has been investigated for the case of solar collectors by many

authors - (e.g. Hollands, 1965, 1973, and 1985); in these studies, a transparent honeycomb panel was mounted between the absorbing plate and the outer glass cover. Analytical and experimental results showed that, under certain conditions, natural convection losses can be suppressed to improve the solar collector efficiency. In this thesis, the same effect will be exploited using a 'slat'-type system, but without affecting the rate of heat transfer by radiation to the chilled ceiling (via control of emissivity). The technique works by controlling the Rayleigh number (which relates the buoyancy to viscous forces) using the depth to width ratio of the attached slats. In effect, the tendency for the cooler air between a given pair of slats to fall countered by the viscous forces present between the air and the slat surfaces; this should result in the 'cell' of cool air remaining in position between the slats. This technique is well understood, and full details can be found in Cengel (1998).

The application of CFD simulation will predict as to which conditions and configuration of the 'honeycomb slat'-type system can suppress natural convection, which will lead to better control of the stratified boundary layer (see figures 1.1-1.3). The CFD predictions will be compared with the experimental data of room air distribution using an experimental facility at

Loughborough University. The implications of the reduced air movement on stabilised condition and air quality will be investigated.

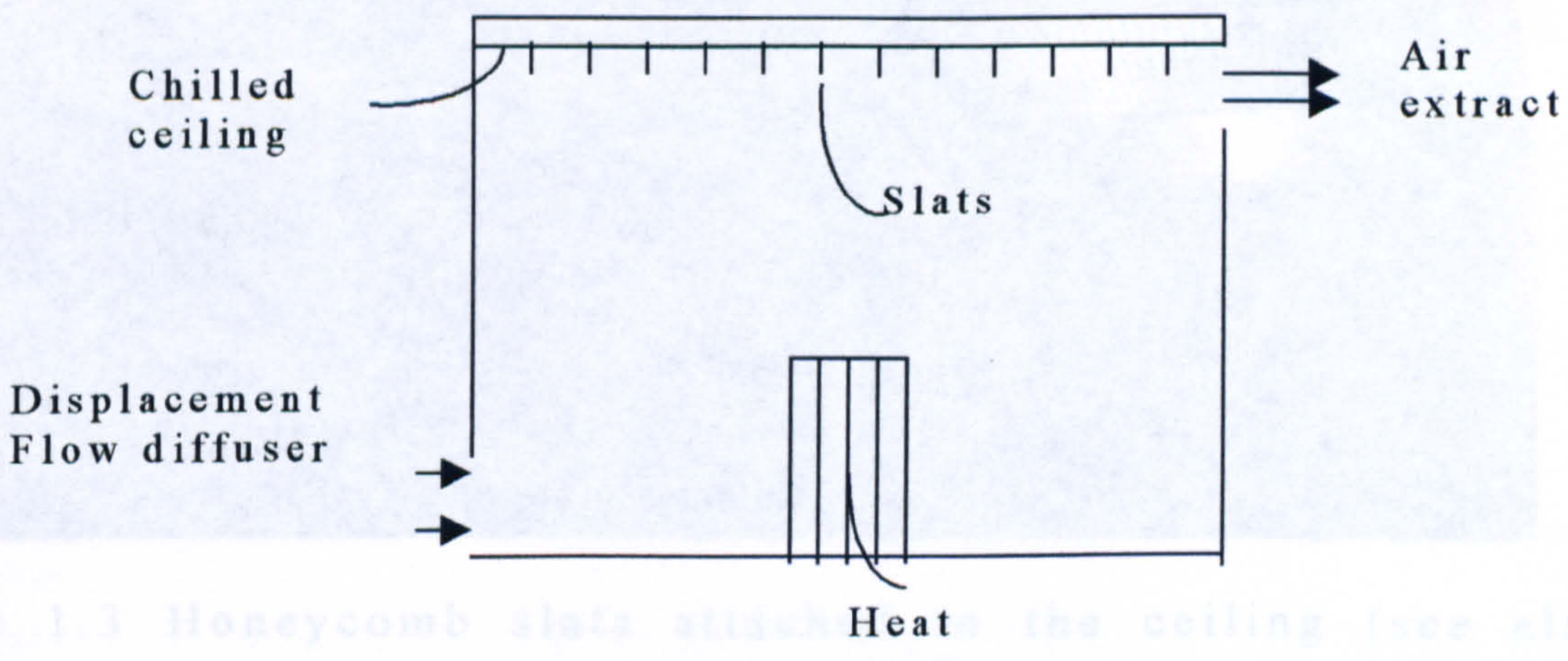

Figure 1.1: Combined slat-clad chilled ceiling and displacement ventilation

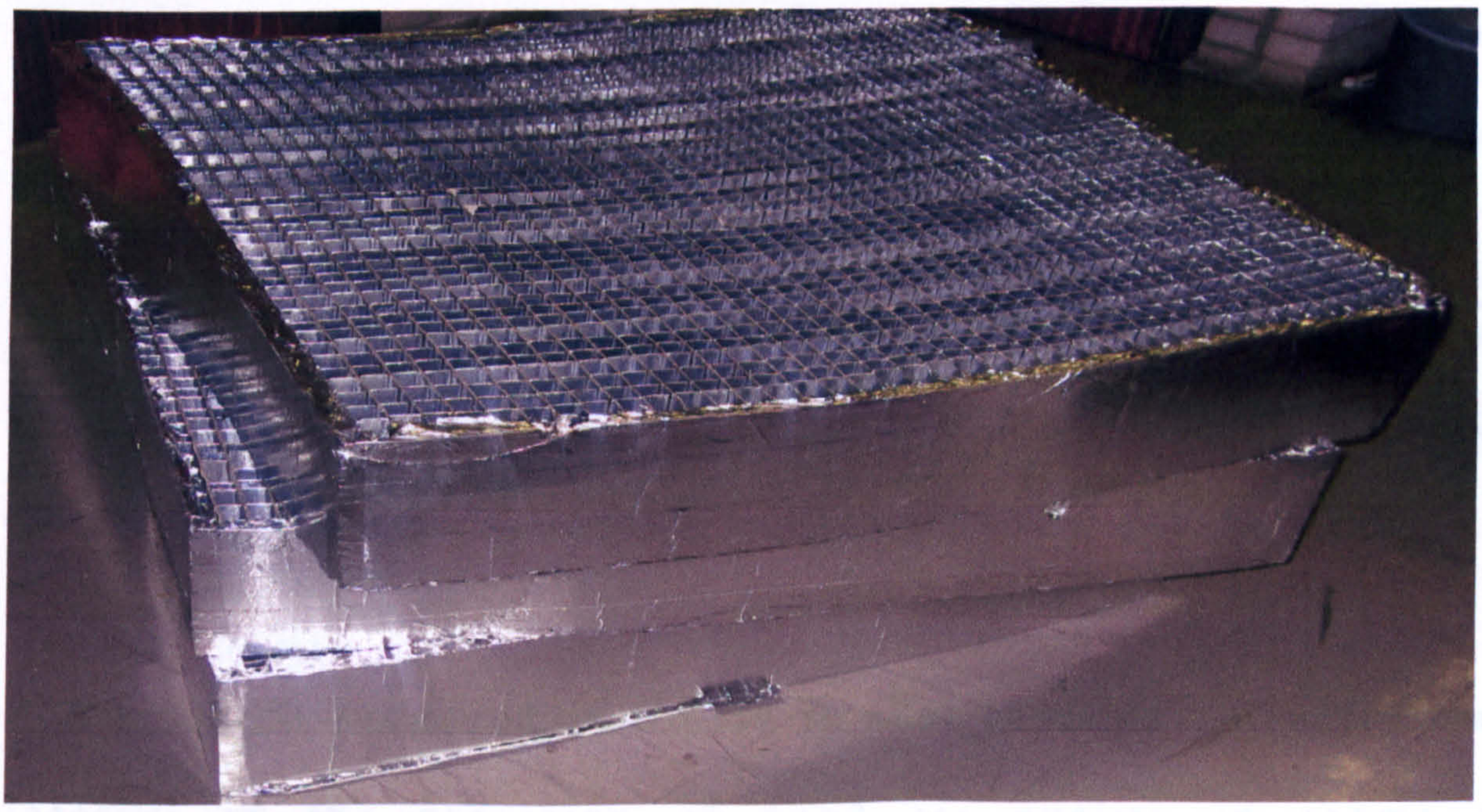

Figure 1.2 Honeycomb slat with Aluminum Foil coating.

Figure 1.3 Honeycomb slats attached to the ceiling (see also figure 5.3).

The above new techniques, once proven by this research, will lead to a total change in the manner of combination of radiant cooling / displacement ventilation systems with the aim of providing thermally stable, comfortable, healthy, habitable spaces to the enhanced satisfaction of the occupants, whilst continuing the international trend towards low energy cooling.

The research proposed is timely in that there is currently much interest in the provision of good air quality in rooms via displacement ventilation (Nielsen 1996). The project also has

very important implications for building energy consumption because displacement ventilation could replace (wherever appropriate) air-conditioning as a means for space cooling. At present, displacement ventilation has limited load removal capacity, as well as suffering from stability problems when combined with conventional chilled ceilings. The proposed thesis will solve these problems.

The existing combination of chilled ceiling and displacement ventilation system experience stability problems that make such integration limited in enhancing air quality. No other research has tried to provide knowledge that can improve the cooling capability of displacement ventilation without destroying the upward air movement characteristics of the system. This thesis proposed would replace the conventional chilled ceiling / displacement ventilation system and provide fundamental understanding of their interaction that can be used in designing good air environment.

1.3. Research objectives

The specific objectives of this thesis are therefore as follows:

(i) To develop an application of CFD for modelling conventional displacement and chilled ceiling environment.

(ii) To repeat item (i) but for the new arrangement consisting of displacement ventilation and 'slat'-clad chilled ceiling environment.

(iii) To determine the optimum slat configuration, using the CFD technique, on the suppression of natural convection of cool air due to chilled ceiling system.

(iv) To validate the CFD predictions for the above conditions using the experimental facility at Loughborough University.

(v) To investigate the potential for a slat system to suppress downward cold convection and hence maintain displacement ventilation.

The deliverables from the project will be identification as to which arrangement can produce the better environment in terms

of confirmation of stabilised conditions, air quality, and hence satisfaction for the occupant, together with sets of performance characteristics and comfort criteria for each system for use by designers. The plan of work is as follows:

(i) The CFD code (Sabre-One), which has been specifically designed to model building airflow and heat transfer, will be used to simulate the conventional chilled ceiling/ displacement ventilation environment. Such computational technique will form the first major phase of the project to develop a suitable thermal model that incorporates the characteristic of displacement ventilation and chilled ceiling system. CFD modelling will be carried out for a range of heating loads and ceiling temperatures to provide fundamental understanding, with high level of detail, of air flow and heat transfer in such environment. The results on this arrangement will form a basis for comparison when the new arrangements are tested. This task will be carried out at De Montfort University.

(ii) Based on heat transfer theory (Hollands, 1965) and performance results predicted, a low emissivity 'slat'-type system will be designed for attachment to the chilled

ceiling, so as to suppress downward currents of cold air from the chilled ceiling whilst allowing radiant transfer with the room to continue unaffected. For this new arrangement, the previous tests will be repeated, and the results will be compared with those from the conventional arrangement, in order to determine the effect of the slat layer on flow patterns and air quality within the room. This task will be carried out at De Montfort University.

(iii) The effect of slat depth/spacing on room airflow including the stability of the stratified boundary layer will be investigated using CFD modelling. The optimum slat configuration will be identified as to which arrangement can produce the better environment in terms of confirmation of stabilised conditions and air quality. The implications of the reduced air movement on air quality will also be investigated. This task will be carried at De Montfort University.

(iv) CFD modelling will be a means of developing a reference model for a new combined chilled ceiling and displacement ventilation system, with a great deal of details, which will

be tested using experimental data using the test room at Loughborough University. This room, which was developed during the EPSRC Contract No. GR/J/46289 is equipped with chilled ceiling and displacement ventilation facilities. This task will be carried at Loughborough University.

(v) The results of the laboratory testing for the Honeycomb slats will be Validated using CFD simulations, which will be carried at De Montfort University.

(vi) The final stage will be an overall analysis of the findings, presented in a format, which can be readily used by designers.

1.4 Structure of the thesis

This thesis will be constructed as mentioned below.

Chapter One, Introduction, objectives and plan of work

Chapter Two, will deal with the literature review.

Chapter Three will highlight the use of CFD code its accuracy in simulating the displacement ventilation and chilled ceiling environment.

Chapter Four will discuss the theory of honeycomb slats, and investigate, if the CFD code can be used to simulate honeycomb slats.

Chapter Five will investigate using CFD simulations to achieve the optimum configuration of the honeycomb slats.

Chapter Six will show details of the manufacturing stages of honeycomb slat and its installation in the test chamber.

Chapter Seven will discuss the experiment method used for the laboratory investigation.

Chapter Eight will present the results obtained from the laboratory investigation and discussion of the results.

Chapter Nine will provide the results of the validation of the laboratory investigation with CFD simulation.

Chapter Ten will provide the conclusion and further recommendations.

Chapter Two

2.0 Literature review

2.1 Introduction

In commercial premises and deep-plan designs with significant internal heat gains, air conditioning has often been specified in order to achieve the required internal space conditions. Air conditioning is widely recognised as an energy-intensive solution. Interest has grown, therefore, in the development of low energy techniques for space cooling, and among these is the use of displacement ventilation and chilled ceiling systems.

2.2 Displacement ventilation

Displacement ventilation is a strategy in which the main intention is to 'partition' room air into upper and lower 'zones', trapping pollutants in the upper zone, and leaving the occupied zone below with a lower pollutant concentration . The height of the partition is known as the stationary zone and it is dependent on the flow from the plumes entering the upper mixed zone being equilibrium with the extract flow. The height of the stationary

boundary is depended on flow in the plumes vary with height, which in turn is dependent on a number of factors. In displacement ventilation system low velocity full fresh air is introduced gently into the occupied zone at low level and at a temperature slightly lower than that of the desired zone air temperature. As a result of density differences, the fresh air forms a cool layer over the floor. The air then rises as it is warmed by heat sources in the zone, and the convective plumes generated by these sources remove heat and contaminants that are extracted at ceiling level this can be seen in figure 2.1. These convection currents entrain air from its surroundings, so that the volume flow increases with the distance from the source. In this way the system is able to provide an environment of improved air quality as compared with mixing of air, which occurs in conventional HVAC systems for the same airflow rate conditions. Further, the same heat load loads can be removed for a supply temperature of typically 19°C as compared with a supply temperature of 13°C in an HVAC system. The system offers enhanced thermal comfort, improved air quality and reduced energy consumption, for removal of the same loads as those removed by a conventional HVAC system (Taki 2005).

2.3 Limitations of displacement ventilation

There are two main limitations that are faced when using displacement ventilation.

(i) In order to remain within the guidelines presented in International Standard ISO 7730 (1994), on thermal comfort (that is, the vertical temperature gradient should be less than 3°C per meter) a displacement ventilation system is limited to removing a convective heat load of up to 25 W/m^2 of floor area (Sandberg and Blomqvist, 1989). However, the typical heating Load in offices frequently exceeds this figure, necessitating the provision of an additional cooling mechanism such as a chilled ceiling.

(ii) The air unit requires a certain amount of wall area, and requires the occupants to be at a certain distance to provide better performance. Hakon Skistad (1994), has suggested that addition to the above two points, the displacement ventilation with buoyancy-driven flows are less effective in the following cases

1. Where ceiling heights are lower than 2.3 metres

2. Where disturbance to room air flows are strong

3. Where the contaminants are colder / denser than the ambient air.

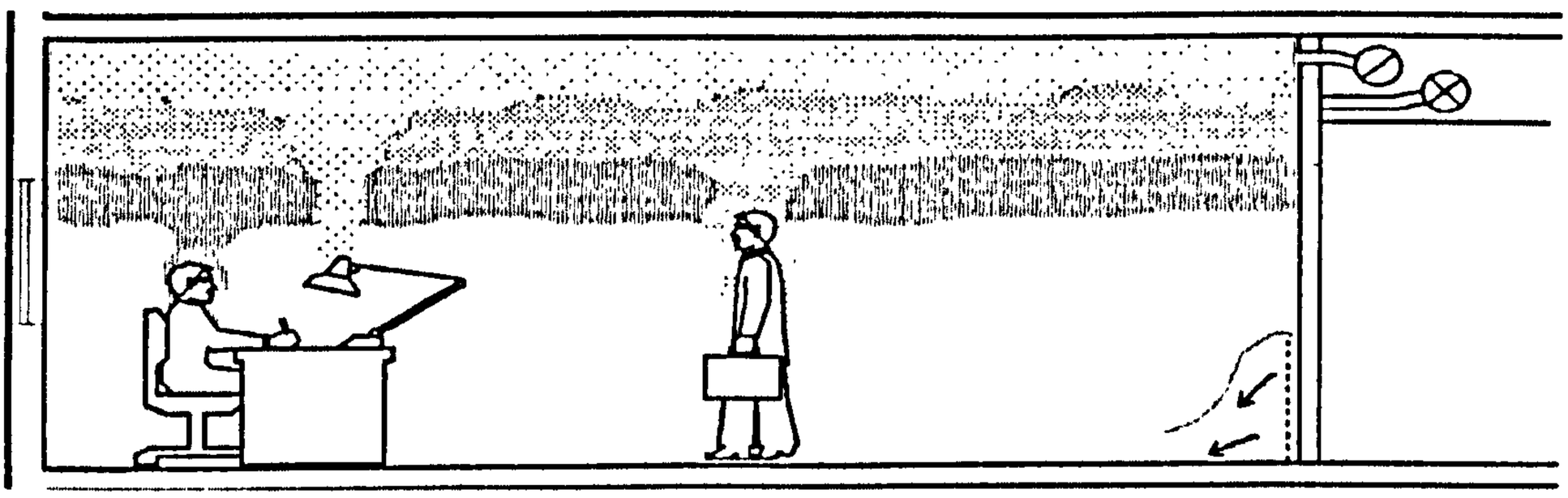

Figure 2.1: Air from different convection sources settle at different levels in the room (Skistad).

2.4 Suitable use of displacement ventilation

- Where the supply air is cooler than the ambient air

- Where contaminants are warm and / or lighter than the surrounding air and associated with a heat source.

- Where the surface temperature of heat sources are high

- Where disturbances to room air flows are weak.

- Where there is sufficient height for the upper mixed zone to be above the occupied space, (in tall rooms, e.g. where the room height are more than 3 meters).

- Improved indoor air quality in the breathing zone due to the result of upward transport of contaminants

- Reduce risk of discomfort due to draught as result of the generally low velocity and turbulence levels in the occupied zone (outside the "near zone" of the diffuser)

- Higher supply air temperature allow the greater use of free cooling either by direct use of outside or indirect evaporative cooling. (higher supply temperatures are

possibly disadvantageous where much dehumidification and reheat is necessary.

- Higher return air temperature resulting in improved heat recovery efficiencies at air handling plant.

- Rather than maintaining uniform air temperature and contaminant concentrations throughout most of the room, vertical gradients of both temperature and contaminant concentration are developed. The result of this is that the occupants in the occupied zone are exposed to temperature and air quality conditions that are similar to the air supply conditions (Jackman 1991).

Due to above advantages it can be understood that displacement ventilation systems have the potential to provide a high quality indoor environment at low flow rate and higher supply air temperature then with traditional mixing ventilation, which mixes the air pollutants throughout the space.

2.5 The chilled ceiling system

In a chilled ceiling system, cool water passes through pipe work, which is bonded to ceiling tiles and is insulated at the rear. This produces a typical ceiling tile surface temperature in the range of 14-19°C. Chilled ceiling system can remove up to 100W/m^2 of floor area by the combined processes of radiation and convection and are considered to enhance the thermal comfort sensation of occupants in a manner analogous to the outdoors and beneath the open sky. Radiant cooling follows the same principles as radiant heating. The heat transfer occurs between the space and the panels through a temperature differential. However, unlike radiant heating, the colder ceiling absorbs the thermal energy radiating from people and their surroundings. The major difference between cooled ceilings and air cooling is the heat transport mechanism. Air cooling uses convection only, whereas cooled ceilings use a combination of radiation and convection. This amount of radiant heat transfer can be as high as fifty five per cent, while convection accounts for the remainder. With cold ceilings, the radiant heat transfer occurs through a net emission of electromagnetic waves from the warm occupants and their surroundings to the cool ceiling. On the other hand, convection

first cools the room air due to contact with the cold ceiling, creating convection currents within the space, which transfers the heat from its source to the ceiling where it is absorbed.

Panel type chilled ceiling systems have been developed in a variety of forms, and includes systems, using air as the cooling source as well as Hydronic systems. Earlier systems, employed ceiling construction of metal planks (extruded aluminium) with copper chilled water pipes clipped to the rear metal planks. Appleby (1998), and Skaret (1987).

Systems are now available that use pressed steel ceiling panels, which are designed to fit closely together and are more easily integrated with other commercial false ceiling construction. This type of chilled ceiling was used for the laboratory investigation. Other chilled ceiling panels are also available and have had investigation on them (Stahl and Keller 1992), (Busweiler 1993), (Niu and Van der kooi 1992,1993), (Niu 1994).

A cooled ceiling operates in direct proportion to the heat load in the room. Typically, a person sitting at a desk will emit sensible and latent (130) watts of energy while a computer emits 90 to 530 Watts to its surroundings. The greater the number of people and /or appliances and exposure to sunlight, the greater the

temperature gradient and therefore an increased capacity of the cold ceiling. Generally, cold ceilings are able to handle up to 100 watts per square meter with up to 50% of the ceiling space utilized for cooling.

One of the disadvantage of the earlier ceiling panels systems was their inability to integrate with other types of architectural ceilings. This has partly overcome by the introduction of metal chilled ceiling panels, which are based on size of standard ceiling tiles.

A limitation on all types of static cooling system using chilled water is the need to avoid condensation at pipe work surfaces. This can impose a limitation on the chilled water flow temperature and hence on the panel load capacity. The possibility of condensation is mainly dependent on the pipe surface temperature and the expected humidity level in the room with the greatest risk probably where the flow pipe work enters. Humidity levels in the room are greatly dependent on the local latent load, infiltration of outside air, and the supply air condition. Laine (1993) has found that condensation will occur at conditions when relative humidity equals 70%, at room air temperature of 23°C, when the chilled water flow temperature of 14°C the pipe surface is about 16°C. However since condensation

of water occurs when the dew point temperature is reached, proper water temperature control can help avoid any condensation. To prevent the formation of condensation, a sensor monitoring the dew point temperature of the room can be used in conjunction with a controller, which modulates the inlet water temperature accordingly. Therefore, if a risk of condensation is present, the water temperature is raised or the water flow is shut off. However, since the lower the panel's inlet temperature is, the more work the panels do, the inlet temperature should be determined to be as close as possible to the room's dew point temperature. Consequently, the cooling capacity of a radiant cooling system is generally limited by the minimum allowable temperature of the inlet water relative to the dew point temperature of the room air.

Panel type chilled ceiling system offer the highest proportion of heat absorption by radiant effect of static cooling systems. The high proportion of radiant cooling has implication for both thermal comfort and the dynamic thermal behaviour of the room. (Rees 1998) Chilled ceiling panel systems, by directly absorbing thermal radiation, will therefore alter the usual dynamic thermal behaviour of the room fabric and system loads, loads with a

radiant component will impose an instantaneous load on the cooling system rather than the lagging.

Rees (1998) has suggested that all air cooling systems invariably give mean radiant temperature a few degrees above the mean air temperature. Udagawa (1993) and Kulpmann (1993) have suggested that chilled ceiling panel systems tend to give room surface temperatures (and thus mean radiant temperatures) closer to the mean air temperature.

The overall heat transfer performance of chilled ceiling panels depends on their ability to promote natural convection in addition to acting as plane radiant collector. In principle the specific heat transfer from a cooled surface by radiation is limited by its emmisvity. (Rees 1998)

The thermal resistance of the ceiling panel is a significant factor in system design and varies with the panel construction. Lower resistance means that the panel surface temperature is closer to the mean chilled water temperature. The chilled water temperature could be limited in practical use due to the need of avoiding condensation.

One possible limitation to the cooling capacity of chilled ceiling panel systems is suggested by the sensitivity of occupants to

asymmetric thermal radiation, a possible sensation of having a cold head. Fanger et al. (1985) has suggested a comfort limit for asymmetric thermal and radiation; Fanger carried out test for different combinations of hot and cold room surfaces. Adopting this method the room can be divided into two half spaces and the so called " half space radiation temperature" be defined for each, so that the thermal comfort limits are defined with reference to the temperature difference. Fanger et al has suggested that for a room with a cool ceiling the half space radiant temperature difference was found to be to the order of 14K for 10% dissatisfied persons. Kulpmann (1993) also carried out tests in rooms with chilled ceiling panels under different load conditions and found that half space radiation temperature difference to be in the region of 5K. Further study are needed in this region to determine if there is a stringent limitation on the chilled ceiling design with relation to the limit of thermal comfort under asymmetrical thermal radiation

2.6 The potential advantages of chilled ceiling panel cooling system

The advantages of can be described as:

- Lower infiltration heat gain resulting from the use of higher operating air temperatures for a given comfort level.

- Greater advantages can be taken of free cooling as a result of the higher chilled water temperatures and vapour compression refrigeration may be avoided in some circumstances.

- Reduced risk of discomfort due to draught can result from lower air change rates required, as the bulk of the sensible loads can be dealt with by the ceiling panels, rather than the ventilation air.

Since air quality must be maintained and radiant panels remove only the sensible heat from the space, radiant cooling panels should be used in conjunction with a small ventilation system.

2.7 Combined chilled ceiling and displacement ventilation system

It can be seen that displacement ventilation and chilled ceiling have a number of features and potential advantages in common. When the both displacement ventilation and chilled ceiling are combined as one system the following advantages may result: -

- The acknowledge limited load capacity of displacement ventilation can be extended by use with static cooling (therefore giving total capacities of the order of 80 W/m^2 of floor area.).

- The potential improved indoor quality benefits of displacement ventilation may be achieved.

- Improved thermal comfort may result from the lower air velocities and turbulence levels inherent in using displacement ventilation and from reduced vertical temperature gradients.

- Improved energy performance may result from taking advantages of higher chilled water temperatures of both these systems, by maximising the amount of free cooling, and the possibilities of using alternatives central plant designs.

Despite the advantages discussed here, this combined system is still relatively new technology lacking long-term trial. Some problems have been reported as mentioned in table 2, and await further investigation. Studies of the combined displacement ventilation and chilled ceiling systems use two main research approaches: Experimental and numerical (computer CFD) modelling. Experimental research is mostly carried out in environmental chambers with some onsite measurements. The measured data is used to assess thermal comfort and air quality; some studies included human subjects for direct validation of thermal comfort models. Results obtained by experimental research are considered to be reliable, but also they are costly and time consuming. As the computer modelling improves its accuracy and speed over time, it is becoming more and more popular.

Main issues of research include thermal comfort, air quality, energy saving, economic, performance of the system, condensation prevention and CFD. Table 2.1 provides a brief summary of the current work related to radiant cooling and displacement ventilation.

RESEARCH AREA	TITLE	AUTHORS	BRIEF SUMMARY OF WORK
Thermal Comfort Air Quality & CFD predicting	The effect of Ceiling Temperatures on Displacement Flow and Thermal Comfort – (experimental and simulation studies)	AH Taki, DL Loveday KC Parson (1996)	The paper provides simulation and experimental data on the combined system of displacement ventilation and chilled ceiling for various heat loads and various ceiling temperatures. The results show that at low ceiling temperature of 14°C the displacement airflow pattern is disturbed but at higher ceiling temperatures of 18-21°C some displacement airflow is present. Also showed that the air quality in the lower zone is reduced at low ceiling temperatures.
	Displacement ventilation environments with chilled ceilings: thermal comfort design within the context of the BSEN ISO7730 versus adaptive debate	DL Loveday KC Parson AH Taki SG Hodder (2001)	The paper provides the results of the laboratory investigation to see if the standard BSEN ISO 7730 is valid to used with the combined system of displacement ventilation and chilled ceiling to predict thermal comfort. The investigation involved 184 human test cases, for 8 test conditions to measure PMV and AMV, for various air changes per hour. The results showed that the ISO 7730 standard is valid and does not require any modification for prediction of thermal comfort.

	Designing for Thermal comfort in combined Chilled ceiling/Displacement Ventilation Environments	DL Loveday KC Parson AH Taki (1998)	The paper deals with the laboratory testing and provides the guidance on design for thermal comfort in displacement ventilation and chilled ceiling system. The results are based on Human subjects. The findings highlight that the combined system at low ceiling temperatures of 14-16°C can caused destruction of the displacement airflow pattern, that Fanger method can be used without modification. High Air change per hour (8) also causes mixing at ceiling temperatures of 18°C.
	Thermal comfort in chilled ceiling and displacement ventilation environments: Vertical radiant temperature asymmetry effects	SG Hodder DL Loveday KC Parson AH Taki (1998)	The paper presents laboratory Investigation on thermal comfort for the combined system of DV &CC. The conclusion is given as that the vertical radiant temperature asymmetry was found to have insignificant effect on the overall thermal comfort of the seated occupant for various ceiling temperatures.
	Ceiling Cooling and Displacement Ventilation in Officers, Thermal Comfort aspects	E Mayer (1995)	Laboratory investigation using psychophysical to measure 54 occupants thermal comfort. The paper concludes that air temperature at ankle should not fall below 22°C and head height should be not exceed 24°C to obtain thermal acceptable thermal comfort.

Thermal Comfort Air Quality & CFD predicting	The Future for Cooling Ceiling	Bunn Roderic and Wyatt Terry (1991)	Paper provides the results of both CFD simulation and laboratory investigation. Concludes that static cooling is an ideal complement to displacement ventilation. Static cooling at ceiling level produces a downward displacement of air which rather then fight the buoyancy of the warm air, slots in underneath the limit of the displacement and lifts it up further also concluded that the radiant components of the chilled beams help to make the occupants feel cool.
	Thermal Comfort and Energy Consumption of the Radiant ceiling panel system compared with the Conventional all Air system	T Imanari T Omori K Bogaki (1999)	The paper compares the two systems in terms of Thermal comfort, energy consumption and cost. The investigation involved both male and female subjects testing in both of the systems. The results showed that the Radiant ceiling creates a superior Radiant environment while cooling and that the radiant ceiling obtained more votes for thermal comfort from the subjects.
	Looking Radiant	Bunn Roderic (1994)	Case study of new offices in UK, having displacement ventilation and chilled Beams. Concluded that the best place for inlet air was under the monitor and back of each desk, this position would drag hot, polluted air away, thus intruding Fresh air over occupants. No data of results were present.

	A Test Time for Chilled Ceiling	Dickson Don (1994)	Laboratory investigation for a combination of displacement ventilation and chilled ceiling. Concluded that heat load of up to 100W/m^2 can be removed and higher inlet temperatures should be used to comply with present standards.
	Static Cooling and Displacement:	Alamdari Farshad (1995)	CFD and Laboratory investigation on the combined system of displacement ventilation and chilled ceiling of heat loads of up to 80W/m^2. Both CFD and laboratory results have a good agreement in temperature and air velocity profiles. Concluded that the system can reduce air quality.
	The Perfect Mix, Finding the Right Mix	Bunn Roderic (1996)	CFD and laboratory investigation on the combined system of displacement ventilation and chilled ceiling and Beams. The findings showed that the combined DV&CC system can lead to an increase in system cooling capacity, over cooling of warm at the level can invert the displacement process and cause downward convection of cold air into the occupied zone. When chilled beams were used the downward convection current was high enough to create a flow field simulation to that of a mixing system.

	Computation of Airflow in a Displacement Ventilation / Chilled Ceiling Environmental	L Jalil AH Taki DL Loveday (2002)	The paper investigates if CFD can be used to simulate a displacement ventilation and chilled ceiling environment. The paper concludes that CFD code can simulate the required environment and also the results agree with other CFD codes results and laboratory investigation. The CFD code results show that the displacement airflow pattern will be disturb at low ceiling temperatures.
	Indoor Climate in Rooms with Cooled Ceiling System	Niu, J Kool jvd (1994)	CFD study on the investigation on the combined of Displacement system ventilation and chilled ceiling having various heat loads. Results show that the DV &CC system give good performance in thermal comfort and ventilation effectiveness at ceiling loads of $50W/m^2$ floor area. The thermal comfort and ventilation effectiveness are almost equivalent to those of Displacement Ventilation system cooling loads of $25W/m^2$.
	A nodal model for Displacement Ventilation and Chilled Ceiling systems in office spaces	Rees, SJ. Haves P. (2001)	Design a new nodal model to present room heat transfer for displacement ventilation and chilled ceiling systems. Laboratory test were carried to verify the results. Nodal model was used to measure heat of plumes.

	Indoor Air Quality in rooms with Cooled Ceiling s. Mixing Ventilation or Rather Displacement Ventilation.	Behne Martin (1999)	Laboratory investigation carried out to establish which of the systems are best to use. The paper provides the pros and cons of each of the systems.
	Numerical Investigation of Transient Buoyant Flow in a Room with A Chilled Ceiling Displacement Ventilation and \system.	Rees SJ, McGuirk JJ Haves P (2001)	CFD and laboratory investigation carried out on the combined DV&CC system. The calculation and laboratory results indicted that for DV&CC system at high loads (45&75W/m^2) the flow becomes Quasi-periodic in nature.
	Cooling Load Dynamics of Rooms with Cooled Ceilings	J Niu J VD Kooi H VD Rees (1998)	Laboratory investigation on Four systems All air, All air total heat recovery Cooled ceiling with Air total heat recovery Cooled ceiling and desiccant cooling. The findings show that the cooled ceiling and desiccant cooling could save up to 44% of energy compared to the All air system

Condensation Problem	The Truth behind Chilled Beams	Butler David (1997)	Four buildings used as offices were investigated having chilled beams. Findings were presented and recommendations are given to prevent condensation.
	Condensation Control for Chilled Ceiling and Beams	Andrew Martin, Farshad Alamdari (1995)	The paper focuses attention on the need to prevent condensation on the ceiling s and their pipe work, and also exam's the extent to which condensation occurs reviews the available control strategies. Also suggests that chilled ceilings offer a useful means of removing heat from rooms, at the same time provide acceptable thermal comfortable environment at high dry bulb temperatures, as well a low draught risk. More energy efficient.
Energy Saving Technique	Energy Saving Possibilities with Cooled Ceiling systems	Niu J, Kooi jvd, Ree Hvd (1995)	Paper presents the findings on the investigation on two systems. Water type cooled ceiling, and convectional all Air system. The findings show that the Water type cooled ceiling system can save much of the fan energy required in the system, and can increase the heat removal rate.

	Chilled Ceiling in Parallel with Dedicated Outdoor Air Systems: Addressing the Concerns of Condensation, Capacity, and Cost	Stanley A Mumma (2002)	The paper explores the primary concerns expressed by the building industry about radiant cooling and its associated problems.
Simulation and Optimization of system Performance	Air Conditioning with a Combination of Radiant Cooling, Displacement and Desiccant Cooling	Busweiler U (1993)	The paper provides the findings of a case study of a conference room in Germany. The findings show that the combined system of chilled ceiling and desiccant cooling can help to solve simultaneously problem in air conditions also the system can save energy and reduce peak electric consumption.
	A Model Performance	Davids Gavin (1994)	Laboratory investigation suggesting that combination of displacement ventilation and chilled ceiling will act as a mixing system, and not as a displacement system. Whereby discomfort could arise from unacceptable combinations o velocity and low temperatures in down flow from the cooling system.

	Beaming Down	Bunn Roderic (1994)	Report on a 12 story office in London, where a combination of displacement ventilation and chilled Ceiling was used and 1200 chilled ceiling panels were installed; expected heat load in offices was in the region of 55W/m^2. It was expected that the system would work better than the a Disenchament with valves system. No results were presented.
	First Among Equalios	Thomas David (1994)	The paper presented a case study where a chilled ceiling system had been working successfully in a London office.
	A Critical Review on the Performance and Design of Combined Cooled Ceiling and Displacement Ventilation system	Novoselac A, Srebric J (2002)	The paper provides a wonderful review of various aspects of the combination system of DV &CC. The paper deals with, thermal comfort, indoor air quality, energy & capital cost and design parameters. The author concludes that the DV&CC system can disturb the displacement airflow pattern but if properly designed can provide better indoor air quality and thermal comfort level than the mixing system.

	Review of Research into and application of chilled ceilings and displacement ventilation systems in Europe	Riffat, S B, Zhao, X Riffat, S B. Zhao, X., Doherty, P. S., (2004)	A very good paper consisting of 29 pages, deals with all possible aspect of DV&CC system. Its origination, Development and Current status. A comprehensive review is presented on the DV&CC system paper. The Author concludes that at high heat loads (70 W/m^2) can disturb the displacement airflow pattern. But correct layout of the chilled ceiling might reduce the downward convective airflow and thus maintain the expected displacement flow in most of occupied zone.
	Displacement Flow and Cooling Ceiling	K Fitzner H Kruhne (1996)	Experimental results are presented for the combined system of DV&CC for heat loads up to 50W/m^2 for various ach. The paper concludes that the combined system can increase the contaminated in lower room zone and disturb the displacement airflow pattern.
	Chilled Ceiling and Displacement Ventilation	F Alamdari DJG Butler PF Grigg MR Shaw (1998)	CFD and Laboratory investigation, concluding that the combined system of DV&CC will disturb the displacement airflow due to the radiant heat transfer between the chilled panel and wall reduces the room surfaces temperatures below the room air temperatures which causes downward convection near the wall therefore transport contamination from upper the region

			into the occupant zone.
	Displacement Ventilation and Cooled Ceilings	F Alamdari (1998)	CFD and laboratory on displacement ventilation and chilled ceiling investigation which concludes on 25W/m^2 heat load can be removed by displacement ventilation.
	Hydronic Radiant Cooling Preliminary Assessment	Feustel HE, Stetiu C (1995)	The paper provides data on radiant cooling and investigates if radiant cooling could perform well in US climate.
	Cooling Load Dynamics of Rooms with Cooled Ceiling	Niu J, (1997)	Paper provides the results for a numerical simulation and laboratory experimental test to validate the number simulation. The paper also deals with the performance of the chilled ceiling and thermal comfort.
	Air Conditioning and Displacement Ventilation: System Analysis	Cost Research and Engineering Services	Two pages breakdown of the cost involved in installing air condition systems and highlights vary cooling systems available.

		Department (1998)	
	Hydronic Radiant Cooling Preliminary Assessment	Helmut.E Feustel Corina Stetiu (1995)	The paper provides data on radiant cooling and investigates if radiant cooling would perform well in the US climate.

Table: 2.1 Showing the outline of review of work carried out by various researcher on the combined displacement ventilation / chilled ceiling systems.

To summaries the current research in more detail from the Graph.

Taki and Loveday (1996) carried out an intense study on the effects of displacement ventilation and chilled-ceiling systems when combined together. The research showed interesting reading. Taki contradicted Kofoed's (1994) finding that when chilled ceiling and displacement ventilation are combined together, the overall system is claimed to offer enhanced thermal comfort, improve air quality. Research carried out by Taki (1996) showed that this was not the case, as the warmer air given off by the displacement ventilation will rise and the cooler air released from the chilled ceiling will fall down as it is denser. This process will act as catalysts for the convection current flow and will produce an invisible layer of contaminated air, which leads to an environment of poor air quality. Taki further went on to suggest that in his studies he found that combination of chilled ceiling and displacement ventilation system could cause destruction of the displacement flow pattern at low ceiling temperatures of 14-16°C. At higher ceiling temperature 18-21°C, some displacement flow is present but the stratified boundary layer is strongly suppressed. He concluded by suggesting that the combination of the system could cause

deterioration in air quality as result of diminished displacement flow pattern.

Kruhne (1993) results showed that when both DV & CC system are combined, the increase value in temperature difference between the room air and ceiling surface the radiation exchange increases. At the walls this leads to a downward buoyant flow of air. Because the air begins to flow downward out of the mixing zone below the ceiling, the contaminated air reaches the zones of fresh air and increases contamination near the floor and in the breathing level, suggesting that this buoyant wall flow forces the contaminants out of the mixing region below the ceiling into the fresh air layer figure 2.2 shows the diagrammatic presentation of the above mentioned motion. This is caused mainly through the radiant heat exchange between room walls and cooled ceiling, the air is then driven downwards by the negative buoyancy, therefore the wall tend to have a lower temperature than room air. Therefore suggesting that contaminant concentration is higher than in the case of " Pure " displacement ventilation.

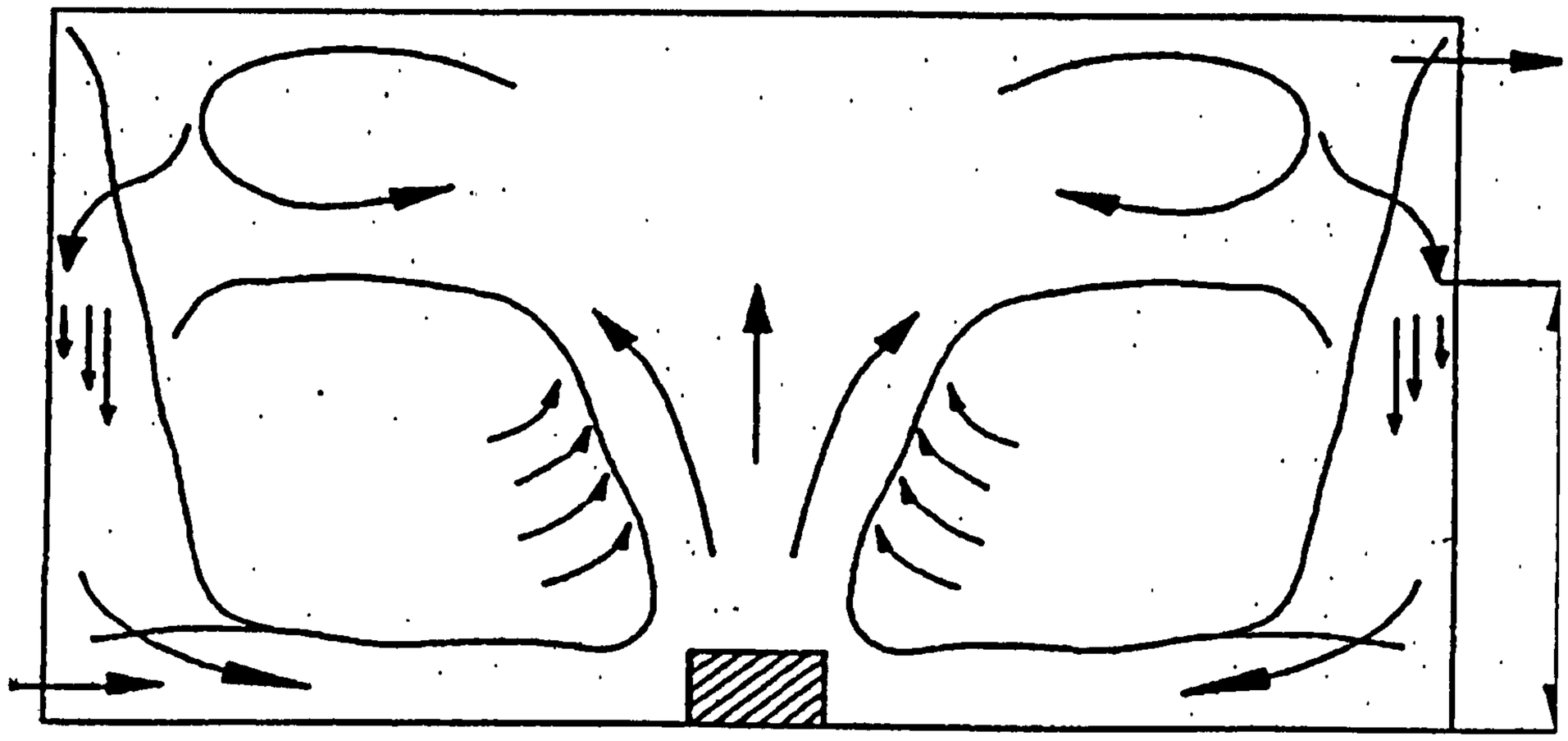

Figure 2.2: Showing the diagrammatic presentation of Kruhne findings that the combined DV&CC system can disturb the displacement airflow pattern.

2.8 Summary

A body of research has been conducted on the combination of displacement ventilation and chilled ceiling as a cooling system. Skaret (1987), Behne (1993), Kruhne (1993), Kulpmann (1993), Skistad (1994, displacement ventilation book), Taki, and Loveday (1996), Rees (1998), Srebric and Novoselac (2001), Riffat, Zhao and Doherty (2004). Which have all concluded that the use of displacement ventilation and chilled ceiling as a combined system can disturb the displacement airflow pattern,

reduce the air quality, and thermal comfort of the occupant. For these both systems to work as one combination, the downward airflow near the walls, as well as in the room needs to be reduced or suppressed. This can be achieved by the use of a 'slat'-type system attached to the chilled ceiling for suppression of the natural convection current of cold air near the ceiling and will preserve the displacement airflow pattern in the room.

The next chapter will discuss the first stage of the research, by introducing CFD model, to simulate the displacement ventilation and chilled ceiling environment and will also highlight the problem associated with the combined displacement ventilation and chilled ceiling systems.

Chapter Three

3.0 Computational Fluid Dynamics (CFD)

3.1 What is Computational Fluid Dynamics (CFD)?

CFD is a computational technique based on the numerical solution of fluid flow equation it is used for predicting what will happen, quantitatively, when fluids flow, often with the complications of:

- Simultaneous flow of heat,
- Mass transfer (eg perspiration, dissolution),
- Phase change (eg melting, freezing, boiling),
- Chemical reaction (eg combustion, rusting),
- Mechanical movement (eg of pistons, fans, rudders),
- Sresses in and displacement of immersed or surrounding solids, and is used for industrial and non industrial applications.

3.2 How does CFD make predictions?

3.2.1 Solver

There are three distinct streams of numerical solution techniques:

- Finite difference
- Finite elements
- Spectral method

The main differences between the three separate stream are associated with the way in which the flow variable are approximated and the discrimination processes.

Like many physical phenomena, fluid flows are governed by mass, momentum and energy balance principles, which are typically expressed in the form of partial differential equations. For example, subsonic flow of air, or flow of water, can be

described using the incompressible Navier-Stoke equations. The Navier-Stokes equations are capable of producing an astounding variety of fluid flows, such as ocean waves, wingtip vortices, whistling of telephone wires in the wind etc. The complexity of fluid behaviour carries with it a certain price: the Navier-Stokes equations are extremely difficult to solve using pen and paper, or *analytically*. Traditionally, this deficit of solutions had to be alleviated by observing the actual fluid in action, or experimentally. But such experiments are quite costly to set up and perform. They also come at a wrong time in the design process—after the wind tunnel model or an actual device has been already built.

In the last 40 years, it became possible to approximately solve the Navier-Stokes equations using a brand-new *computational* approach. Here, the Navier-Stokes equations are broken down into pieces, each simpler to analyze. These pieces, which can number in the millions, are then put together with the help of a computer to form a coherent whole. The necessary step is the reduction of the continuum, i.e. the velocity and pressure at every of the infinite number of points of interest, to the *discrete* set of values, which is finite. The common discrimination methods are:

3.2.2 Finite difference method

The infinite set of points is replaced by a finite set of points, called *nodes*, and the Navier-Stokes equations are enforced only at these points. The local form of the equations takes the shape of stencils, which relate velocity and pressure values at one node to the values at neighbouring nodes. Formation of the stencils requires that the nodes be connected in a *structured* mesh, so that each node is able to identify its neighbours to the south, north, east, west etc.

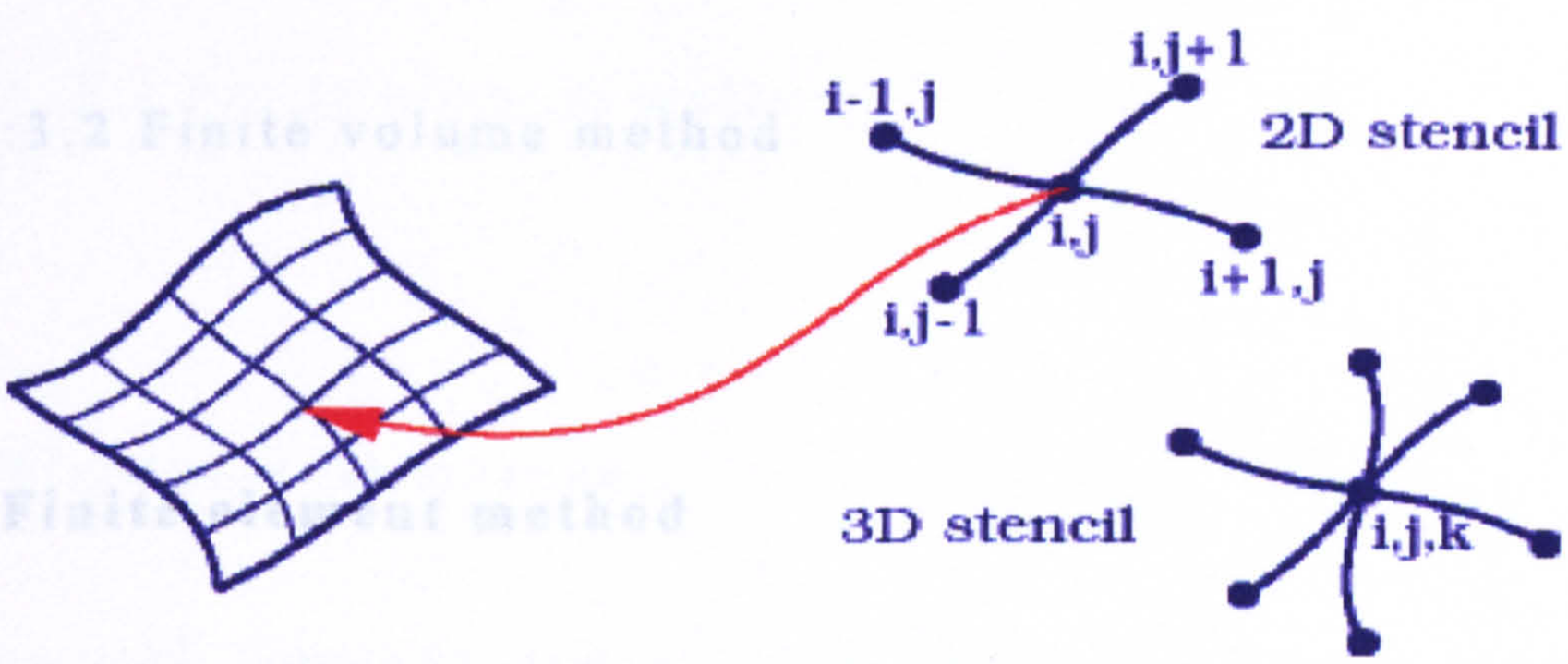

Figure: 3.1 Finite difference method

3.2.3 Finite volume method

The volume taken by the fluid is divided into a finite number of volumes, or *cells* and Navier-Stokes equations are converted into

equivalent integral forms are applied to each cell. The local form of the equations balances mass and momentum *fluxes* across the faces of each individual cell. The shape of the cells may be irregular, or *unstructured*.

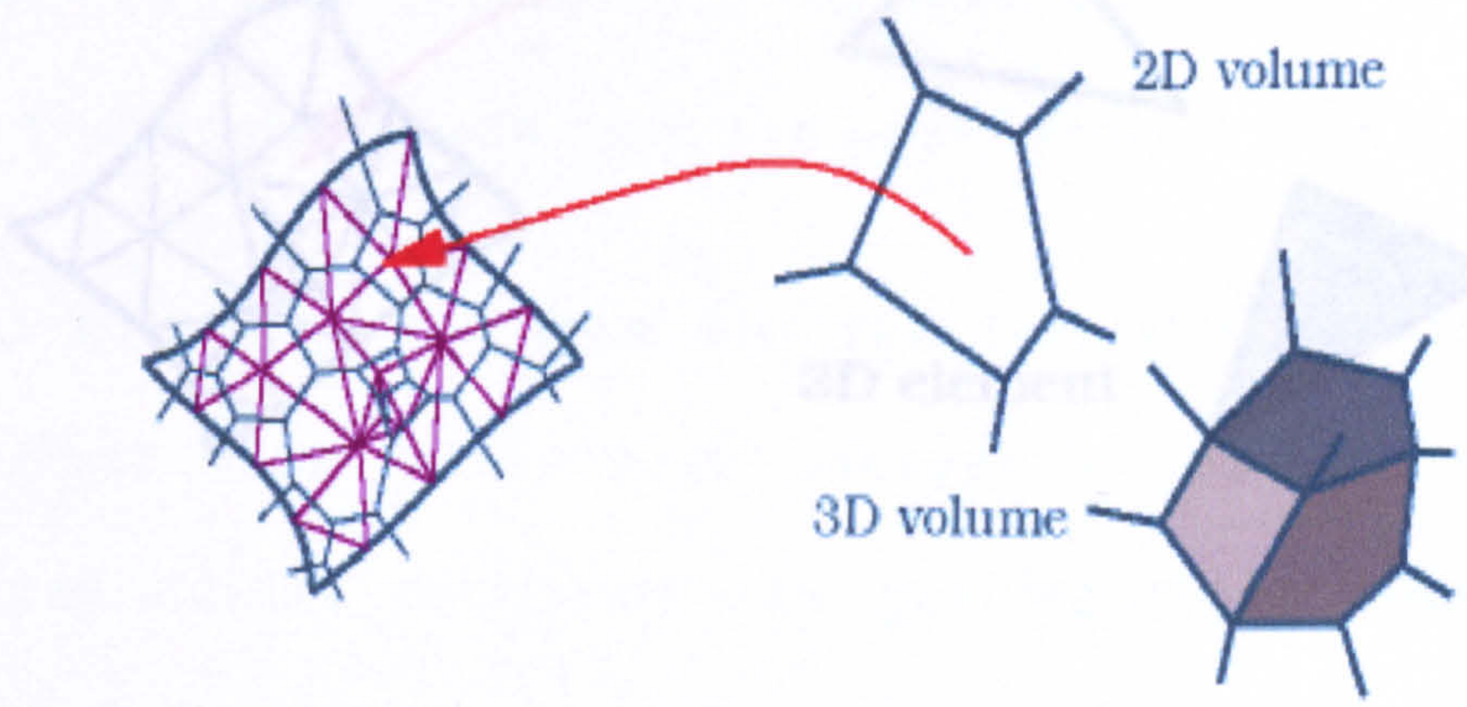

Figure:3.2 Finite volume method

3.2.4 Finite element method

A large but finite number of known functions are proposed as the representation of the flow field, and Navier-Stokes equations are used to select the one with best approximation properties. The candidate functions are constructed from simple interpolation functions within each *element* into which the domain is divided.

The value of the function everywhere inside the element is determined by values at the *nodes* of that element. The elements combine to form a mesh, which can be also unstructured.

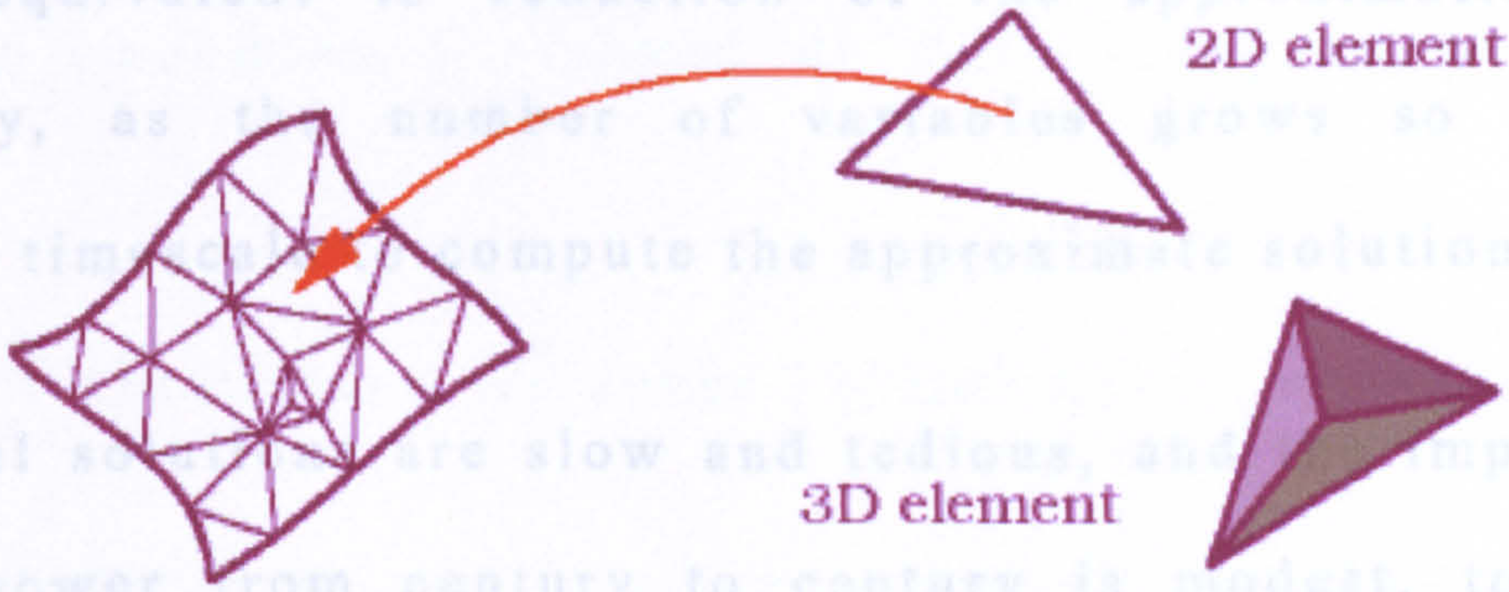

Figure: 3.3 Finite element method

3.2.5 The spectral method

The Spectral methods approximate the unknowns by means of truncated Fourier series or series of Chebyshev Polynominals. Unlike the Finite difference or Finite element approach the approximations are not local but valid throughout the entire computational domain.

All the methods, if properly applied, will give better and better approximation to the actual solution of Navier-Stokes equation as the number of variables is increased. This is known as 'convergence' of the approximate solution to the real solution, and is equivalent to reduction of the approximation error. Obviously, as the number of variables grows so does the computer timescale to compute the approximate solution.

Analytical solutions are slow and tedious, and the improvement in brainpower from century to century is modest, to say the least. Experimental facilities are getting more capable every year, but only incrementally. By contrast, the power of computers has been growing exponentially, fuelled at first by weapons and transportation research budgets, and more recently, by a vast general-purpose computing market.

3.4 Can CFD be trusted?

In solving the fluid problems we need to be aware that the underlying physics is complex and the results generated by a CFD code at the best as good as the physics and chemistry embedded in it and at worst as good as its operator.

CFD-based predictions are never 100%-reliable, because:

- the input data may involve too much guess-work or imprecision;
- the available computer power may be too small for high numerical accuracy (this is often the case);
- the scientific knowledge base may be inadequate (so is this).

The reliability is greater:

- For laminar flows rather than turbulent ones
- For single-phase flows rather than multi-phase flows;
- Or chemically-inert rather than chemically-reactive materials;
- For single chemical reactions rather than multiple ones;

- For simple fluids rather than those of complex composition.

Therefore, coal-fired furnaces represent an extreme of uncertainty; but CFD is nevertheless used increasingly in their design because the uncertainties resulting from its non-use is even greater.

3.5 CFD code used for the simulations.

Sabre One CFD code was used for the CFD simulation. Sabre One CFD code was chosen over other commercially available CFD codes because it has been specifically designed to model building air environment, as the research involves modelling of indoor air environment. Sabre One code uses the finite volume method for numerical solution. The CFD simulations carried out for the required boundary conditions were conducted by the two turbulence models, Eddy-viscosity or K-epsilon.

3.5.1 Eddy Viscosity

A sample model of turbulence is that of a constant Eddy-viscosity model. Where the diffusion coefficient is defined by input data is a constant throughout the flow field. For further reading see whittle (1996)

3.5.2 K-e model

The most widely used method of representing turbulence is the two-equation K-e model. This is an eddy viscosity model where the diffusion coefficient is computed independently for each cell in the calculation domain. The turbulence diffusion coefficient is predicted from values of "k", the kinetic energy of turbulence, and "e", its dissipation rate. The disadvantages are that both "k" and "e" require the solution of one additional convection diffusion equation each. This increases the computational demand due to the need to solve the extra equations and also because the diffusion coefficients "evolve" with the solution variables thus increasing the time to taken to achieve a converged solution. (for further reading see Whittle (1996)

3.6 Validating the CFD code (SABRE-One)

To assess the accuracy of the SABRE-One CFD code used it was compared with other CFD codes available, CFX, FLOVENT and , laboratory test results of Taki et al (1996) and other researchers.

Cook (1997) used CFX code for his finding in natural ventilation work, similar boundary conditions were set, where a room 5.1m in length, 1.0m in width and 2.55m in height. Having two opening, one in the floor and the other in the ceiling to allow the air in and out by natural ventilation with a line heat source of 200 watts distributed in the centre of the room having an area of 0.1m width x 1.0m length.

The results showed similar flow pattern and temperature in the room. The temperature at and above the stratification boundary layer is the same, the only difference is in the displacement flow curve leading to the stratification boundary layer, this could have been caused by inaccurate simulation of the correct size of the openings inlet and outlet (figure 3.5).

The code was further compared with FLOVENT CFD code that was used by Alamdari and Eagels (1996) in their investigation with displacement ventilation and chilled ceiling. Similar

boundary conditions were simulated to that of Alamdari work. Room size 4.5m in length, 2.7m in height and 4.5m in width, having two dummies with 20W/m^2 heat load imposed on them, with 19 ^{0}C supply air temperature with 3.5 ACH. The results showed very good agreement with the Flovent CFD code, both having similar airflow pattern, and temperature gradient (see figure 3.6)

The code was compared to Taki et al (1996) laboratory results. The same boundary conditions were simulated using the CFD code, room size 5.4m length, 3.m width and 2.8m height, with four work dummies each having various heat loads imposed on them ranging from 15-25-35-50 and 60 W/m^2. The supply temperature was 19 ^{0}C with 3.9 ACH. The results at first showed large differences in temperature, and airflow patterns, this was due to heat transmission and heat accumulation in the building and only a part of the heat gain inside the room was removed by ventilation. (Theses heat losses were calculated as being in the region of 40% of the heat loads). These heat losses were incorporated into the CFD simulation to represent correct heat loads in the lab. The results from this simulation showed very good agreement both in temperature and airflow pattern (see figure 3.7)

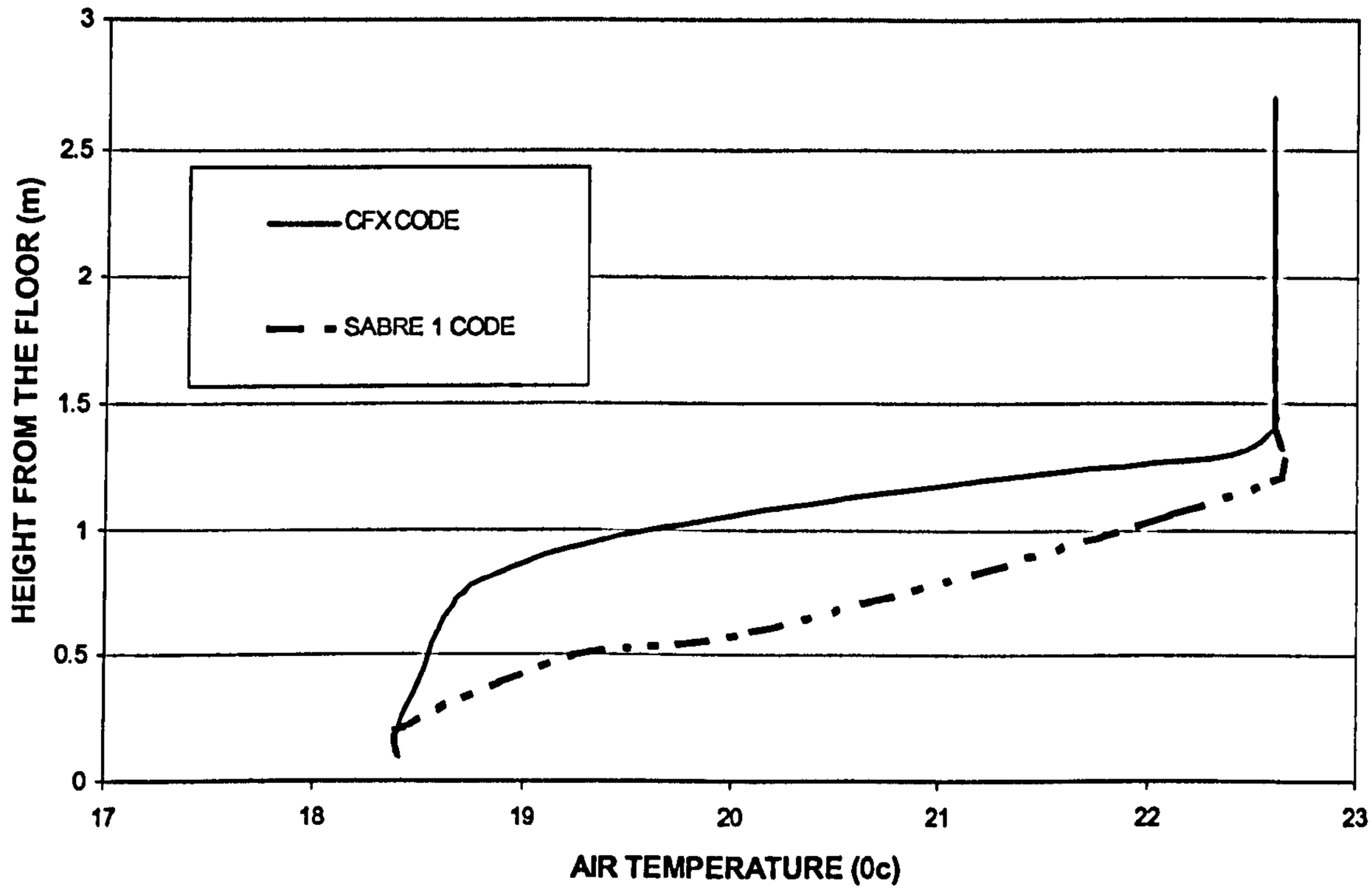

COMPARISON OF RESULTS BETWEEN CFX AND SABRE1 CFD CODE TO REPRESENT NATURAL VENTILATION

Figure 3.4: Showing the comparison of results between CFD used by Cook (1997) and Sabre-One CFD model. It can be seen that the code has predicted the same height of the stratified boundary layer and similar air temperature to the ceiling height.

.

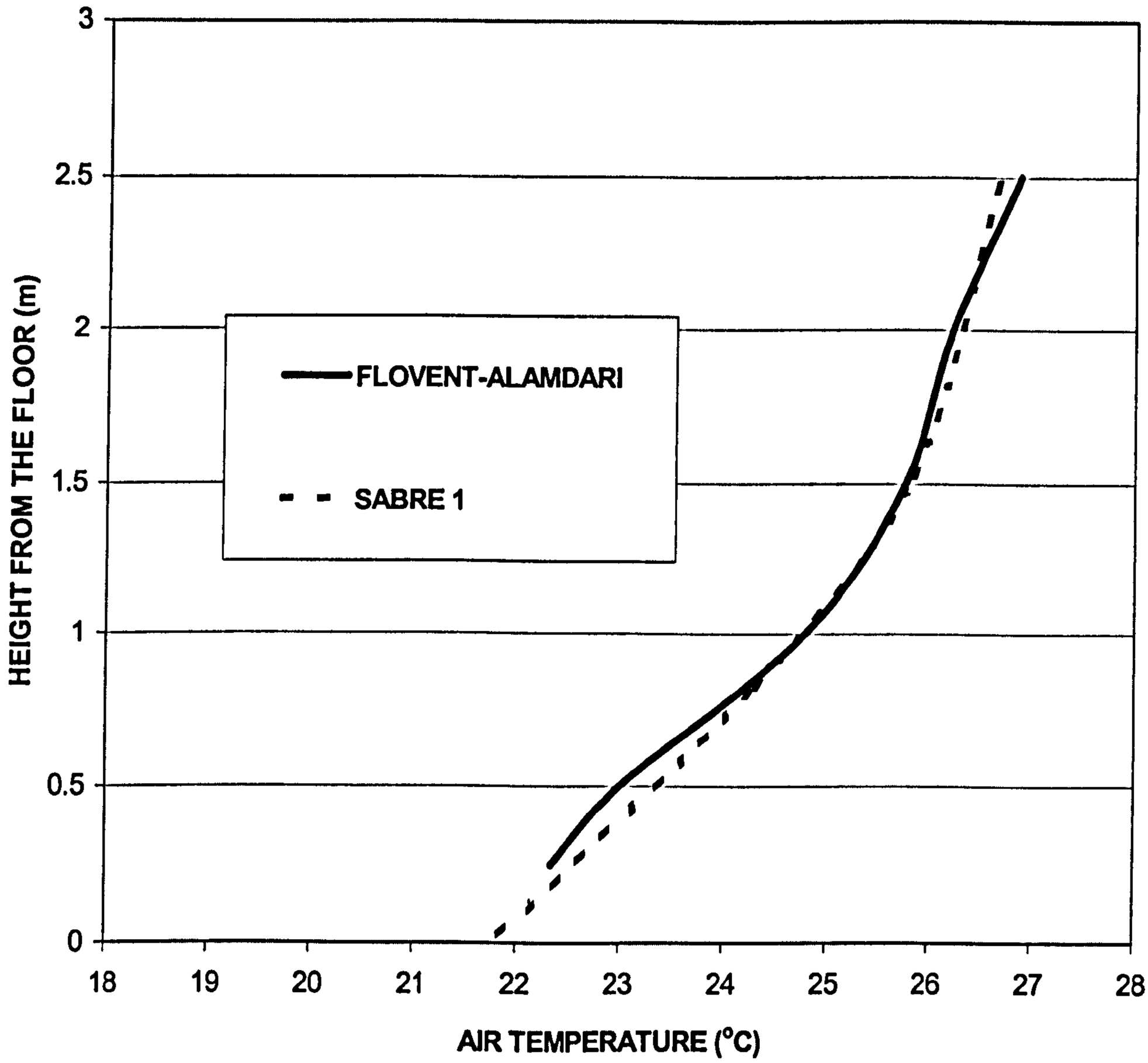

Figure 3.5: Showing the results between the Flovent Code used by Alamdari (1998), and the Sabre-One CFD code. The results show the same air temperature profile, which suggests that Sabre One CFD code will produce results similar to other commercially available CFD codes.

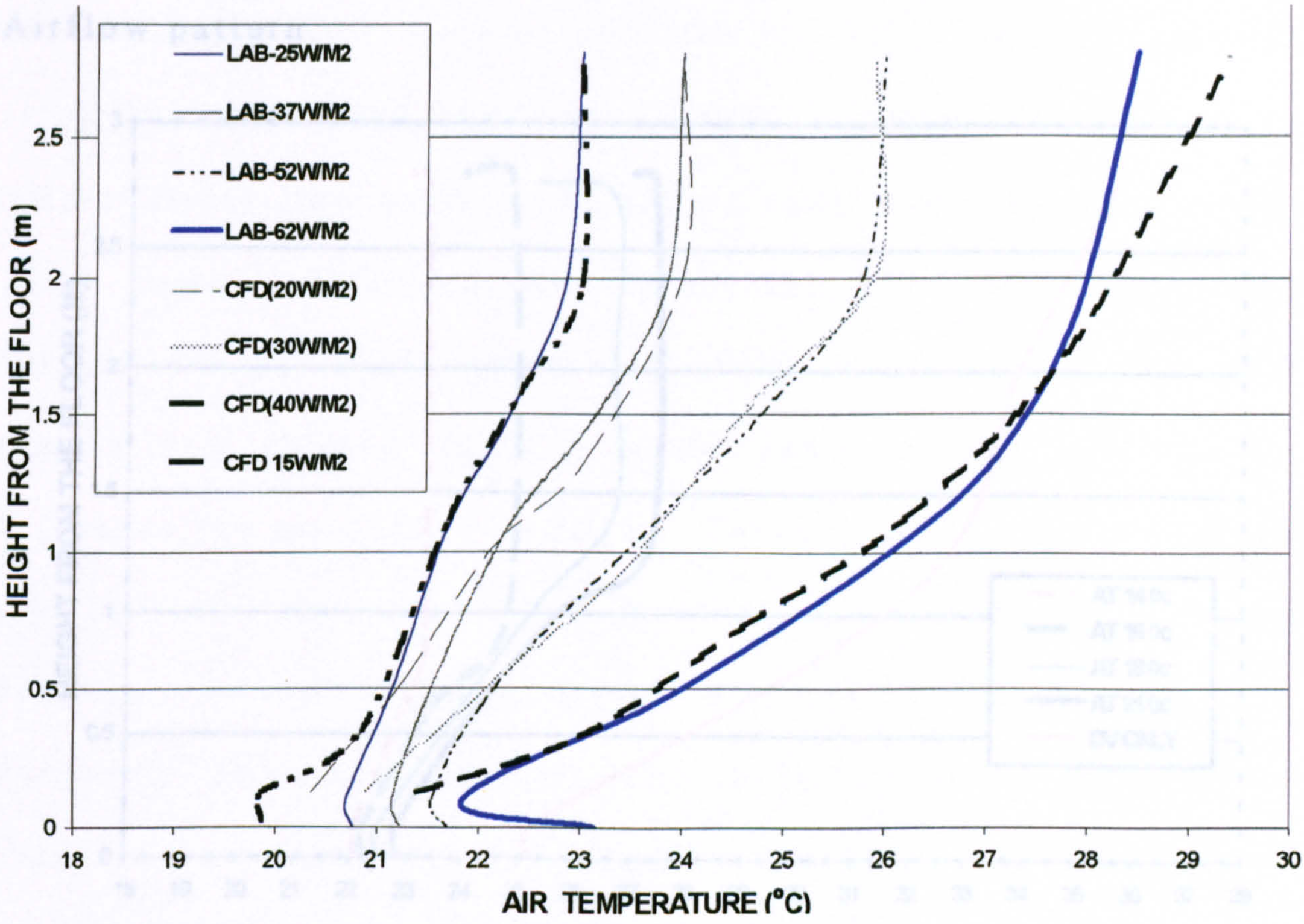

Figure 3.6: Graph showing the comparison between the results of Taki et al (1996) and the predictions of the CFD code. When various heat loads of 25-37-52-and 62W/m^2 were imposed on the dummies. The results show similar temperature profiles.

As above results confirm the accuracy of the CFD model, computational fluid dynamics simulations were carried out for displacement ventilation and chilled ceiling system having different Boundary condition to assess what effects the chilled

ceiling systems have on the Air quality and Displacement Airflow pattern.

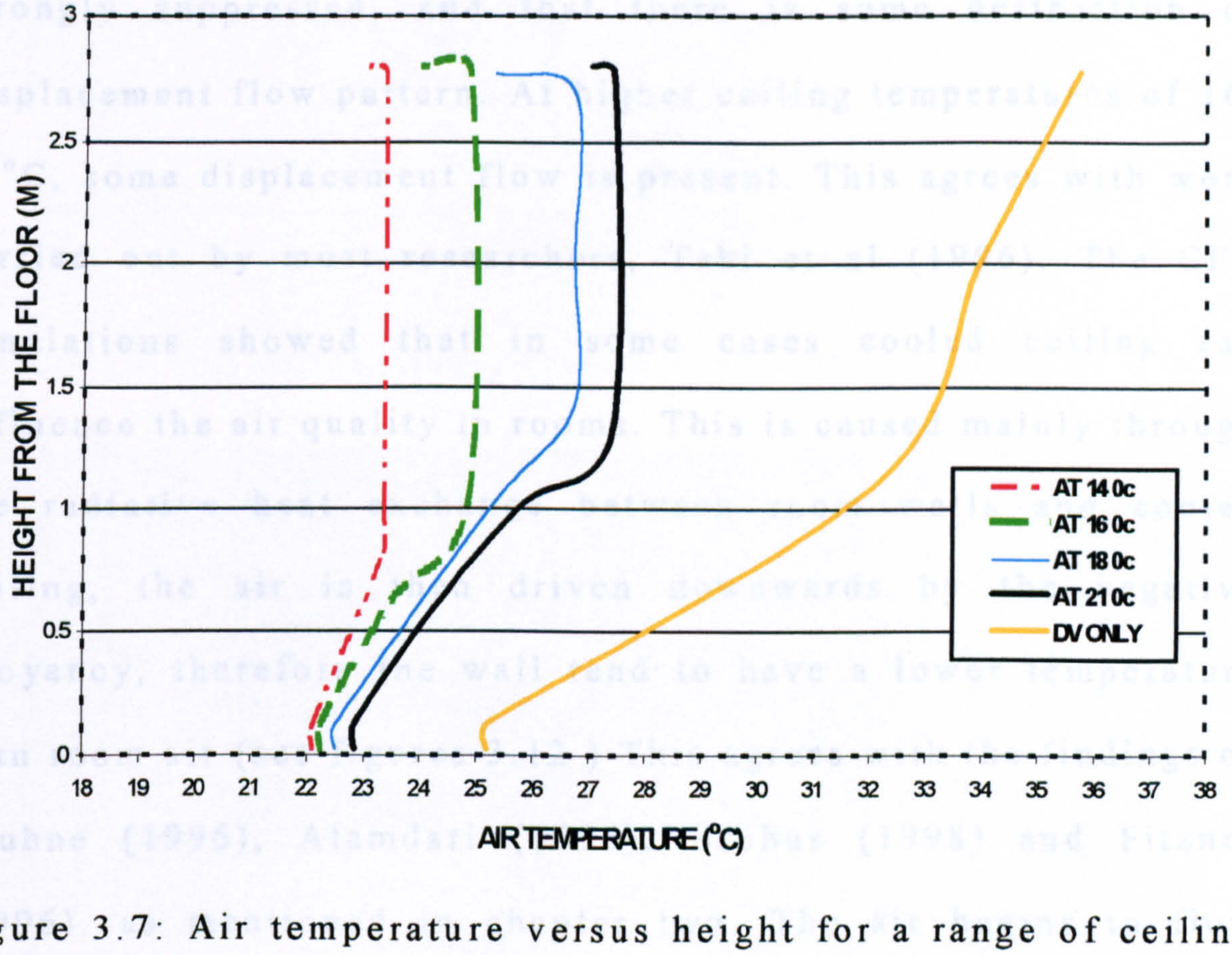

Figure 3.7: Air temperature versus height for a range of ceiling surface temperature at a heat load of 60W/m^2 and supply air temperature is 19°C.

Figure 3.7 shows the results of CFD simulation, vertical temperature profiles in the room, for a range of ceiling temperatures (14, 16, 18 and 21°C) at a fixed heat load of 60W/m^2. Figure 3.8 also shows the predictions of temperature profile for the case of displacement ventilation only (where

there was no chilled ceiling). The CFD simulation shows that at low ceiling temperatures of 14°C the stratified boundary layer is strongly suppressed, and that there is some destruction of displacement flow pattern. At higher ceiling temperatures of 16-21°C, some displacement flow is present. This agrees with work carried out by most researchers, Taki et al (1996). The CFD simulations showed that in some cases cooled ceiling can influence the air quality in rooms. This is caused mainly through the radiative heat exchange between room walls and cooled ceiling, the air is then driven downwards by the negative buoyancy, therefore the wall tend to have a lower temperature than room air (see figures 3.12) This agrees with the findings of Kruhne (1996), Alamdari (1996), Brohus (1998) and Fitzner (1996), as mentioned in chapter two. The air begins to flow downward out of the mixing zone below the ceiling; the contaminated air reaches the zones of fresh air and increases contamination near the floor and in the breathing level.

Figure 3.9 shows the diagrammatic presentation of Figure 3.10, Figure 3.10 shows CFD simulation showing the above mention scenario and Figure 3.11 shows the temperature profile in the room highlighting that the air temperatures at the walls tend to have a lower air temperature than the room air temperature.

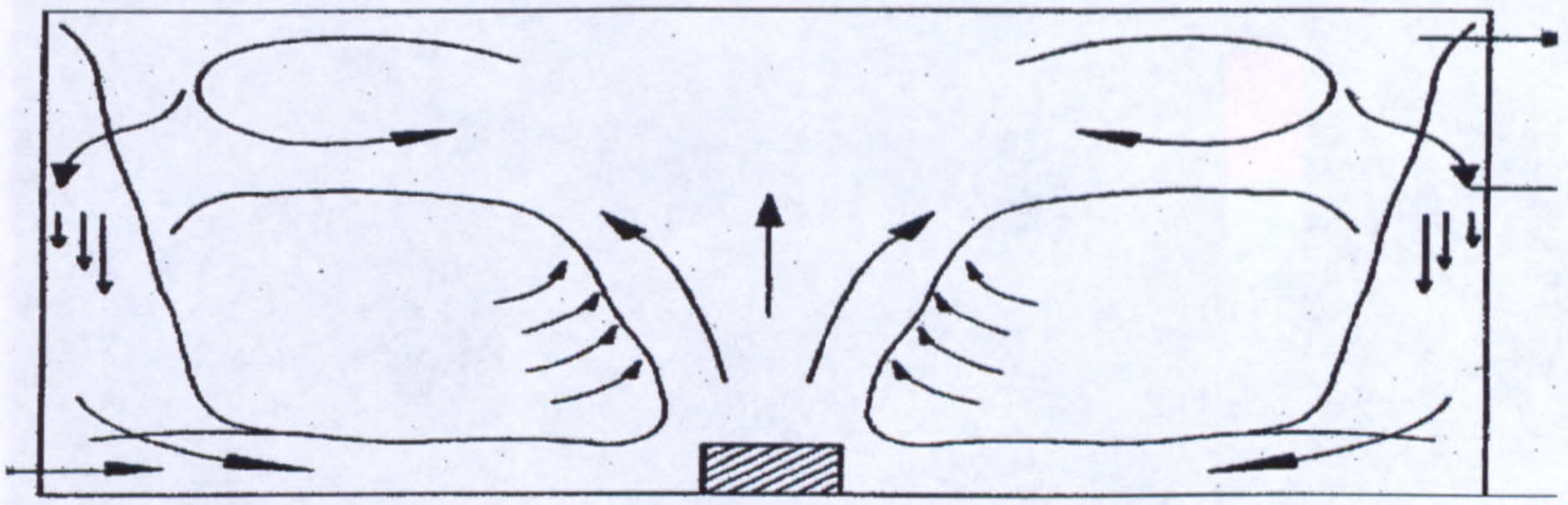

Figure 3.8 Shows the diagrammatic presentation of Figure 3.9

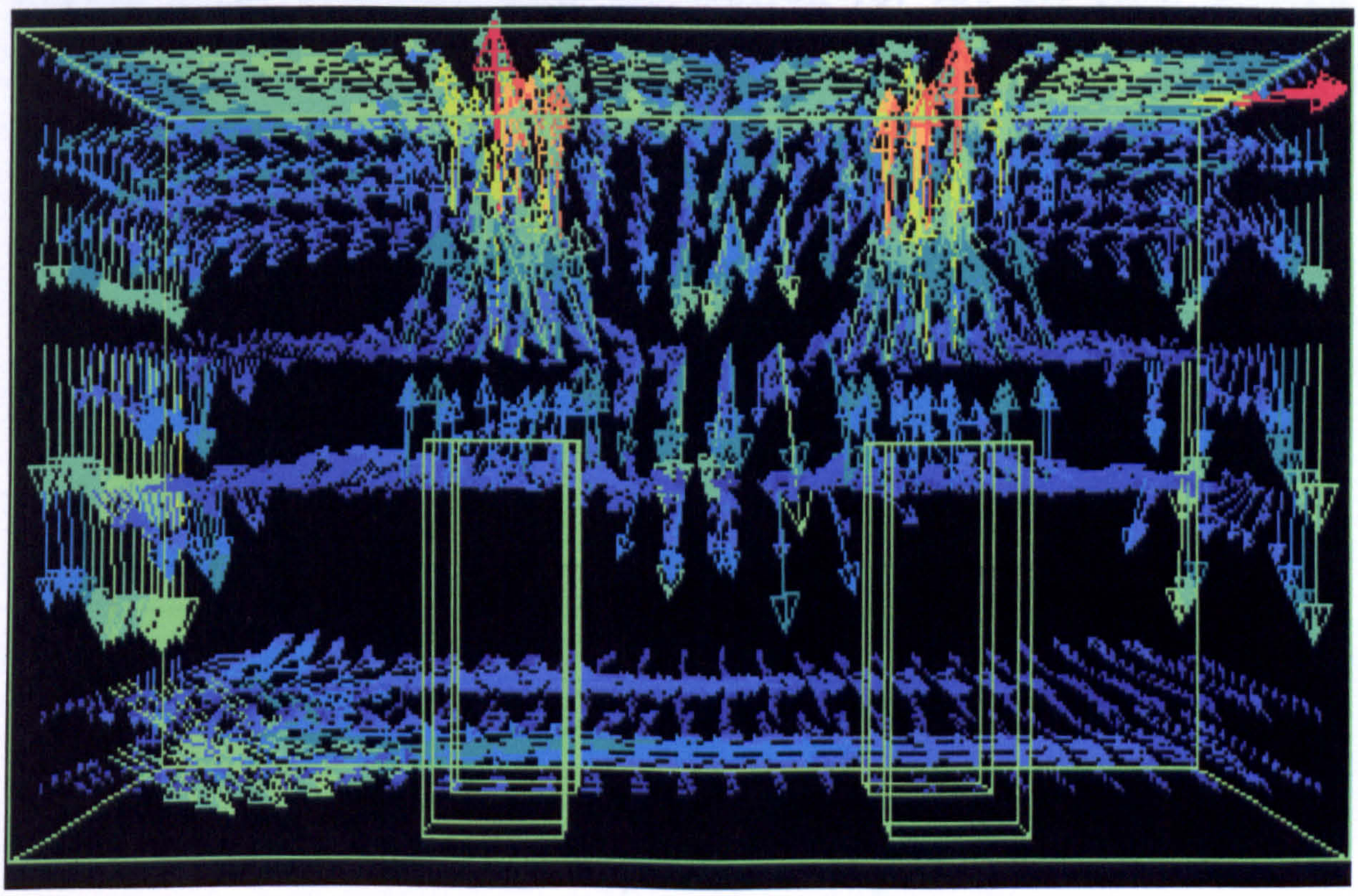

Figure 3.9: Showing that due to the chilled ceiling cold air is driven downwards along the walls transporting the mixed air in to the fresh area zone and disturbs the displacement air flow pattern

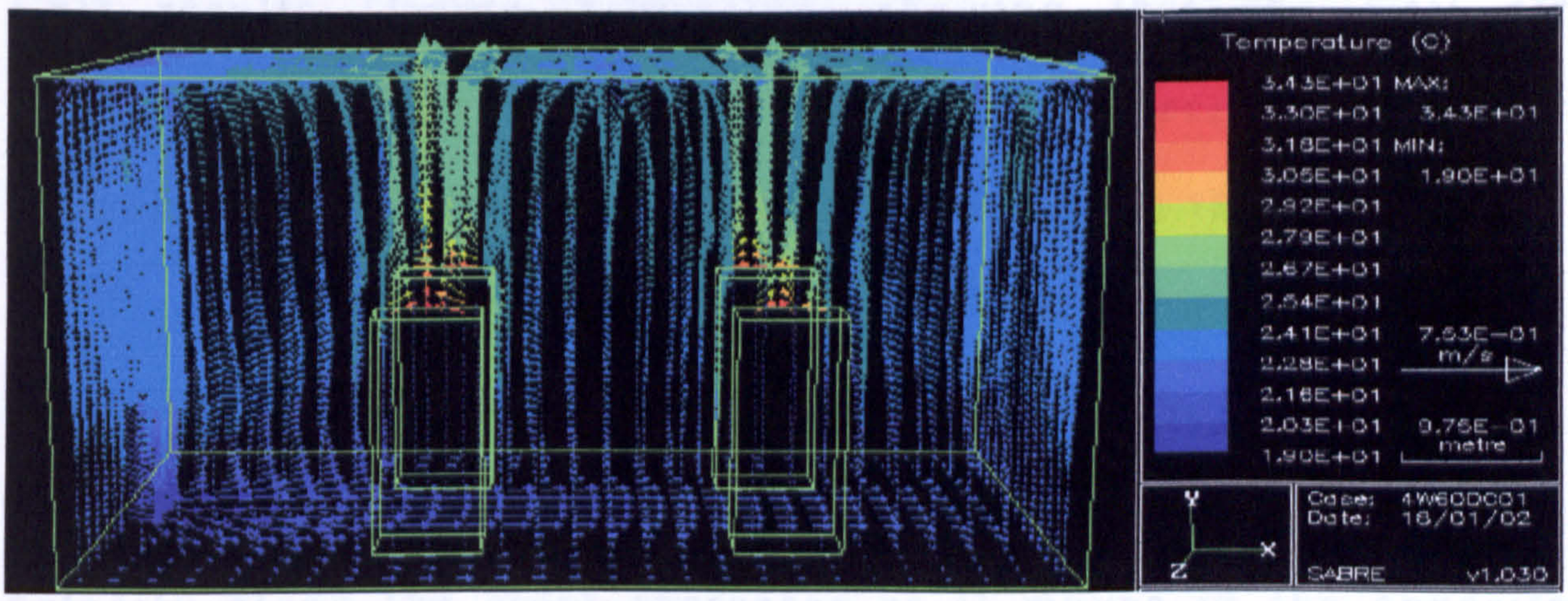

Figure 3.10: Showing CFD simulation for the air flow motion in the room, also it can be seen that the walls have a lower temperature than the room air temperature

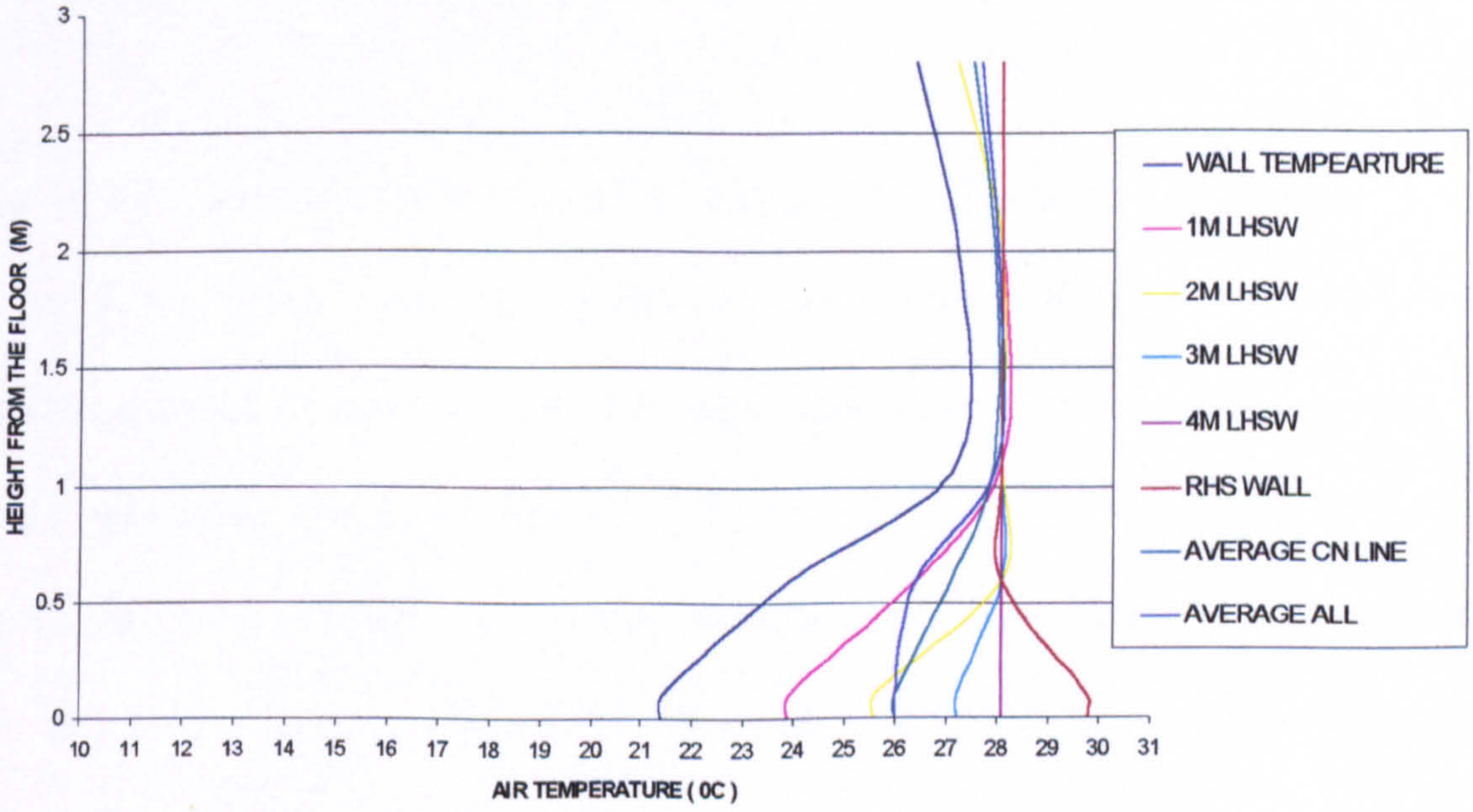

Figure 3.11: Graph results showing that wall air temperature is lower than the room air temperature when air temperature was taken at different distance from the walls

CFD results (figure 3.10,3.11), showing that the wall air temperature is lower than the room air temperature when air temperature was taken at different distance from the walls.

Using the same boundary conditions as above, the velocity along the floor was investigated. The CFD simulations showed that velocity along the floor increases as it moves in the opposite direction to the diffuser until it reaches it maximum and then it reduces back down as shown in figure 3.12; these results also agree with Skistad (1994).

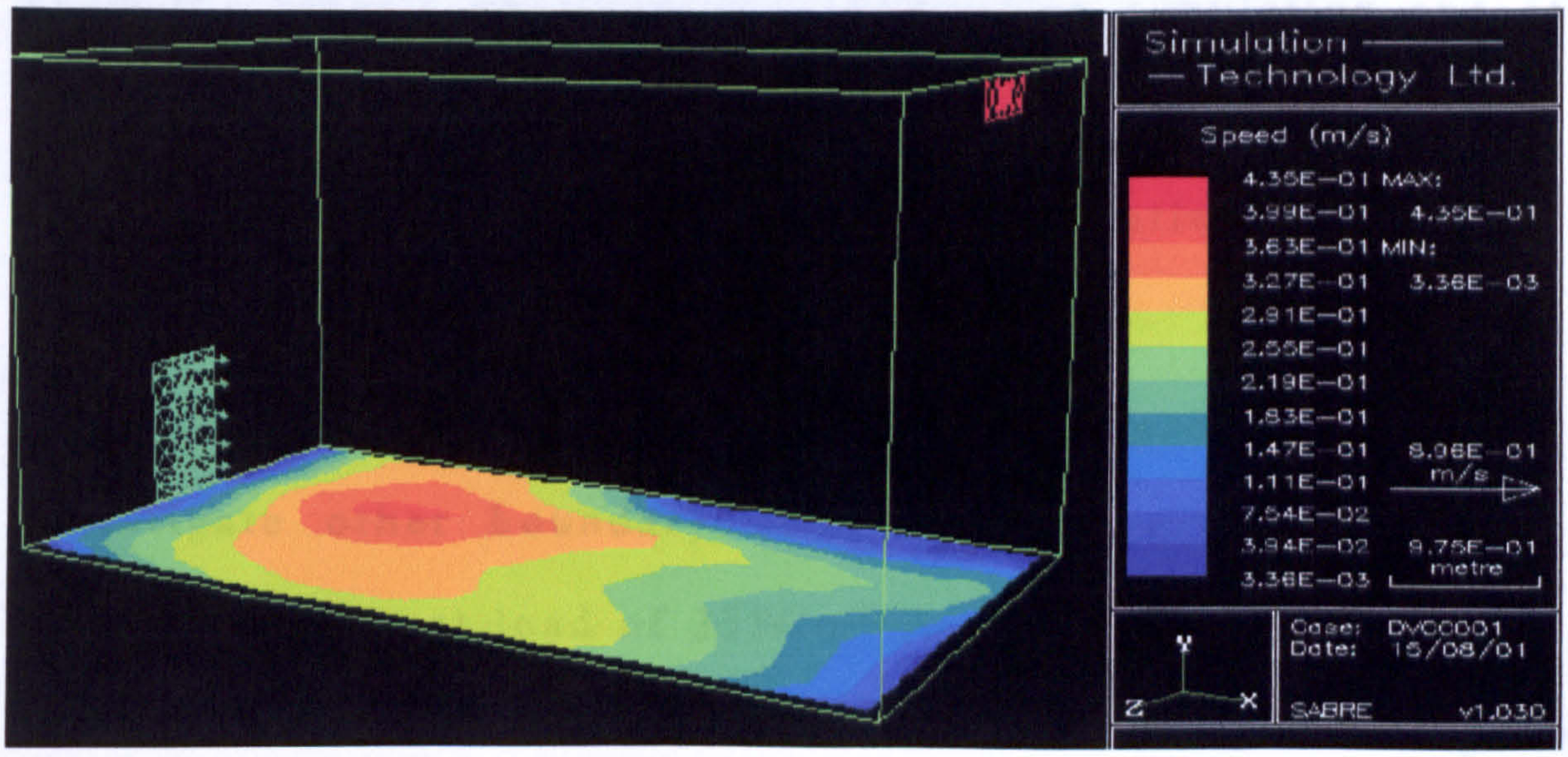

Figure 3.12: CFD Simulation agreeing with skistad that air velocity along the floor increases with distances from the supply unit until it reaches its maximum.

The CFD simulation results (Figures 3.16,3.17) show a good agreement with others (Taki et al 1996, Alamdari, 1998) that displacement ventilation is not capable of removing the heat loads greater than 35 W/m^2 (figure 3.17). The results show that the room is divided into two layers one the clean layer of air and the second layer, which is the mixed air, layer (contaminated air). The two layers are divided by the stratified boundary layer. The height of the stratified boundary layer plays an important part in determining the cleanness of the air in the room.

From the results obtained from Sabre-One simulation and other codes it can be concluded that the Sabre-One CFD code is as accurate as any other CFD code currently available.

Further simulations were carried out using the CFD code to investigate other boundary conditions. Figure 3.14 show the effects of the heat load of $25W/m^2$ imposed on the top surface of the dummies at 1.4m, 1.0m and 0.6m above the floor height and at floor level. It can be clearly seen that when the heat load is imposed at 1.4m above the floor the temperature profile gradient is the most steepest, then when the heat loads are imposed at 0.6m or at floor level. The results show that the room air temperature in the fresh zone is lower when the heat load is imposed at 1.4m height above the floor and the room air temperature is higher when heat is located near the floor. When the heat load is located at 1.4m height above the floor the temperature difference between the supply temperature and temperature at ankle height was found to be in the region of 26% of total temperature difference. Where in the case of heat load located at the floor surface the figure was in the region of 78% of total temperature difference this can be clearly seen in figure 3.15 and figure 3.16. Therefore it can be concluded that height

of the heat load can influence the temperature profile gradient and the rate of heat removed.

The results have raised a question on the findings of researches and the ISO standard 7730 (1994). The ISO standard 7730 states that for occupants to have clean air and experience thermal comfort the temperature gradient at ankle and noise height (1.1m) should not exceed 3°C/m. The results in figure 3.14 clearly show that when heat load is imposed at 1.4m above the floor the temperature gradient is within the requirements but when the heat load is imposed on 1.0m and at 0.6m above the floor, the temperature gradient exceed the requirements. Suggesting that displacement ventilation is not able to remove heat loads of 25W/m^2. Where we know this is not true, as figure 3.7 shows that displacement ventilation can remove heat loads of up to 35W/m^2. Therefore it is very important to consider the height of the heat loads when evaluating vertical temperature gradient. The air velocity for the case when heat Load imposed on the floor reached it maximum value. While lowest values were produced when the height of load was at 1.4m above the floor this can be seen in figure 3.17 This suggests that the displacement ventilation can only influence the airflow pattern at low heights. The results of the CFD simulation showed that

approximately 50% of the temperature difference between supply and extract air tock place at ankle height. This should be regarded as an estimate only and for some cases this may not be true.

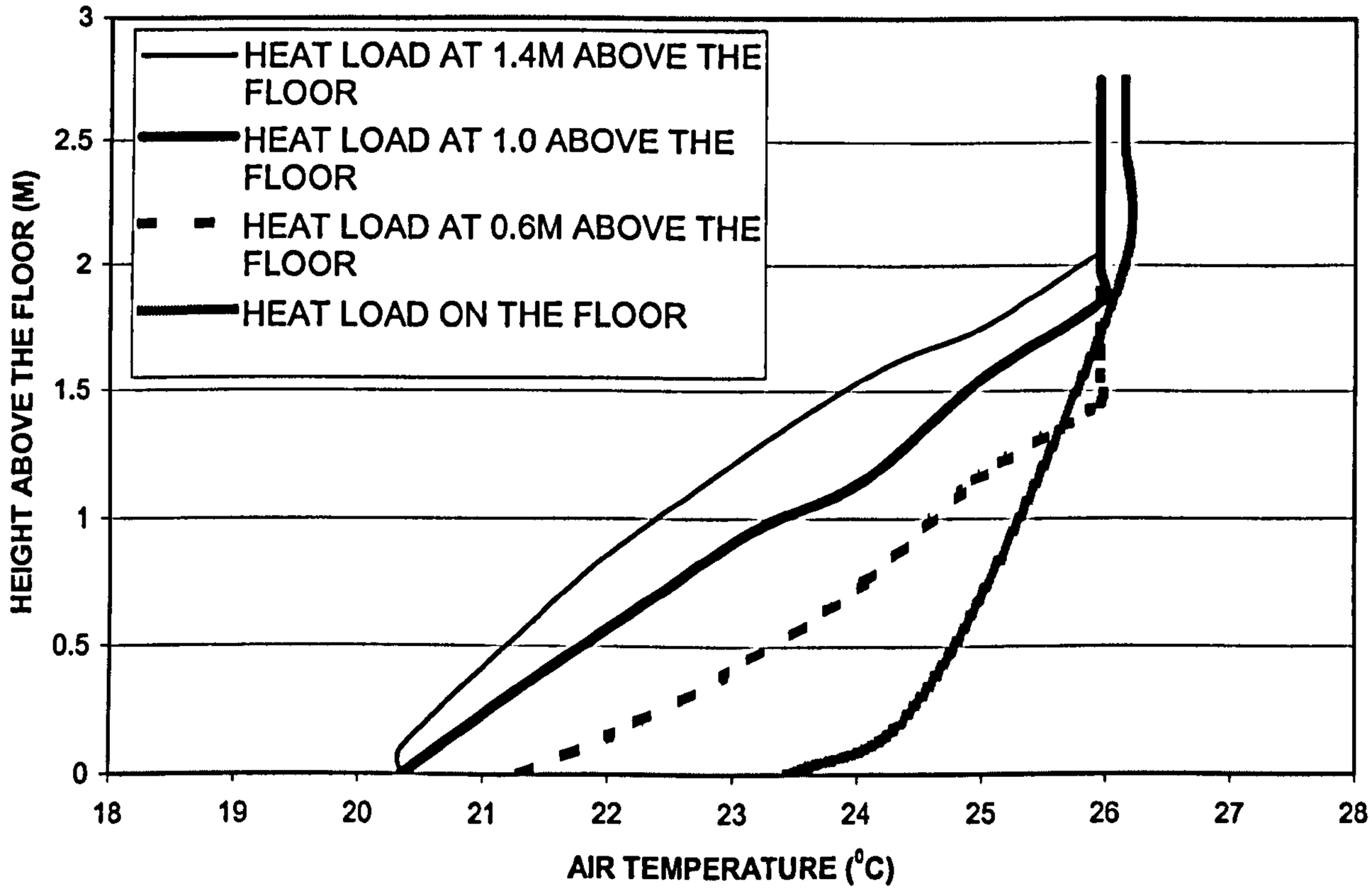

Figure 3.13: Graph showing the height of the stratified boundary layer, when heat load of 25W/m^2 is impose at different heights.

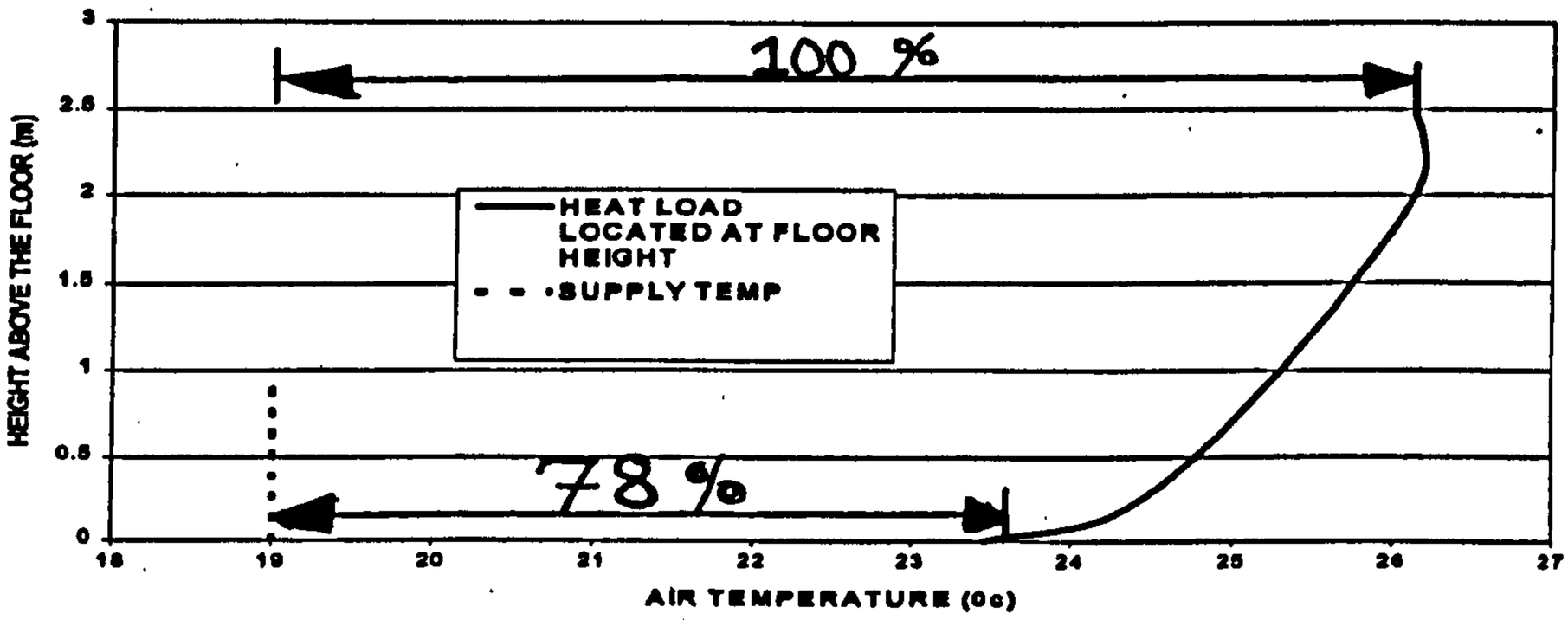

TEMPERATURE DISTRIBUTION WITH HEAT LOAD OF 25W/M2 LOCATED AT FLOOR HEIGHT

Figure 3.14: Showing the temperature profile when heat load of 25W/m^2 is imposed at floor height. The results indicates that the air temperature difference between the supply temperature and the ankle height is 78% of the total temperature difference.

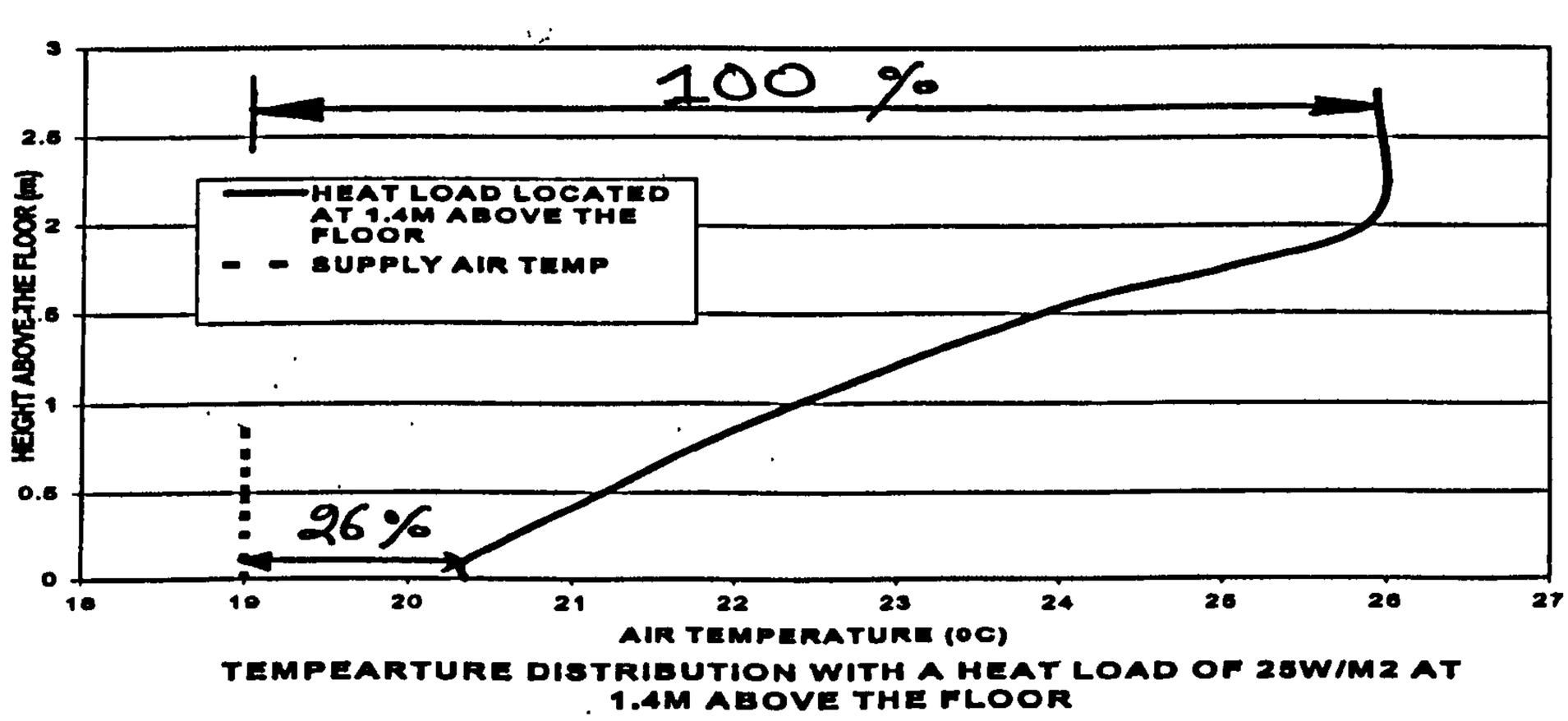

TEMPEARTURE DISTRIBUTION WITH A HEAT LOAD OF 25W/M2 AT 1.4M ABOVE THE FLOOR

Figure 3.15: Showing the temperature profile when heat load of 25W/m^2 is imposed at height of 1.4m above the flow. The results show the temperature difference between the supply temperature and the ankle height is 26% of the total temperature difference

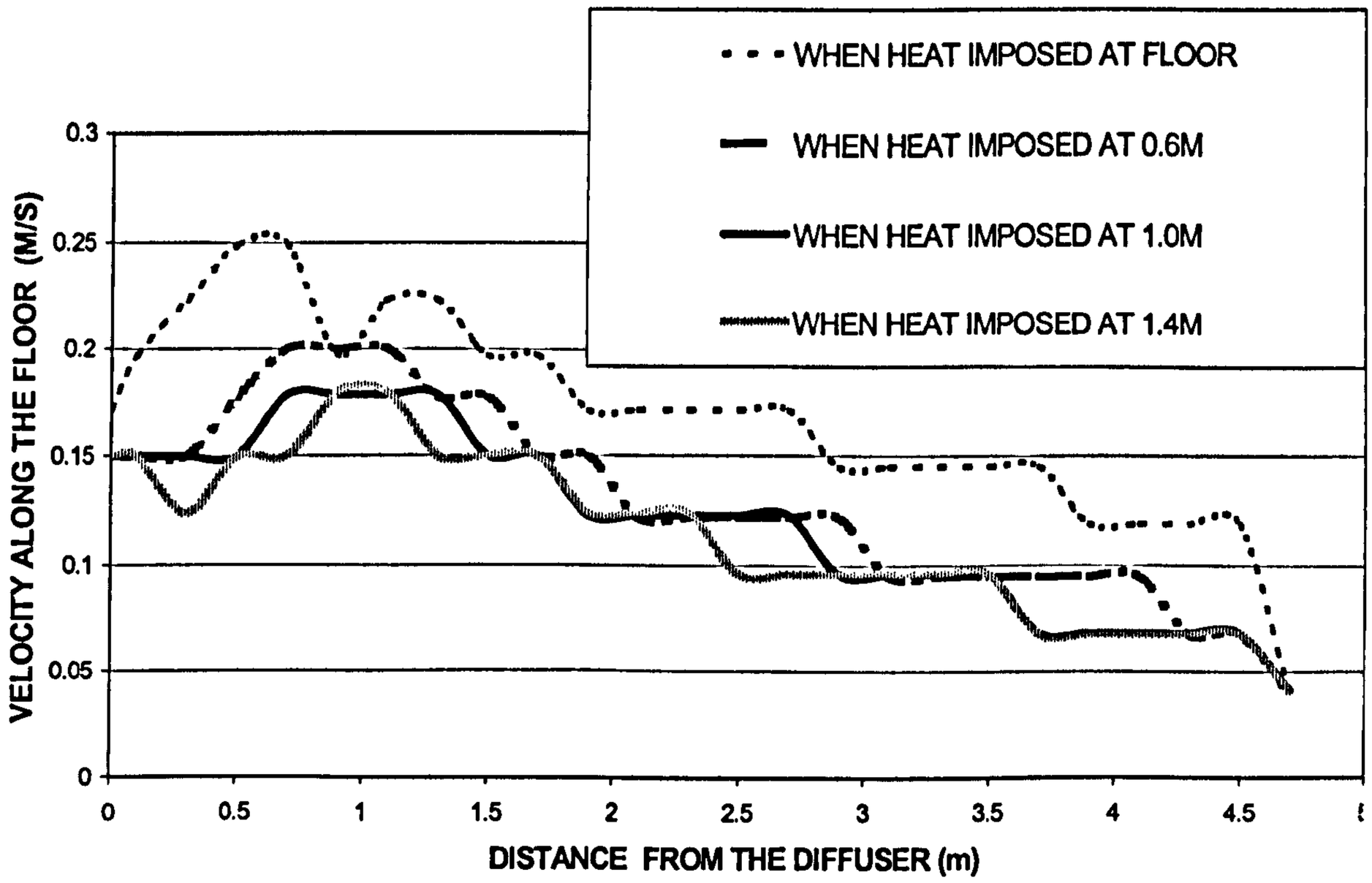

VELOCITY PROFILE FOR HEAT LOAD OF 25W/M^2 IMPOSED AT VARIOUS HEIGHTS. THE VELOCITY RECORDED AT ANKLE HEIGHT (SUPPLY VELOCITY 0.182 M/S)

Figure 3.16: The graph represents the velocity at floor level for the same conditions as seen in figure 3.4.

It can be clearly seen in figure 3.16, that the when heat load of 25W/m^2 is imposed at floor height the increase in velocity is the greatest and the lowest for when heat load is imposed at 1.4m above the floor.

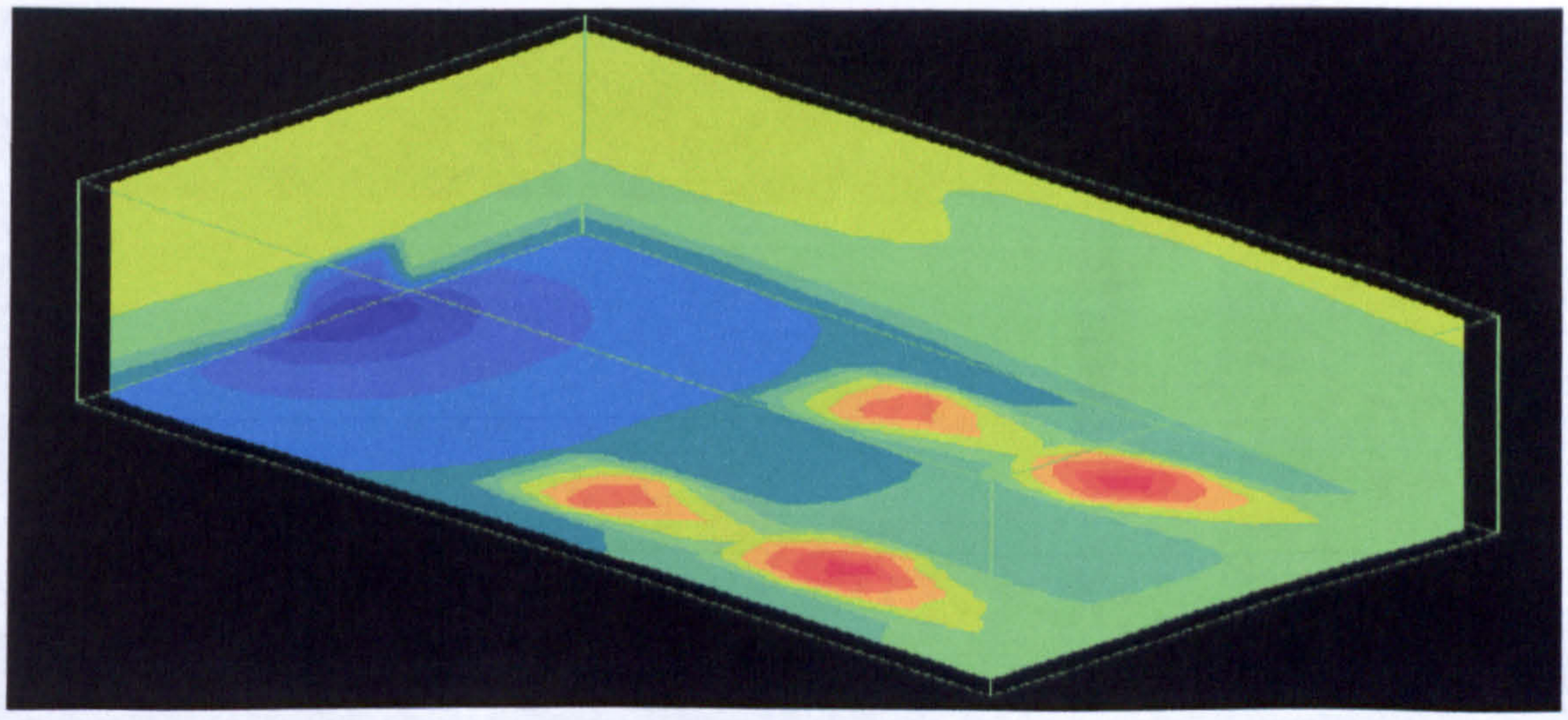

Figure 3.17 CFD simulations showing the temperature contour profile when heat load of 25W/m^2 was imposed on four stations at floor height level. No heat plume can be seen above the four heat stations.

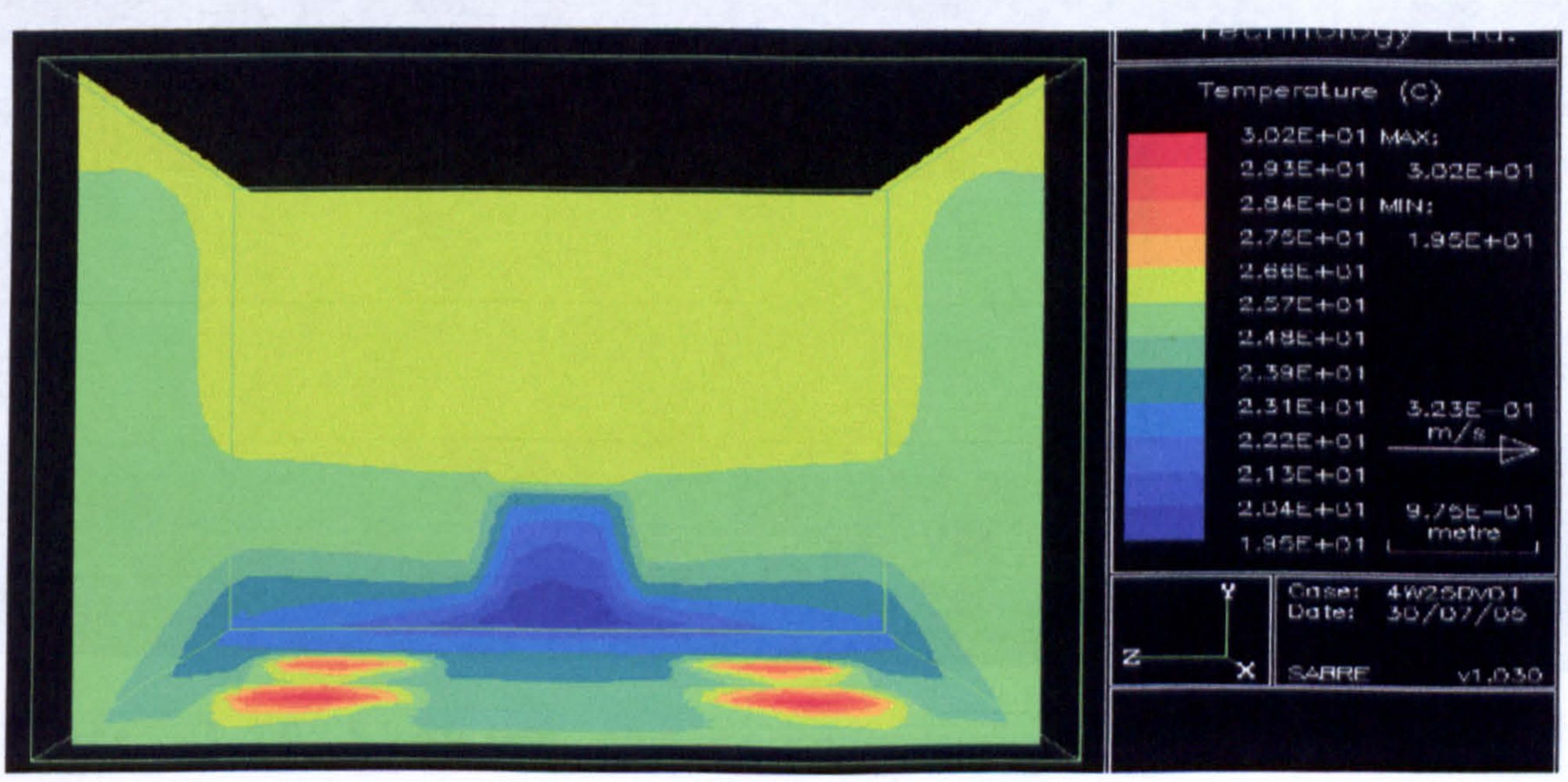

Figure: 3.18 CFD simulations showing the temperature contour profile when heat load of 25W/m^2 was imposed on four stations at floor height level. No heat plume can be seen above the four heat stations.

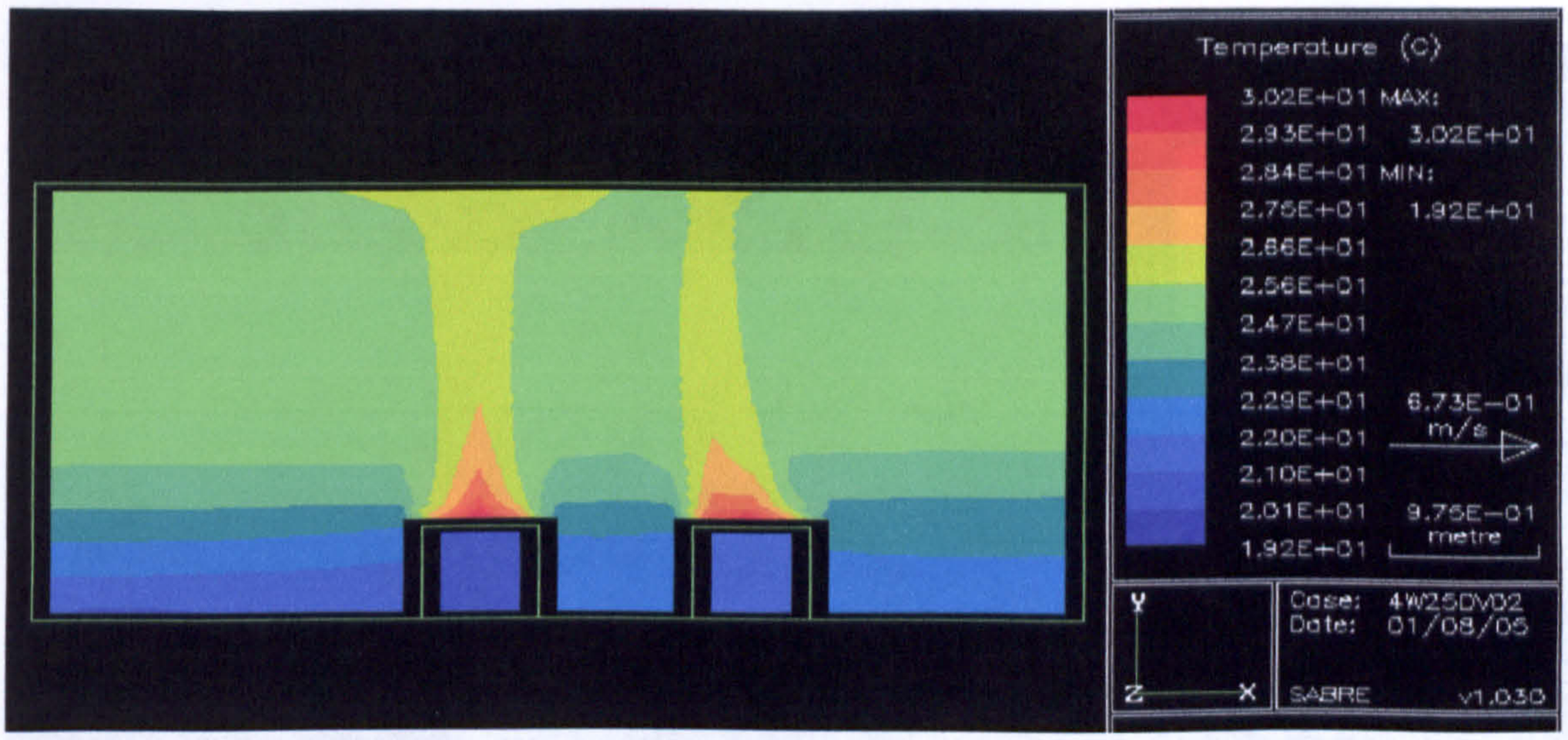

Figure: 3.19 Showing the temperature contour profile when heat load of 25W/m^2 was imposed on four stations at a height of 0.6m above floor height. The height of the plume can be seen.

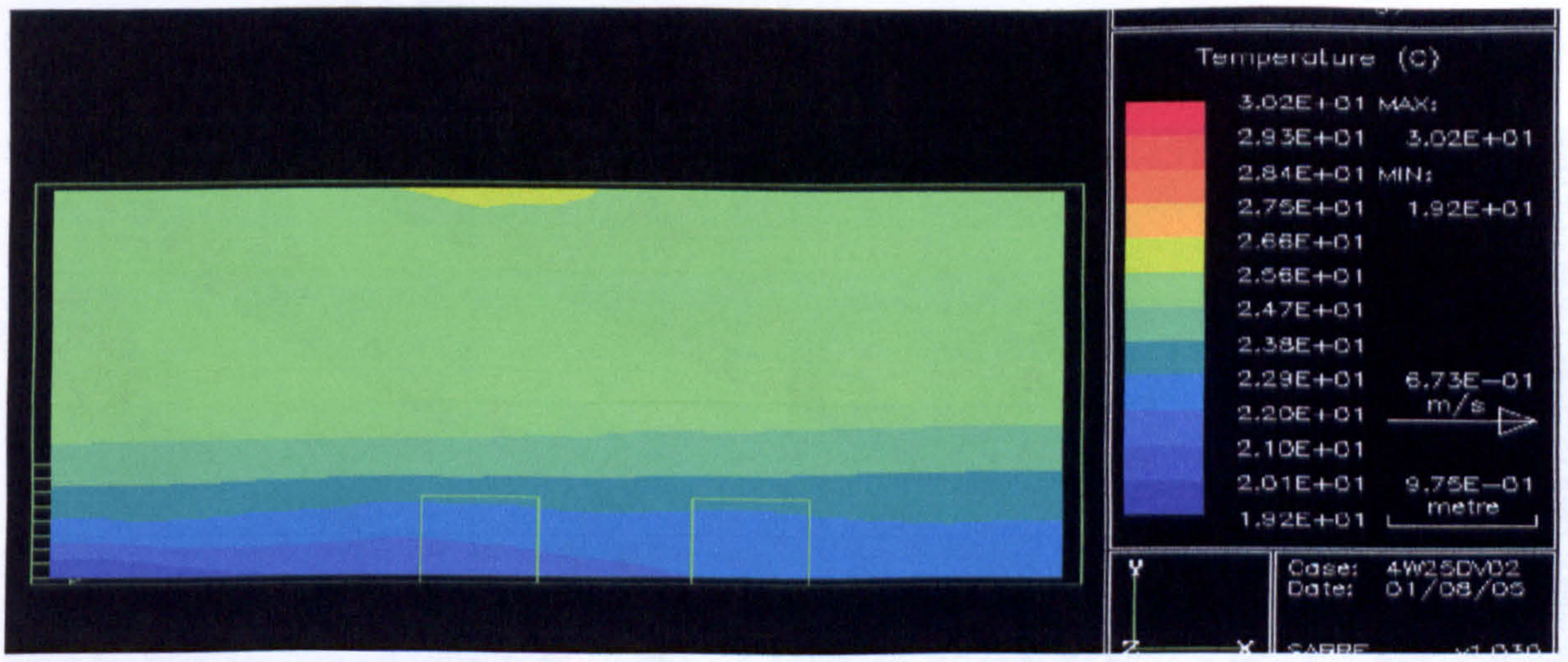

Figure: 3.20 Showing the temperature contour profile at the centre of the room away from the heat loads station, when heat load of 25W/m^2 was imposed on four stations at a height of 0.6m above floor height. No heat plume is seen but a displacement air temperature is seen.

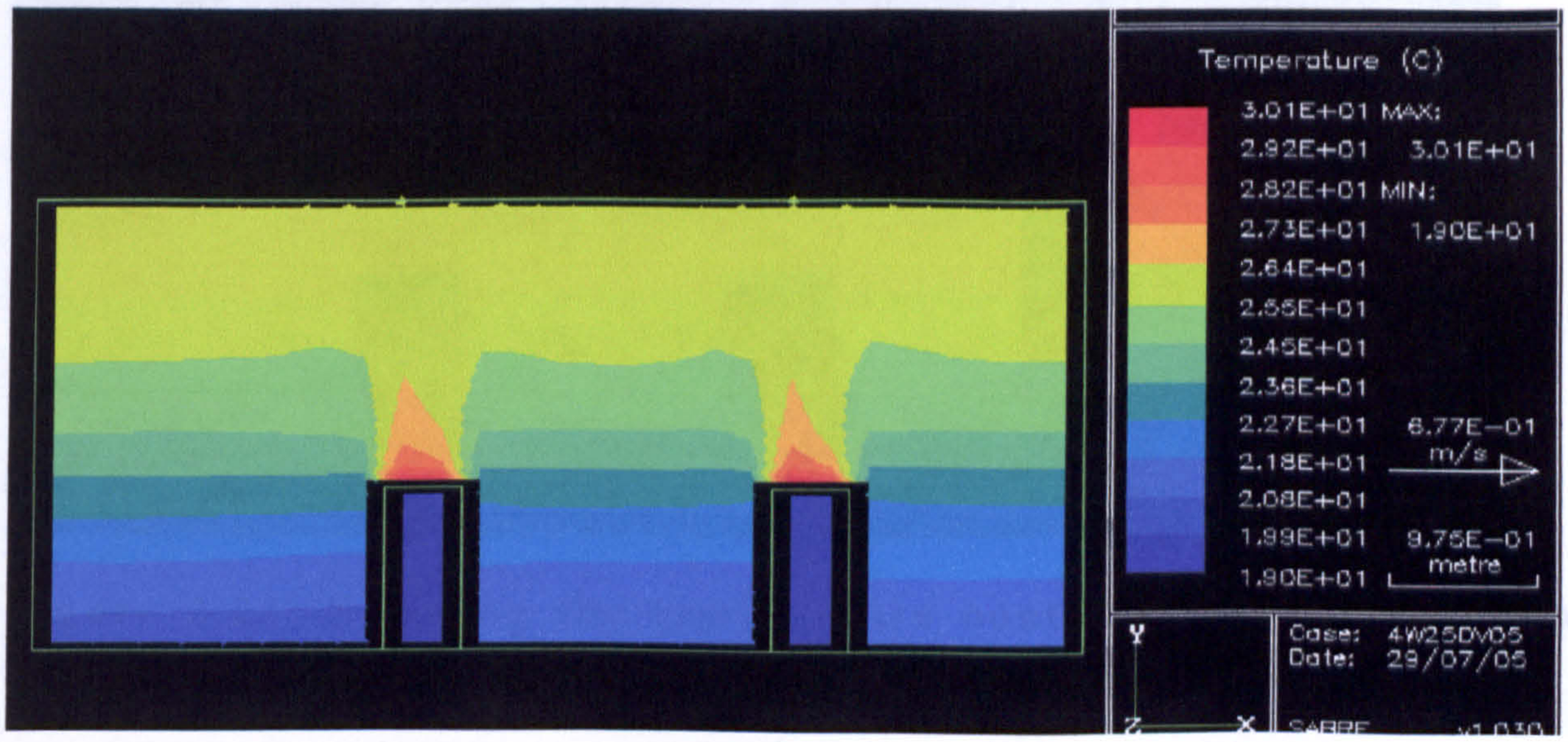

Figure 3.21: Showing the temperature contour profile when heat load of 25W/m^2 was imposed on four stations at a height of 1m above floor height. The height of the plume can be seen.

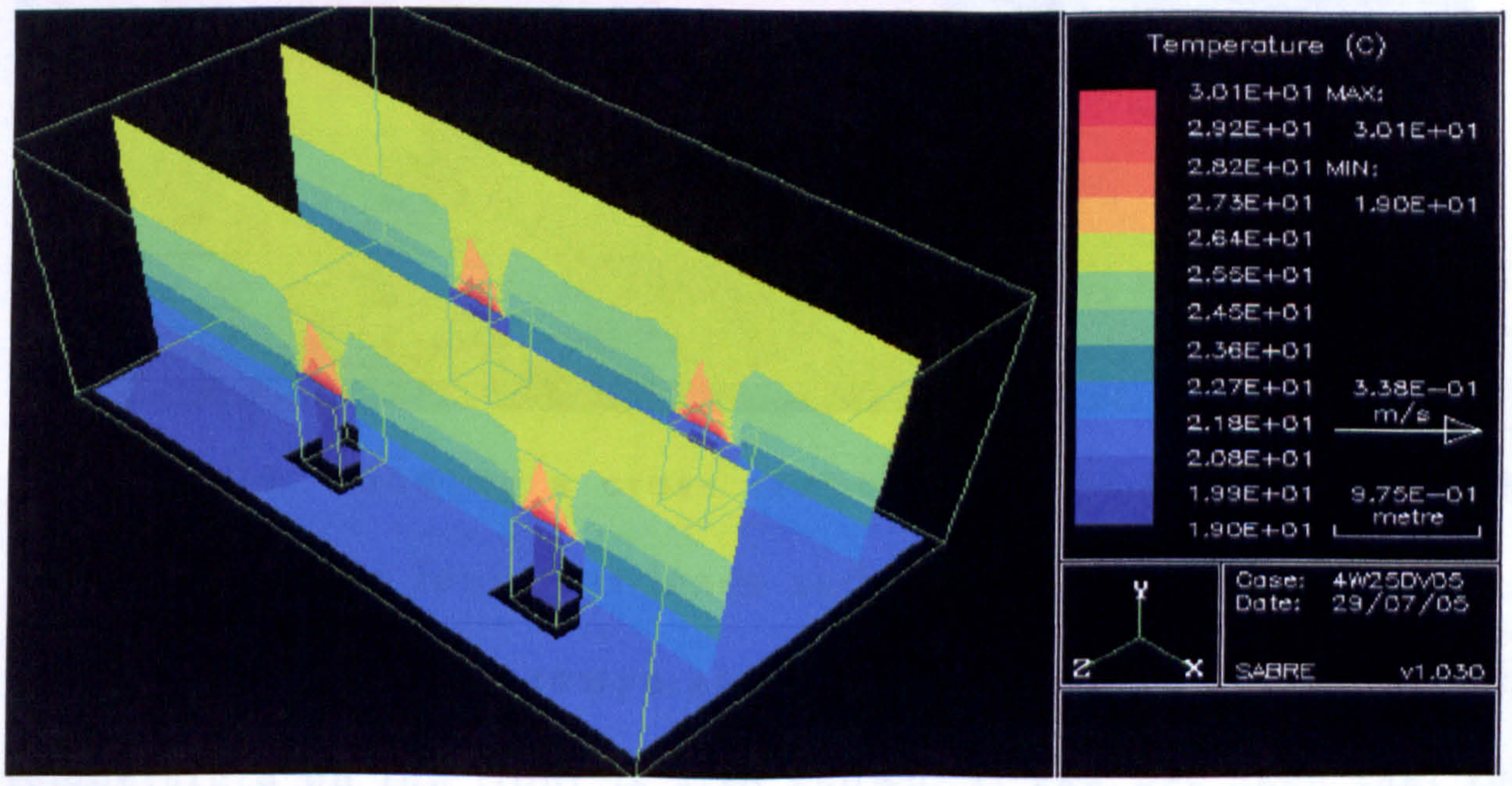

Figure 3.22 Showing a cross section view of the above figure 3.21. Four heat loads and their air temperature plume are seen.

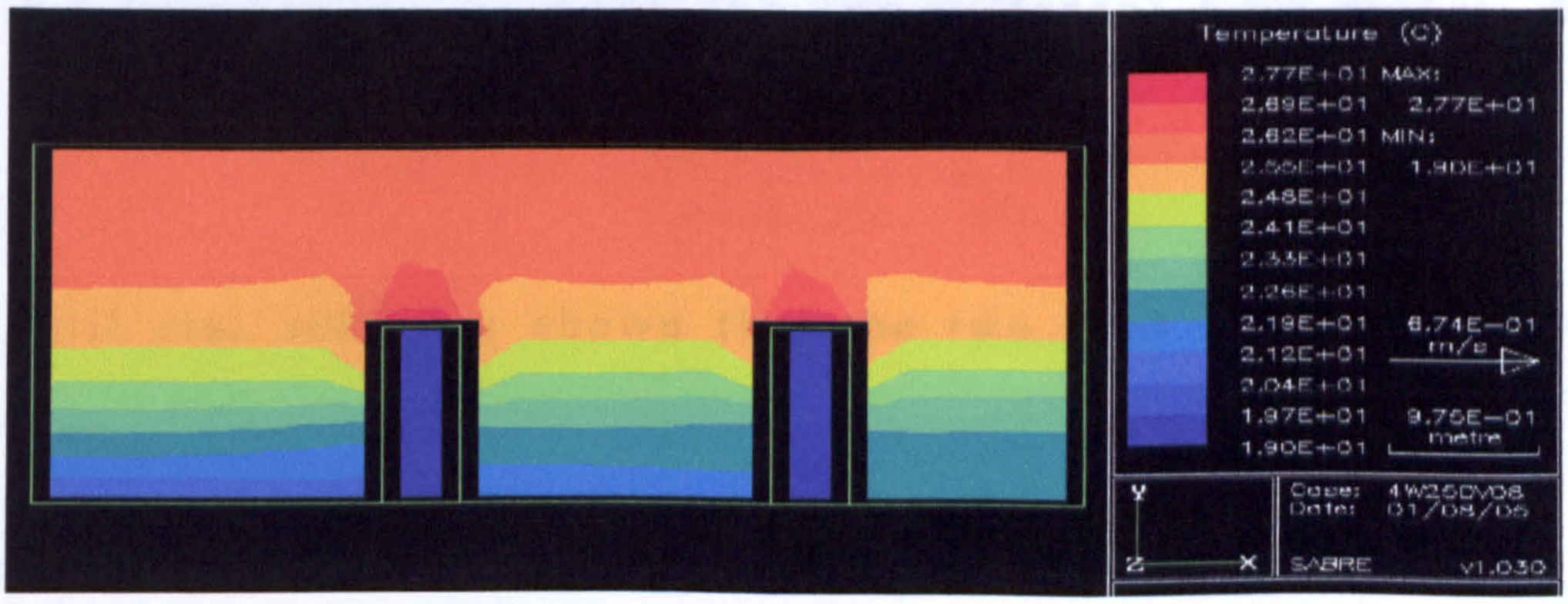

Figure 2.23: Showing the temperature contour profile when heat load of 25W/m^2 was imposed on four stations at a height of 1.4 meters above floor height. The height of the plume can be seen.

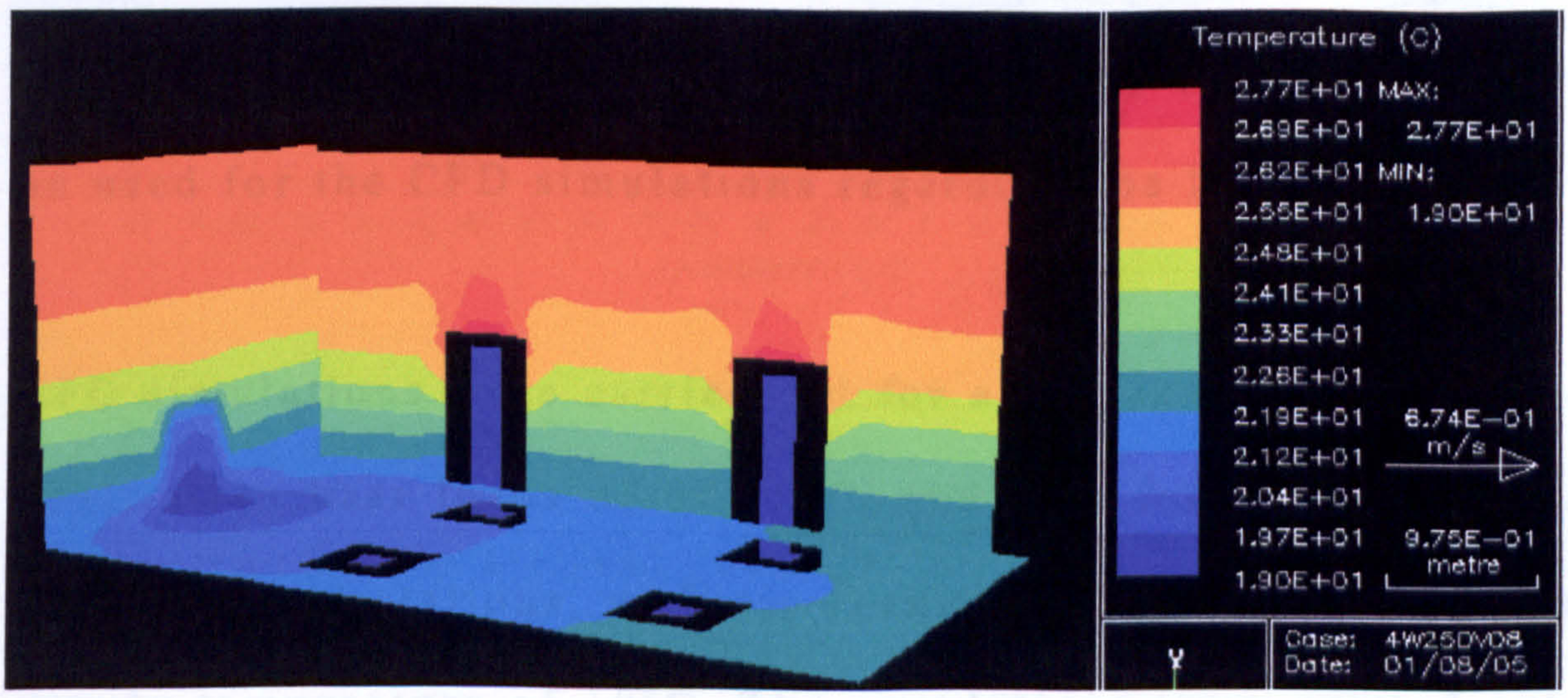

Figure 3.24: Showing a cross section view of the above figure 3.24. Beside the four heat loads and their air temperature plume are seen, the air inlet temperature contour is also visible; the air temperature on the floor is also shown. It can bee seen that the air temperature at the two different walls are similar due to the displacement airflow pattern.

3.7 Comparison between the two different CFD models Eddy viscosity and K-epsilon.

Jalil etal 2002 has shown that the two CFD models in Sabre – One,

1) K-epsilon model

2) Eddy viscosity model

Produce different results in the free zone but provide similar results in the mixing zone and in the region of the SB layer. Tests were needed to establish which of the two models should be used for the CFD simulations regarding the investigation.

CFD simulations were carried out for a test case of displacement ventilation heat loads of $62W/m^2$ and also for $40W/m^2$ imposed on seven heat stations, with air change per hour (ACH) of 4, and supply temperature of 19°C. The simulations were carried out on both K-epsilon and Eddy model. Figure 3.26 and figure 3.27 show the CFD simulation result plotted in a graph for the above mentioned test cases.

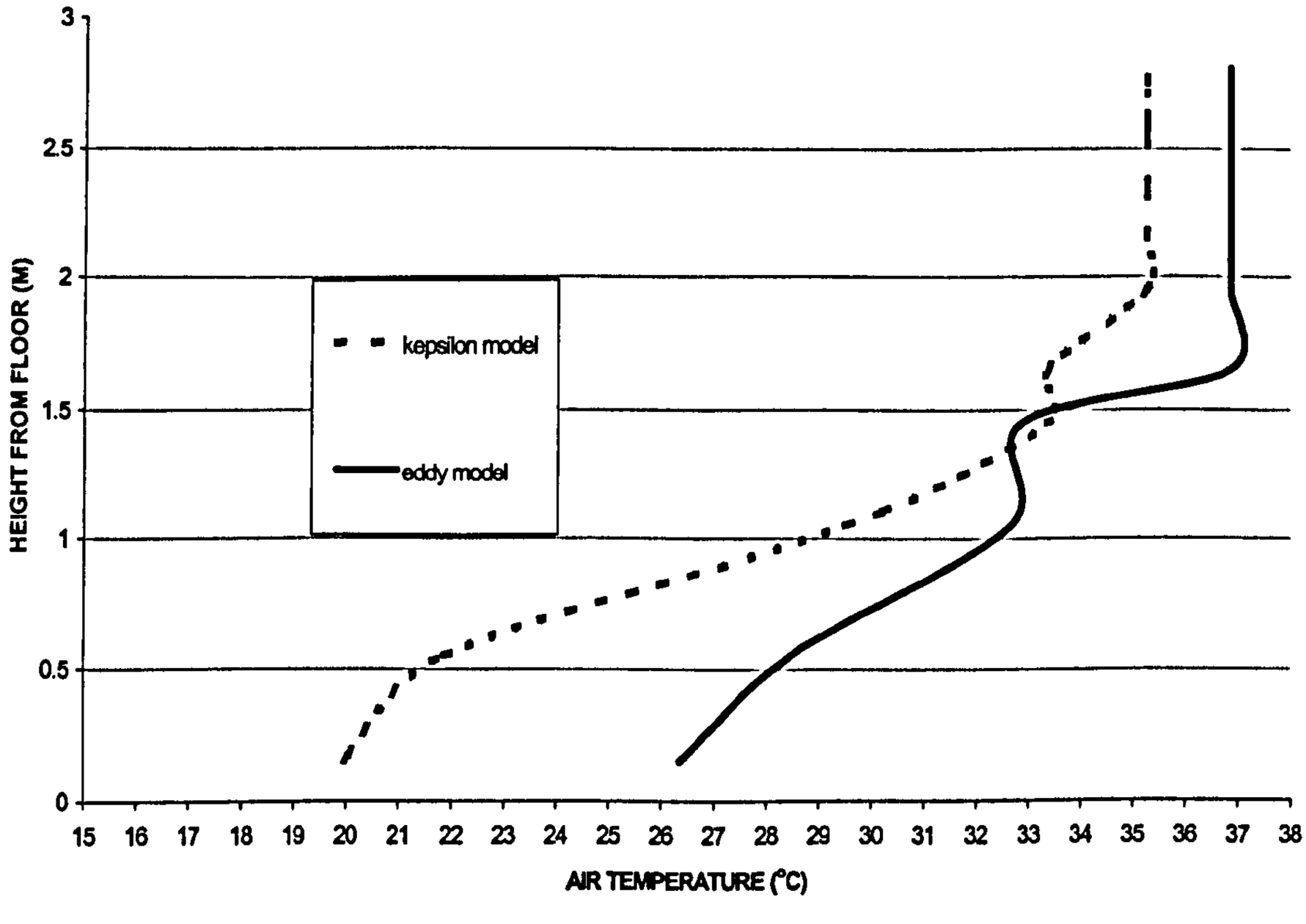

Figure 3.25: Showing the results of Heat load of 62W/m^2 imposed on 7 heat stations

From the results it can be seen that for the same boundary condition both of the models produces results that were different. The air temperature at the ankle height has a temperature difference of 6°C between the two models. And a temperature difference of 2°C at the ceiling height.

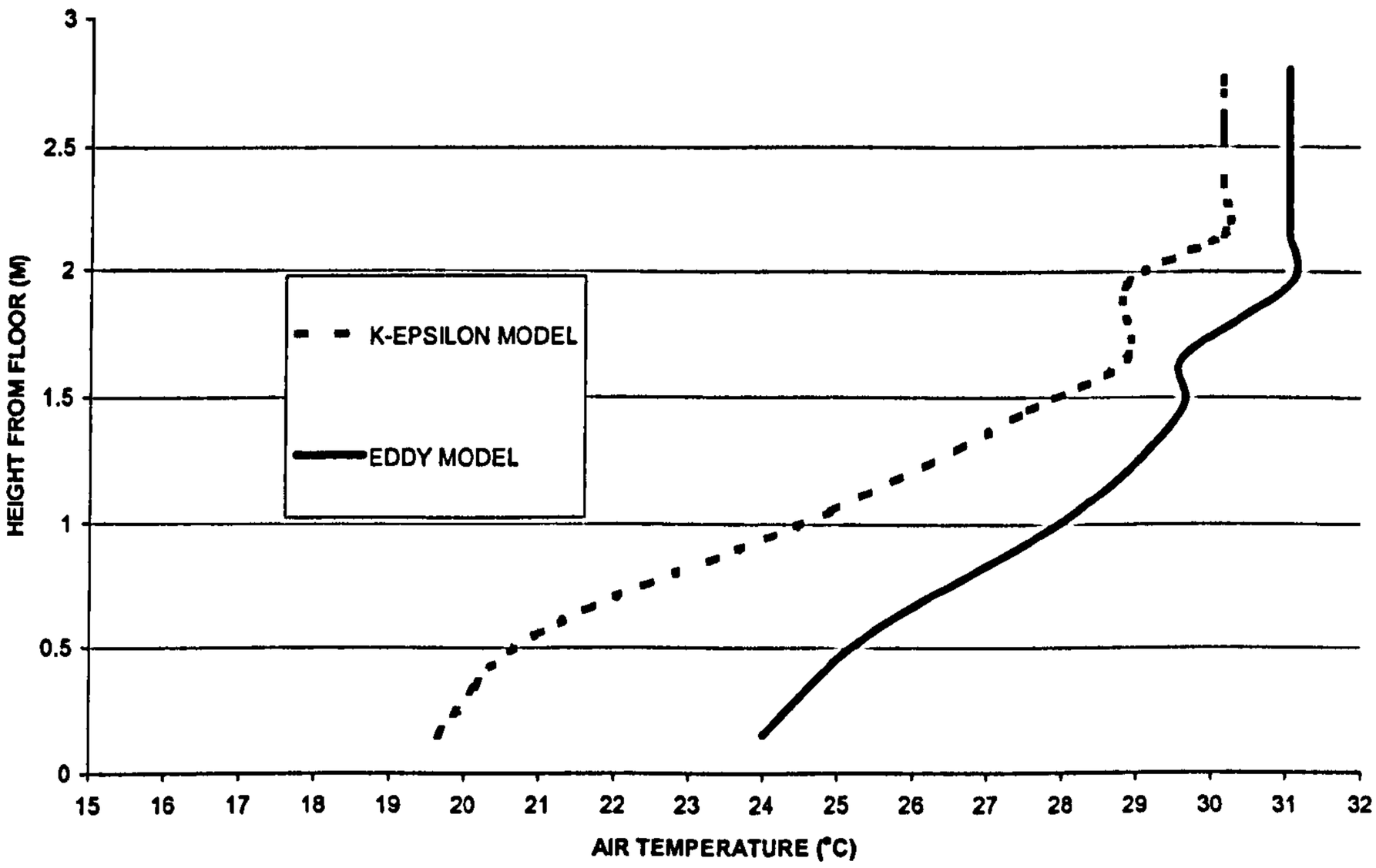

Figure 3.26: Showing the results of Heat load of 40W/m² imposed on 7 heat stations).

The results again show similarity as figure 3.26 but the temperature difference at ankle height and at ceiling height is lower.

From both sets of results it can be concluded that both K-epsilon model and Eddy model produce results that were different so it is important to know which of the two models will produce the results that agree with the laboratory results. We know that the

laboratory results obtain by Taki etal, Kruhne (1996), Alamdari (1996), Brohus (1998) and Fitzner (1996), Rees (2001) show that the temperature at the ankle height is not in the region of 19°C but is higher.

Both graphs show that for the K-epsilon model the temperature at the ankle height for both heat loads of 40W/m^2 and 60W/m^2 are in the region of 19.65°C and 19.95°C where for the case of Eddy viscosity model there is a difference of 2.5°C (See table 3.1).

Model	Heat load	Temperature at ankle height °C
K-epsilon	*40 W/m^2* *62W/ m^2*	*19.65 °C* *19.95 °C*
Eddy	*40 W/ m^2* *62 W/ m^2*	*23.5 °C* *26 °C*

Table 3.1: Showing the temperature at ankle height (0.1m above the floor) for the same boundary conditions but for different CFD models.

Further tests were carried out to confirm that the Eddy model produces better results then that of K-epsilon model for the whole room environment. Simulations were carried out on different size diffusers, which would result in different air velocity for the inflow, the smaller the diffuser size the greater the inflow is required to achieve ACH of 4.

Two different inlet diffuser sizes were used for the same conditions as before (heat load of 40W/m^2 imposed on 7 heat stations, having a supply temperature of 19°C and an air inflow having an ACH =4.

Two different diffuser size were

1) 0.7m x 0.4m

2) 0.9m x 0.6m

For the smaller size diffuser need to have an inflow velocity of 0.3m/s at 50% face free to achieve ACH of 4.

For the larger size diffuser the inflow velocity required to achieve ACH of 4 was 0.186 m/s. Figure 3.19 show the findings

of the CFD simulation for the above mentioned test cases. Figures 3.28 to 3.32 show the CFD simulations representing the room air temperature profile.

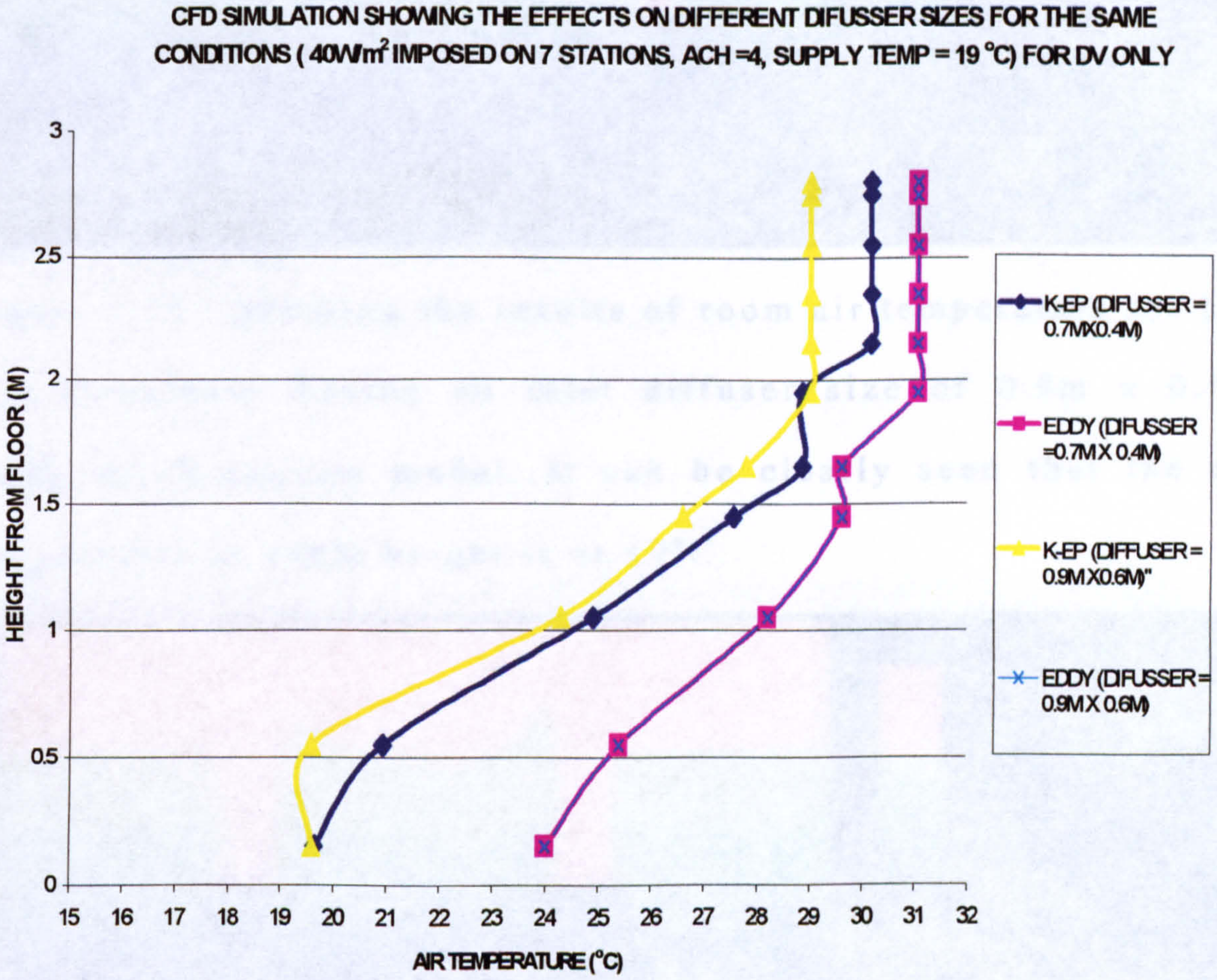

Figure 3.27: Showing the effects of different size Diffuser on the room air temperature profile obtained by CFD simulations for 40 W/m^2 heat loads impose on seven heat stations having inlet air supply temperature of 19°C.

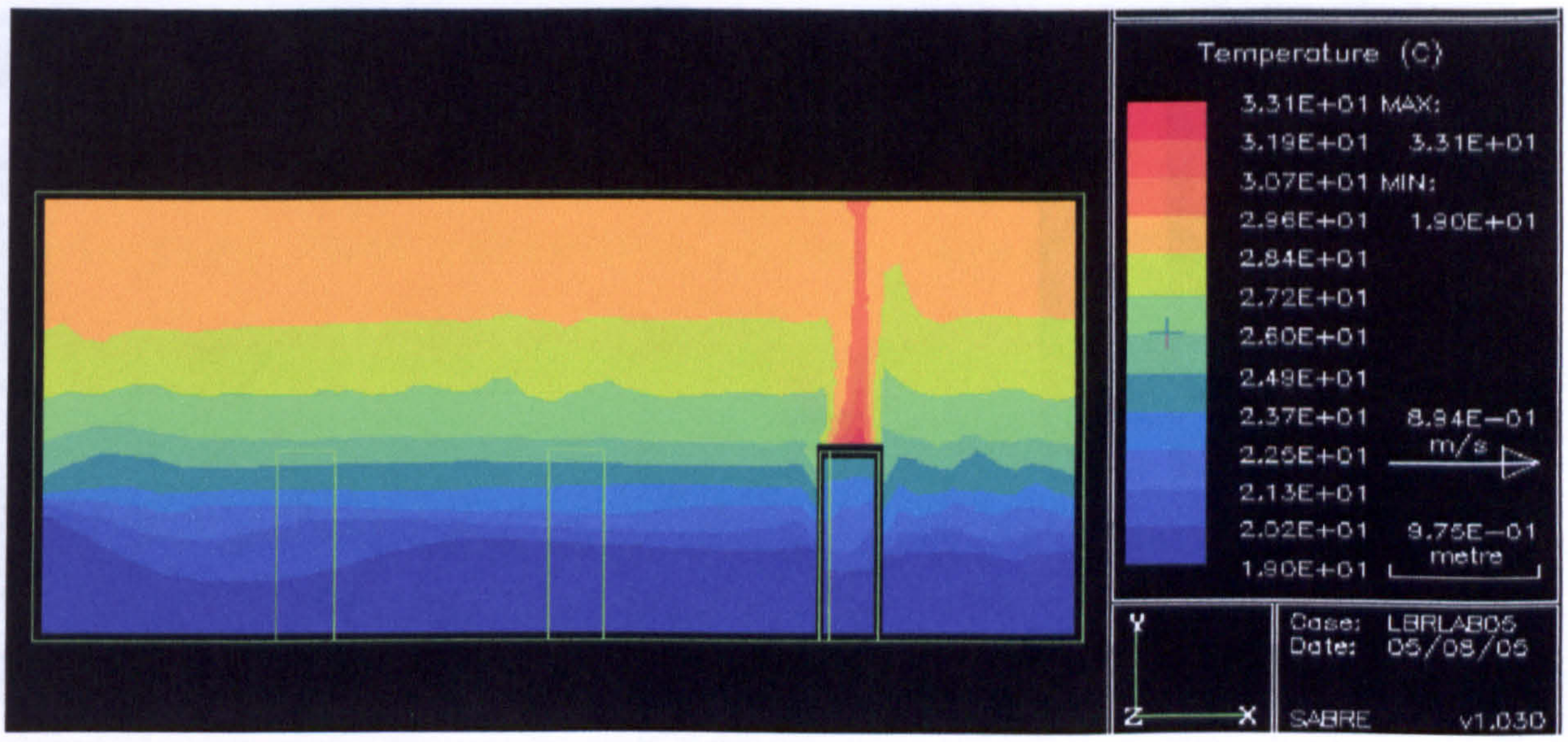

Figure 3.28: Showing the results of room air temperature for the test conditions having an inlet diffuser size of 0.9m x 0.6m using the K-epsilon model. It can be clearly seen that the air temperature at ankle height is at 19°C.

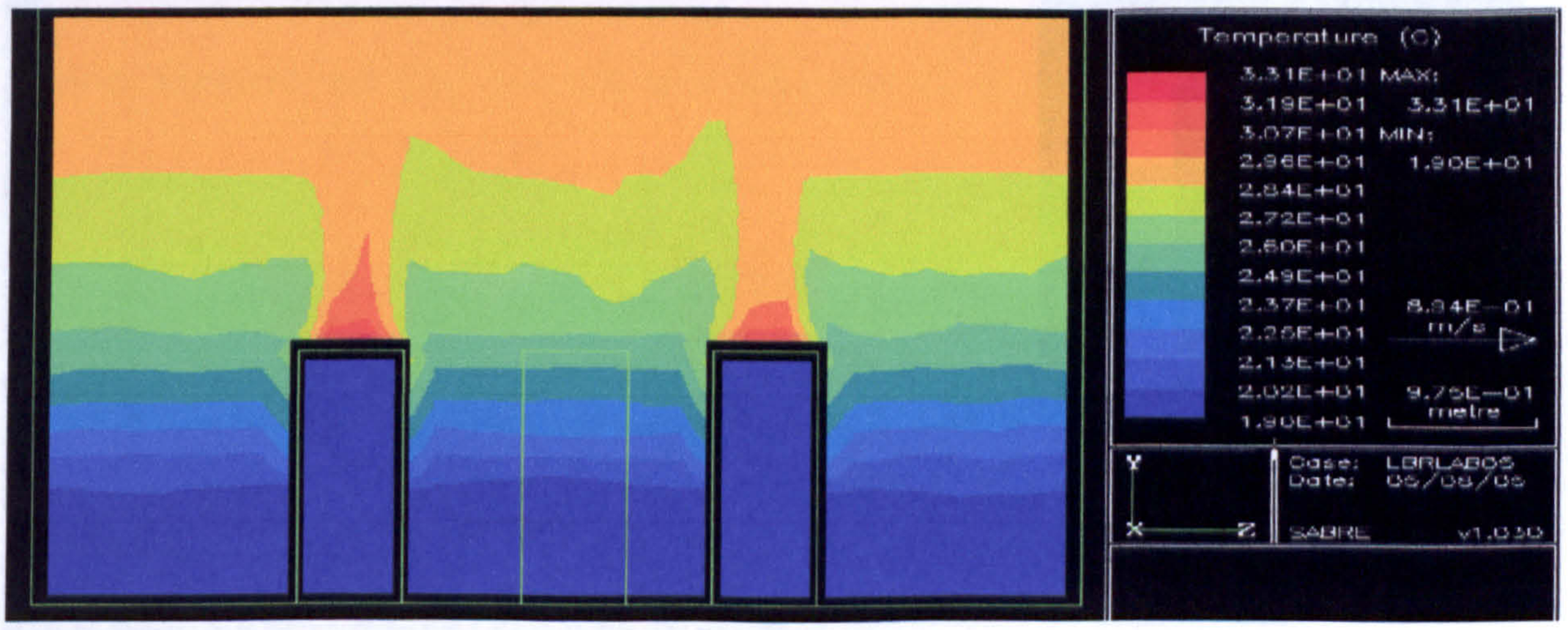

Figure 3.29: Showing the results of room air temperature for the test conditions having an inlet diffuser size of 0.9m x 0.6m using the K-epsilon model. It can be clearly seen that the air temperature at ankle height is at 19°C.

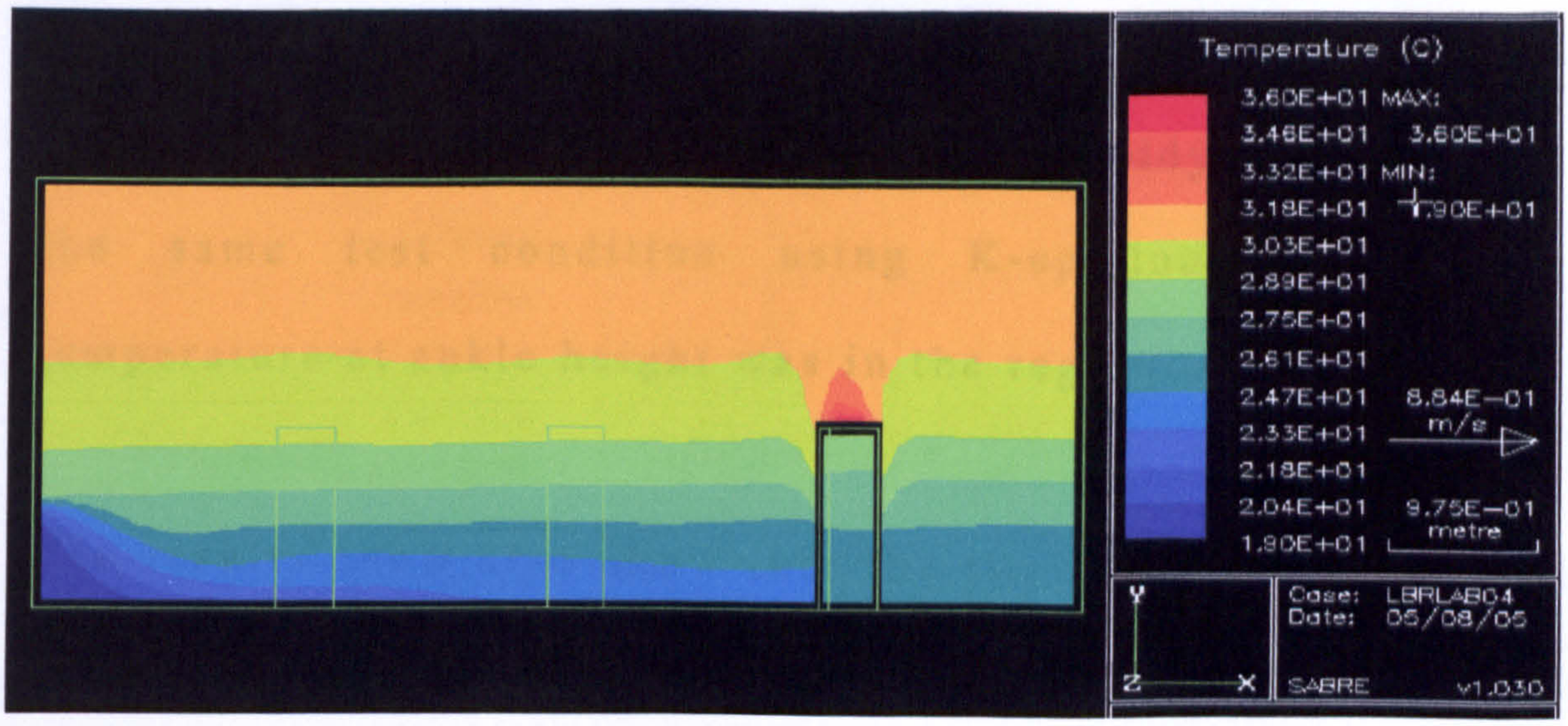

Figure 3.30: Showing the results of room air temperature for the test conditions having an inlet diffuser size of 0.9m x 0.6m using the Eddy viscosity model.

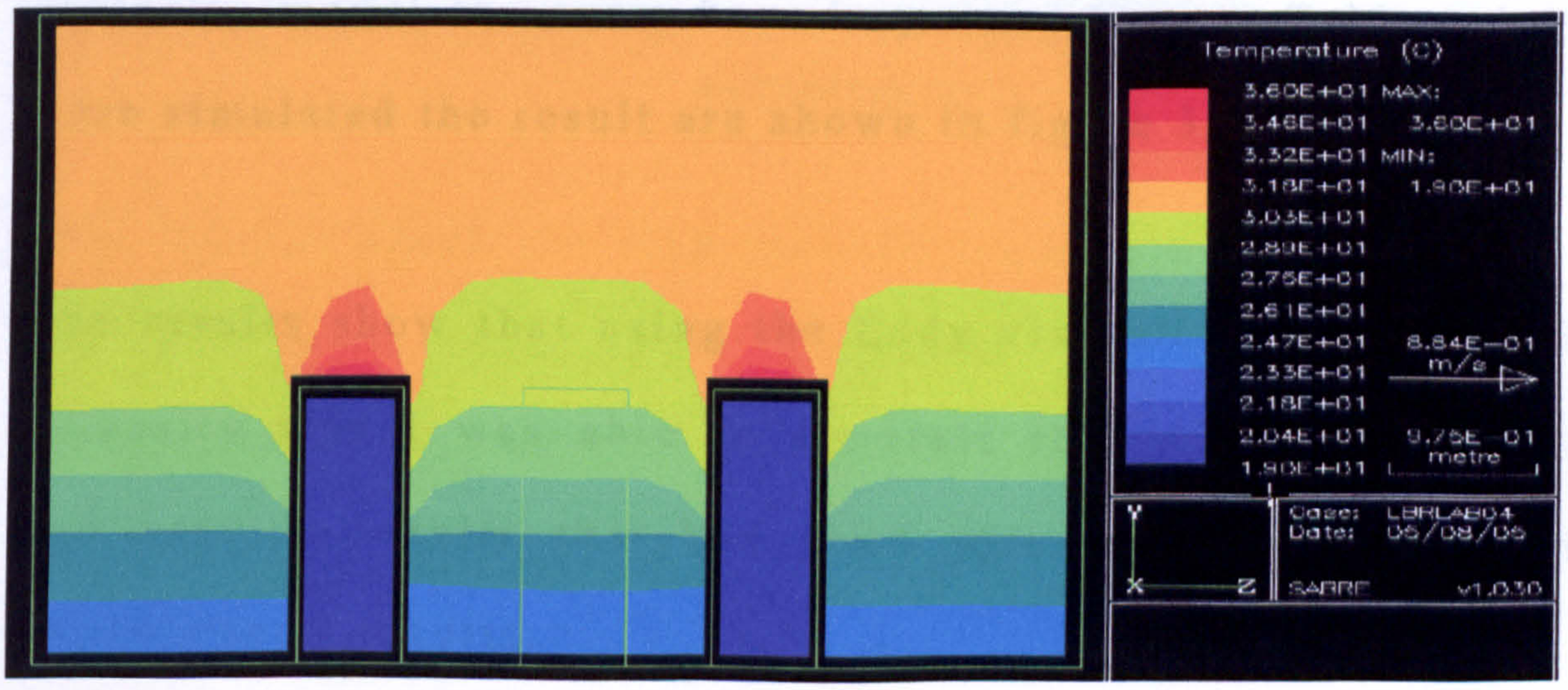

Figure 3.31: Showing the results of room air temperature for the test conditions having an inlet diffuser size of 0.9m x 0.6m using the Eddy viscosity model.

It can be clearly seen in figure 3.27 that the air temperature at ankle height is in the region of 24°C for Eddy model, where for the same test condition using K-epsilon model the air temperature at ankle height was in the region of 19°C.

The results show also show that the two different size diffusers had some effect on the K-epsilon model where for the Eddy model the results were of 100% same, therefore suggesting that the Eddy model produced identical results. Also it can be concluded that the change in velocity does not have much influence after a certain distance from the diffuser. Using Eddy viscosity model the same boundary condition as Taki etal 1996 were simulated the result are shown in figure 3.33.

The results show that using the Eddy viscosity model, the eddy viscosity model was able to simulate the boundary conditions and provide results that had good agreements with Taki 1996 experimental results.

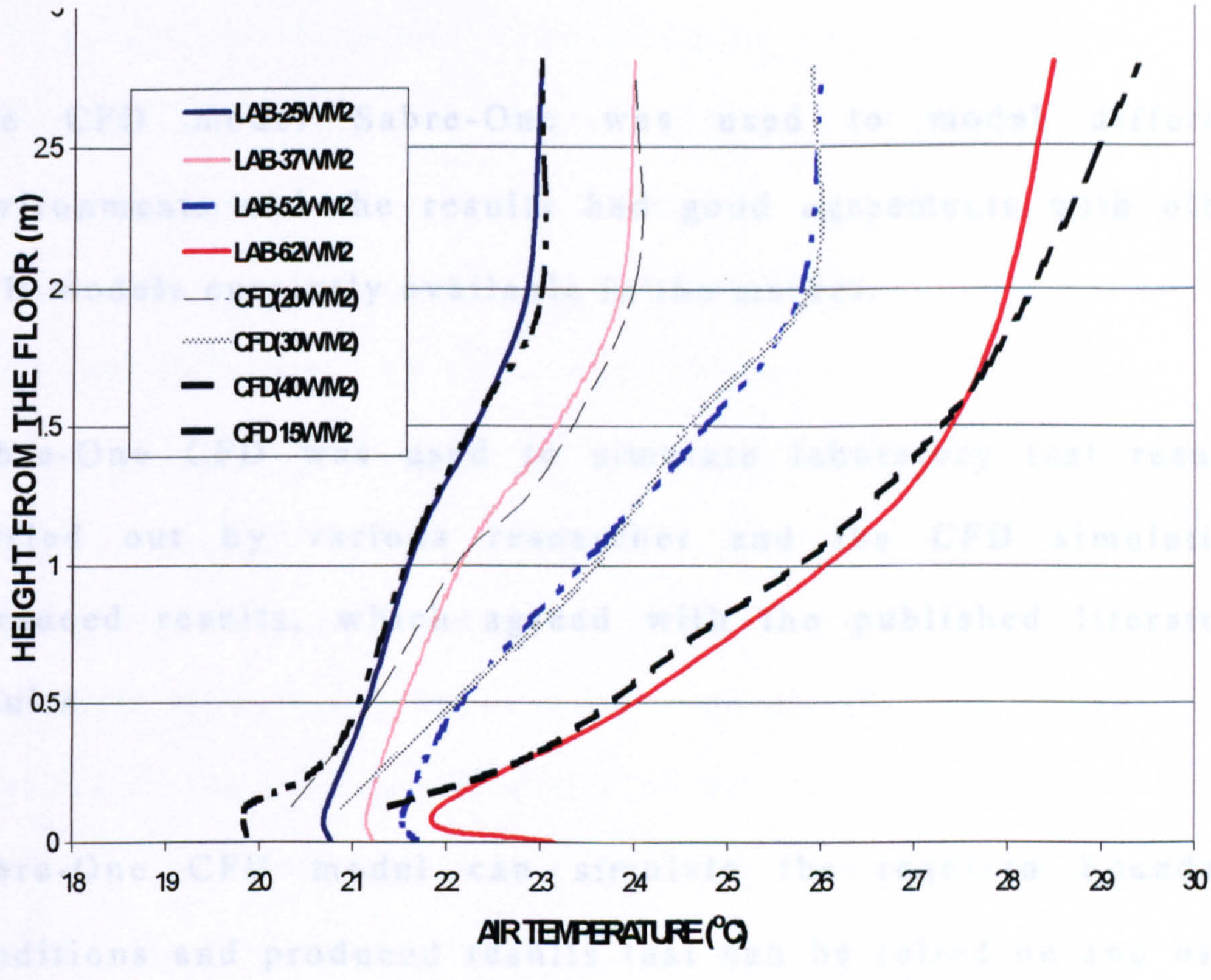

Figure 3.32: Graph showing that the results obtained using Eddy viscosity model had good agreement with Taki etal (1996) laboratory results.

Therefore it can be concluded that the eddy model produces results that agree with the laboratory results, and thus Eddy viscosity model should be used for the CFD simulations required for the investigations.

3.8 Summary

The CFD model Sabre-One was used to model different environments and the results had good agreements with other CFD models currently available in the market.

Sabre-One CFD was used to simulate laboratory test results carried out by various researcher and the CFD simulation produced results, which agreed with the published literature results.

Sabre-One CFD model can simulate the required boundary conditions and produced results that can be relied on and used for guidance for other research work.

CFD simulations were carried out for various boundary conditions using both K-epsilon and Eddy viscosity model, the results obtained using Eddy viscosity model were deemed to be more accurate as it agreed with both the laboratory results and CFD simulations results obtained by various CFD models (CFX and Flovent).

CFD results have raised a question in connection to the ISO 7730 (1994). Namely that if heat load o f 25W/m^2 is imposed on various heights above the floor, in some cases the air temperature gradient will exceed the requirements set out in ISO 7730 (1994) figure 3.13 shows the findings.

In the next chapter, honeycomb slats theory will be discussed. Also CFD model will be used to simulate the honeycomb slats attached to the ceiling and will provide the optimum depth width ratio for the manufacturing of the honeycomb slats to be use in the laboratory testing.

Chapter Four

4.0 Honeycomb slats and heat transfer

4.1 Principles of heat transfer

To understand how the principles and concepts involved in the proposed honeycomb slats system will work as regards the suppression of natural convection, it is first necessary to understand some relevant basic heat transfer principle.

There are three modes of heat transfer: conduction, radiation, and convection. Conduction and radiation are fundamental physical mechanisms, while convection is really conduction as affected by fluid flow.

4.1.1 Conduction

It is an exchange of energy by direct interaction between molecules of a substance containing temperature differences. It occurs in gases, liquids, or solids and has a strong basis in the

molecular kinetic theory of physics further details can be found in Cengel 1998.

4.1.2 Convection

Convection is the most heavily studied problem in heat transfer: More than three-quarters of all published heat transfer papers deal with convection. This is because convection is a difficult subject, being strongly influenced by geometry, turbulence, and fluid properties. A brief description of convection current is that, convection is the transfer of heat in fluid, such as air, caused by the movement of the heated air or fluid. In a building space, warm air rises and cold air settles to create a convection loop and is termed free convection. Convection can also be caused mechanically, (termed forced convection), by a fan or by wind.

In natural convection fluid motion is due solely to local buoyancy differences caused by the presence of the hot or cold body surface. A convection current entrains air from its surroundings, so that the volume flow increases with the distance from the source. Most fluids near a hot wall, for example, will have their density decreased, and an upward near-wall motion will be induced. Natural convection velocities are

relatively gentle and the resultant wall heat flux will generally be less than in forced motion.

4.1.3 Radiation

All surfaces radiate heat no transport medium is required. Energy is transported by electromagnetic waves an example is solar energy which reaches the earth by radiation. For the purpose of understanding heat transfer, electromagnetic radiation is conveniently divided into 'Short-wave radiation' and 'Longwave radiation'. Shortwave radiation has wavelengths less than 1000nm and is associated with very hot sources such as the sun. Visible light is in this category. Longwave radiation (sometimes called the long infrared) is associated with much cooler surfaces such as that occur normally within buildings. The two types of radiation often interact with materials in very different ways. (This thesis considers heat transfer by long-wave radiation).

The amount of heat radiated by a surface depends on its temperature. Thus the heat radiated by a person is circa 430 W/m^2. The heat radiation by a window with an indoor surface temperature of 10°C is *circa* 330W/m^2. The person radiates heat to the glass and the glass radiates heat to the person. So on

balance there will be a net heat transfer by radiation from the warmer surface of the person to the colder surface of the glass. The extent of heat radiation from a surface is dependant on the fourth power of its temperature. Thus the net transfer between two surfaces depends on the difference in their temperatures and on the emissivity 'e' of the surfaces. The emmisivity is a measure of how good a surface is at emmitting radiation. Most materials other than metals are good emmitters. When long-wave (heat) radiation falls on a surface part of it is reflected and part is absorbed.

There are two terms commonly encountered while discussing radiant heat transfer:

4.1.3.1 Emittance (or emissivity) is meaning in comparison to that from a black body the ability of a material's surface to give off radiant energy. All materials have emissivities ranging from zero to one. The lower the emittance of a material, the lower the heat radiated from its surface. Aluminum foil has a very low emittance, which explains its use in reflective insulation. Emissivity therefore can be described as the ratio of the radiant energy emitted from a surface at a given temperature to the energy emitted by a black body at the same temperature.

4.1.3.2 Reflectance (or reflectivity) refers to the fraction of incoming radiant energy that is reflected from the surface. Reflectivity and emissivity are related and a low emmittance is indicative of a highly reflective surface. For example, aluminium with an emmittance of 0.03 has a reflectance of 0.97. Table 4.1 shows the Emmittance values for various material surfaces.

MATERIAL SURFACE	EMMITTANCE
Asphalt	0.90-0.98
***Aluminum foil**	**0.03-0.05**
Brick	0.93
Concrete	0.85-0.95
Fiberglass / Cellulose	0.8-0.90+
Glass	0.95
Iron (polished)	0.06
Iron (rusty)	0.85
Limestone	0.36-0.90
Marble	0.93
Paint: white lacquer	0.80
Paint: white enamel	0.91
Paint: black lacquer	0.80
Paint: black enamel	0.91
Paper	0.92
Plaster	0.91
Silver	0.02
Steel (mild)	0.12
Wood	0.90

Table 4.1: The Emittance of various surfaces is listed in the table. Further reading on heat transfer and it modes can be found in Cengel, 1998.

4.2 Introduction to Rayleigh number

Rayleigh number can be briefly described as; that in Fluid mechanics, the Rayleigh number for a fluid is a dimensionless number associated with the heat transfer within the fluid. The Rayleigh number is defined as the product of the Grashof number, (which describes the relationship between Buoyancy and Inertia within a fluid), and the Prandlt number, (which describes the relationship between the viscosity of a fluid and its temperature).

When Rayleigh number is below the critical value for the fluid, heat transfer is primarily in the form of Conduction; when the value exceeds the critical value, heat transfer is primary in the form of convection. The Rayleigh number formula is as follow.

$$Ra = \frac{g\beta\,(T_1-T_2)\,L^3}{V^2}\,Pr$$

Equation 4.1 Rayleigh number

where β is the coefficient of volume expansion, g is the acceleration due to gravity, L is the length of the geometry,

T_1 and T_2 are temperature difference and V is the kinematic viscosity, Pr is the Prandtl number and the parameter Ra is called the Rayleigh number, which represents the ratio of the destabilizing effect of buoyancy force to the stabilizing effect of viscous force.

In the 1900's Benard investigated a fluid, with a free surface, heated from below in a dish, and noticed a rather regular cellular pattern of hexagonal convection cells. Rayleigh explained this in 1916 in terms of a bouyancy driven instability, by doing a linear expansion of the equations in the fluid velocities.

The critical Rayleigh number between two horizontal parallel plates was found to be Ra = 1708. This is the point at where the convection current between the two parallel plates no longer exist. When the critical Rayleigh number is exceeded and as instability sets in, the hot layer tries to go up simultaneously when the cold upper layer tries to come down. Both things will not happen at the same time and the fluid avoids this stale mate by separating itself into a pattern of convective cells. In each cell the fluid rotates in a closed orbit and the direction of rotation alternates with successive cells. Above the Critical Rayleigh number the convection current cells are present the

following figures 4.1 and 4.2 show the convection cell between two parallel plates.

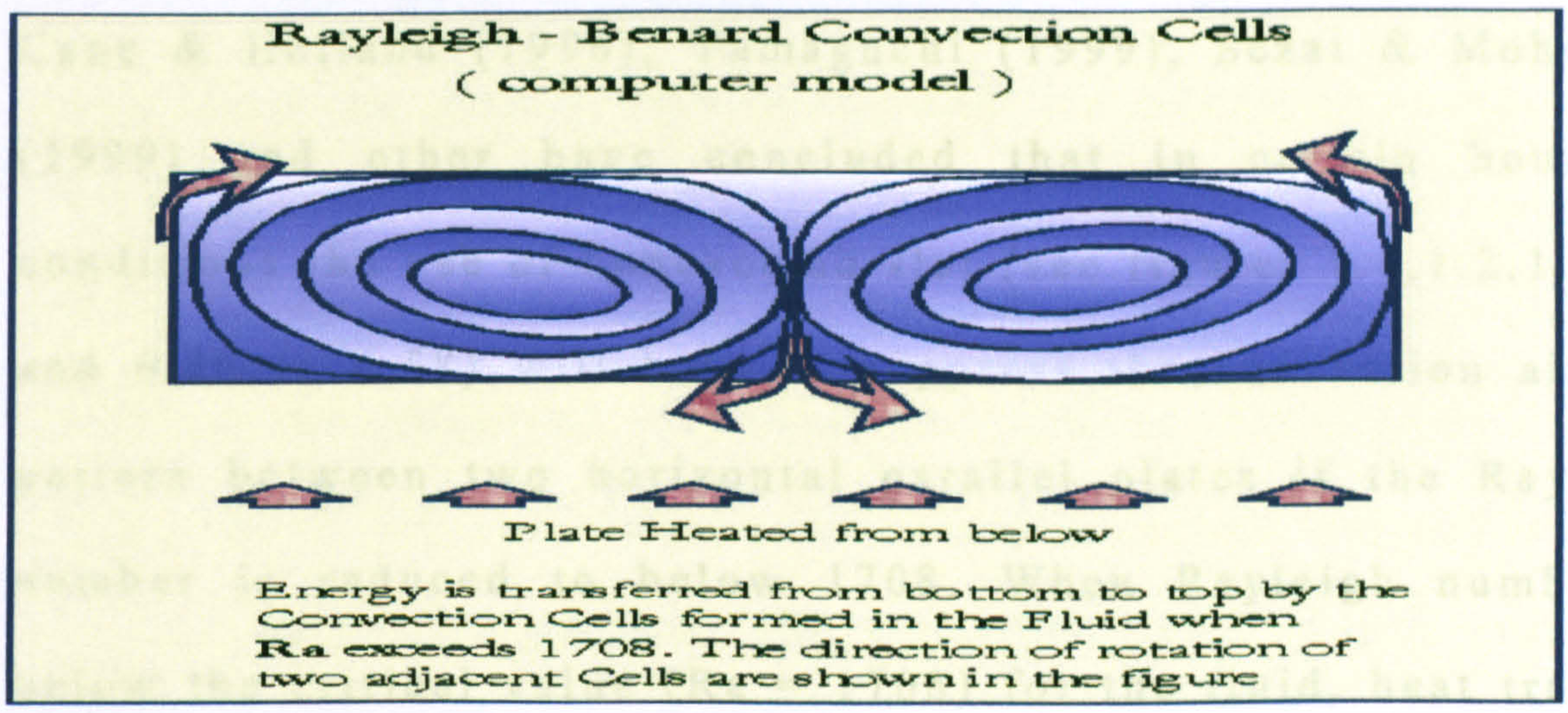

Figure : 4.1 Convection current cells diagram shows the cells in the two-dimensional view.

Cross-sectional view of cell illustrating convection rolls

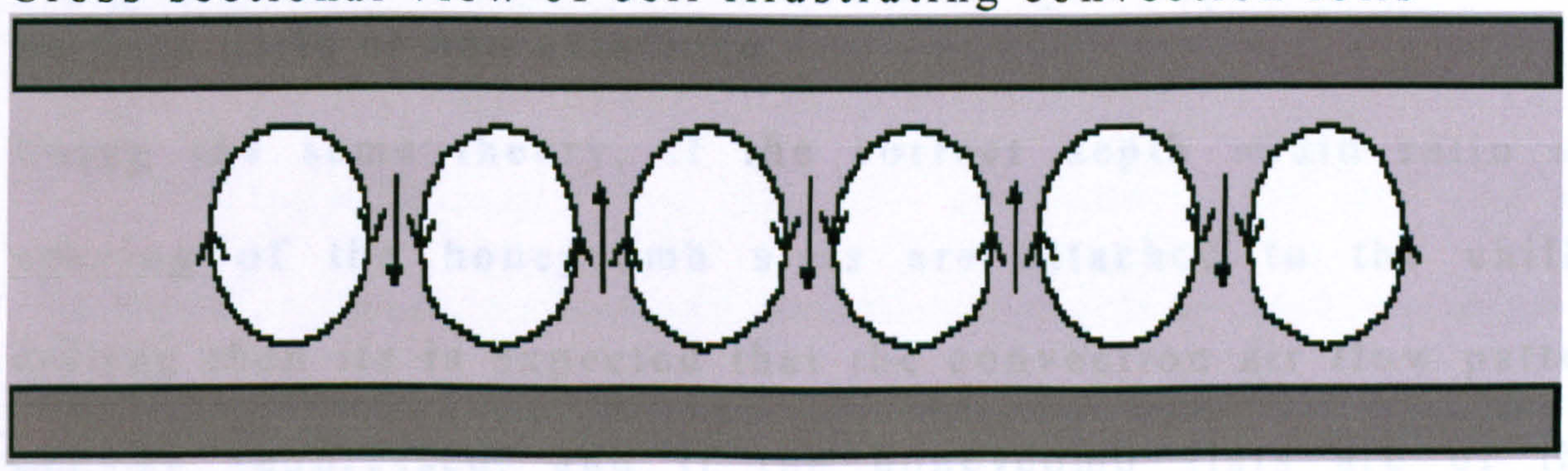

Figure : 4.2 Showing convection cells circulating in opposite directions. Indicating that the heat transfer will be by convection.

4.3 Honeycomb slats

Researchers such as Hollands (1965,1973,1985), Platzer (1992), Cane & Holland (1996), Yamaguchi (1999), Sezai & Mohmmad (1999) and other have concluded that in certain boundary conditions the use of honeycomb slat (see figures 1.1,1.2,1.3,5.1 and 6.40 to 6.58) will help to suppress the convection airflow pattern between two horizontal parallel plates if the Rayleigh number is reduced to below 1708. When Rayleigh number is below the critical value (Ra = 1708) for the fluid, heat transfer is primary in the form of conduction; when the value exceeds the critical value, heat transfer is primary in the form of convection, Holland has further suggested that if the thickness of the honeycomb slat is minimum than heat transfer by conduction will be very little or non existence.

Using the same theory, if the correct depth width ratio and spacing of the honeycomb slats are attached to the chilled ceiling then its is expected that the convection air flow pattern can be suppressed, and if the honeycomb slats are of thin thickness then heat transfer by conduction will be non existence. Heat transfer can now only be transfer by radiation, if shinny/polish aluminium material is used for the honeycomb slats then the emmisivity will be in the region 0.03m, which will

allow the chilled ceiling radian cooling to operate and thus transfer the heat by radiant cooling.

The chapter will highlight research carried out by various researchers on honeycomb slats and its usage in suppression airflow between plates and in porous environment. The results of CFD simulation will also be presented which were used to simulate the required boundary conditions for various depth width ratios of the honeycomb slats attached to the chilled ceiling. This will provide the optimum depth width ratio for manufacturing the honeycomb slats to be attached to the ceiling for the laboratory testing.

Francia (1961) carried out research on the honeycomb devices in 1961 and found that, the honeycomb devices can effectively reduce the radiation losses from a solar collector and concluded that for certain condition the use of honeycomb devices can results in suppression of the natural convection current. Francia (1961) works was carried out on very high temperatures, which led him to use honeycomb depth width ratios of the order of 25 and honeycomb depth of the order of ten inches (254mm).

Hollands (1965) continued research work on the honeycomb devices in flat plate solar collectors. Hollands work was based on lower temperatures, stationary, flat -plate solar collectors,

using honeycomb depths of about two inches and depth to width ratios in the neighbourhood of four. Holland concluded that by inserting the honeycomb devices between two surfaces under certain conditions natural convection can be suppressed and the radiation heat loss from the absorber can be reduced.

Two other factors of importance in the performance of Honeycomb flat plate's collector's device are

A) heat losses due to conduction directly through the honeycomb wall material

B) the transmittance of the honeycomb to solar radiation.

Both of the above factors are primary determined by the thickness of the honeycomb walls.

Wall thickness plays a major part in the efficiency of honeycomb devices. If the honeycomb cell wall are sufficiently thin, heat losses by conduction directly through the honeycomb wall materials need not be important (will have very little effect), and a high transmittance to solar radiation can be achieved.

4.3.1 Natural convection heat transfer

The experiments of Holland (1965) included the case of a layer of fluid, unbounded in the horizontal direction and bounded top and bottom by two horizontal, rigid surfaces, the lower surface was maintained at a higher temperature than the upper as this would encourage convection current, in this configuration no honeycomb device was present. The stability of the layer was a classical stability problem, which was highly research by Lord Rayleigh as mention in section 4.2, the research concludes and had good agreement with Rayleigh as mention in section (4.2)

Holland's experimental findings show that if the fluid is unconstrained in the horizontal direction and the Rayleigh number is slowly increased from zero, the fluid will first become unstable and convection current will start when the lowest Rayleigh number on the neutral stability plot, ie Ra=1707.8 is reached. He further suggested that this corresponds to a cell depth to width ratio of approximately one-half. If a thin walled honeycomb structure is mounted in the fluid between the horizontal boundaries, and the Rayleigh number is again increased slowly from Zero convection current will no longer commence at Ra =1708. This is due to the fact that the cellular

motion corresponding to this Rayleigh number would not satisfy the zero-velocity boundary conditions demanded by the rigid honeycomb walls. The fluid will remain stable until a value of the Rayleigh number is reached where the corresponding incipient fluid motion has a cell depth width ratio that will allow it to satisfy the boundary conditions demanded by inserted honeycomb structure. Figure 4.3 shows the stability plot calculated by Holland. (based on the work carried out by Pneuli).

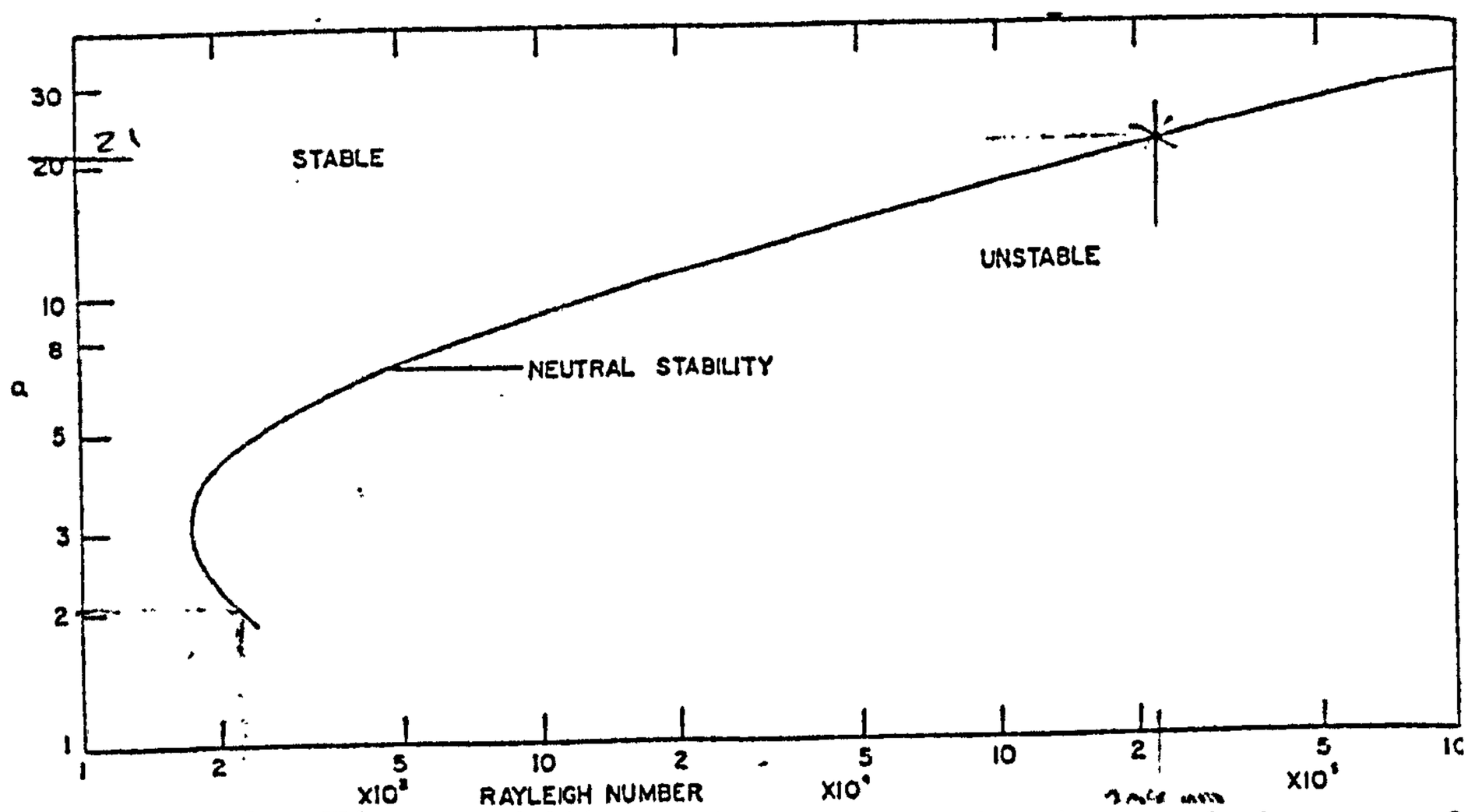

Figure 4.3: The stability plot for a horizontal layer of fluid heated from below.

Using figure 4.3 Holland suggested that if the honeycomb is of square array, convection currents can be suppressed in the above mentioned method until a Rayleigh number is reached

corresponding to the following equation: for suppression of convection current

$$a = \pi \sqrt{5.}\ (d/w)$$ Equation 4.2:

Where w is the width and d is the depth of the honeycomb cells. The value of a on the plot of neutral stability is given by the equation 4.2.

For example, a honeycomb structure of cell depth to width ratio of three has a value of the parameter (a) of

$$a = \pi \sqrt{5.}\ (3) = 21.1$$

From figure 4.3 the stability plot convection currents are suppressed for a values of Rayleigh number below 209,000.

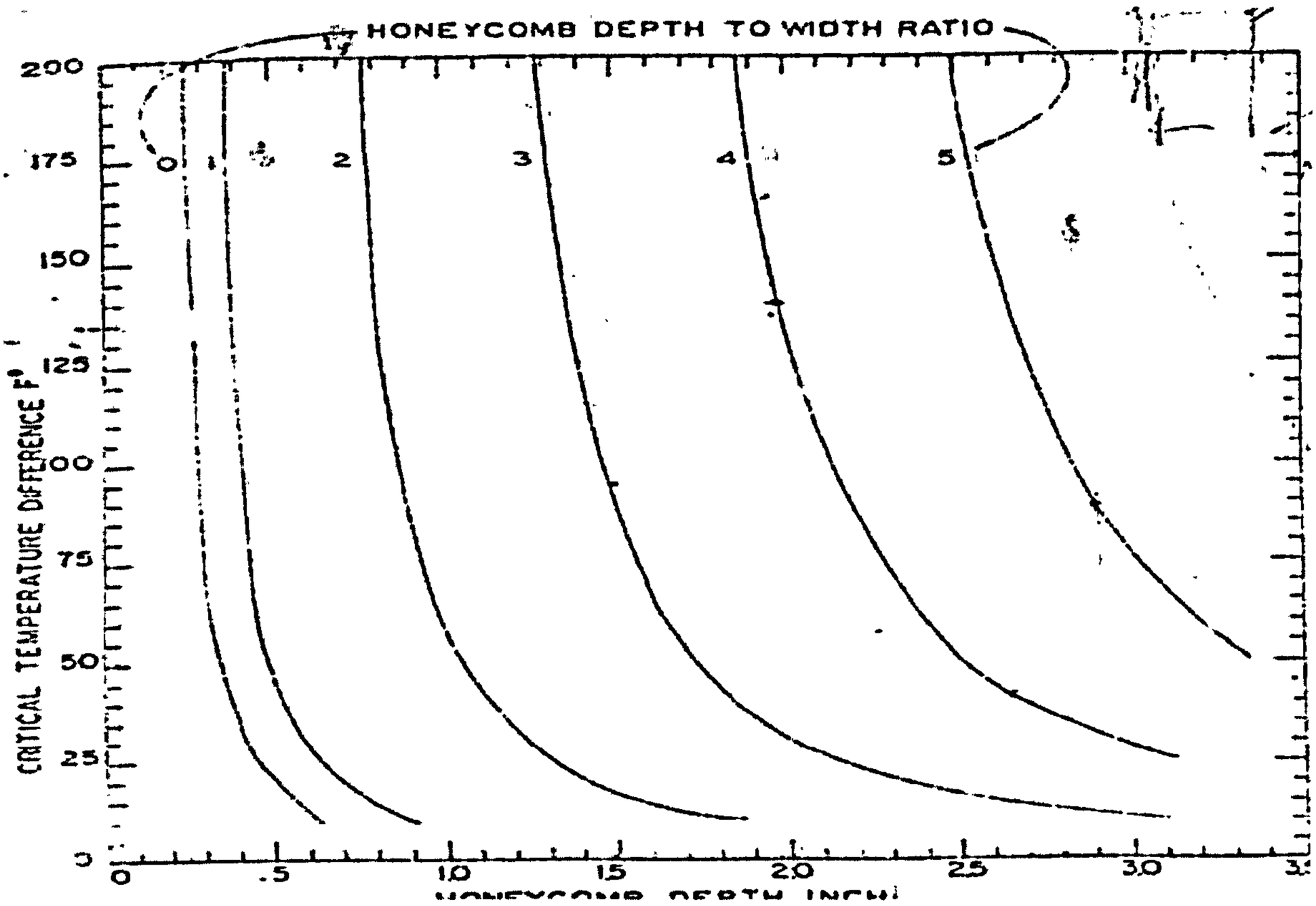

Figure 4.4: Original plot showing critical temperature difference below which convection current are suppressed.

The above graph produced by Holland (figure 4.4) which shows the relationship between the maximum temperature difference across the fluid layer below which convection currents are suppressed, for various fluid layer depths and honeycomb cell depth to width ratios.

The previous graph (figure 4.3) showed the corresponding Rayleigh number and the depth width ration of honeycomb to suppress the convection current. Using the graph (figure 4.4) it is possible to establish at what temperature difference (between the horizontal plates) and its corresponding honeycomb depth width ratio, where suppression of the convection current can be achieved. For example if A two-inch deep honeycomb panel with a cell depth-to-width ratio of four will suppress convection up to temperature differences of 135 °F (57.23°C).

Hollands findings suggest that if the convection currents are suppressed, the fluid can transfer heat by conduction only and the Nusselt number for natural convection is unity. Therefore if and when convection, current starts it helps to transfer heat through the fluid, and the Nusselt number increases.

4.3.2 Radiant heat transfer

Provided the walls of honeycomb are sufficiently thin and black to long -wave radiation. No heat transfer from one cell to another is expected. The radiant heat exchange between the two

faces of the honeycomb panel can be reduced to the treatment of radiant exchange in a single isolated cell of the honeycomb. As no heat exchange is expected from one cell to another the sides of the isolated cell can be assumed to be insulated.

4.3.3 Overall heat transfer coefficient

If the convection is suppressed, the Nusselt number for natural convection is unity then the natural convection heat transfer coefficient is given by

$$ha = \frac{ka}{d}$$

Equation 4.3:

where ka is the thermal conductivity of air and d is the depth of the honeycomb.

Holland carried out four test cases to show magnitude of the above Heat transfer coefficients to those that exist with and without honeycomb present.

Case 1 - Both horizontal surfaces are black, with no honeycomb

Case 2 - Same as case one but one bounding surface has an emissivity of 0.15.

Case 3 - Both bounding surfaces are black, and a honeycomb structure fabricated from sheet glass, 0.01 inches thick, and with a depth-width ratio of four is inserted between the horizontal surfaces.

Case 4 - Same as case 3 except that one of the bounding surfaces has an emissivity of 0.15.

The following results were obtained

Cases	1	2	3	4
Honeycomb	NO	NO	YES	YES
Emissivity	1.0	0.15	1.0	0.15
Convective heat transfer coefficient	0.548	0.548	0.112	0.112
Radiative heat transfer coefficient	1.56	0.234	0.358	0.156
Honeycomb conductive heat transfer coefficient	N/A	N/A	0.155	0.155
Overall, heat transfer coefficient	2.108	0.782	0.625	0.423

Table 4.2 Magnitude of the heat transfer coefficient for the four cases. (Holland 1965)

The table results show a reduction in the overall heat transfer coefficient due to the glass honeycomb. The reduction in overall heat transfer coefficient from case (3) to case (4) indicates that despite the use of honeycomb, if a lower emissivity surface is used it will further reduce the overall heat transfer coefficient.

Other researchers have also studied the effect of honeycomb devices and their effect on the heat transfer and convection current.

Edwards (1969) also discovered that by inserting parallel vertical walls (slats) on the onset of convection in a cavity heated from below and cooled from above, would help to reduced heat transfer

Charters and Peterson (1972) studied the effects of honeycomb Cellular materials in relationship to free convection suppression and found that the use of honeycomb may be effective in suppressing convection in the horizontal cases

Buchberg, Catton, and Edward (1976) reviewed the effects of honeycomb structure in used between absorbers and glass cover

to suppress natural convection, and concluded that for effective suppression, the honeycomb should have an optimum geometry.

Siebers and Viskanta,(1979) studies the use of honeycomb in solar collectors and concluded that the use of honeycomb is very effective in reducing the free convection.

Hoogendoorn etal (1985), Studied in the effect of honeycomb devices on radiation, conduction and convection. The study found that heat transfer by conduction through the low conducting ribs (slats) is less than 2.4% of the total heat transfer for Rayleigh numbers between 10^5 to 10^7 indicating that the radiation heat transfer on the rib surfaces, which is eventually conducted through the ribs, will have a negligible effect on the total heat transfer to or from the plate surface. The study further concluded that the poor conducting Ribs on the surface merely act as convection suppressors.

Sharma and Kaushika (1987) carried out tests on the effect of the performance characteristics of honeycomb in use of solar ponds and concluded that the best results showed that the optimum depth of the honeycomb should be between 12-17 cm.

Kangni, etal (1991) carried out research on natural convection and conduction in enclosures with multiple vertical partitions, where they concluded that by increasing A number of partitions (slat/honeycomb) resulted in the degreasing of heat transfer.

Platzer (1992) in his studies on the calculation procedure for collectors with different size honeycomb found that a honeycomb of 5cm having Aspect ratio of 5 to 8 and for honeycomb of 10cm the with aspect ratio of and about 12, will effectively suppress the convection.

E.K.Lakhal etal,(1994) carried out research on natural convection heat transfer in honeycomb enclosures with perfect conducting fins, and also concluded that the use of long fins can help to suppress the convection current.

Schweiger, etal (1995) carried out numerical experiments on laminar natural convection in rectangular cavities with and without honeycomb structures and found that the use of Honeycomb can help to reduce convection heat transfer.

Asako, etal (1996) carried out research on the use of Hexanagonal honeycomb core of negligible thickness and found

that the combined convection heat transfer rate is affected by radiation. The total heat transfer rate increases with an in the emissivity. Therefore the emissivity should be made as low as possible to decrease the heat transfer rate.

Cane and Holland (1997) etal found that free convection heat transfer across an air layer can be effectively suppressed by a thin-walled square or hexagonal celled honeycomb even in the inclined position.

Sezai and Mohmamad (1999) also carried out test on different methods of suppressing free convection with adding poor conductor ribs (slats); and concluded that by inserting ribs on the surface can reduced the rate of free convection heat transfer as much as 75% compare with a bare plate. Sezai & Mohmamad also found that for Ra $=10^5$, a reduction of natural convection heat transfer is as high as 50% when a heights of the ribs are in the region of 5cm. The study also suggested that to minimize radiation heat transfer aluminium foil should be used.

Yamaguchi etal (1999) have (further) suggested that when simulating three-dimension heat transfer for natural convection in a vertical porous layer with a Hexagonal honeycomb core, if

the porous layer is very long and wide in both the vertical and horizontal direction, the velocity and temperature fields repeat themselves in the successive enclosures except at the end boundaries of the layer. Therefore, it is possible to solve the natural convection and radiation in only one hexagonal honeycomb porous enclosure.(This is what will be done for CFD simulation to determine the depth width ratio honeycomb). There also found that if the walls of the honeycomb have thin thickness the honeycomb walls will act as poor conductors and conduction will be negligible.

Holland carried out a large body of research on the use of honeycomb in various research and concluded that the used of honeycomb will suppressed the convection current, in 1985, Holland and Iynkaran carried out test on honeycomb where a 10mm air gap was introduced between the plate and the honeycomb, and concluded that the an air gap of about 10mm does not invalidate the honeycomb's ability to suppress free convection heat transfer. No other literature was available on the effect of the honeycomb where the gap between the honeycomb and the floor was in the area of 2.6m, this is the area gap for the distance between the floor and the end of the honeycomb slat for the test room.

To simulate the effect of attaching the honeycomb to chilled ceiling for different depth width ratio would be time consuming and costly, therefore a single cell of depth width ratio were simulated using the CFD simulation, as suggested by Yamaguchi etal, (1999). First it was important to establish if the CFD model was able to simulate the required boundary conditions. To establish this various test simulations were carried out.

Research on the honeycomb and its effect on the heat transfer and convection current can be summerised as follows:

- The use of honeycomb can help suppress the natural convection current for various cases.

- The effectiveness of the honeycomb is strongly influence by the thickness of the honeycomb wall, since both the conduction loss and solar transmittance is dependent on this.

- If the honeycomb cell walls are sufficiently thin, heat losses by conduction directly through the honeycomb wall will be negiable.

- A low emissivity surface will help to reduce the overall heat transfer coefficient.

- A shining surface will help in transmittance of the solar radiation.

The honeycomb will help to suppress the convection current and as the honeycomb slats will be of negligible thickness, conduction can not occur therefore heat transfer can only occur via radiation, if the side's walls of the honeycomb are shinny the radiant cooling ceiling will be able to see the room surfaces.

4.4 Development of CFD simulation regarding slats

CFD simulations were carried out to determine whether the CFD code can produce results for the use of slats/ honeycomb in the room. The simulations carried out so far as discussed in previous chapters have only been simulated for the whole room environment. It was not known if the CFD code could simulate and produce results for small regions near the ceiling.

CFD simulation were carried out on two horizontal parallel flat plates, having a temperature difference of 10°C (16 °C impose on the top plate and 26°C impose on the bottom plate.) to encourage convection current, the length of the parallel plates was at 4m and height distance between the two plate at 1m in 2D model (case:slats102) the results showed two complete identical circular convection cells. When the number of mesh cells were increase in the size of the circular cell changed, one became larger than the other (case:slats103).

It was decided to determine at what point (height) between the two horizontal parallel plates the airflow becomes stable, therefore the height was reduced from 1m to 0.5m (case :slats104) the results showed 3 circular cells as seen in figure 4.5.

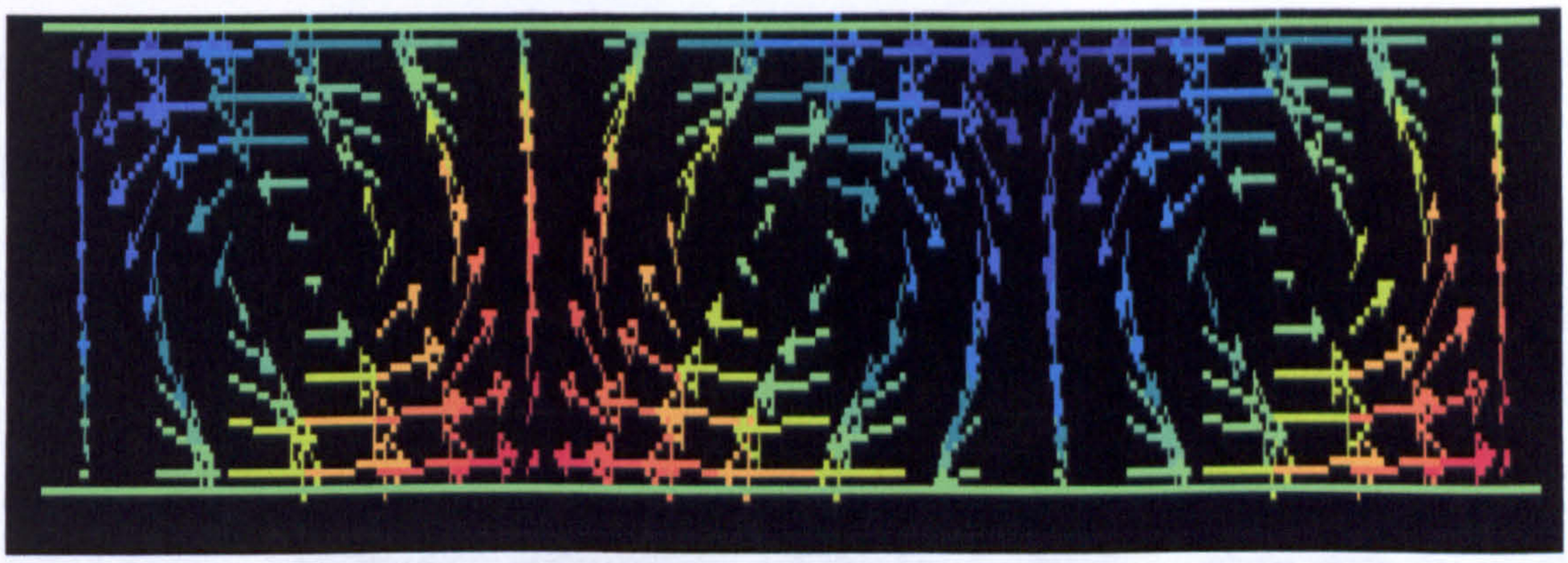

Figure 4.5: Ref: slats104 CFD simulation results for 2 horizontal parallel plates (0.5m height, 4m length ,1m width 2D model) shows 3 circles of convection current, (temp different set at 26-16 (10 °C)

Figure 4.6:

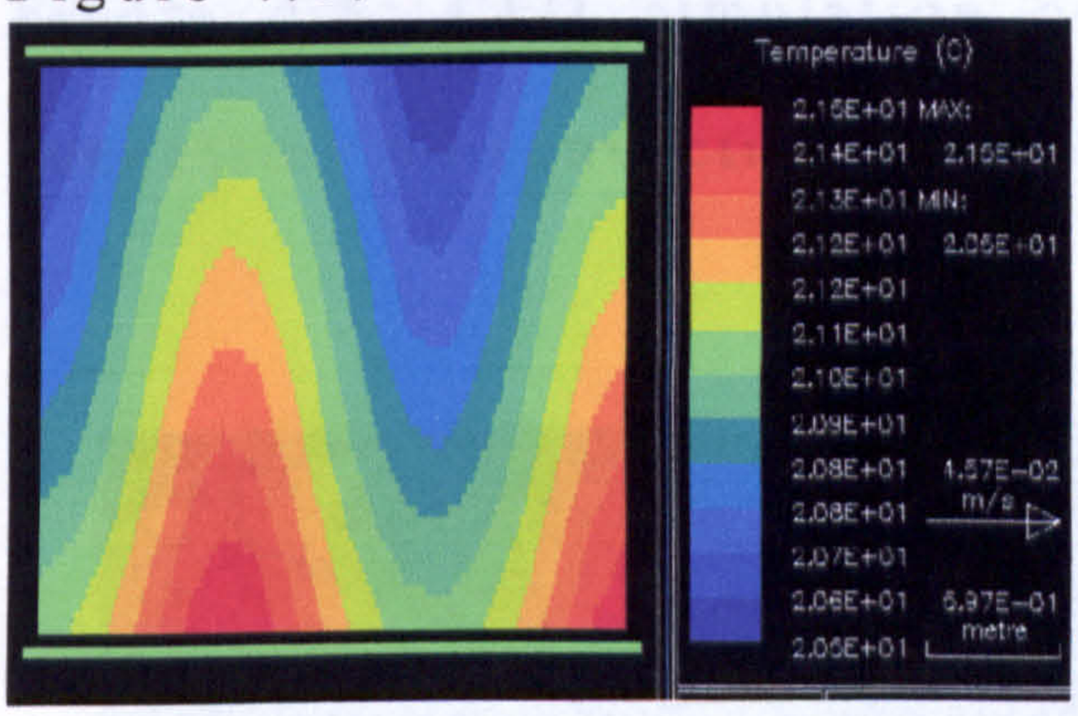

Figure 4.7

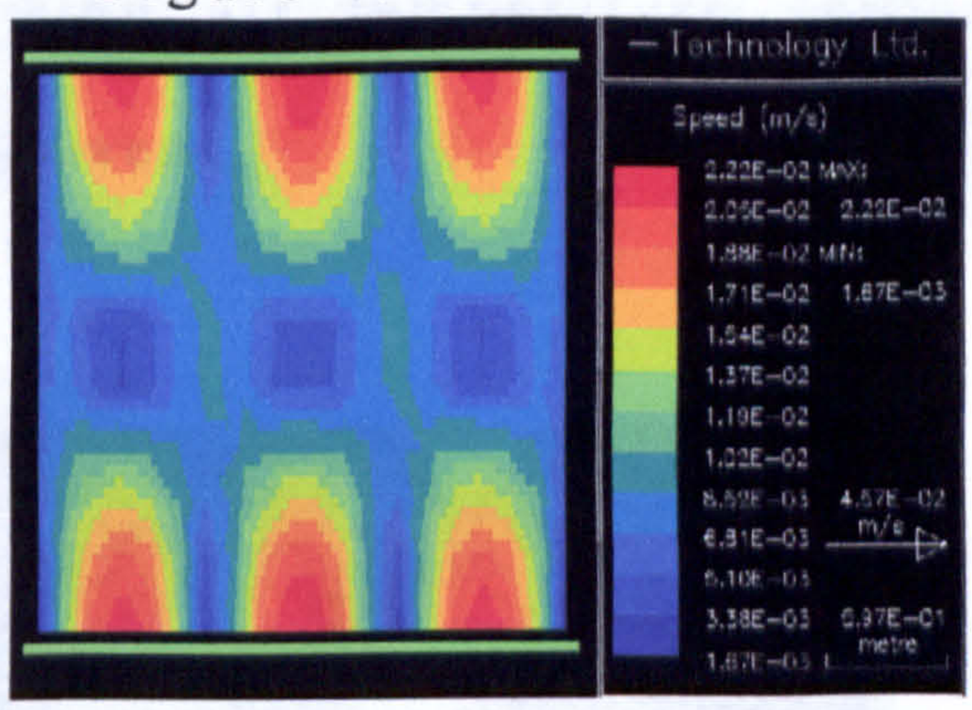

Figure: 4.6: CFD simulation showing air temperature contours of convection current of simulation shown in the figure 4.5

Figure: 4.7: CFD simulation showing air velocity contours of convection current of simulation shown in the figure 4.5

The height was further reduced to 0.25m the results showed no circular cells and showed NO airflow pattern as seen in figures 4.8 and 4.9,

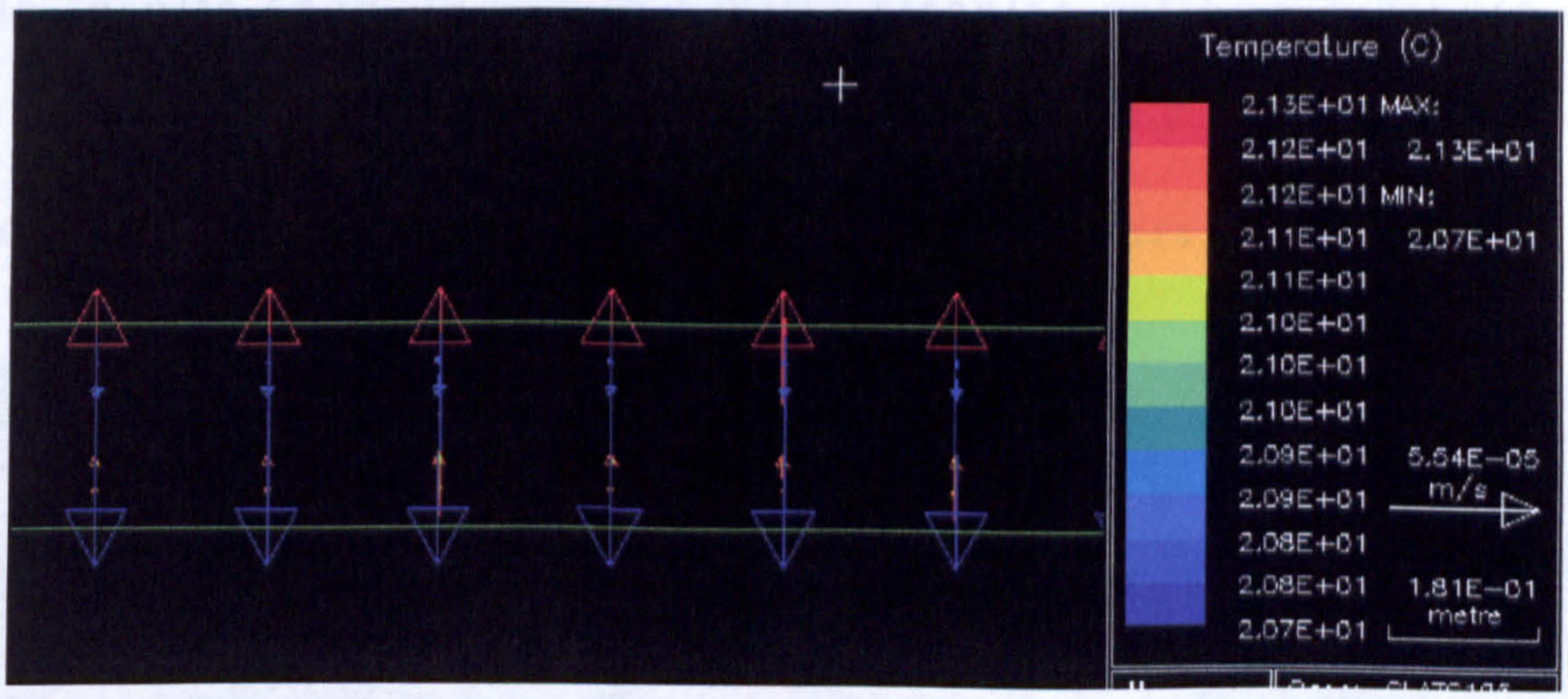

Figure 4.8: CFD simulation showing air temperature contour suggesting no convection current present.

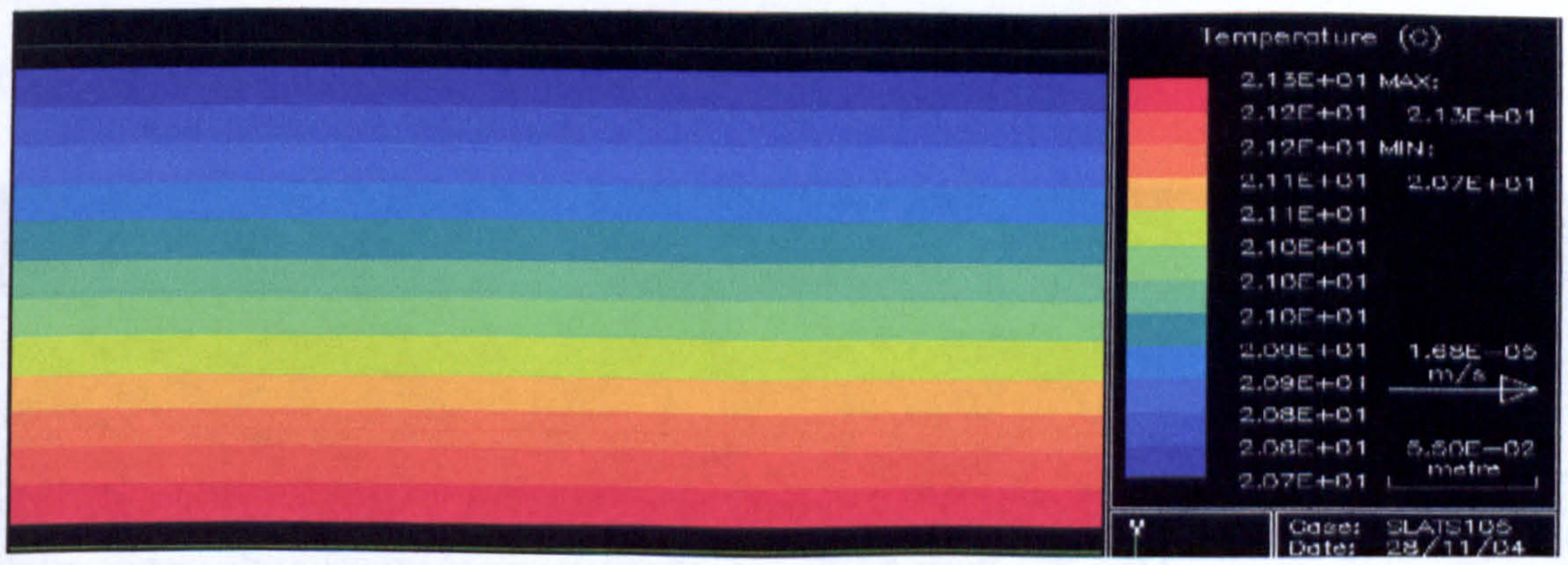

Figure 4.9 : CFD simulation showing no convection current present

The height between the two parallel plates was increase from 0.25m to 0.375m (half way between 0.5m and 0.25m),this was carried out to determine at what point the airflow became stable. The results showed four complete circular cells, see Figure 4.10 to Figure 4.14. These figures show the airflow pattern in various forms including line contour, velocity contours.

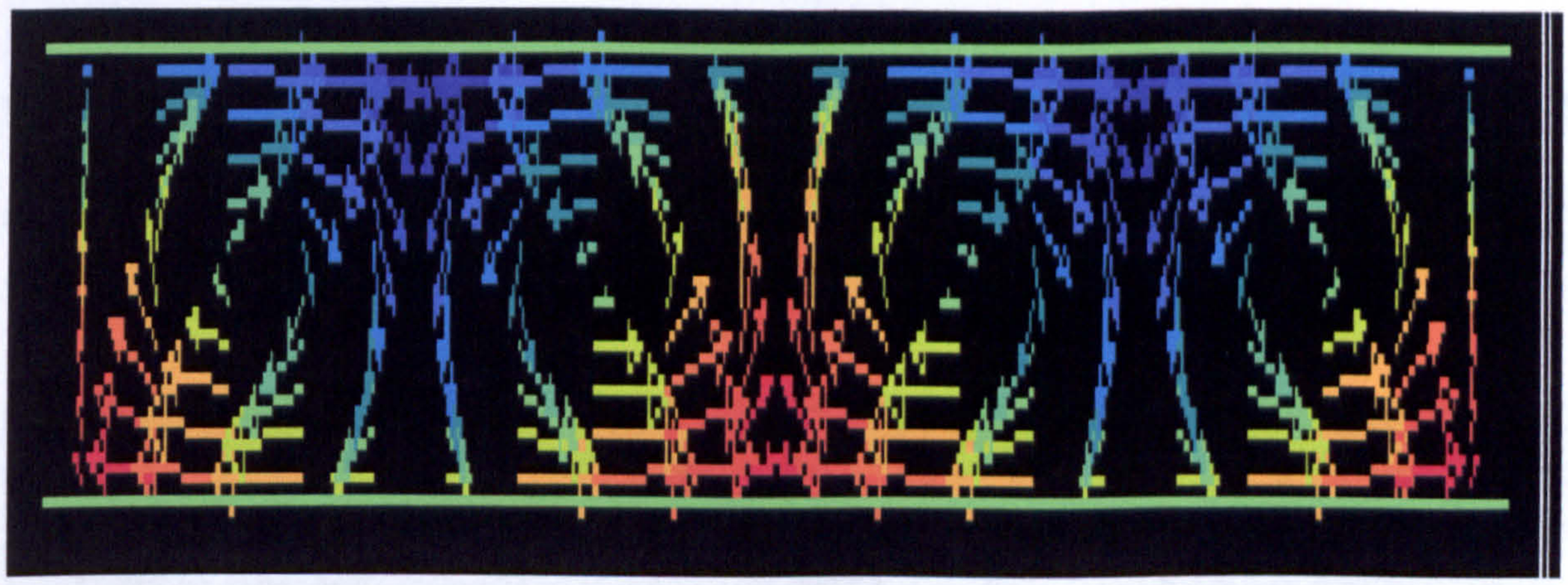

Figure: 4.10: CFD simulation showing airflow consisting of four circular convection current cells.

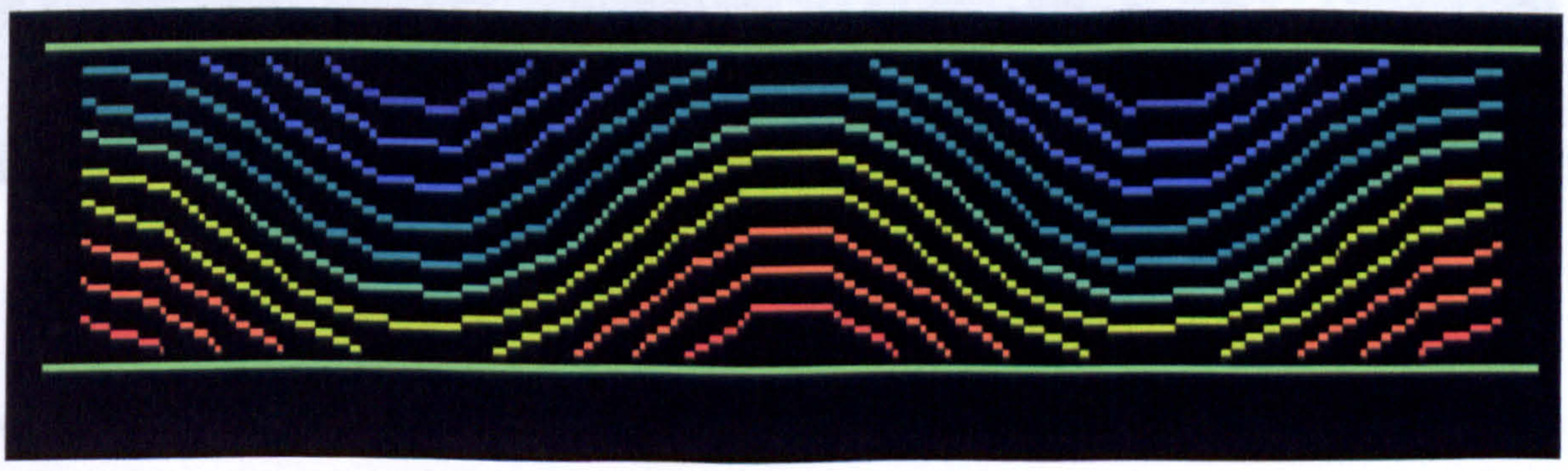

Figure 4.11: CFD simulation showing airflow with four circular convection current cells, in line contours

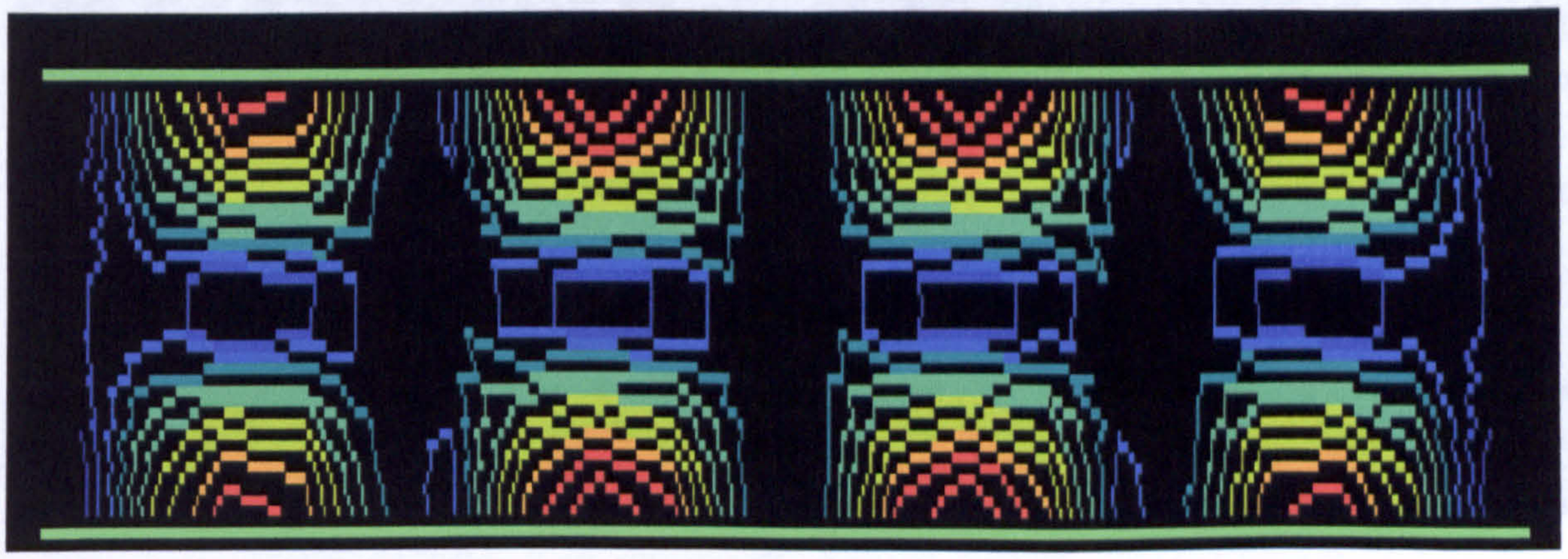

Figure : 4.12: CFD simulation showing airflow with four circular convection current cells, in line contours

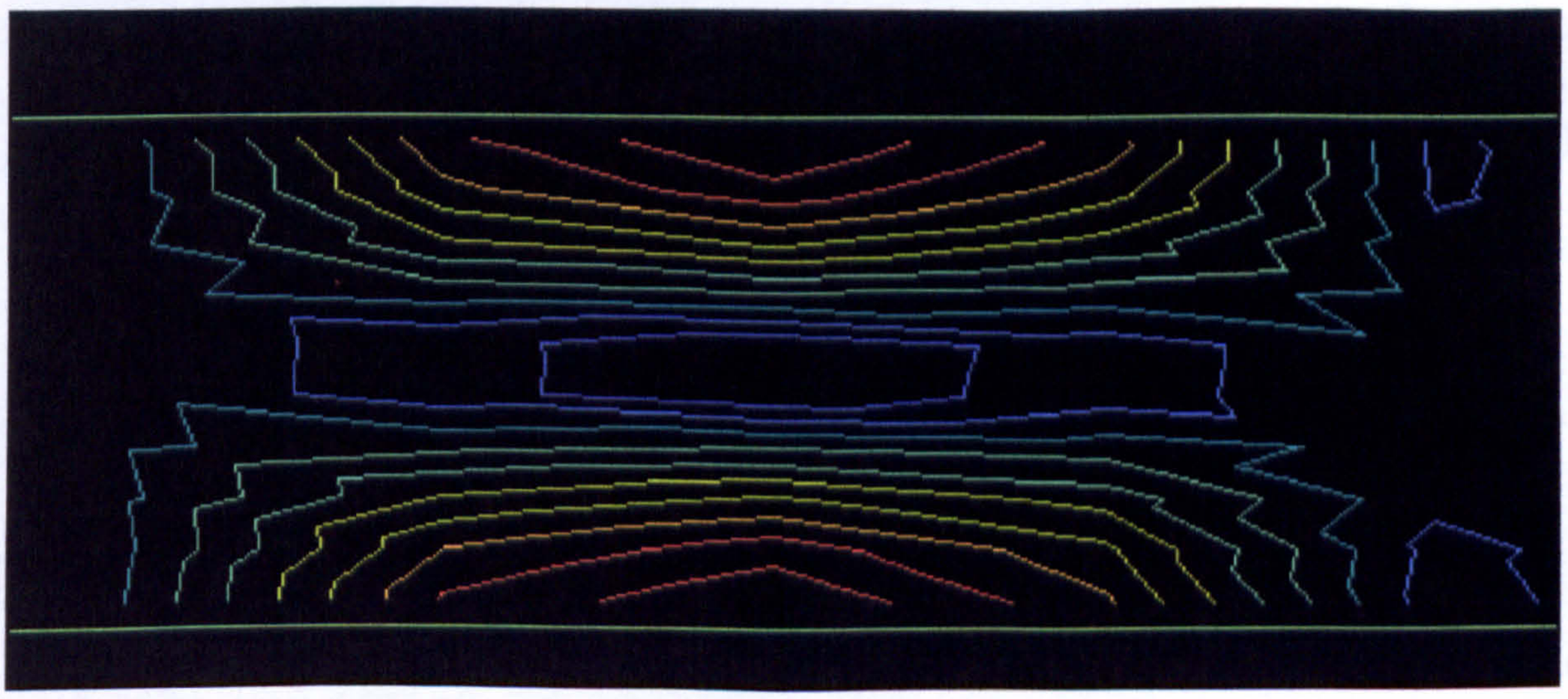

Figure: 4.13: CFD simulation showing a section of one of the convection current in line contour for velocity.

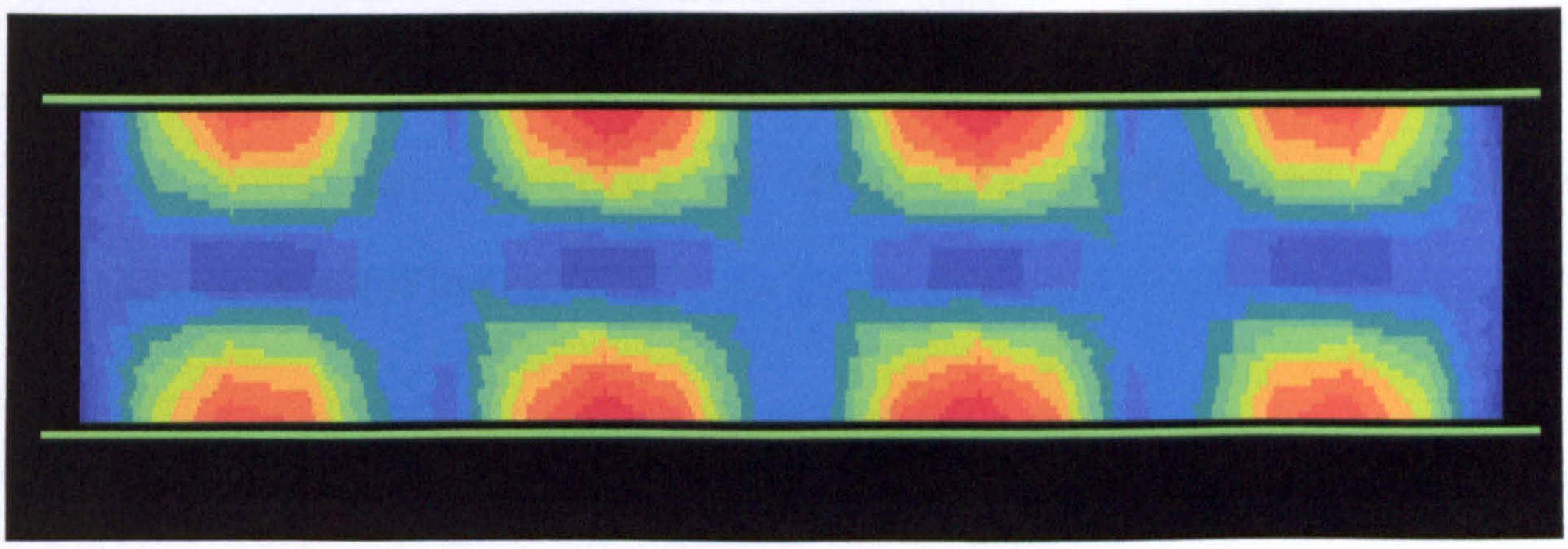

Figure 4.14: CFD simulation showing four airflow circular convection current cells, in line contours for velocity

Therefore the height was reduced from 0.375m to 0.3125m (this is the middle of 0.25m and 0.375m), the results also showed that no airflow was present, therefore suggesting that for two horizontal parallel flats at a distance between the two plates of 0.3125m the airflow becomes stable.

It was intended to investigate the effects of adding vertical plates at the two ends of the horizontal parallel plates would have on the airflow. As we know that at a height difference of 0.375m between the two parallel plates showed 4 circular cells (case: slats106) therefore the two vertical plates were added at the two ends, the results showed the airflow no longer existed

(case:slats108), thus suggesting that by inserting extra resistance to the plates the airflow has become suppressed, this agreed with the findings of Hollands (1965) and all other researchers mentioned.

It was decided to model the 2D simulation into 3D modelling (case slat114). Using the (case:slat102), the simulation was modeled in 3D modelling, this meant that in Z direction the numbers of cells were increased from 1 to 7 cells. The results showed 1 large circular cell in Z direction, which is shown in figure 4.15, where in test case slat102, the results showed two equal size circular cells.

3D simulation was carried (slat114) out to compare with 2D simulation of (case slat104), the results again showed difference in airflow. Table 4.3 shows the findings and the CFD simulation result are shown in figures 4.15 to 4.17.

File name	Model	Results
Slats102	2D	2 Cells
Slats114	3D	1 Cells

Table 4.3 showing the comparison of the results for the same boundary conditions for 2D and 3D modelling. Figure 4.18 shows the CFD simulation results showing one complete convection circular cell

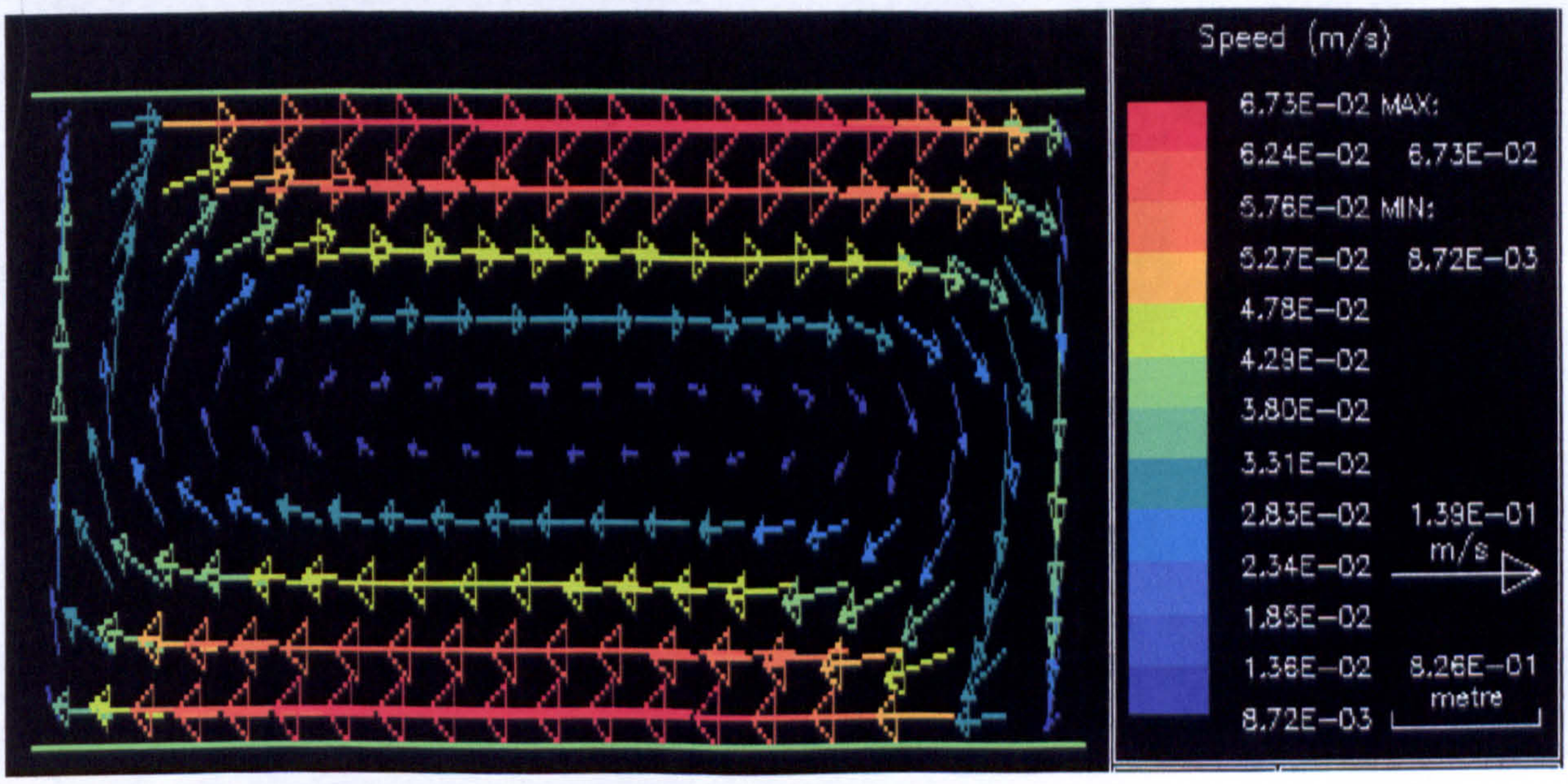

Figure 4.15: CFD simulation showing one complete convection current cell (case slats114)

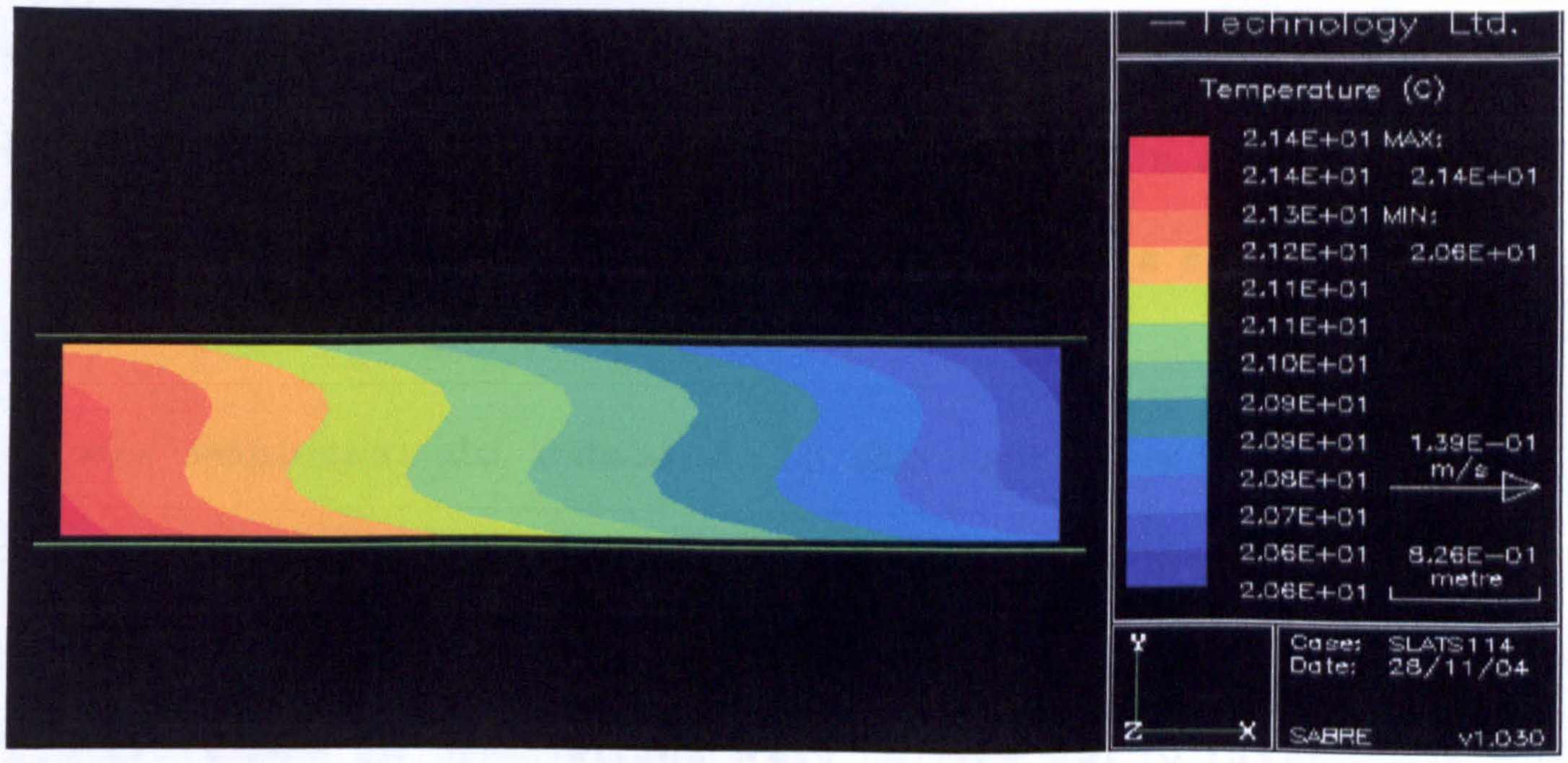

Figure 4:16 CFD simulation showing air temperature contour of one complete convection current cell (case slats114)

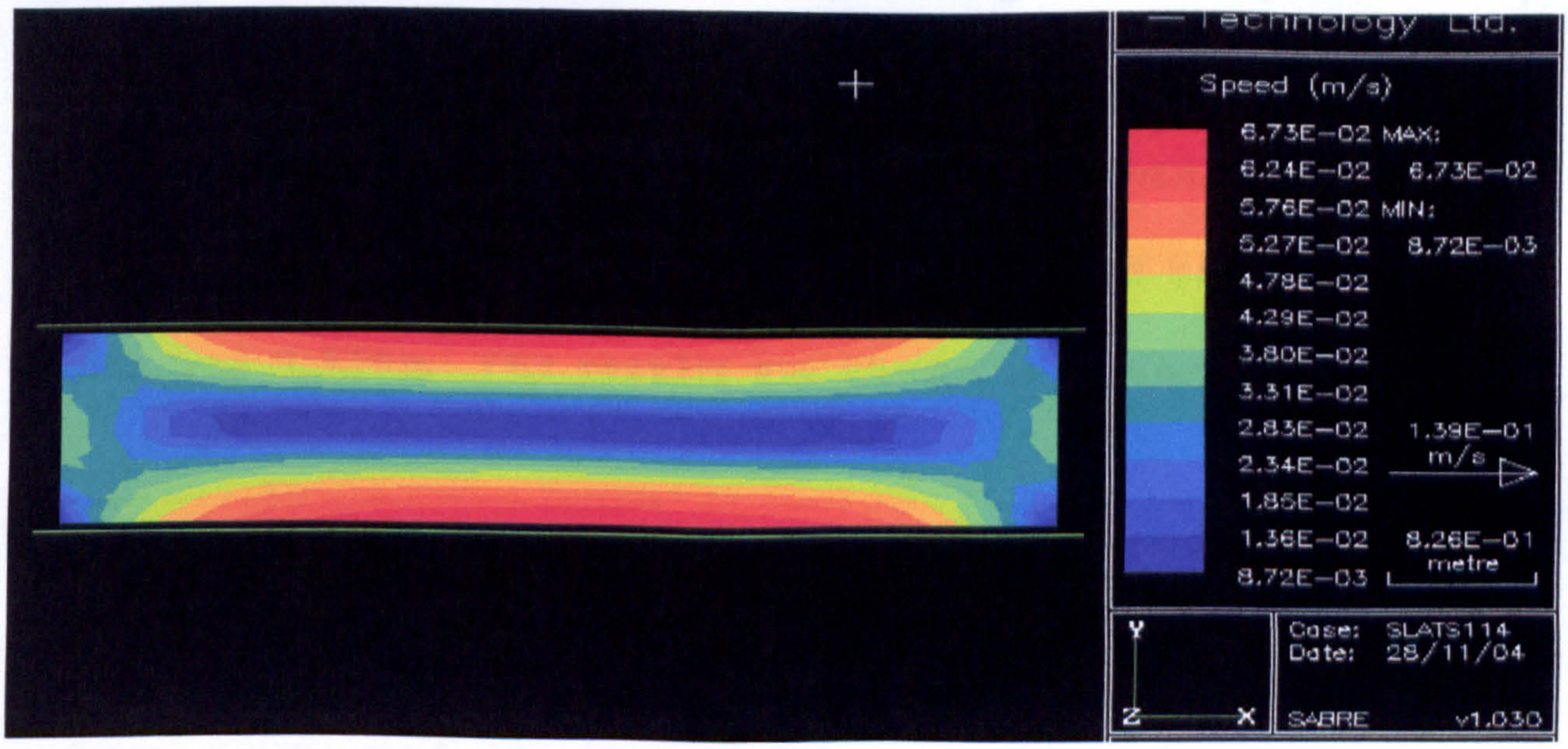

Figure 4.17: CFD simulation showing air velocity contour of one complete convection current cell (case slats114)

Case slat118 was simulated in 2D model having the same boundary conditions as case slat116. The results for this 2D and 3D, agreed that no airflow movement-convection air was present.

It was important do establish if the length and width of the horizontal parallel plates can effect the airflow pattern.

Therefore two 2D simulations were carried out to investigate the above question.

Case slat120 was simulated having a length of the plate 8m by 1m width, and height between the two plates 0.375m. The results were compared with the case slat106 which had the boundary conditions of length = 4m by width = 1m, height between the two plates was 0.375m. The results are shown in table 4.4.

File name and Boundary Condition	Result
Slat106 (4m x 1 m)	4 cells
Slat120 (8m x 1m)	No Air movement

Table: 4.4 showing the effects that are seen when horizontal parallel plate length is changed Figures 4.21 and Figure 4.22 show CFD simulation results for the case study of slat106 showing four circular cells.

The result suggesting that change in length of the horizontal plate can influence the airflow.

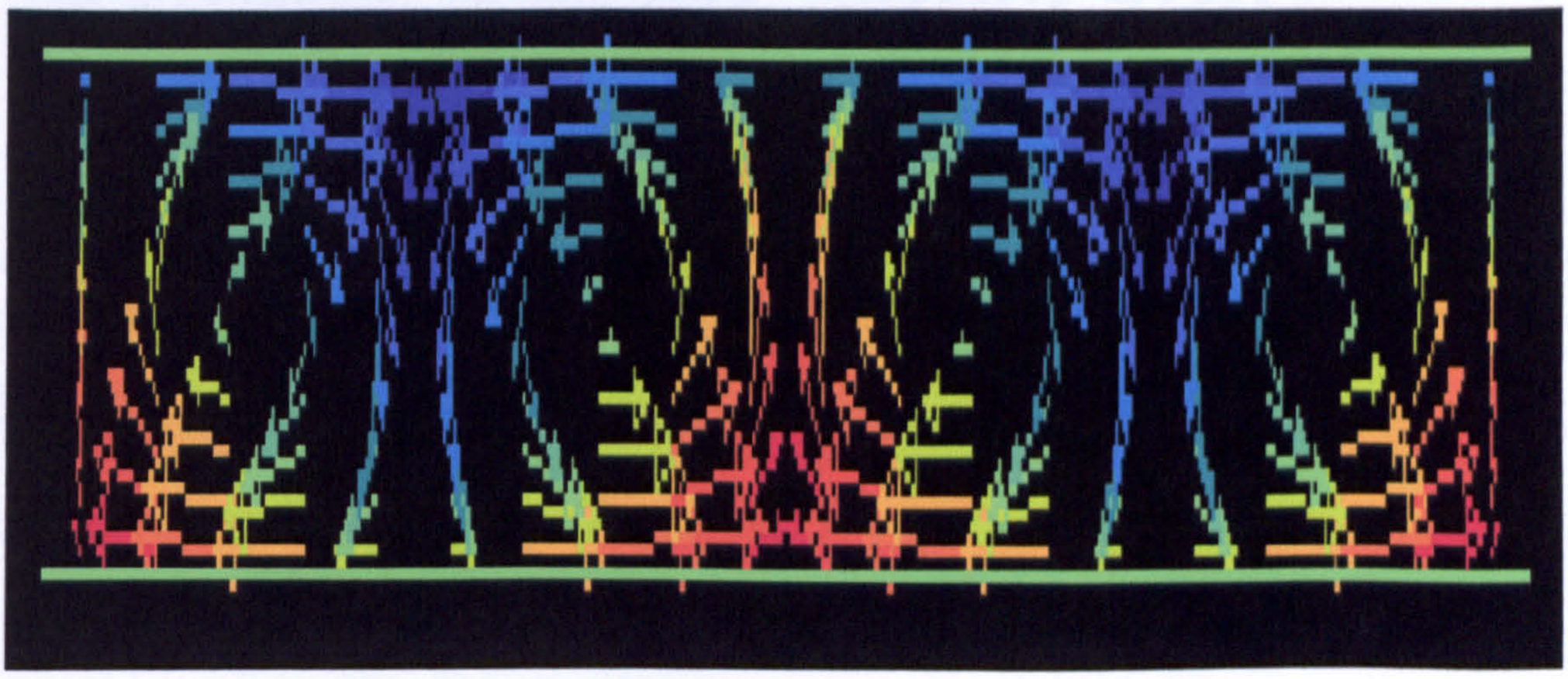

Figure 4.18: CFD simulation showing 4 complete circular convection cells suggesting heat transfer by convection (for case slats106)

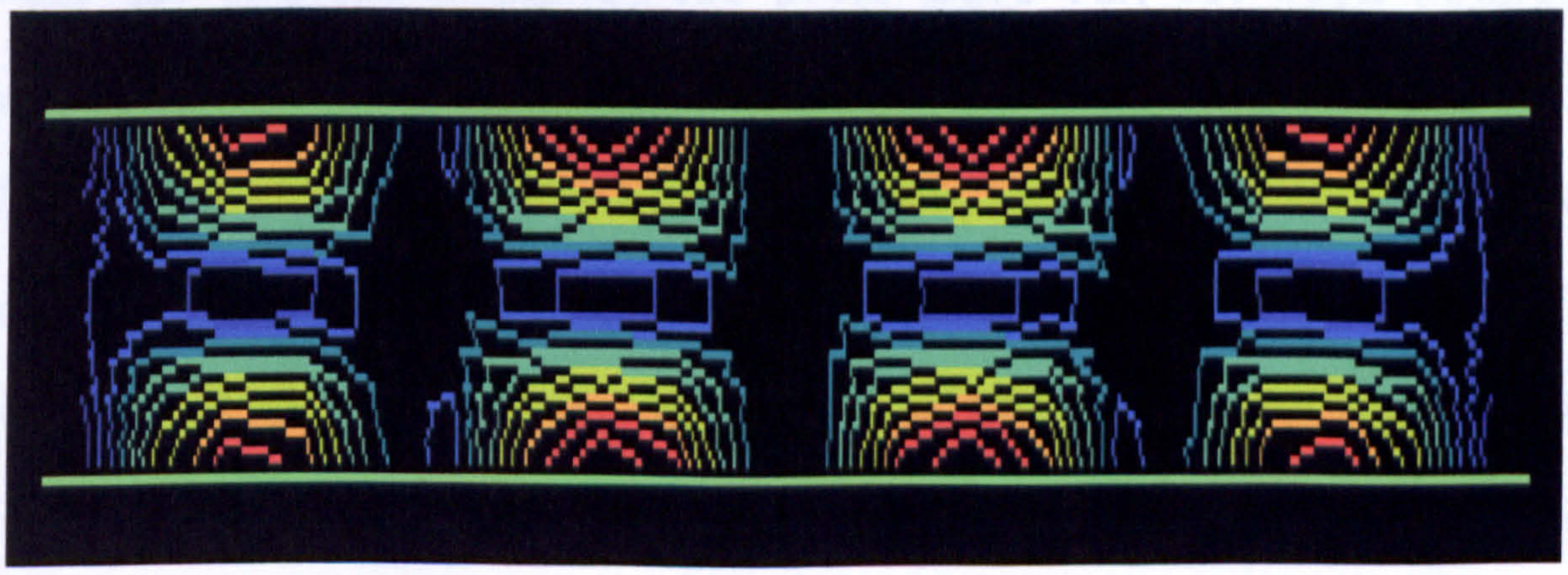

Figure 4.19: CFD simulation showing air velocity contours Showing Four (4) complete circular convection cells (case:slats106)

4.5 K-epsilon versus Eddy viscosity model

CFD Simulation were carried out using the K- epsilon model to compare with the Eddy Model, as we know from previous work (chapter Three see figures 3.25 to 3.32) Eddy model produce Results that were more accurate then the K-epsilon model, when applied for large spaces.

Case slat123 was simulated using the same boundary conditions as case slat105 where the height difference between the two parallel horizontal plates was 0.25m, the length of the plates were 4m and the width of the plate were 1m, for such boundary condition the air flow showed no airflow movement using the Eddy model see figure 4.8 and 4.9, and suppression of the airflow occurs The results for the K-epsilon model showed the results of air movement in figure 4.20 and 4.21. Both of the model produced results that contradict each other. It was important to establish which of the two models produce the correct results.

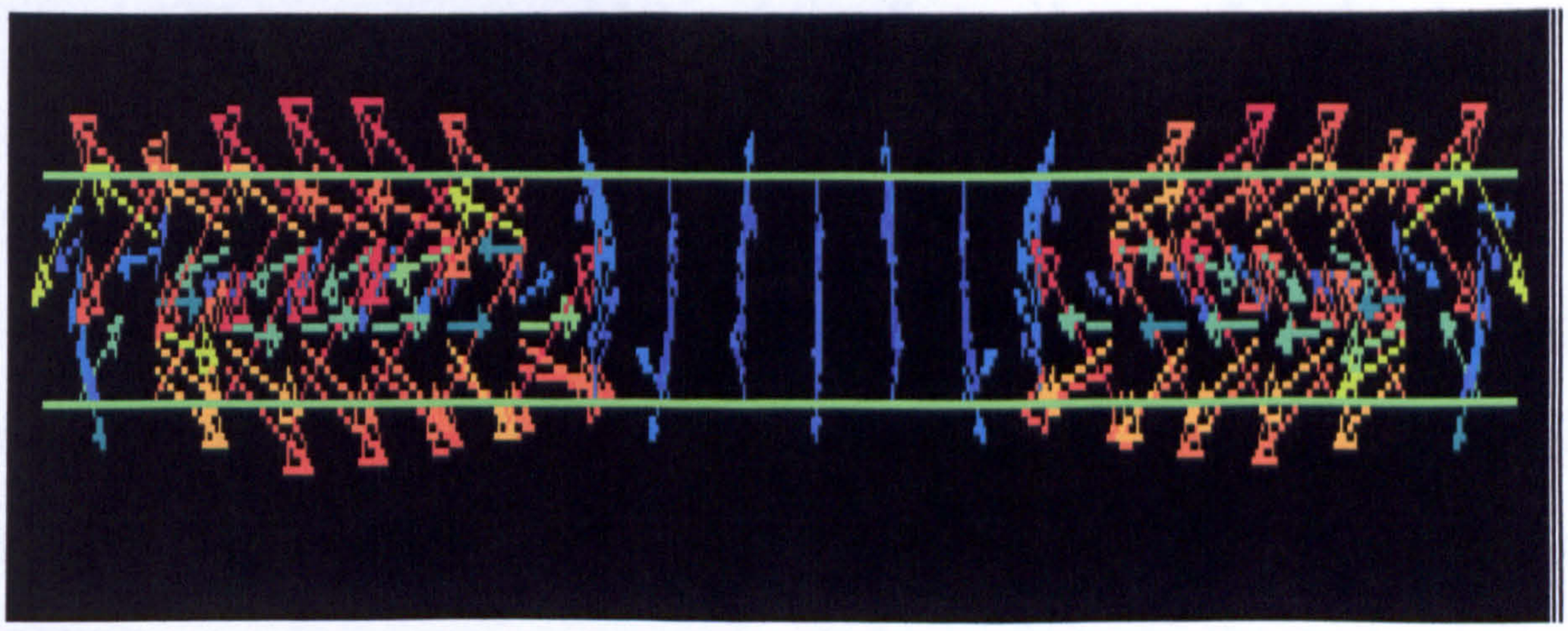

Figure 4.20: CFD simulation showing the results for case slats 123 in 2D k-epsilon model, 4mx0.25x1m results show convection where for the same boundary condition in Eddy viscosity model show no convection current.

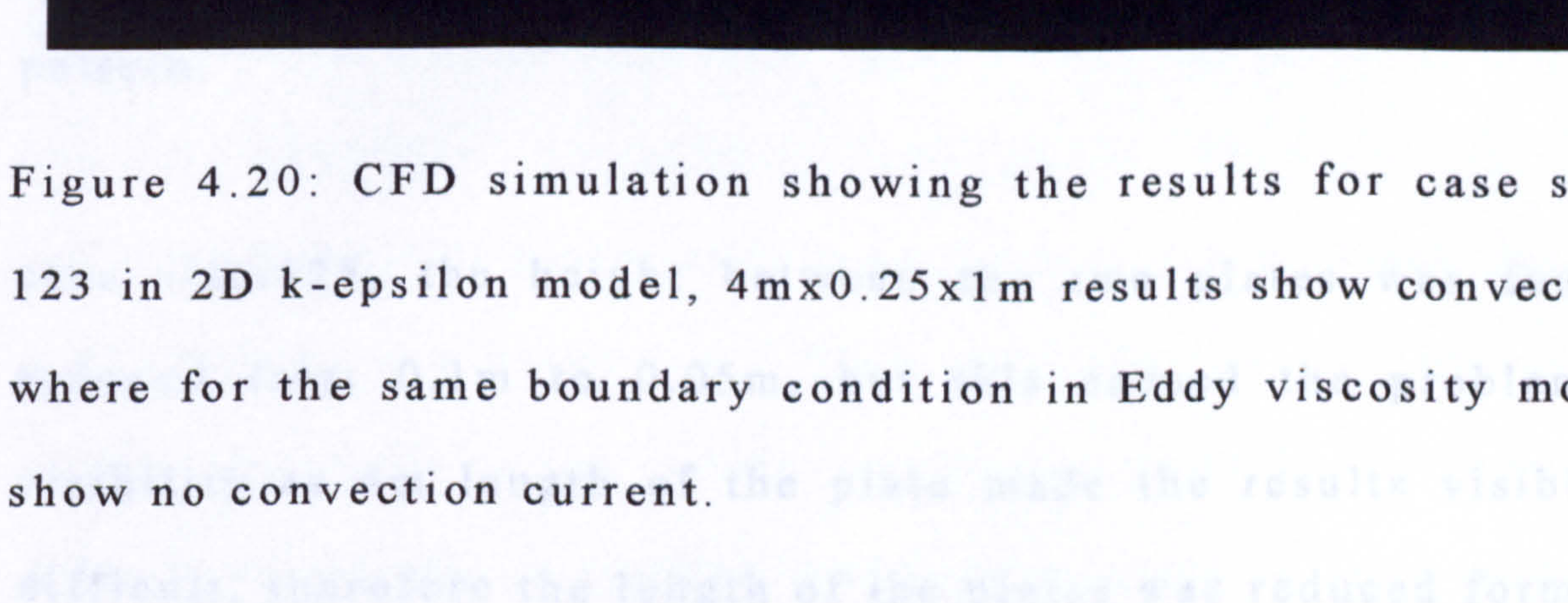

Figure 4.21: CFD simulation showing simulation results for case slats123: the results are showing the air temperature line contour profile

It was important to establish if the K-epsilon model also had any limitation.

Case slats124 , the length of the slats was kept at 4m and width at 1m. But the height between the two horizontal parallel was reduce from 0.25m to 0.1m, the results again produce airflow pattern.

case slats125, the height between the two plates was further reduced from 0.1m to 0.05m, but this caused the problem in visibility as 4m length of the plate made the results visibility difficult, therefore the length of the plates was reduced form 4m to 0.4m, but the width of the plates was kept at 1m.The result again produced Airflow.

As we know that at a Rayleigh number of 1708 the convection current will become stable between two horizontal parallel plates.

Using the standard formula for Rayleigh numbers

$$Ra = \frac{g\beta(T_1-T_2)L^3}{V^2} Pr \qquad \text{Equation 4.1}$$

It was found that to obtain a Rayleigh number of 1708 for the current boundary conditions the height between the two horizontal parallel plates should be 0.012m. Case (Slats126) was simulated with a height of 0.012m between the two horizontal plates, the result of the simulation showed no airflow, (therefore suggestion that the K-epsilon model is accurate in its simulation of the required boundary conditions).

Other simulation were needed to verify the about statement that the K-epsilon model can accurately model the required boundary conditions, therefore the height between the two horizontal parallel plate was increased to 0.015m, we know that at this height there should be some convection current as, the critical Rayleigh number is no longer 1708 for the new boundary condition. The results produced convection current between the two horizontal Parallel plates as expected (see figure 4.22).

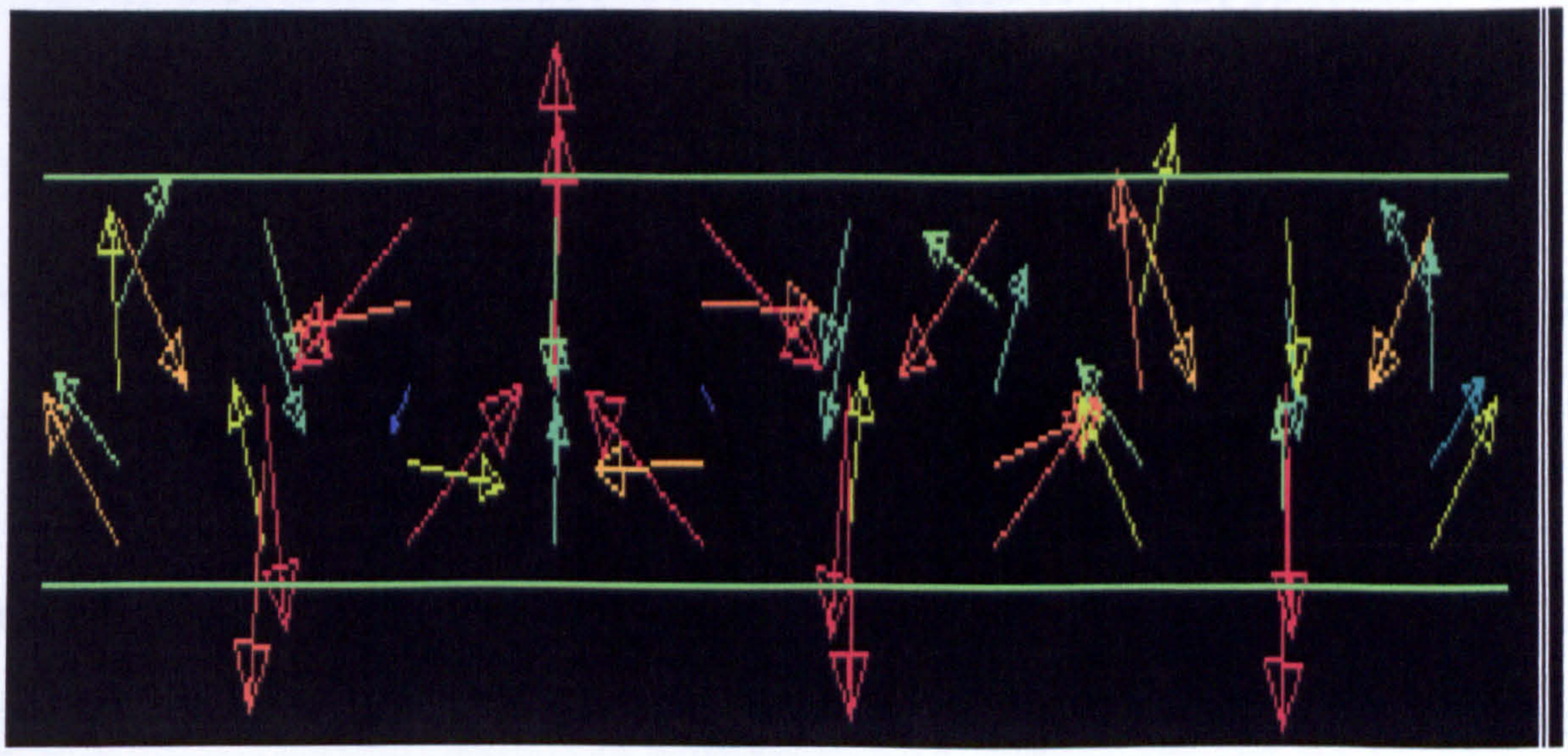

Figure 4.22: CFD simulation showing case slats127 which is in 2D K-epsilon model, showing convection current for Rayleigh numbers above 1708, (distance between plates 0.15m) temperature difference from 26-20°C (10°C). The result shows the break up of the convection cell as it is near the critical Rayleigh number.

From the formula to achieve Rayleigh number, we know that at Rayleigh number of 1708, the distance between the two horizontal parallel plates is 0.012m where convection current is suppressed when temperature difference is 10 °C. If we have a temperature difference of 0.5 °C then the distance between the two horizontal parallel plates will be 0.032m to achieve the

critical Rayleigh number of 1708, to achieve suppression of the convection current.

Case nwslat14, was simulated in 2D model the results produced agreed with the theory that at this height between the two parallel plates the convection current was suppressed.

If we changed the temperature difference from 0.5°C to 5°C, and keeping the same distance between the two parallel plates (0.032m), we should expect the result to show convection current. (case nwslat15) the result produced, agreed with the theory and thus produced convection current as seen in figure 4.23, Figure 4.24 and figure 4.25.

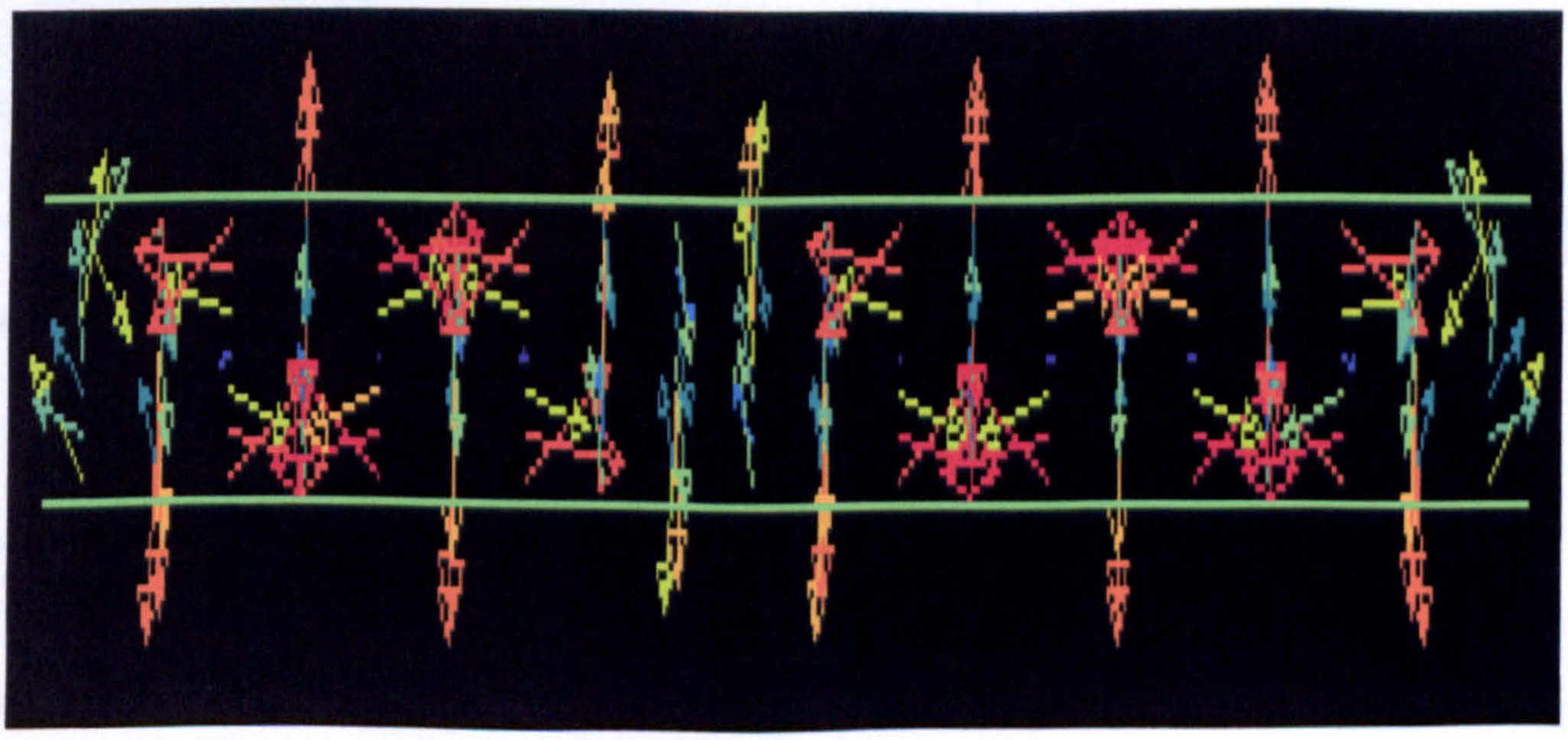

Figure: 4.23: CFD simulation showing convection current present when change in temperature is introduced.

The results show that by changing the temperature difference between the two horizontal parallel plates which has a height difference of 0.032m, (in fact will changes the critical Rayleigh number), convection current will appear as suggested by lord Rayleigh.

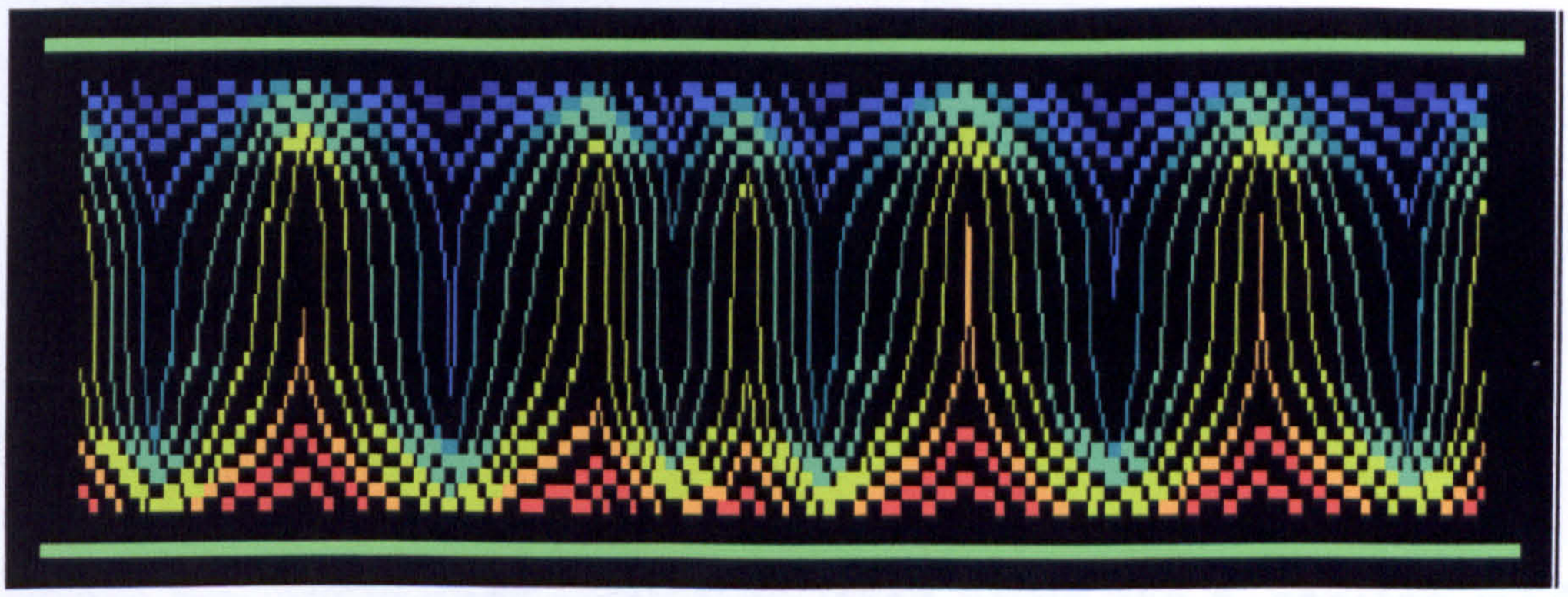

Figure: 4.24: CFD simulation showing air temperature line contours for the case nwslat15, (air temperature line contour representation of the air temperature flow seen in figure 4.23)

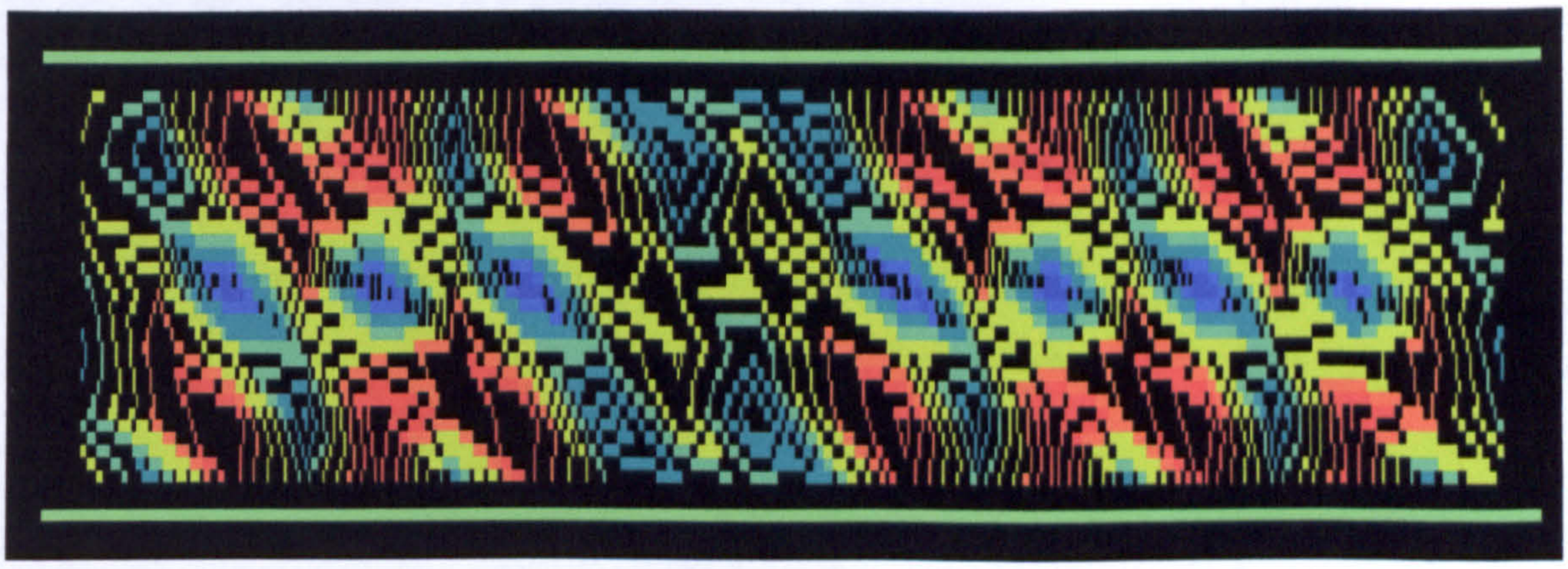

Figure: 4.25: CFD simulation showing: air velocity contours for the case nwslat15, (a velocity line contour representation of the air temperature flow seen in figure 4.23)

Many test conditions were simulated using the K-epsilon model. The results of the simulation suggest that the change in the length and height between the two plates and the change in temperature difference between the two plates can have an influence on the airflow between the two horizontal plates. Table 4.5 shows some of the results obtained when the temperature difference between the two plates is changed for the same length between the two plates; the first simulation shows (case nwslat14) that at temperature difference of 0.5°C we should expect suppression.

Case name	Boundary condition	Temperature Difference (^{o}C)	Results
Nwslat14	Length= 0.4m Width =0.1m Height = 0.032m	0.5°C	SUPPRESSION
Nwslat15	Length= 0.4m Width =0.1m Height = 0.032m	10°C	CONVECTION CURRENT
Nwslat16	Length= 0.4m Width =0.1m Height = 0.032m	5°C	CONVECTION CURRENT
Nwslat17	Length= 0.4m Width =0.1m Height = 0.032m	2.5°C	CONVECTION CURRENT

Table 4.5: The change in temperature difference can influence the airflow between the two parallel plates.

Case name	Boundary condition	Temperature Difference (°C)	Results
Nwslat 21	Height = 0.025m Width = 0.1m **Length = 0.1m**	1°C	CONVECTION CURRENT
Nwslat 22	Height = 0.025m Width = 0.1m **Length = 0.2m**	1°C	CONVECTION CURRENT
Nwslat 28	Height = 0.025m Width = 0.1m **Length = 0.3m**	1°C	CONVECTION CURRENT
Nwslat 26	Height = 0.025m Width = 0.1m **Length = 0.35m**	1°C	CONVECTION CURRENT
Nwslat 20	Height = 0.025m Width = 0.1m **Length = 0.4m**	1°C	CONVECTION CURRENT

Table 4.6: The change in the length of the two horizontal parallel plates can influence the airflow between the two plates.

It was uncertain from the results why at a specific length of the plates the convection current between the two horizontal parallel plates becomes suppressed.

The results were further analyzed where we can a pattern appearing as seen in table 4.7.

Case name	Length of the two plates (m)	Results	Velocity of the airflow (m/s)	Temperature Difference (°C)
Nwslat20	0.4m	Suppressed	Max = $9.35x10^{-4}$ Min = $6.66x10^{-6}$	1°C
Nwslat26	0.35m	Suppression	Max = $6.04x10^{-4}$ Min = $5.26x10^{-6}$	1°C
Nwslat28	0.3m	Suppression / convection current	Max $=2.16x10^{-4}$ Min = $4.01x10^{-6}$	1°C
Nwslat	0.2m	Convection current	Max = 7.86^{-4} Min = $1.02x10^{-5}$	1°C
Nwslat	0.1m	Convection current	Max = $2.13x10^{-3}$ Min = $3.43x10^{-5}$	1°C

Table 4.7: Showing that the increase in the length of the two horizontal parallel plates can influence the convection current between the two plates.

From table 4.7 it can be concluded that the air velocity of the airflow (convection current) is suppressed when the velocity of the airflow between the two plates is reduced to below 10^{-4} thus, as the length of the plate is increased, the airflow velocity is decreased, leading to reduction in the convection current between the two plates.

The results suggest that the CFD code using K-epsilon turbulence model could accurately predict air distribution and the suppression of convection current.

From the results of case slat126 at height of 0.012m between the two horizontal parallel plates, we know that the airflow becomes stable at a RA = 1708. The CFD simulation produced the suppression of the airflow in 2D model and also in 3D model (case slat130).

4.6 Summary

- The K-epsilon CFD simulation model was able to simulate and produce the critical Rayleigh number, for two horizontal parallel plates.

- The results of test cases slats126, slats127, and other simulations carried out. The simulation results suggest that K-epsilon model can model the required boundary conditions and it can produce accurate results, and should be used instead of Eddy model for these boundary conditions.

- It can be concluded that the K-epsilon model is accurate and should be used for the simulation of the honeycomb / slat boundary conditions.

- The K- epsilon CFD model can simulate the required boundary conditions and has good agreement with other research work.

The next chapter will investigate using CFD K-epsilon model simulations to establish the optimal configuration of the honeycomb slats that needs to be manufactured in order to suppress the convection current near the ceiling, and therefore stabilizing the airflow and reintroducing the displacement airflow pattern.

CHAPTER FIVE

5.0 Optimum configuration of the honeycomb slats

5.1 CFD simulation to achieve optimum configuration of the honeycomb slats.

The previous chapter dealt with CFD simulation with regards to two parallel horizontal plates and its corresponding Rayleigh number for suppression of convection. This chapter will deal with the whole room environment and using CFD simulations will help to provide an optimum depth to width ratio for the honeycomb slat to be attached to the cooled ceiling to suppress the convection current near the cooled ceiling.

The K-epsilon CFD model will be used to simulate the honeycomb slats attached to the chilled ceiling to provide the optimal depth width ratio.

Before the whole room environment could be simulated it was important to carry out CFD simulation between two horizontal parallel plates for conditions where convection current would exist, and insert slats between the two plates to establish if the

convection current can be suppressed. (Case slat142): was simulated in 2D model for the height of 0.015m between the two parallel plates having a length and width of the plates at 0.4m. Five (5) slats were added at distances of 0.0m, 0.1m, 0.2m, 0.3m, and 0.4m along the length of the plates, the temperature difference was 10°C (16°C at the top plate and 26°C on the bottom plate). The results showed that by inserting the slats we were able to create friction which resulted in the convection current being reduced.

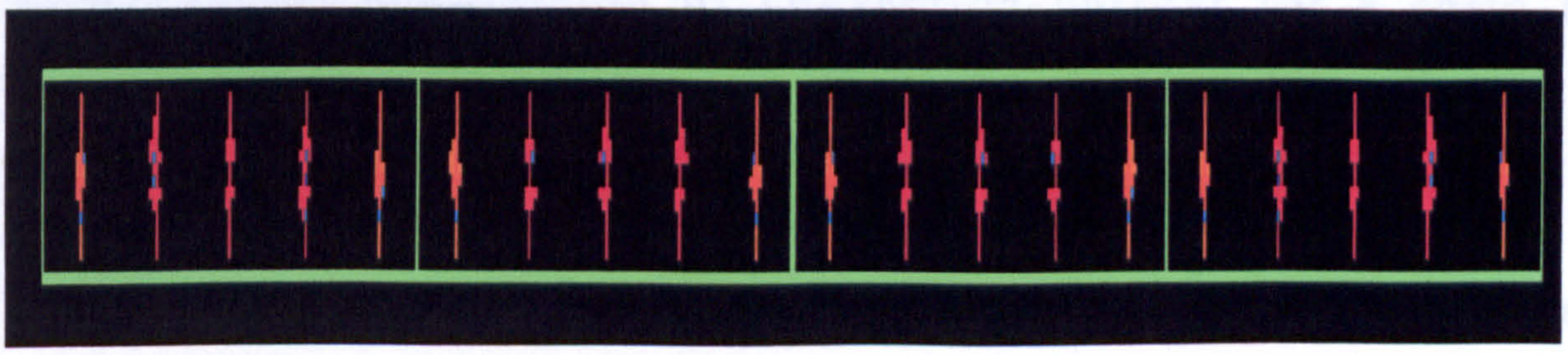

Figure 5.1: showing convection current being suppressed when slats are inserted between two horizontal parallel plates.

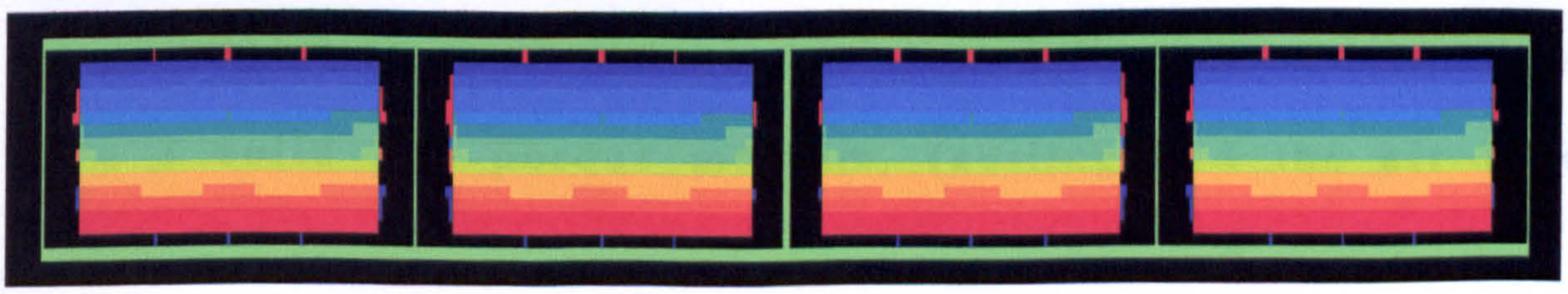

Figure 5.2: showing air temperature contours showing convection current suppressed when slats are inserted between two horizontal parallel plates.

From the literature review it was concluded that no formula was found to determine the Rayleigh number at where the convection current becomes suppressed for a solid and porous boundary. But experiments carried out by Holland and Iynkaran (1985) having a 10mm air gap between the plate and the honeycomb, and concluded that the gap does not invalidate the honeycomb's ability to suppress free convection heat transfer. In the case of the whole room environment the gap between the honeycomb and the floor is in the area of 2.6m. No literature was available for study on the suppression of convection current for a solid and porous environment.

As the CFD code is accurate in predicting the airflow between two horizontal parallel plates (chapter 4), and as we have no formula to determine the airflow between a solid and Porous medium it was decided to use the CFD code to determine this. For the solution to the problem of the airflow in reality we will have a solid and porous medium, (ceiling and the air in the room).

Simulations were carried out to determine at what height between a solid surface and a porous medium whereby the airflow would become stable.

It was decided to simulate a solid - porous environment, as this is what will be expected in the real scenario. The top area will represent the chilled ceiling surface (solid) and the bottom space will represent the porous area the air surface from below. From the CFD and laboratory test the results of the displacement ventilation and chilled ceiling system; we can predict the air temperature in the room both near the ceiling and in the rest of the room (see chapter two for some results).

Due to limitation of time and computer software and hardware it was decided to simulate one honeycomb and not the whole room with the honeycombs as this will require more time for the computation to be completed (figure 5.3)

It was decided to set 200 mm height of the honeycomb slats as the maximum, as this height will allow suffusion space between the occupant's heads and the end of the honeycomb slat.
The following boundary conditions were used, 200 mm height of the slat/honeycomb, temperature difference at 5 °C (16 °C - 21 °C). HTC imposed. CFD simulations were carried out for various depth / width (d/w) ratio to see the effect, the changes in ratio will have on the airflow in the room especially near the chilled ceiling.

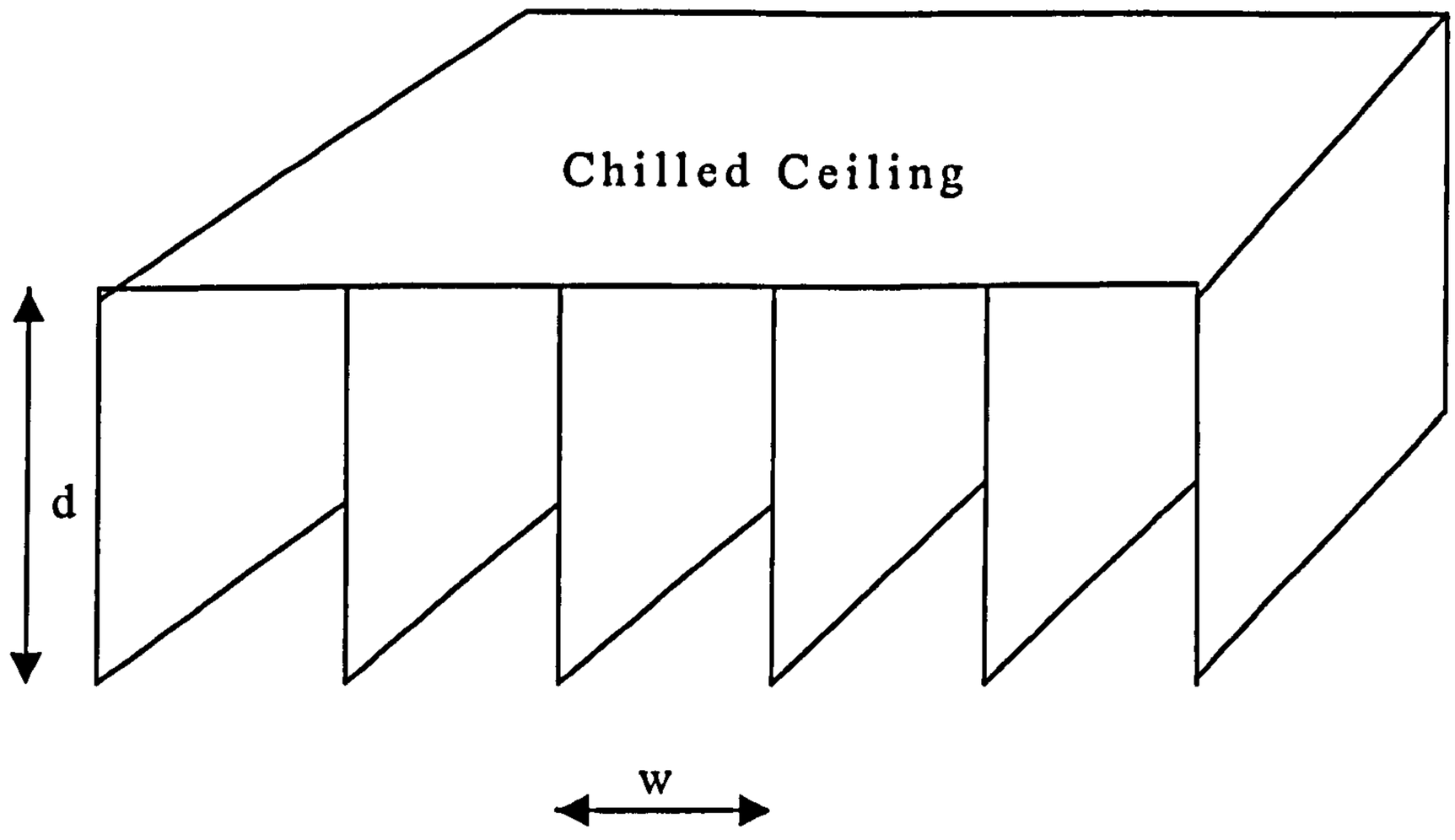

Figure 5.3: shows the diagrammatic of depth width ratio (d/w) for the honeycomb slat. The top solid surface represents the chilled ceiling and the opening at the bottom represents the porous environment (also see figures 1.1 to 1.5 for honeycomb slat).

The simulation results showed that by inserting honeycomb slats at different depth width ratios it has a major influence on the airflow pattern. As the depth width ratio increases, it causes the decreasing of velocity of the airflow in the honeycomb thus reducing the effect on the airflow, which helps to introduce convection current process.

The results show (table 5.3) that an increase in depth width ratio from 1 to 2, the air velocity is reduced by 25%. The greatest drop in the air velocity is observed when d/w ratio 9 to 10 is imposed; this has resulted in velocity drop of over 95%. This suggests that a depth width ratio of 9 is the transition point where the convection current is becoming suppressed for this particular test case. It was also found that at d/w of 10 to 11 for most Rayleigh numbers showed only 10% of reduction in the velocity airflow. Table 5.1 shows the relationship between the depth width ratio and the drop in air velocity in the honeycomb slat for the above mentioned test case.

Maximum Air Velocity (m/s)	Depth Width ratio (d/w)	Percentage drop of Velocity % (m/s)
0.0593	1	0
0.0448	2	24.45
0.0404	3	9.82
0.0.312	4	22.77
0.026	5	16.67
0.0184	6	29.23
0.0143	7	22.28
0.00885	8	38.11
0.000358	9	95.95
0.000315	10	12.01
0.000303	11	3.8
0.00217	12	28.38

Total drop of air velocity % from depth width ratio 1 to 10 = 99.47%

Table: 5.1 show the relationship between the depth width ratio and the drop in air velocity measured between the honeycomb slats in percentage.

Table 5.1 shows that if depth width ratio of 10 is used then the total drop in air velocity in the honeycomb slat is over 99%.

It can be concluded that to obtain suppression of convection current a depth width ratio of above 9 ideally should be used.

Using a d/w ratio of 10, it is possible to reduce the air velocity in the honeycomb slat by 95%. At depth width ratio of 1 to 11 and 1 to 12 also produced a total drop in Air velocity of above 95%. Therefore it is found that d/w of 10 is the optimum configuration for honeycomb slat for suppressing the convection current of air, which is due to chilled ceiling.

Figures 5.4, 5.5, 5.6, 5.7, and 5.8 show airflow motion of convection current for different depth width ratio of honeycomb slat. Figure 5.7 showing the CFD simulation showing that the convection current has been suppressed at a depth width ratio of 10.

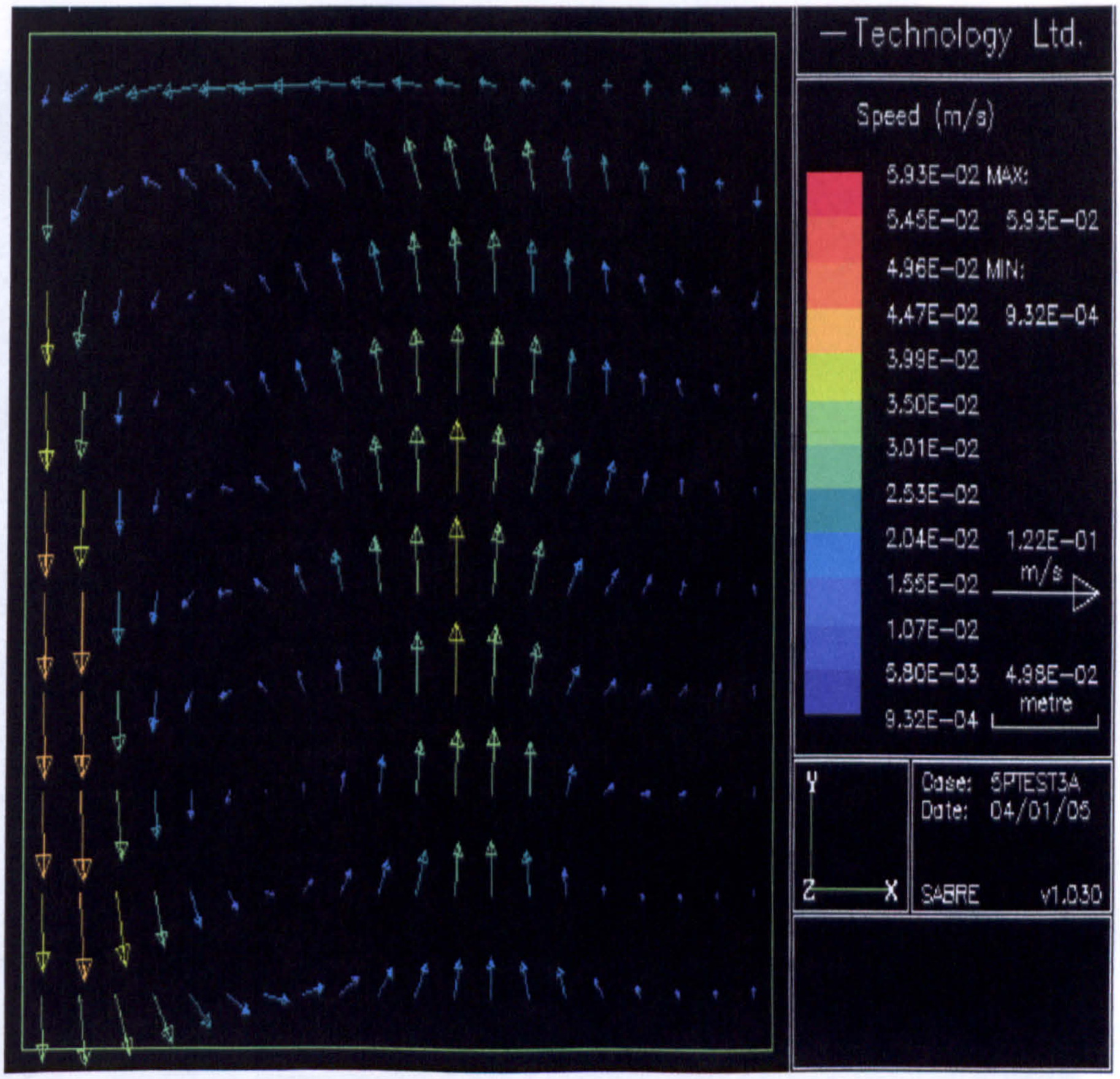

Figure: 5.4: CFD simulation results for depth width ratio of one

CFD simulation showing the airflow between the honeycomb slats when a depth width ratio of one is use. It can be clearly seen that the convection current is present at low depth width ratio, as expected.

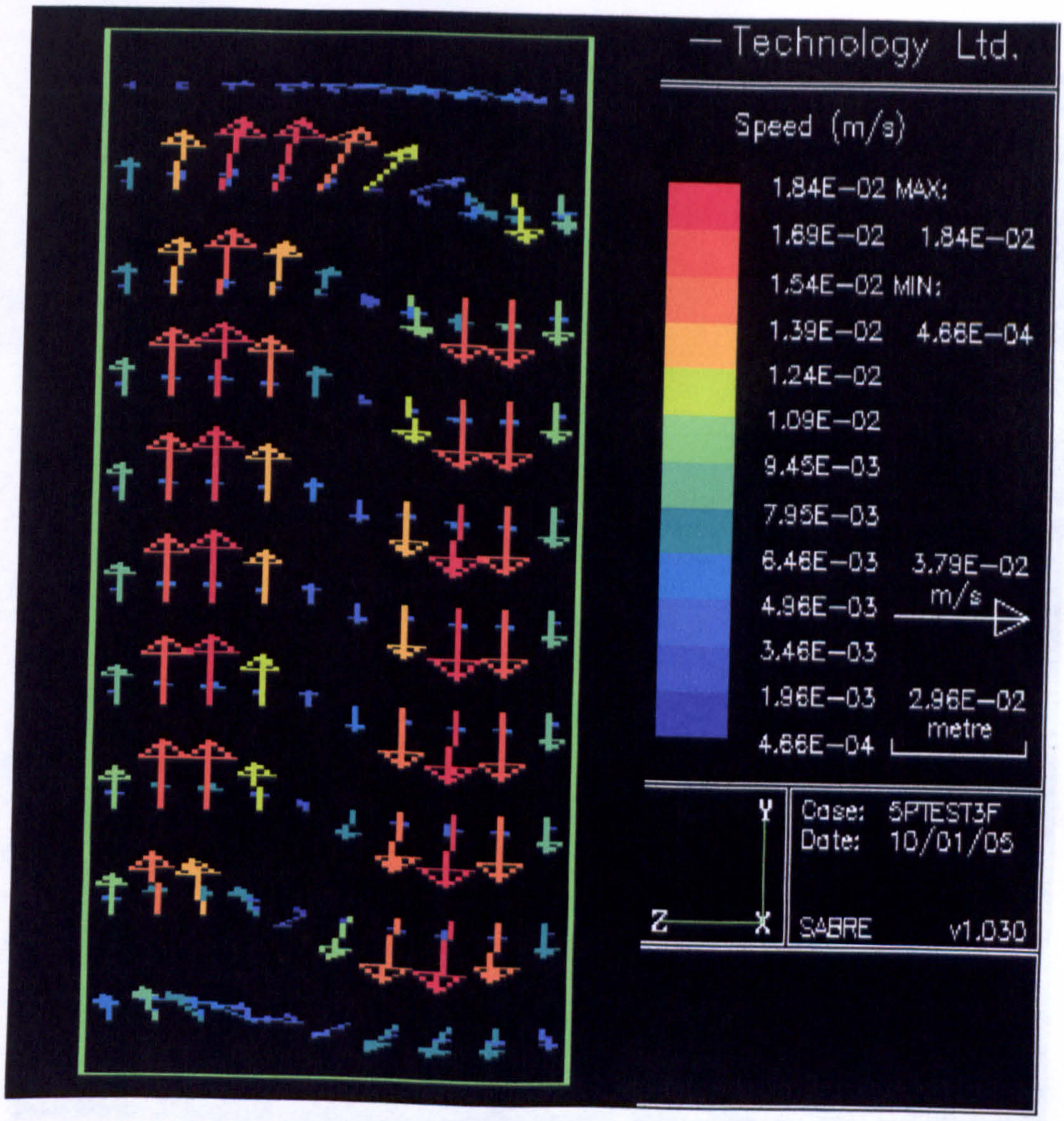

Figure 5.5: CFD simulation showing that the convection current is present between the honeycomb slats for depth width ratio of six.

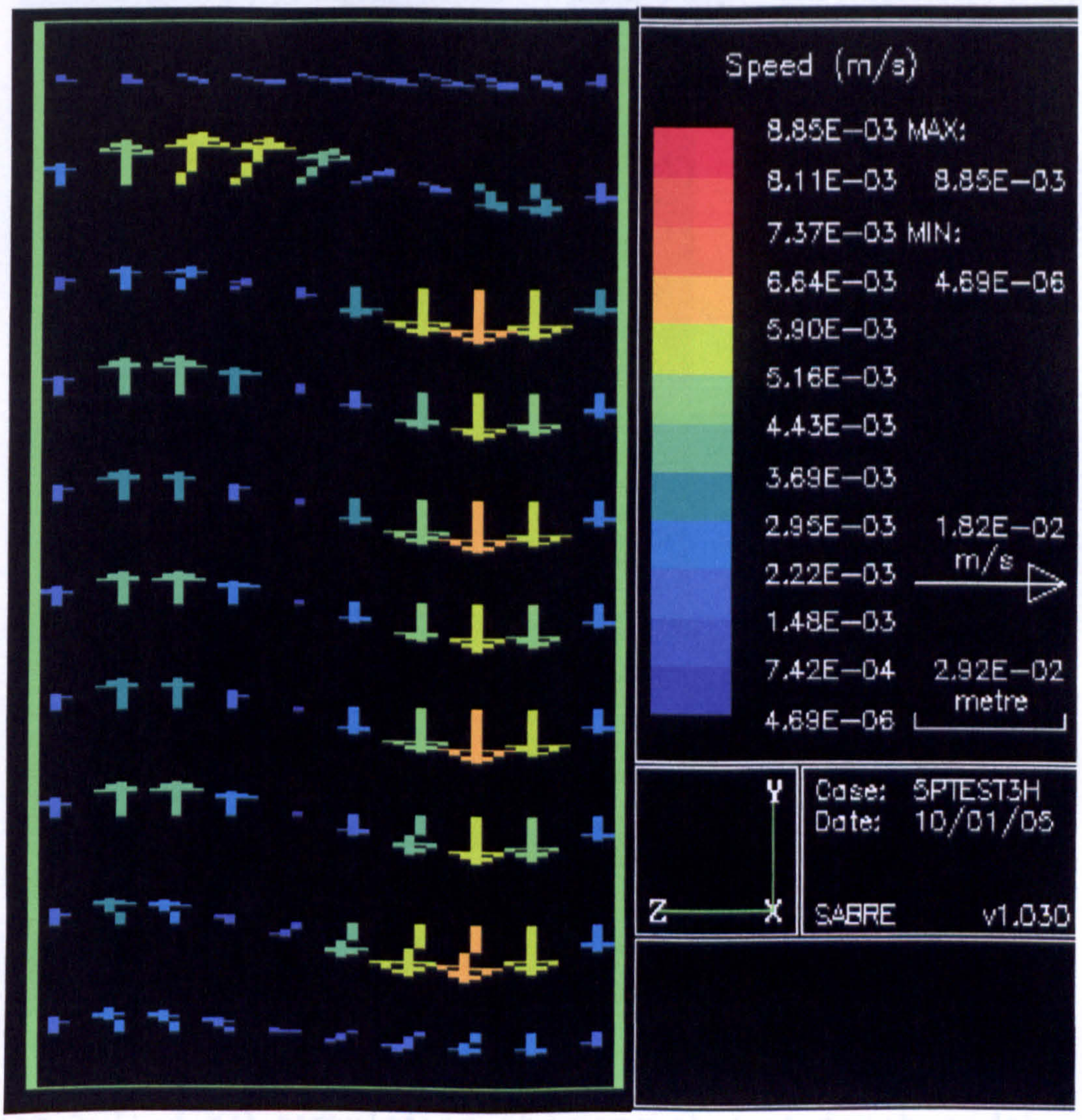

Figure 5.6: CFD simulation showing that convection current is present between the honeycomb slats for depth width ratio of eight (8). The simulation also show that the maximum air velocity in the honeycomb slat 10^{-3}.

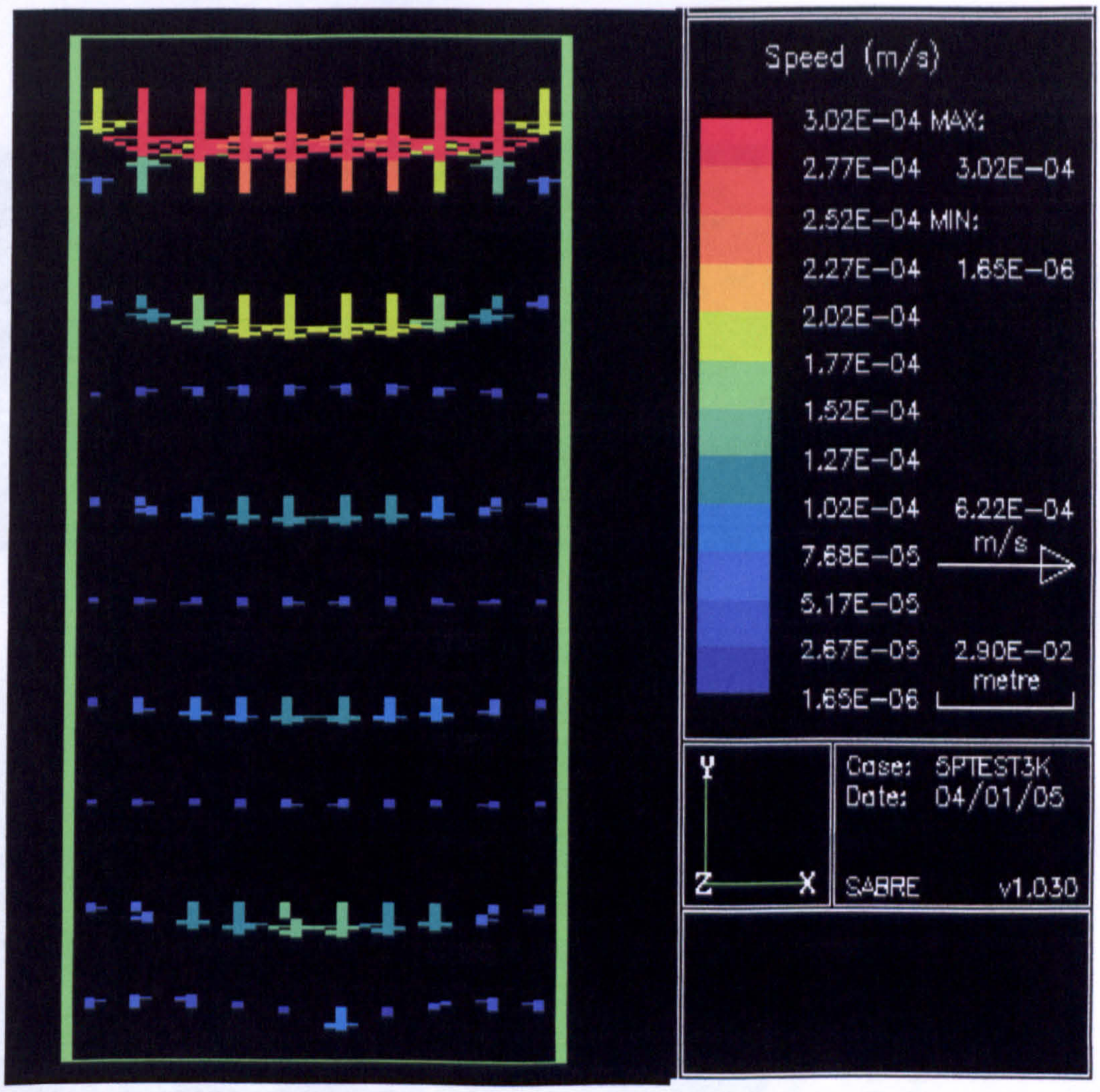

Figure 5.7: CFD simulation showing that at depth width ratio of ten (10), we can see that the convection is no longer present between the honeycomb slats. And the maximum air velocity between the honeycomb slats is $3x10^{-4}$, where most of the airflow is in the region of $2.67x10^{-6}$, therefore suggesting that due to the depth width ratio of 10, it is possible to suppress the convection current.

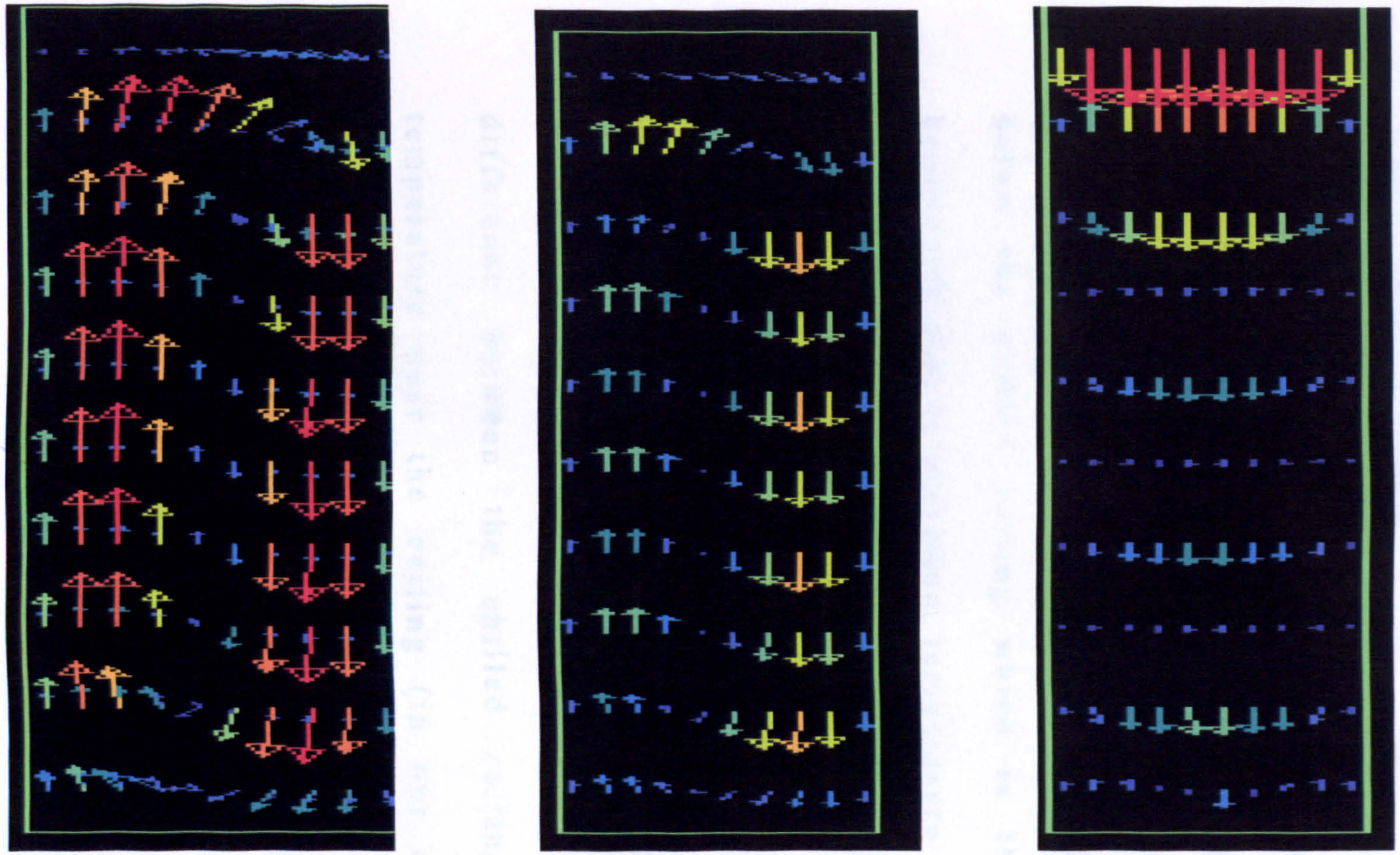

Depth width ratio 6 Depth width ratio 8 Depth width ratio 10

Figure 5.8: CFD simulation showing the stages of convection current being suppressed between the honeycomb slats for various depth width ratios.

From the CFD simulations (figures 5.4 to 5.8), it can be seen that as the depth width ratio increases the convection current air flow decreases, this can also be seen by the reduction of the air flow velocity,

It was decided to simulate different boundary conditions relating to Rayleigh numbers, which will be base on the temperature difference between the chilled ceiling and at a height of 200mm below the chilled ceiling which is the end height of the honeycomb slat (a maximum temperature difference between the chilled ceiling and the room temperature of up to 18°C was used. Table 5.9 shows all the possible

From the displacement ventilation and chilled ceiling CFD simulation it was possible to predict the air temperature difference between the chilled ceiling and the room air temperature near the ceiling (in our case 200mm from the ceiling). This information can be used to set the temperatures difference between the chilled ceiling and at the open end of the honeycomb slats.

5.2 CFD simulations in relationship to Rayleigh numbers

Figure 5.8 and Figure 5.9 show the relationship between Rayleigh numbers and the corresponding average temperature difference in the room (that is the average temperature difference between the ceiling air temperature and room air temperature).

The next set of CFD simulation will be based on Rayleigh number and its corresponding air temperatures (that is air temperatures at the ceiling and the in the room see table 5.9 and 5.10).

It can be seen from the graph 5.8 the relationship between Rayleigh numbers and the corresponding average temperature difference in the room, which shows that the bulk of the boundary conditions falls between the average temperature difference in the room of 13°C to 24°C, and below Rayleigh number of 6 million.

The graph 5.9 shows a large quantity of boundary conditions relating to Rayleigh numbers and temperature Difference. It would be timely to simulate all the boundary conditions.

Previous simulations (table 5.1) show that at honeycomb length of 200mm having temperature difference of 5°C, (21-16) for depth width ratio of 10 produced suppression of the convection current. It was decided to simulate the honeycomb height of 200mm for various depth width ratio, corresponding to its relating Rayleigh number, simulation were carried out for Rayleigh number one to nine million.

Tables are presented in the appendix A showing all the possible test cases for the various Rayleigh numbers.

Figures 5.11 to 5.18 present the results for various Rayleigh numbers and its corresponding depth width ratios.

DATA SHOWING THE RELATIONSHIP BETWEEN AVERAGE TEMPERATURE DIFFERENCE AND RAYLEIGH NUMBER

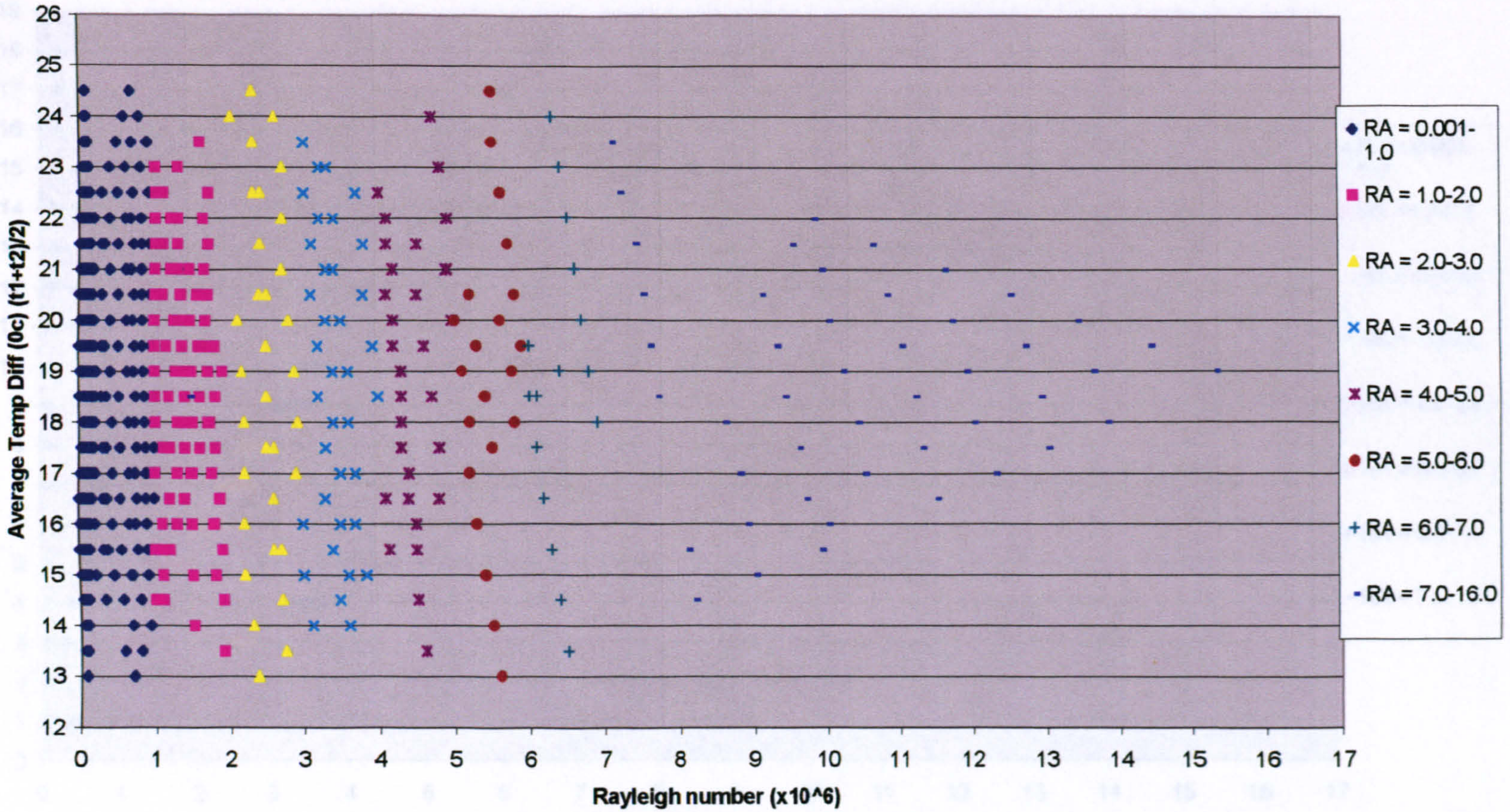

Figure 5.9: Graph showing the relationship between the average air temperature and its corresponding Rayleigh number.

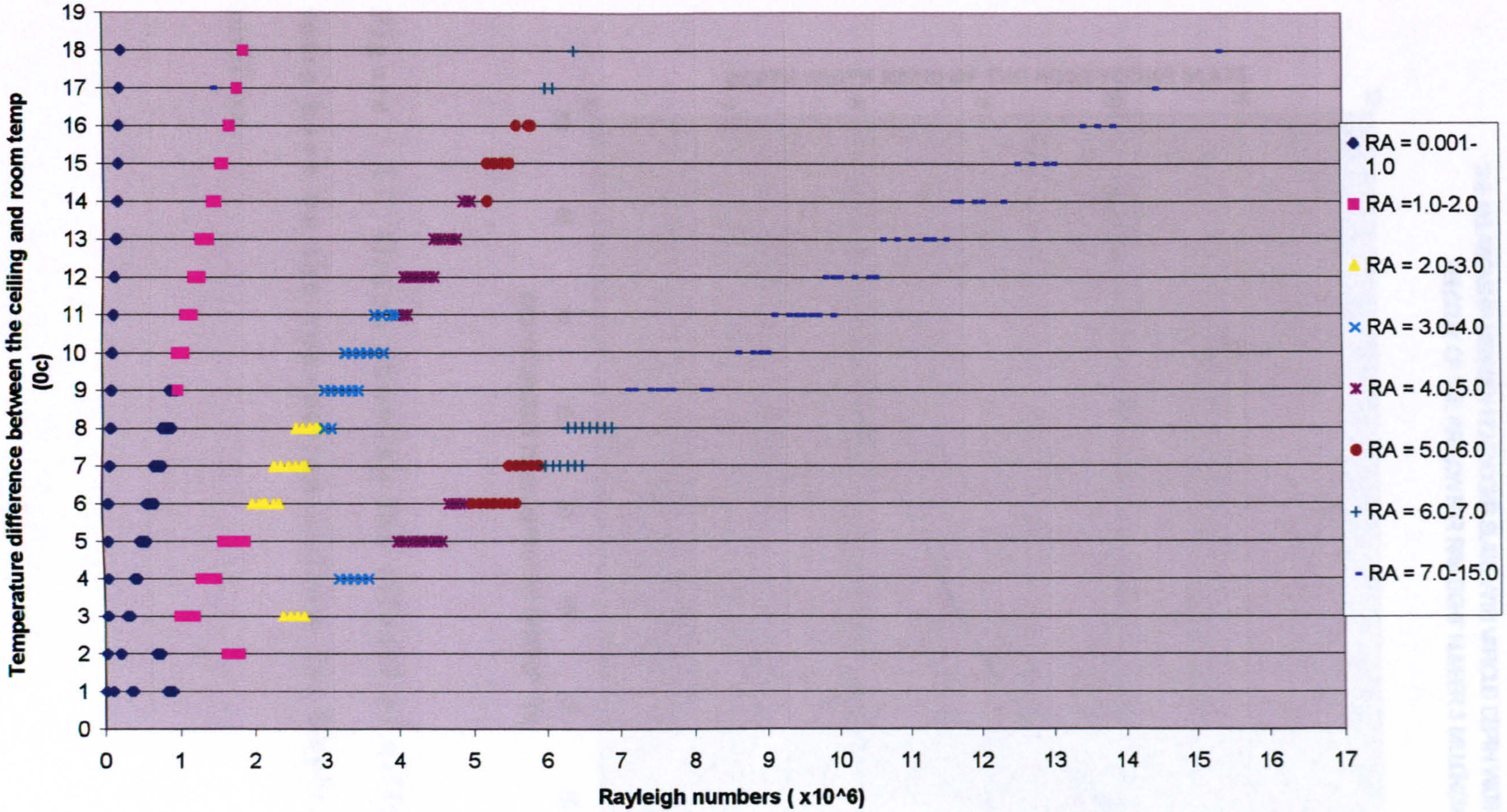

Figure 5.10: Graph showing the relationship between the temperature difference between the chilled ceiling temperature and the room air temperature.

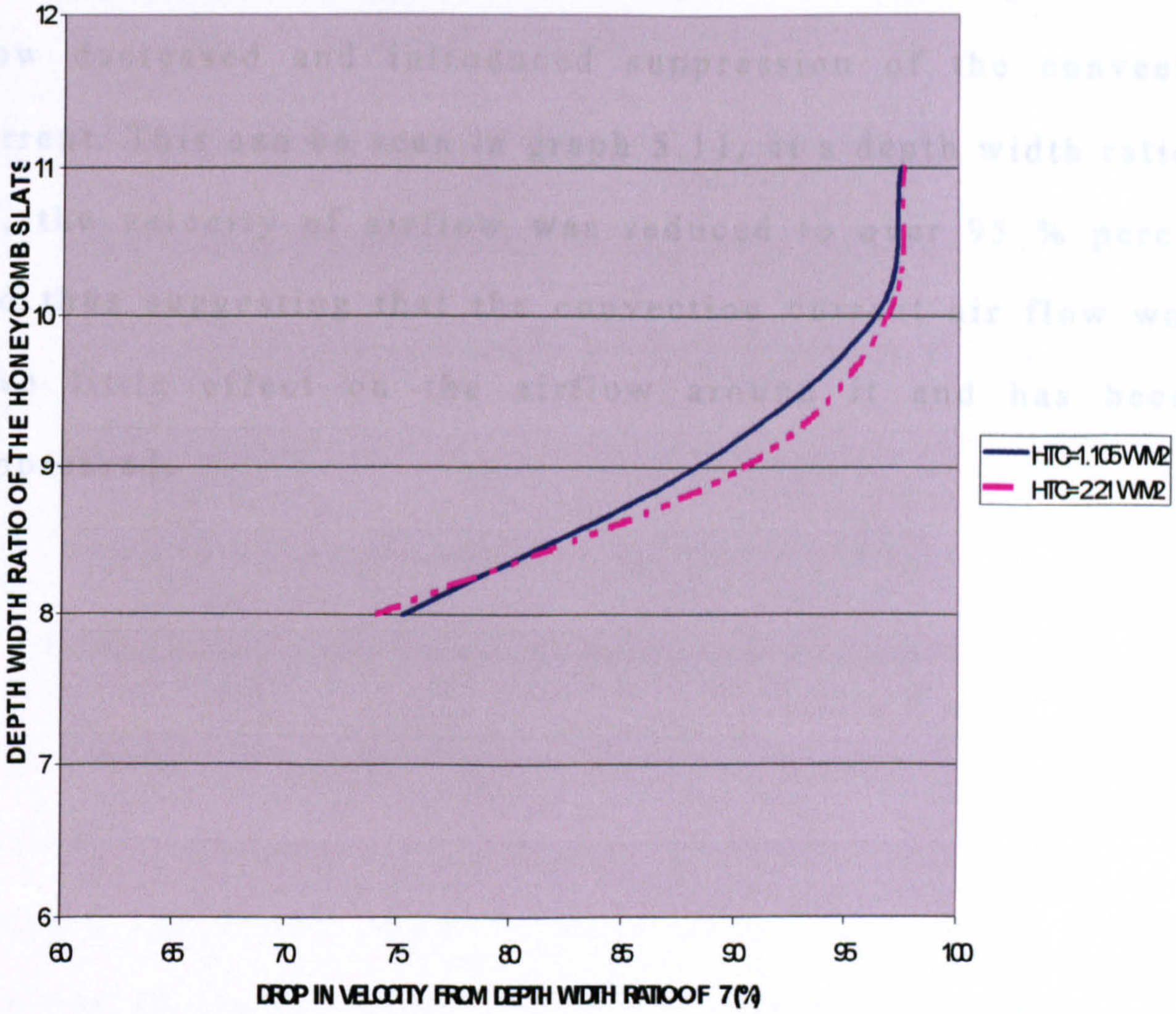

Figure 5.11: Graph showing the effects of different depth width ratio have on the convection airflow for Rayleigh number of 3 million.

The simulations showed that little effect was seen on the convection current up to depth width ratio of seven (7), as the dept width ratio increased the drop in the velocity of the air flow decreased and introduced suppression of the convection current. This can be seen in graph 5.11, at a depth width ratio of 10, the velocity of airflow was reduced to over 95 % percent, and thus suggesting that the convection current air flow would have little effect on the airflow around it and has become suppressed.

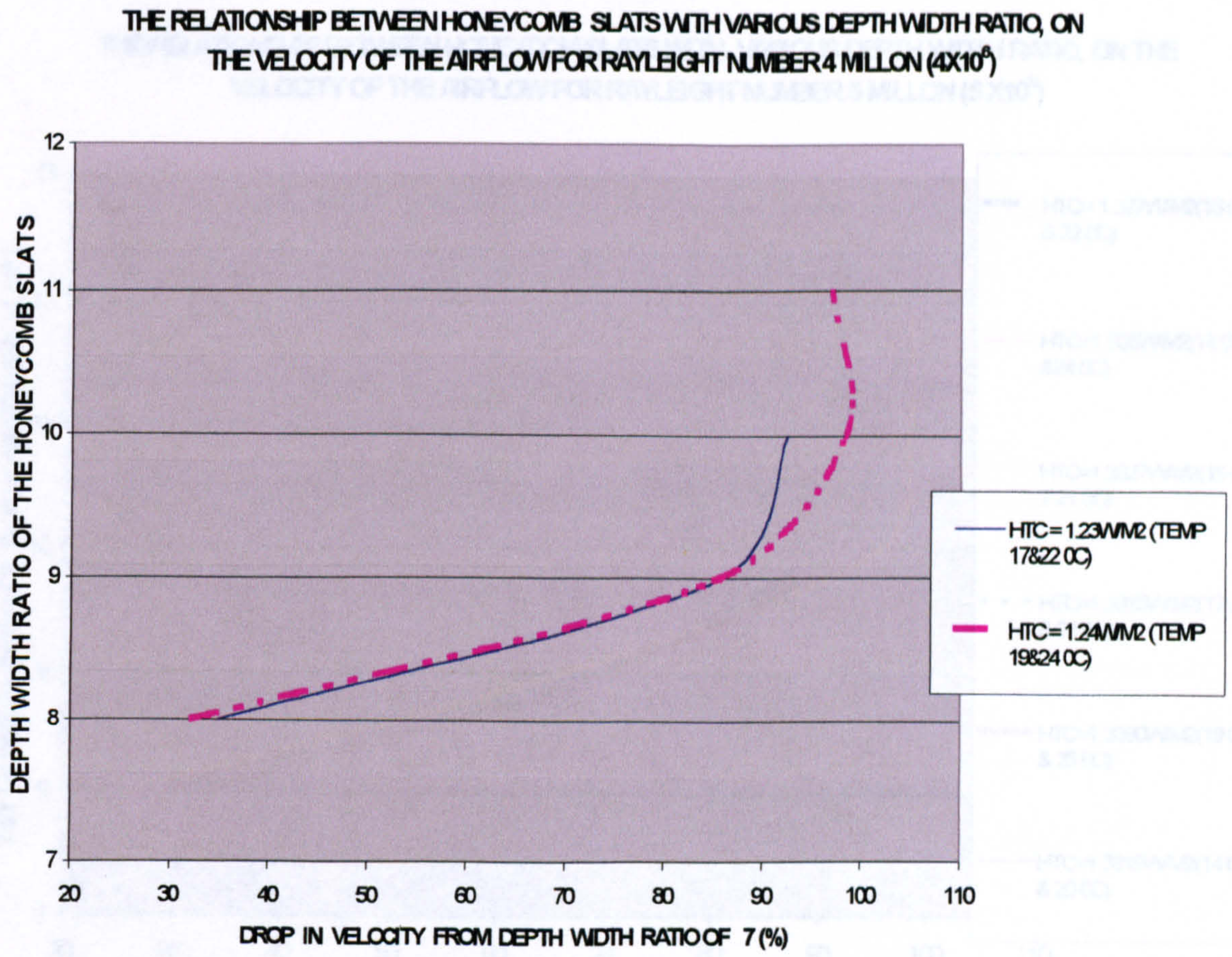

Figure 5.12: Graph showing the effect different depth width ratio has on the convection airflow for Rayleigh number of four (4) million.

The results (figure 5.12) indicate that at a depth width ratio of 10, over 90% reduction in the air velocity is seen between the honeycomb slats.

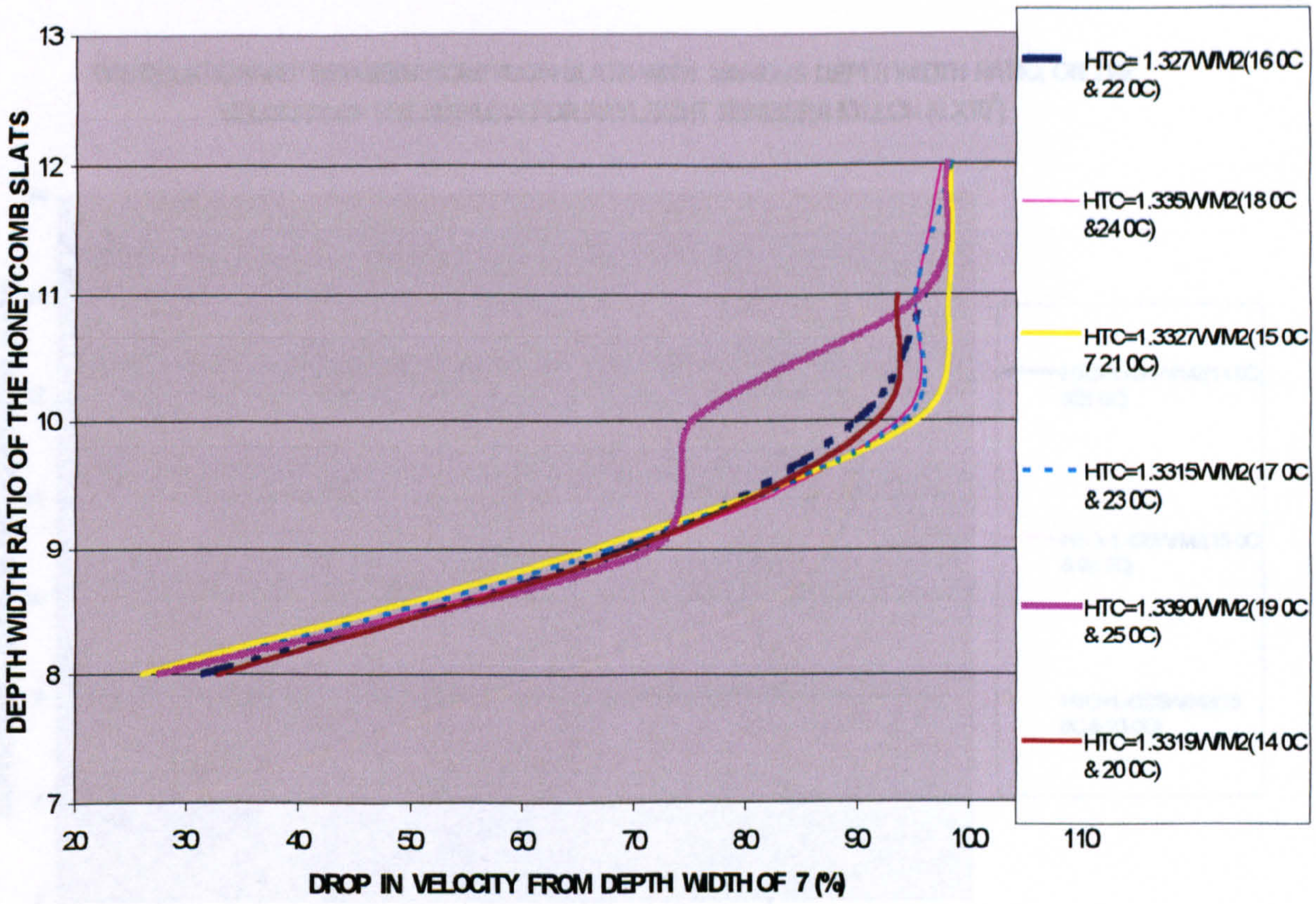

Figure 5.13: Graph showing the effects different depth width ratios have on the convection airflow for Rayleigh number of 5 million.

The results (figure 5.13) are based on six cases having a temperature differences corresponding to a Rayleigh number of 5 million. The results again also show that for a Rayleigh number of 5 million, the results indicate that at a depth width

ratio of 10, over 90% reduction in the air velocity is seen between the honeycomb slats

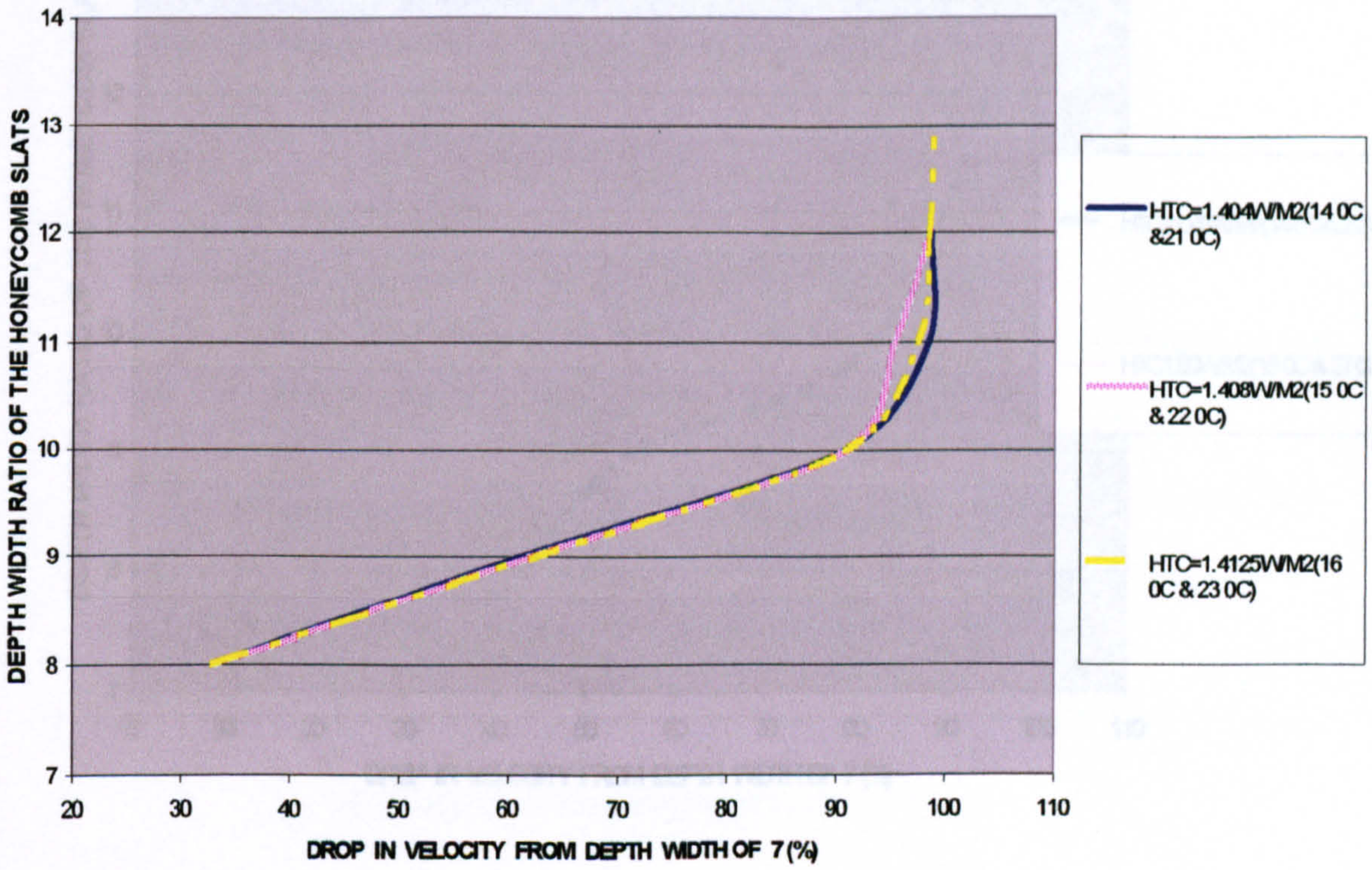

Figure 5.14: Graph showing the effects different depth width ratio have on the convection airflow for Rayleigh number of 6 million.

The results (figure 5.14) are based on three cases having a temperature differences corresponding to a Rayleigh number of 6 million. The results (figure 5.14) indicate that at a depth width ratio of 10, over 90% reduction in the air velocity is seen between the honeycomb slats

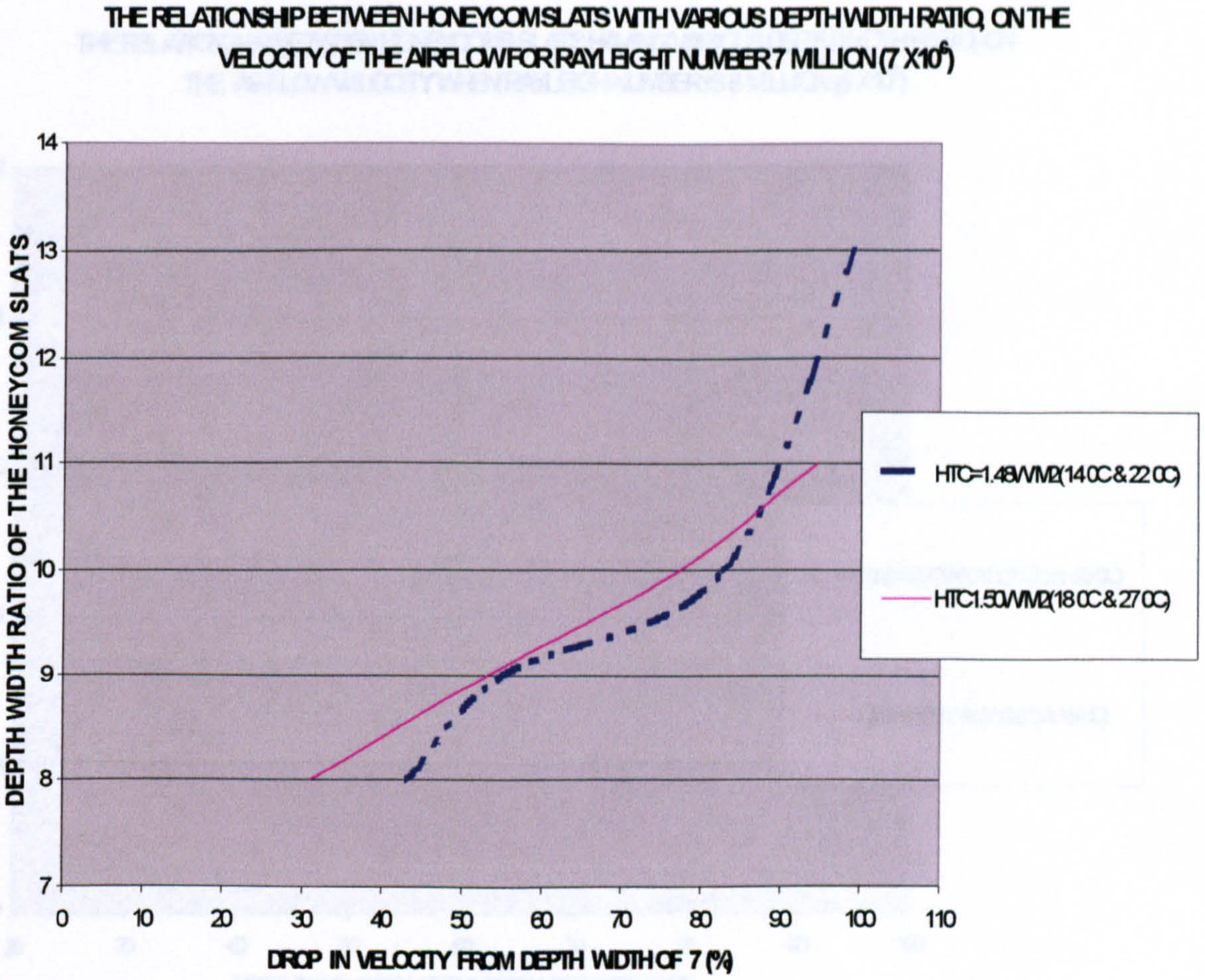

Figure 5.15: Graph showing the effects different depth width ratio has on the convection airflow for Rayleigh Number of 7 million.

The results (figure 5.15) for the two boundary conditions that correspond to a Rayleigh number of 7 million show that a depth width of 10 will reduced over 80% of the airflow between the honeycomb slats.

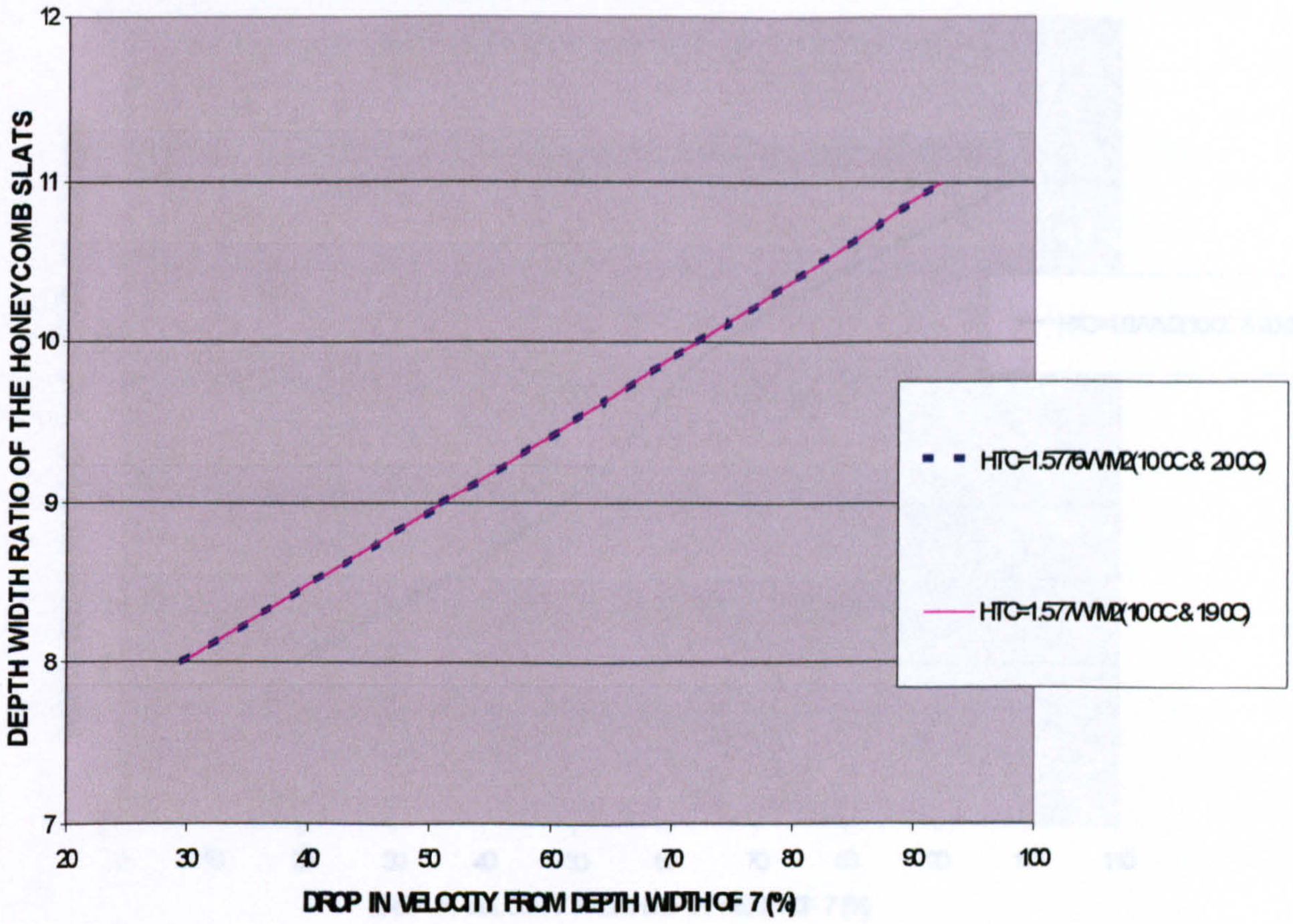

Figure 5.16: Graph showing the effects different depth width ratio; have on the convection airflow for Rayleigh number of 8 million.

The results (figure 5.16) show that for cases that correspond to a Rayleigh number of 8 million. To obtain a reduction of 90% of airflow between the honeycomb slats, a depth width of 11 and above will be need.

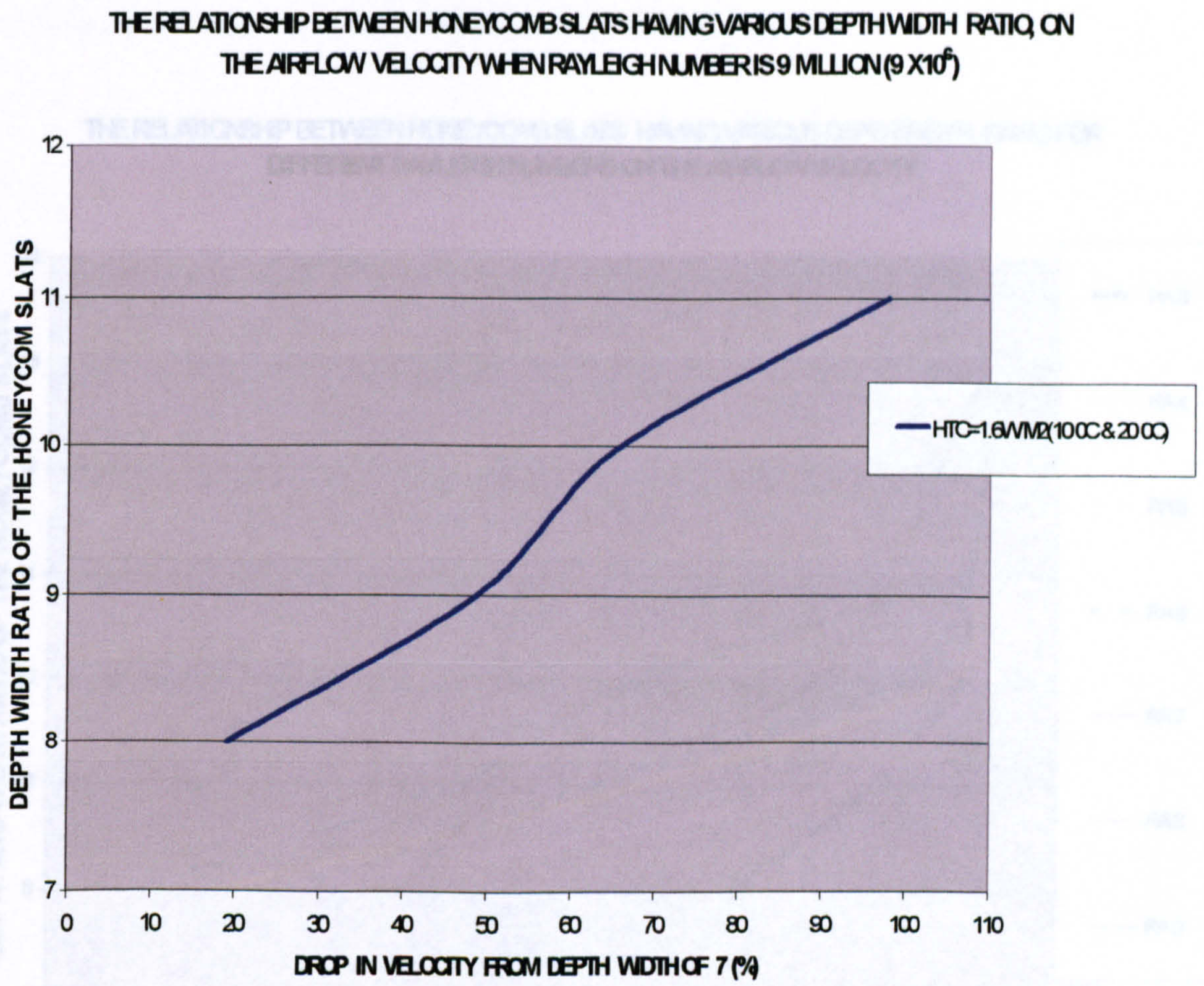

Figure 5.17: Graph showing the effects different depth width ratio have on the convection airflow for Rayleigh number of 9 million.

For this case (figure 5.17) the depth width ratio of 10 will only reduce air velocity by 65%, where depth width of 11 will reduce the airflow by 90%. Therefore the optimum configuration of 11 is need for test cases that corresponds to Rayleigh number of 9 million.

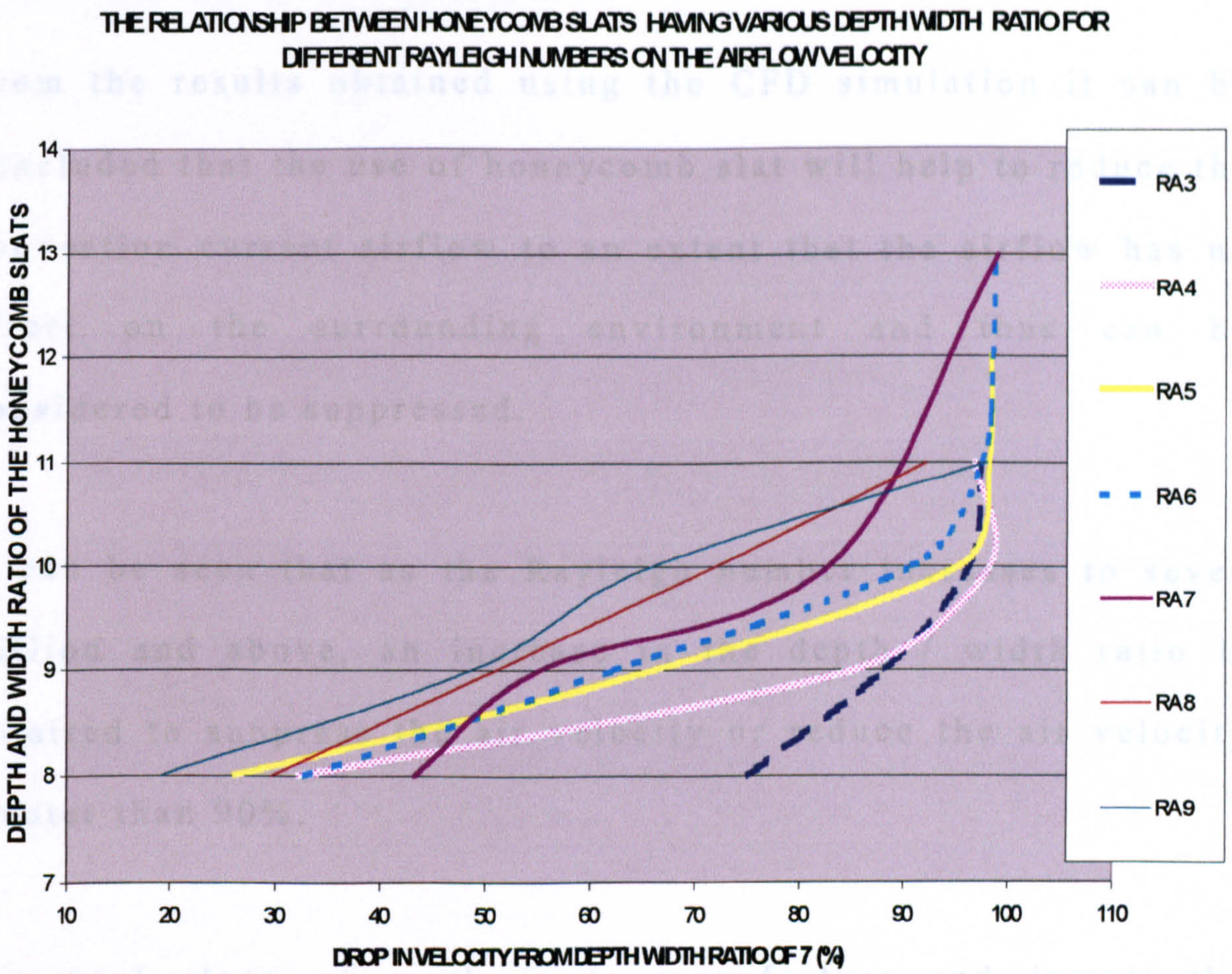

Figure 5.18: Graph showing the effects different depth width ratio have on the convection air flow for different Rayleigh numbers ranging form 3 million to 9 million

5.3 Optimum configuration of the honeycomb slats for manufacturing the honeycomb Slats

From the results obtained using the CFD simulation it can be concluded that the use of honeycomb slat will help to reduce the convection current airflow to an extent that the airflow has no effect on the surrounding environment and thus can be considered to be suppressed.

It can be seen that as the Rayleigh number increases to seven million and above, an increase in the depth / width ratio is required to suppress the air velocity or reduce the air velocity greater than 90%.

The next stage of work is to manufacture and install the Honeycomb with a depth / width ratio of 10, to see if the experimental results agree with the CFD simulation.

The next chapter will present the results of the material samples sent for testing to establish the emmisivity of the material. The material with the lowest emmissivity was used for coating the cardboard used to manufacture the honeycomb slats.

The manufacturing stages of the honeycomb slat and the installation of the honeycomb slat in the test chamber are also described in the next chapter.

Chapter Six

6.0 Manufacturing and installation of honeycomb slats

6.1 Manufacturing of honeycomb slats

From the CFD simulation in chapter 5, it was found that honeycomb slats at an optimum depth / width ratio causes velocity of convection current airflow to be reduced leading to suppression of the airflow. From the CFD simulation a depth / width ratio of 10 produced the best configuration. The literature review on honeycomb devices has suggested that it is essential that the honeycomb must have the following characteristic to achieve best results.

- The thickness of the honeycomb must be as minimal as possible due to the fact that the efficiency of the honeycomb is strongly influence by the thickness of the honeycomb walls, since both the conduction loss and solar transmittance is dependent on this.

- A low emissivity surface will help to reduce the overall heat transfer coefficient.

- A shining surface will help in transmittance of the solar radiation.

- The honeycomb slats should be light in weight, as the honeycomb slat will be attached to the chilled ceiling.

Due to the fact that the honeycomb slats have to be light in weight, it was decided to use corrugated cardboards. These would be strong and hard and would still be light in weight.

The corrugated cardboard was manufactured by Fast Pack International and had a brown surface. The corrugated cardboard surface needed to be a shiny and have a low emissivity to help reduce the overall heat transfer (as mentioned in chapter 4).

Many specialist companies were contacted to obtain a paint with known low emmissivity and a shiny surface that could be used to coat the corrugated cardboard.

The companies were unable to provide any technical data on emmisivity of the paints. Therefore a paint survey was conducted to collect a range of possible low emmisivity paints, such paints and aluminium foil needed to be scientifically tested to determine their properties. The paints or aluminium foil with lowest emmisivity will be selected and used to coat the honeycomb slats. Oxford Brooks university, Oxford, England was chosen for the scientific testing for the materials, due to their established experiment facility.

The list of materials tested for the their scientific data were

Humbrol metal coat (polished) (figure6.1)

Firlex aluminium paint (figure 6.2)

Silver aluminium applied finish (figure 6.3)

Aluminium foil (figure 6.4)

Uncoated cardboard (figure 6.5)

Figures 6.7 to figure 6.10 show the experimental facilities and test equipment needed to carry out the relevant testing to obtain the scientific data on the materials.

The following pages show pictures and the results for of the materials tested, at the test facilities at Oxford Brooks university Oxford, England

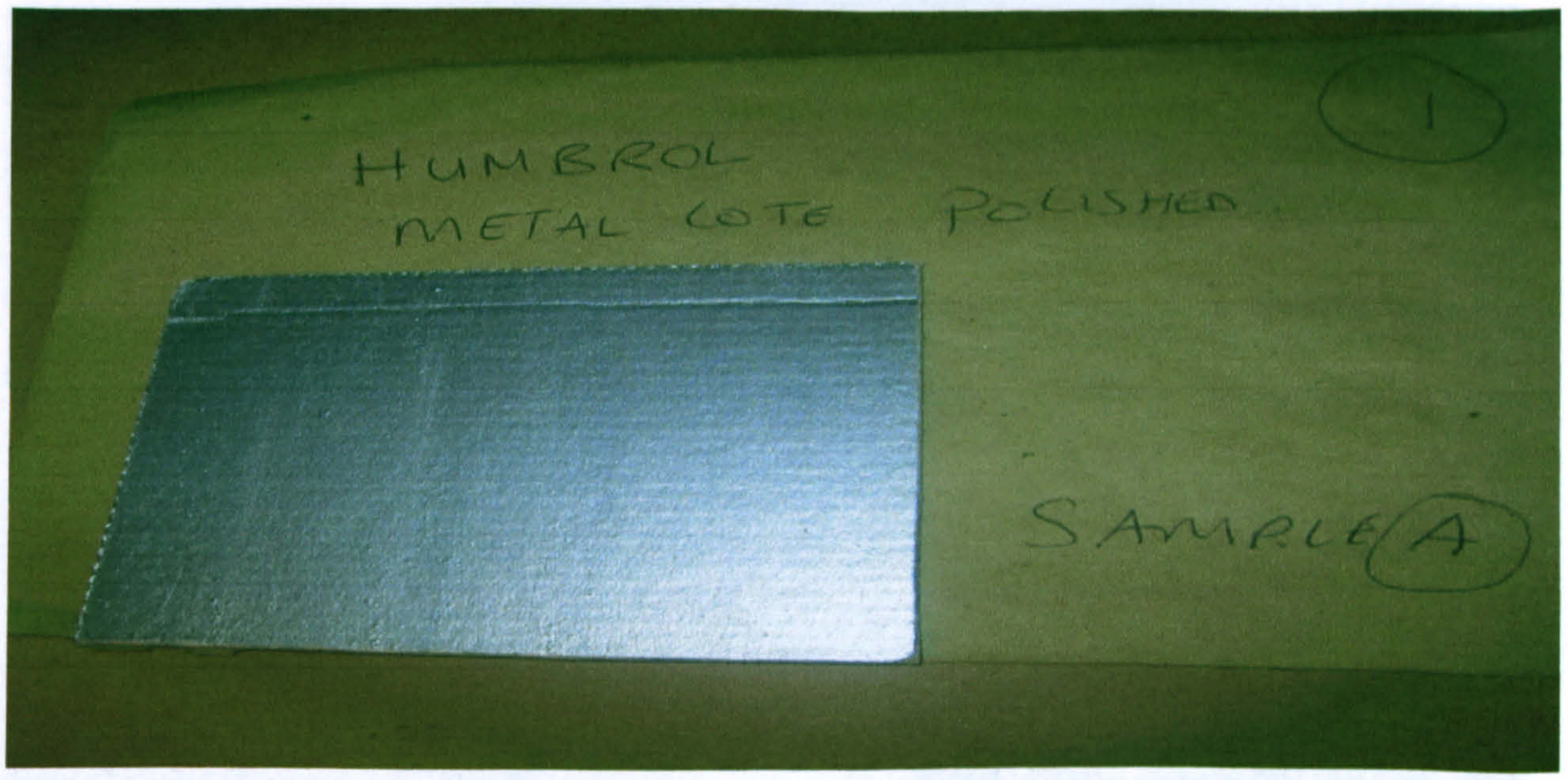

Figure 6.1: Cardboard coated with Humbrol metal coat (polished) sent for testing

Figure 6.2: Cardboard coated with aluminium foil sent for testing

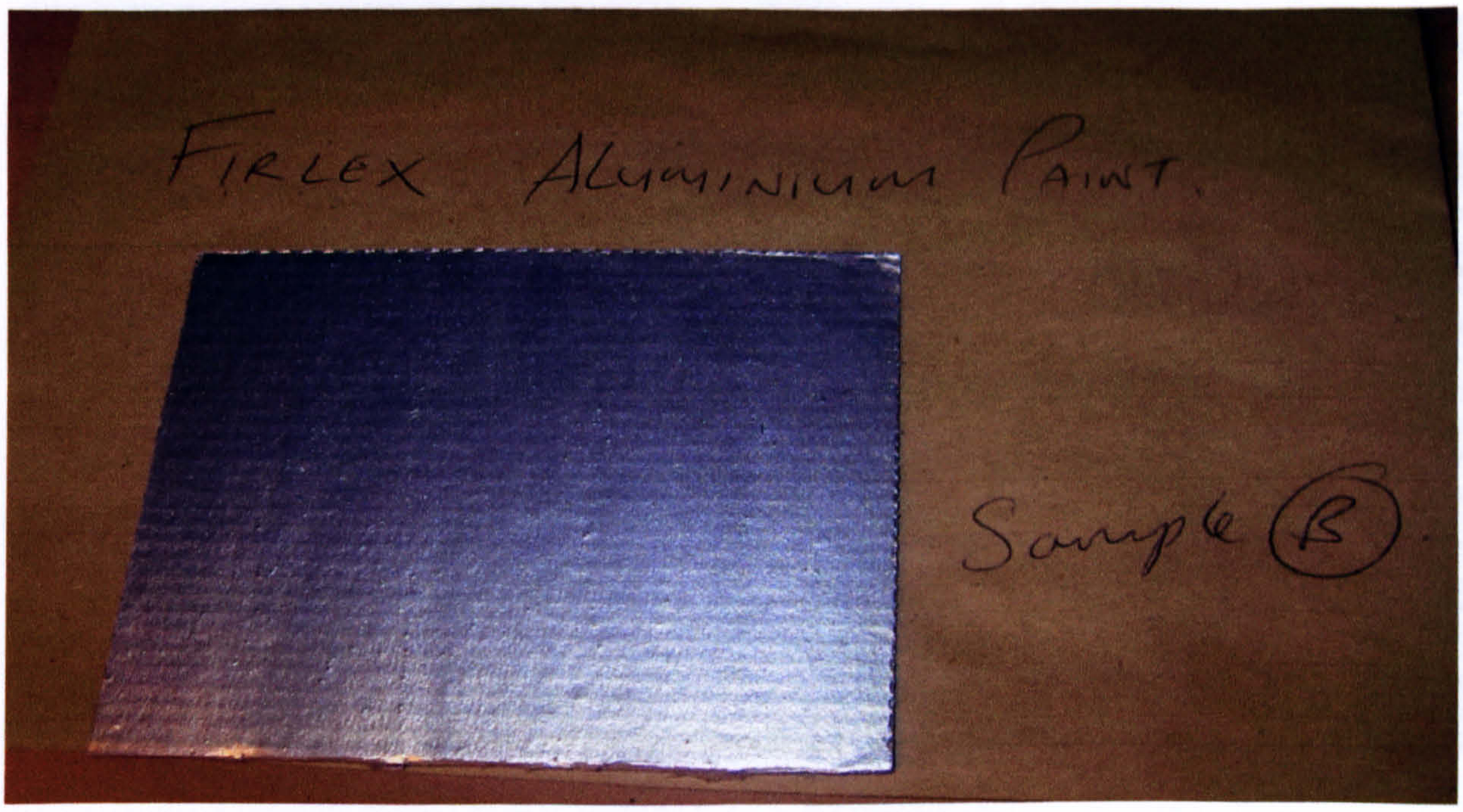

Figure 6.3: Cardboard coated with aluminium Paint sent for testing

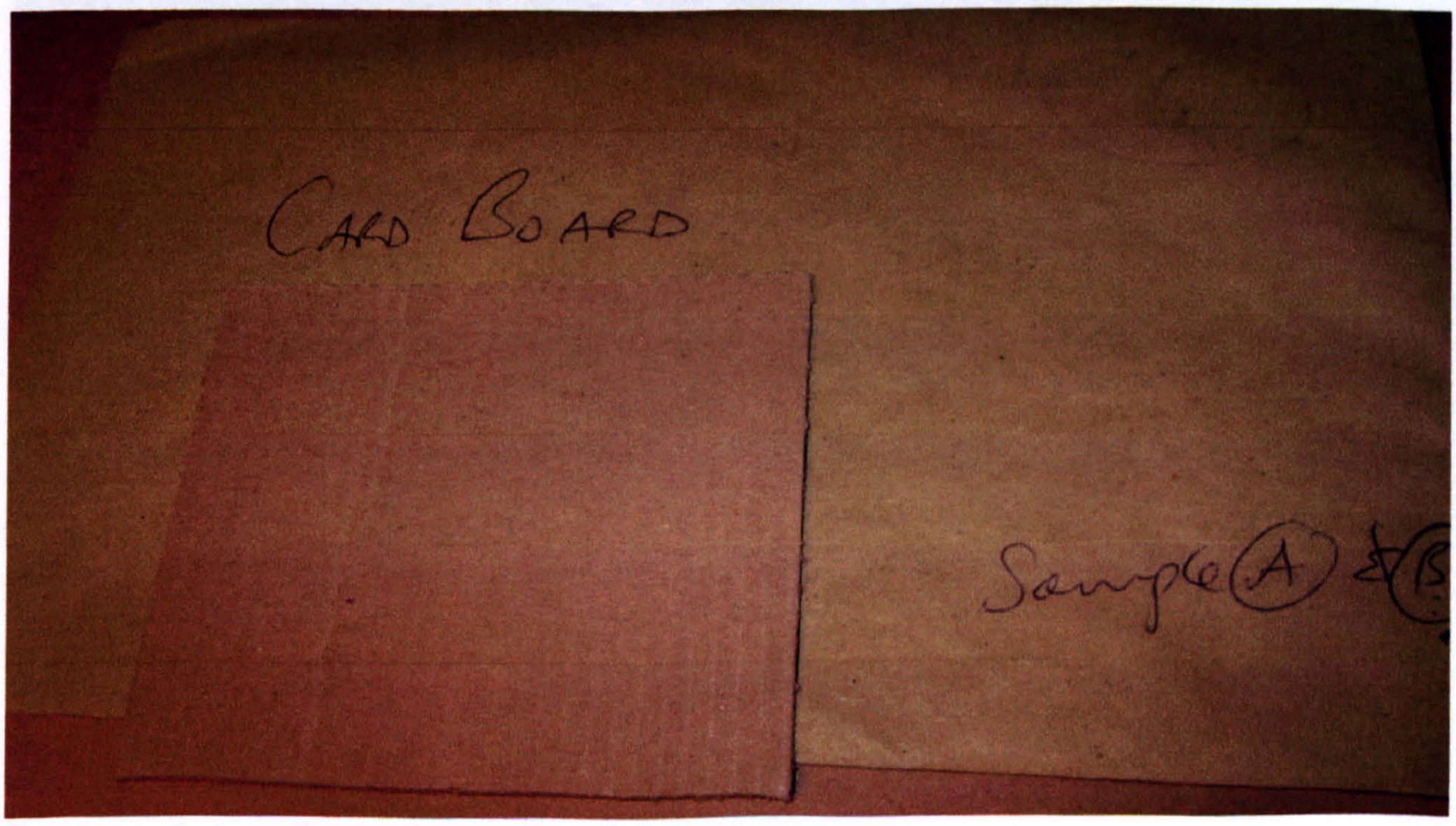

Figure 6.4: Plain uncoated cardboard sent for testing.

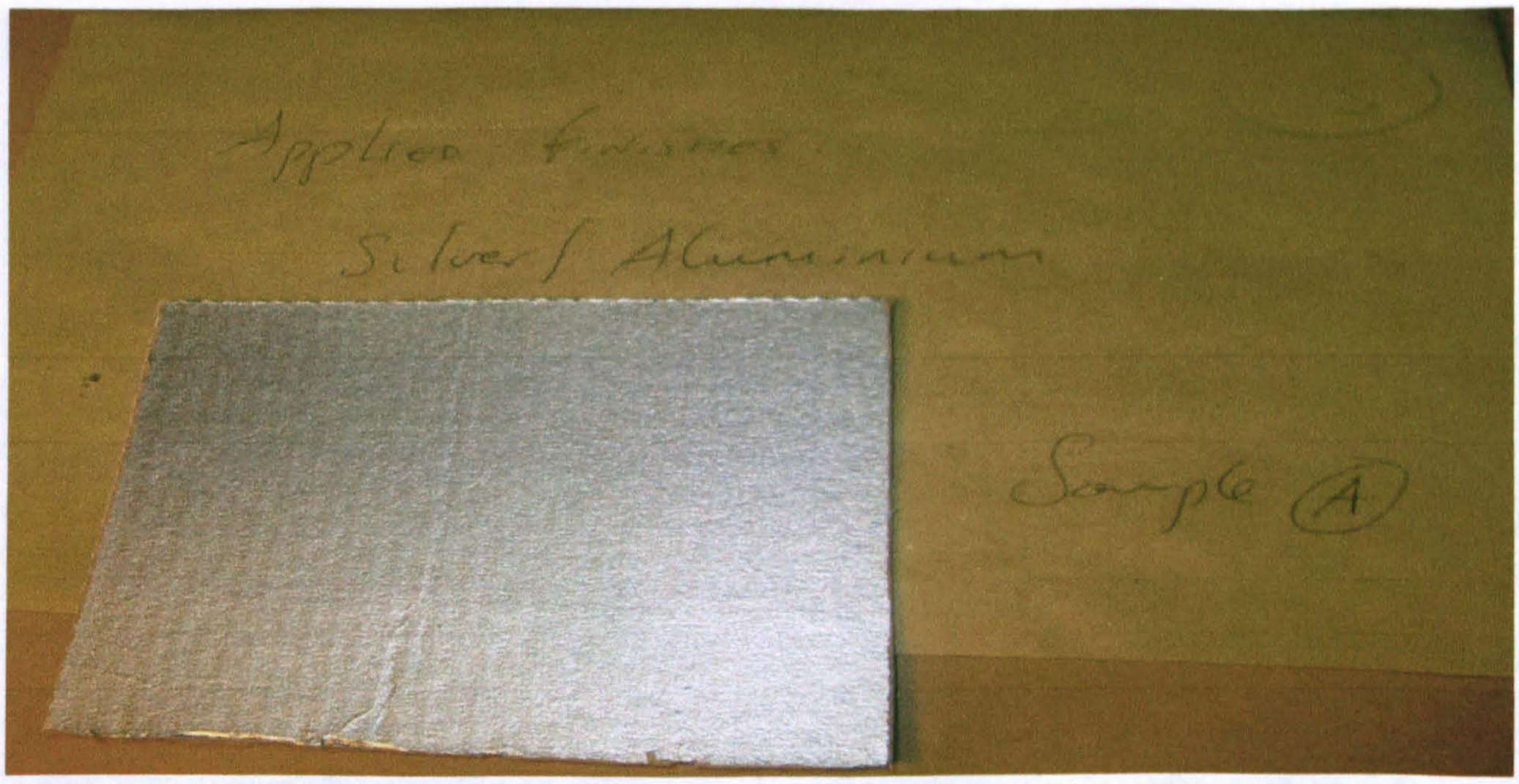

Figure 6.5: Cardboard coated with silver aluminium applied finish

Figure 6.6: Samples sent for testing

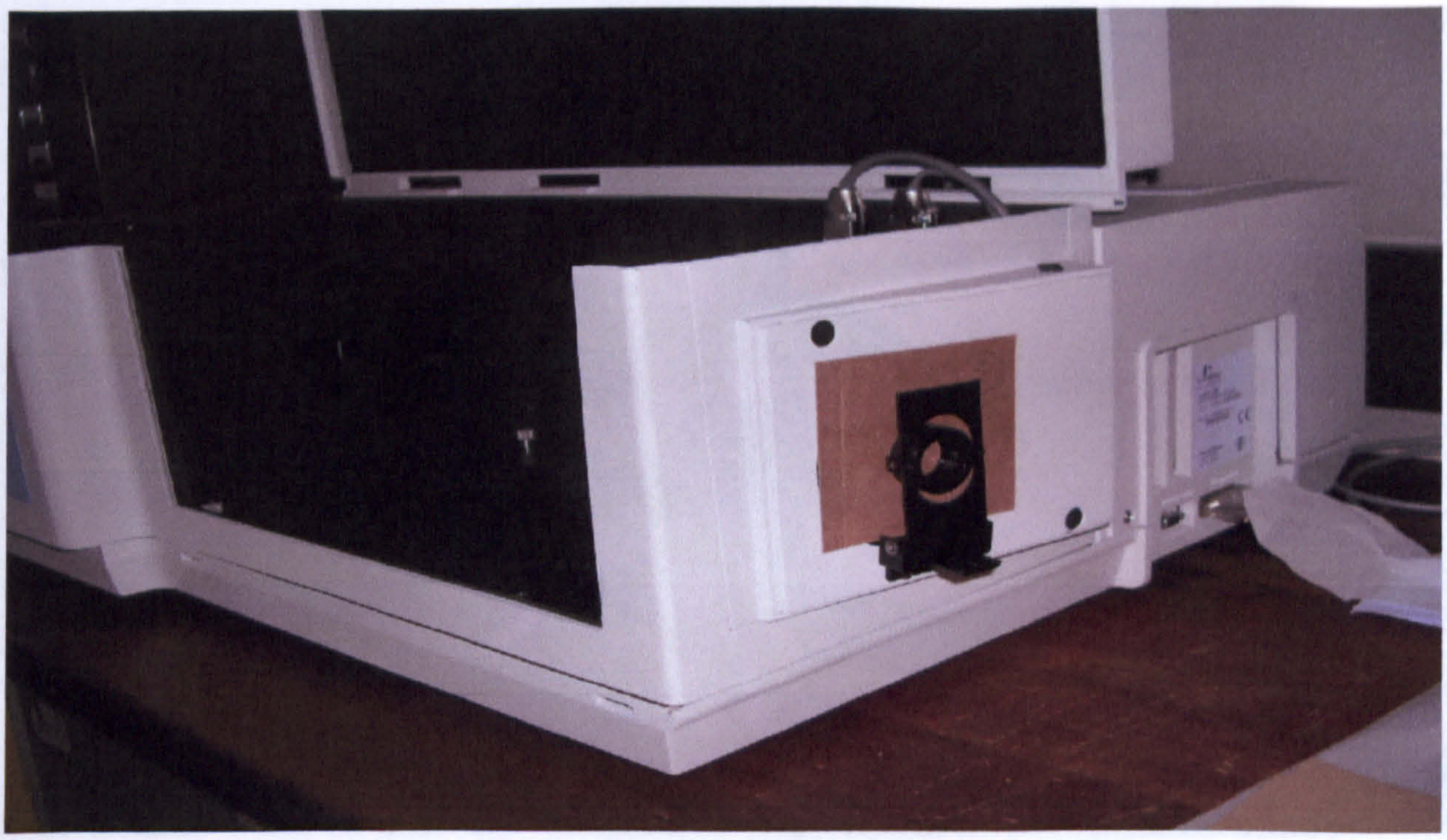

Figure 6.7: Testing equipment at Oxford Brooks university.

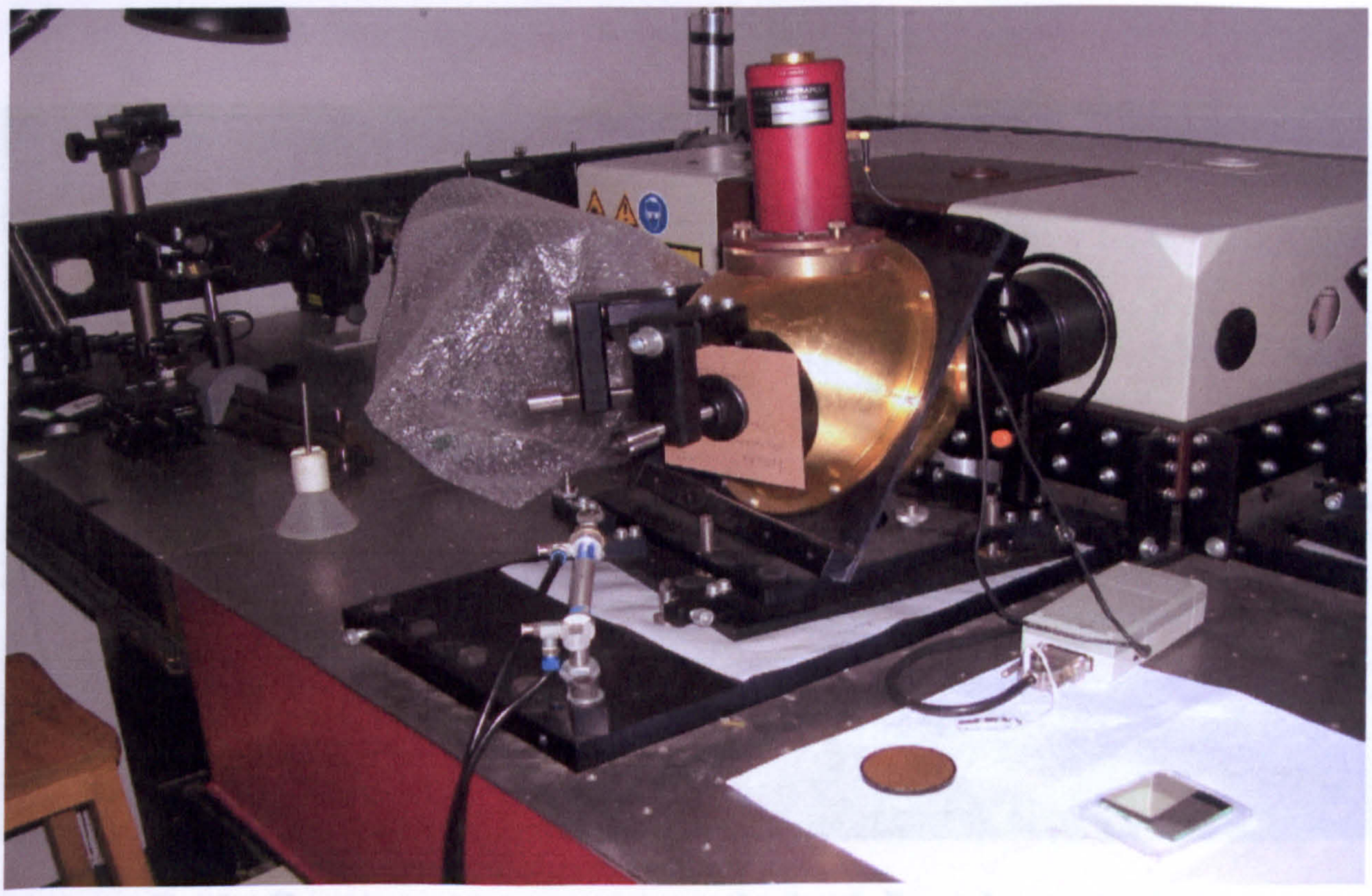

Figure 6.8: Testing equipment at Oxford Brooks university.

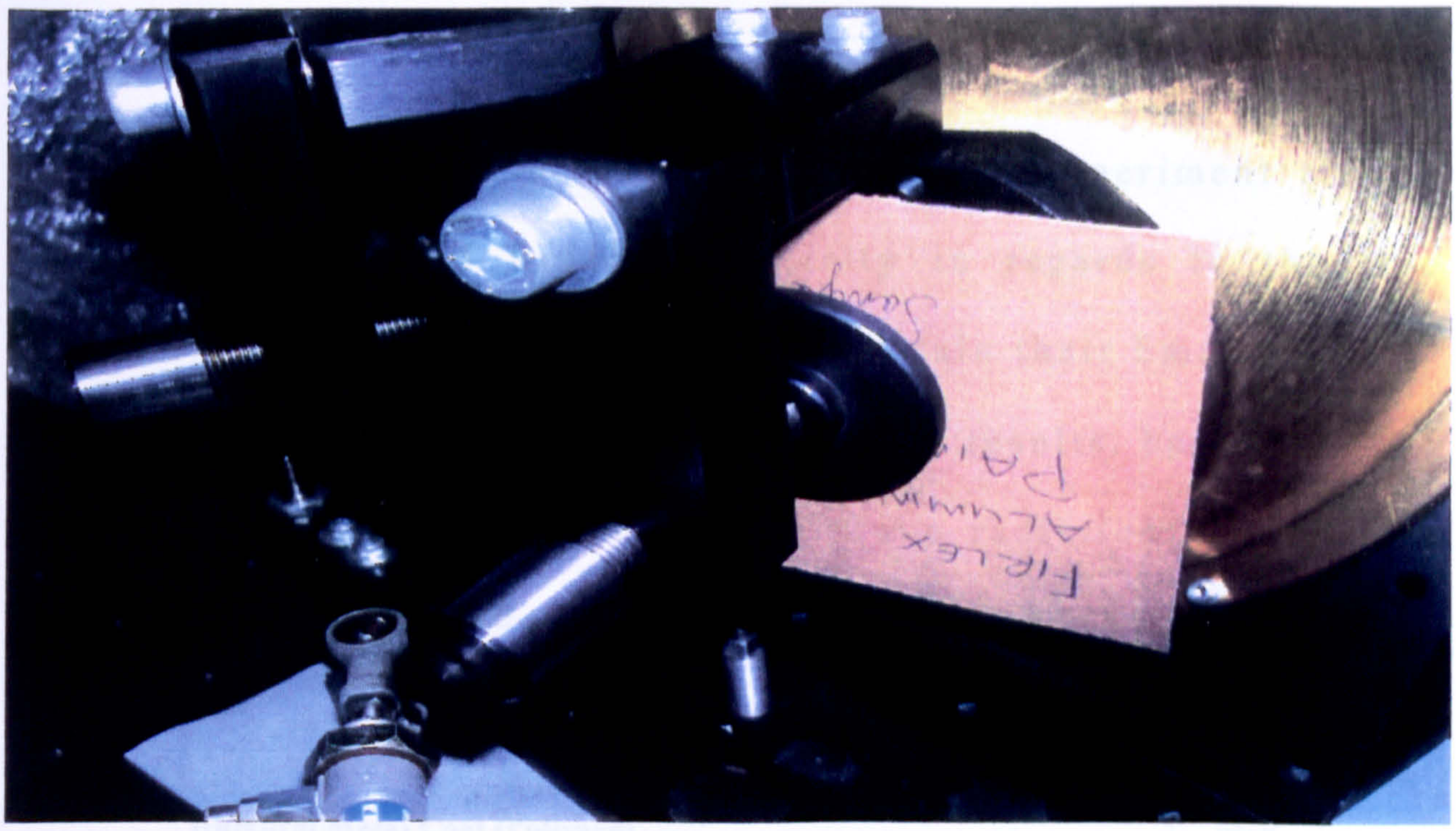

Figure 6.9: Testing equipment at Oxford Brooks university.

Figure 6.10: Testing equipment at Oxford Brooks university.

6.2 Experimental results.

The following graphs 6.11 to 6.20 show the experiment results provided by Oxford Brooks university in regards to the five materials that were sent for testing to obtain their Emmisivity. Figures 6.11 to figures 6.15 show the results based on the reflectance of the material to long wave radiation and figures 6.16 to figures 6.20 results are based on the short wave radiation.

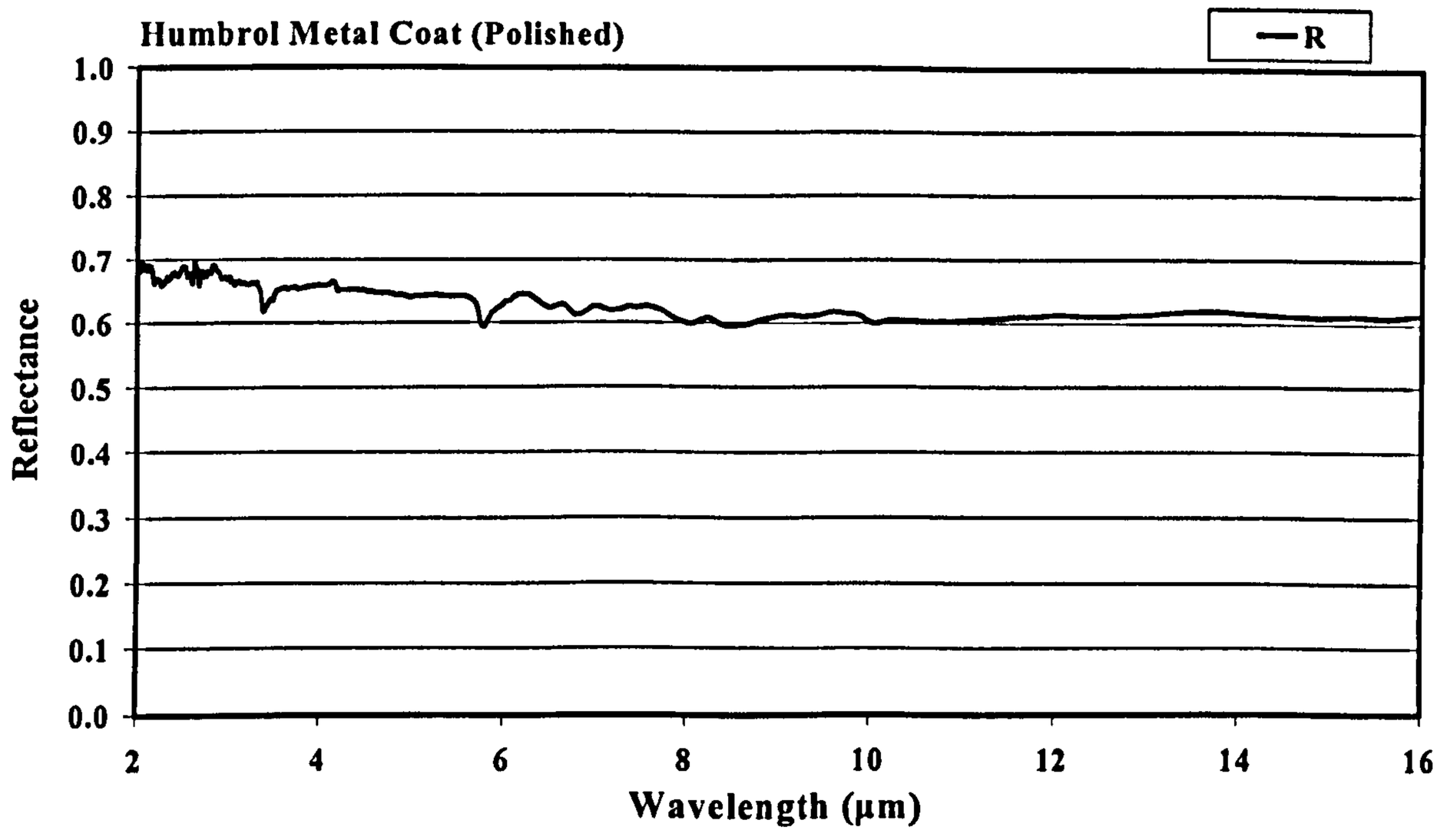

Figure 6.11: Results for the total near-normal hemispherical infrared spectral reflectance of Humbrol metal coat (polished) sample.

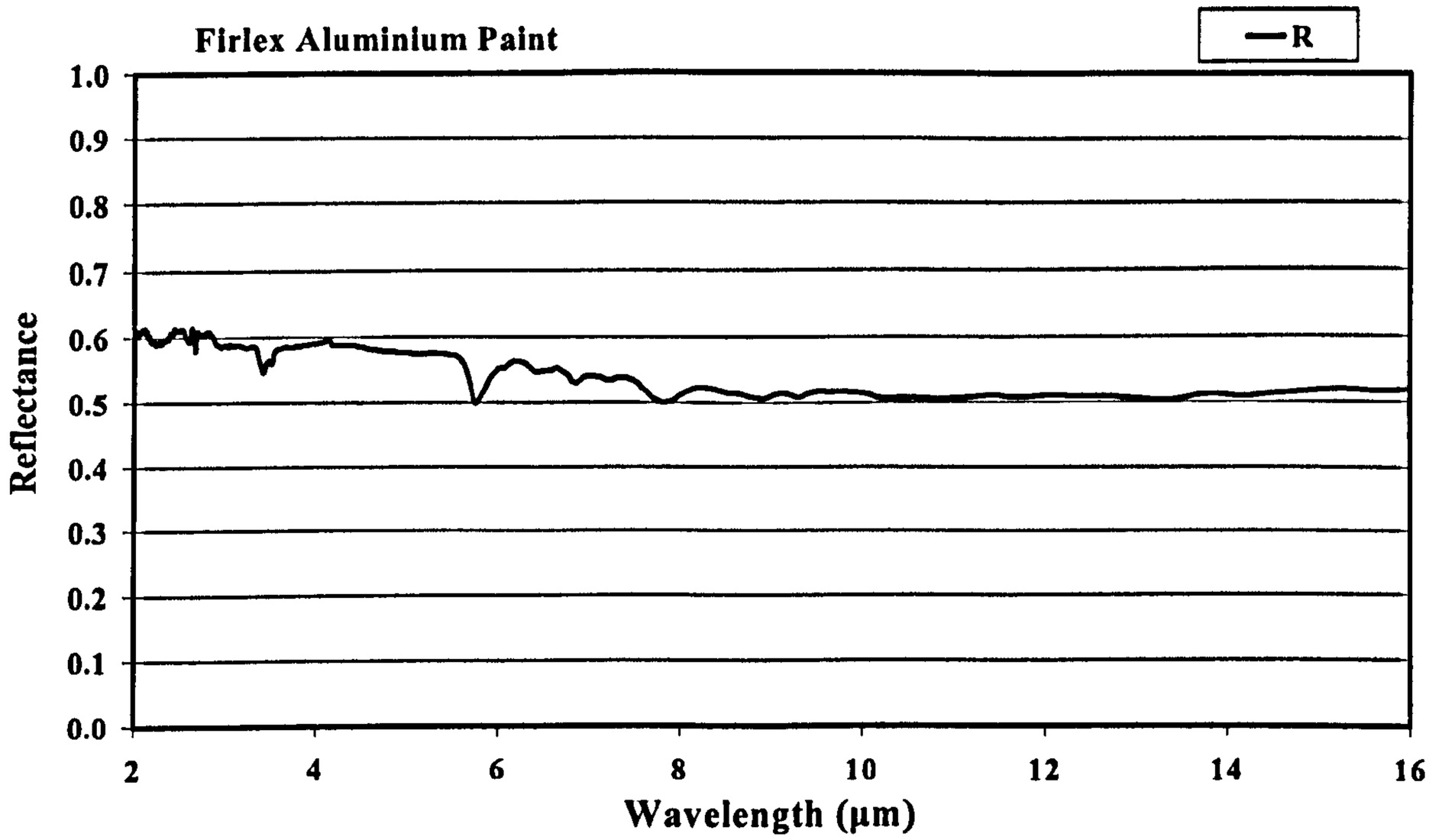

Figure 6.12: Results for the total near-normal hemispherical infrared spectral reflectance of Firlex aluminium paint sample.

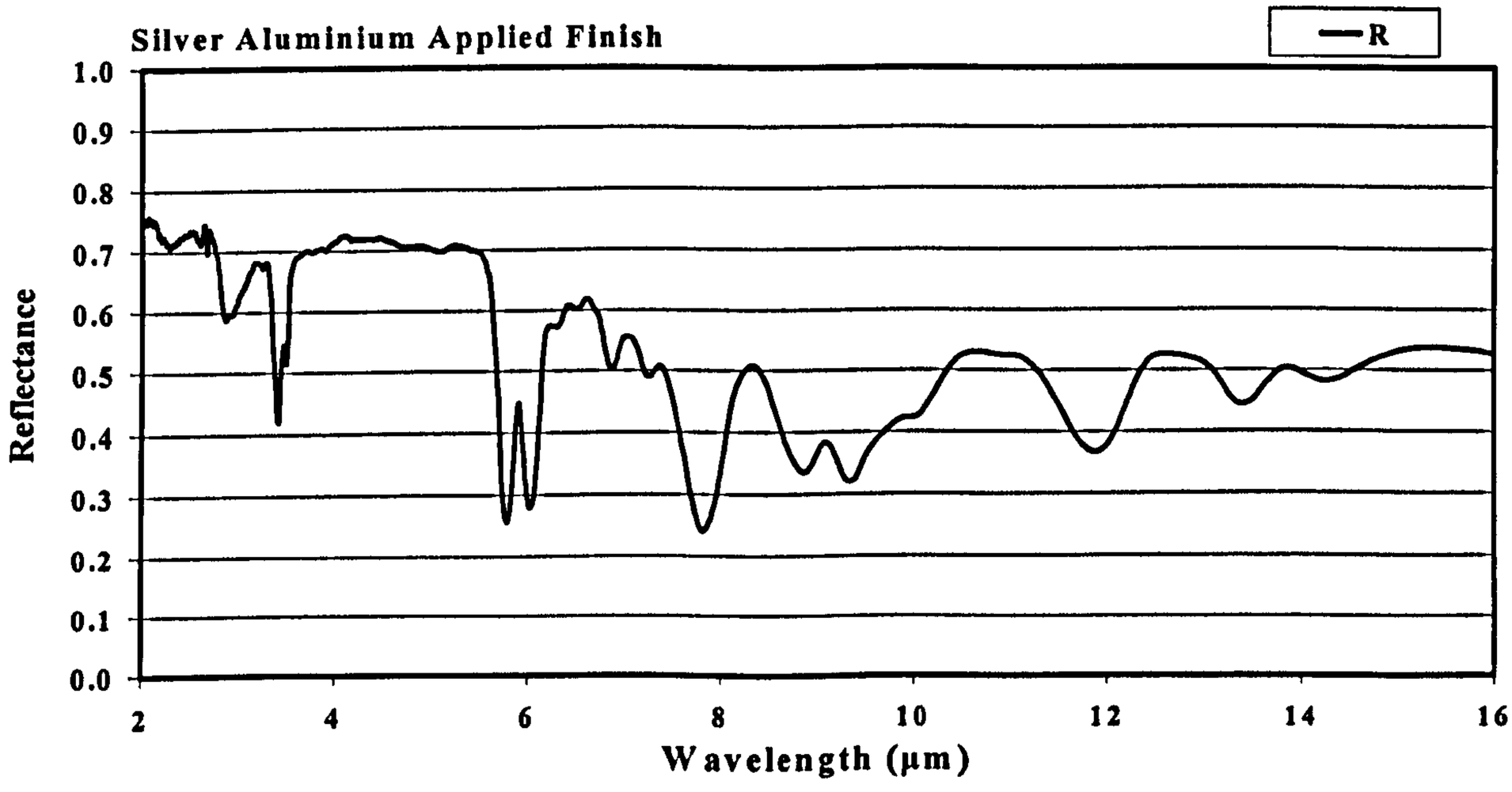

Figure 6.13: Results for the total near-normal hemispherical infrared spectral reflectance of silver aluminium applied finish sample.

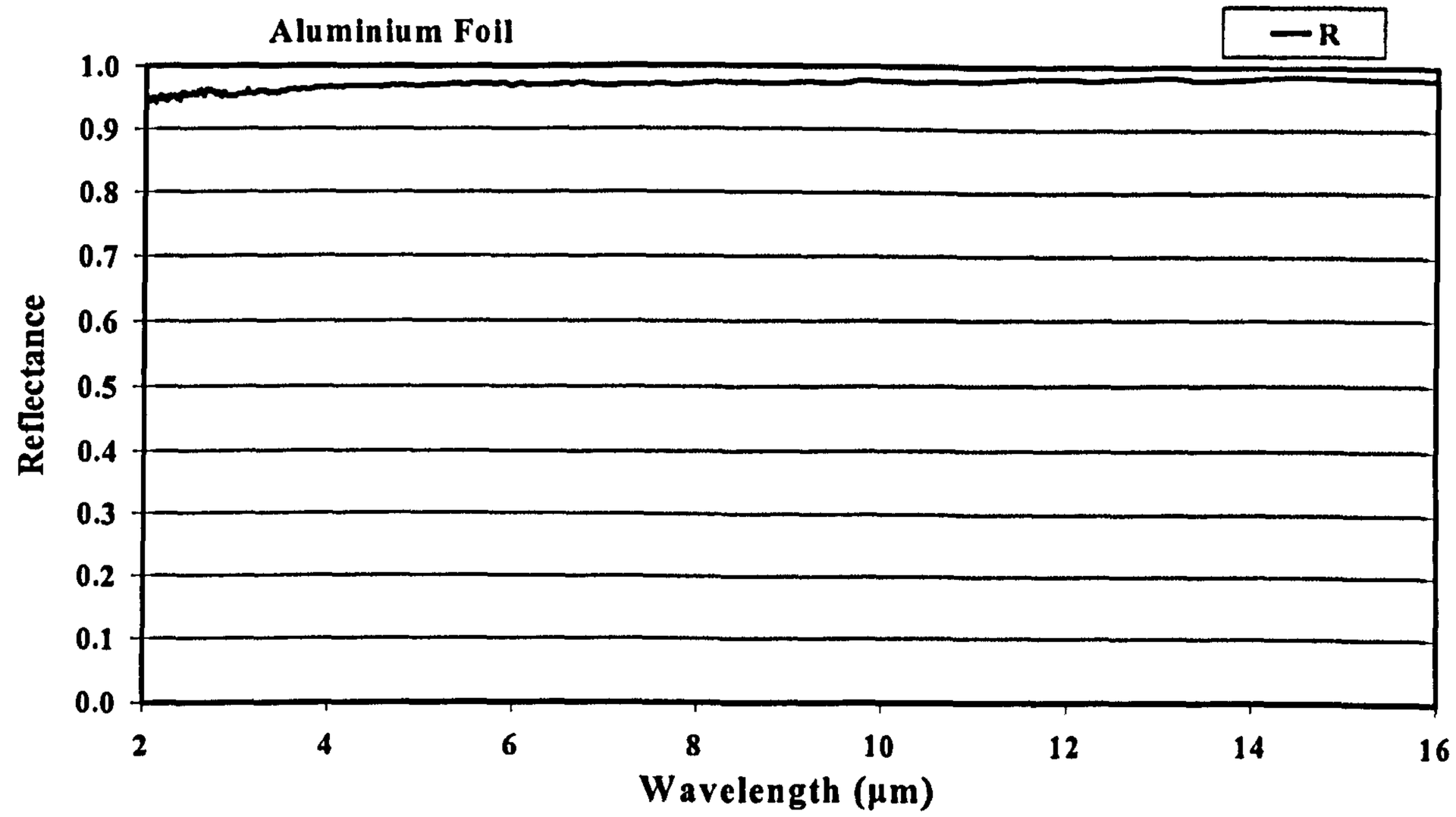

Figure 6.14: Results for the total near-normal hemispherical infrared spectral reflectance of aluminium foil sample.

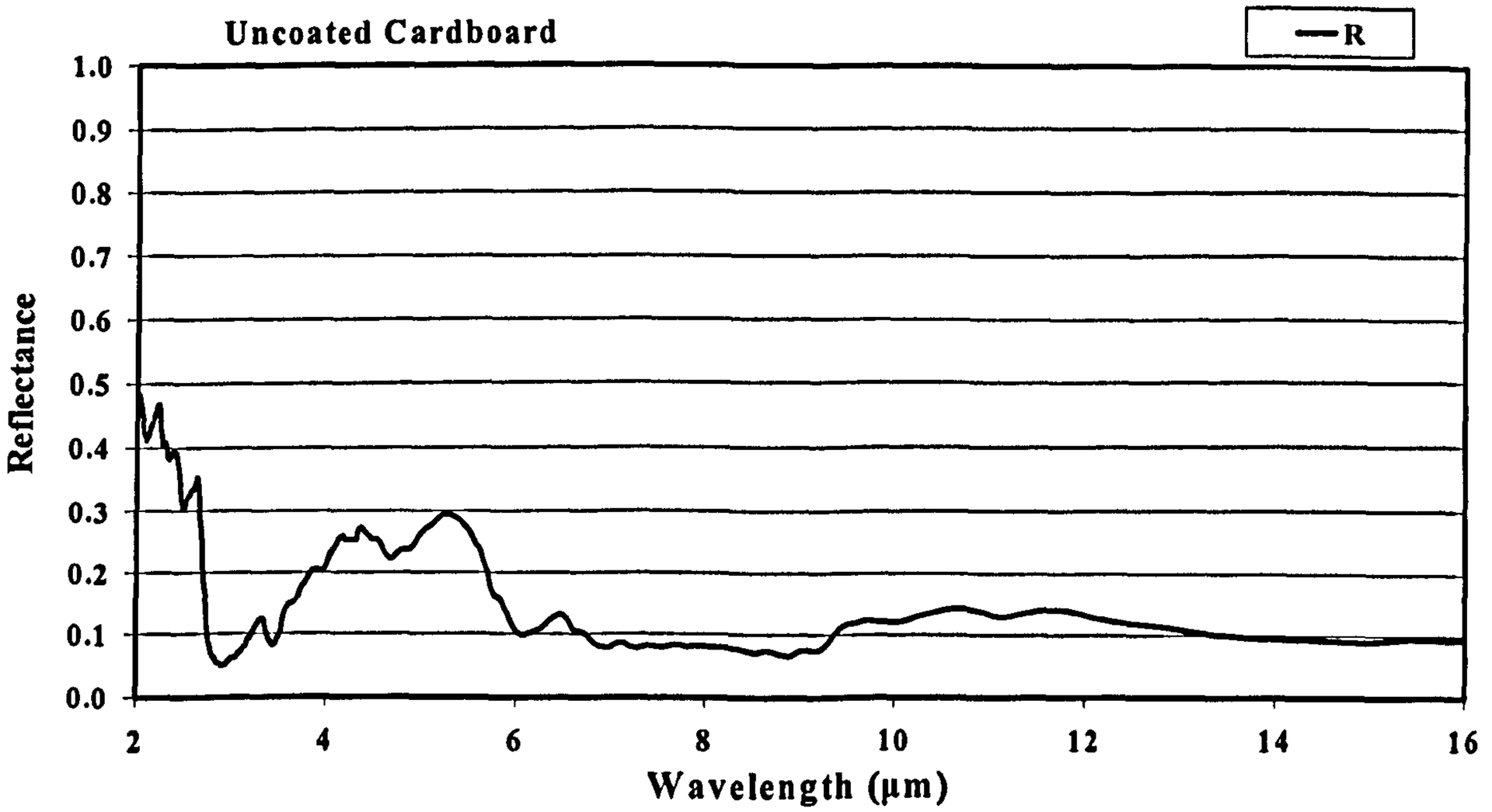

Figure 6.15: Results for the total near-normal hemispherical infrared spectral reflectance of uncoated cardboard sample.

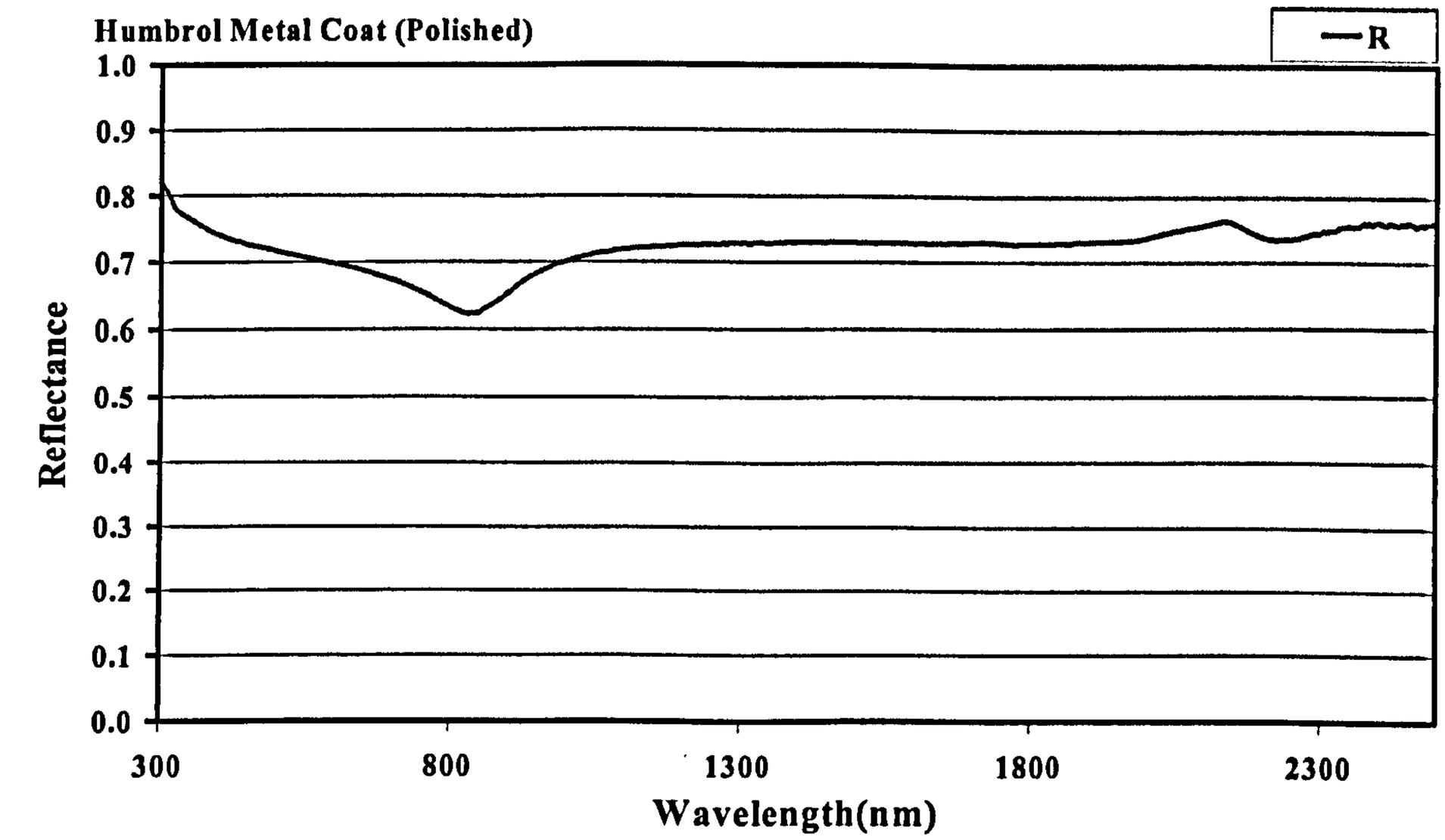

Figure 6.16: Results for the total near-normal hemispherical spectral reflectance of Humbrol metal coat (polished) sample.

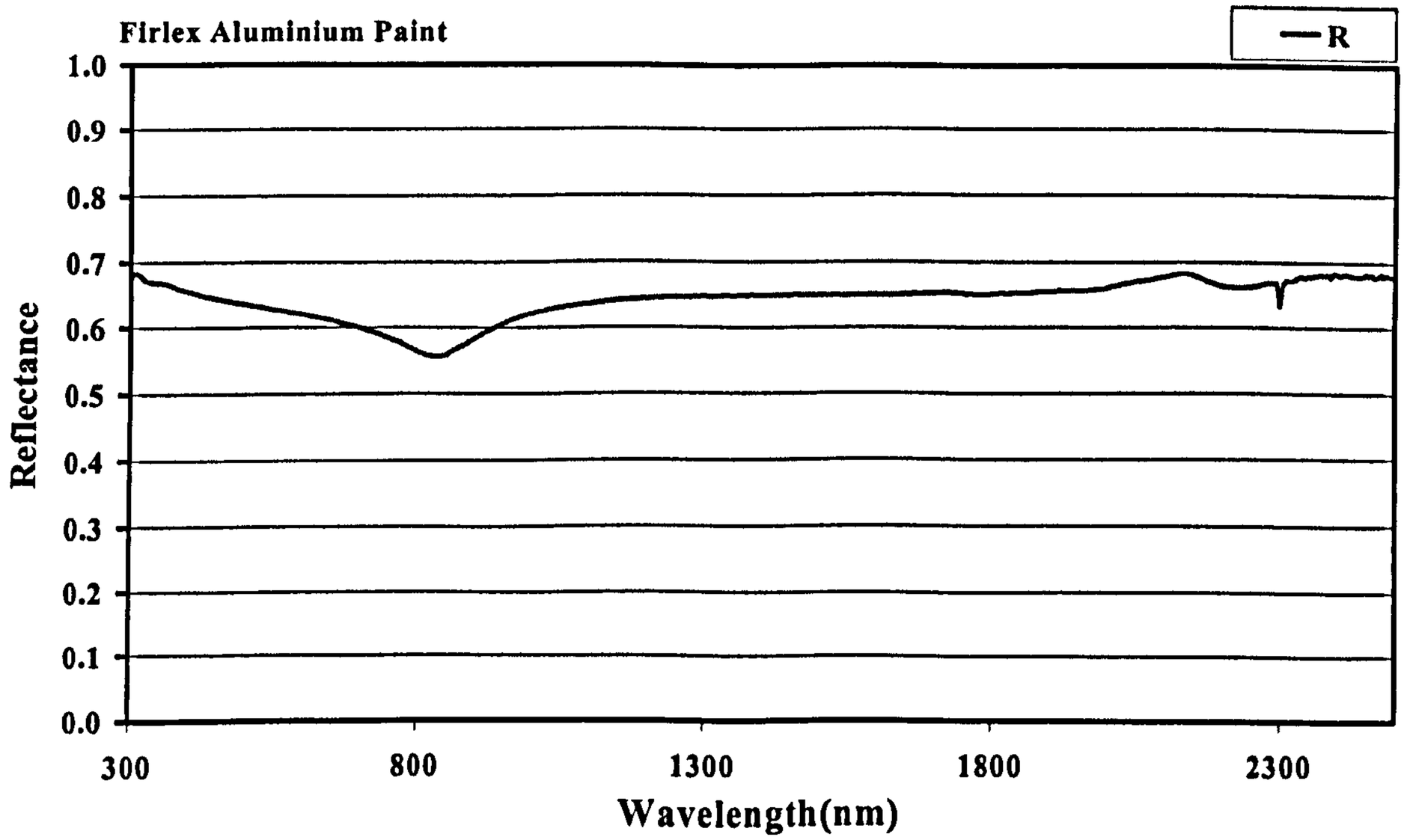

Figure 6.17: Results for the total near-normal hemispherical spectral reflectance of Firlex aluminium paint sample.

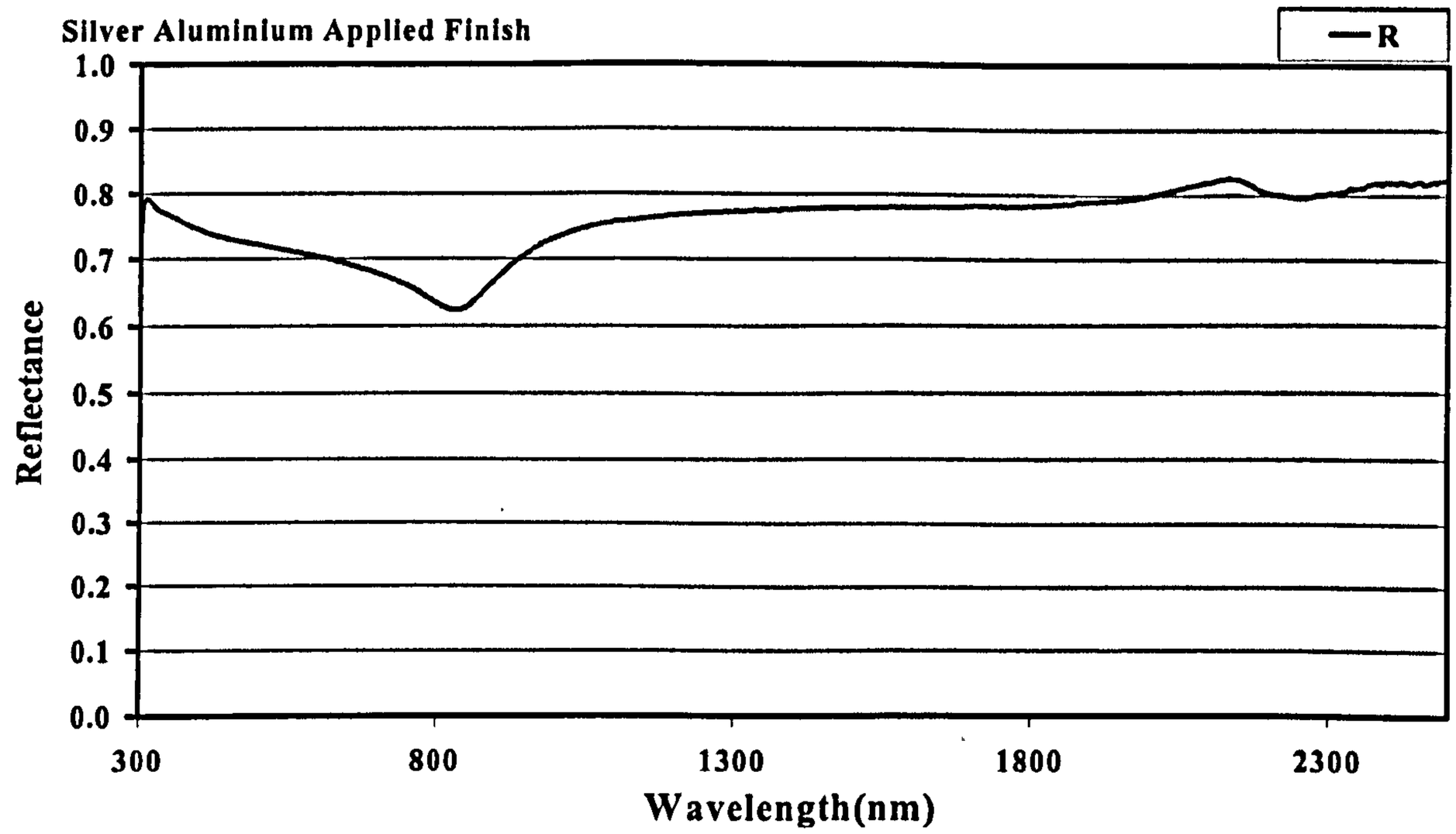

Figure 6.18: Results for the total near-normal hemispherical spectral reflectance of Silver aluminium applied finish sample.

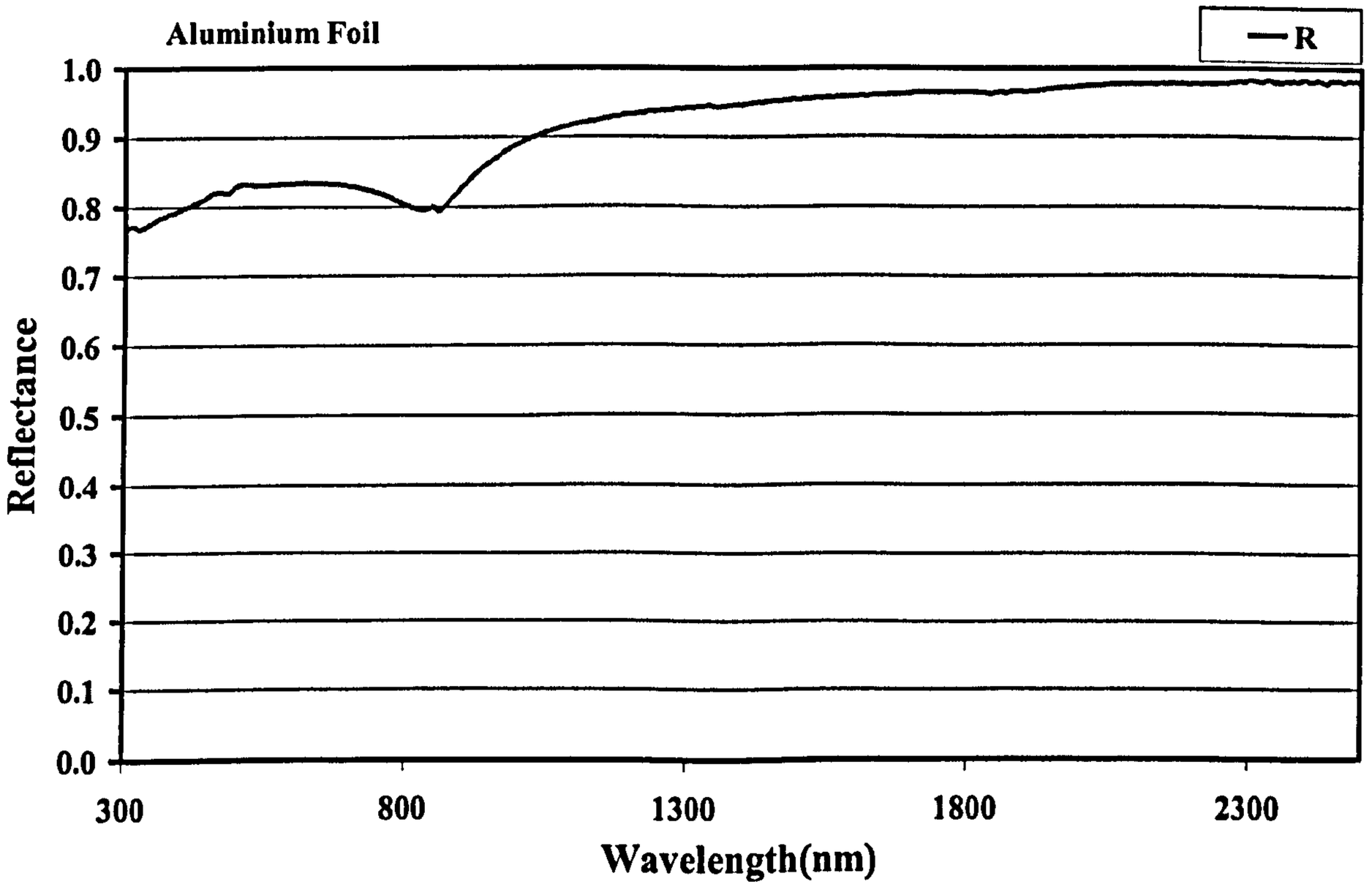

Figure 6.19: Results for the total near-normal hemispherical spectral reflectance of aluminium foil sample.

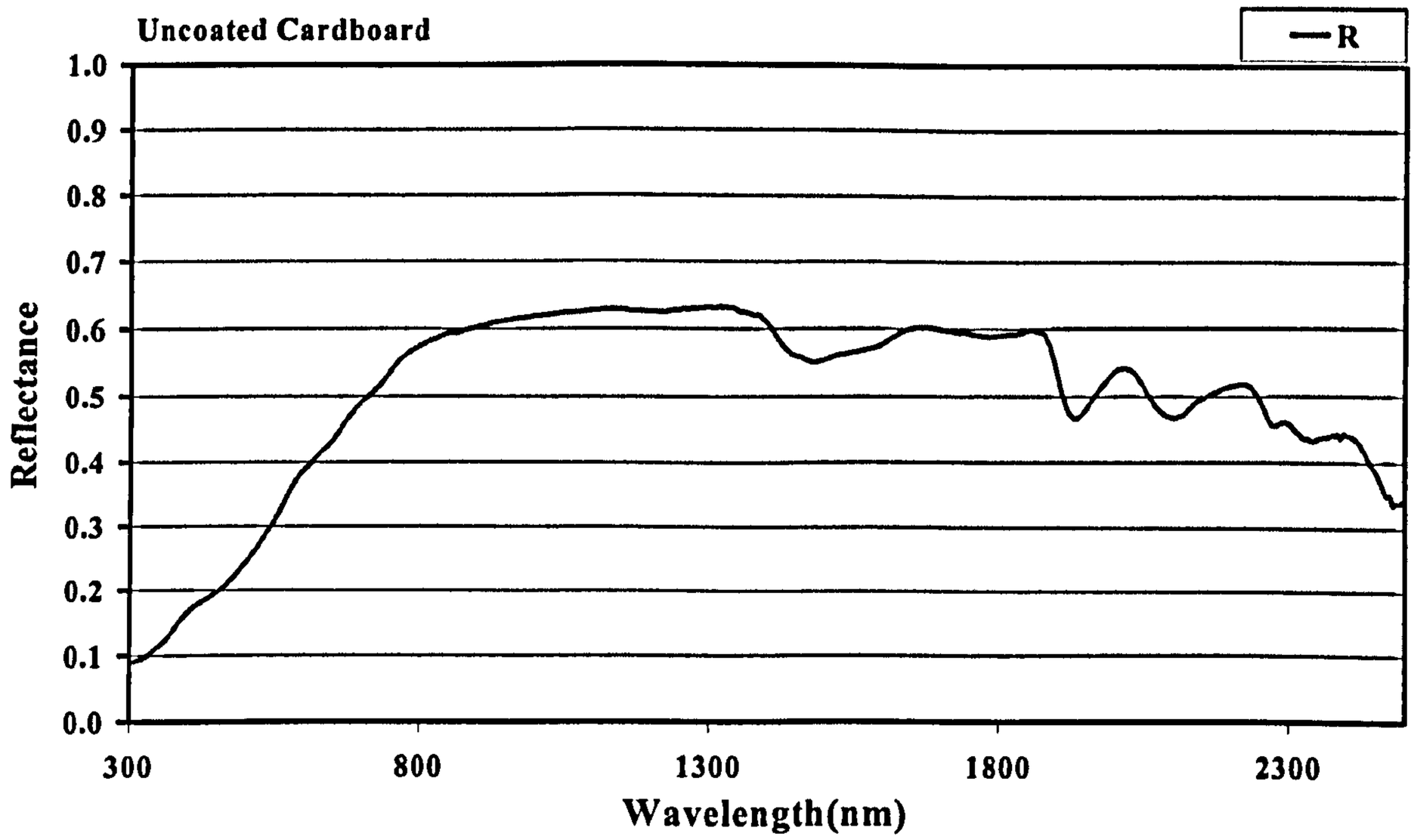

Figure 6.20: Results for the total near-normal hemispherical spectral reflectance of uncoated cardboard sample.

SAMPLE NAME	RS	RV	EMITTANCE
Humbrol Metal Coat (Polished)	0.70	0.71	0.39
Firlex Aluminium Paint	0.62	0.63	0.48
Silver Aluminium Applied Finish	0.72	0.71	0.50
Aluminium Foil	0.85	0.83	0.02
Uncoated Cardboard	0.45	0.32	0.89

Table 6.1: Showing the Emittance of the five samples. (Table presentation of the ten graphs (figures 6.11 to 6.20)).

The test results (figure 6.11 to 6.25) are summarized in table 5.1 and it is concluded that the aluminium foil has the lowest emissivity and also has the most shiny surface. For the method of the material testing and further explanation of the results can be achieved by contacting the material test lab at Oxford Brooks university.

The next stage of the research involved manufacturing the honeycomb slat, and coating the corrugated cardboard, which are presented in the following figures.

The correct mould size was designed and the corrugated cardboard was cut to the correct size and then aluminium foil tape was coated on all the honeycomb slat manually, this was very time taking as the honeycomb slats need to be coated both sided in a smoothly finish.

Section 5.2 shows the various stages of manufacturing and installation of the honeycomb slats to the test chamber.

6.2 The manufacturing process of the honeycomb slats

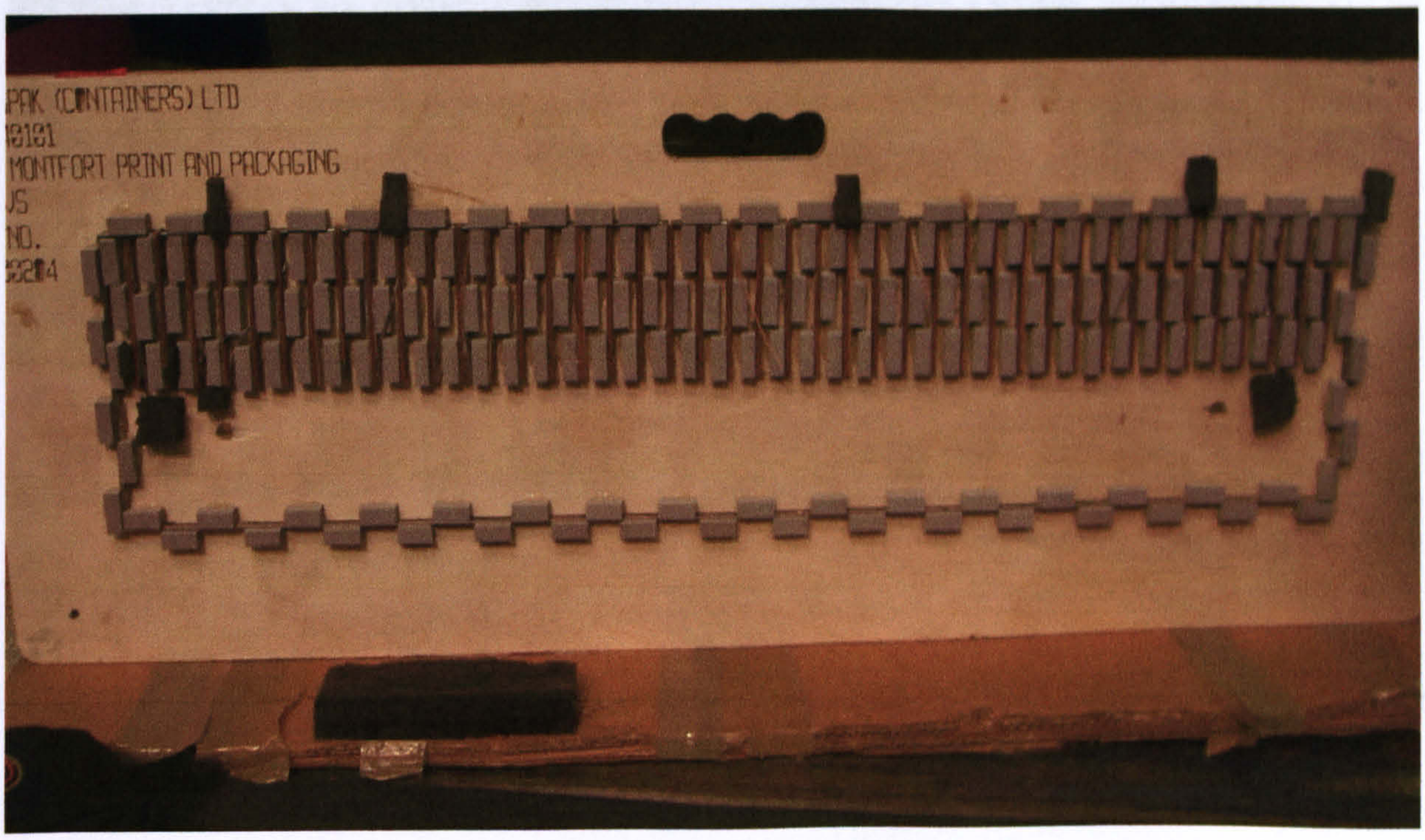

Figure: 6.21: Honeycomb slats mold,

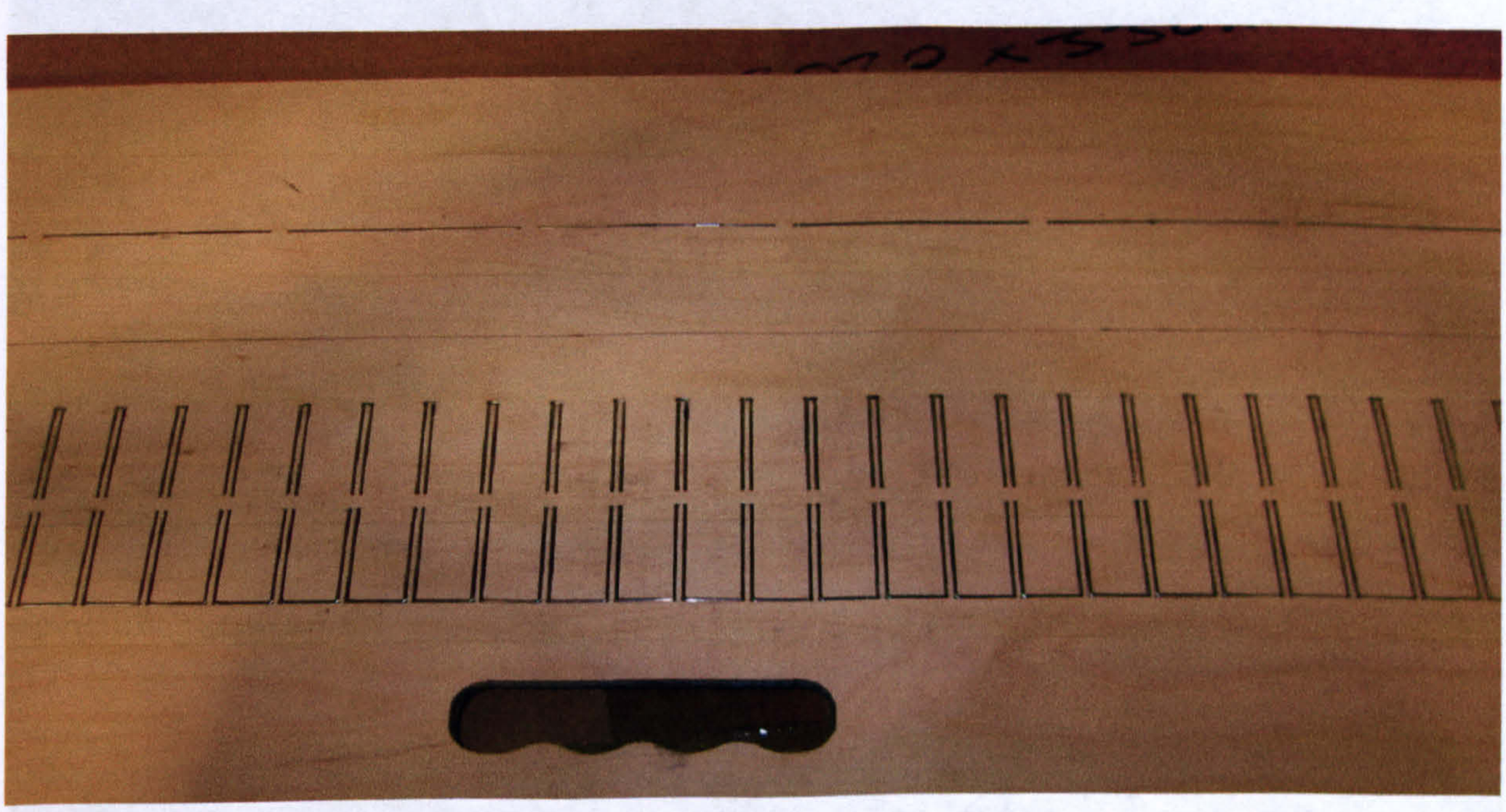

Figure: 6.22: Honeycomb slats design to correct dimensions on timber.

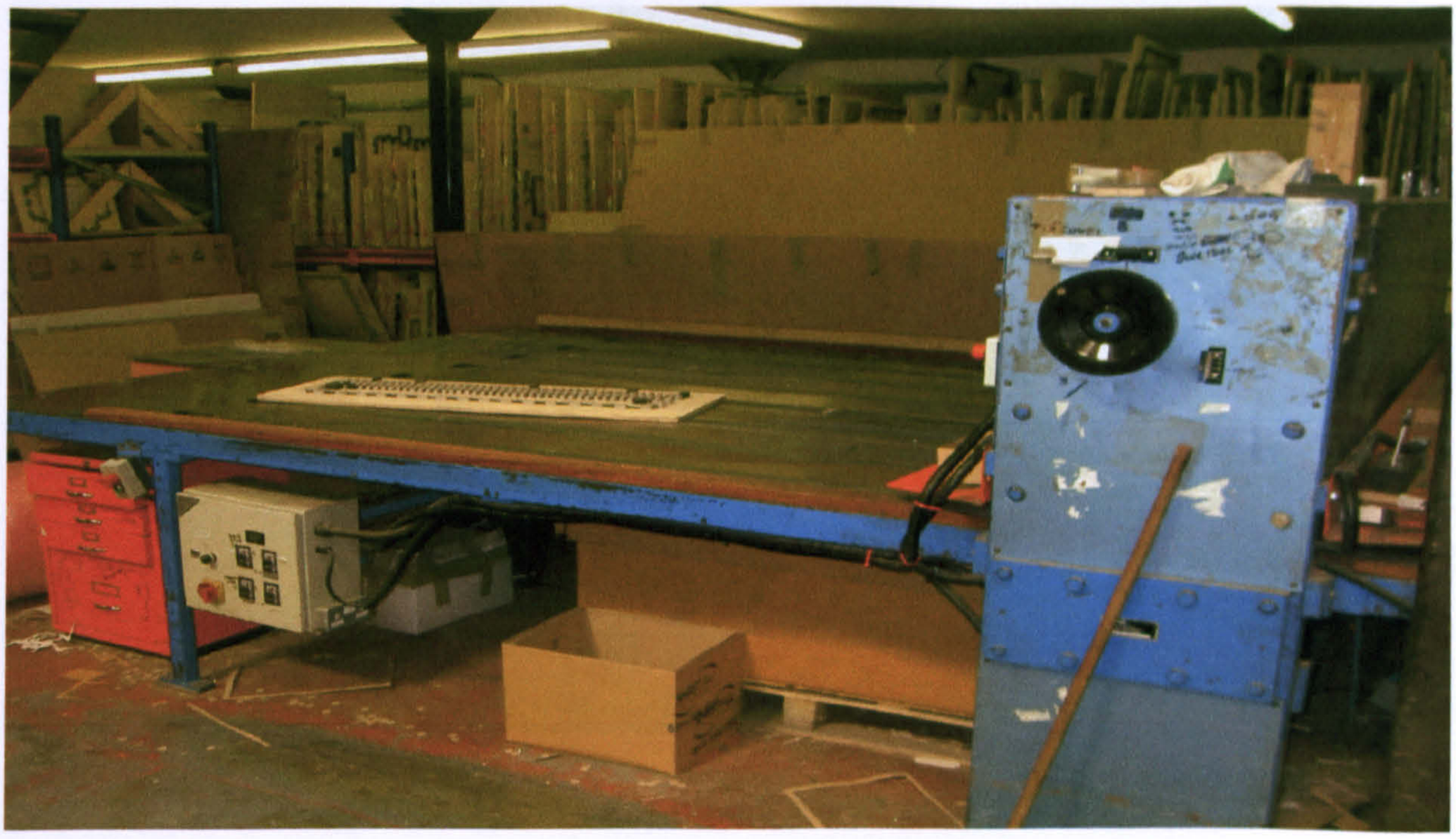

Figure 6.23: Machine cutting the honeycomb to correct size

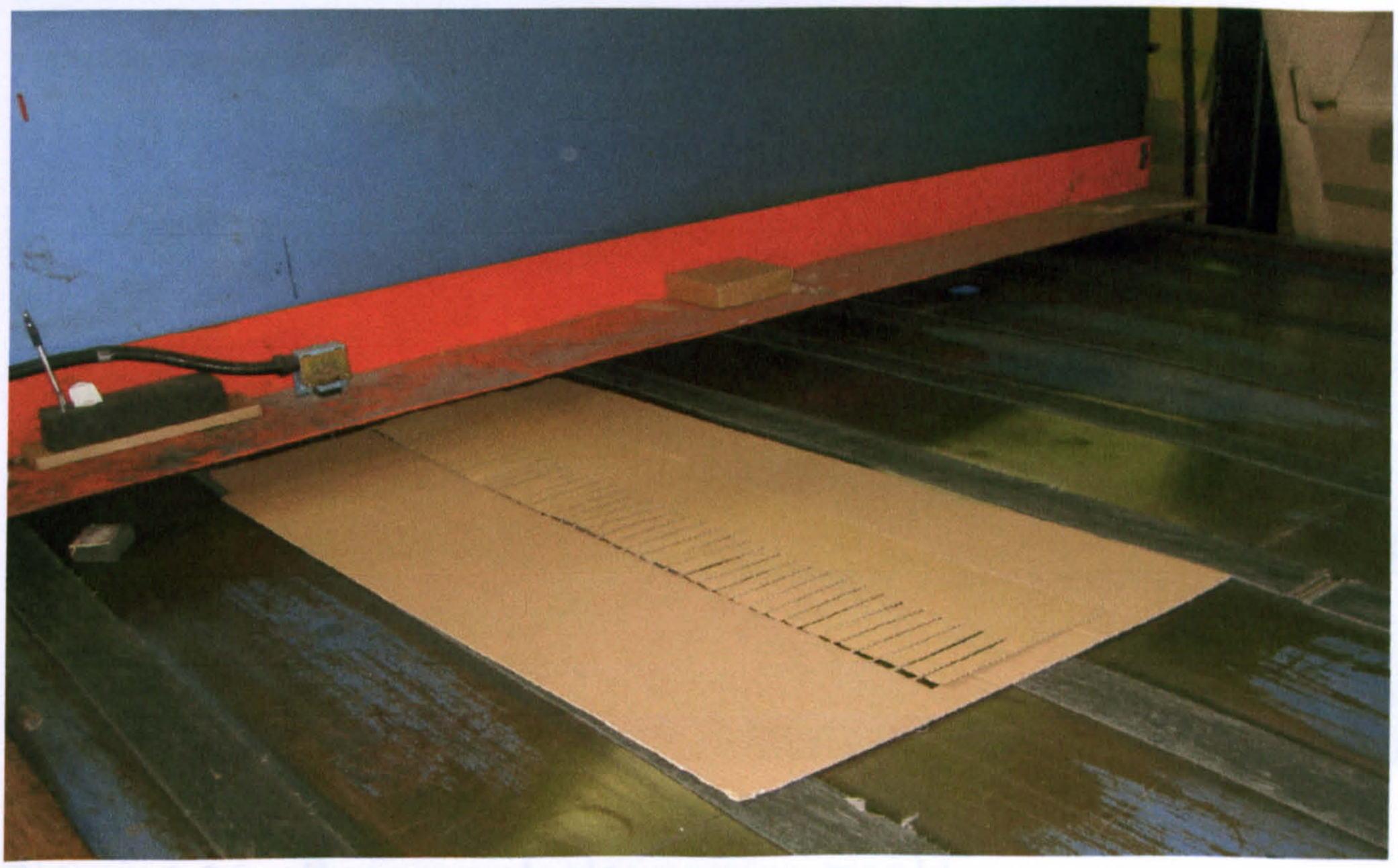

Figure 6.24: Machine cutting the honeycomb to correct size

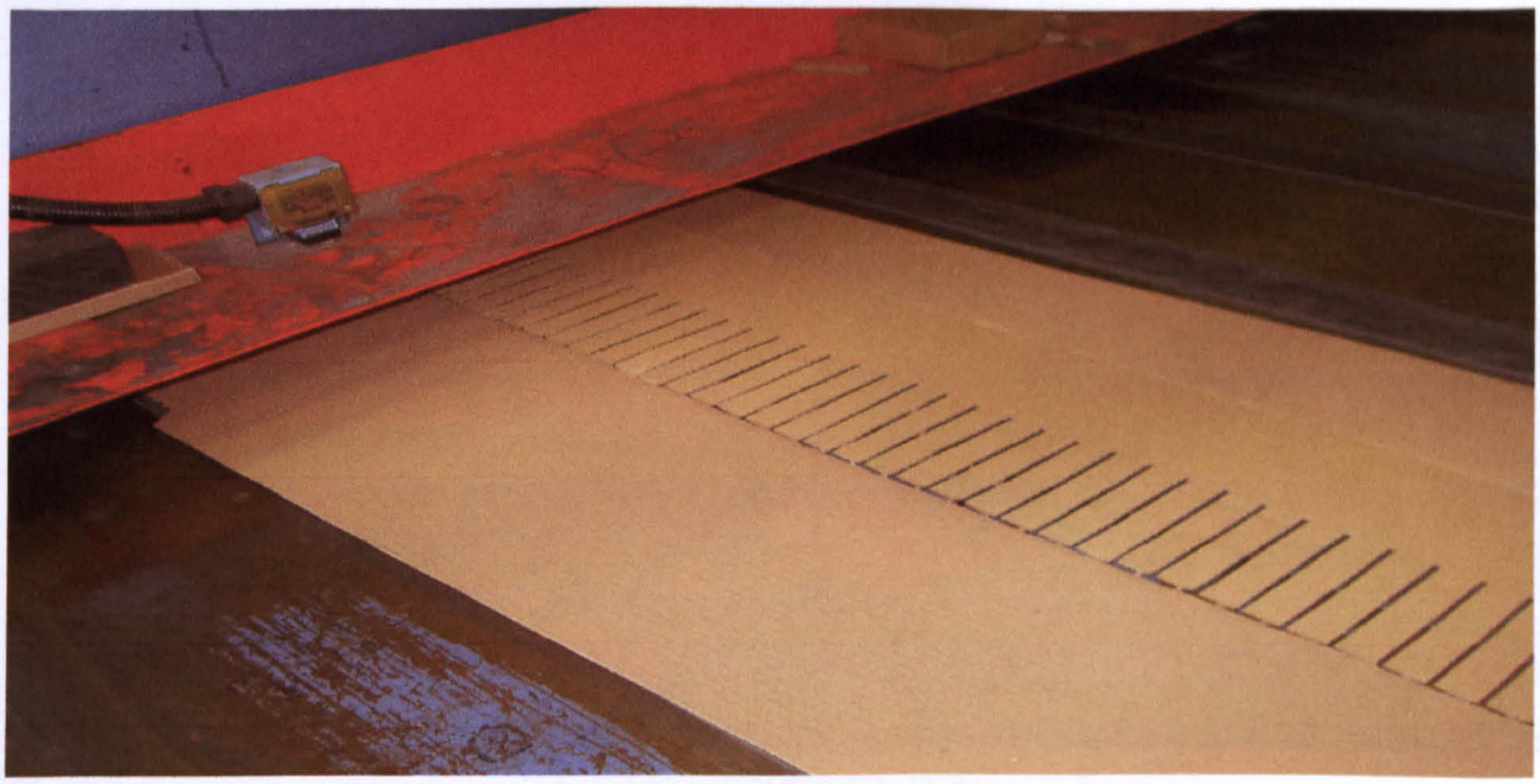

Figure 6.25: Machine cutting the honeycomb slats

Figure 6.26: Honeycomb slat cutting mould

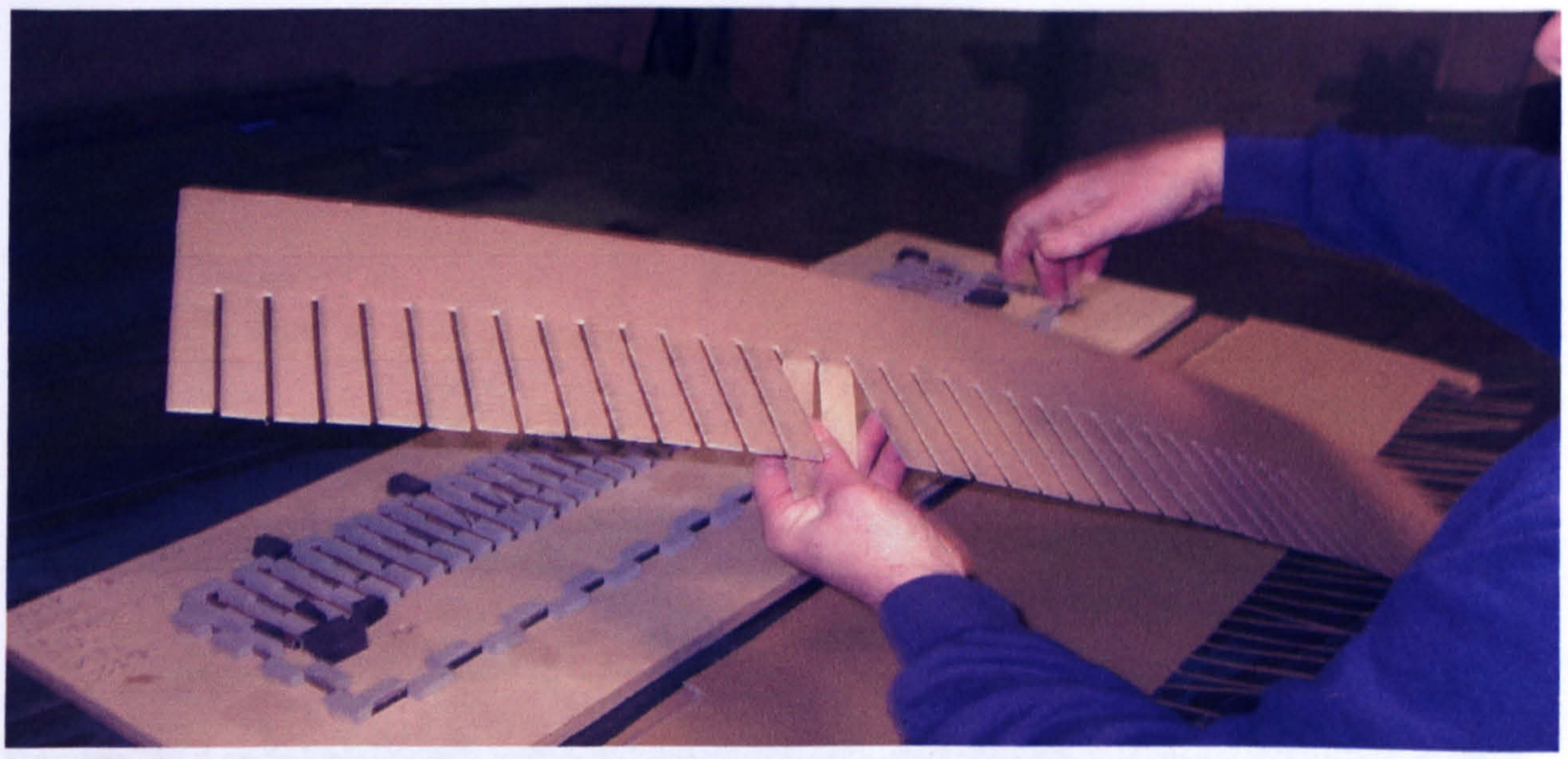

Figure 6.27: Honeycomb slats with the mould

Figure 6.28: Cutting the aluminium foil tape to correct size for coating the cardboard.

Figure 6.29: Cutting the aluminium foil tape to correct size for coating the cardboard.

Figure 6.30: Pealing the aluminium foil tape.

Figure 6.31: Coating the cardboard with aluminium foil tape.

Figure 6.32: Coating the cardboard with aluminium foil tape.

Figure 6.33: Coating the top of the cardboard

Figure 6.34: Coating the cardboard with the second aluminium foil tape.

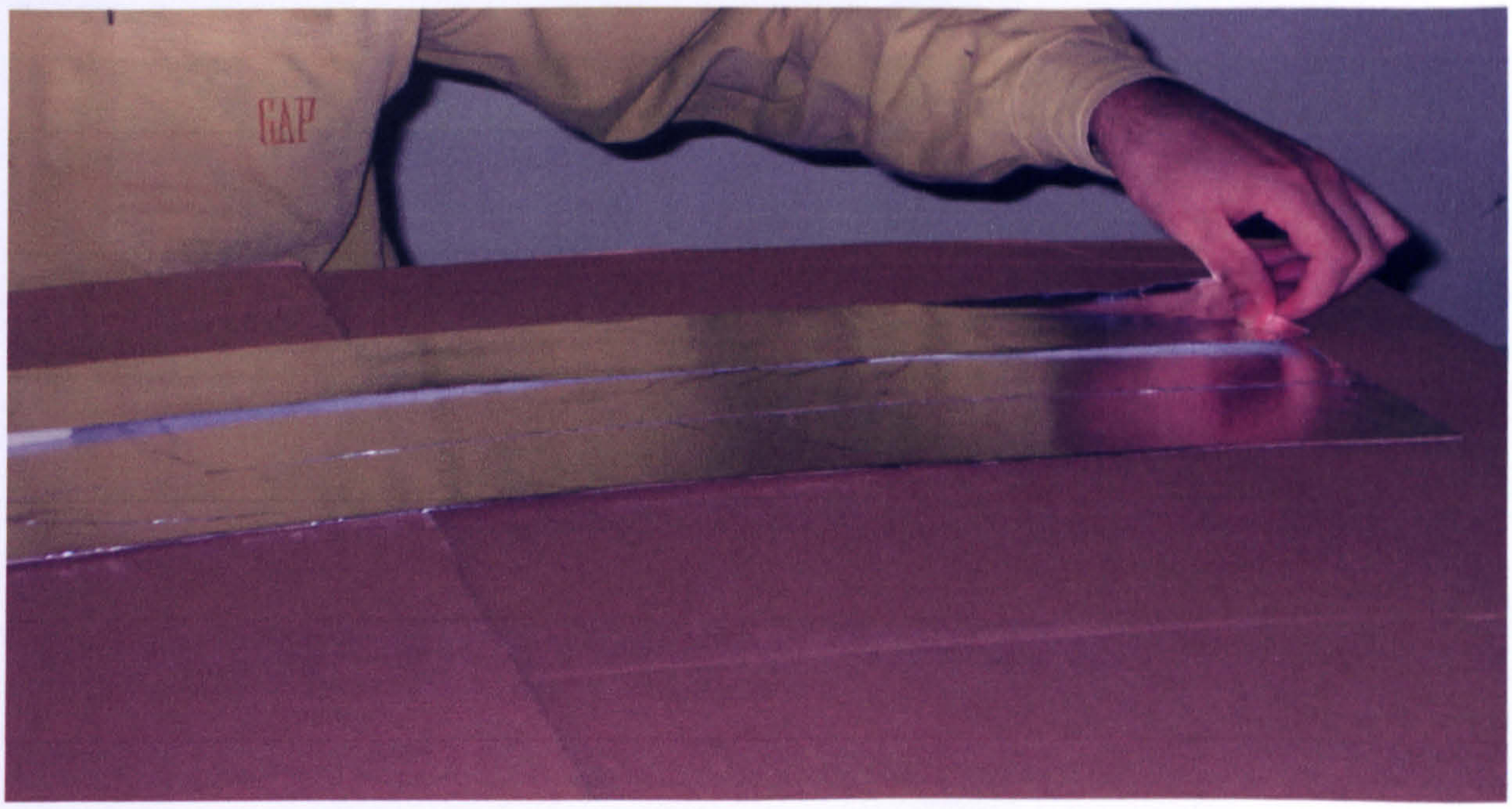

Figure 6.35: Coating the cardboard with the third aluminium foil tape

Figure 6.36: Uncoated and coated card board.

Figure 6.37: Coated and uncoated cardboard.

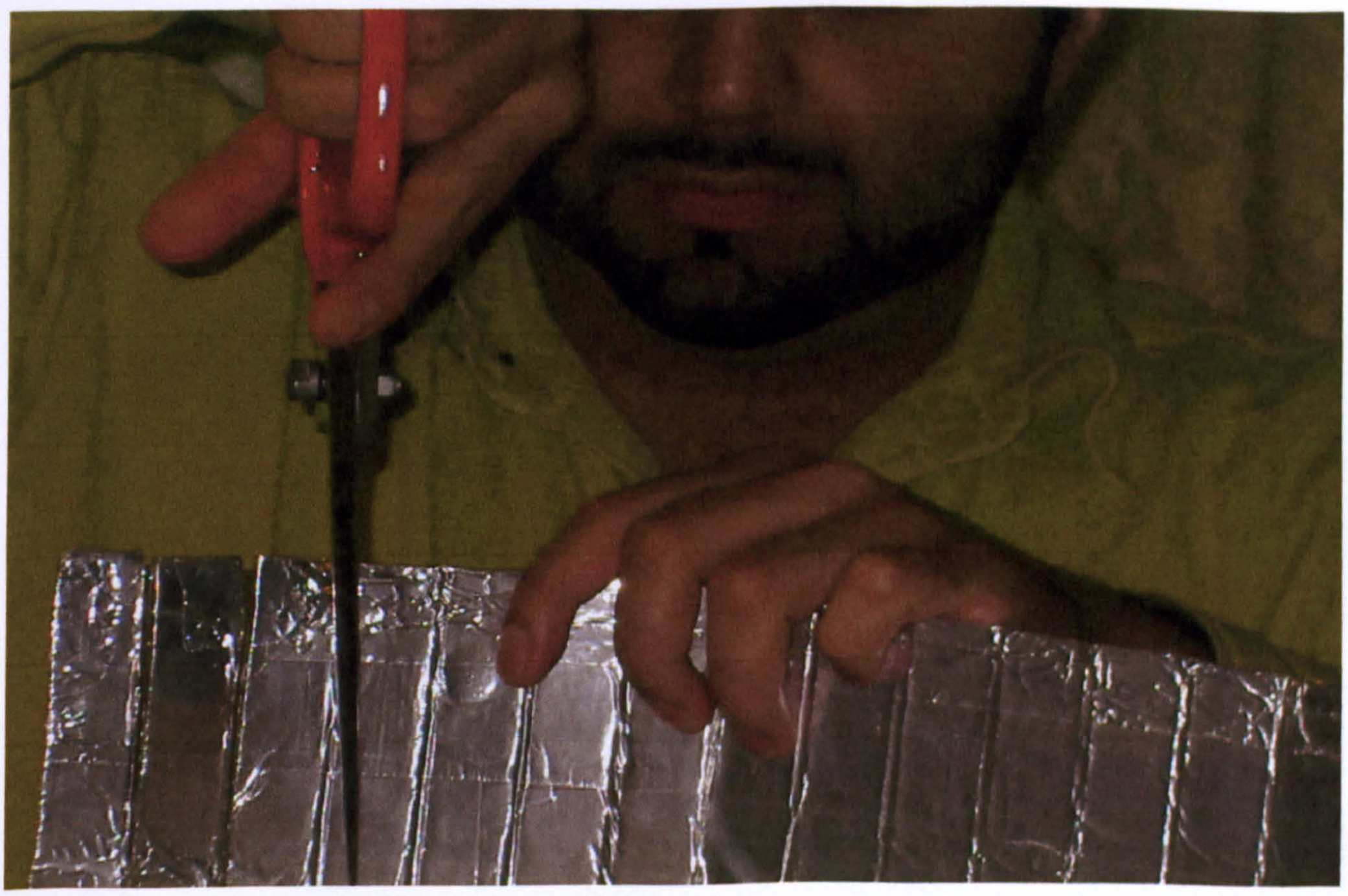

Figure 6.38: Cutting the coated cardboard to the correct size for fixing.

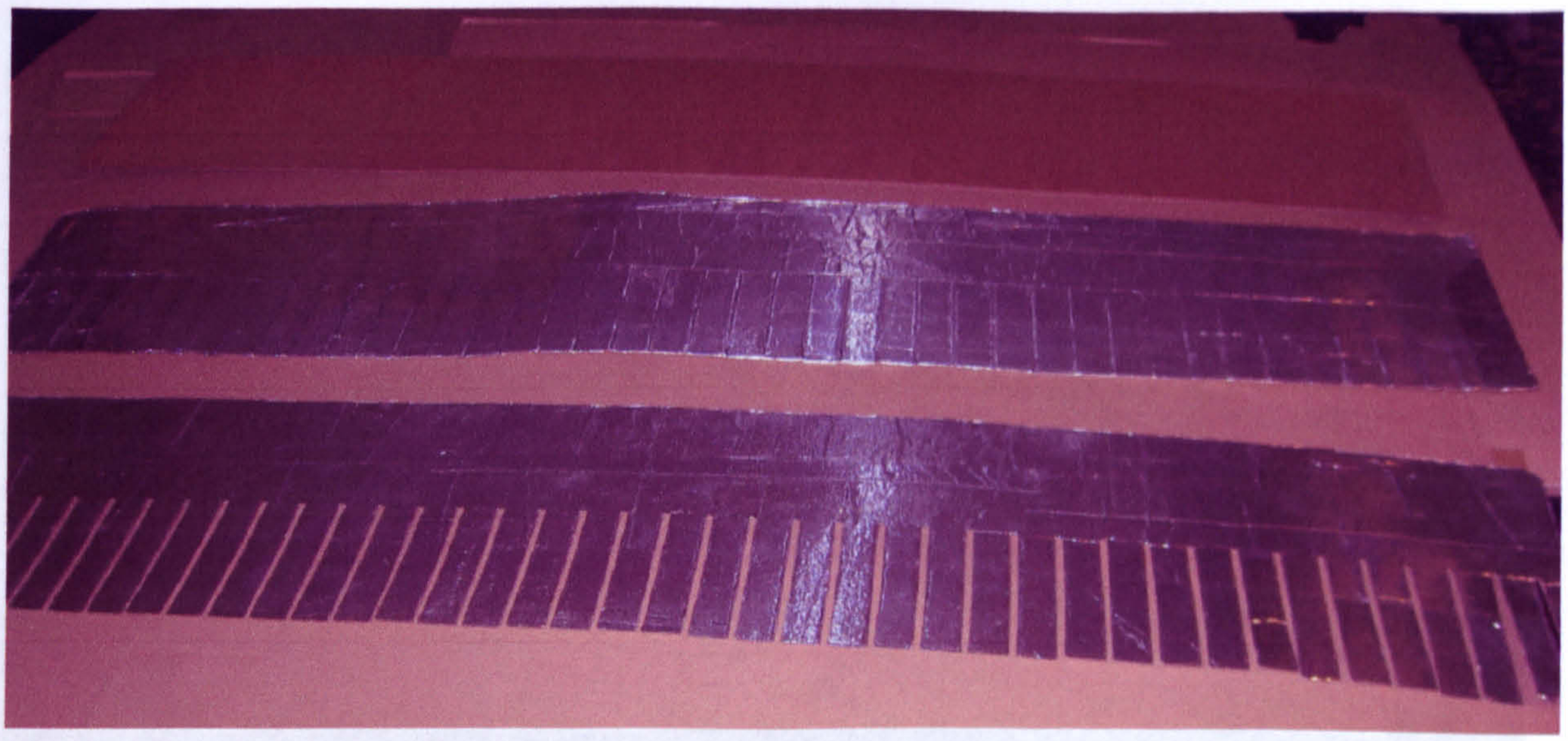

Figure 6.39: Showing uncoated cardboard, coated cardboard, cut to correct size honeycomb slat sheet.

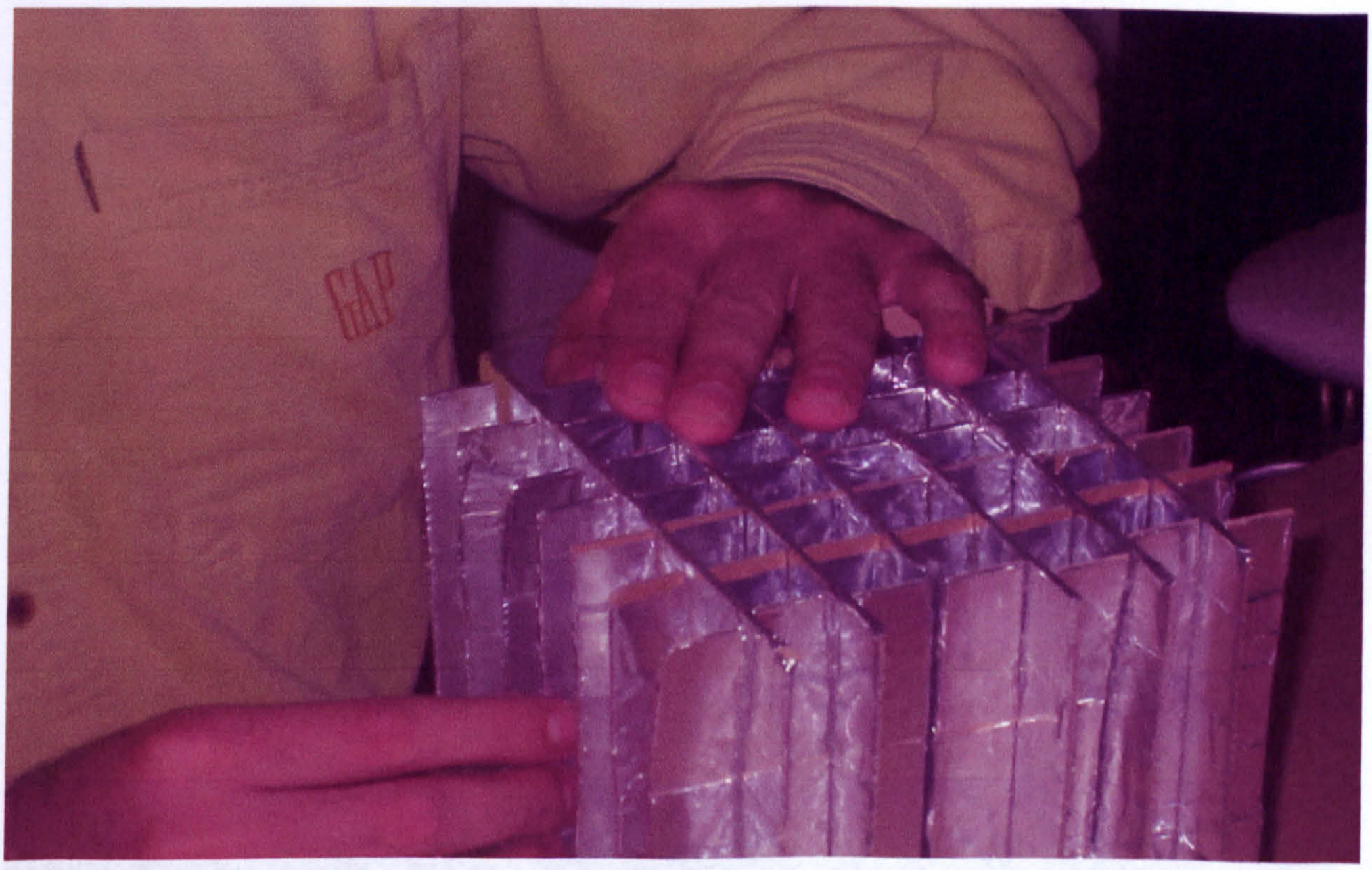

Figure 6.40: Making the small model of the honeycomb slat model.

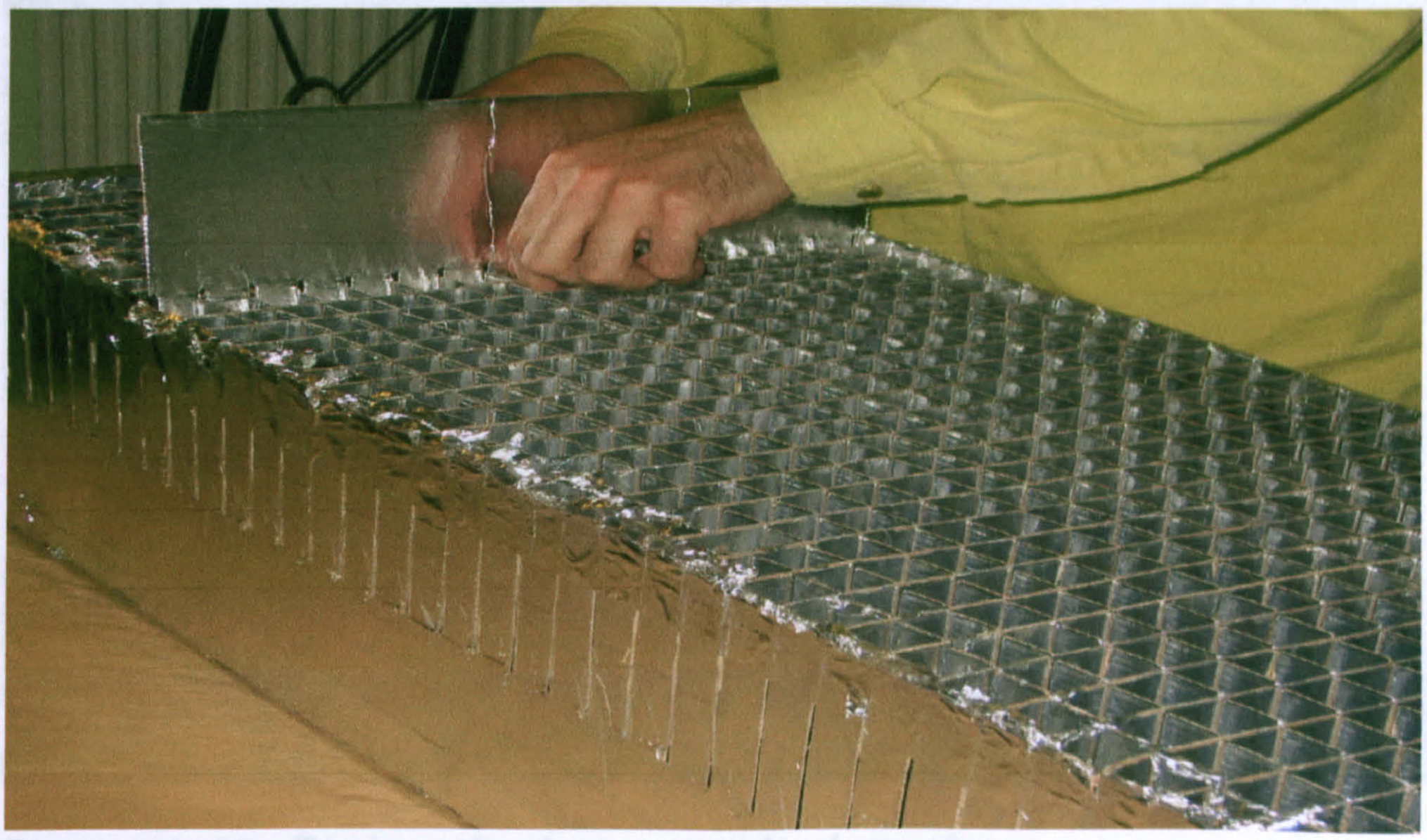

Figure 6.41: Fixing the honeycomb slats sheet.

Figure 6.42: Fixing the honeycomb slats sheet.

Figure 6.43: Fixing the honeycomb slats sheet.

Figure 6.44: Complete section of the honeycomb slats to be attached to the chilled ceiling.

Figure 6.45: Measuring the honeycomb slat section to the correct size.

Figure 6.46: Measuring the honeycomb slat section to the correct size.

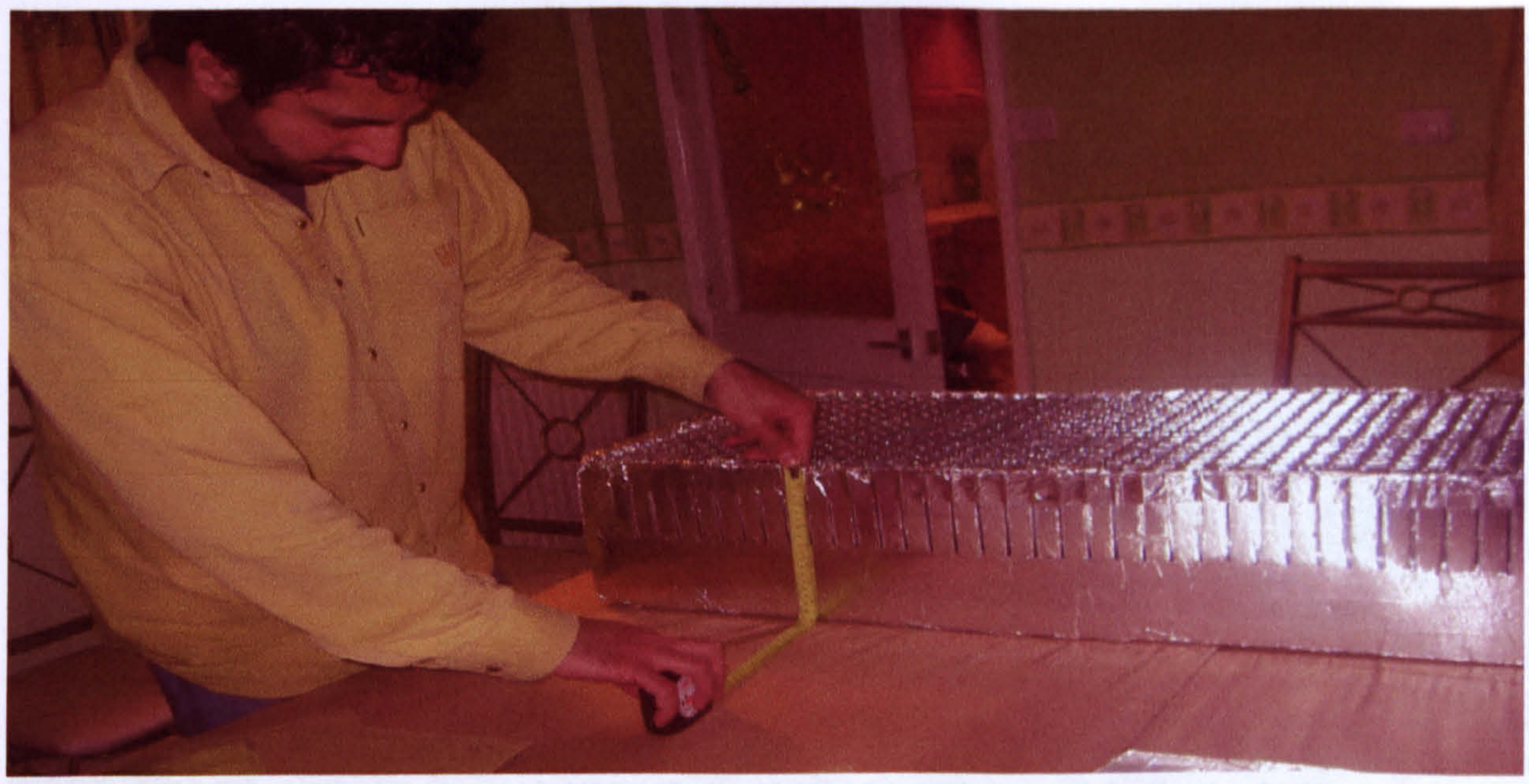

Figure 6.47: Measuring the honeycomb slat section to the correct size.

Figure 6.48: Measuring the honeycomb slat section to the correct size.

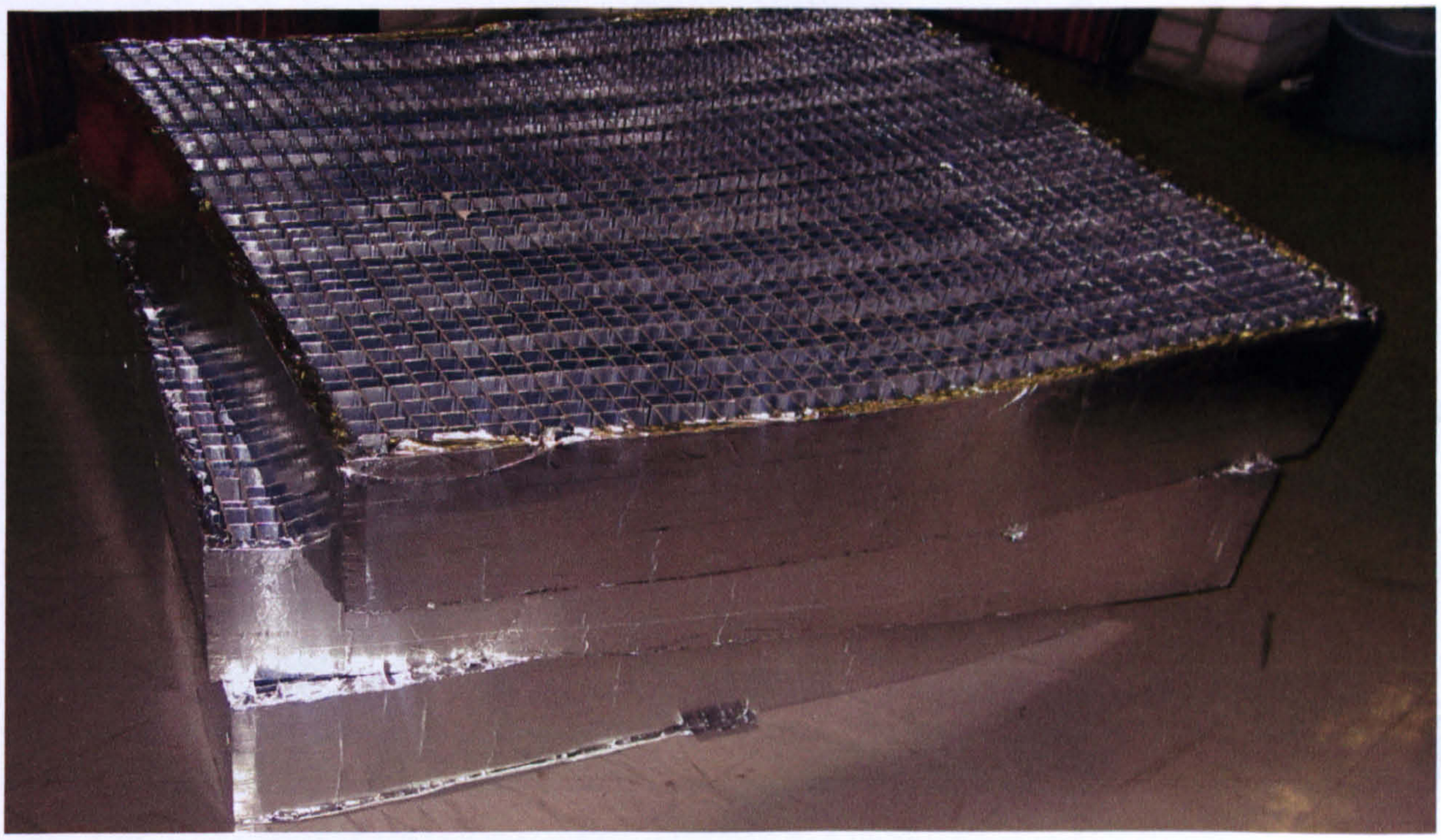

Figure 6.49: Honeycomb slats, before attaching to the chilled ceiling.

Figure 6.50: Honeycomb slats fixed to the ceiling around the inlet diffuser.

Figure 6.51: Honeycomb slats being attached to the ceiling

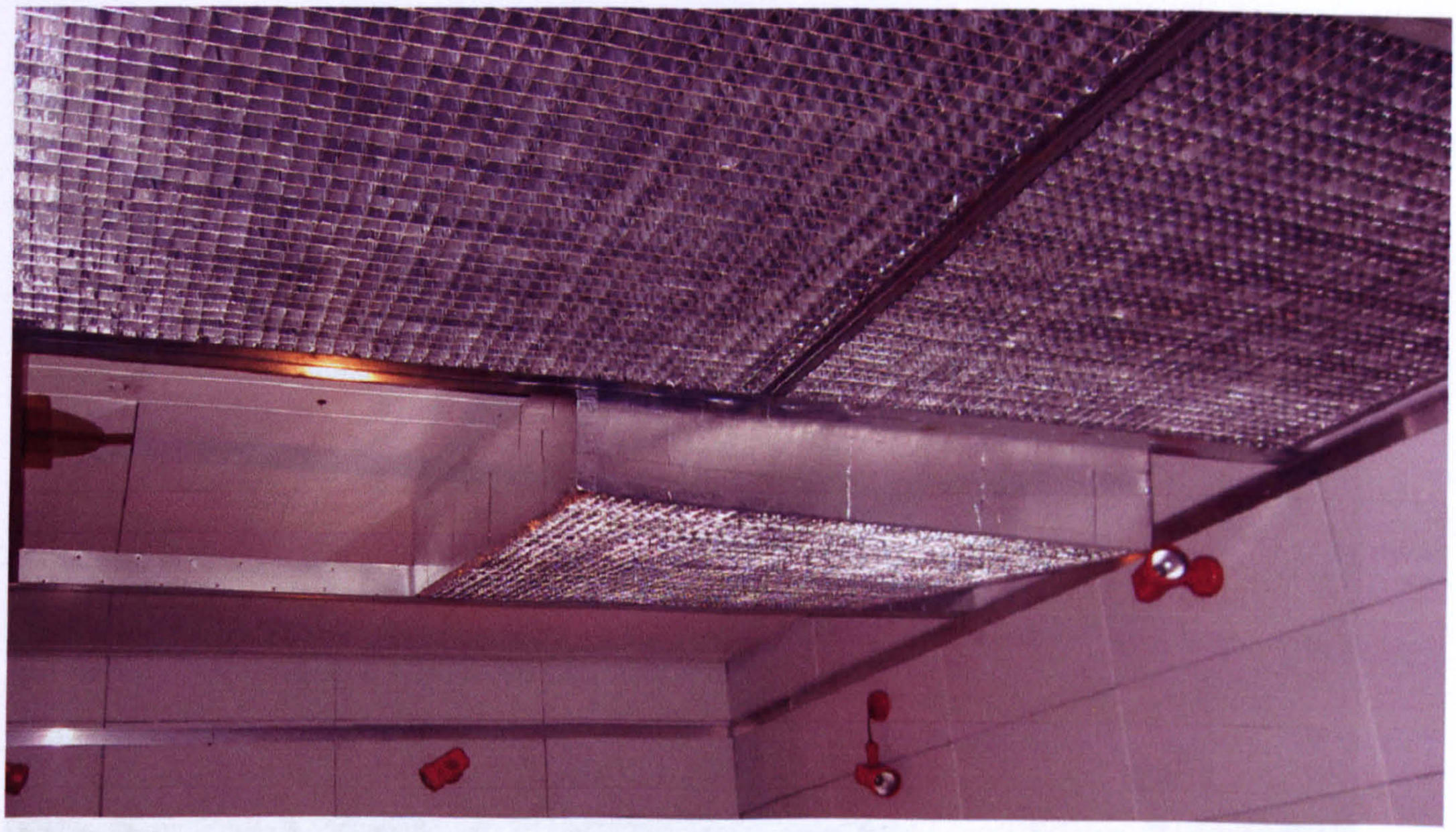

Figure 6.52: Honeycomb slats attached to the ceiling.

Figure 6.53: Honeycomb slats attached to the ceiling.

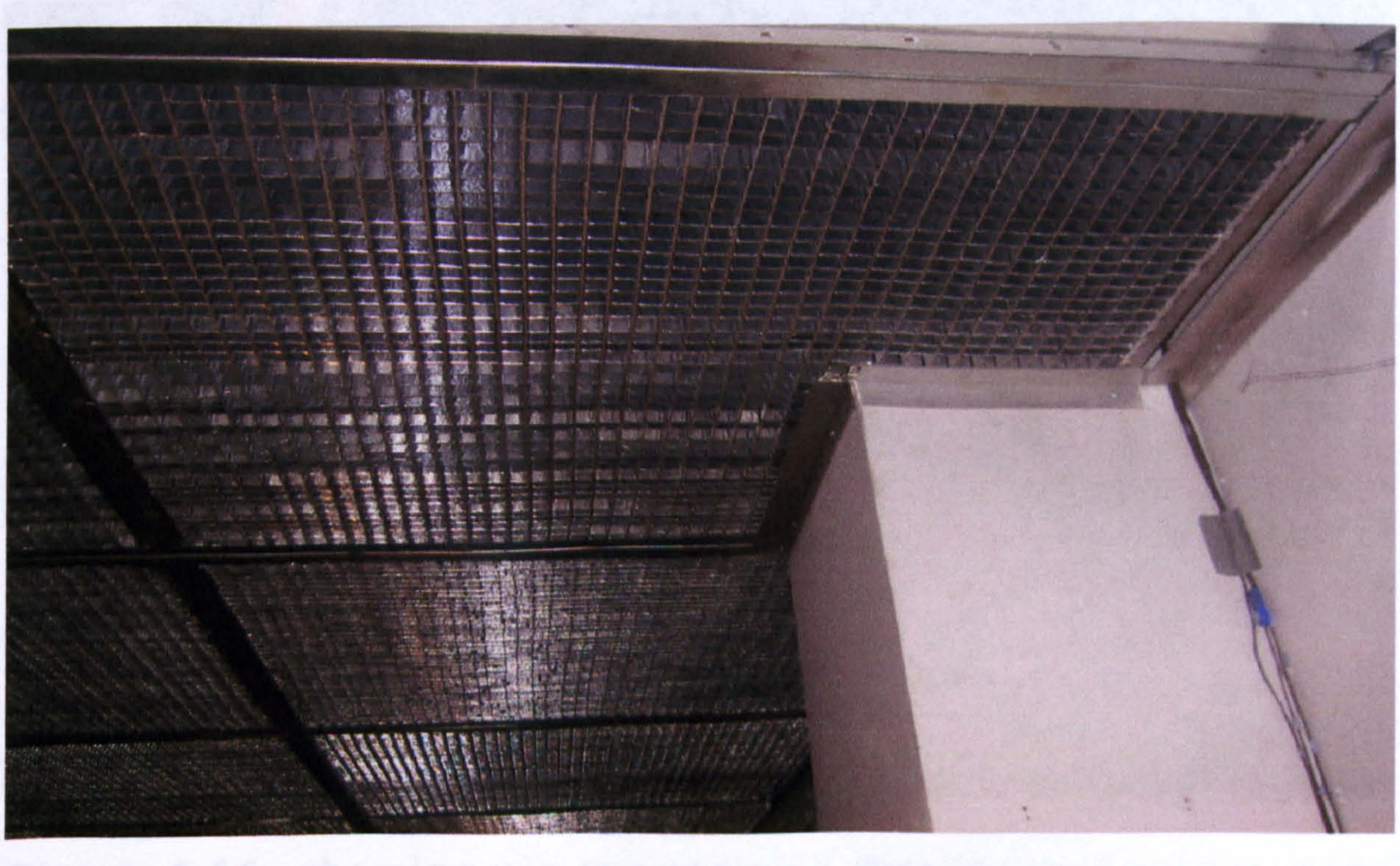

Figure 6.54: Honeycomb slats attached to the ceiling.

Figure 6.55: Honeycomb slats attached to the ceiling with Air temperature measurement equipment attached to the stall.

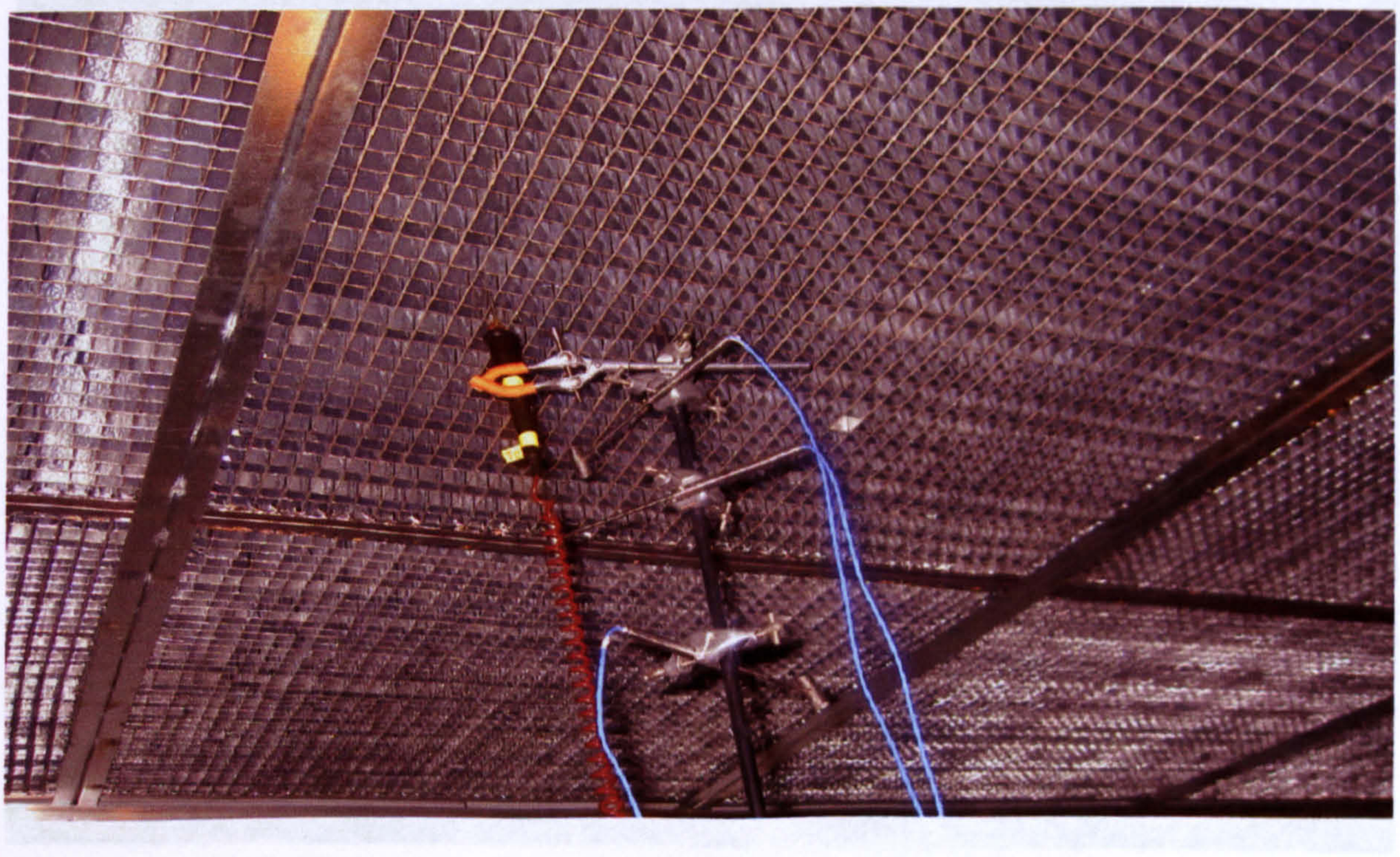

Figure 6.56: showing air temperature measuring sensors inserted between the honeycomb slats and the chilled ceiling.

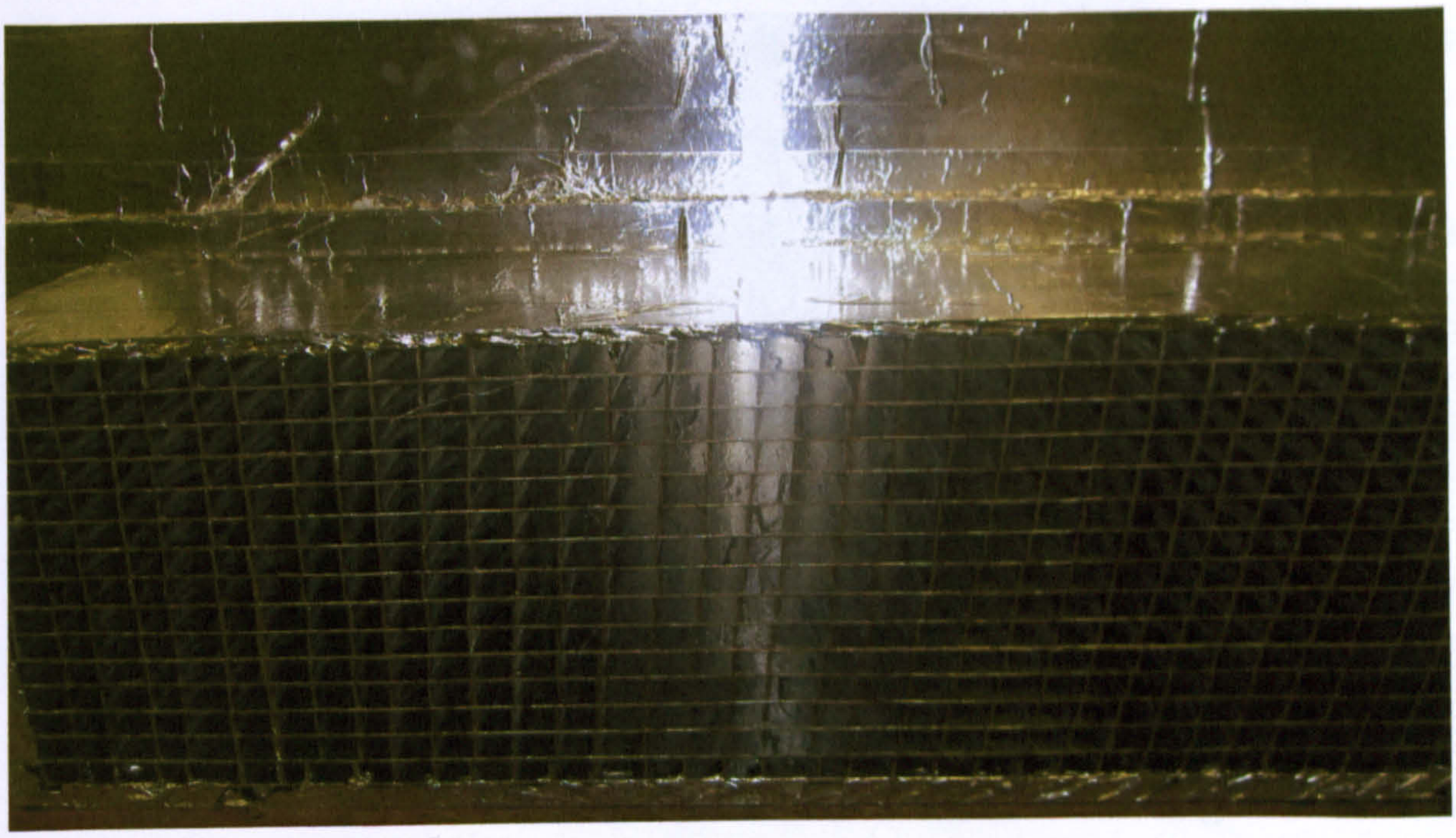

Figure 6.57: Showing the end of the honeycomb slat with light reflecting on it.

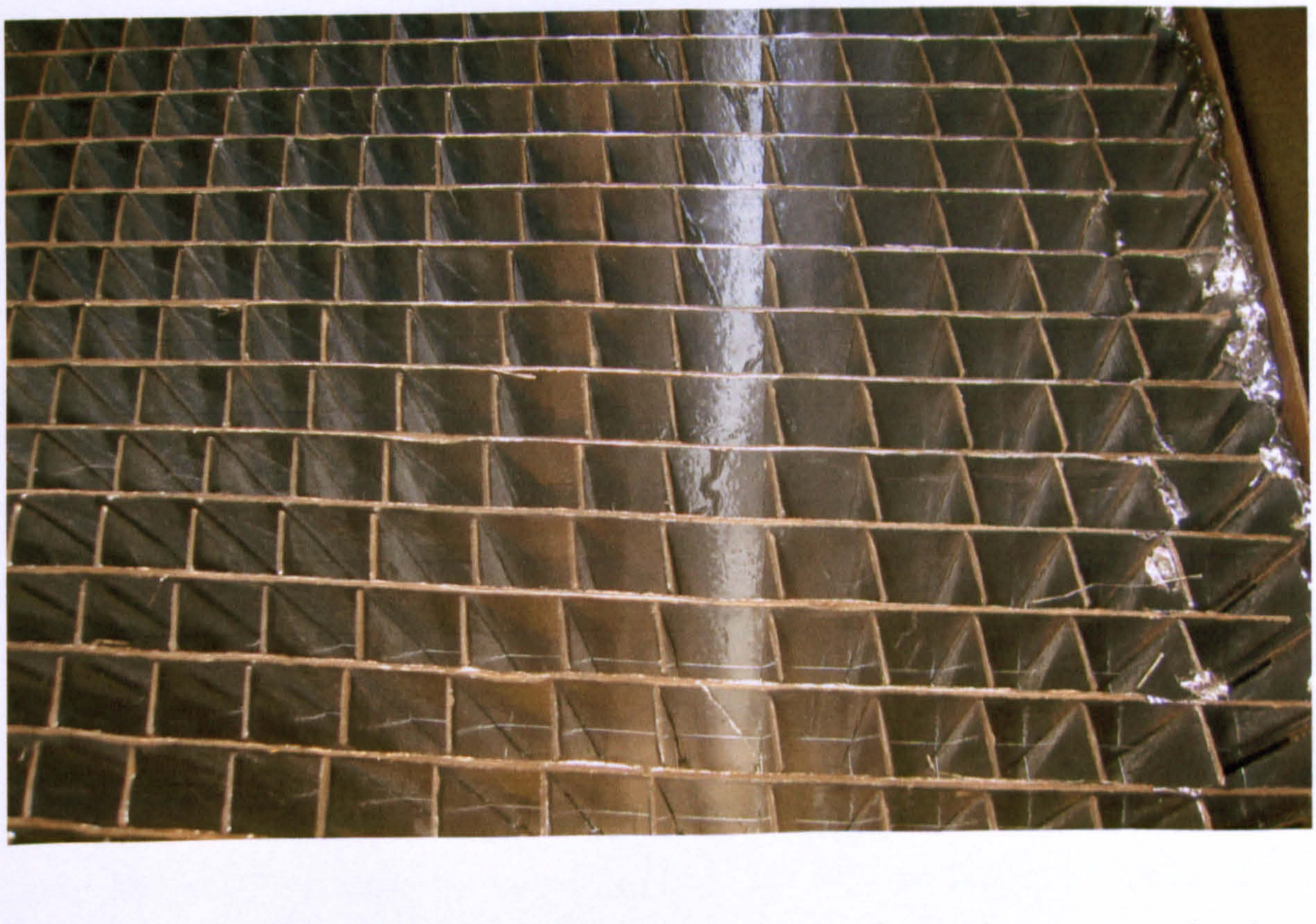

Figure 6.58: Showing the bird eye view of the honeycomb slats.

The total amount of corrugated cardboard needed for coating was in the region of 3420m^2. Each honeycomb slat was 1000mm in length by 200mm in height with 10mm thickness. Therefore a total of 1750 honeycomb slat were to be coated both sided with the aluminium foil tape. This process of coating the honeycomb Slats had taken over three months to complete.

The next chapter Seven will deal with the experimental method and will also deal with the honeycomb installing in the test chamber and the laboratory investigation into the effect that displacement ventilation and chilled ceiling as one system have on the airflow pattern without and with honeycomb slat attached to the ceiling.

Chapter Seven

7.0 Experimental method

7.1 The experimental facility

The experiments were conducted in the experimental test chamber at the department of Civil and Building Engineering at Loughborough university, England. The environmental test chamber is of a size representative of a two-person office and has internal dimension of 5.4m long, 3.0m wide and 2.8m height (figure 7.1). The long axis of the room is aligned nearly West-East. The room is not quite symmetrical owing to a column part way along the south wall and has a net floor area of 16.2m^2. The chamber is constructed on the first floor of a laboratory building with its southerly wall formed by the external wall of the building and has two small windows, which have seven panels on wood and steel frame, to allow day lighting for some experiments. The walls of the chamber are constructed of plywood with insulating panels on a wood and steel frame. The test chamber floor is constructed from commercial raised floor panels over the laboratory floor slab (having a void space

between the test chamber floor and the laboratory floor of approximately 75mm); the test chamber floor is carpeted. The roof of the test chamber is constructed with a plywood outer skin and insulating panels on a steel frame with a plenum of 325mm depth containing ventilation ductwork suspended over the false ceiling. The distance between the roof of the laboratory and the test chamber roof is approximately 1.5m.

The displacement ventilation system is formed by a semicircular diffuser on the centre-line of the shorter east wall of the test chamber and an "egg-crate" type extract grille above the door located at the other end of the room. The extract grill is 200mm high and 600mm long located above the door, at 2.5m above the floor level and is shown in figure 7.4.

The supply diffuser is 700mm high and 400mm diameter and is of type QL-180 manufactured by Trox Brother Ltd. The supply grille is constructed with a perforated metal face with square holes and a foam rubber sheet behind, having a free area in the region of 80 % and is shown in figure 7.5.

The chilled ceiling is constructed from a proprietary system of metal tiles 1.65m long 0.3m wide occupying above 88% of the

total ceiling area (this is the maximum active area that could be achieved after allowing space for the ceiling support system).

The panels are of type WK-DU-M manufactured by Trox Brother Ltd. and consist of an array of copper tubes fixed to a perforated metal sheet. The tubes are in contact with the rear of the metal ceiling tile and are oval in shape to increase the contact area. Foil insulating panel approximately 25mm thick is attached onto the top of the tile over the tubes and backing plate. (See figure 7.6 and 7.7)

The air supply for the displacement ventilation system is ducted from the laboratory air handling plant consisting of a fresh air inlet and filter, a direct expansion cooling coil, a thermistor controlled electric heating element, and a variable speed supply air fan and exhausted directly to outside (figure 7.2). Cooling to the air stream is provided using a direct expansion heat exchanger connected to a refrigeration plant with a compressor and water-cooled condenser (figure 7.3). The heater batteries and cooling coil are controlled via electronic controllers connected to thermocouple sensors. The temperature of the air stream can be controlled to $(\pm)0.1°C$. The airflow rate through

the supply and extract streams is measured with a multi-hole orifice device with the pressure drop measured on a fluorocarbon manometer.

Chilled water is supplied to the ceiling panel system from a central chilled water buffer tank. Water is circulated from the tank by a fixed speed pump through a three port mixing valve which is used to control the temperature of the water entering the chilled ceiling panel circuits.

The valves have an electric actuator controlled from a separate electronic PID controller using a thermocouple sensor. The pump flow rate is high enough to ensure a temperature difference of only 2-3K across the chilled ceiling panel system and so minimise any temperature difference across the ceiling surface. The chilled water supply temperature is divided into six parallel circuits that are in turn connected to groups of five ceiling panels connected in series. Each of the six secondary circuits has a rota meter flow measuring device to enable the division of the flow to be checked and recorded.

Internal heat loads were simulated using two sizes of cuboids boxes containing single domestic light bulbs of various wattages

(ranging form 60 Watts to 150 Watts). The boxes were 300mm cube of 2m height (figure 7.8), and the other is 300mm x 300mm x 300mm height standing on a table (figure 7.9). The boxes were painted matt black and had a series of ventilation holes around the sides to allow some airflow through the box by natural convection.

7.2 Air temperature measurements

The test chamber air temperature was taken using Type "T" copper constantan thermocouples giving an accuracy of $^{+}$.0.2°C, mounted on a vertical stand at various heights, to allow measurements of the vertical room air temperature. The air temperature were recorded manually and then later plotted. The sensors were closely spaced near the floor and ceiling where the air temperature gradient is expected can been seen in Figures 7.10, 7.11, and 7.12.

7.2.1 Air velocity measurements

Air velocity accurate to $^{+}$.0.1 ms^{-1} was taken using a hand held measurer at the same height as the temperature sensor points.

7.2.2 Mean radiant temperature

The mean radiant temperatures were taken at three heights 0.1m 0.6m and 1.1m in the centre of the room. The mean radiant temperature was established using a B&K indoor climate analyser.

7.2.3 Relative humidity

The wet bulb and dry bulb temperatures were taken in the room and then using the psychometric chart to determine relative humidity.

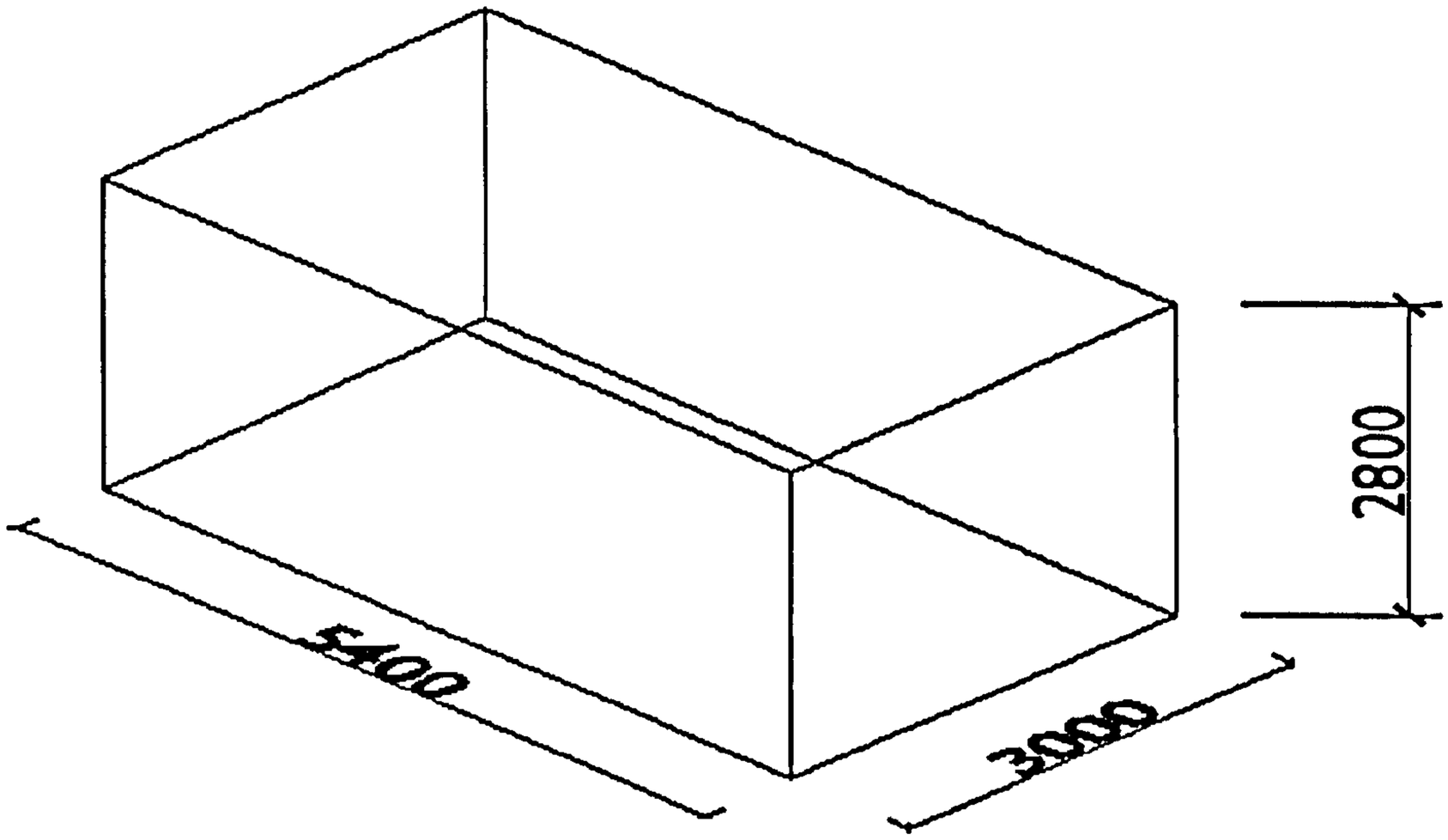

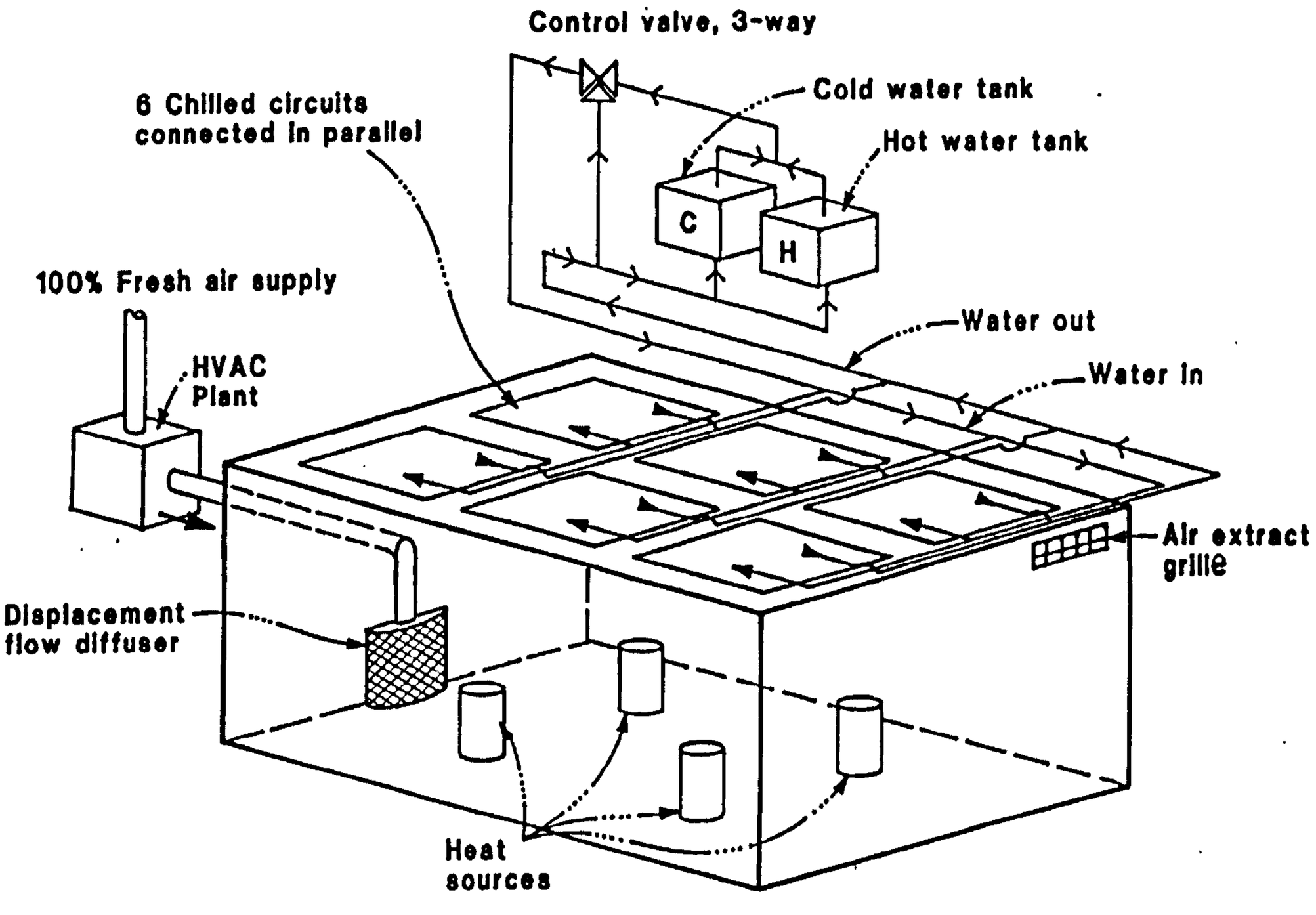

Figure 7.1. Schematic diagram of the room being modelled

Figure 7.2: Showing the test chamber in the laboratory

Figure 7.3: Air heating unit, supplying the inlet air to the test chamber.

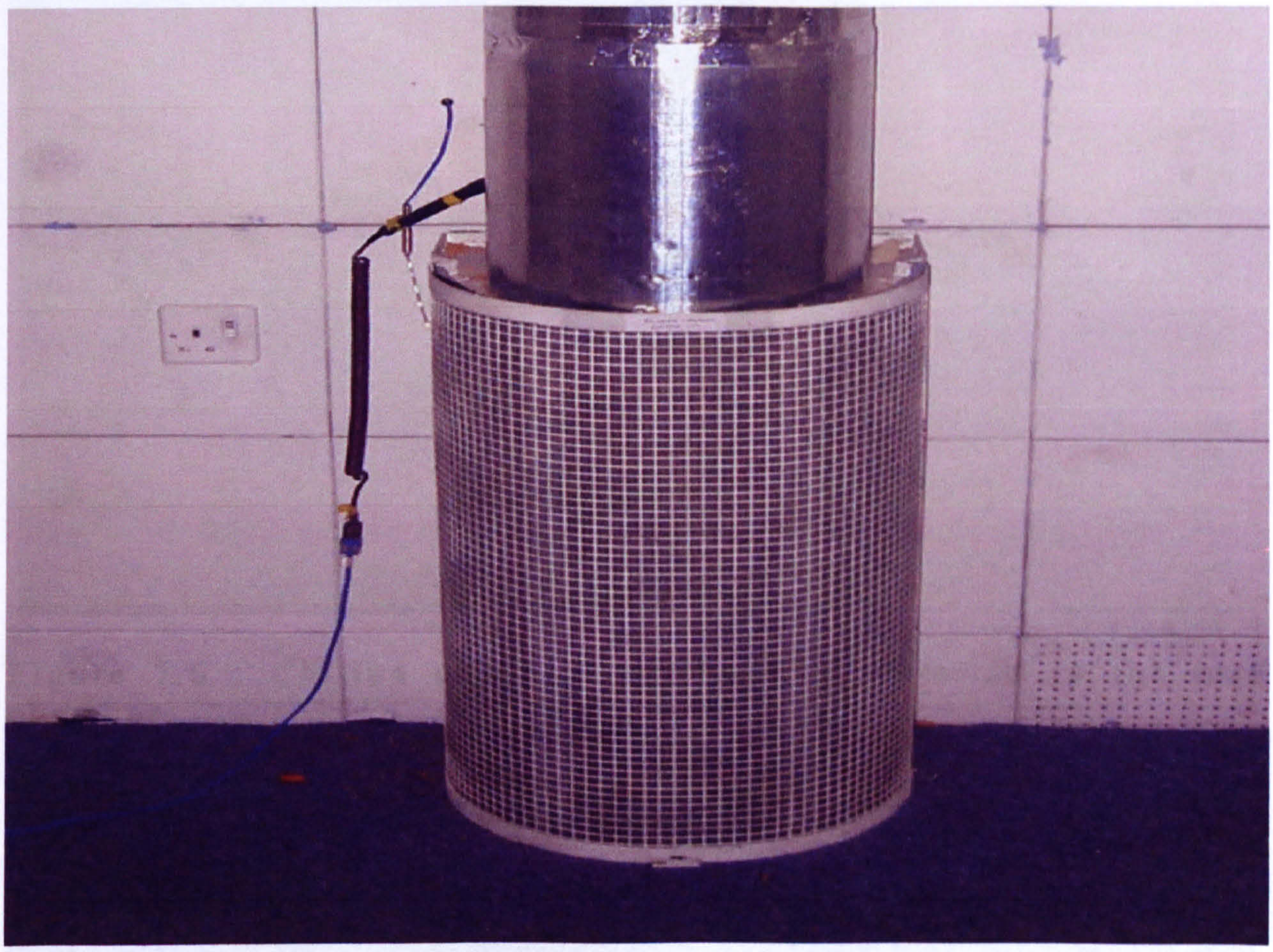

Figure 7.4 : Displacement ventilation supply air inlet with a temperature sensor monitoring the room air inlet temperature.

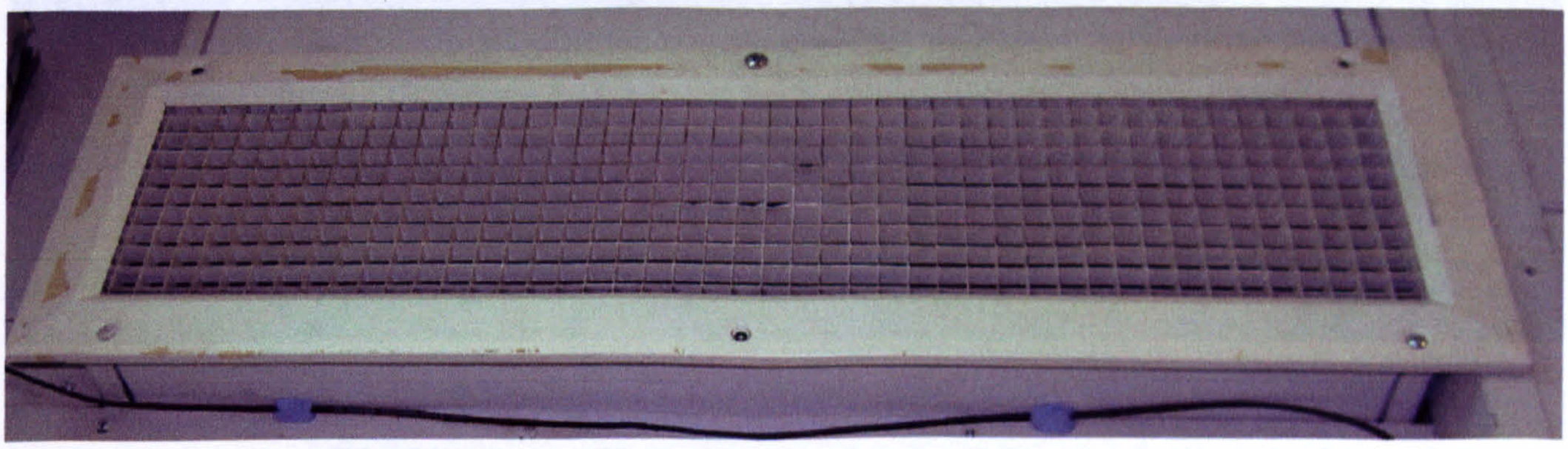

Figure 7.5 : Extract air vent, used to extract the room air flow.

Figure 7.6 : Chilled ceiling panel being installed in the test chamber.

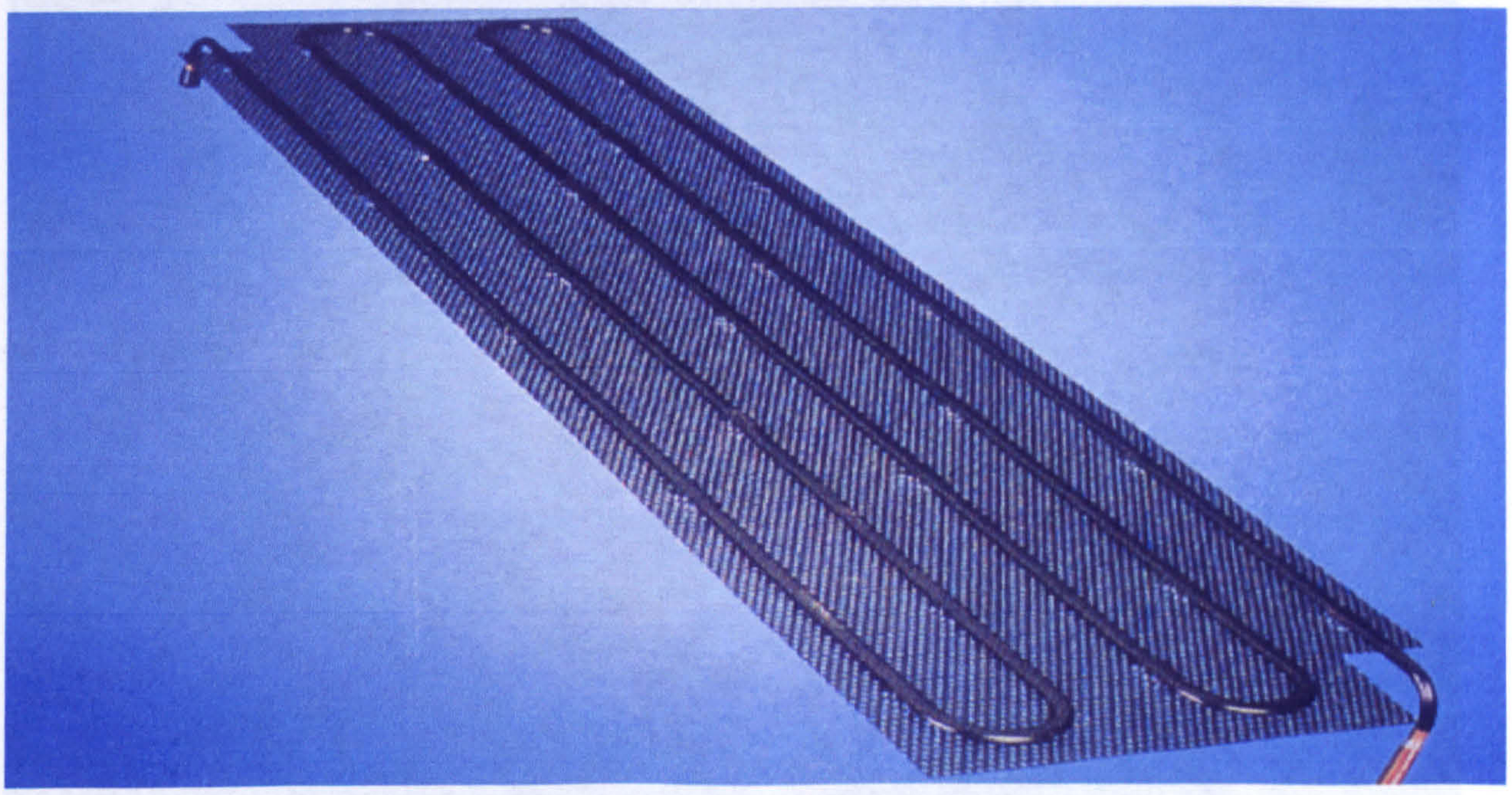

Figure 7.7 : Chilled ceiling panel showing pipe work, without the external metal panel.

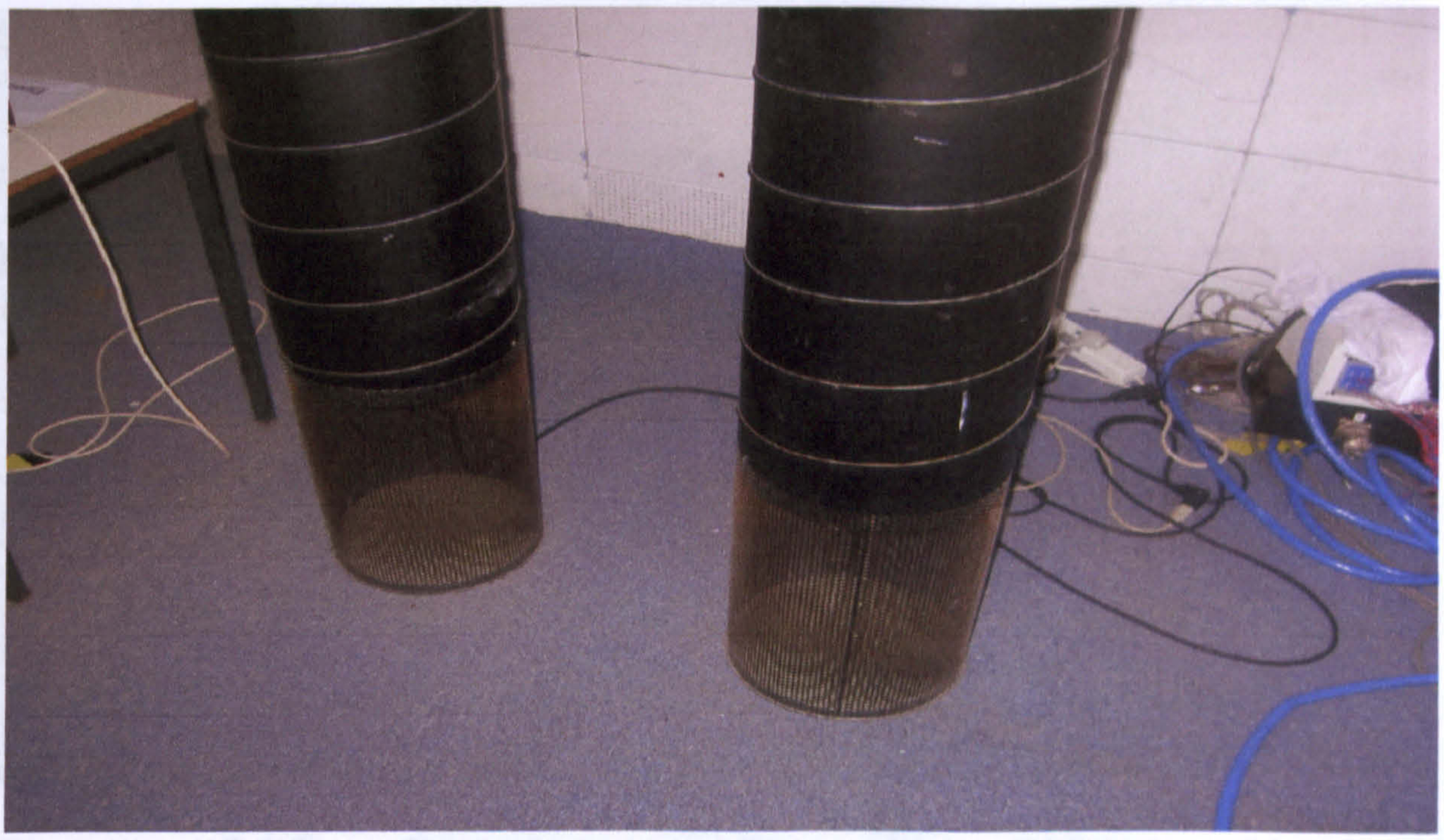

Figure 7.8: Heat sources (dummies) used for the experiments

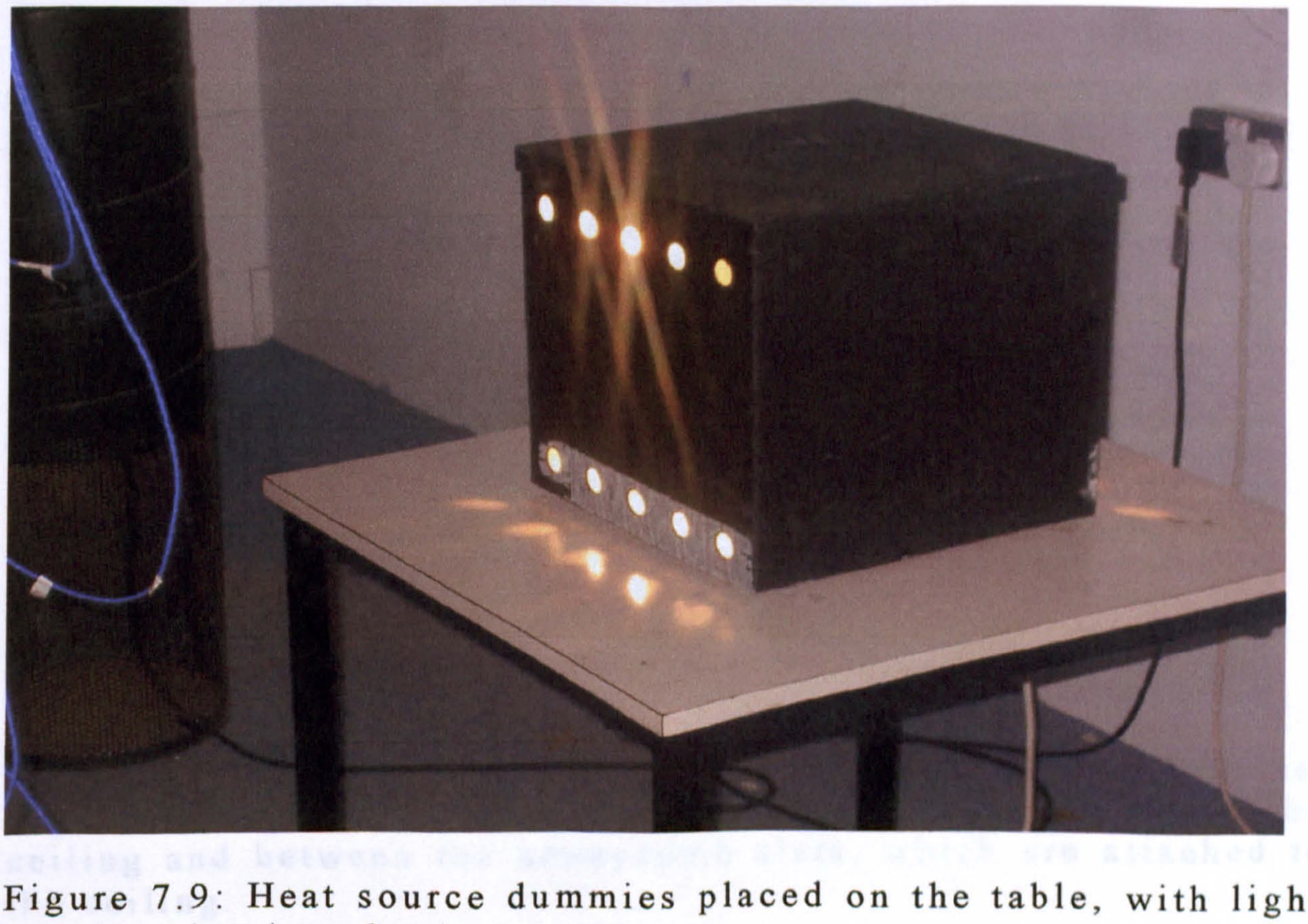

Figure 7.9: Heat source dummies placed on the table, with light representing heat load.

Figure 7.10: Showing Type "T" copper constantan thermocouples, mounted on vertical stand at various heights, to allow measurements of the vertical room air temperature. Also the honeycomb slat attached to the ceiling are seen.

Figure 7.11: showing type "T" copper constantan thermocouples, mounted on vertical stand to measure air temperature near the ceiling and between the honeycomb slats, which are attached to the ceiling.

7.3 Experimental procedure and test conditions.

The aim of the first stage of the lab work was to characterise the room conditions and establish if such conditions can be reproduced. The first set of results showed that the condition were not in agreement with those that were produce by Taki and Loveday (1996). It was also found that the air change per hour (ACH) was fluctuating through the experiment.

It was found that outside air entering the external opening of the displacement ventilation unit resulted in the fluctuation of the air rate. This led to a situation where it was difficult to accurately control air changes per hour. To overcome this problem it was decided that the air should to be drawn from the laboratory space and be used for the test chamber. This would provide a stable and more accurate airflow rate for the test conditions.

For the designer (first) test conditions it was found that due to the above change it was possible to achieve a constant required air velocity for all the test conditions.

The test conditions were sometimes difficult to reproduce due to the incidental solar heat gain across the wall, which is exposed to the outside environment. It was decided that the test chamber should only be used in the evening and night, as this would reduce the possibility of such heat gains giving better controlled conditions. The designer (first) test conditions were carried out after 3:30pm, which resulted in two test conditions each day. The test room was left in operation over night prior to each experiment to achieve steady state conditions and 4 hours were allowed between 2 consecutive test conditions.

A set of boundary conditions were set in the test chamber, to gain confidence in the test chamber performance and the laboratory equipment. It was essential that all the test conditions carried out can be reproduced at a later date for verification and further testing.

The following boundary conditions were tested, heat load of 62w/m^2 imposed using seven heat dummies (figure 7.8, 7.9). An inlet air change rate of 4 ACH, for both combined chilled ceiling and displacement ventilation operation and also for chilled ceiling only operation figure 7.13 show the test chamber layout.

The chilled ceiling temperatures tested were 21, 18, 16 14 and 12°C. The above test conditions were set, and the vertical air temperature profiles were recorded. The first set of results in figure 7.12 are shown with A next to the ceiling boundary conditions and the second test conditions results are shown with B next to the ceiling temperature in figure 7.12.

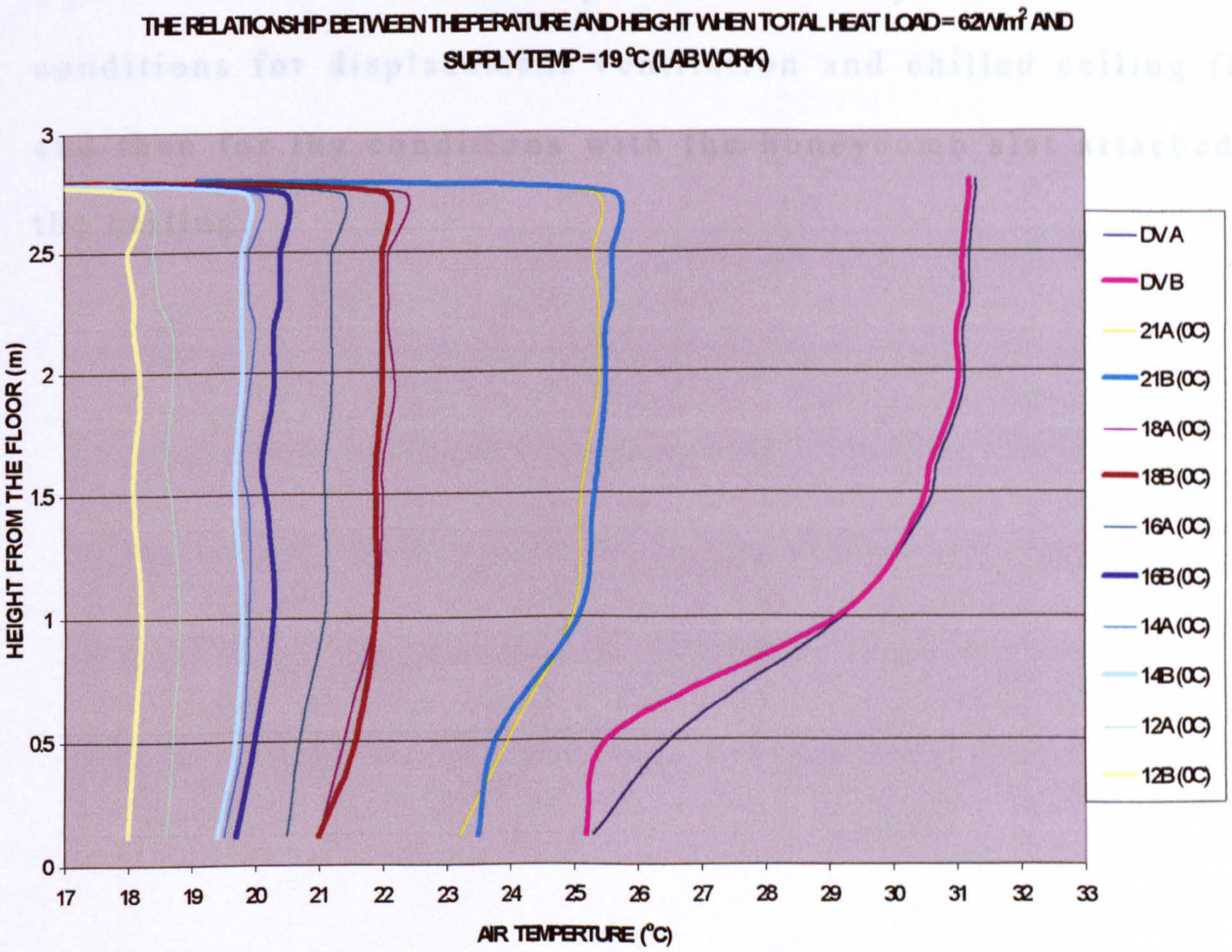

Figure 7.12: Graph showing results that the same test conditions can be repeated and obtain similar results.

The results in figure 7.12 show that for the same imposed test conditions it is possible to recreate the same room thermal conditions in terms of the identical air temperature profiles. The results also show that at low ceiling temperatures the displacement airflow pattern is strongly disturbed.

The results mean that it is possible to carry out the entire test conditions for displacement ventilation and chilled ceiling first and then for the conditions with the honeycomb slat attached to the ceiling.

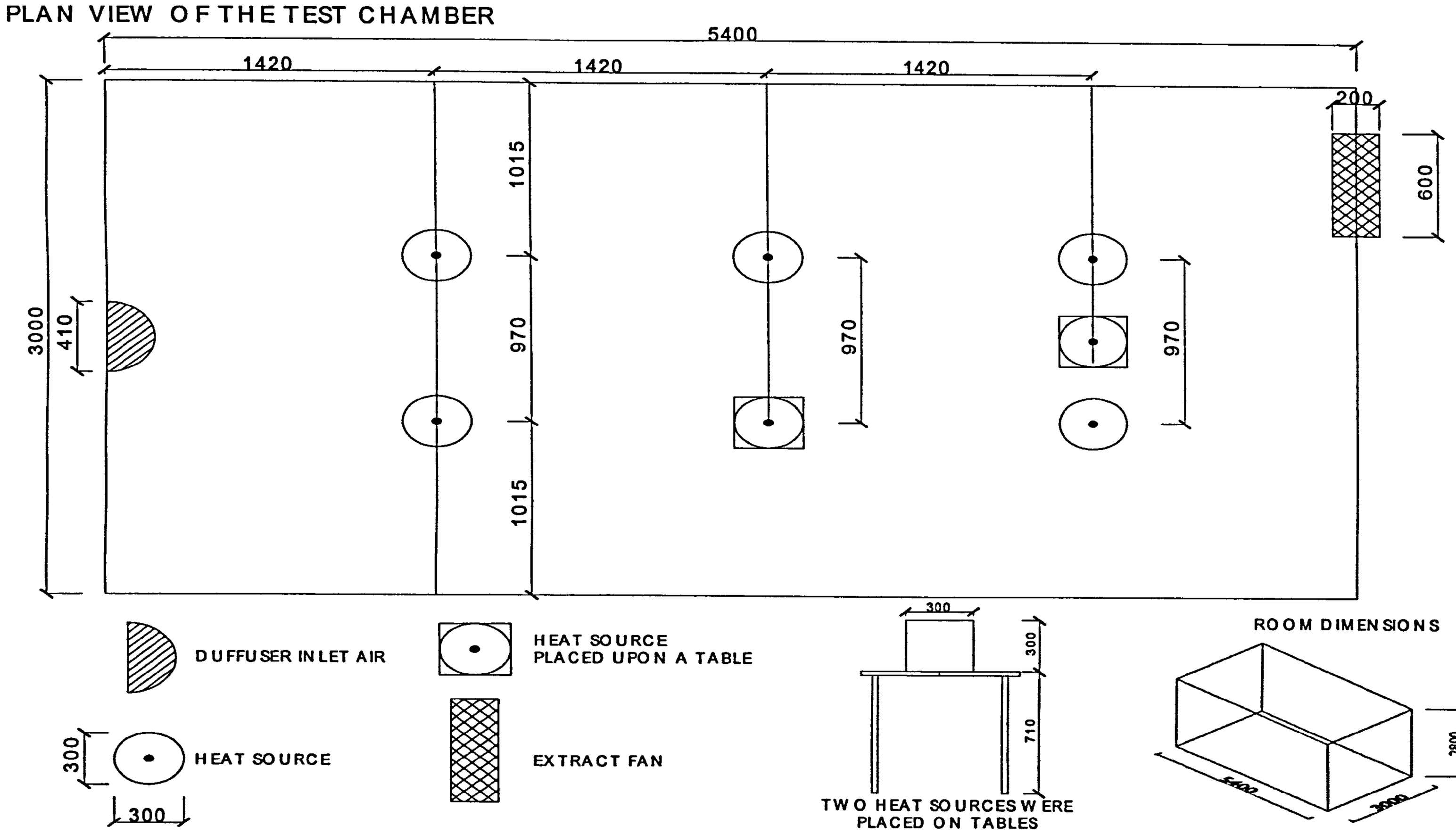

Figure 7.13 showing the test chamber dimensions with the relevant equipment.

7.4 Summary

- To set up conditions of displacement ventilation for at least 12 hours.

- When setting up the next chilled ceiling temperature conditions a minimum of 3.5 hours is required for the test chamber to be fully settled.

- Try to set the chilled ceiling temperature conditions in order of temperatures as this would save time for the conditions to settle in the test chamber (i.e. 21°C–18°C–16°C etc).

- To record the Air temperature results of test chamber before entering the room to measure velocity of the Diffuser, the Extract and the ceiling temperature.

- To take ceiling temperature measurements at the centre of each chilled ceiling circuit. (there are six circuit in the test chamber) Important not to take ceiling temperature

directly above a heat source as this will give inaccurate results of the ceiling temperature.

- It is important to use the correct measuring equipment, the equipment should comply with the requirement as prescribed in ISO 7730.

- To summaries it is possible to recreate the same test conditions and obtain similar results

The next chapter will investigate the experimental measurement for displacement ventilation system, the combined system of displacement ventilation and chilled ceiling without and with Honeycomb slat attached to the ceiling for various ceiling temperatures and various air changes per hours (ACH). Also it will discuss findings on the use of honeycomb slat in the combined system.

Chapter Eight

8.0 Experimental results

8.1 Introduction

The experimental results that were carried out in the test chamber at Loughborough university, are presented and discussed in this chapter. The experiments were conducted with two main purposes in mind.

To investigate the performance of the chilled ceiling and displacement ventilation systems operated together and for the displacement ventilation system generated alone.

To investigate a new technique for achieving stable conditions for displacement airflow. The technique used here was the attachment of a honeycomb slat system to the chilled ceiling, for suppressing downward cool natural convection and hence re introducing the displacement airflow pattern.

The principle results presented primarily in the form of tables and graphs showing air temperature profiles above the floor for a range of conditions. These profiles contain a large amount of data regarding the performance of the system and provide an indication of the extent of mixing or stratification of the air at different heights.

The room vertical temperature profiles in all cases are based on Thermocouple measurements taken after a minimum of 4 hours between test conditions, and are recorded manually and then later plotted.

8.2 Test conditions

A series of measurements was undertaken to confirm the displacement floor pattern in the absence of the chilled ceiling and Honeycomb slat system. The experimental procedure adopted was to measure the vertical air temperature profile in the room for the set of design conditions mentioned in table 8.1; for all the test conditions, the inlet air supply temperature introduced into the room was 19°C.

Test case	Heat load (W/m^2)	ACH= 2	ACH= 4	ACH= 6	ACH= 8
1	32	X	X		
2	43	X	X	X	X
3	52	X	X	X	X
4	62	X	X	X	X

Table 8.1: list of experimental test conditions carried for the Displacement ventilation systems only.

The results for the above test cases are shown in figures 8.1 to figure 8.4.

8.2.1. The displacement ventilation test cases.

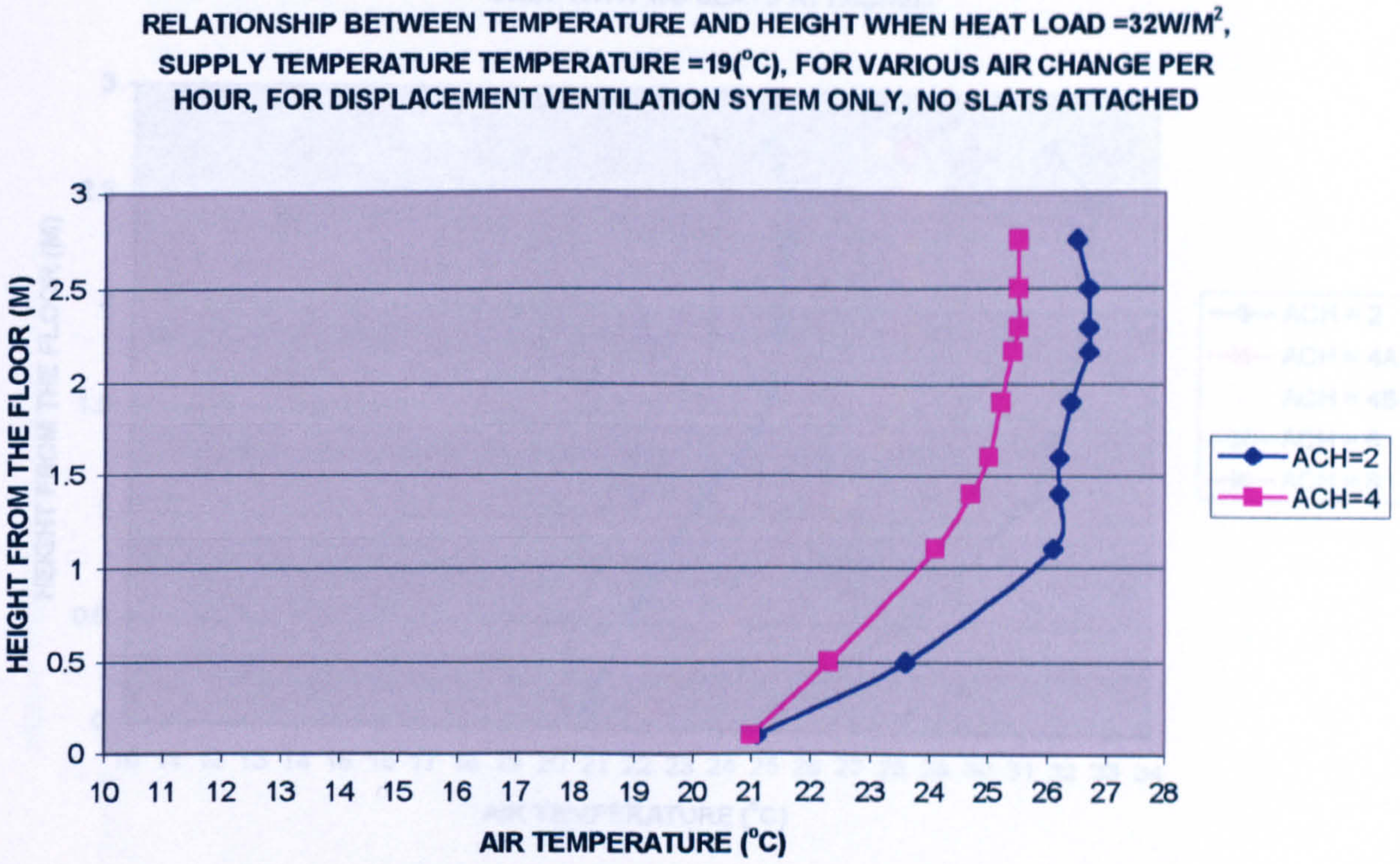

Figure 8.1: Graph showing the results for test case 1

The result shows that at a heat load of 32W/m^2, the displacement ventilation profile is clearly seen. The stratification can also be seen and is at 1.5m height above the floor. It can also be seen that at ACH of 2 and 4, the displacement ventilation system is unable to meet the guidelines of the International Standards (ISO 7730) 1994, on thermal comfort, that is the vertical temperature gradient should be less than 3°C per metre. (the temperature difference between head and foot for a seated person).

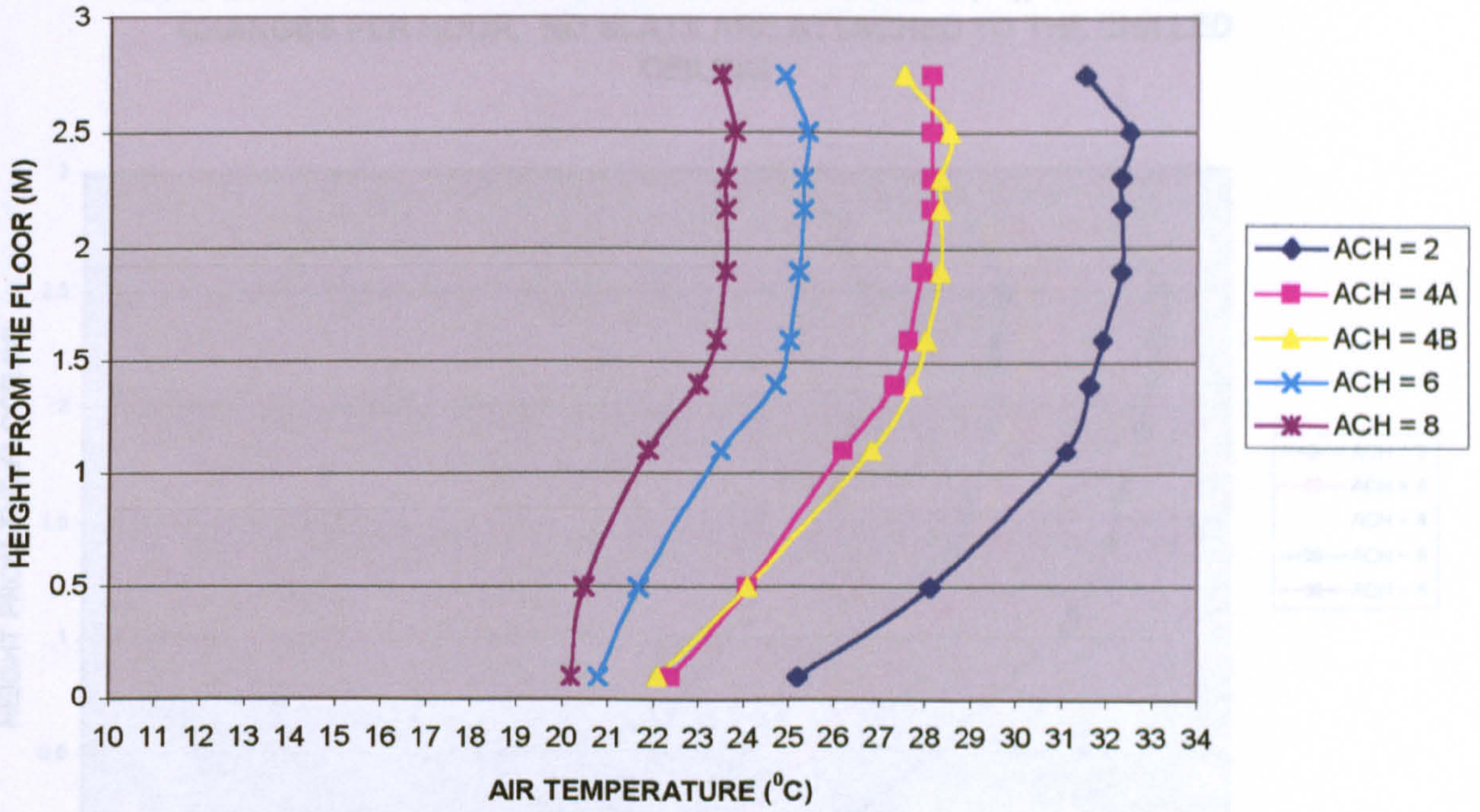

Figure 8.2: Showing the results for test case 2

The result shows that at a heat load of 43W/m^2 the displacement ventilation profile is also clearly seen. The stratification can also be seen and is above 1.5 heights from the floor. The graph also shows that at low ACH, i.e. 2 and 4 the displacement ventilation system is unable to meet the guidelines of the International Standards (ISO 7730) 1994. But at higher ACH such as 6 and 8 the displacement ventilation system is able to satisfy the requirement. At ach of 8 the displacement airflow pattern and the air temperature gradient is reduced to 1°C for 1 metre height, where for ach of 2, this gradient is 6°C.

THE RELATIONSHIP BETWEEN THE AIR TEMPERATURE AND HEIGHT WHEN HEAT LOAD = 52W/M^2, SUPPLY AIR TEMPERATURE 19(^{0}C), DIFFERENT AIR CHANGES PER HOUR, NO SLATS ARE ATTACHED TO THE CHILLED CEILING

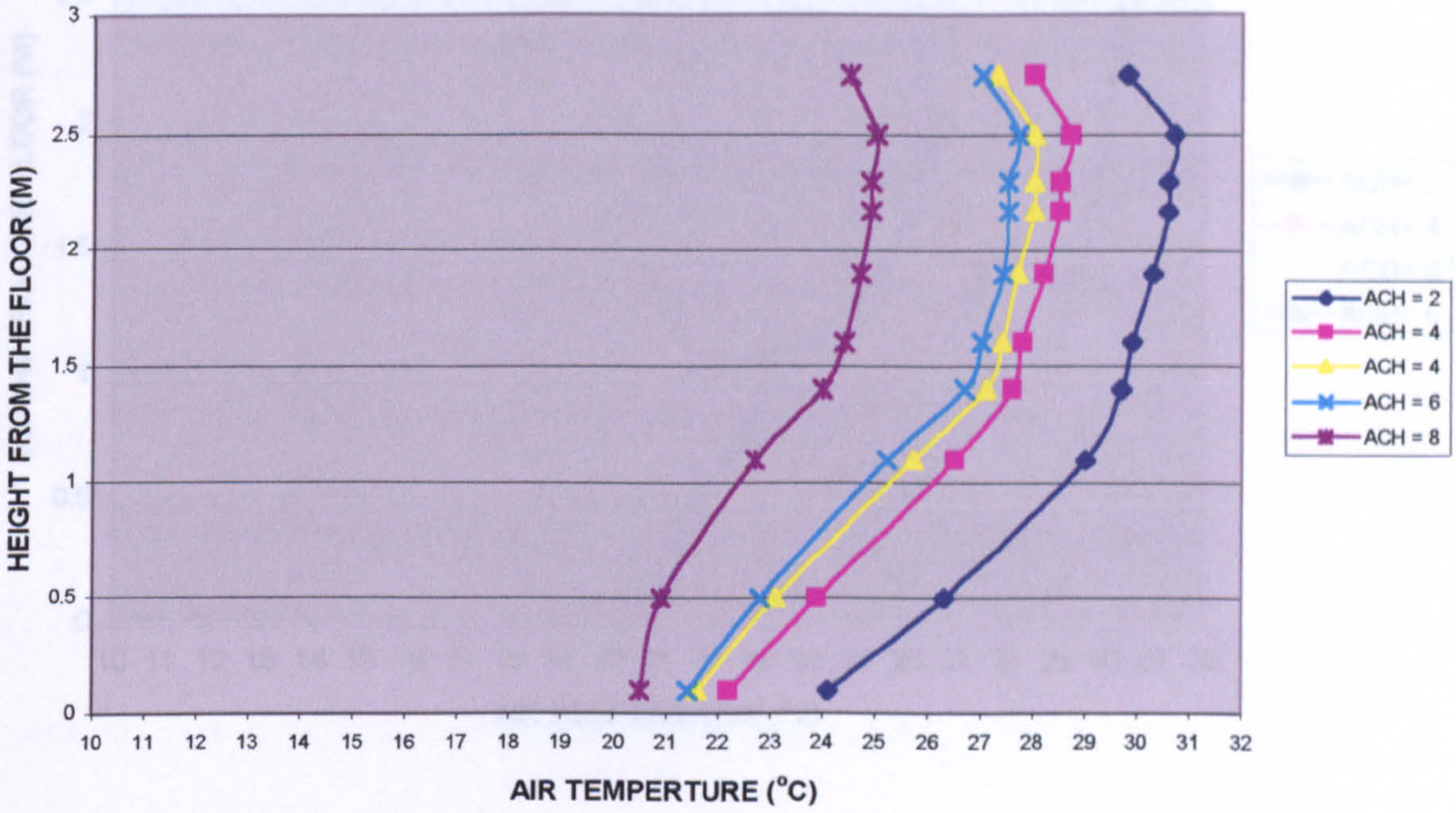

Figure: 8.3 Showing the results for test case3.

The results for air temperature profile for various ach suggest that the results for ach of 8 only meet the guidelines of the International Standards (ISO 7730) 1994.

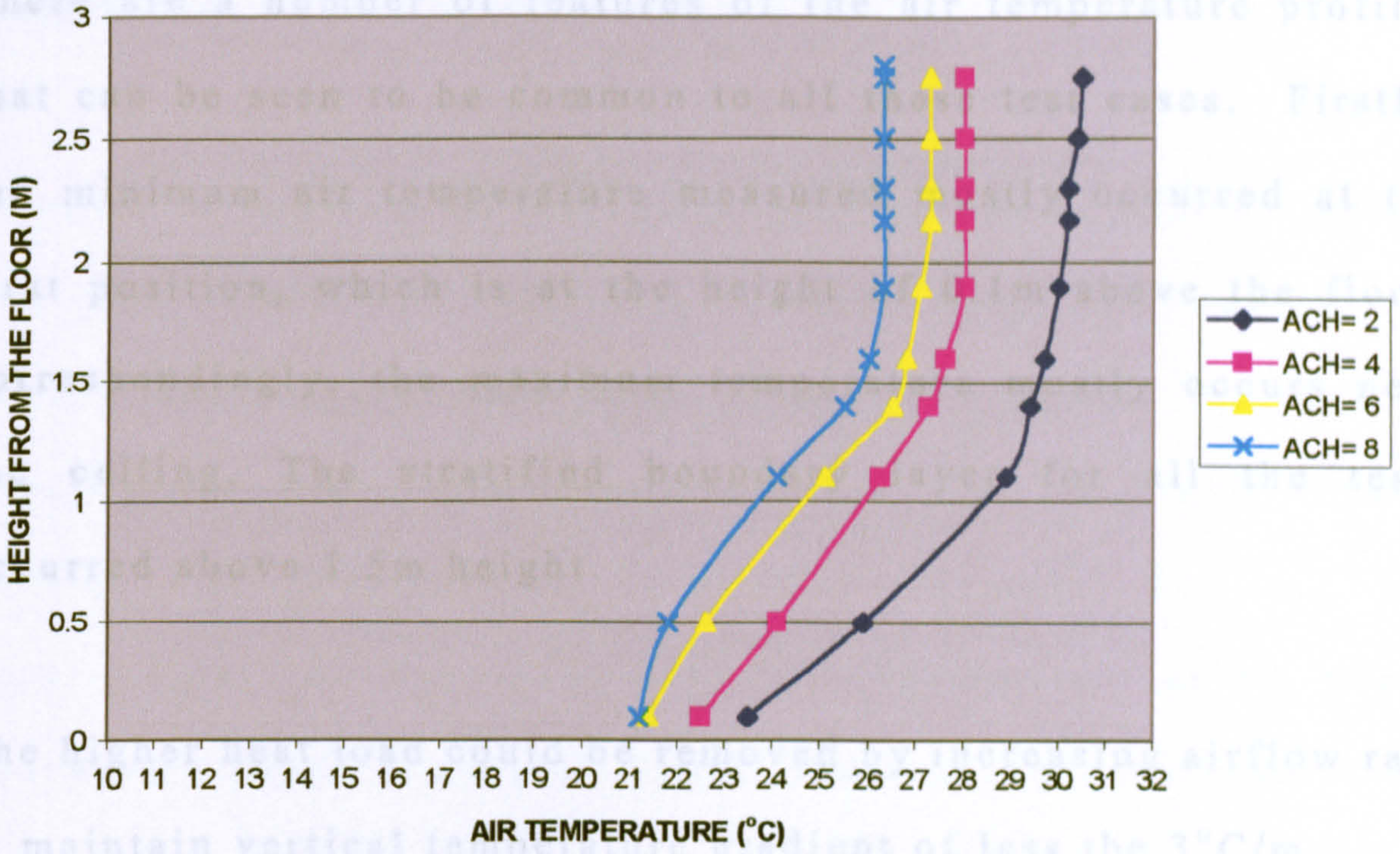

Figure: 8.4 Showing the results for test case4.

Figure 8.4 provides the results of the test case 4, showing air temperature profiles for different ACH. The results show that to remove a typical office heat load of 62W/m^2 even high ach is not effective in removing the heat load. Additional cooling system is required if this heat load is needed to be removed. This additional system is radiant cooling (chilled ceilings).

8.3 Summary of the result for displacement ventilation

There are a number of features of the air temperature profiles that can be seen to be common to all these test cases. Firstly, the minimum air temperature measured mostly occurred at the first position, which is at the height of 0.1m above the floor. correspondingly, the maximum temperature mostly occurs near the ceiling. The stratified boundary layer for all the tests occurred above 1.5m height.

The higher heat load could be removed by increasing airflow rate to maintain vertical temperature gradient of less the 3°C/m.

To conform to the (ISO 7730) additional heat removing system is needed. One can either increase the number of diffusers but this will in return reduce the room space, or use chilled ceiling combined with displacement ventilation system.

8.4 The displacement ventilation and chilled ceiling test cases

8.4.1 Effect of ceiling temperature

In order to conform to the ISO 7730, the use of chilled ceiling was introduced with the displacement ventilation system to remove the higher heat load. Table 7.2 shows the list of experiments that were conducted for the combined chilled ceiling and displacement ventilation system. For all the experimental test cases the heat load is constant at 62 W/m^2, which represents a typical office cooling load, with inlet air temperature set at 19°C, having different ACH and ceiling temperature.

Test case	ACH	Ceiling temperature 18°C	Ceiling temperature 16°C	Ceiling temperature 14°C	Ceiling temperature 12°C	Ceiling temperature 21°C
5	2	X	X	X	X	
6	4	X	X	X	X	X
7	6	X	X	X		
8	8	X	X			

Table 8.2: shows the list of experimental test conditions carried for the combined displacement ventilation and chilled ceiling system.

Figures 8.5 to figure 8.8 show the results of the above tested cases in the form of room air temperatures profiles measured at various height in the room.

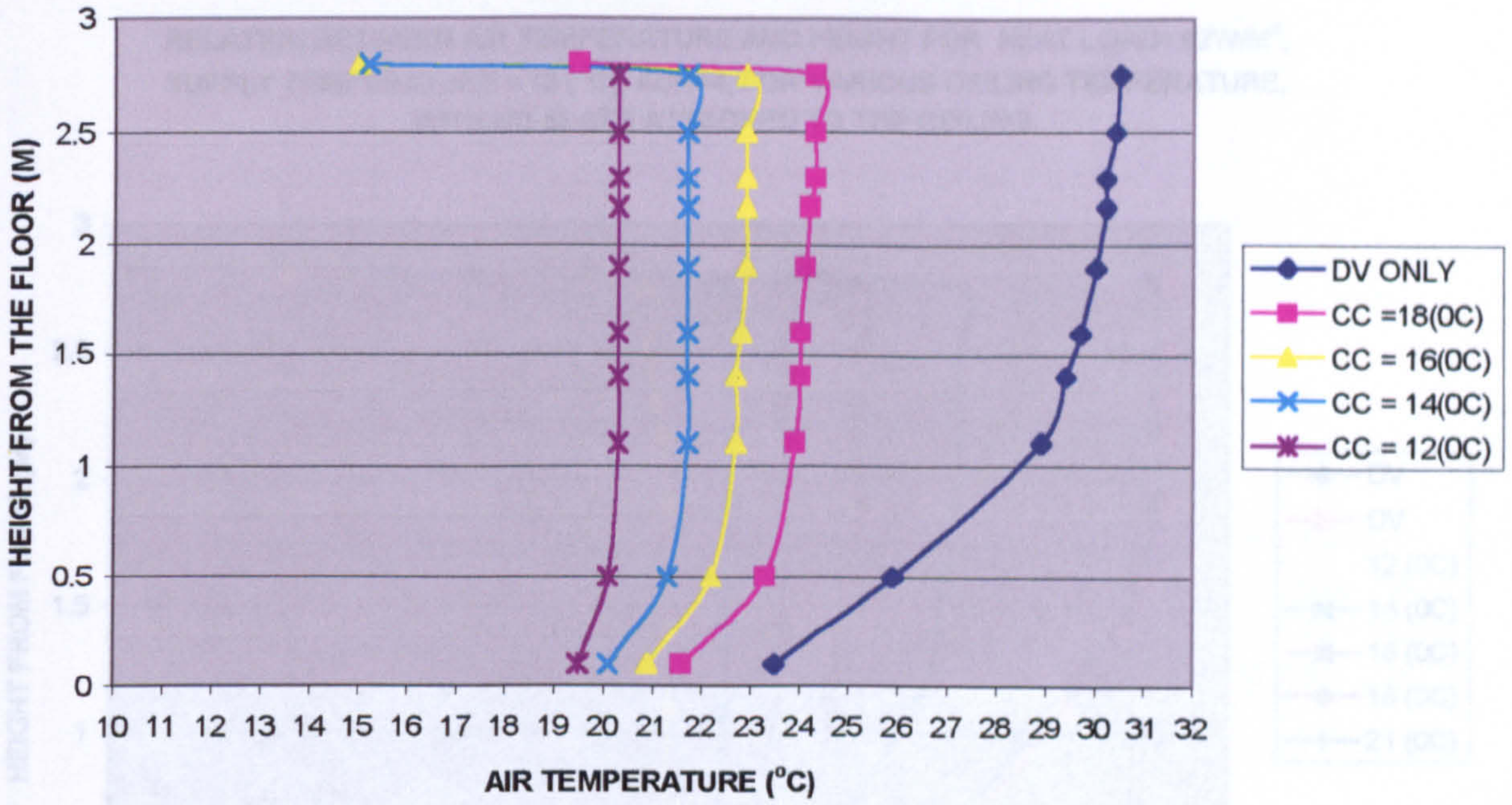

Figure 8.5: Shows the experimental test results for test case 5.

The results (figure 8.5) clearly show that in chilled ceiling/ displacement ventilation environments, higher heat loads could be removed and the requirements as presented in ISO 7730 standard could be met. However the results also show that the displacement flow pattern is disturbed and the stratified boundary layer has lowered towards the floor. Thus the mixing is occurring in the occupied zone resulting in a poorer air quality

environment. This takes place when the ceiling temperature is below 18°C.

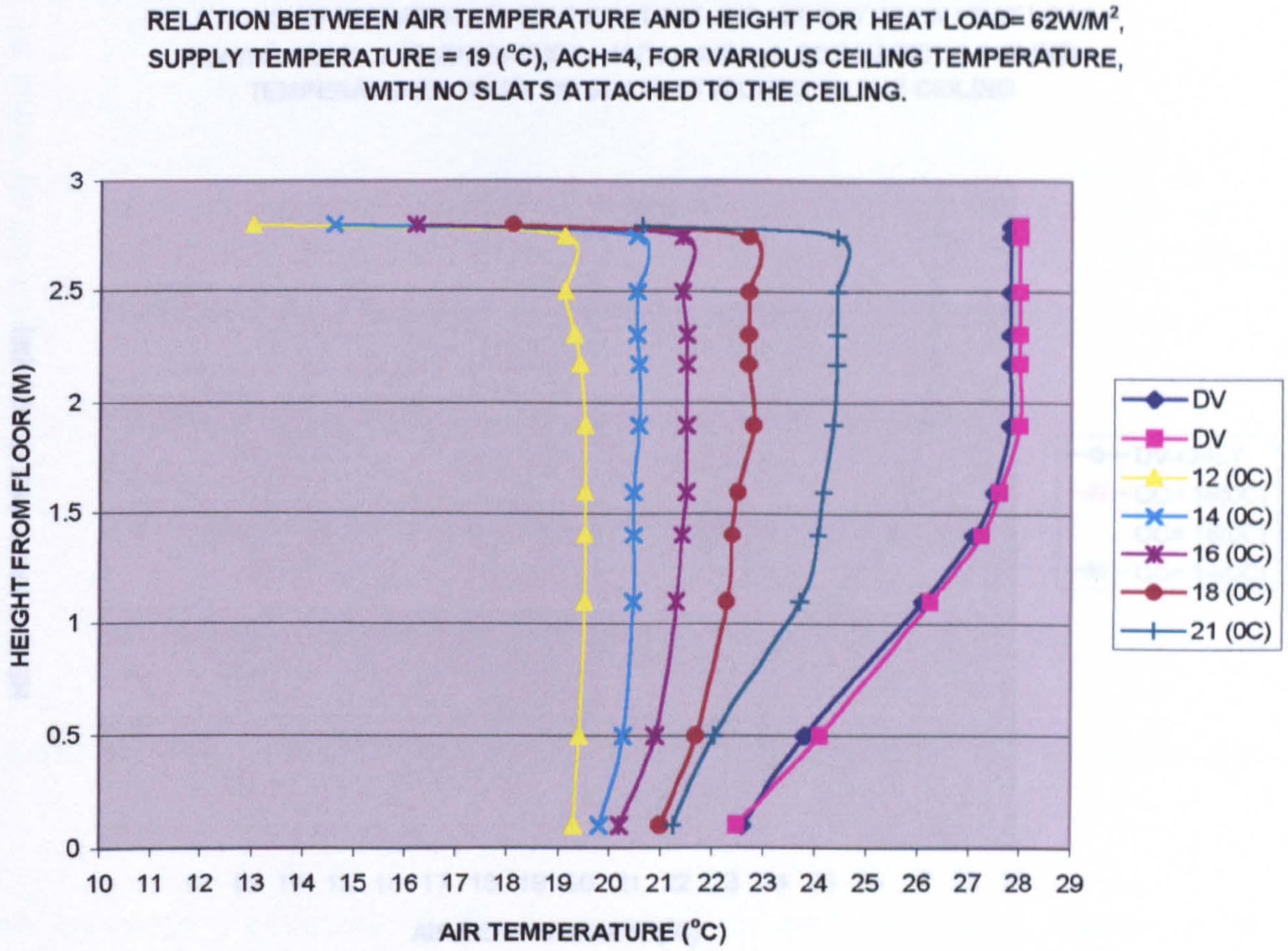

Figure 8.6: Shows the experimental test results for test case 6.

The results (figure 8.6) show that the increase in ACH from 2 to 4 has resulted in the distorting of the displacement airflow pattern for ceiling test conditions for 12°C 14°C 16°C and 18°C. Where as for ACH of 2 the displacement ventilation flow pattern is still present for these same ceiling air temperatures (figure

8.5), but for higher ceiling temperature of 21°C displacement airflow pattern is still present.

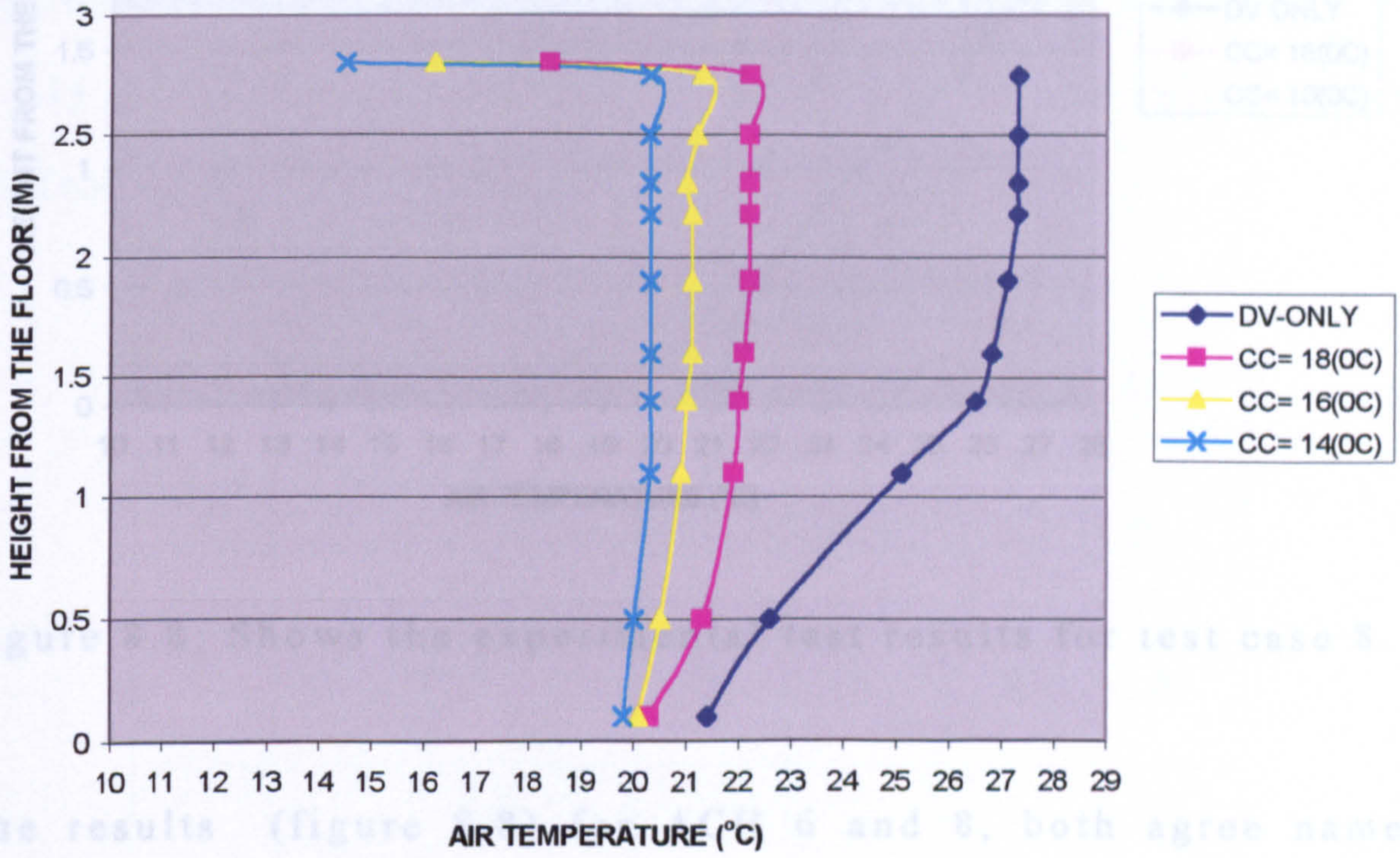

Figure 8.7: Shows the experimental test results for test case 7.

The results obtained were as expected, and show that when the ACH is increased to 6 it has an effect on the air temperature profile, it disturbs the displacement airflow pattern thus results in potentially poorer air quality in the occupied zone.

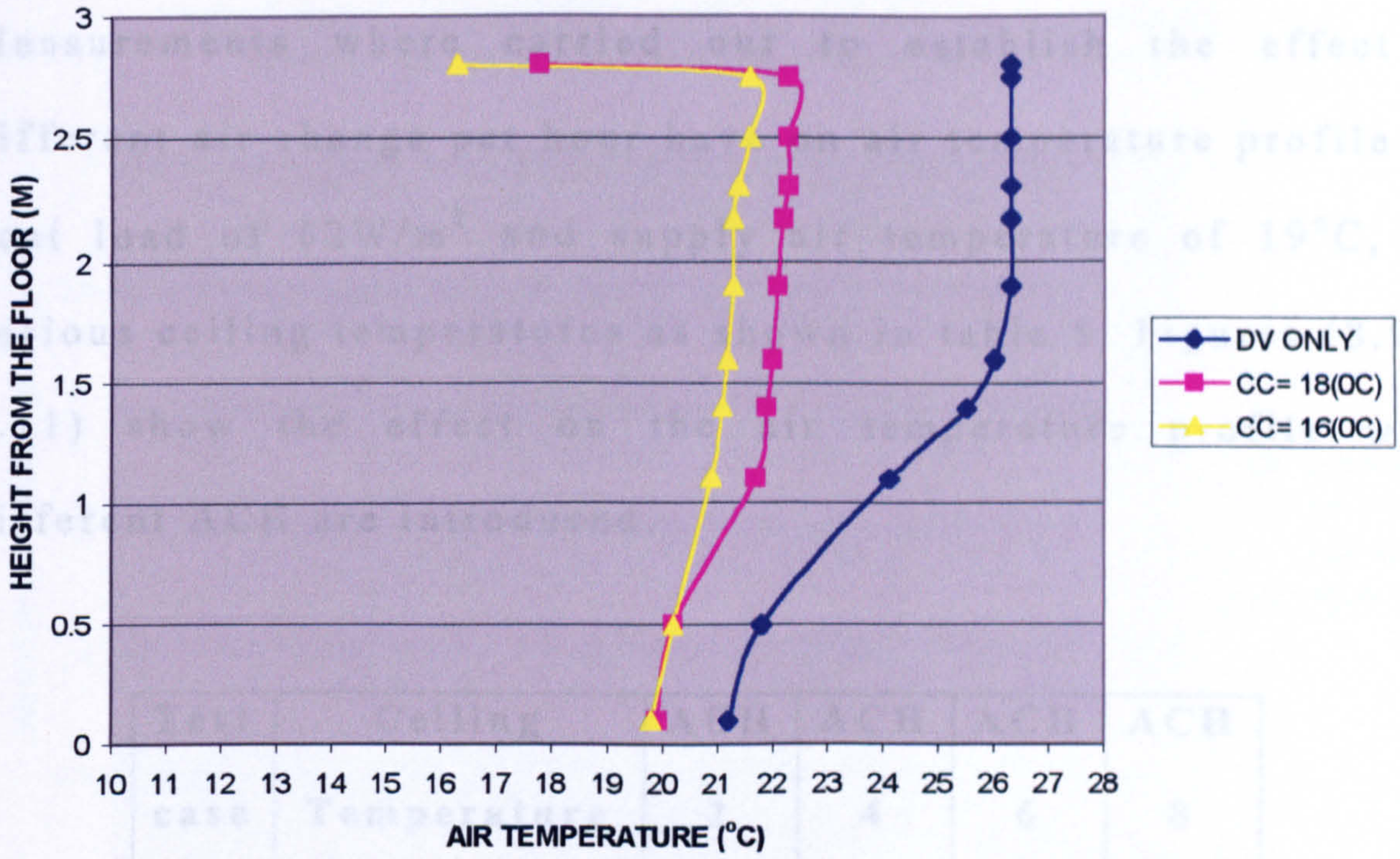

Figure 8.8: Shows the experimental test results for test case 8.

The results (figure 8.8) for ACH 6 and 8, both agree namely that at lower ceiling temperatures of 14°C and 16°C the displacement ventilation flow pattern has be completely distorted, but at ceiling temperature of 18°C some sign of displacement flow pattern can be still seen.

8.4.2 Effect of air changes per hours (ACH)

Measurements where carried out to establish the effect of different air change per hour have on air temperature profile for heat load of 62W/m^2 and supply air temperature of 19°C, for various ceiling temperatures as shown in table 8. Figures (8.9 to 8.11) show the effect on the air temperature profile when different ACH are introduced.

Test case	Ceiling Temperature	ACH 2	ACH 4	ACH 6	ACH 8
9	18°C	X	X	X	X
10	16°C	X	X	X	X
11	14°C	X	X	X	

Table 8.3 shows the test conditions that were carried out to investigate the effect of air change per hour for various ceiling temperatures.

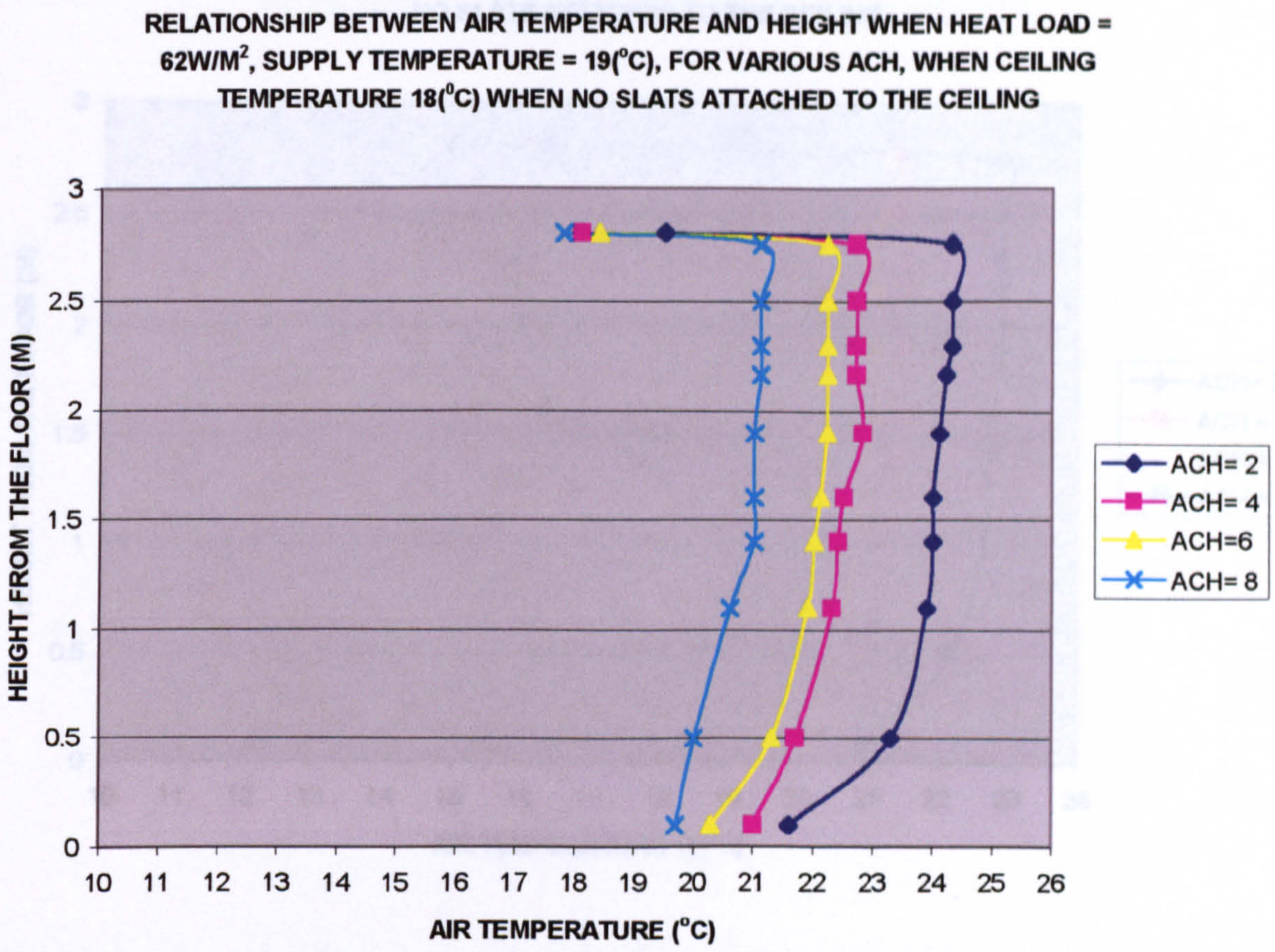

Figure 8.9: Showing the air temperature profile in the room for test case 9.

The results (figure 8.9) show that when ceiling temperature is set at 18°C. All the ach will comply with the requirements of ISO 7730, and for ACH of 2 and 4, a good displacement airflow pattern is seen. Therefore to remove the heat load even low ACH can be used thus saving on energy consumption.

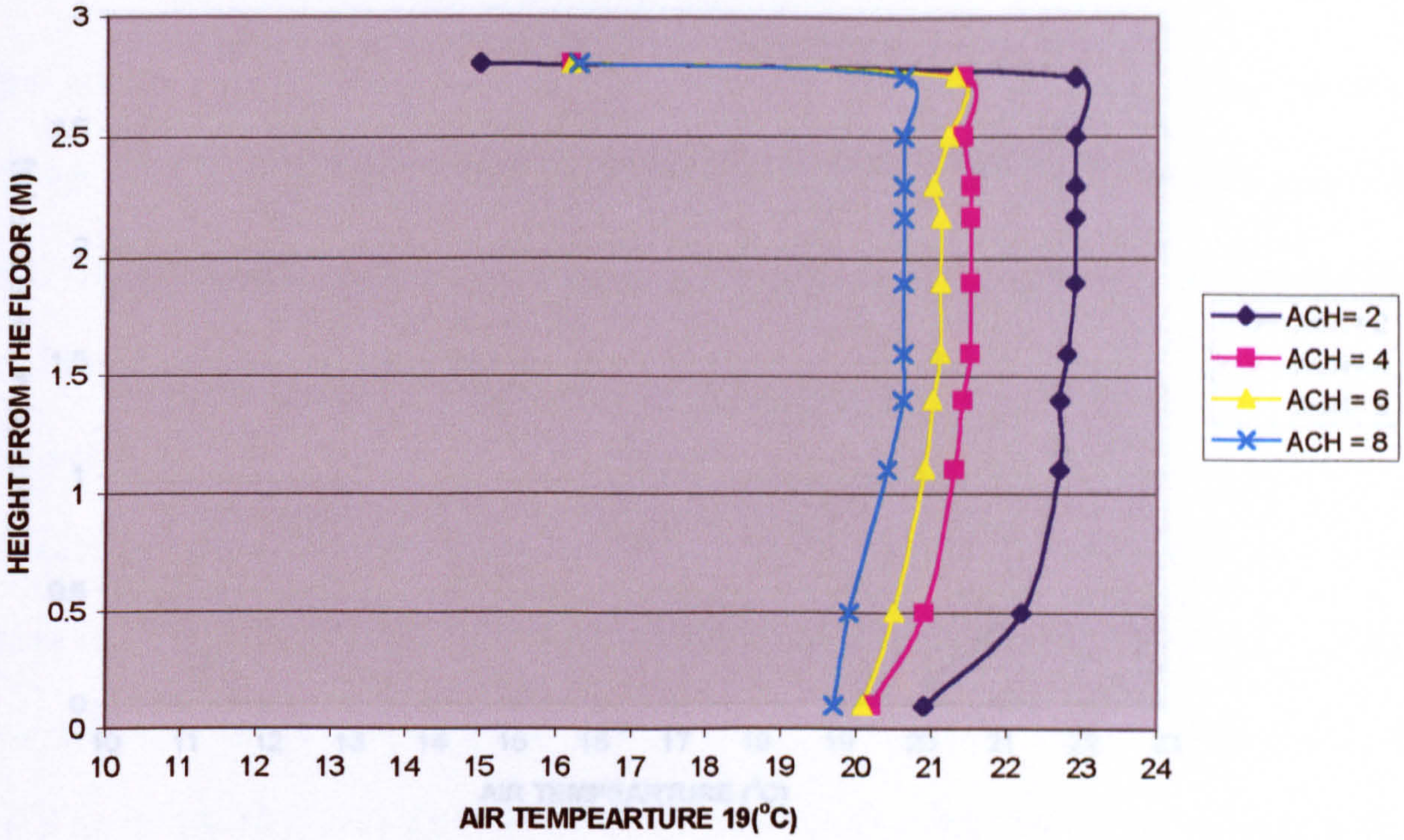

Figure 8.10: Showing the air temperature profile in the room for test case 10.

The results (figure 8.10) show that for ceiling temperature of 16°C, the displacement airflow pattern is disturbed at high ACH but at low ACH very good displacement airflow pattern is seen. The results also suggest that to remove the heat load low ACH can be used which will make it more energy efficient.

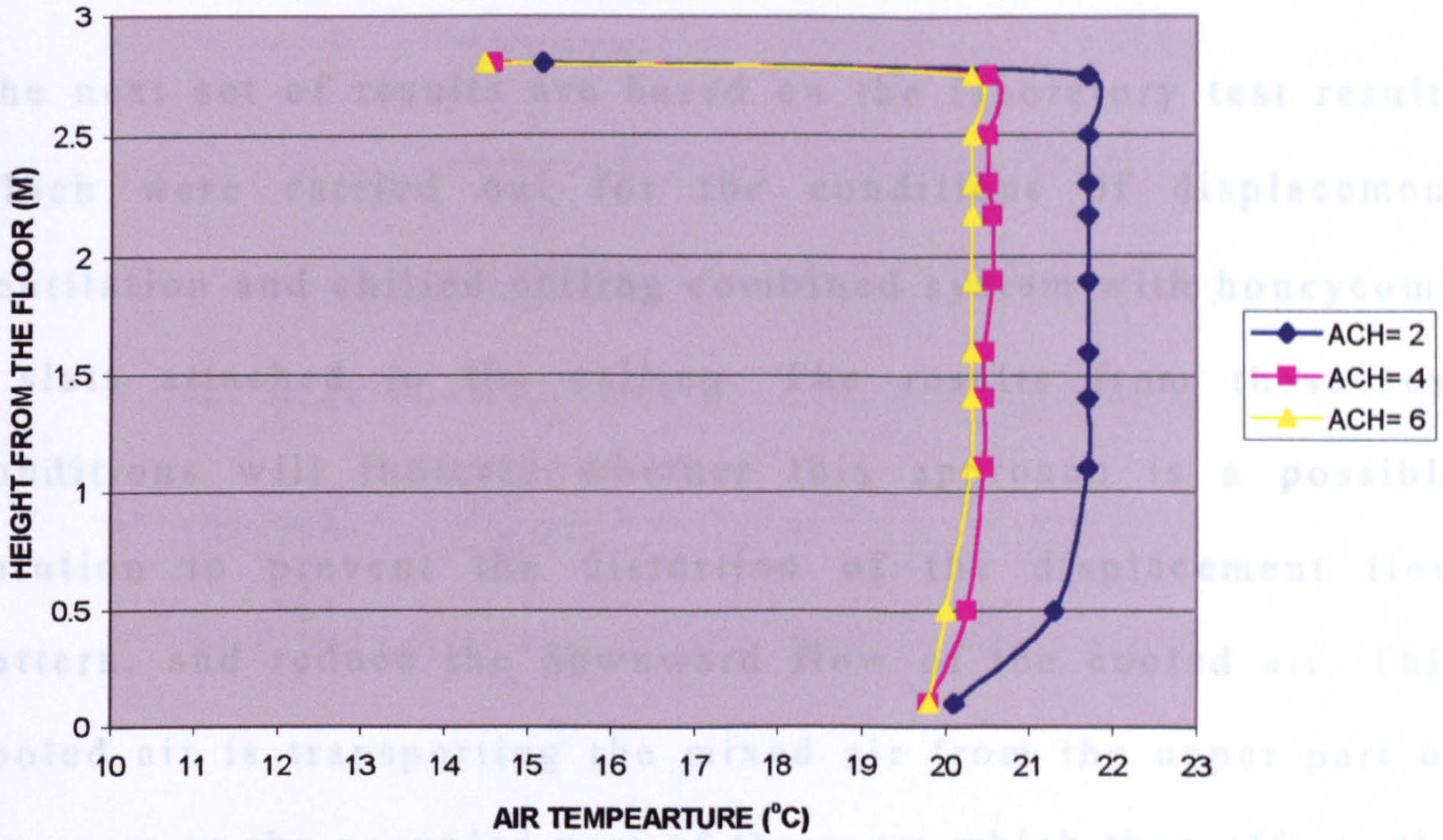

Figure 8.11: Showing the air temperature profile in the room for test case 11.

The results (figure 8.11) highlight that for ceiling temperature of 14°C, the displacement airflow pattern is completely disturbed at ACH of 4 and 6. The stratified boundary layer is reduced well below 1 meter above the floor. Only at low ACH of 2 some signs of displacement airflow pattern is seen. The results also suggest that to remove the heat load low ach can be used which will make it more energy efficient.

8.5 The displacement ventilation and chilled ceiling tests with honeycomb / slats attached to the ceiling

The next set of results are based on the laboratory test results which were carried out for the conditions of displacement ventilation and chilled ceiling combined system with honeycomb / slats attached to the ceiling. The results from these test conditions will indicate whether this approach is a possible solution to prevent the distortion of the displacement flow pattern, and reduce the downward flow of the cooled air. This cooled air is transporting the mixed air from the upper part of the room to the occupied part of the room which then affects the air quality of the in the occupied zone. The procedure adopted to investigate the affects the honeycomb slats will have on the airflow, was by attaching the honeycomb slat to the ceiling as discussed in chapter five. From the CFD investigation discussed in chapter Five the optimum depth width ratio for the honeycomb slat was found to be in region of ten to one (10:1). The test conditions carried out are stated in table 8.4.

The results of the attachment of the honeycomb slats to the ceiling are presented in figures 8.12 to 8.34.

TEST CASE	ACH	DV ONLY	CEILING TEMP 21°C	CEILING TEMP 18°C	CEILING TEMP 16°C	CEILING TEMP 14°C	CEILING TEMP 12°C
12	2	X	X	X	X	X	X
13	4	X	X	X	X	X	X
14	6	X	X	X	X	X	X
15	8	X	X	X	X		

Table 8.4: Shows the test conditions that were carried out to investigate the effects of honeycomb slat attached to ceiling.

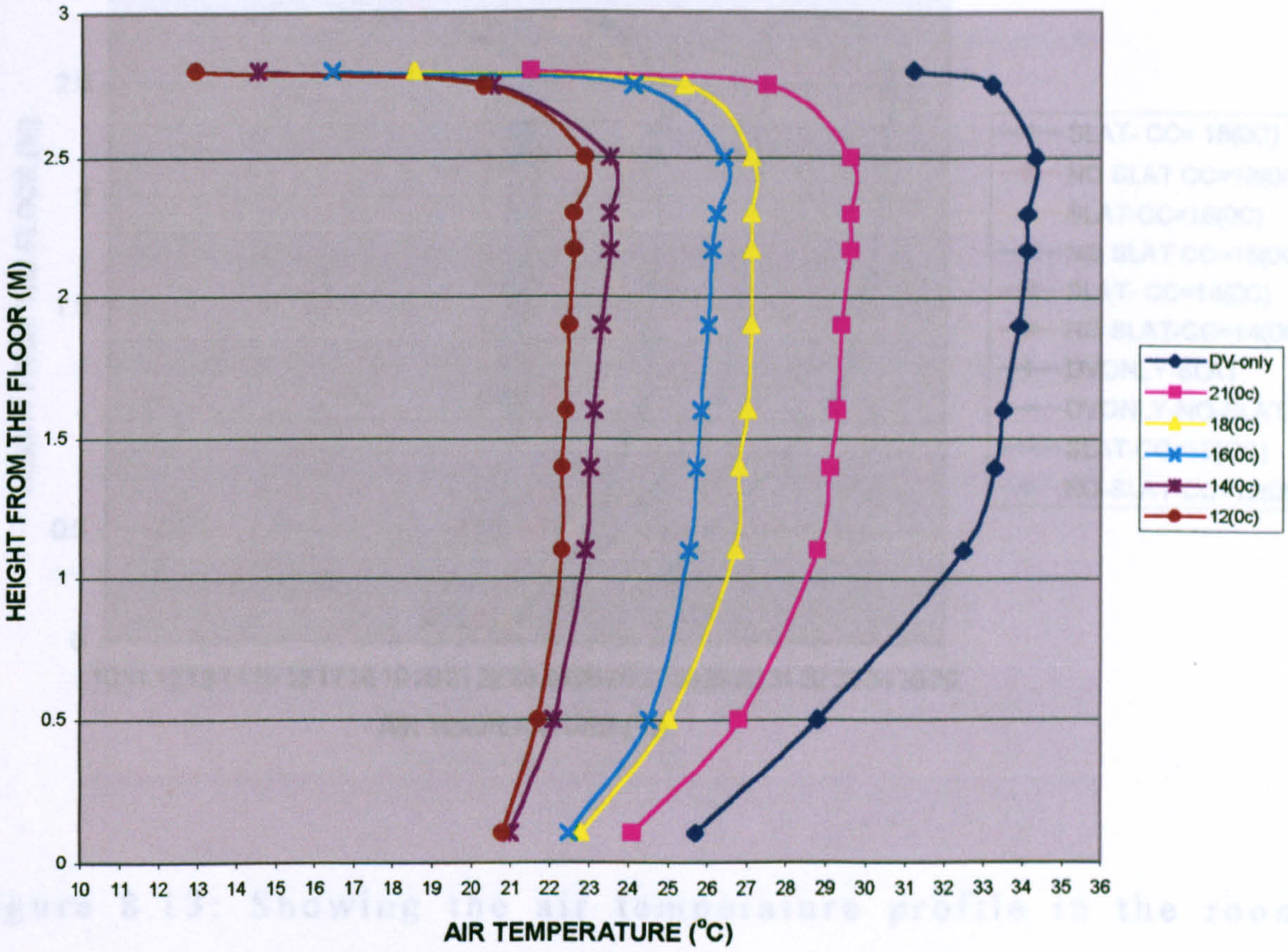

Figure 8.12: showing the air temperature profile in the room for test case 12

It is very interesting to see that by attaching the honeycomb slats to the ceiling the airflow displacement pattern can be preserved even at low ceiling temperatures (figure 8.12). This can be further seen in following figures 8.13 to 8.16.

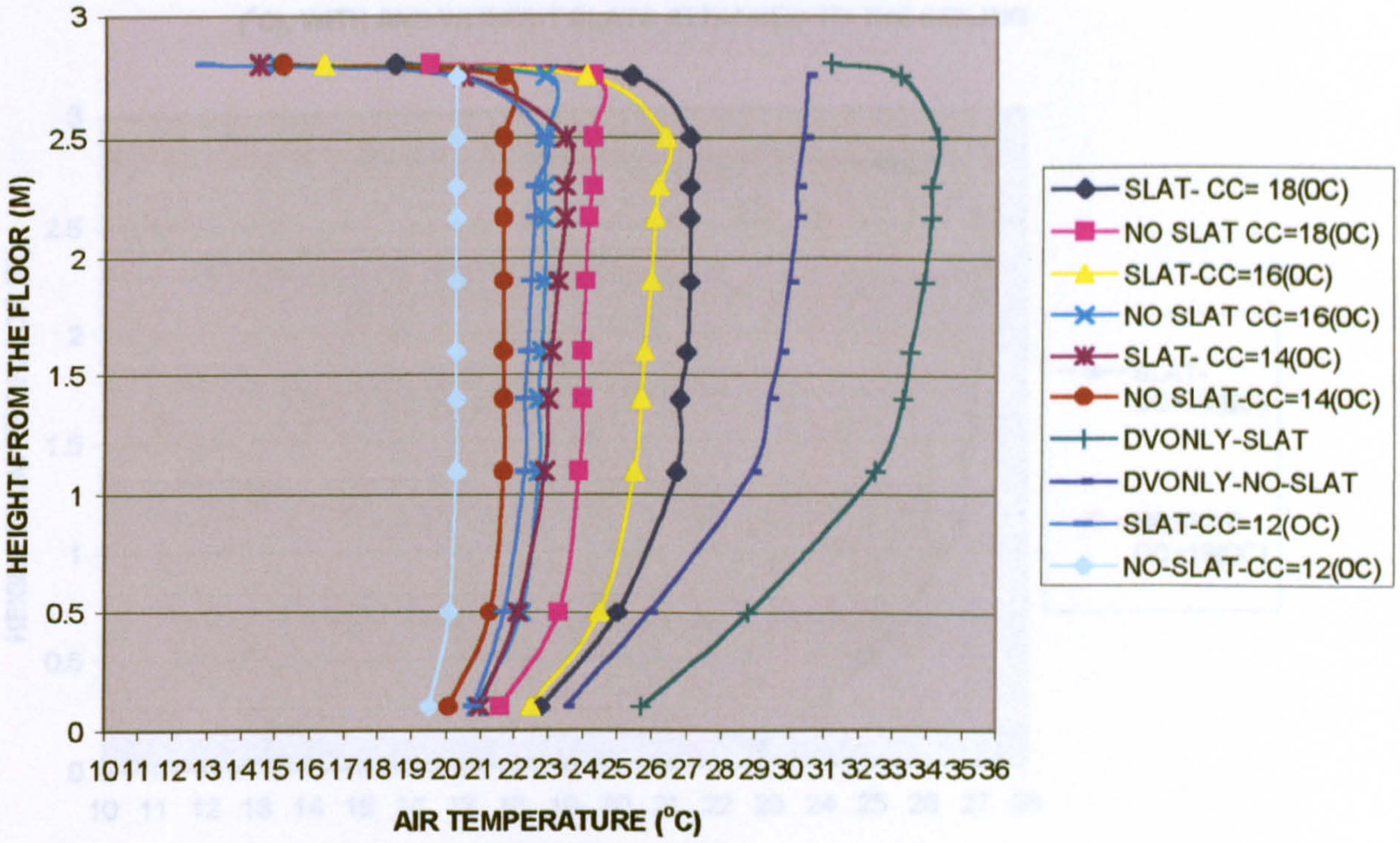

Figure 8.13: Showing the air temperature profile in the room for test case 12.

Figure 8.13 shows both results for air temperature profile with and without honeycomb slats attached to the ceiling. The results clearly show that for low ceiling air temperatures the use of honeycomb slats can help to preserve the displacement airflow pattern, which had been disturbed for same boundary conditions without the use of honeycomb slats.

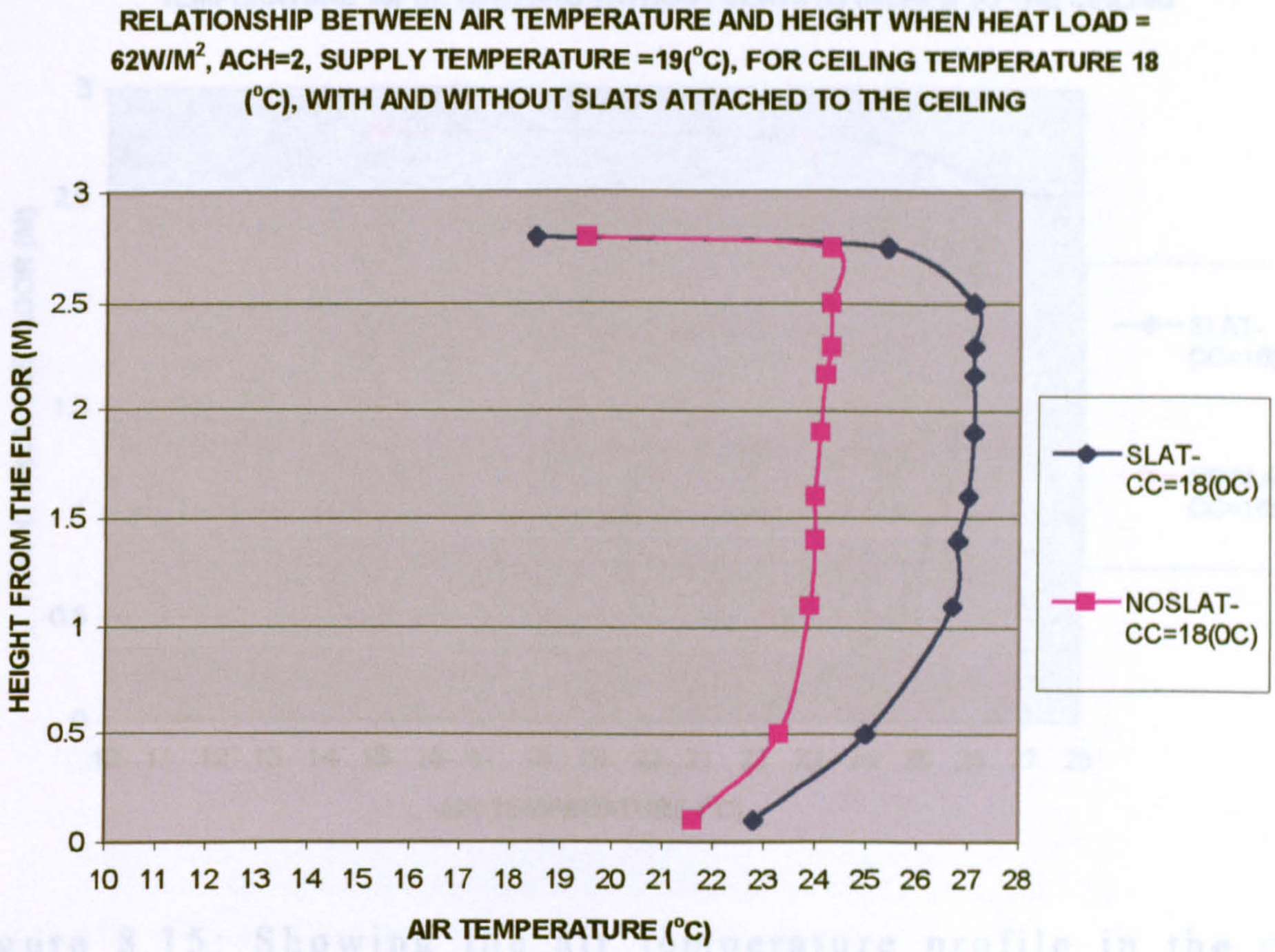

Figure 8.14: Showing the air temperature profile in the room for test case 12 with comparison between ceiling temperatures for with without the honeycomb slats attached to the ceiling for the ceiling temperature of 18°C.

The results in figure 8.13 indicated that when the honeycomb slats are attached to the ceiling for 2 ACH. The result do not meet the requirements set out ISO 7730, which suggest that when using low ACH for ceiling temperature of 18°C to remove large heat loads it is better not to use the honeycomb slats.

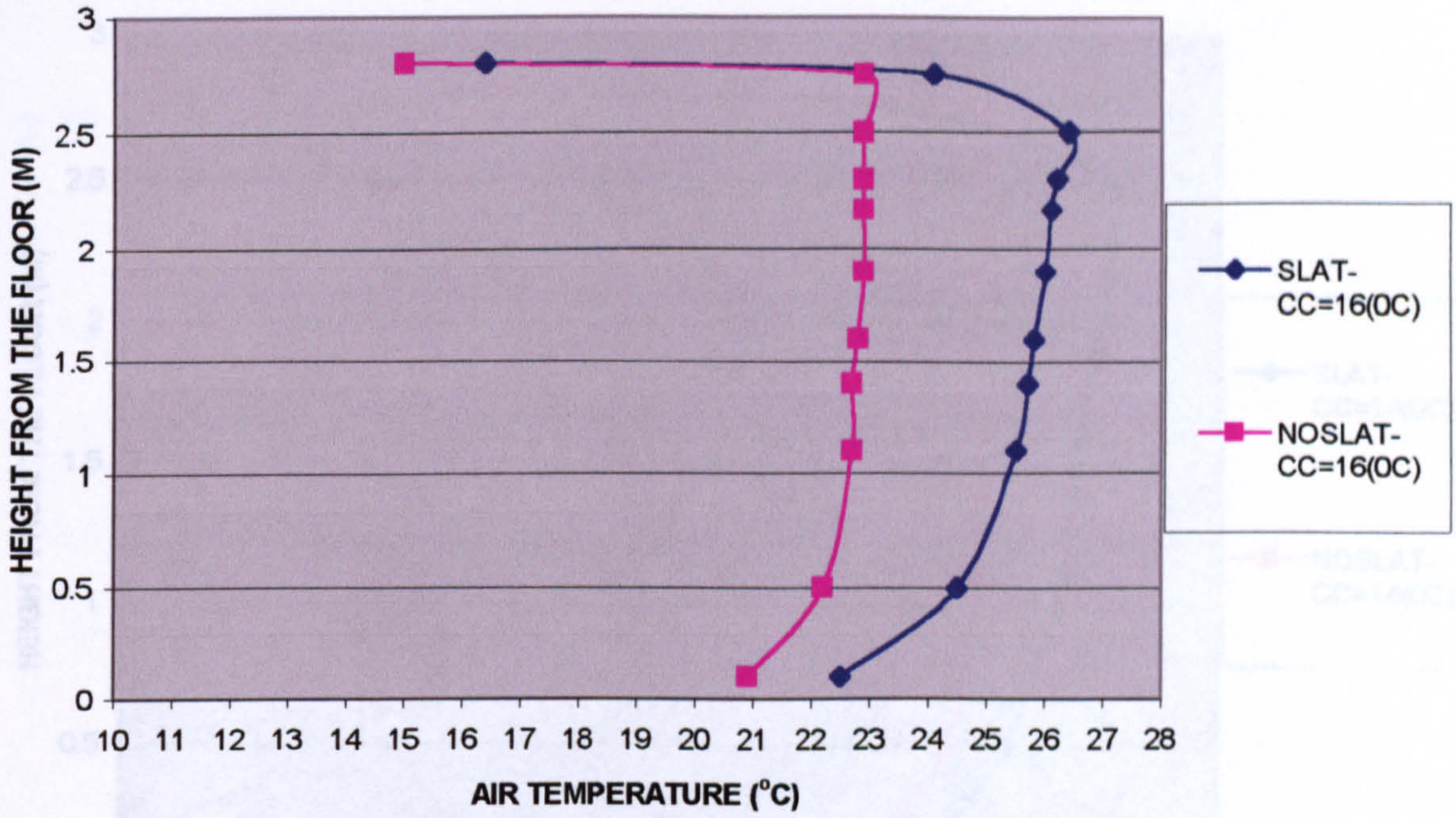

Figure 8.15: Showing the air temperature profile in the room for test case 12 with comparison between ceiling temperatures for with without the honeycomb slats attached to the ceiling for the ceiling temperature of 16°C.

The results indicate that for a ceiling temperature of 16°C and ACH of 2. The use of honeycomb slat, have reintroduced the displacement airflow pattern, which had been disturbed by the lower air ceiling temperature.

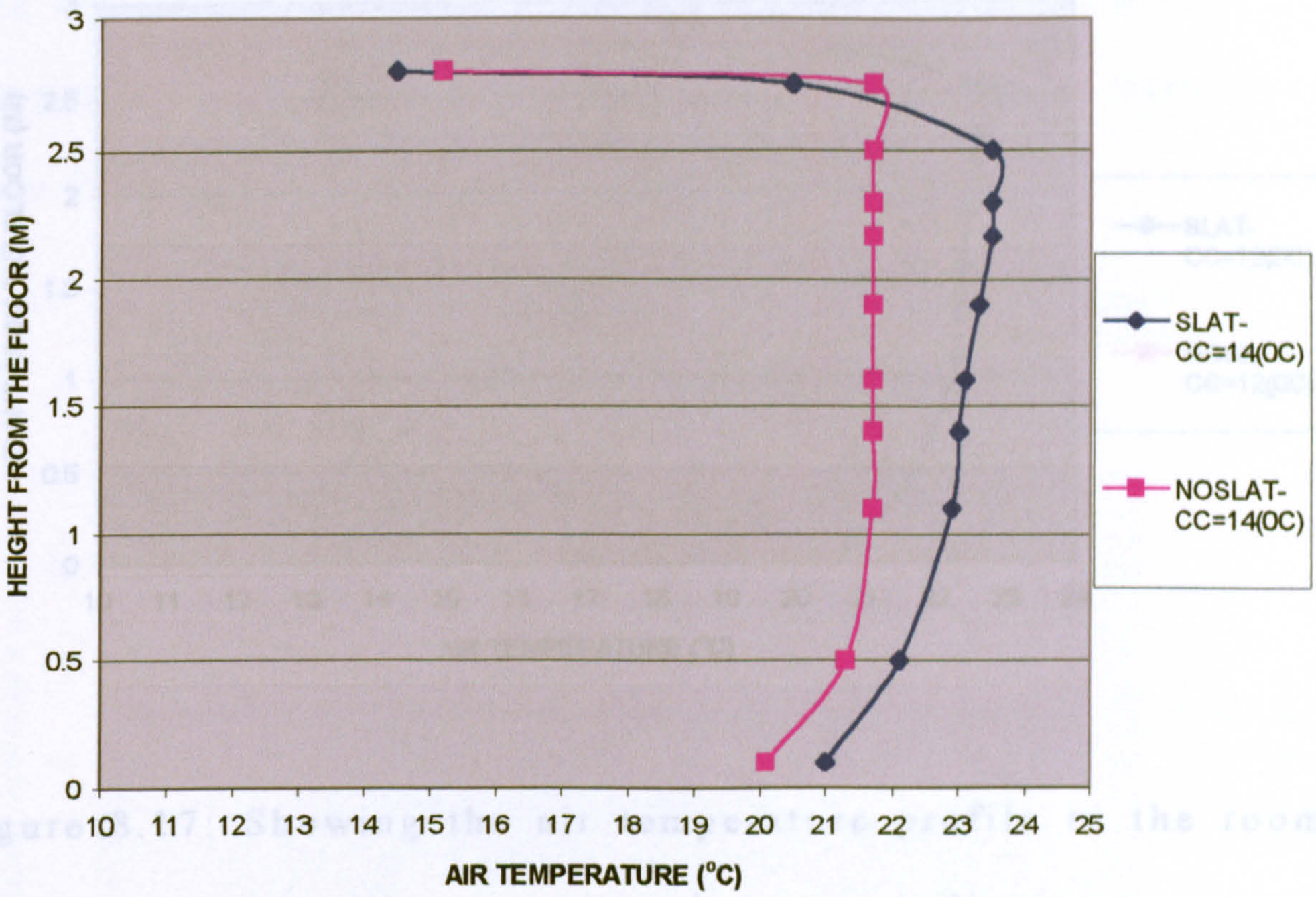

Figure 8.16: Showing the air temperature profile in the room for test case 12 with comparison between ceiling temperatures for with without the honeycomb slats attached to the ceiling for the ceiling temperature of 14°C.

The results show that for low ceiling air temperature of 14°C, and low ACH of 2, without the honeycomb slats the displacement airflow pattern is disturbed.

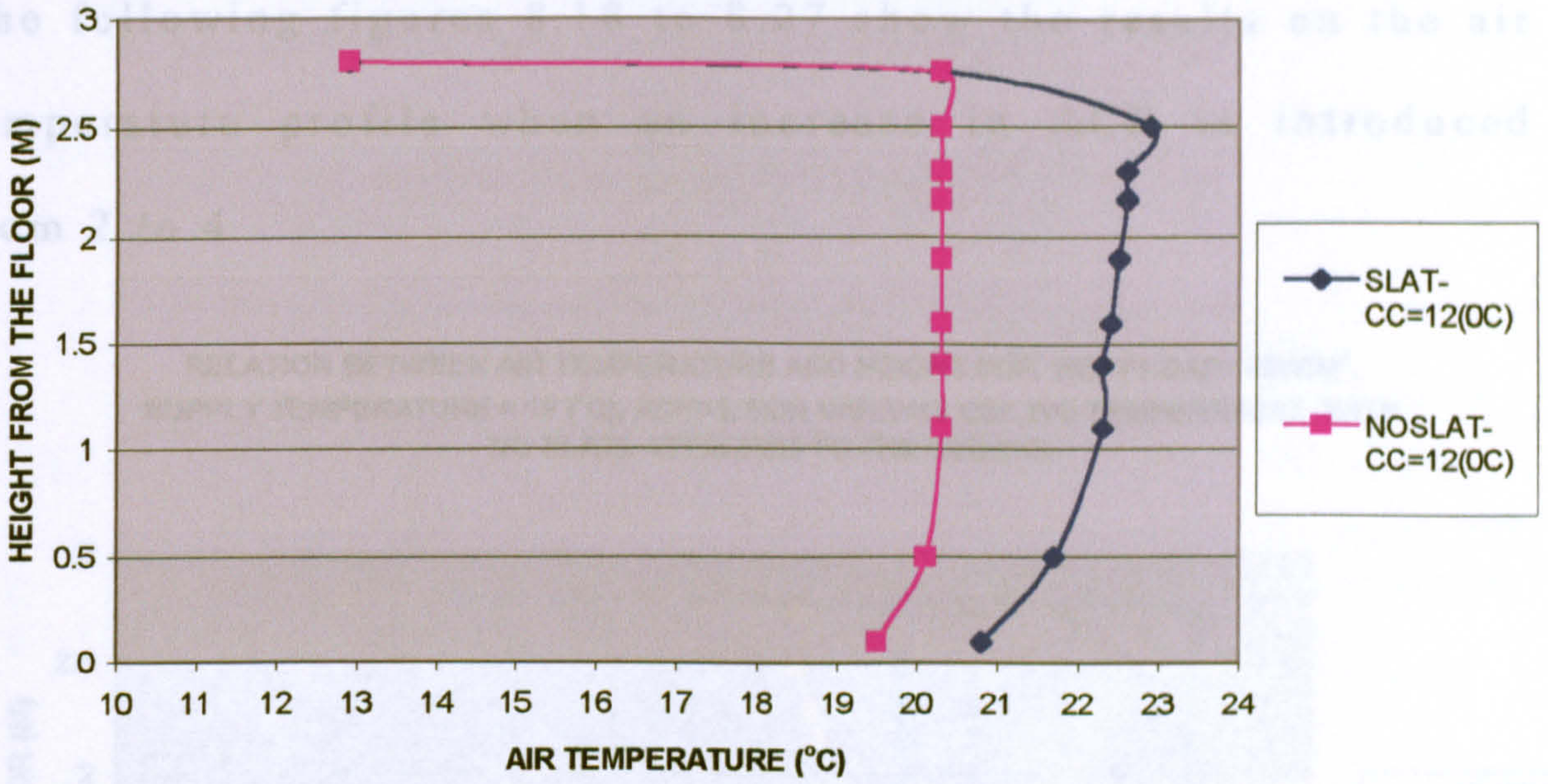

Figure 8.17: Showing the air temperature profile in the room for test case 12 with comparison between ceiling temperatures for with without the honeycomb slats attached to the ceiling for the ceiling temperature of 12°C

The results show that for all the chilled ceiling temperatures the attachment of the slats to the ceiling can contribute to the suppression of downward cold air and thereby preserving the displacement airflow pattern. The effect of air change per hours of 4,6 and 8 on air temperature profile are also carried out these are presented in figures 8.18 to 8.39.

8.5.1 Effect of change in ACH

The following figures 8.18 to 8.27 show the results on the air temperature profile when an increase in ACH is introduced from 2 to 4.

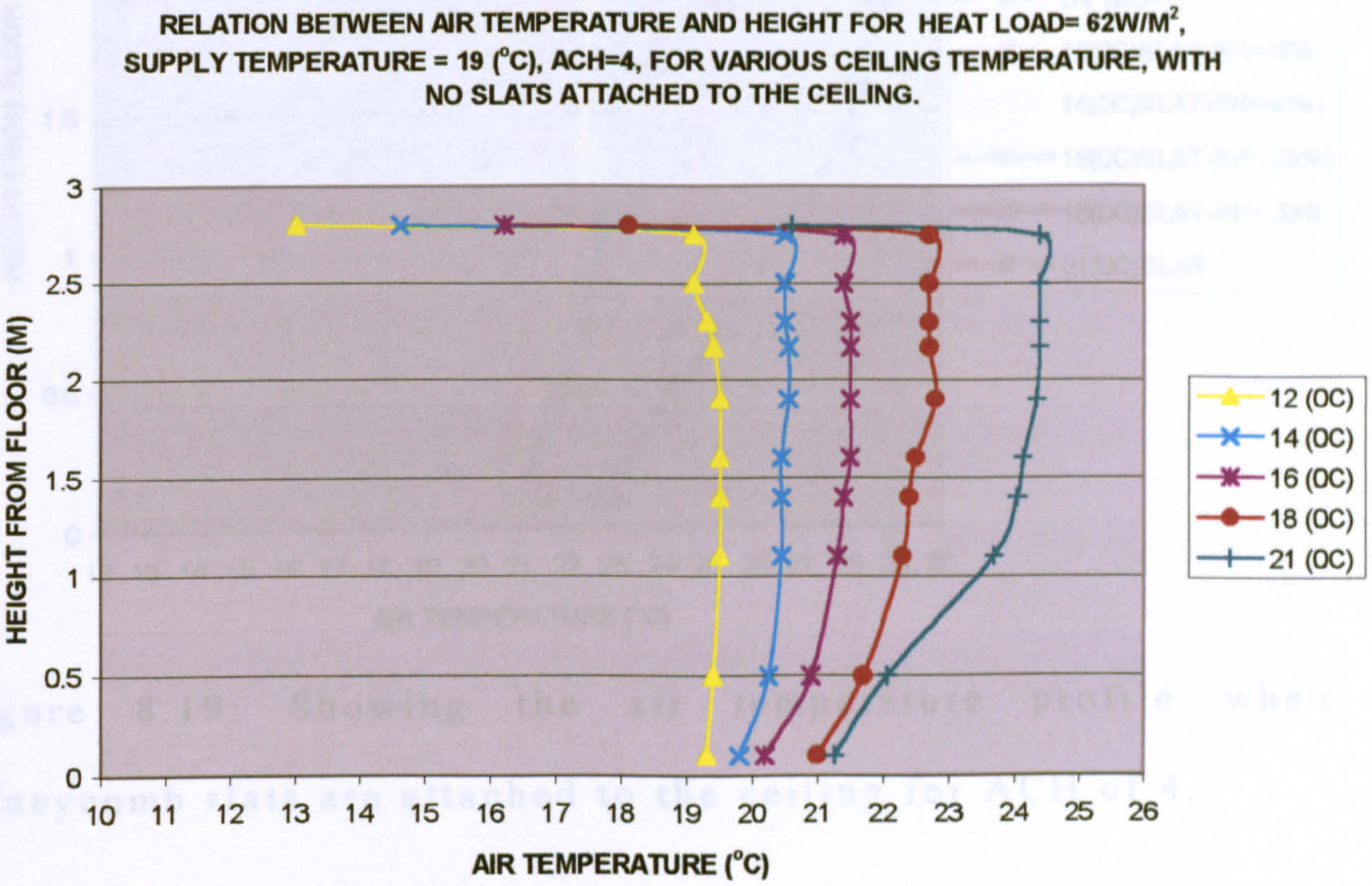

Figure 8.18 representing the air temperature profile for ach of 4 without the attachment of honeycomb slats attached to the ceiling.

It can be seen that without the use of honeycomb slats at low ceiling temperatures the displacement airflow pattern is completely disturbed.

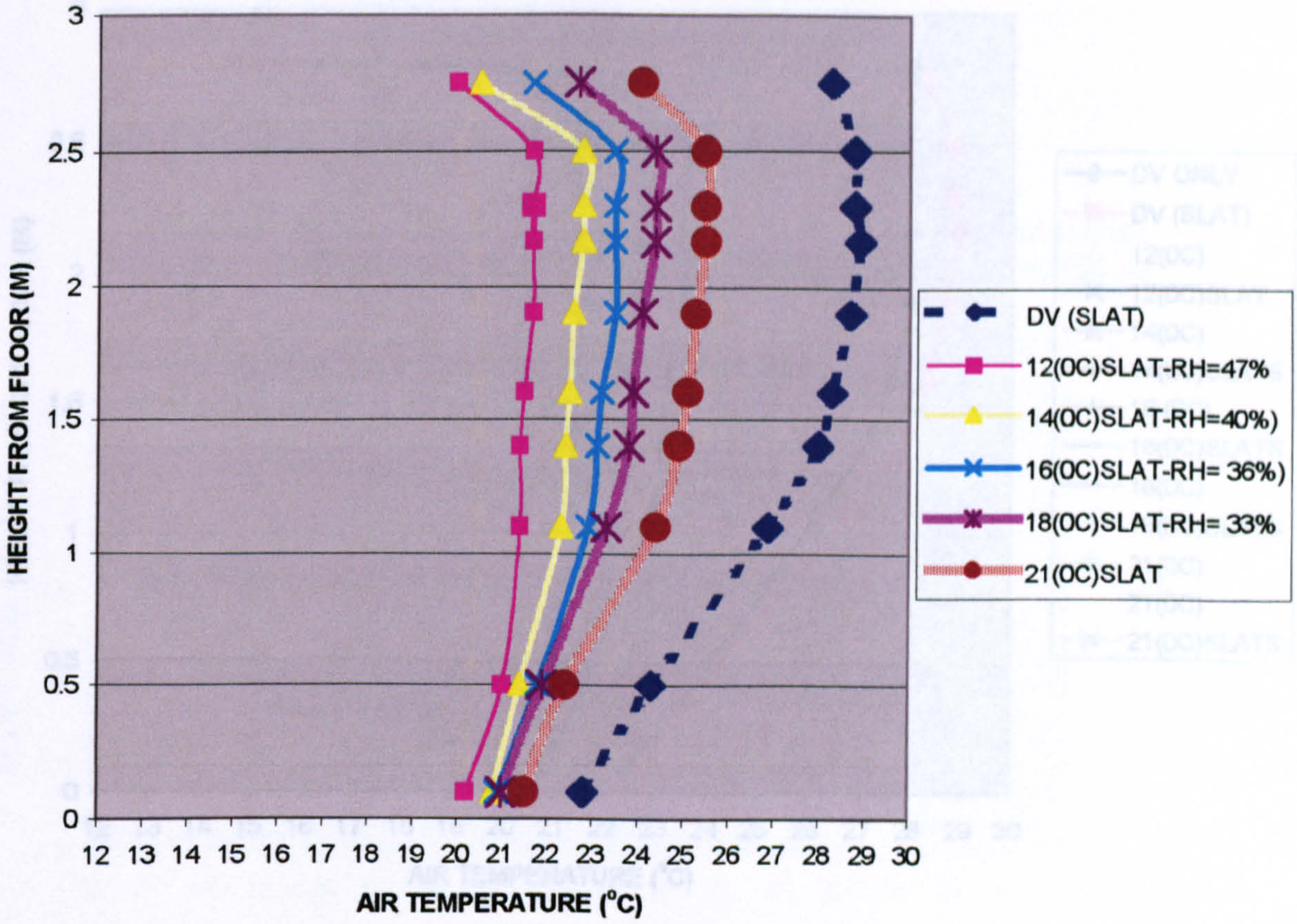

Figure 8.19: Showing the air temperature profile when honeycomb slats are attached to the ceiling for ACH of 4.

The result clearly show that the by attaching the honeycomb slat to the ceiling, for ACH of 4, at low ceiling temperatures the displacement airflow pattern can be preserved. These finding also agree with those when ACH was set at 2, figures 8.20 to 8.25.

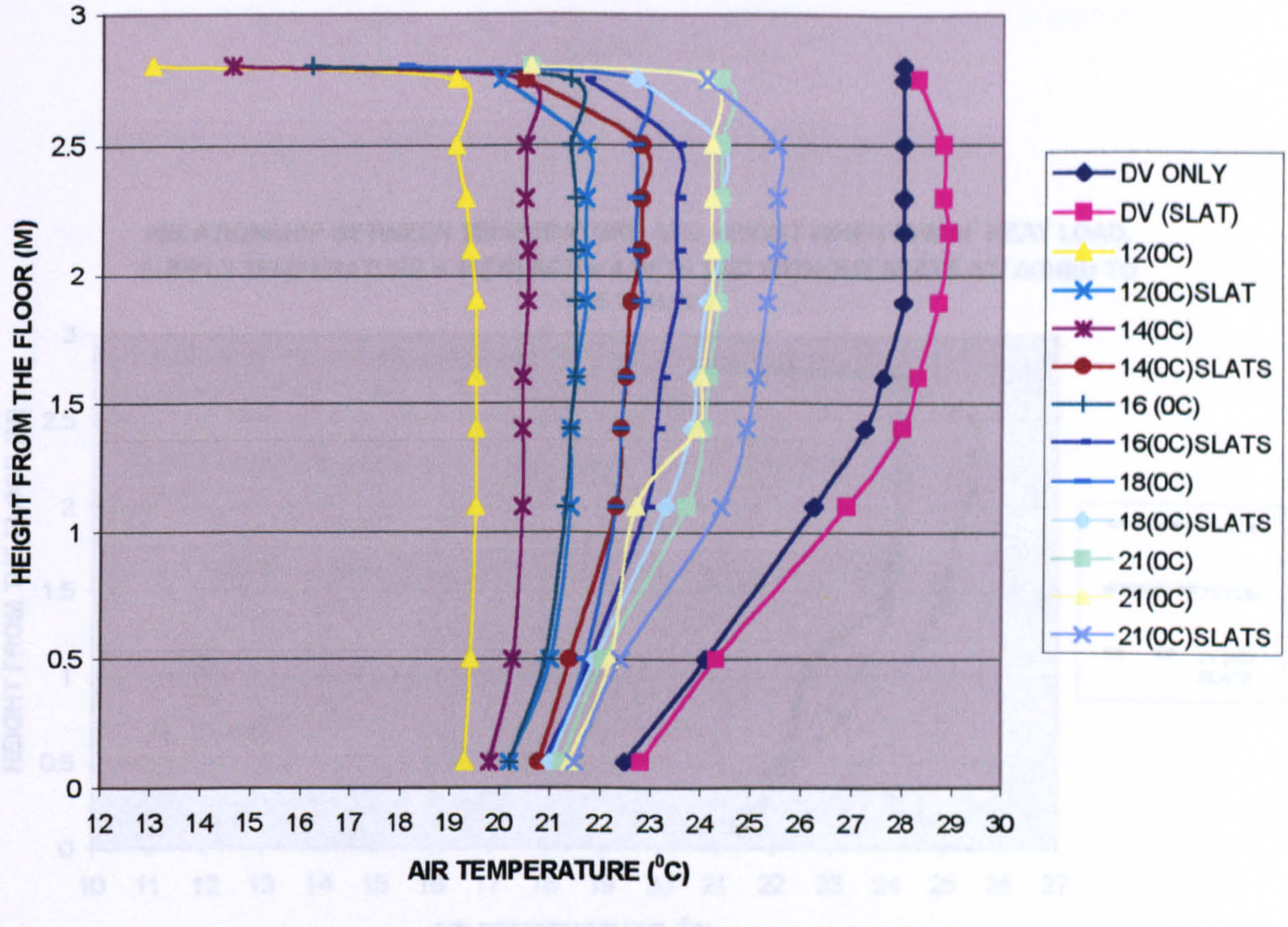

Figure 8.20: Showing the results of air temperature profile for figures 8.18 and 8.19.

The results are shown for both with and without honeycomb slat attached to the ceiling. The results show that the honeycomb slats have a major impact on the downward cold ceiling air flow. The honeycomb helps to suppress the convection current and therefore allows the preservation of the displacement airflow pattern. Figures 8.21 to 8.25 show the individual comparison with and without honeycomb slats

attached to the ceiling for the heat load of 62W/m^2 for various ceiling temperatures for an ACH of 4.

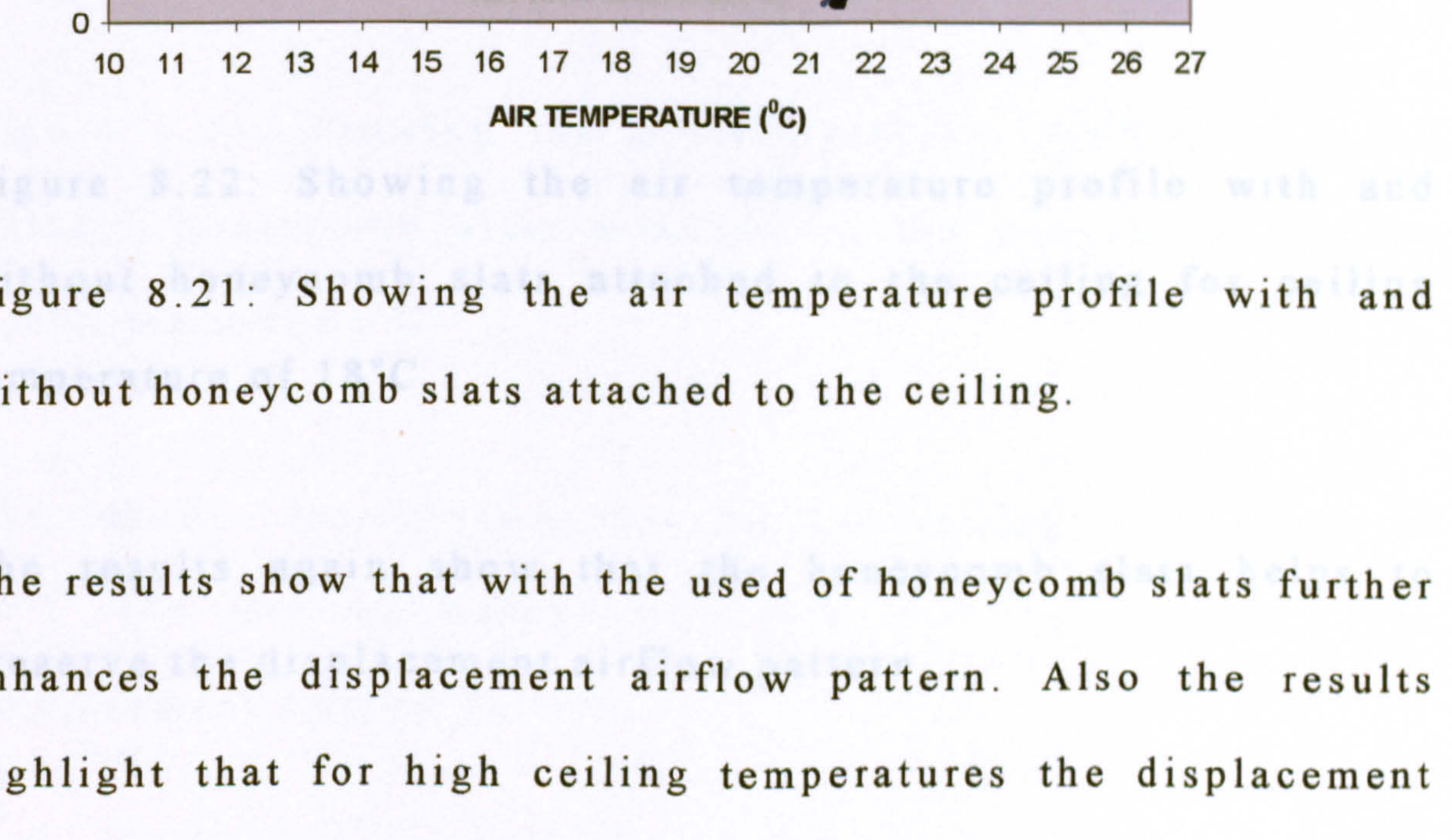

Figure 8.21: Showing the air temperature profile with and without honeycomb slats attached to the ceiling.

The results show that with the used of honeycomb slats further enhances the displacement airflow pattern. Also the results highlight that for high ceiling temperatures the displacement airflow pattern is preserved and the air temperature profile also complies with the standard set out by ISO 7730 even without the use of honeycomb slats.

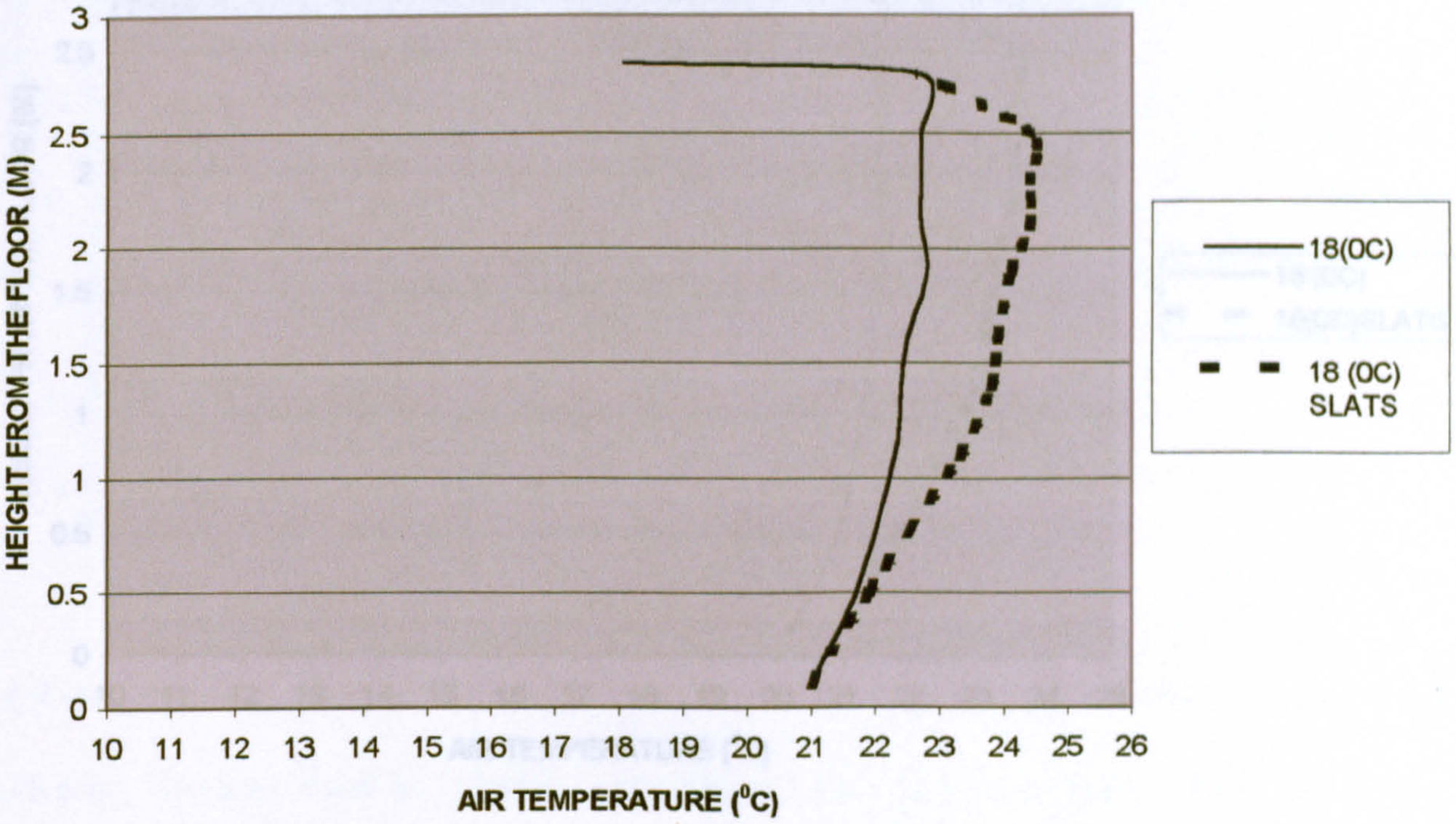

Figure 8.22: Showing the air temperature profile with and without honeycomb slats attached to the ceiling for ceiling temperature of 18°C.

The results again show that the honeycomb slats helps to preserve the displacement airflow pattern.

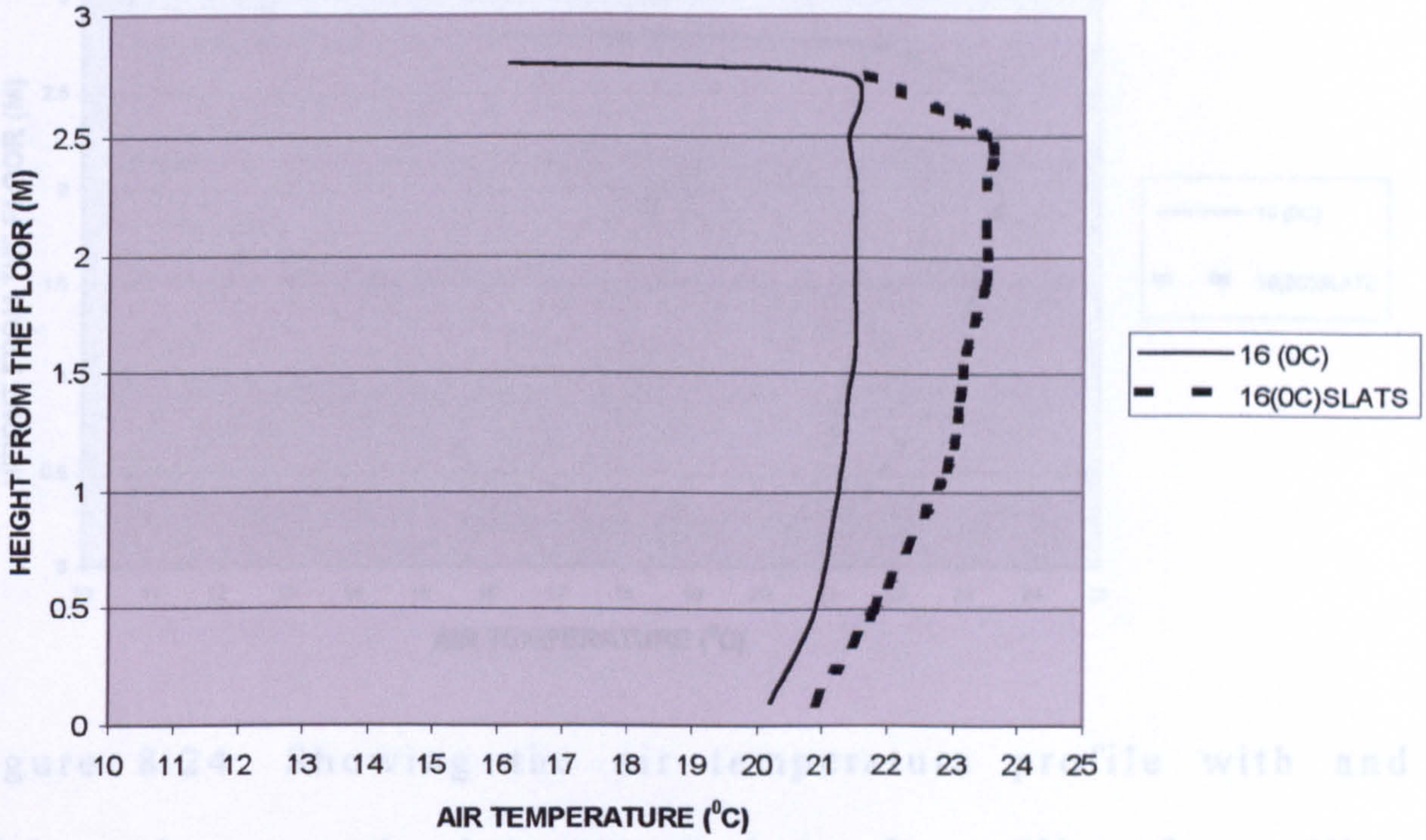

Figure 8.23: Showing the air temperature profile with and without honeycomb slats attached to the ceiling for ceiling temperature of 16°C.

The results clearly show that for the ceiling temperature of 16°C the use of honeycomb slats will re introduce the displacement airflow pattern.

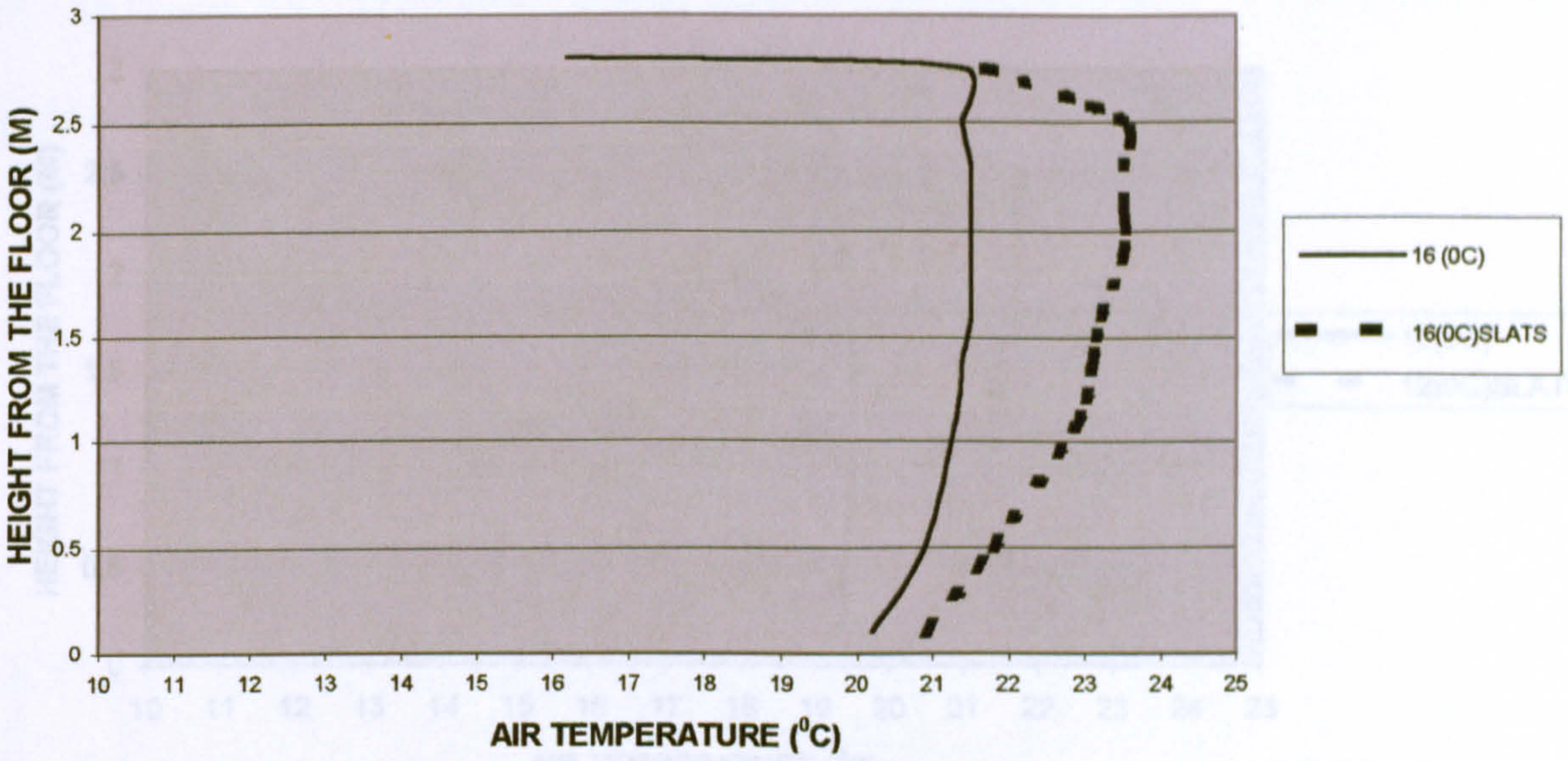

Figure 8.24: Showing the air temperature profile with and without honeycomb slats attached to the ceiling for ceiling temperature of 14°C.

The results clearly shows that for the test case where the ceiling temperature of 14°C and without the use of honeycomb slats the displacement airflow pattern is completely disturb. The results also show that with the attachment of the honeycomb slats a good displacement airflow pattern is seen.

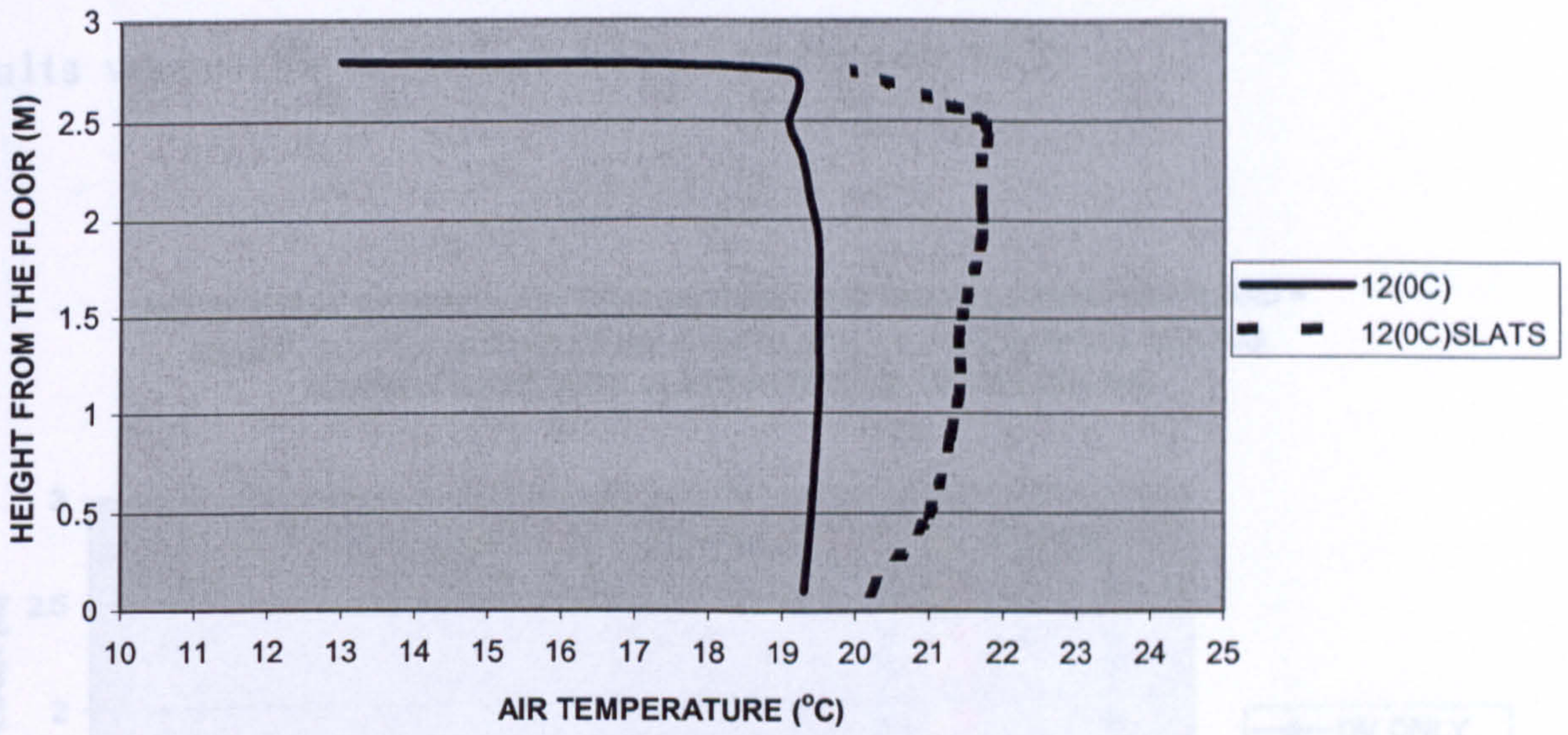

Figure 8.25: Showing the air temperature profile with and without honeycomb slats attached to the ceiling for ceiling temperature of 12°C.

The results clearly show (figure 8.25) that for the ceiling temperature of 12°C without the use of honeycomb slats the displacement airflow pattern is completely disturb. The room air temperature profile is almost at right angle. The air temperature difference from ankle height to breathing height is below 0.3°C, where it is 1.3°C when the honeycomb slats are used. The results also show that with the attachment of the honeycomb slats a good displacement airflow pattern can be reintroduced into the room.

8.5.2 Effect of ACH of 6.

The following figures 8.28 to 8.32 show the experimental results when the ACH has been increased to 6.

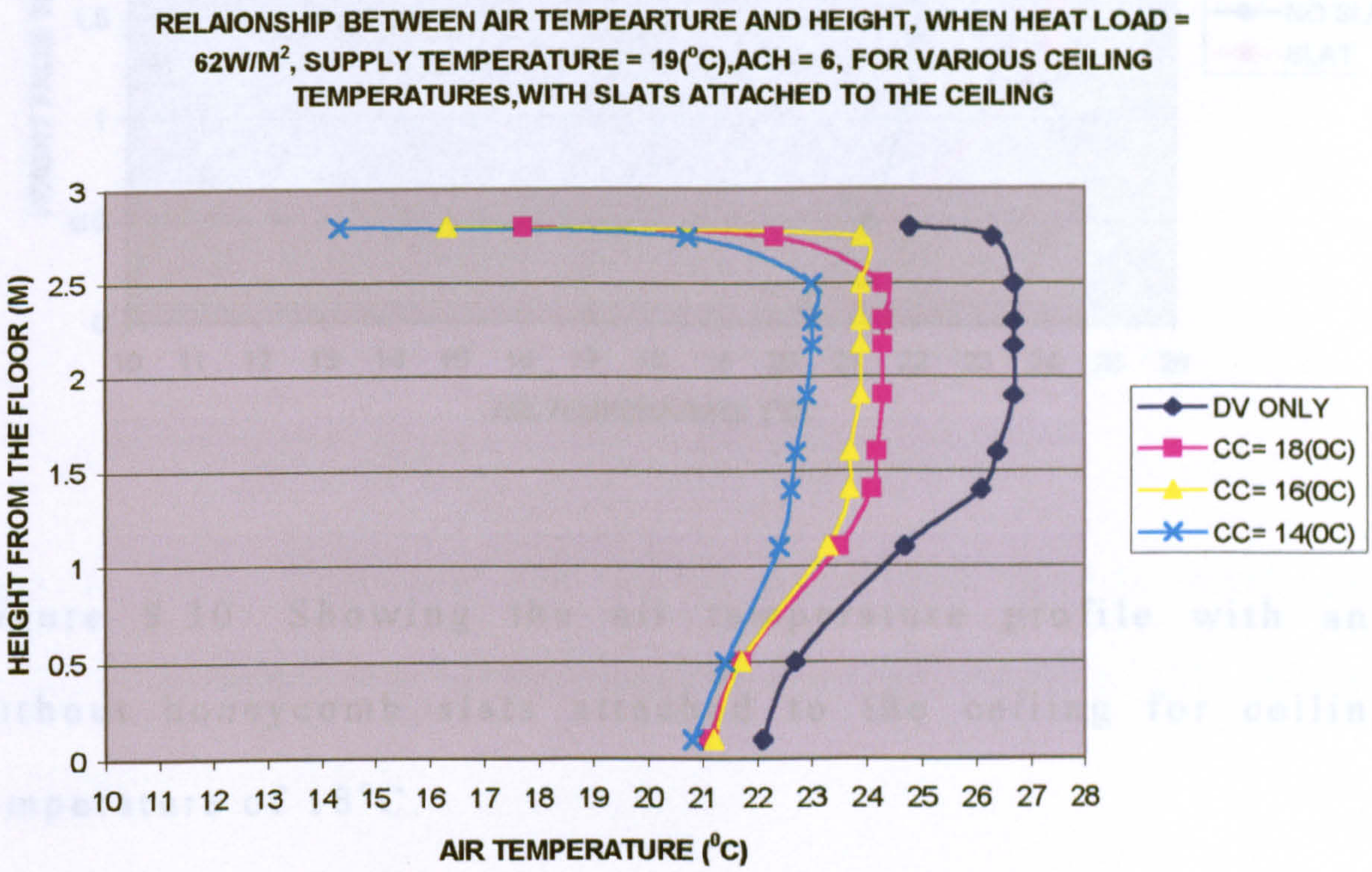

Figure 8.28: Showing the air temperature profile when honeycomb slats are attached to the ceiling for ACH of 6

These results are further show in figures 8.30 to 8.32 where each individual test case is compared for with and without honeycomb slats attached to the ceiling.

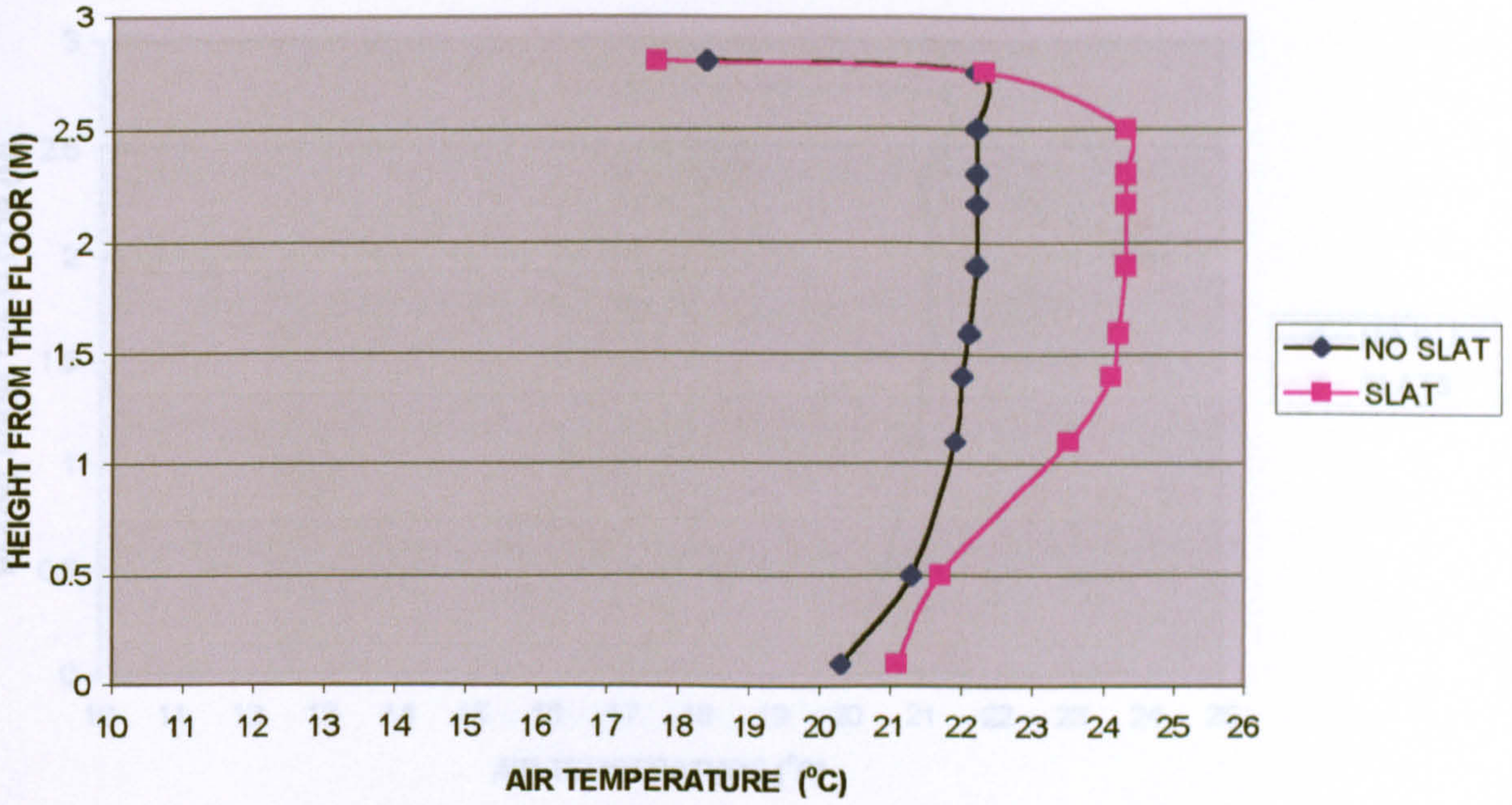

Figure 8.30: Showing the air temperature profile with and without honeycomb slats attached to the ceiling for ceiling temperature of 18°C.

The results indicate that for ceiling temperatures of 18°C, and ACH of 6. The system will produce a good displacement airflow pattern and the need for honeycomb is not required.

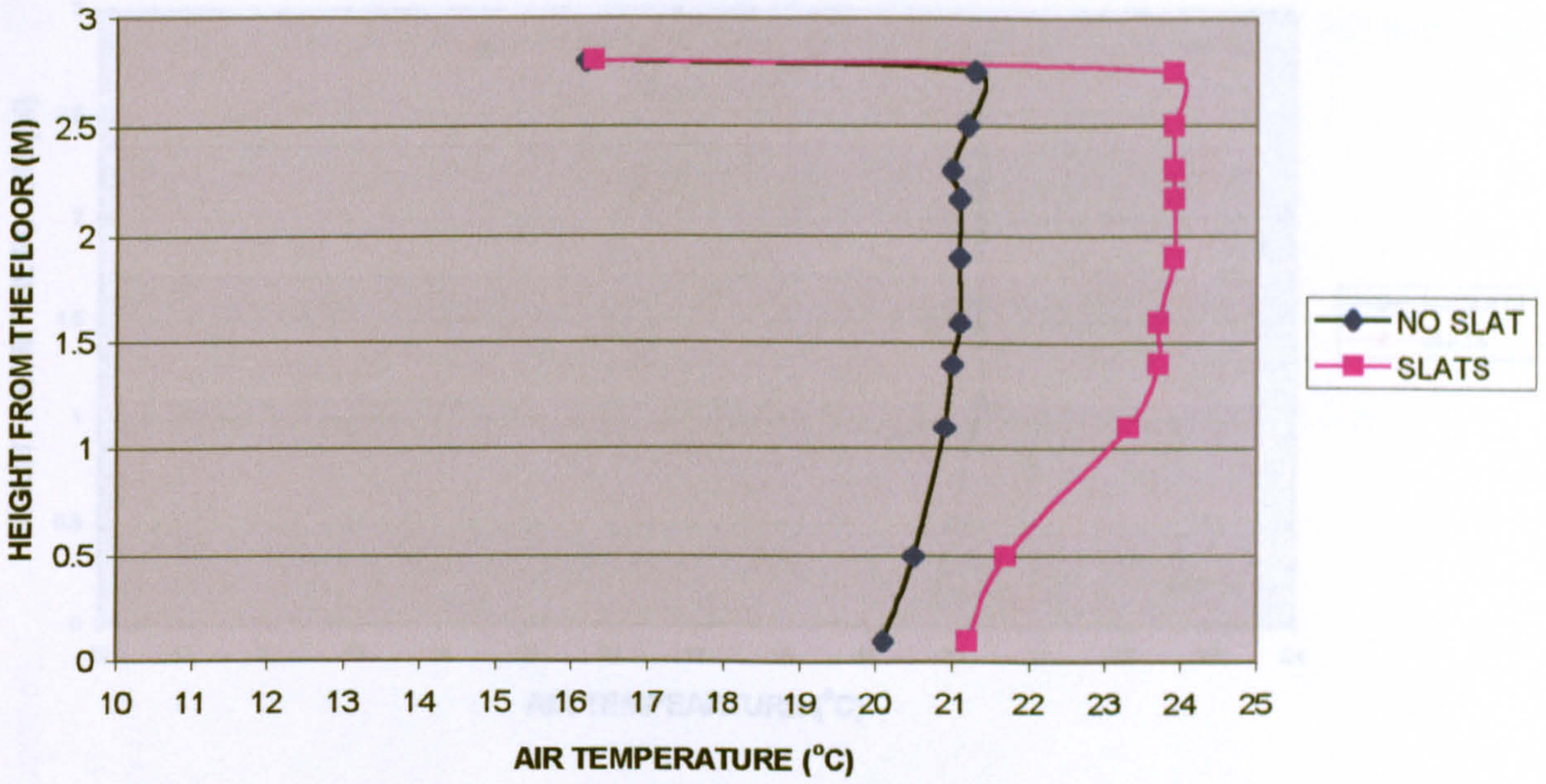

Figure 8.31: Showing the air temperature profile with and without honeycomb slats attached to the ceiling for ceiling temperature of 16°C.

The results indicate that for ceiling temperatures of 16°C, and ACH of 6. The system will affect the displacement airflow pattern. To improve the displacement airflow pattern the use of Honeycomb is need.

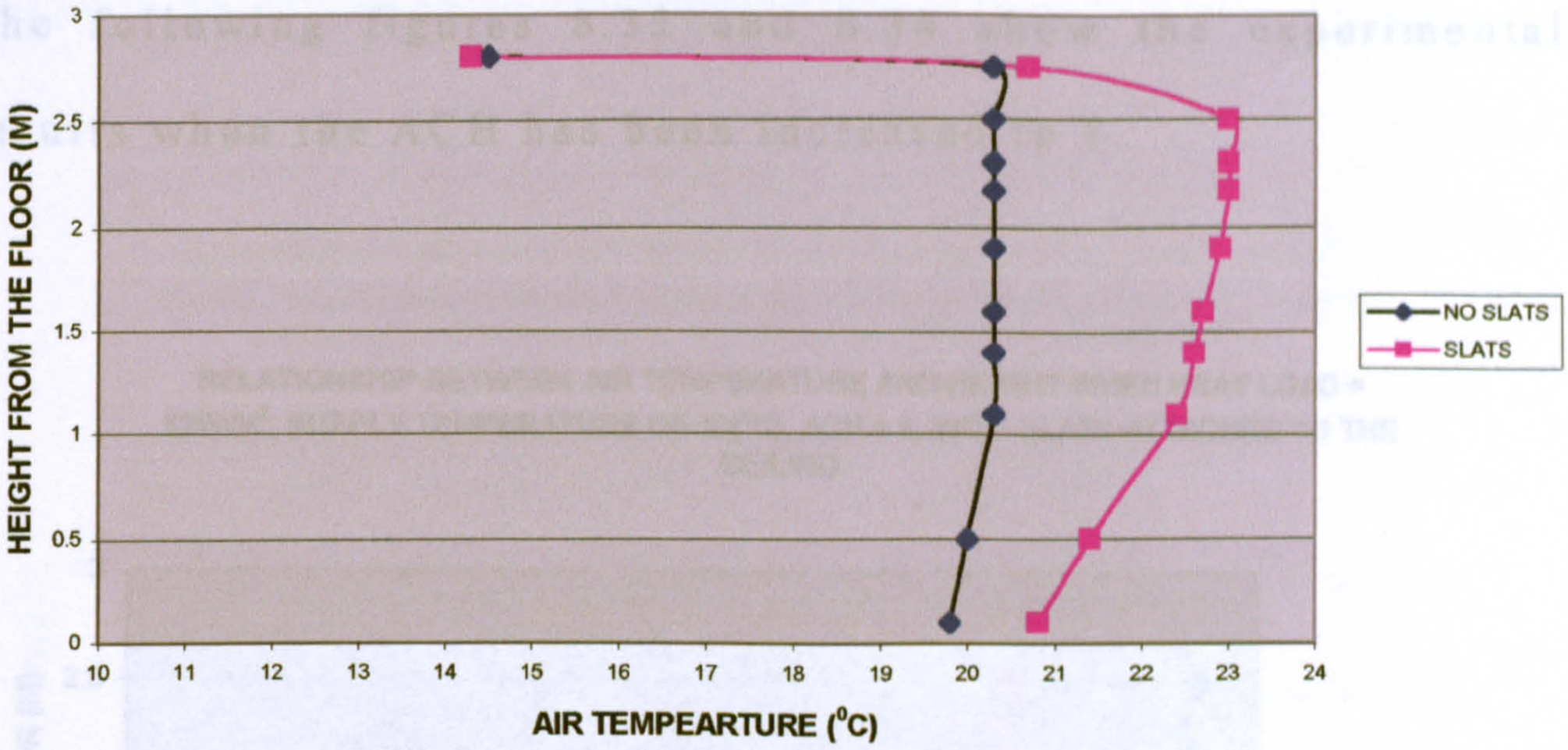

Figure 8.32: Showing the air temperature profile with and without honeycomb slats attached to the ceiling for ceiling temperature of 14°C.

The results indicate that for ceiling temperatures of 14°C, and ACH of 6. The system will disturb the displacement airflow pattern; this can be seen by the almost vertical air temperature profile. The results also show by attaching the honeycomb slats to the ceiling the displacement airflow pattern will be re introduced. The temperature difference between ankle and head height for the case without the honeycomb slats is below 0.5°C, where for when the honeycomb slats are attached this temperatures rises to over 1.5°C.

8.5.3 Effect of ACH of 8

The following figures 8.33 and 8.34 show the experimental results when the ACH has been increased to 8.

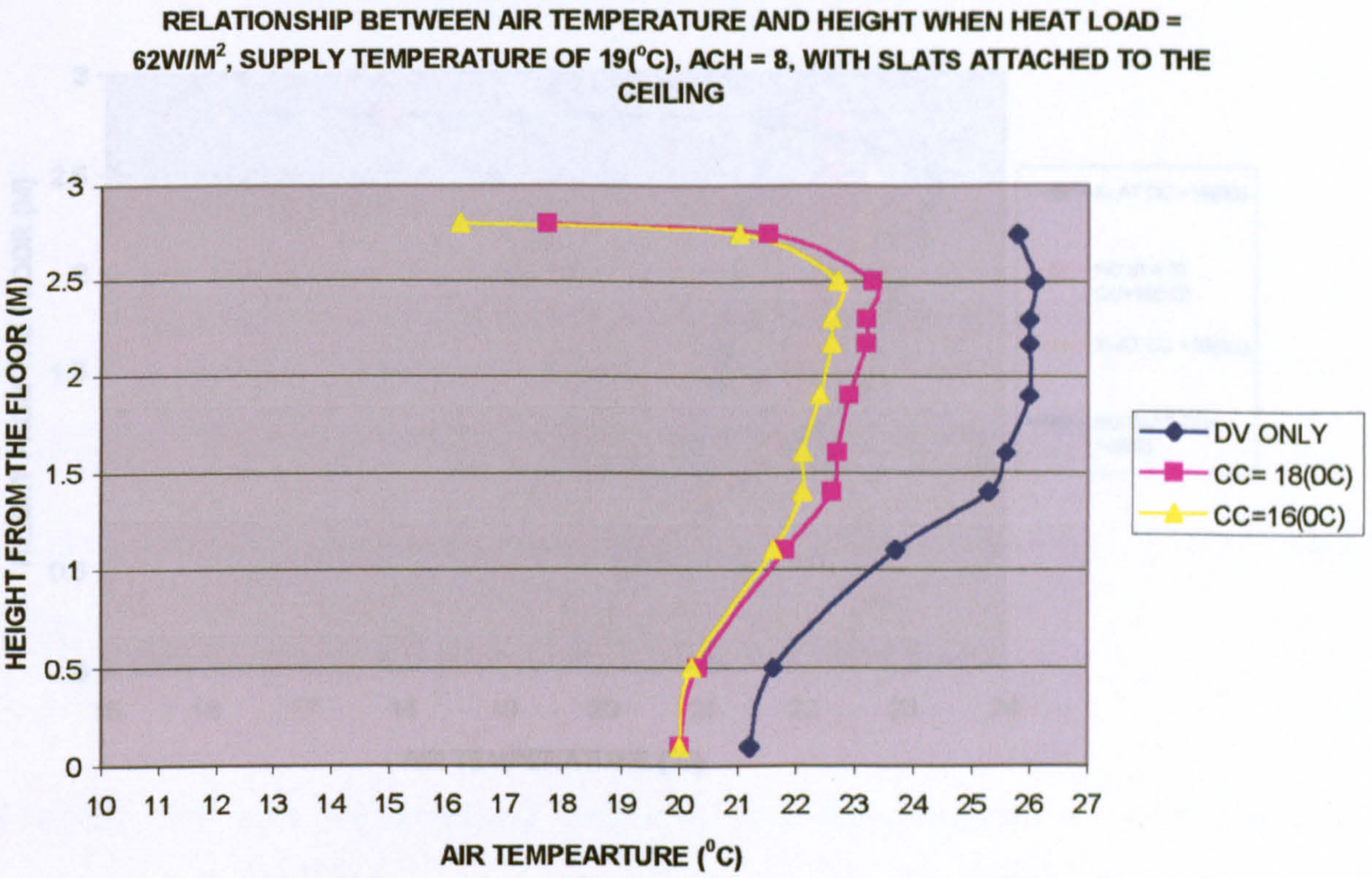

Figure 8.33: Showing the air temperature profile when honeycomb slats are attached to the ceiling for ACH of 8.

The results for ACH of 8 show interesting findings, it can be seen from the graph that the results for both ceiling temperatures of 16°C and 18°C are very similar; the room air temperature at ankle and head height is almost the same.

Figure 8.34 shows the comparison of results for these two ceiling temperatures corresponding to with and without honeycomb attached to the ceiling.

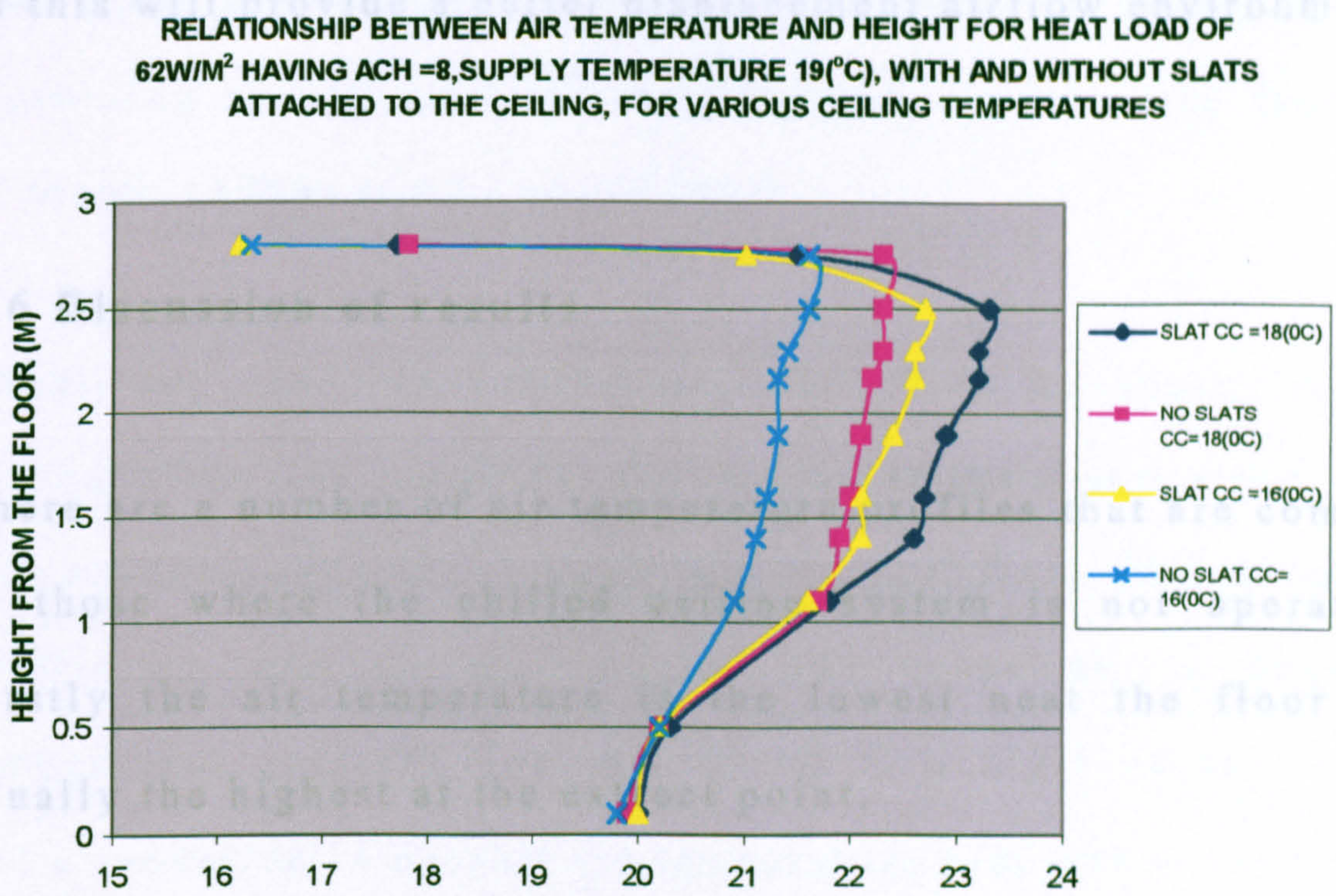

Figure 8.34: Showing the air temperature profile for the test conditions with and without honeycomb slats attached to the ceiling for ceiling temperature of 14°C and 16°C.

The results show that when the ceiling temperature of 18°C is used the system will produce a displacement airflow pattern therefore the use of honeycomb slat is not needed. But at case where the lower ceiling temperature of 16°C is used the

displacement pattern is present the temperature difference between ankle and head height is 1°C where for the same case when honeycomb slats are used the temperature difference is 2°C. Therefore it would be better to use the honeycomb slat, as this will provide a better displacement airflow environment.

8.6 Discussion of results

There are a number of air temperature profiles that are common to those where the chilled ceiling system is not operating. Firstly the air temperature is the lowest neat the floor and usually the highest at the extract point.

Without the use of chilled ceiling the displacement ventilation system is unable to remove heat loads of 62W/m^2 even at high air change per hour.

The combined chilled ceiling and displacement ventilation system, the displacement flow could be preserved under low cooling load e.g. loads under 40W/m^2.

The temperature profiles at high ceiling temperatures have a displacement flow pattern, where low ceiling temperatures disturb the displacement airflow pattern.

The floor air temperature ratio was found to decrease with increasing supply airflow rate, this concurs with the findings of Mundt (1990) and Li *et al.*(1993).

Conditions near the ceiling were found to be approximately adiabatic in the case of the displacement ventilation only experiments. In the cases where the both displacement ventilation and chilled ceiling was operating, a negative temperature gradient was introduced in a layer of air stream and a reduction in overall air temperature gradient in the room.

Reduction of the ceiling temperature in the displacement ventilation and chilled ceiling experiments caused a reduction in the proportion of the load transferred to the air stream and a reduction in the overall air temperature gradient in the room, this agrees with Loveday, Taki (1998), and Rees (1998).

In the test results for displacement ventilation and chilled ceiling combined. The results show that greater mixing was evident in the upper part of the room as indicated by reduced air temperature gradients above a height of approximately 1.2m.

The combination of displacement ventilation and chilled ceiling system with out the honeycomb slats can cause the destruction of the displacement flow pattern. Thus reducing the air quality this agrees with the finding of Kruhne, Taki, loveday, Bunn, (1996) and also the CFD simulation for the test conditions of displacement ventilation and chilled ceiling system.

The experimental results indicate that by attachment of the Honeycomb slats at the optimum configuration to the ceiling at low ceiling temperatures 12°C, 14°C, and 16°C the displacement airflow pattern can be reintroduced into the room. Therefore producing better air quality which had been reduced in the absent of the honeycomb slats.

It can be concluded that the use of displacement ventilation and chilled ceiling system will disturb the displacement

ventilation and reduce the air quality in the room, both in the occupied zone and in the zone near the ceiling. Where as the attachment of a honeycomb slat system can raise the general air temperature in the space and permit some displacement ventilation to occur (as shown by the presence of an inclined temperature gradient in the vertical direction) in situations where, without the slats, it would have been completely destroyed. This can be explained by the suppression of the cool downward air currents as a result of the honeycomb slat-clad ceiling system.

CHAPTER NINE

9.0 CFD simulation of laboratory results

9.1 CFD simulations to verify laboratory results

This chapter deals with the verification of the experimental laboratory work with the use of CFD simulation. Chapter five provided the optimum depth width ratio for the honeycomb slats to be attached to the ceiling. The CFD simulation carried out in chapter five were based on individual honeycomb slat investigation and did not provide / show the results for the whole room environment.

The optimum depth width ration of 10:1 which was simulated in chapter Five and then manufactured and installed in the test chamber for experimental investigation (chapter 6,7 and 8) did indeed produce the results that were predicted by the CFD code as mentioned in chapter Five.

Due to vast complexity and the number of cells required to simulated the whole room environment with the honeycomb slats attached to the ceiling for the optimum depth width ratio

the Sabre-One CFD as well as CFX5 was not able to simulate the required environment. However Sabre-One CFD code was able to simulate a lower depth width ratio for the honeycomb slats attached to the ceiling. Figures 9.1 to 9.14 show the CFD simulation.

The results of CFD simulations do indicate that with the attachment of the honeycomb slats to the ceiling, does effect the airflow movement near the ceiling this is clearly visible in the airflow vectors shown in the above mentioned figures. Figure 9.1 and 9.2 show the results for the case study where honeycomb slat of $1m^2$ section was simulated in the centre of the room. The CFD simulations results show that with out the honeycomb slats (figure 9.1) the airflow at the centre of the room near the ceiling is producing a convection current that would transport contamination into the low room zone. Figure 9.2 shows that by attaching the honeycomb slat in the centre of the room can disturb the convection current process directly below the honeycomb slats, this is because of the suppression of the convection current airflow between the honeycomb slats.

Figure 9.3 show the airflow vectors in the centre of the room for the case without honeycomb slats. The CFD simulation clearly show that in the centre of the room large convection

current cells are produced and also the cold ceiling air is also moving away from the ceiling in a downward direction from the ceiling and is transporting contaminants in to the lower zone. Figure 9.4 shows the CFD simulation results for the same test case but with the use of honeycomb slats. The results indicate that by inserting the honeycomb slat in the centre of the room it disturbed the convection current near the ceiling and prevents the cold ceiling air from travelling downward towards the lower zone of the room and thus reduce the transportation of the contaminated air. Figures 9.5 to 9.12 show the CFD simulations results for the test case where the whole room has honeycomb slats attached to the ceiling. As expected the results show that by attaching the honeycombs slats to the chilled ceiling, the convection current can be suppressed near the ceiling (between the honeycombs slats) and prevent the cold air transporting contaminants towards the lower zone of the room. Figure 9.5 shows the CFD simulations for the room without honeycomb slats attached to the ceiling. In figure 9.5 it can be seen that at the ends of the walls large convection current airflow cells are present and smaller convention current cells between the heat sources. Figure 5.6 shows the CFD simulations for the case with the whole room having honeycomb slats attached to the ceiling. The results show that

the large convention current airflow cells near the walls are not seen and also the smaller convection cells between the heat sources are also not seen, thus indicating that by attaching the honeycombs slats to the ceiling the convection current can be suppressed and a displacement airflow pattern can be re established in the room. Figures 9.7 and 9.8 show the detail CFD simulation of the airflow above the heat source and near the ceiling.

Figures 9.9 and 9.10 show the airflow and airflow line vectors above the heat sources and in the room for both without and with the honeycomb slats attached to the ceiling. It can be seen that for the case without the honeycomb slats large convection current cells are seen near the end walls were these convection current cells are not seen for the case where honeycomb slats are attached to the ceiling.

Figure 9.11 to 9.14 show the temperature contour for both cases without and with honeycombs slats attached to the ceiling.

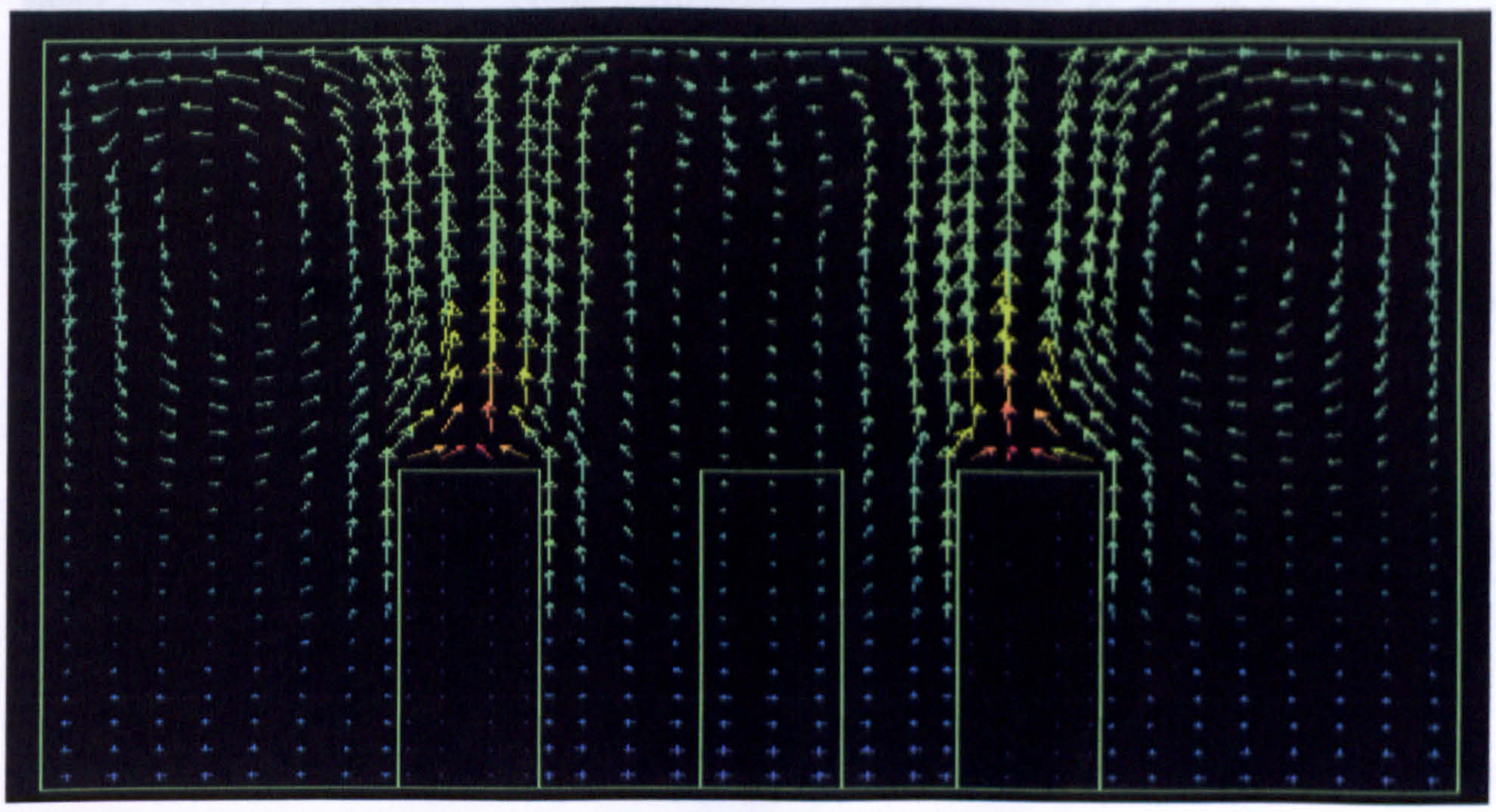

Figure 9.1: Showing airflow vectors above two the heat source without honeycomb slats, convection current cells can be seen.

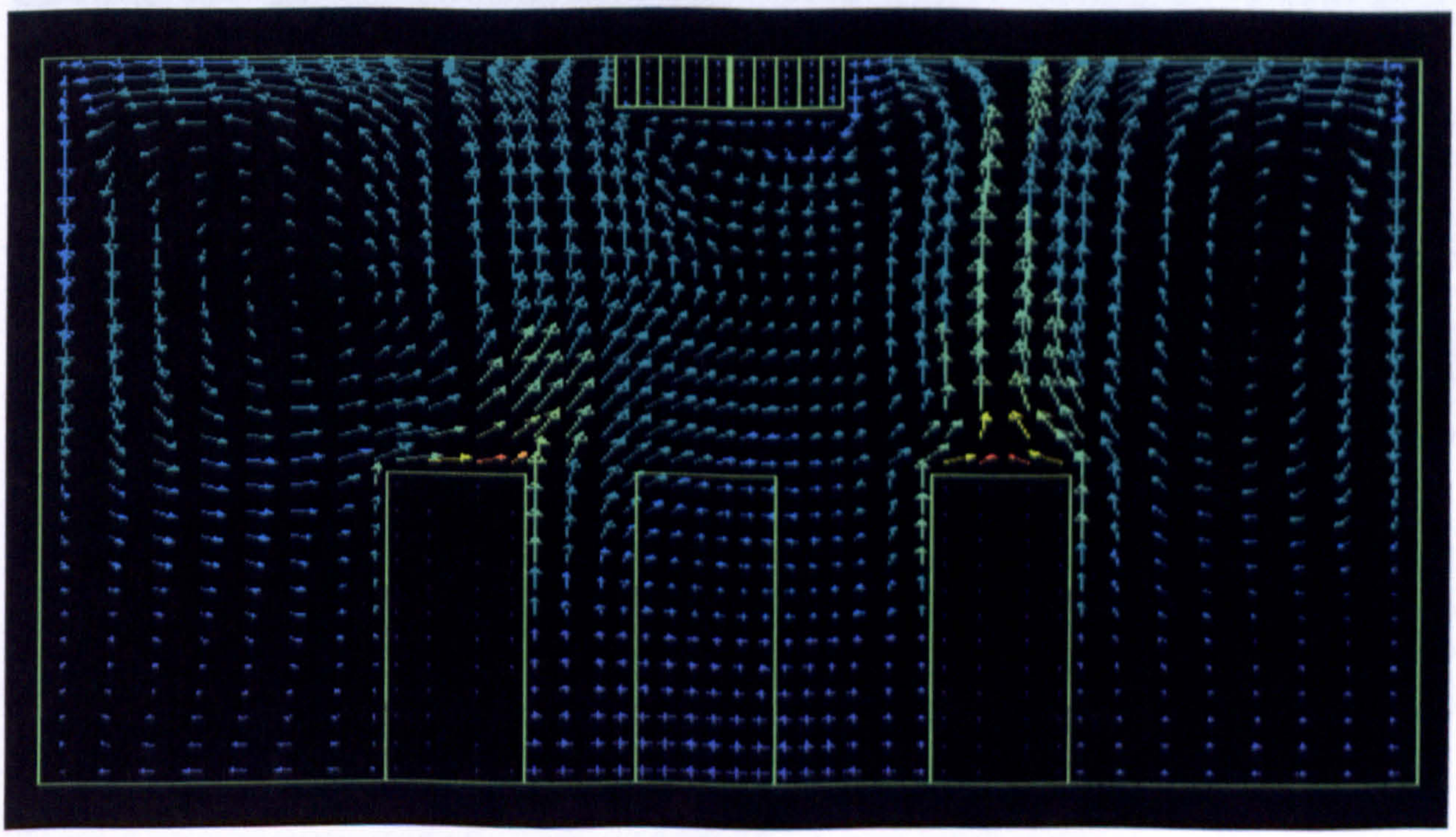

Figure 9.2: Showing airflow vectors above two heat sources with honeycomb slats attached to ceiling.

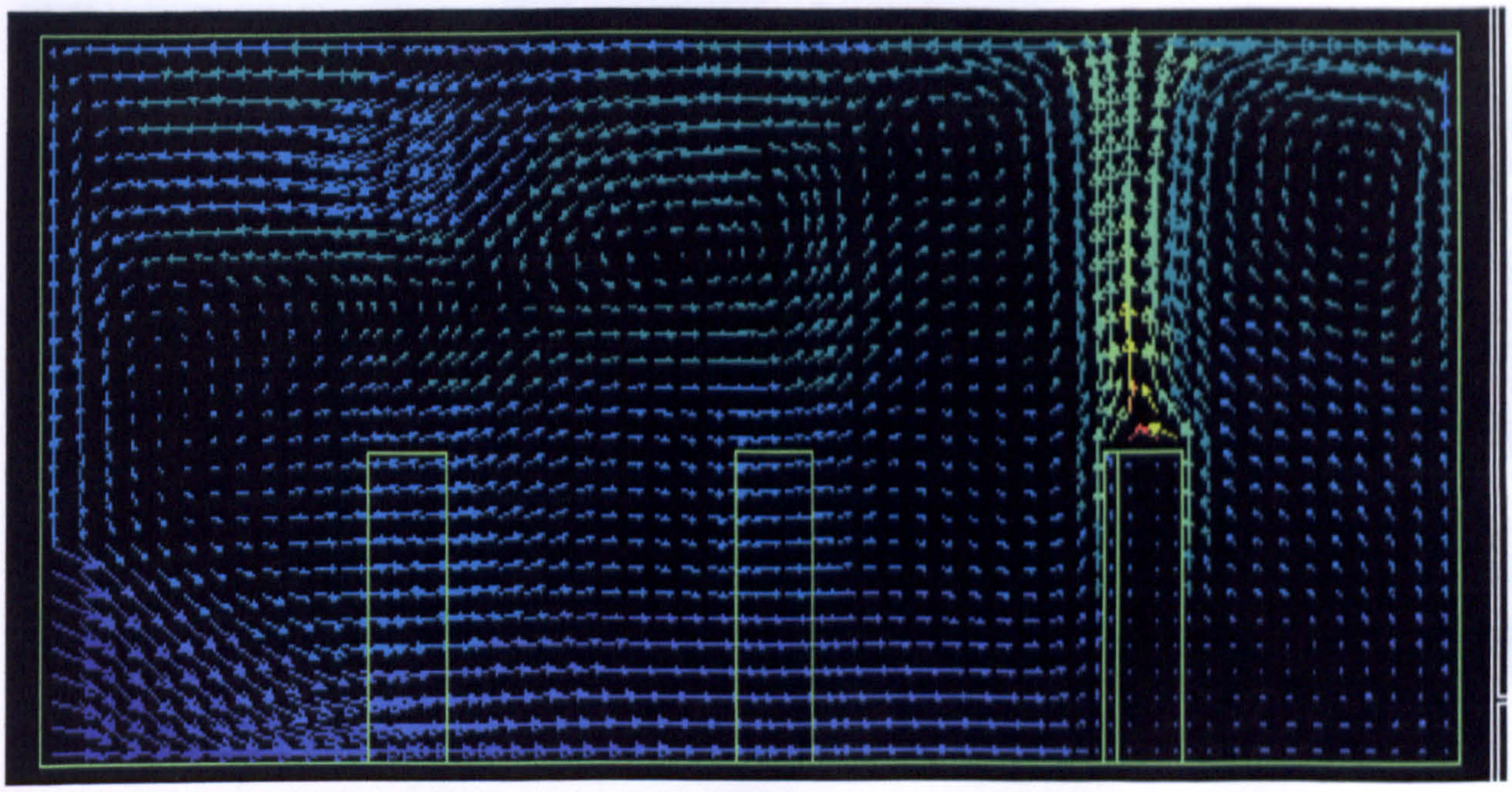

Figure 9.3: Showing airflow vectors in the room and above a heat source without honeycomb slats, convection current cells can be seen

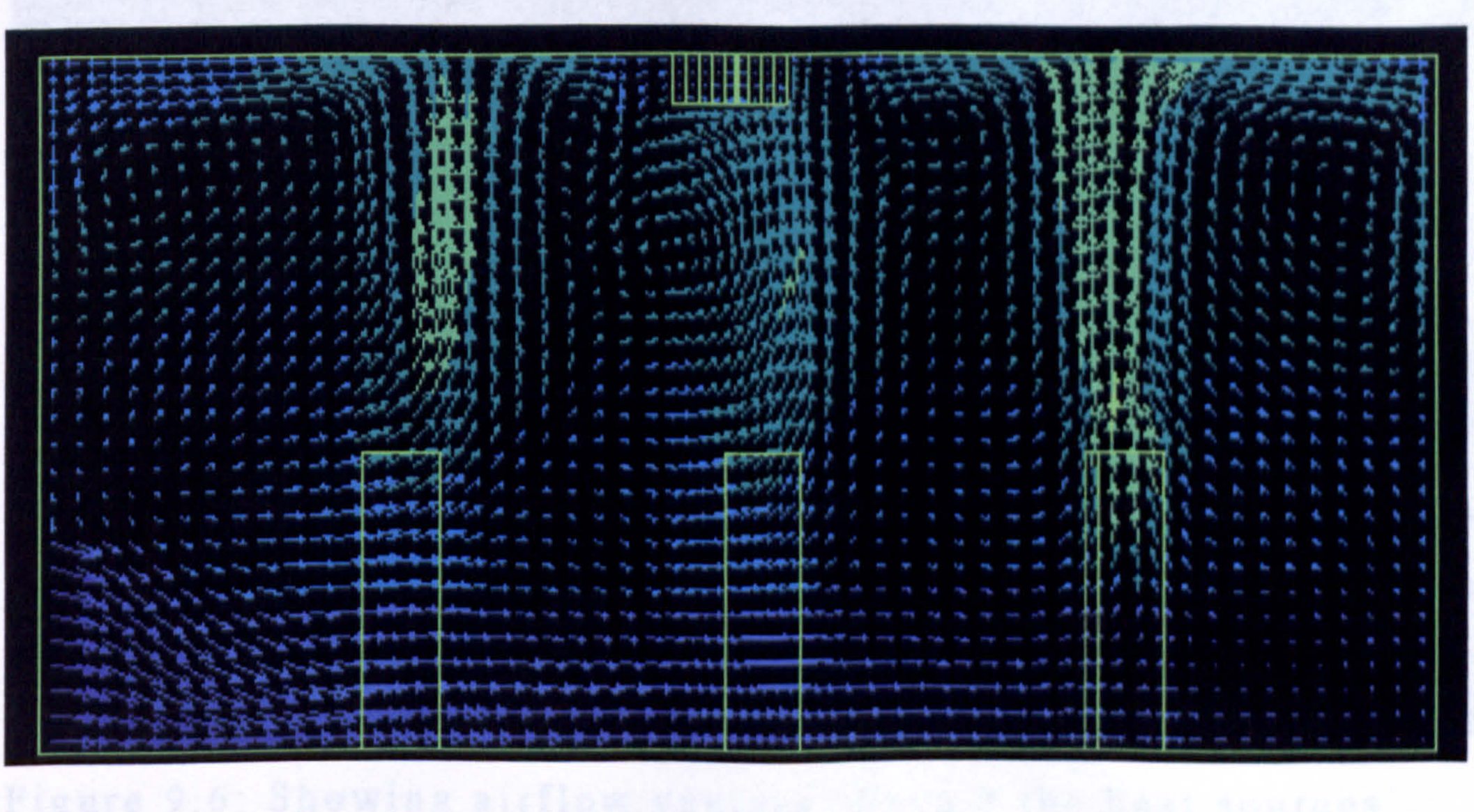

Figure 9.4: Showing airflow vectors above two the heat sources with honeycomb slats attached to ceiling.

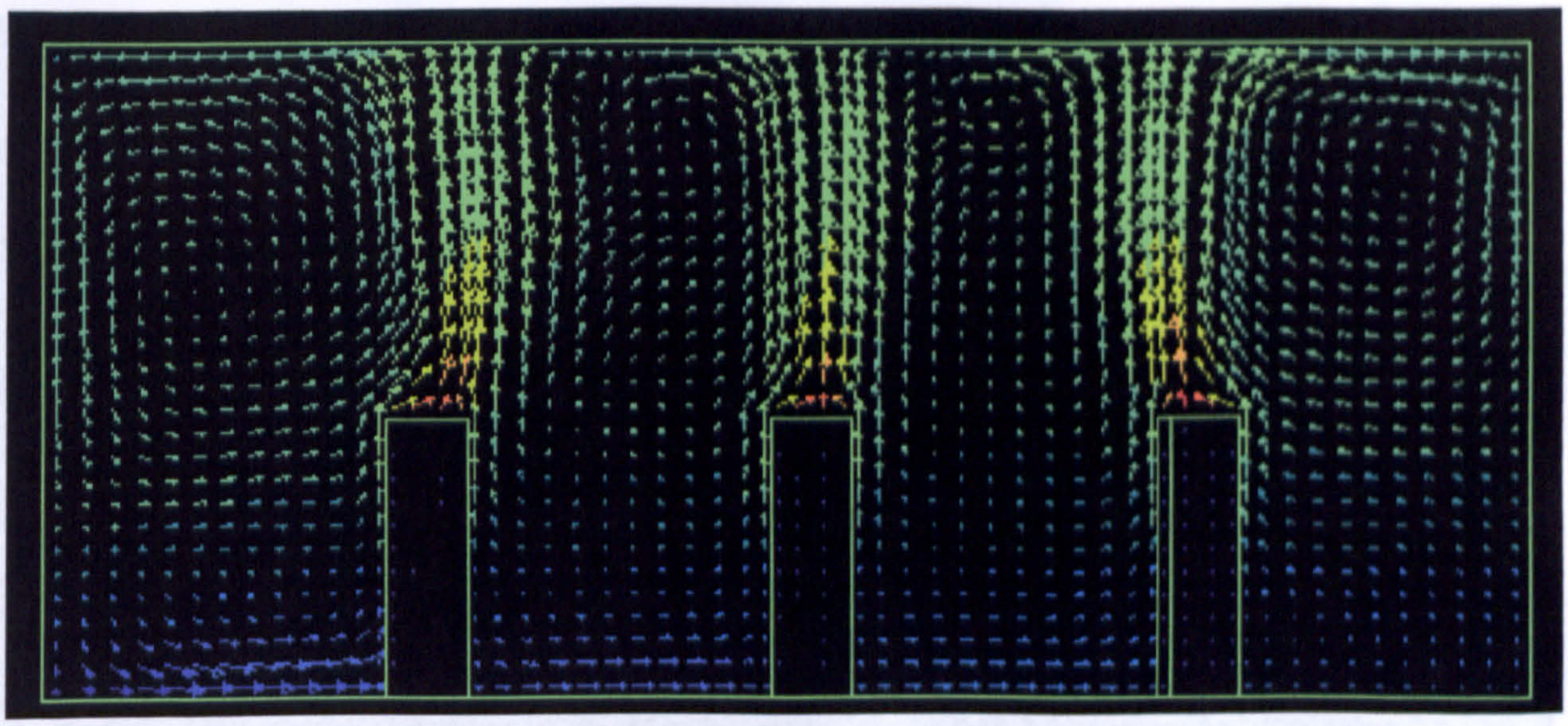

Figure 9.5: Showing airflow vectors in the room and above 3 heat sources without honeycomb slats, convection current cells can be seen.

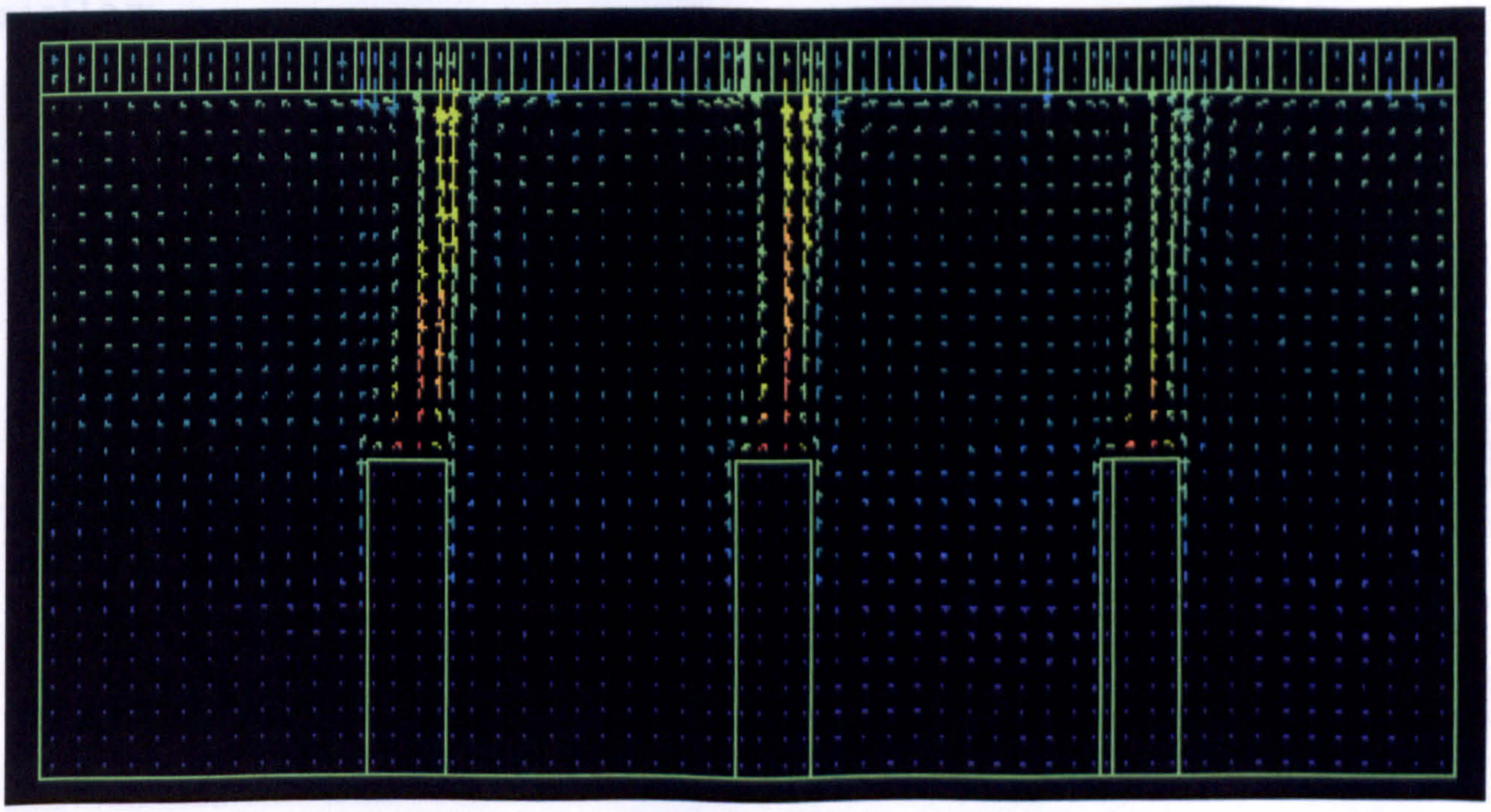

Figure 9.6: Showing airflow vectors above 3 the heat sources with honeycomb slats attached to ceiling the convection currents have been suppressed.

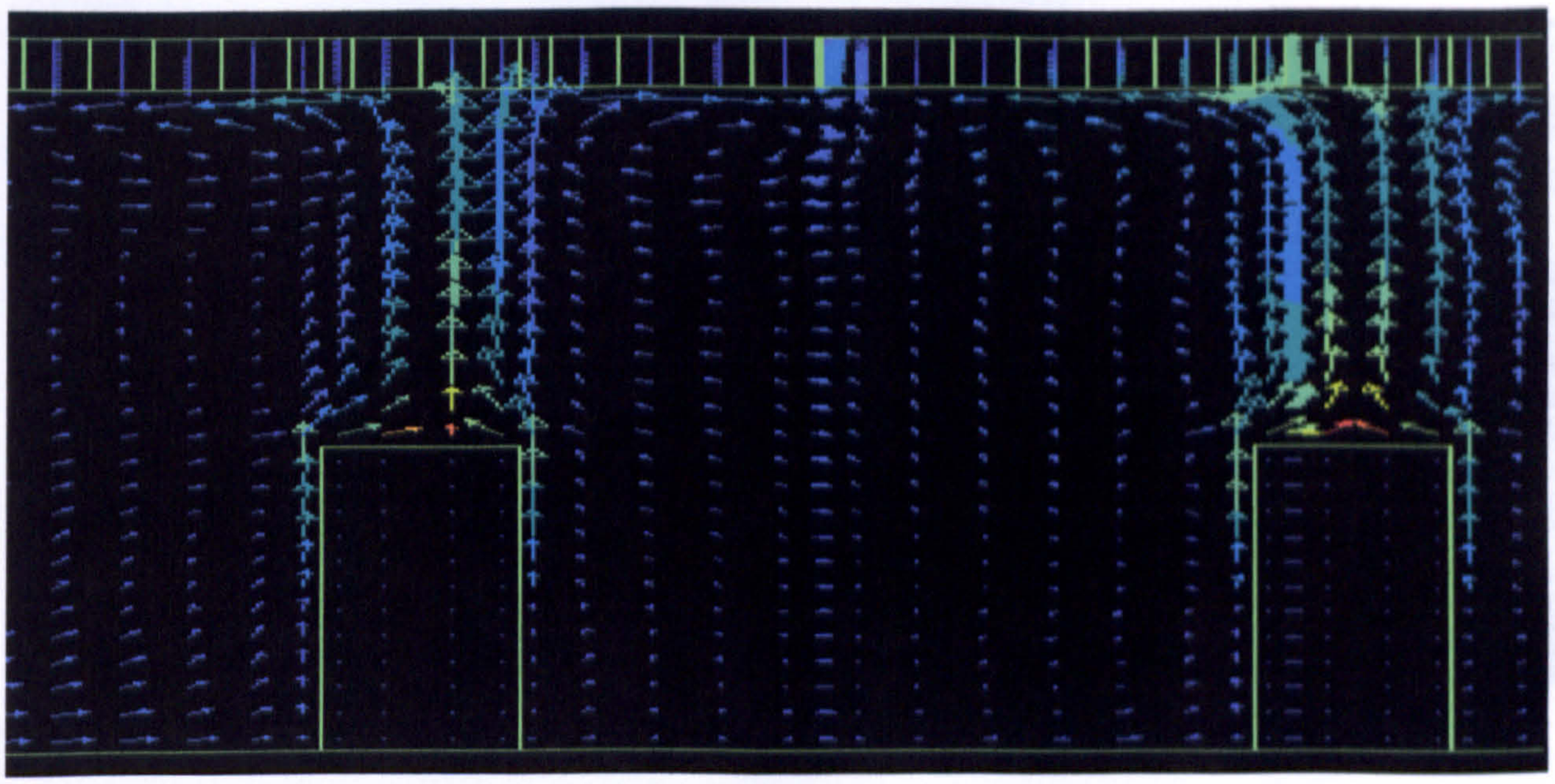

Figure 9.7: CFD simulation with honeycomb slats attached and the effects the honeycomb slats have on the heat plume and airflow

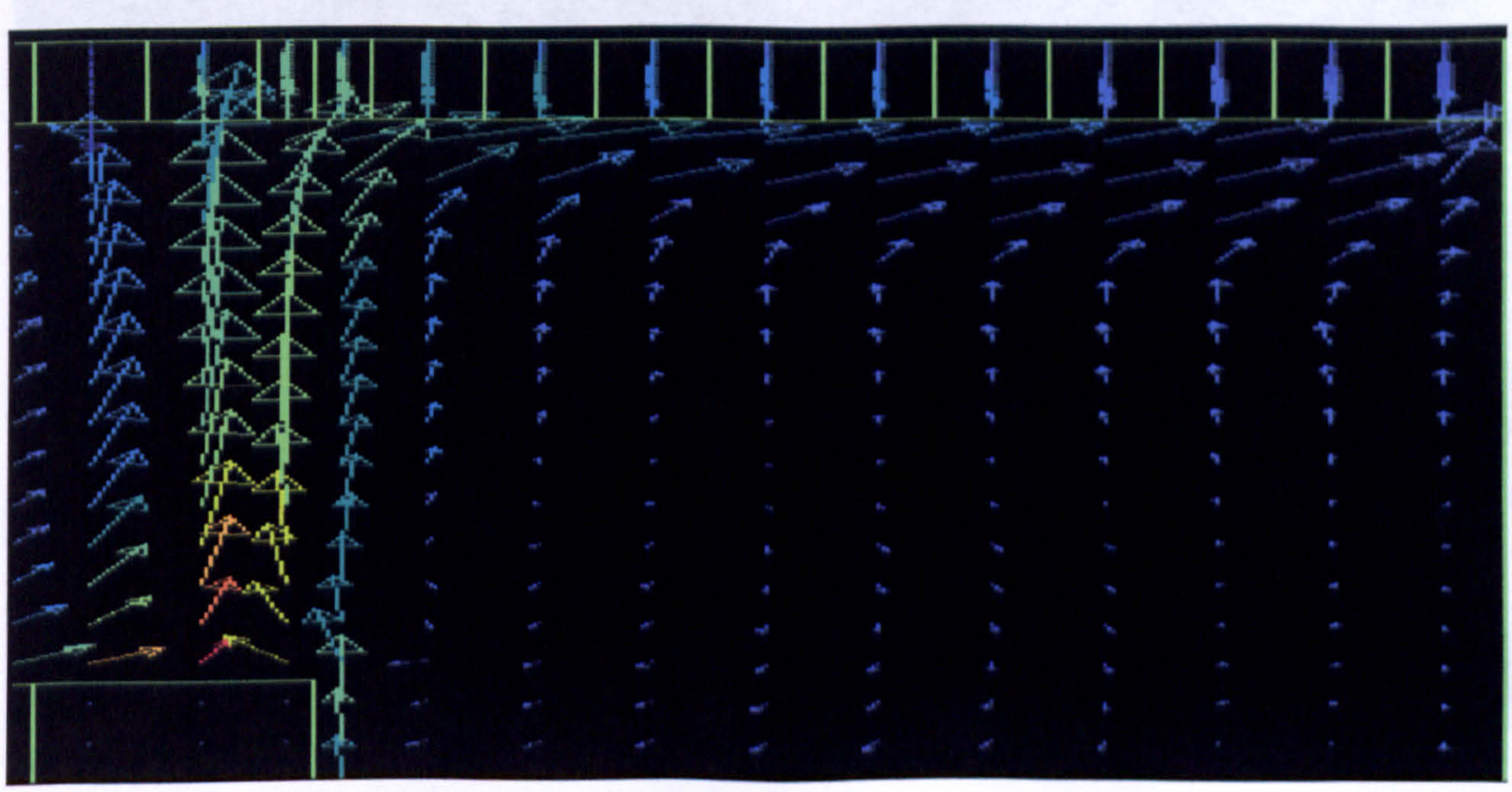

Figure 9.8: CFD simulations showing the airflow near the ceiling and near the honeycomb slats

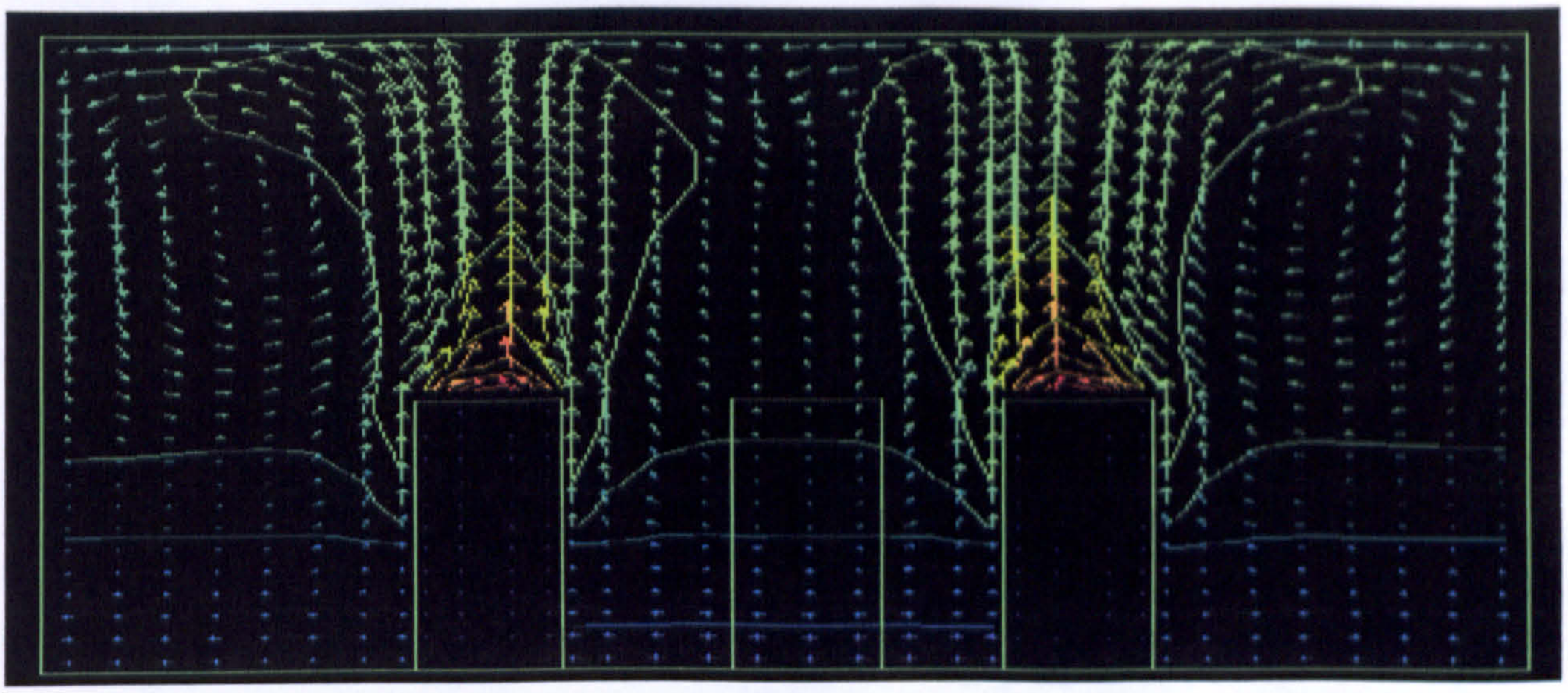

Figure 9.9: Showing airflow vectors, airflow line contours above two the heat source without honeycomb slats, convection current cells can be seen.

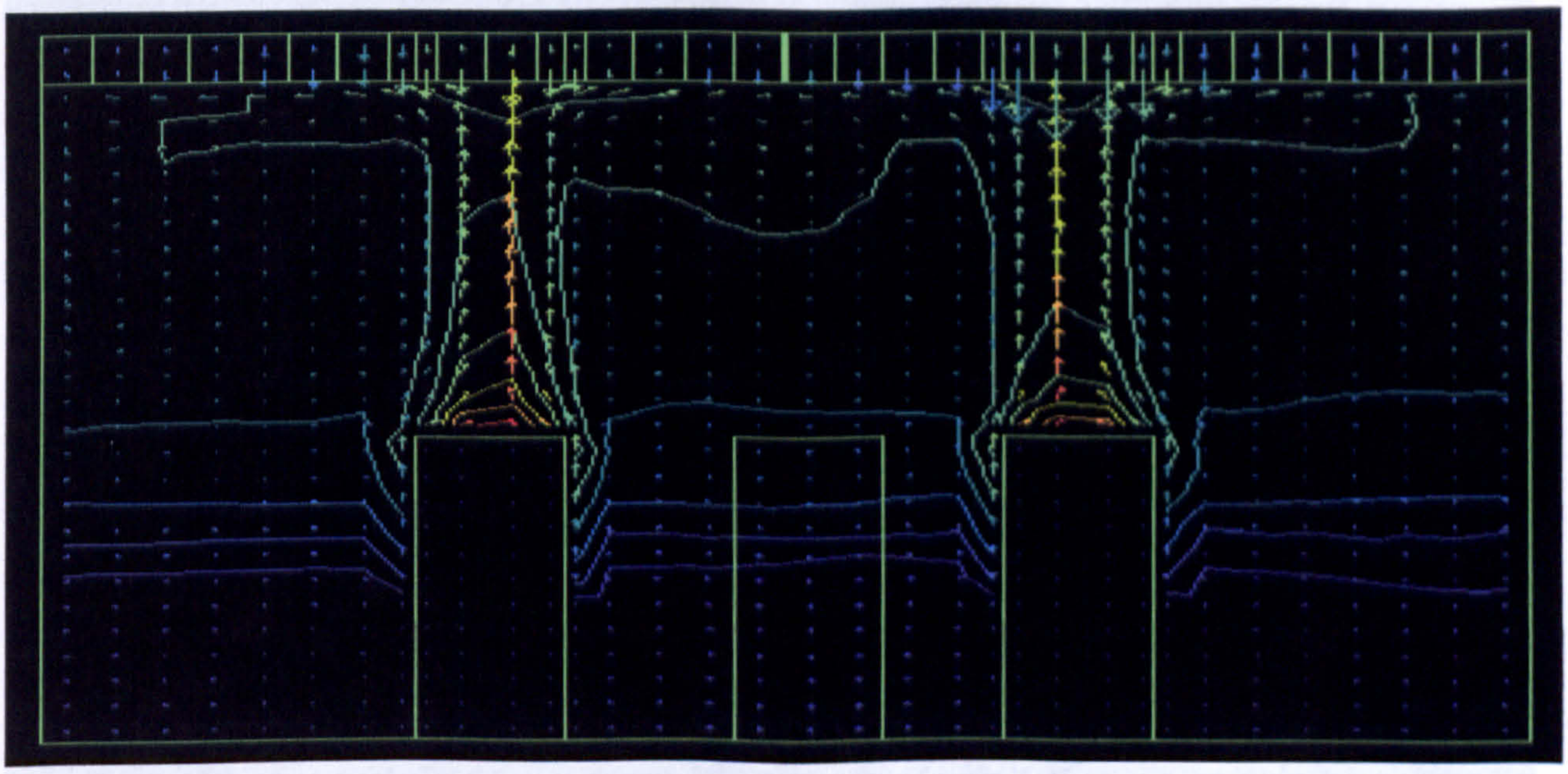

Figure 9.10: Showing airflow vectors, airflow line contours above two the heat source with honeycomb slats, convection current cells have been suppressed.

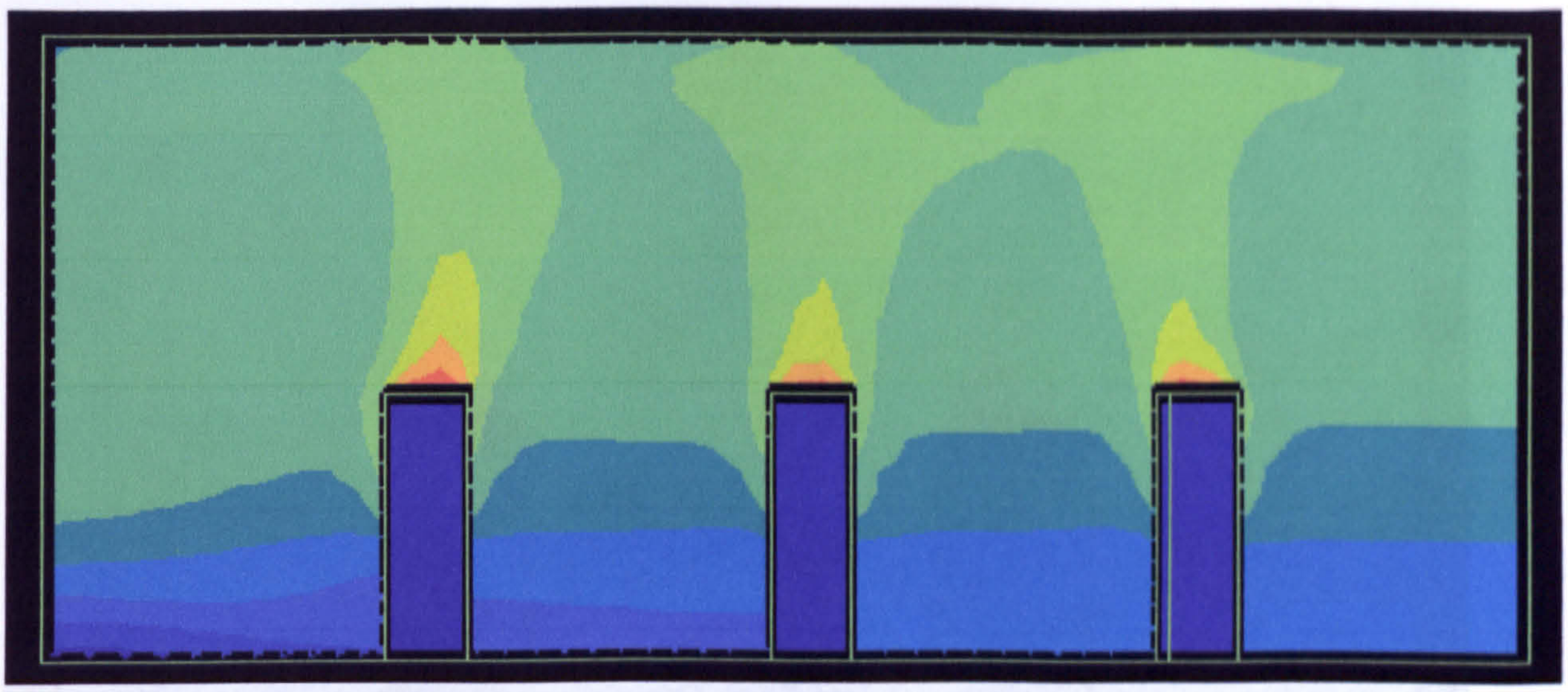

Figure: 9.11: Airflow temperature contours in the room above 3 heat sources without honeycomb slats attached to the ceiling.

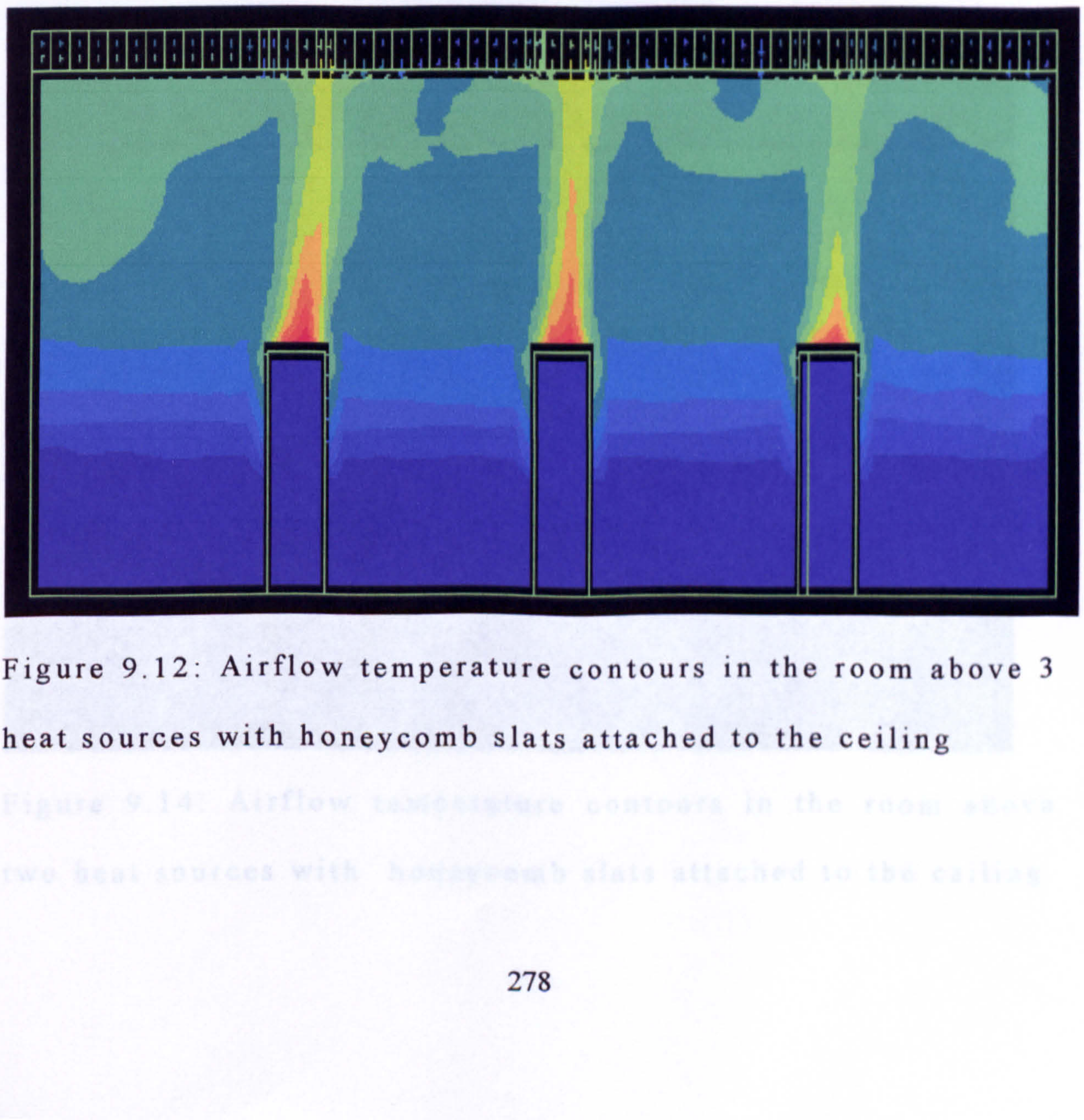

Figure 9.12: Airflow temperature contours in the room above 3 heat sources with honeycomb slats attached to the ceiling

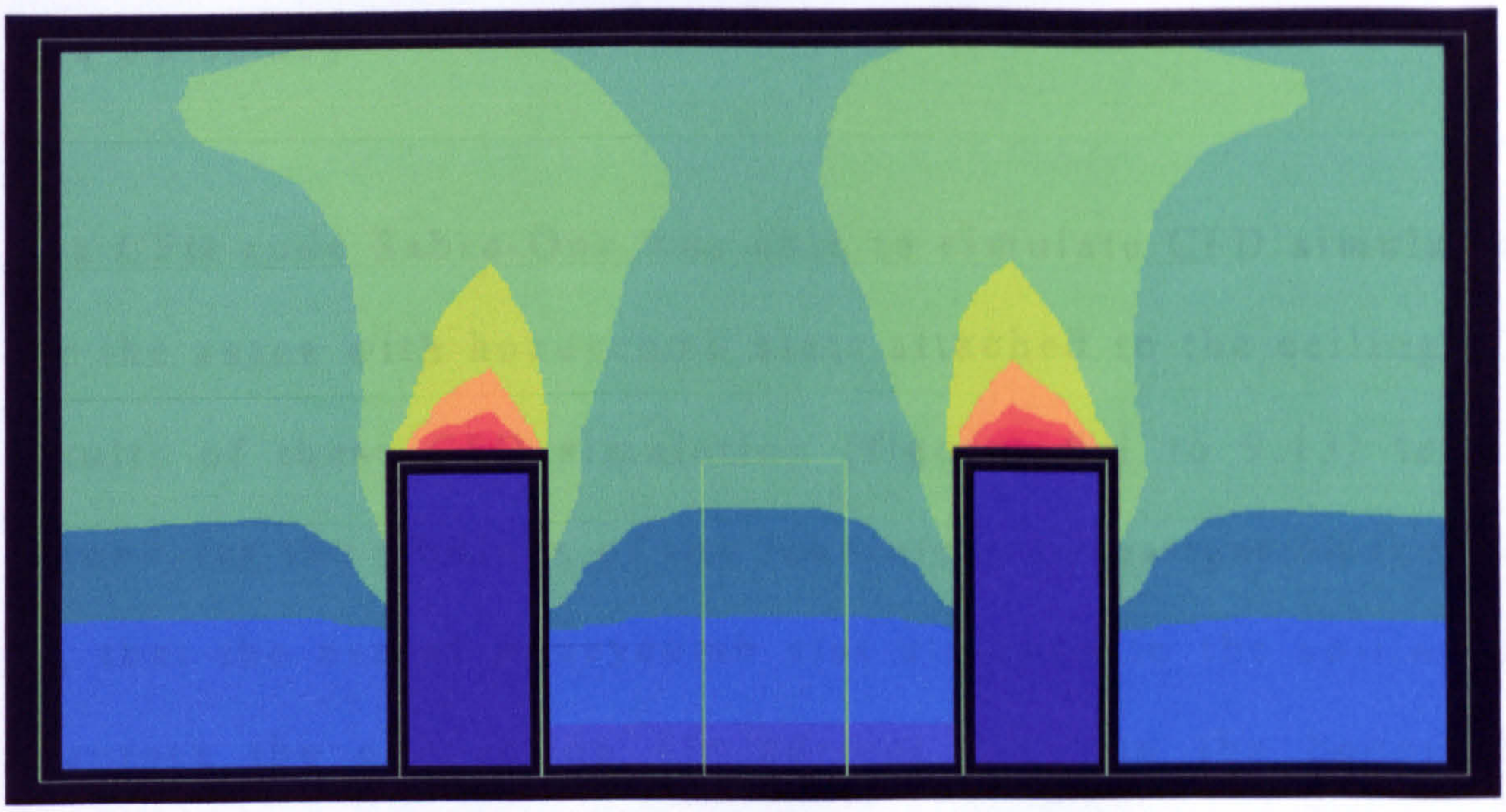

Figure 9.13: Airflow temperature contours in the room above two heat sources without honeycomb slats attached to the ceiling.

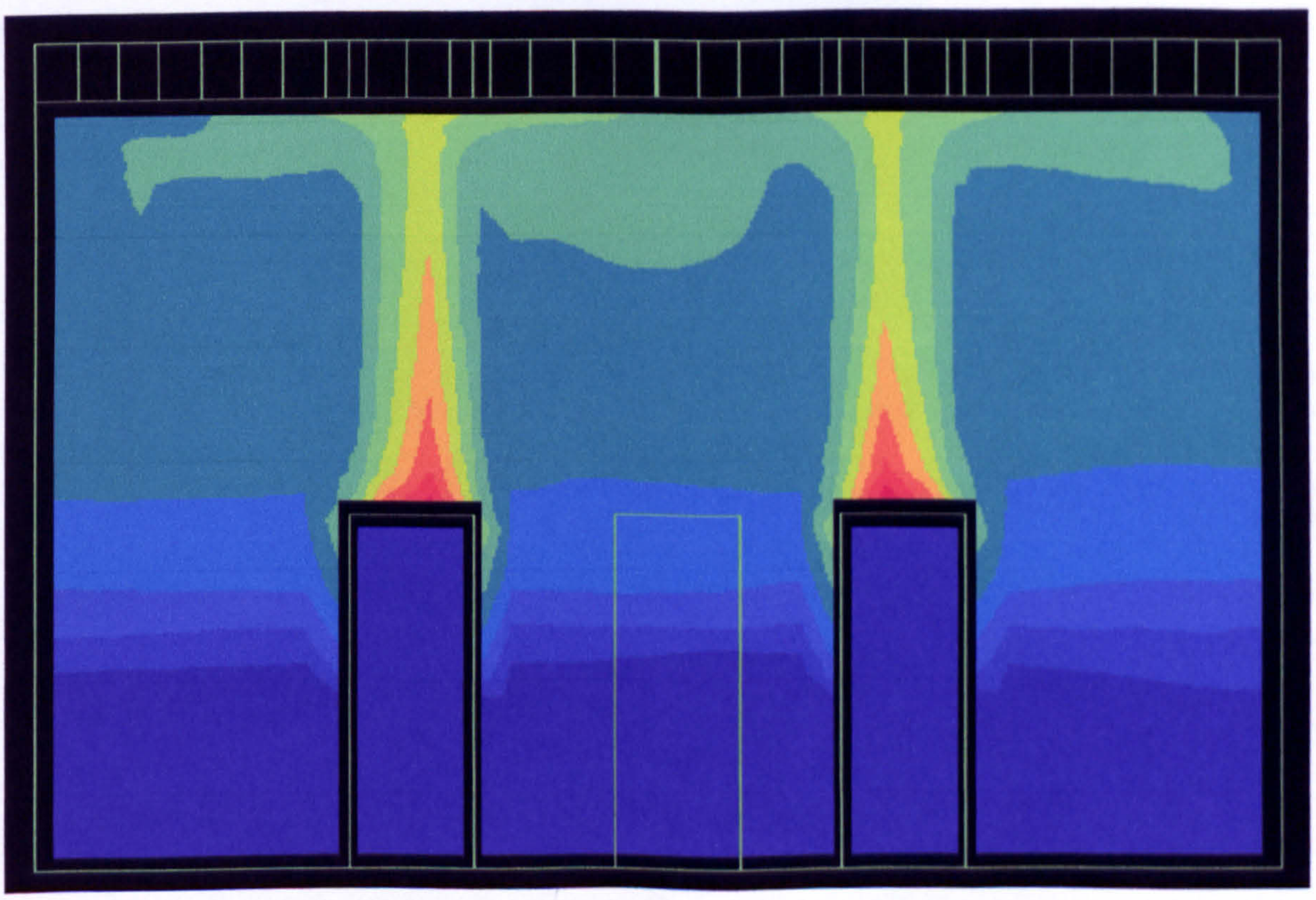

Figure 9.14: Airflow temperature contours in the room above two heat sources with honeycomb slats attached to the ceiling.

9.2 Summary

The CFD code Sabre-One was able to simulate CFD simulations for the cases with honeycomb slats attached to the ceiling. The results of these CFD simulation (figures 9.1 to 9.13) tend to agree with the findings of the laboratory investigation (chapter 8), that the use of honeycomb slat attached to the ceiling can suppress the convection air current between the honeycomb slats and re introduce the displacement airflow pattern in the room, thus improve the air quality.

CHAPTER TEN

10.0 Conclusions and recommendations

10.1 Conclusions

The literature review in chapter two highlighted that the current situation with the combined displacement ventilation and radiant cooling systems at low ceiling temperatures can disturb the displacement airflow pattern and thus transport the contaminated air near the ceiling to the occupied zone, also causing the height of the stratified boundary layer to be reduced.

Both CFD simulations and experiments have been carried out to test the use of a honeycomb slat system for suppressing downward cool air currents in a combined chilled ceiling / displacement ventilation environment. The following conclusions may be drawn from this thesis:

- The CFD model Sabre-One was successful in modelling the required environments and the results had good agreements with both, other CFD codes and experimental

findings found in published literature as those reported by (Taki et al, 1996), (Kruhne, 1993), (Alamdari and Eagles, 1996), and (Fitzner, 1996). This proves that the CFD code can be regarded as an effective tool for accurately predicting airflow and temperature distributions, and for assessing the adverse effect on the air quality in such combination environments.

- Both CFD simulations and experimental findings conclude that without the use of chilled ceiling the displacement ventilation system is unable to remove heat loads of $62 W/m^2$ even at high air changes per hour, in order to meet the criteria as presented in ISO 7730.

- CFD results have raised a question in connection to the ISO 7730 (1994). That if heat load of $25 W/m^2$ is imposed on various heights above the floor, in some cases the air temperature gradient could exceed the requirements of $3°C/m$.

- In the absence of slats, both the CFD and experimental results show that the combination of a chilled ceiling with a displacement ventilation system can potentially

destroy the displacement flow pattern. This is particularly the case at ceiling temperatures of 16°C or below, and is caused by downward currents of cool air producing mixing of the room airflow. At a ceiling temperature of 18°C and above, displacement flow is evident. Such a combination therefore requires careful design to work effectively (see also Loveday et al, 1998). The findings also show that greater mixing was evident in the upper part of the room as indicated by reduced temperature gradients.

- The K-epsilon CFD simulation model was able to simulate accurately the critical Rayleigh number (1708), for two horizontal parallel plates as reported by lord Rayleigh (1916).

- The CFD simulation was able to produce the optimum configuration (depth to width ratio of 10:1) for the honeycomb slats to suppress the air convection current for Rayleigh numbers range from 10^6 to $7x10^6$. For higher Rayleigh numbers the optimum configuration depth to width ratio would be greater than 11:1.

- Both CFD and experimental results show that the attachment of a honeycomb slat system can raise the general air temperature in the space and permit some displacement ventilation to occur (as shown by the presence of an inclined temperature gradient in the vertical direction) in situations where, without the slats, it would have been completely destroyed. This can be explained by the suppression of the cool downward air currents as a result of the honeycomb slat-clad ceiling system.

- The work presented here has confirmed the feasibility of the slat system approach as a means for preserving displacement flow in the presence of a chilled ceiling.

The research work carried out has a significant contribution in the field of improving better air quality and thermal comfort in a combined displacement ventilation and radiant cooling system.

The research work described in this thesis can have a major contribution to the following areas:

- The designers of radiant cooling/displacement ventilation systems will benefit as a result of the knowledge gathered by this study. The work will enhance knowledge in the application of CFD for designing such environments

- CFD modellers and developers in academia and industry will benefit from the work in producing general advice for modelling and simulating such new cooling system. They will be able to use the findings for validation of CFD codes and other (zonal) models.

- Building occupants will enjoy improved air quality and thermal comfort, leading to potential improvements in their health and productivity

The above new technique, has been proven by this thesis, can be used as general advice for designers as regards the combination of radiant cooling/displacement ventilation systems with the aim of producing thermally stable, comfortable, healthy, and good air quality spaces to the enhanced satisfaction of the occupants. In addition, the work

will enhance knowledge related to the international trend towards low energy cooling technologies.

10.2 Further recommendations

- Work from this study can potentially lead to further research to investigate the relationship between energy consumption and thermal comfort together with indoor quality. In addition thermal performance of the chilled ceiling in such new environments could be further analysed to produce new set of guidelines relating to heat removal by both convection and radiation.

- The effects of different materials that could be used to manufacture the honeycomb slats could be further investigated.

REFERENCES

Alamdari Farshad, (1995), Static Cooling and Displacement, Building Services Journal, July 1995, pp 29-30

Alamdari, F and Eagles, N, (1996), 'Displacement Ventilation and Chilled Ceilings', *BSRIA, Technical Note TN2/96*, March 1996.

Alamdari F, (1998), Displacement Ventilation and Cooled Ceilings, Room vent 98 6th international conference on air distribution in rooms, Stochohm, Sweden, June 14-17, 1998 pp 197-205.

Alamdari F, D.J.G. Butler, P.F. Grigg and M.R. Shaw, (1998) Chilled Ceiling and Displacement Ventilation, Renewable Energy, vol 15, 1998, pp 300-305.

Andrew Martin, Farshad Alamdari, (1997), Condensation Control for Chilled Ceiling and Beams, Building Services Journal, Oct. 1997, pp, 45-47,

Antonopoulo KA, (1998), Experimental Evaluation of Energy Savings in Air-Conditioning Using Metal Ceiling Panels, Applied Thermal Engineering, Nov 1998, V 18, No. 11 pp 1129-1138

Asako.Y, Y.Yamaguchi and L Chen, (1996), Combined Natural Convection and Radiation Heat Transfer in A Vertical Air Cavity with Hexagonal Honeycomb Core of Negligible Thickness, Numberical Heat Transfer, Part A, 30: 73-85, 1996.

Behne Martin, (1999), Indoor Air Quality in rooms with Cooled Ceiling s. Mixing Ventilation or Rather Displacement Ventilation. Energy and Building Vol 30, 1999, pp 155-166

Behue Martin, (1995), Is There a Risk of Draft in Rooms with Cooled Ceiling, ASHRAE Transactions, 1995, Vol 101,No. PT 2, pp 744-752

Birol I. Kilkis, Coolp, (1995),A Computer Program for the Design and Analysis of Ceiling Cooling Panels, ASHRAE Transactions, 1995, V 101 No. Pt 2, pp. 703-710

Brohus H.(19980 Influence of a cooled ceiling on Indoor air quality in Displacement Ventilation room examined by means of Computational Fluid Dynamics, Proceedings of Room vent 98, Stockholm 1998 pp 53-57

Brubk MF, (1993), Cooling Ceiling: an Opportunity to Reduce Energy Costs by Way of Radiant Cooling, ASHRAE Transactions, 1993, Vol 99, Pt 2 pp 479-487.

Buchberg H, I.Catton, D.K. Edwards, (1997), Natural Convection in Enclosed Spaces- a Review of application to Solar Energy Collection, Journal of Heat Transfer 98 (1997) pp 182-188.

Bunn Roderic and Wyatt Terry, (1991), The Future for Cooling Ceiling The Future, Building Services Journal, Nov- 1991, pp, 33-36

Bunn Roderic, (1994), Beaming Down, Building Services Journal, June 1994 pp 33-34

Bunn Roderic, (1995), Chilled Lessons-Active Versus Passive Beams, Building Services Journal, May 1995 pp 37-39

Bunn Roderic, (1994), Looking Radiant, Building Services Journal, June 1994, pp, 21-24

Bunn Roderic, (1996), The Perfect Mix , Finding the Right Mix, Building Services Journal, August,1996, pp 43-44

Busweiler U, (1993), Air Conditioning with a Combination of Radiant Cooling, Displacement and Dessicant Cooling, ASHRAE Transactions, 1993, v99 No. Pt 2, pp. 503-510

Butler David, (1997), The Truth behind Chilled Ceiling, Building Services Journal, June 1997, pp, 53-55

Cane R.L.D, K.G.T Hollands, G.D. Raithby, T.E. Unny, (1997), Fee Convection Heat Transfer Across Inclined Honeycomb Panel. Journal of Heat Transfer, February 1977 pp 86-91,.

Cengel, YA, (1998), 'Heat Transfer- A Practical Approach International Edition, McGraw-Hill Companies, Inc., 1998.

Charters W.W.S., L.F.Peterson, (1972), Free Convection Suppression Using Honeycomb Cellular Materials, Solar Energy, Vol 13, 1972, pp 353-361.

Cook MJ (1998), An Evaluation of Computational Fluid Dynamics for Modelling Buoyancy Driven Displacement Ventilation Ph.D. Thesis De Montfort University England.

Cost Research and Engineering Services Department, (1998), Air Conditioning and Displacement Ventilation: System Analysis, Building Services Journal, Sep, 1998, pp 18-21

Davids Gavin, (1994), A Model Performance, Building Services Journal, June 1994 pp 29-30

Dickson Don, (1994), A Test Time for Chilled Ceiling, Building Services Journal, June 1994, pp, 31-32

Faber, T. E. (1995) Fluid Dynamics for Physicists. New York: Cambridge University Press, 1995.

Fanger P.O. BM Langllde.G. Olesen Christensen N.K. and Tanabes (1998). Comfort limit for Asymmetric Thermal Radiation. Energy and Building 1998 Vol 8: pp 225 236

Feustel HE, Stetiu C, (1995), Hydronic Radiant Cooling Preliminary Assessment, Energy and Building, Aug 1995, V 22, No. 3, pp 193-205

Fitzner, K, (1996), 'Displacement Ventilation and Cooled Ceilings, Results of Laboratory Tests and Practical Installation', The Seventh International Conference on Indoor Air Quality and Climate, Indoor Air '96, Nagoya, Japan, July 1996 pp 41-50.

Fitzner F, H Kruhne, (1995), Displacement Flow and Cooling Ceiling, Proceedings of Healthy Buildings, Milan, September 1995.

Francia, G, (1961) " Un Noveau Collecteur de L'Energie Rayonnante Solaire- Theories ET Verification Experimentales", United National Conference on New Sources of Energy, E/Conf. 35/S/71, 1961

Helmut E Feustel, Corina Stetiu, (1995), Hydronic Radiant Cooling Preliminary Assessment, Energy and Buildings vo 22, 1995, pp 193-205

Hodder SG, DL Loveday, KC Parson, AH Taki, (1998), Thermal Comfort in Chilled Ceiling and Displacement Ventilation Environment: Vertical Radiant Temperature Asymmetry Effects, Energy and Building 1998, V 27, No. 2, pp 167-173

Holger Kruhne, (1993), Effect of Cooled Ceilings in Rooms with Displacement Ventilation on the Air Quality, Proceeding of Indoor Air 93, Vol 5, 6th Int' conf, on Indoor Air Quality & Climate pp 395- 400

Hollands K G T, (1965), 'Honeycomb Devices in Flat-Plate Solar Collectors', *Solar Energy* Vol.9, No.3, 1965 pp 159-165.

Hollands, K G T, (1973), 'Natural Convection in Horizontal Thin-Walled Honeycomb Panels', *Journal of Heat Transfer*,1973 PP 439-444.

Hollands, K G T, (1973), 'Natural Convection in Horizontal Thin-Walled Honeycomb Panels', *Journal of Heat Transfer*, 1973 pp 439-444,.

Hollands, K G T, (1985), 'Proposed for a Compound-Honeycomb Collector', *Solar Energy* Vol.34, No.4/5, 1985. pp 309-316.

Hollands, K.G.T, (1965), " Honeycomb Devices in Flat-Plate Solar Collectors, Presented at the Solar Energy Society Conference, Phoenix, Arizona, March 15-17, 1965. Vol. 9, No 3, 1965

Hollands K.G.T. and K. Iynkaran, (1985), Proposal For A Compound-Honeycomb Collector, Solar Energy. Vol 34. No 4/5, 1985 pp 309-316,.

Hoogendoorn CJ, (1985), Natural Convection Suppression in Solar Collectors, in : S.Kakac, W.Aung, R.Viskanta, (EDS.), Natural Convection, Fundamentals and Applications, Hemisphere Publication Corp, New York, 1985 pp 940-960

Hottel, H.C. and Keller, J D, (1993)," Effect of Reradiation on Heat Transmission in Furnaces and through Openings", Trans, ASME, IS55-6 (1933)

Imanari T, T Omori, K Bogaki, (1999), Thermal Comfort and Energy Consumption of the Radiant ceiling panel system compared with the Conventional all Air system, Energy and Buildings vol 30 1999 pp 167-175.

ISO 7730 (1994), 'Moderate Thermal Environments - Determination of the PMV and PPD indices and specification of the conditions for thermal comfort, Geneva: *International Standards Organisation*, 1994.

Jalil L, Taki AH, Loveday, DL, (2002), Computation of Airflow in a Displacement Ventilation / Chilled Ceiling Environmental, IndoorAir 2002, 9th Int' Conference on Indoor Air Quality and Climate, June 30th-July-5th 2002, Monterey, California, USA.

Jones P.J, G.E.Whittle, Computational Fluid Dynamics for Building Air Flow Prediction- Current Status and Capabilities.

Kangni A, R. Ben Yedder, and E. Bilgen. (1991), Natural convection and conduction in enclosures with Multiple Vertical Partitions, Journal Heat Mass Transfer, Vol. 34. NO. 11, 1991, pp 2819-2825.

Kruhne Holger (1993), Effects of Cooled Ceilings in Rooms with Displacement Ventilation on the Air Quality. 6th International Conference on Indoor Air Quality and climate Proceedings of Indoor Air 93 Vol 5, pp 395-400.

Kulpmann RW, (1995) Thermal Comfort and Air Quality in Rooms with Cooled Ceilings, ASHRAE Transactions, 1995, Vol 99,No. PT 2, PP 488-502

Lakhal EL, M.Hasnaoui, E.Bilgen and P.Vasseur, (1994) Natural Convection Heat Transfer In Honeycomb Enclosures With Perfectly Conducting Fins. International Conference on Fluid and Thermal Energy Conversion 94, Indonesia, December 12-15,1994.

Lord Rayleigh, (1916) " On Convection Currents in a Horizontal Layer of Fluid, when the Higher Temperature id on the Underside", *Phil. Mag., Ser. 6,32, 1916 p 529*

Loveday DL, Parsons, KC Taki AH, (1998) Designing for Thermal Comfort in Combined Chilled Ceiling / Displacement Ventilation Environment, ASHRAE Transactions, 1998, Vol 104, No. Pt 1B pp 901-910

Loveday, DL, Parsons, KC, Taki, AH, and Hodder, SG,(2001) Validation of ISO 7730 for Thermal Comfort Design of Chilled Ceiling/Displacement Ventilation Environments, International Conference on Moving Thermal Comfort Standards into 21st Century, Windsor, UK, 2001 pp323-334.

Loveday, DL, Parsons, KC, Taki, AH, Hodder, SG and Jeal, LD (1998), 'Designing for Thermal Comfort in Combined Chilled Ceiling/Displacement Ventilation Environments', *ASHRAE Transactions* vol.104, pt.1B, pp901-911, SF-98-4-4, ISSN 0001-2505.1998.

Mayer E, (1995) Ceiling Cooling and Displacement Ventilation in Officers, Thermal Comfort aspects, Proceedings of Health Buildings 95, pp 1209-1214.

Nielsen, P V, (1996) 'Temperature Distribution in a Displacement Ventilation Room', *The Fifth International Conference on Air Distribution in Rooms, Room Vent '96,* Yokohama, Japan July 1996, pp 323-330,.

Niu J, JVD Kooi, H VD Rees (1998), Cooling Load Dynamics of Rooms with Cooled Ceiling, Building Services Journal, Sep, 1998, pp 201-207

Niu J, Kooi jvd, Ree Hvd, (1995) Energy Saving Possibilities with Cooled Ceiling systems, Energy and Buildings, Dec. 1995, V23, No.2, pp 147-158

Niu, J Kool jvd, (1994) Indoor Climate in Rooms with Cooled Ceiling System, Building and Environment, July 1994, V29, No 3, pp 283-290

Niu J, J VD Kooi, H VD Rees, (1997) Cooling Load Dynamics of Rooms with Cooled Ceilings, Proce, CIBSEA: Building Services Engineers research technol 18 (4) 1997 pp 201-207

Novoselac A, Srebric j, (2002) Cooled Ceiling and Displacement Ventilation system, Energy and Building Vol 34, 2002 pp 497-509

Platzer W.J, (1992) Calculation Procedure For Collectors with a Honeycomb Cover Of Rectangular Cross Section. Solar Energy. Vol 48. No 6 pp 381-393, 1992

Pneuli,D., (1962) " The Thermal Instability of Confined Fluids", PhD thesis, case Institute of Technology, 1962. Jan-Feb 1979 pp 8-15.

Rees SJ, McGuirk JJ Haves P, (2001) Numerical Investigation of Transient Buoyant Flow in a Room with A Displacement Ventilation and Chilled Ceiling system. International Journal of Heat and Mass Transfer vol 44 2001, pp 3067-3080

Rees, SJ. Haves P. (2001) A nodal model for Displacement Ventilation and Chilled Ceiling systems in office spaces Building and Environment, v 36, 2001, pp 753-762

Riffat, S B, Zhao, X Riffat, S B. Zhao, X., Doherty, P. S (2004), Review of Research into and application of chilled

ceilings and displacement ventilation systems in Europe, International Journal of Energy Research, Nov 2004 no28 , pp 257-286

Scheiger H, A.Oliva, M. Costa, C.D. Perez Segarra and A.Ivancic, (1995) Numerical Experiments on Laminar Natural Convection in Rectangular Cavities with and without Honeycomb-Structures, International Journal Num Meth Heat Fluid Flow, Vol 5, pp 423-443 1995

Sezai I, A.A.Mohamad, (1999) Suppressing Free Convection from a Flat Plate with Poor Conductor Ribs. International Journal of Heat and Mass Transfer 42 (1999) pp 2041-2051.

Sharma MS, N.D. Kaushika, (1987) Design And Performance Characteristics of Honeycomb Solar Pond, Energy Convers Mgmt Vol 27, no 1 1987 pp-111-116.

Siebers DL, R. Viskanta, (1979) Thermal Analysis of Some Flat-Plate Solar Collector Designs For Improving Performance, Journal of Energy, Vol 3, No 1, Jan-Feb 1979, pp 8-15

Skaret .E. (1987) Displacement Ventilation, Proceedings of Room vent 87 Sweden 1987.

Skistad Hakon (1994), Displacement Ventilation, ISBN 086380 1471 Research Studies Press Ltd. Taunton, Somerset, England 1994.

Smale, S. (2000) "Mathematical Problems for the Next Century." In Mathematics: Frontiers and Perspectives 20000821820702 (Ed. V. Arnold, M. Atiyah, P. Lax, and B. Mazur). Providence, RI: Amer. Math. Soc., 2000.

Sprecher P, Gasser B, Bock O, Kofoed P, (1995) Control Strategy for Cooled Ceiling panels, ASHRAE Transactions, 1995,Vol 101, Pt 2 pp711-716

Sprecher P, etal, (1996) Chilled Ceiling for Hot Heads, Sulzer Technical Review, Jan. 1996, pp. 15-17

Stanley A Mumma, (2002) Chilled Ceiling in Parallel with Dedicated Outdoor Air Systems: Addressing the Concerns of Condensation, Capacity, and Cost, ASRAE Transactions Research 2002, vol 108, part 2, pp 220-231.

Stetiu Corina, etal, (1995) Development of a Nodal to Simulate the Performance of Hydronic Radiant Cooling ceiling, ASHRAE Transactions, 1995, V 101 No. Pt 2, pp. 730-743

Steven. L.Marcus, (1983) An Approximate Method for Calculating The Heat Flux Through A Solar Collector Honeycomb, Solar Energy, Vol. 30. No. 2. pp 127-131, 1983.

Symons J.G, (1982), The Solar Transmittance of Some Convection Suppression Devices for Solar Energy Applications: An Experimental Study, Journal of Solar Energy Engineering, Vol 104, August 1982. pp 251-256.

Taki AH, Loveday DL, Parsn KC, (1996) The effects of Ceiling Temperature on Displacement Flow and Thermal Comfort –Experimental and Simulation. RoomVent 1996, July 17-19, 5th Int' Conference on Air Distribution in Rooms.

Taki, AH, Loveday, DL and Parsons, KC, (1996) The Effect of Chilled Ceiling Temperatures on Displacement Flow and Thermal Comfort- experimental and simulation studies, The Fifth International Conference on Air Distribution in Rooms-

RoomVent '96, Yokohama -Japan, vol. 3, pp307-314, 1996, ISBN 492455701 3.

Taki, AH, Loveday, DL, Parsons, KC and Hodder, S, (1997) Thermal Comfort Assessment in Chilled Ceiling and Displacement Ventilation Environments, The Second International CIB Conference on Buildings and the Environment, Paris, vol. 1, 1997 pp397-404.

Taki AH, Jalil L and Loveday DL (2002) Use of Computational FluidDynamics for Modelling Displacement Ventilation Environments. The International Conference on Research Trends in Science and Technology, Beirut, Lebanon March 4th to march 8th 2002.

Taki AH, Jalil L and Loveday DL, (2005) Stabilising Airflows in Chilled Ceiling / Displacement Ventilation Environments. 22nd International Conference on Passive Low Energy Architecture (PLEA), Beirut, Lebanon, November 2005.

Thomas David, (1994), First Among Equalios, Building Services Journal, June 1994 pp 27-28

Tritton, D. J. (1998) Physical Fluid Dynamics, 2nd ed. Oxford, England: Clarendon Press, pp. 52-53 and 59-60, 1988.

Udagawa M, (1993) Simulation of Panel Cooling Systems with Linear Subsystem Model, ASHRAE Transactions, 1993, v99 No. Pt 2, pp. 534-544

Whittle G.E., (1986) Computation of Air Movement and Convective Heat Transfer within Building, International Journal of Ambient Energy, volume 7, number3 July 1986, pp 151-164

Whittles, GE and Jones, PJ, (1992) Computational Fluid Dynamics (CFD) for Buildings Airflow Predictions-Current status and capabilities. Building and Environment Vol. 27 no 3,1992 pp 321-338.

Yamaguchi Y, Asako Y and M Faghri, (1999) Natural Convection and Radiation Heat Transfer in a Vertical Porous Layer with a Hexagonal Honeycomb Core (Part 1: Numerical Analysis) Heat Transfer-Asian Research,28(4), 1999.

Zweifei G, etal (1993) Simulation of Displacement Ventilation and Radiant Cooling with DOE-2, ASHRAE Transactions, 1993, v99 No. Pt 2, pp. 548-555

World wide web References

http://en.wikipedia.org/wiki/Computational_fluid_dynamics

http://manila.cats.rwth-aachen.de/developer/tools/intro (for Figure 3.4)

APPENDICES

Appendix A

Table showing the Rayleigh numbers one million to sixteen million and the corresponding air temperatures difference between the Honeycomb Slats (200mm from the ceiling) and the ceiling temperatures. The Rayleigh numbers are calculated based on 200mm height (depth) of the honeycomb slat with change in air temperatures.

The following table shows all the possible test conditions based on their Rayleigh numbers.

The table is split into 12 columns the

First column (cc temp) represents the ceiling temperature in (°C)

Second column (room temp) represents the room air temperature in (°C)

Third column (rm- cc) represents the temperature difference between the ceiling and the room air temperature in (°C).

Fourth column (av-room temp) represents the average room air temperature in (°C)

Fifth column (Kelvin) represents the average room air temperature in Kelvin

Sixth column (g) represents the acceleration due to gravity

Seventh column (β) represents coefficient of thermal expansion

Eighth column (L) represents the depth in cubed (L^3)

Ninth column (**Pr**) represents the Prandtl number

Tenth column (V^2) represents the Kinematic viscosity squared (V^2)

Eleventh column (**Ra**) represents the equivalent Rayleigh number

The last column (**Ra**) represents the Rayleigh number multiplied by a million ($x10^6$)

RAYLEIGH NUMBERS FROM 100,000 TO 1 MILLION

Cc temp	Room temp	rm-cc	av-room temp	kelvin	*g*	β	L	*Pr*	V^2	*Ra*	Ra
21	22	1	21.5	**294.5**	9.81	0.003396	0.000125	0.712875	*2.3085E-10*	**12858.11**	0.0128
21	23	2	22	**295**	9.81	0.00339	0.000125	0.71275	*2.32181E-10*	**25520.947**	0.025
21	24	3	22.5	**295.5**	9.81	0.003384	0.000125	0.712625	*2.33517E-10*	**37991.469**	0.037
21	25	4	23	**296**	9.81	0.003378	0.000125	0.7125	*2.34856E-10*	**50272.583**	0.05
21	26	5	23.5	**296.5**	9.81	0.003373	0.000125	0.712375	*2.36198E-10*	**62367.151**	0.062
21	27	6	24	**297**	9.81	0.003367	0.000125	0.71225	*2.37545E-10*	**74277.983**	0.074
21	28	7	24.5	**297.5**	9.81	0.003361	0.000125	0.712125	*2.38896E-10*	**86007.843**	0.086
20	21	1	20.5	**293.5**	9.81	0.003407	0.000125	0.713125	*2.28199E-10*	**13056.394**	0.013
20	22	2	21	**294**	9.81	0.003401	0.000125	0.713	*2.29523E-10*	**25913.493**	0.025
20	23	3	21.5	**294.5**	9.81	0.003396	0.000125	0.712875	*2.3085E-10*	**38574.331**	0.038
20	24	4	22	**295**	9.81	0.00339	0.000125	0.71275	*2.32181E-10*	**51041.894**	0.051
20	25	5	22.5	**295.5**	9.81	0.003384	0.000125	0.712625	*2.33517E-10*	**63319.114**	0.063
20	26	6	23	**296**	9.81	0.003378	0.000125	0.7125	*2.34856E-10*	**75408.875**	0.075
20	27	7	23.5	**296.5**	9.81	0.003373	0.000125	0.712375	*2.36198E-10*	**87314.011**	0.087

20	28	8	24	297	9.81	0.003367	0.000125	0.71225	2.37545E-10	99037.31	0.099
19	20	1	19.5	292.5	9.81	0.003419	0.000125	0.713375	2.25563E-10	13258.777	0.0132
19	21	2	20	293	9.81	0.003413	0.000125	0.71325	2.26879E-10	26314.132	0.026
19	22	3	20.5	293.5	9.81	0.003407	0.000125	0.713125	2.28199E-10	39169.181	0.039
19	23	4	21	294	9.81	0.003401	0.000125	0.713	2.29523E-10	51826.985	0.051
19	24	5	21.5	294.5	9.81	0.003396	0.000125	0.712875	2.3085E-10	64290.552	0.064
19	25	6	22	295	9.81	0.00339	0.000125	0.71275	2.32181E-10	76562.842	0.076
19	26	7	22.5	295.5	9.81	0.003384	0.000125	0.712625	2.33517E-10	88646.76	0.086
18	19	1	18.5	291.5	9.81	0.003431	0.000125	0.713625	2.22942E-10	13465.367	0.0134
18	20	2	19	292	9.81	0.003425	0.000125	0.7135	2.24251E-10	26723.078	0.026
18	21	3	19.5	292.5	9.81	0.003419	0.000125	0.713375	2.25563E-10	39776.33	0.039
18	22	4	20	293	9.81	0.003413	0.000125	0.71325	2.26879E-10	52628.265	0.052
18	23	5	20.5	293.5	9.81	0.003407	0.000125	0.713125	2.28199E-10	65281.969	0.065
18	24	6	21	294	9.81	0.003401	0.000125	0.713	2.29523E-10	77740.478	0.077
18	25	7	21.5	294.5	9.81	0.003396	0.000125	0.712875	2.3085E-10	90006.773	0.09
17	21	4	19	292	9.81	0.003425	0.000125	0.7135	2.24251E-10	53446.156	0.053
17	22	5	19.5	292.5	9.81	0.003419	0.000125	0.713375	2.25563E-10	66293.884	0.066
17	23	6	20	293	9.81	0.003413	0.000125	0.71325	2.26879E-10	78942.397	0.078

17	24	7	20.5	293.5	9.81	0.003407	0.000125	0.713125	2.28199E-10	91394.757	0.091
16	17	1	16.5	289.5	9.81	0.003454	0.000125	0.71415	2.17858E-10	13885.041	0.013
16	18	2	17	290	9.81	0.003448	0.000125	0.714	2.1904E-10	27566.765	0.027
16	19	3	17.5	290.5	9.81	0.003442	0.000125	0.713875	2.20337E-10	41028.822	0.041
16	20	4	18	291	9.81	0.003436	0.000125	0.71375	2.21936E-10	54208.246	0.054
16	21	5	18.5	291.5	9.81	0.003431	0.000125	0.713625	2.22942E-10	67326.833	0.067
16	22	6	19	292	9.81	0.003425	0.000125	0.7135	2.24251E-10	80169.234	0.08
16	23	7	19.5	292.5	9.81	0.003419	0.000125	0.713375	2.25563E-10	92811.437	0.092
15	16	1	15.5	288.5	9.81	0.003466	0.000125	0.71445	2.15502E-10	14091.361	0.014
15	17	2	16	289	9.81	0.00346	0.000125	0.7143	2.16678E-10	27975.393	0.027
15	18	3	16.5	289.5	9.81	0.003454	0.000125	0.71415	2.17858E-10	41655.124	0.047
15	19	4	17	290	9.81	0.003448	0.000125	0.714	2.1904E-10	55133.529	0.057
15	20	5	17.5	290.5	9.81	0.003442	0.000125	0.713875	2.20337E-10	68381.37	0.068
15	21	6	18	291	9.81	0.003436	0.000125	0.71375	2.21936E-10	81312.369	0.081
15	22	7	18.5	291.5	9.81	0.003431	0.000125	0.713625	2.22942E-10	94257.566	0.094
14	16	2	15	288	9.81	0.003472	0.000125	0.7146	2.1433E-10	28392.092	0.028
14	17	3	15.5	288.5	9.81	0.003466	0.000125	0.71445	2.15502E-10	42274.082	0.042
14	18	4	16	289	9.81	0.00346	0.000125	0.7143	2.16678E-10	55950.787	0.055

14	19	5	16.5	289.5	9.81	0.003454	0.000125	0.71415	2.17858E-10	69425.207	0.069
14	20	6	17	290	9.81	0.003448	0.000125	0.714	2.1904E-10	82700.294	0.082
14	21	7	17.5	290.5	9.81	0.003442	0.000125	0.713875	2.20337E-10	95733.918	0.095
13	16	3	14.5	287.5	9.81	0.003478	0.000125	0.71475	2.1316E-10	42905.294	0.042
13	17	4	15	288	9.81	0.003472	0.000125	0.7146	2.1433E-10	56784.183	0.056
13	18	5	15.5	288.5	9.81	0.003466	0.000125	0.71445	2.15502E-10	70456.804	0.07
13	19	6	16	289	9.81	0.00346	0.000125	0.7143	2.16678E-10	83926.18	0.083
13	20	7	16.5	289.5	9.81	0.003454	0.000125	0.71415	2.17858E-10	97195.29	0.097
12	16	4	14	287	9.81	0.003484	0.000125	0.7149	2.11994E-10	57634.119	0.057
12	17	5	14.5	287.5	9.81	0.003478	0.000125	0.71475	2.1316E-10	71508.823	0.071
12	18	6	15	288	9.81	0.003472	0.000125	0.7146	2.1433E-10	85176.275	0.08
12	19	7	15.5	288.5	9.81	0.003466	0.000125	0.71445	2.15502E-10	98639.525	0.09
11	16	5	13.5	286.5	9.81	0.00349	0.000125	0.71505	2.1083E-10	72581.774	0.07
11	17	6	14	287	9.81	0.003484	0.000125	0.7149	2.11994E-10	86451.179	0.08
10	16	6	13	286	9.81	0.003497	0.000125	0.7158	2.0967E-10	87825.131	0.087

Rayleigh no' from 0.1 x10^6 (100'000) to 0.5x10^6 (500'000)

Cc temp	Room temp	rm-cc	av-room temp	kelvin	*g*	β	L	*Pr*	V^2	*Ra*	Ra
19	27	8	23	**296**	9.81	0.003378	0.000125	0.7125	*2.34856E-10*	**100545.17**	0.1
19	28	9	23.5	**296.5**	9.81	0.003373	0.000125	0.712375	*2.36198E-10*	**112260.87**	0.11
18	26	8	22	**295**	9.81	0.00339	0.000125	0.71275	*2.32181E-10*	**102083.79**	0.1
18	27	9	22.5	**295.5**	9.81	0.003384	0.000125	0.712625	*2.33517E-10*	**113974.41**	0.11
18	28	10	23	**296**	9.81	0.003378	0.000125	0.7125	*2.34856E-10*	**125681.46**	0.125
17	25	8	21	**294**	9.81	0.003401	0.000125	0.713	*2.29523E-10*	**103653.97**	0.1
17	26	9	21.5	**294.5**	9.81	0.003396	0.000125	0.712875	*2.3085E-10*	**115722.99**	0.11
17	27	10	22	**295**	9.81	0.00339	0.000125	0.71275	*2.32181E-10*	**127604.74**	0.127
17	28	11	22.5	**295.5**	9.81	0.003384	0.000125	0.712625	*2.33517E-10*	**139302.05**	0.139
16	24	8	20	**293**	9.81	0.003413	0.000125	0.71325	*2.26879E-10*	**105256.53**	0.1
16	25	9	20.5	**293.5**	9.81	0.003407	0.000125	0.713125	*2.28199E-10*	**117507.54**	0.11
16	26	10	21	**294**	9.81	0.003401	0.000125	0.713	*2.29523E-10*	**129567.46**	0.129
16	27	11	21.5	**294.5**	9.81	0.003396	0.000125	0.712875	*2.3085E-10*	**141439.22**	0.14
16	28	12	22	**295**	9.81	0.00339	0.000125	0.71275	*2.32181E-10*	**153125.68**	0.15
15	23	8	19	**292**	9.81	0.003425	0.000125	0.7135	*2.24251E-*	**106892.31**	0.1

									10		
15	24	9	19.5	292.5	9.81	0.003419	0.000125	0.713375	2.25563E-10	119328.99	0.11
15	25	10	20	293	9.81	0.003413	0.000125	0.71325	2.26879E-10	131570.66	0.13
15	26	11	20.5	293.5	9.81	0.003407	0.000125	0.713125	2.28199E-10	143620.33	0.14
15	27	12	21	294	9.81	0.003401	0.000125	0.713	2.29523E-10	155480.96	0.15
15	28	13	21.5	294.5	9.81	0.003396	0.000125	0.712875	2.3085E-10	167155.44	0.16
14	22	8	18	291	9.81	0.003436	0.000125	0.71375	2.21936E-10	108416.49	0.1
14	23	9	18.5	291.5	9.81	0.003431	0.000125	0.713625	2.22942E-10	121188.3	0.12
14	24	10	19	292	9.81	0.003425	0.000125	0.7135	2.24251E-10	133615.39	0.13
14	25	11	19.5	292.5	9.81	0.003419	0.000125	0.713375	2.25563E-10	145846.54	0.14
14	26	12	20	293	9.81	0.003413	0.000125	0.71325	2.26879E-10	157884.79	0.15
14	27	13	20.5	293.5	9.81	0.003407	0.000125	0.713125	2.28199E-10	169733.12	0.16
14	28	14	21	294	9.81	0.003401	0.000125	0.713	2.29523E-10	181394.45	0.18
13	21	8	17	290	9.81	0.003448	0.000125	0.714	2.1904E-10	110267.06	0.1
13	22	9	17.5	290.5	9.81	0.003442	0.000125	0.713875	2.20337E-10	123086.47	0.12
13	23	10	18	291	9.81	0.003436	0.000125	0.71375	2.21936E-10	135520.62	0.13
13	24	11	18.5	291.5	9.81	0.003431	0.000125	0.713625	2.22942E-10	148119.03	0.14
13	25	12	19	292	9.81	0.003425	0.000125	0.7135	2.24251E-10	160338.47	0.16
13	26	13	19.5	292.5	9.81	0.003419	0.000125	0.713375	2.25563E-	172364.1	0.17

									10		
13	27	14	20	293	9.81	0.003413	0.000125	0.71325	2.26879E-10	184198.93	0.18
13	28	15	20.5	293.5	9.81	0.003407	0.000125	0.713125	2.28199E-10	195845.91	0.19
12	20	8	16	289	9.81	0.00346	0.000125	0.7143	2.16678E-10	111901.57	0.1
12	21	9	16.5	289.5	9.81	0.003454	0.000125	0.71415	2.17858E-10	124965.37	0.12
12	22	10	17	290	9.81	0.003448	0.000125	0.714	2.1904E-10	137833.82	0.13
12	23	11	17.5	290.5	9.81	0.003442	0.000125	0.713875	2.20337E-10	150439.01	0.15
12	24	12	18	291	9.81	0.003436	0.000125	0.71375	2.21936E-10	162624.74	0.16
12	25	13	18.5	291.5	9.81	0.003431	0.000125	0.713625	2.22942E-10	175049.77	0.17
12	26	14	19	292	9.81	0.003425	0.000125	0.7135	2.24251E-10	187061.55	0.18
12	27	15	19.5	292.5	9.81	0.003419	0.000125	0.713375	2.25563E-10	198881.65	0.19
12	28	16	20	293	9.81	0.003413	0.000125	0.71325	2.26879E-10	210513.06	0.2
11	18	7	14.5	287.5	9.81	0.003478	0.000125	0.71475	2.1316E-10	100112.35	0.1
11	19	8	15	288	9.81	0.003472	0.000125	0.7146	2.1433E-10	113568.37	0.11
11	20	9	15.5	288.5	9.81	0.003466	0.000125	0.71445	2.15502E-10	126822.25	0.12
11	21	10	16	289	9.81	0.00346	0.000125	0.7143	2.16678E-10	139876.97	0.13
11	22	11	16.5	289.5	9.81	0.003454	0.000125	0.71415	2.17858E-10	152735.46	0.15
11	23	12	17	290	9.81	0.003448	0.000125	0.714	2.1904E-10	165400.59	0.16
11	24	13	17.5	290.5	9.81	0.003442	0.000125	0.713875	2.20337E-	177791.56	0.17

									10		
11	25	14	18	291	9.81	0.003436	0.000125	0.71375	2.21936E-10	189728.86	0.18
11	26	15	18.5	291.5	9.81	0.003431	0.000125	0.713625	2.22942E-10	201980.5	0.2
11	27	16	19	292	9.81	0.003425	0.000125	0.7135	2.24251E-10	213784.62	0.21
11	28	17	19.5	292.5	9.81	0.003419	0.000125	0.713375	2.25563E-10	225399.21	0.22
10	17	7	13.5	286.5	9.81	0.00349	0.000125	0.71505	2.1083E-10	101614.48	0.1
10	18	8	14	287	9.81	0.003484	0.000125	0.7149	2.11994E-10	115268.24	0.11
10	19	9	14.5	287.5	9.81	0.003478	0.000125	0.71475	2.1316E-10	128715.88	0.12
10	20	10	15	288	9.81	0.003472	0.000125	0.7146	2.1433E-10	141960.46	0.14
10	21	11	15.5	288.5	9.81	0.003466	0.000125	0.71445	2.15502E-10	155004.97	0.15
10	22	12	16	289	9.81	0.00346	0.000125	0.7143	2.16678E-10	167852.36	0.16
10	23	13	16.5	289.5	9.81	0.003454	0.000125	0.71415	2.17858E-10	180505.54	0.18
10	24	14	17	290	9.81	0.003448	0.000125	0.714	2.1904E-10	192967.35	0.19
10	25	15	17.5	290.5	9.81	0.003442	0.000125	0.713875	2.20337E-10	205144.11	0.2
10	26	16	18	291	9.81	0.003436	0.000125	0.71375	2.21936E-10	216832.98	0.21
10	27	17	18.5	291.5	9.81	0.003431	0.000125	0.713625	2.22942E-10	228911.23	0.22
10	28	18	19	292	9.81	0.003425	0.000125	0.7135	2.24251E-10	240507.7	0.24
21	22	1	21.5	294.5	9.81	0.003396	0.003375	0.712875	2.3085E-10	347168.98	0.34

19	20	1	19.5	**292.5**	9.81	0.003419	0.003375	0.713375	*2.25563E-10*	**357986.97**	0.35
18	19	1	18.5	**291.5**	9.81	0.003431	0.003375	0.713625	*2.22942E-10*	**363564.9**	0.36
17	18	1	17.5	**290.5**	9.81	0.003442	0.003375	0.713875	*2.20337E-10*	**369259.4**	0.36
16	17	1	16.5	**289.5**	9.81	0.003454	0.003375	0.71415	*2.17858E-10*	**374896.12**	0.37
15	16	1	15.5	**288.5**	9.81	0.003466	0.003375	0.71445	*2.15502E-10*	**380466.74**	0.38
21	22	1	21.5	**294.5**	9.81	0.003396	0.001	0.712875	*2.3085E-10*	**102864.88**	0.1
21	23	2	22	**295**	9.81	0.00339	0.001	0.71275	*2.32181E-10*	**204167.58**	0.2
21	24	3	22.5	**295.5**	9.81	0.003384	0.001	0.712625	*2.33517E-10*	**303931.75**	0.3
21	25	4	23	**296**	9.81	0.003378	0.001	0.7125	*2.34856E-10*	**402180.67**	0.4
21	26	5	23.5	**296.5**	9.81	0.003373	0.001	0.712375	*2.36198E-10*	**498937.21**	0.49
20	21	1	20.5	**293.5**	9.81	0.003407	0.001	0.713125	*2.28199E-10*	**104451.15**	0.1
20	22	2	21	**294**	9.81	0.003401	0.001	0.713	*2.29523E-10*	**207307.94**	0.2
20	23	3	21.5	**294.5**	9.81	0.003396	0.001	0.712875	*2.3085E-10*	**308594.65**	0.3
20	24	4	22	**295**	9.81	0.00339	0.001	0.71275	*2.32181E-10*	**408335.15**	0.4
19	20	1	19.5	**292.5**	9.81	0.003419	0.001	0.713375	*2.25563E-10*	**106070.21**	0.1
19	21	2	20	**293**	9.81	0.003413	0.001	0.71325	*2.26879E-10*	**210513.06**	0.21
19	22	3	20.5	**293.5**	9.81	0.003407	0.001	0.713125	*2.28199E-10*	**313353.45**	0.31
19	23	4	21	**294**	9.81	0.003401	0.001	0.713	*2.29523E-10*	**414615.88**	0.41

18	19	1	18.5	291.5	9.81	0.003431	0.001	0.713625	2.22942E-10	107722.93	0.1
18	20	2	19	292	9.81	0.003425	0.001	0.7135	2.24251E-10	213784.62	0.21
18	21	3	19.5	292.5	9.81	0.003419	0.001	0.713375	2.25563E-10	318210.64	0.31
18	22	4	20	293	9.81	0.003413	0.001	0.71325	2.26879E-10	421026.12	0.42
18	19	1	18.5	291.5	9.81	0.003431	0.001	0.713625	2.22942E-10	107722.93	0.1
18	20	2	19	292	9.81	0.003425	0.001	0.7135	2.24251E-10	213784.62	0.21
18	21	3	19.5	292.5	9.81	0.003419	0.001	0.713375	2.25563E-10	318210.64	0.31
18	22	4	20	293	9.81	0.003413	0.001	0.71325	2.26879E-10	421026.12	0.42
17	21	4	19	292	9.81	0.003425	0.001	0.7135	2.24251E-10	427569.25	0.42
17	18	1	17.5	290.5	9.81	0.003442	0.001	0.713875	2.20337E-10	109410.19	0.1
17	19	2	18	291	9.81	0.003436	0.001	0.71375	2.21936E-10	216832.98	0.2
17	20	3	18.5	291.5	9.81	0.003431	0.001	0.713625	2.22942E-10	323168.8	0.3
16	17	1	16.5	289.5	9.81	0.003454	0.001	0.71415	2.17858E-10	111080.33	0.11
16	18	2	17	290	9.81	0.003448	0.001	0.714	2.1904E-10	220534.12	0.22
16	19	3	17.5	290.5	9.81	0.003442	0.001	0.713875	2.20337E-10	328230.58	0.32
16	20	4	18	291	9.81	0.003436	0.001	0.71375	2.21936E-10	433665.97	0.43
15	16	1	15.5	288.5	9.81	0.003466	0.001	0.71445	2.15502E-10	112730.89	0.11
15	17	2	16	289	9.81	0.00346	0.001	0.7143	2.16678E-10	223803.15	0.22

15	18	3	16.5	**289.5**	9.81	0.003454	0.001	0.71415	*2.17858E-10*	**333240.99**	0.33
15	19	4	17	**290**	9.81	0.003448	0.001	0.714	2.1904E-10	**441068.24**	0.44
14	16	2	15	**288**	9.81	0.003472	0.001	0.7146	*2.1433E-10*	**227136.73**	0.22
14	17	3	15.5	**288.5**	9.81	0.003466	0.001	0.71445	*2.15502E-10*	**338192.66**	0.33
14	18	4	16	**289**	9.81	0.00346	0.001	0.7143	*2.16678E-10*	**447606.3**	0.44
13	16	3	14.5	**287.5**	9.81	0.003478	0.001	0.71475	*2.1316E-10*	**343242.35**	0.34
13	17	4	15	**288**	9.81	0.003472	0.001	0.7146	*2.1433E-10*	**454273.46**	0.45

Rayleigh no' from $1x10^6$ (1'000'000) to $2.0x10^6$ (2'000'000)

Cc temp	Room temp	rm-cc	av-room temp	kelvin	*g*	β	L	*Pr*	V^2	*Ra*	Ra
18	28	10	23	**296**	9.81	0.003378	0.001	0.7125	*2.34856E-10*	**1005451.7**	1
17	27	10	22	**295**	9.81	0.00339	0.001	0.71275	*2.32181E-10*	**1020837.9**	1
17	28	11	22.5	**295.5**	9.81	0.003384	0.001	0.712625	*2.33517E-10*	**1114416.4**	1.1
16	26	10	21	**294**	9.81	0.003401	0.001	0.713	*2.29523E-10*	**1036539.7**	1
16	27	11	21.5	**294.5**	9.81	0.003396	0.001	0.712875	*2.3085E-10*	**1131513.7**	1.1
16	28	12	22	**295**	9.81	0.00339	0.001	0.71275	*2.32181E-10*	**1225005.5**	1.2
15	25	10	20	**293**	9.81	0.003413	0.001	0.71325	*2.26879E-10*	**1052565.3**	1
15	26	11	20.5	**293.5**	9.81	0.003407	0.001	0.713125	*2.28199E-10*	**1148962.7**	1.1
15	27	12	21	**294**	9.81	0.003401	0.001	0.713	*2.29523E-10*	**1243847.6**	1.2
15	28	13	21.5	**294.5**	9.81	0.003396	0.001	0.712875	*2.3085E-10*	**1337243.5**	1.3
14	24	10	19	**292**	9.81	0.003425	0.001	0.7135	*2.24251E-10*	**1068923.1**	1
14	25	11	19.5	**292.5**	9.81	0.003419	0.001	0.713375	*2.25563E-10*	**1166772.4**	1.16
14	26	12	20	**293**	9.81	0.003413	0.001	0.71325	*2.26879E-10*	**1263078.4**	1.26
14	27	13	20.5	**293.5**	9.81	0.003407	0.001	0.713125	*2.28199E-10*	**1357865**	1.35
14	28	14	21	**294**	9.81	0.003401	0.001	0.713	*2.29523E-*	**1451155.6**	1.45

									10		
13	23	10	18	291	9.81	0.003436	0.001	0.71375	2.21936E-10	1084164.9	1
13	24	11	18.5	291.5	9.81	0.003431	0.001	0.713625	2.22942E-10	1184952.3	1.18
13	25	12	19	292	9.81	0.003425	0.001	0.7135	2.24251E-10	1282707.7	1.28
13	26	13	19.5	292.5	9.81	0.003419	0.001	0.713375	2.25563E-10	1378912.8	1.37
13	27	14	20	293	9.81	0.003413	0.001	0.71325	2.26879E-10	1473591.4	1.47
13	28	15	20.5	293.5	9.81	0.003407	0.001	0.713125	2.28199E-10	1566767.3	1.56
12	22	10	17	290	9.81	0.003448	0.001	0.714	2.1904E-10	1102670.6	1
12	23	11	17.5	290.5	9.81	0.003442	0.001	0.713875	2.20337E-10	1203512.1	1.2
12	24	12	18	291	9.81	0.003436	0.001	0.71375	2.21936E-10	1300997.9	1.3
12	25	13	18.5	291.5	9.81	0.003431	0.001	0.713625	2.22942E-10	1400398.1	1.4
12	26	14	19	292	9.81	0.003425	0.001	0.7135	2.24251E-10	1496492.4	1.49
12	27	15	19.5	292.5	9.81	0.003419	0.001	0.713375	2.25563E-10	1591053.2	1.59
12	28	16	20	293	9.81	0.003413	0.001	0.71325	2.26879E-10	1684104.5	1.68
11	20	9	15.5	288.5	9.81	0.003466	0.001	0.71445	2.15502E-10	1014578	1
11	21	10	16	289	9.81	0.00346	0.001	0.7143	2.16678E-10	1119015.7	1.1
11	22	11	16.5	289.5	9.81	0.003454	0.001	0.71415	2.17858E-10	1221883.6	1.2
11	23	12	17	290	9.81	0.003448	0.001	0.714	2.1904E-10	1323204.7	1.3
11	24	13	17.5	290.5	9.81	0.003442	0.001	0.713875	2.20337E-	1422332.5	1.4

									10		
11	25	14	18	291	9.81	0.003436	0.001	0.71375	2.21936E-10	1517830.9	1.5
11	26	15	18.5	291.5	9.81	0.003431	0.001	0.713625	2.22942E-10	1615844	1.6
11	27	16	19	292	9.81	0.003425	0.001	0.7135	2.24251E-10	1710277	1.7
11	28	17	19.5	292.5	9.81	0.003419	0.001	0.713375	2.25563E-10	1803193.6	1.8
10	19	9	14.5	287.5	9.81	0.003478	0.001	0.71475	2.1316E-10	1029727	1
10	20	10	15	288	9.81	0.003472	0.001	0.7146	2.1433E-10	1135683.7	1.1
10	21	11	15.5	288.5	9.81	0.003466	0.001	0.71445	2.15502E-10	1240039.7	1.2
10	22	12	16	289	9.81	0.00346	0.001	0.7143	2.16678E-10	1342818.9	1.3
10	23	13	16.5	289.5	9.81	0.003454	0.001	0.71415	2.17858E-10	1444044.3	14
10	24	14	17	290	9.81	0.003448	0.001	0.714	2.1904E-10	1543738.8	1.5
10	25	15	17.5	290.5	9.81	0.003442	0.001	0.713875	2.20337E-10	1641152.9	1.6
10	26	16	18	291	9.81	0.003436	0.001	0.71375	2.21936E-10	1734663.9	1.7
10	27	17	18.5	291.5	9.81	0.003431	0.001	0.713625	2.22942E-10	1831289.9	1.8
10	28	18	19	292	9.81	0.003425	0.001	0.7135	2.24251E-10	1924061.6	1.9
21	24	3	22.5	295.5	9.81	0.003384	0.003375	0.712625	2.33517E-10	1025769.7	1
21	25	4	23	296	9.81	0.003378	0.003375	0.7125	2.34856E-10	1357359.8	1.3
21	26	5	23.5	296.5	9.81	0.003373	0.003375	0.712375	2.36198E-10	1683913.1	1.6

20	23	3	21.5	**294.5**	9.81	0.003396	0.003375	0.712875	*2.3085E-10*	**1041507**	1
20	24	4	22	**295**	9.81	0.00339	0.003375	0.71275	*2.32181E-10*	**1378131.1**	1.3
20	25	5	22.5	**295.5**	9.81	0.003384	0.003375	0.712625	*2.33517E-10*	**1709616.1**	1.7
19	22	3	20.5	**293.5**	9.81	0.003407	0.003375	0.713125	*2.28199E-10*	**1057567.9**	1
19	23	4	21	**294**	9.81	0.003401	0.003375	0.713	*2.29523E-10*	**1399328.6**	1.3
19	24	5	21.5	**294.5**	9.81	0.003396	0.003375	0.712875	*2.3085E-10*	**1735844.9**	1.7
18	21	3	19.5	**292.5**	9.81	0.003419	0.003375	0.713375	*2.25563E-10*	**1073960.9**	1
18	22	4	20	**293**	9.81	0.003413	0.003375	0.71325	*2.26879E-10*	**1420963.2**	1.4
18	23	5	20.5	**293.5**	9.81	0.003407	0.003375	0.713125	*2.28199E-10*	**1762613.2**	1.7
17	20	3	18.5	**291.5**	9.81	0.003431	0.003375	0.713625	*2.22942E-10*	**1090694.7**	1
17	21	4	19	**292**	9.81	0.003425	0.003375	0.7135	*2.24251E-10*	**1443046.2**	1.4
17	22	5	19.5	**292.5**	9.81	0.003419	0.003375	0.713375	*2.25563E-10*	**1789934.9**	1.7
16	19	3	17.5	**290.5**	9.81	0.003442	0.003375	0.713875	*2.20337E-10*	**1107778.2**	1.1
16	20	4	18	**291**	9.81	0.003436	0.003375	0.71375	*2.21936E-10*	**1463622.6**	1.4
16	21	5	18.5	**291.5**	9.81	0.003431	0.003375	0.713625	*2.22942E-10*	**1817824.5**	1.8
15	18	3	16.5	**289.5**	9.81	0.003454	0.003375	0.71415	*2.17858E-10*	**1124688.4**	1.2
15	19	4	17	**290**	9.81	0.003448	0.003375	0.714	2.1904E-10	**1488605.3**	1.48
15	20	5	17.5	**290.5**	9.81	0.003442	0.003375	0.713875	*2.20337E-10*	**1846297**	1.8

14	17	3	15.5	288.5	9.81	0.003466	0.003375	0.71445	2.15502E-10	1141400.2	1.1
14	18	4	16	289	9.81	0.00346	0.003375	0.7143	2.16678E-10	1510671.2	1.5
14	19	5	16.5	289.5	9.81	0.003454	0.003375	0.71415	2.17858E-10	1874480.6	1.87
13	16	3	14.5	287.5	9.81	0.003478	0.003375	0.71475	2.1316E-10	1158442.9	1.1
13	17	4	15	288	9.81	0.003472	0.003375	0.7146	2.1433E-10	1533172.9	1.5
13	18	5	15.5	288.5	9.81	0.003466	0.003375	0.71445	2.15502E-10	1902333.7	1.9
12	16	4	14	287	9.81	0.003484	0.003375	0.7149	2.11994E-10	1556121.2	1.5
12	17	5	14.5	287.5	9.81	0.003478	0.003375	0.71475	2.1316E-10	1930738.2	1.9
11	16	5	13.5	286.5	9.81	0.00349	0.003375	0.71505	2.1083E-10	1959707.9	1.9
21	23	2	22	295	9.81	0.00339	0.008	0.71275	2.32181E-10	1633340.6	1.63
20	22	2	21	294	9.81	0.003401	0.008	0.713	2.29523E-10	1658463.5	1.65
19	21	2	20	293	9.81	0.003413	0.008	0.71325	2.26879E-10	1684104.5	1.68
18	20	2	19	292	9.81	0.003425	0.008	0.7135	2.24251E-10	1710277	1.71
17	19	2	18	291	9.81	0.003436	0.008	0.71375	2.21936E-10	1734663.9	1.73
16	18	2	17	290	9.81	0.003448	0.008	0.714	2.1904E-10	1764272.9	1.76
15	17	2	16	289	9.81	0.00346	0.008	0.7143	2.16678E-10	1790425.2	1.79
14	16	2	15	288	9.81	0.003472	0.008	0.7146	2.1433E-10	1817093.9	1.8

Rayleigh no' from $2x10^6$ (2'000'000) to $3.0x10^6$ (3'000'000)

Cc temp	Room temp	rm-cc	av-room temp	kelvin	*g*	β	L	*Pr*	V^2	*Ra*	Ra
21	27	6	24	297	9.81	0.003367	0.003375	0.71225	*2.37545E-10*	2005505.5	2
21	28	7	24.5	297.5	9.81	0.003361	0.003375	0.712125	*2.38896E-10*	2322211.8	2.3
20	27	7	23.5	296.5	9.81	0.003373	0.003375	0.712375	*2.36198E-10*	2357478.3	2.3
20	28	8	24	297	9.81	0.003367	0.003375	0.71225	*2.37545E-10*	2674007.4	2.6
19	26	7	22.5	295.5	9.81	0.003384	0.003375	0.712625	*2.33517E-10*	2393462.5	2.3
19	27	8	23	296	9.81	0.003378	0.003375	0.7125	*2.34856E-10*	2714719.5	2.7
18	25	7	21.5	294.5	9.81	0.003396	0.003375	0.712875	*2.3085E-10*	2430182.9	2.4
18	26	8	22	295	9.81	0.00339	0.003375	0.71275	*2.32181E-10*	2756262.3	2.7
17	23	6	20	293	9.81	0.003413	0.003375	0.71325	*2.26879E-10*	2131444.7	2.1
17	24	7	20.5	293.5	9.81	0.003407	0.003375	0.713125	*2.28199E-10*	2467658.4	2.4
17	25	8	21	294	9.81	0.003401	0.003375	0.713	*2.29523E-10*	2798657.2	2.7
16	22	6	19	292	9.81	0.003425	0.003375	0.7135	*2.24251E-10*	2164569.3	2.16
16	23	7	19.5	292.5	9.81	0.003419	0.003375	0.713375	*2.25563E-10*	2505908.8	2.5
16	24	8	20	293	9.81	0.003413	0.003375	0.71325	*2.26879E-10*	2841926.3	2.8
15	21	6	18	291	9.81	0.003436	0.003375	0.71375	*2.21936E-*	2195434	2.19

									10		
15	22	7	18.5	291.5	9.81	0.003431	0.003375	0.713625	2.22942E-10	2544954.3	2.5
15	23	8	19	292	9.81	0.003425	0.003375	0.7135	2.24251E-10	2886092.4	2.88
14	20	6	17	290	9.81	0.003448	0.003375	0.714	2.1904E-10	2232907.9	2.2
14	21	7	17.5	290.5	9.81	0.003442	0.003375	0.713875	2.20337E-10	2584815.8	2.5
14	22	8	18	291	9.81	0.003436	0.003375	0.71375	2.21936E-10	2927245.3	2.92
13	19	6	16	289	9.81	0.00346	0.003375	0.7143	2.16678E-10	2266006.9	2.2
13	20	7	16.5	289.5	9.81	0.003454	0.003375	0.71415	2.17858E-10	2624272.8	2.6
13	21	8	17	290	9.81	0.003448	0.003375	0.714	2.1904E-10	2977210.6	2.9
12	18	6	15	288	9.81	0.003472	0.003375	0.7146	2.1433E-10	2299759.4	2.2
12	19	7	15.5	288.5	9.81	0.003466	0.003375	0.71445	2.15502E-10	2663267.2	2.6
11	17	6	14	287	9.81	0.003484	0.003375	0.7149	2.11994E-10	2334181.8	2.3
11	18	7	14.5	287.5	9.81	0.003478	0.003375	0.71475	2.1316E-10	2703033.5	2.7
10	16	6	13	286	9.81	0.003497	0.003375	0.7158	2.0967E-10	2371278.5	2.37
10	17	7	13.5	286.5	9.81	0.00349	0.003375	0.71505	2.1083E-10	2743591	2.74
21	24	3	22.5	295.5	9.81	0.003384	0.008	0.712625	2.33517E-10	2431454	2.4
20	23	3	21.5	294.5	9.81	0.003396	0.008	0.712875	2.3085E-10	2468757.2	2.4
19	22	3	20.5	293.5	9.81	0.003407	0.008	0.713125	2.28199E-10	2506827.6	2.5

18	21	3	19.5	292.5	9.81	0.003419	0.008	0.713375	2.25563E-10	2545685.1	2.5
17	20	3	18.5	291.5	9.81	0.003431	0.008	0.713625	2.22942E-10	2585350.4	2.5
16	19	3	17.5	290.5	9.81	0.003442	0.008	0.713875	2.20337E-10	2625844.6	2.6
15	18	3	16.5	289.5	9.81	0.003454	0.008	0.71415	2.17858E-10	2665927.9	2.6
14	17	3	15.5	288.5	9.81	0.003466	0.008	0.71445	2.15502E-10	2705541.3	2.7
13	16	3	14.5	287.5	9.81	0.003478	0.008	0.71475	2.1316E-10	2745938.8	2.7

Rayleigh no' from $3x10^6$ (3'000'000) to $4.0x10^6$ (4'000'000)

Cc temp	Room temp	rm-cc	av-room temp	kelvin	*g*	β	L	*Pr*	V^2	*Ra*	Ra
19	28	9	23.5	**296.5**	9.81	0.003373	0.003375	0.712375	*2.36198E-10*	**3031043.5**	3
18	27	9	22.5	**295.5**	9.81	0.003384	0.003375	0.712625	*2.33517E-10*	**3077309**	3
18	28	10	23	**296**	9.81	0.003378	0.003375	0.7125	*2.34856E-10*	**3393399.4**	3.3
17	26	9	21.5	**294.5**	9.81	0.003396	0.003375	0.712875	*2.3085E-10*	**3124520.9**	3.1
17	27	10	22	**295**	9.81	0.00339	0.003375	0.71275	*2.32181E-10*	**3445327.9**	3.4
17	28	11	22.5	**295.5**	9.81	0.003384	0.003375	0.712625	*2.33517E-10*	**3761155.4**	3.7
16	25	9	20.5	**293.5**	9.81	0.003407	0.003375	0.713125	*2.28199E-10*	**3172703.7**	3.1
16	26	10	21	**294**	9.81	0.003401	0.003375	0.713	*2.29523E-10*	**3498321.5**	3.4
16	27	11	21.5	**294.5**	9.81	0.003396	0.003375	0.712875	*2.3085E-10*	**3818858.8**	3.8
15	24	9	19.5	**292.5**	9.81	0.003419	0.003375	0.713375	*2.25563E-10*	**3221882.8**	3.2
15	25	10	20	**293**	9.81	0.003413	0.003375	0.71325	*2.26879E-10*	**3552407.9**	3.5
15	26	11	20.5	**293.5**	9.81	0.003407	0.003375	0.713125	*2.28199E-10*	**3877749**	3.8
14	23	9	18.5	**291.5**	9.81	0.003431	0.003375	0.713625	*2.22942E-10*	**3272084.1**	3.2
14	24	10	19	**292**	9.81	0.003425	0.003375	0.7135	*2.24251E-10*	**3607615.5**	3.6

14	25	11	19.5	292.5	9.81	0.003419	0.003375	0.713375	2.25563E-10	3937856.7	3.93
13	22	9	17.5	290.5	9.81	0.003442	0.003375	0.713875	2.20337E-10	3323334.6	3.3
13	23	10	18	291	9.81	0.003436	0.003375	0.71375	2.21936E-10	3659056.6	3.6
13	24	11	18.5	291.5	9.81	0.003431	0.003375	0.713625	2.22942E-10	3999213.9	3.99
12	20	8	16	289	9.81	0.00346	0.003375	0.7143	2.16678E-10	3021342.5	3
12	21	9	16.5	289.5	9.81	0.003454	0.003375	0.71415	2.17858E-10	3374065.1	3.3
12	22	10	17	290	9.81	0.003448	0.003375	0.714	2.1904E-10	3721513.2	3.7
11	19	8	15	288	9.81	0.003472	0.003375	0.7146	2.1433E-10	3066345.9	3
11	20	9	15.5	288.5	9.81	0.003466	0.003375	0.71445	2.15502E-10	3424200.7	3.4
11	21	10	16	289	9.81	0.00346	0.003375	0.7143	2.16678E-10	3776678.1	3.7
10	18	8	14	287	9.81	0.003484	0.003375	0.7149	2.11994E-10	3112242.4	3.11
10	19	9	14.5	287.5	9.81	0.003478	0.003375	0.71475	2.1316E-10	3475328.8	3.475
10	20	10	15	288	9.81	0.003472	0.003375	0.7146	2.1433E-10	3832932.4	3.83
21	25	4	23	296	9.81	0.003378	0.008	0.7125	2.34856E-10	3217445.3	3.2
20	24	4	22	295	9.81	0.00339	0.008	0.71275	2.32181E-10	3266681.2	3.2
19	23	4	21	294	9.81	0.003401	0.008	0.713	2.29523E-10	3316927	3.3
18	22	4	20	293	9.81	0.003413	0.008	0.71325	2.26879E-10	3368209	3.3
17	21	4	19	292	9.81	0.003425	0.008	0.7135	2.24251E-	3420554	3.4

									10		
16	20	4	18	291	9.81	0.003436	0.008	0.71375	2.21936E-10	3469327.7	3.4
15	19	4	17	290	9.81	0.003448	0.008	0.714	2.1904E-10	3528545.9	3.5
14	18	4	16	289	9.81	0.00346	0.008	0.7143	2.16678E-10	3580850.4	3.5
13	17	4	15	288	9.81	0.003472	0.008	0.7146	2.1433E-10	3634187.7	3.6
12	16	4	14	287	9.81	0.003484	0.008	0.7149	2.11994E-10	3688583.6	3.6

Rayleigh no' from $4x10^6$ (4'000'000) to $5.0x10^6$ (5'000'000

Cc temp	Room temp	rm-cc	av-room temp	kelvin	*g*	β	L	*Pr*	V^2	*Ra*	Ra
16	28	12	22	**295**	9.81	0.00339	0.003375	0.71275	*2.32181E-10*	**4134393.4**	4.1
15	27	12	21	**294**	9.81	0.003401	0.003375	0.713	*2.29523E-10*	**4197985.8**	4.19
15	28	13	21.5	**294.5**	9.81	0.003396	0.003375	0.712875	*2.3085E-10*	**4513196.8**	4.5
14	26	12	20	**293**	9.81	0.003413	0.003375	0.71325	*2.26879E-10*	**4262889.5**	4.2
14	27	13	20.5	**293.5**	9.81	0.003407	0.003375	0.713125	*2.28199E-10*	**4582794.2**	4.5
14	28	14	21	**294**	9.81	0.003401	0.003375	0.713	*2.29523E-10*	**4897650.1**	4.89
13	25	12	19	**292**	9.81	0.003425	0.003375	0.7135	*2.24251E-10*	**4329138.6**	4.3
13	26	13	19.5	**292.5**	9.81	0.003419	0.003375	0.713375	*2.25563E-10*	**4653830.7**	4.6
13	27	14	20	**293**	9.81	0.003413	0.003375	0.71325	*2.26879E-10*	**4973371**	4.97
12	24	12	18	**291**	9.81	0.003436	0.003375	0.71375	*2.21936E-10*	**4390867.9**	4.3
12	25	13	18.5	**291.5**	9.81	0.003431	0.003375	0.713625	*2.22942E-10*	**4726343.7**	4.7
11	22	11	16.5	**289.5**	9.81	0.003454	0.003375	0.71415	*2.17858E-10*	**4123857.3**	4.1
11	23	12	17	**290**	9.81	0.003448	0.003375	0.714	2.1904E-10	**4465815.9**	4.4
11	24	13	17.5	**290.5**	9.81	0.003442	0.003375	0.713875	*2.20337E-10*	**4800372.2**	4.8
10	21	11	15.5	**288.5**	9.81	0.003466	0.003375	0.71445	*2.15502E-10*	**4185134.1**	4.15

10	22	12	16	289	9.81	0.00346	0.003375	0.7143	2.16678E-10	4532013.7	4.5
10	23	13	16.5	289.5	9.81	0.003454	0.003375	0.71415	2.17858E-10	4873649.5	4.8
21	27	6	24	297	9.81	0.003367	0.008	0.71225	2.37545E-10	4753790.9	4.7
20	26	6	23	296	9.81	0.003378	0.008	0.7125	2.34856E-10	4826168	4.8
20	25	5	22.5	295.5	9.81	0.003384	0.008	0.712625	2.33517E-10	4052423.3	4
19	24	5	21.5	294.5	9.81	0.003396	0.008	0.712875	2.3085E-10	4114595.4	4.1
19	25	6	22	295	9.81	0.00339	0.008	0.71275	2.32181E-10	4900021.9	4.9
18	23	5	20.5	293.5	9.81	0.003407	0.008	0.713125	2.28199E-10	4178046	4.1
18	24	6	21	294	9.81	0.003401	0.008	0.713	2.29523E-10	4975390.6	4.9
17	22	5	19.5	292.5	9.81	0.003419	0.008	0.713375	2.25563E-10	4242808.6	4.2
16	21	5	18.5	291.5	9.81	0.003431	0.008	0.713625	2.22942E-10	4308917.3	4.3
15	20	5	17.5	290.5	9.81	0.003442	0.008	0.713875	2.20337E-10	4376407.7	4.3
14	19	5	16.5	289.5	9.81	0.003454	0.008	0.71415	2.17858E-10	4443213.2	4.4
13	18	5	15.5	288.5	9.81	0.003466	0.008	0.71445	2.15502E-10	4509235.4	4.5
12	17	5	14.5	287.5	9.81	0.003478	0.008	0.71475	2.1316E-10	4576564.7	4.5
11	16	5	13.5	286.5	9.81	0.00349	0.008	0.71505	2.1083E-10	4645233.5	4.6

Rayleigh no' from $5x10^6$ (5'000'000) to $6.0x10^6$ (6'000'000)

Cc temp	Room temp	rm-cc	av-room temp	kelvin	*g*	β	L	*Pr*	V^2	*Ra*	Ra
13	28	15	20.5	**293.5**	9.81	0.003407	0.003375	0.713125	*2.28199E-10*	**5287839.5**	5.2
12	27	15	19.5	**292.5**	9.81	0.003419	0.003375	0.713375	*2.25563E-10*	**5369804.6**	5.3
12	28	16	20	**293**	9.81	0.003413	0.003375	0.71325	*2.26879E-10*	**5683852.6**	5.6
11	26	15	18.5	**291.5**	9.81	0.003431	0.003375	0.713625	*2.22942E-10*	**5453473.5**	5.4
11	27	16	19	**292**	9.81	0.003425	0.003375	0.7135	*2.24251E-10*	**5772184.9**	5.77
10	24	14	17	**290**	9.81	0.003448	0.003375	0.714	2.1904E-10	**5210118.5**	5.2
10	25	15	17.5	**290.5**	9.81	0.003442	0.003375	0.713875	*2.20337E-10*	**5538891**	5.5
10	26	16	18	**291**	9.81	0.003436	0.003375	0.71375	*2.21936E-10*	**5854490.6**	5.8
21	28	7	24.5	**297.5**	9.81	0.003361	0.008	0.712125	*2.38896E-10*	**5504501.9**	5.5
20	27	7	23.5	**296.5**	9.81	0.003373	0.008	0.712375	*2.36198E-10*	**5588096.7**	5.5
19	26	7	22.5	**295.5**	9.81	0.003384	0.008	0.712625	*2.33517E-10*	**5673392.6**	5.6
18	25	7	21.5	**294.5**	9.81	0.003396	0.008	0.712875	*2.3085E-10*	**5760433.5**	5.7
17	23	6	20	**293**	9.81	0.003413	0.008	0.71325	*2.26879E-10*	**5052313.4**	5
17	24	7	20.5	**293.5**	9.81	0.003407	0.008	0.713125	*2.28199E-10*	**5849264.4**	5.8
16	22	6	19	**292**	9.81	0.003425	0.008	0.7135	*2.24251E-*	**5130831**	5.1

									10		
16	23	7	19.5	292.5	9.81	0.003419	0.008	0.713375	2.25563E-10	5939932	5.9
15	21	6	18	291	9.81	0.003436	0.008	0.71375	2.21936E-10	5203991.6	5.2
14	20	6	17	290	9.81	0.003448	0.008	0.714	2.1904E-10	5292818.8	5.2
13	19	6	16	289	9.81	0.00346	0.008	0.7143	2.16678E-10	5371275.5	5.3
12	18	6	15	288	9.81	0.003472	0.008	0.7146	2.1433E-10	5451281.6	5.4
11	17	6	14	287	9.81	0.003484	0.008	0.7149	2.11994E-10	5532875.5	5.5
10	16	6	13	286	9.81	0.0035	0.008	0.7158	2.0967E-10	5620808.4	5.6

Rayleigh no' from $6x10^6$ (6'000'000) to $7.0x10^6$ (7'000'000)

Cc temp	Room temp	rm-cc	av-room temp	kelvin	*g*	β	L	*Pr*	V^2	*Ra*	Ra
11	28	17	19.5	**292.5**	9.81	0.003419	0.003375	0.713375	*2.25563E-10*	**6085778.5**	6
10	27	17	18.5	**291.5**	9.81	0.003431	0.003375	0.713625	*2.22942E-10*	**6180603.3**	6.1
10	28	18	19	**292**	9.81	0.003425	0.003375	0.7135	*2.24251E-10*	**6493708**	6.4
20	28	8	24	**297**	9.81	0.003367	0.008	0.71225	*2.37545E-10*	**6338387.9**	6.3
19	27	8	23	**296**	9.81	0.003378	0.008	0.7125	*2.34856E-10*	**6434890.7**	6.4
18	26	8	22	**295**	9.81	0.00339	0.008	0.71275	*2.32181E-10*	**6533362.5**	6.5
17	25	8	21	**294**	9.81	0.003401	0.008	0.713	*2.29523E-10*	**6633854.1**	6.6
16	24	8	20	**293**	9.81	0.003413	0.008	0.71325	*2.26879E-10*	**6736417.9**	6.7
15	22	7	18.5	**291.5**	9.81	0.003431	0.008	0.713625	*2.22942E-10*	**6032484.3**	6
15	23	8	19	**292**	9.81	0.003425	0.008	0.7135	*2.24251E-10*	**6841108**	6.8
14	21	7	17.5	**290.5**	9.81	0.003442	0.008	0.713875	*2.20337E-10*	**6126970.8**	6.1
14	22	8	18	**291**	9.81	0.003436	0.008	0.71375	*2.21936E-10*	**6938655.5**	6.9
13	20	7	16.5	**289.5**	9.81	0.003454	0.008	0.71415	*2.17858E-10*	**6220498.5**	6.2
12	19	7	15.5	**288.5**	9.81	0.003466	0.008	0.71445	*2.15502E-10*	**6312929.6**	6.3
11	18	7	14.5	**287.5**	9.81	0.003478	0.008	0.71475	*2.1316E-10*	**6407190.5**	6.4

10	17	7	13.5	286.5	9.81	0.0035	0.008	0.7151	2.1083E-10	6503326.9	6.5

Rayleigh no' from $7x10^6$ (7'000'000) to $8.0x10^6$ (8'000'000)

Cc temp	Room temp	rm-cc	av-room temp	kelvin	G	B	D	PR	V2	RA	RA
19	28	9	23.5	296.5	9.81	0.003373	0.008	0.712375	2.36E-10	7184695.79	7.1
18	27	9	22.5	295.5	9.81	0.003384	0.008	0.712625	2.34E-10	7294361.98	7.2
17	26	9	21.5	294.5	9.81	0.003396	0.008	0.712875	2.31E-10	7406271.64	7.4
16	25	9	20.5	293.5	9.81	0.003407	0.008	0.713125	2.28E-10	7520482.84	7.5
15	24	9	19.5	292.5	9.81	0.003419	0.008	0.713375	2.26E-10	7637055.43	7.6
14	23	9	18.5	291.5	9.81	0.003431	0.008	0.713625	2.23E-10	7756051.19	7.7
13	23	10	18	291	9.81	0.003436	0.008	0.71375	2.22E-10	8673319.37	8.6
12	22	10	17	290	9.81	0.003448	0.008	0.714	2.19E-10	8821364.7	8.8
11	20	9	15.5	288.5	9.81	0.003466	0.008	0.71445	2.16E-10	8116623.77	8.11
11	21	10	16	289	9.81	0.00346	0.008	0.7143	2.17E-10	8952125.91	8.9
10	19	9	14.5	287.5	9.81	0.0035	0.008	0.7148	2E-10	8237816.38	8.2

Rayleigh no' from $9x10^6$ (9'000'000) to $10.0x10^6$ (10'000'000)

Cc temp	Room temp	rm-cc	av-room temp	kelvin	*g*	β	L	*Pr*	V^2	*Ra*	Ra
16	27	11	21.5	**294.5**	9.81	0.003396	0.008	0.712875	*2.31E-10*	**9052109.79**	9.5
16	28	12	22	**295**	9.81	0.00339	0.008	0.71275	*2.32E-10*	**9800043.72**	9.8
15	26	11	20.5	**293.5**	9.81	0.003407	0.008	0.713125	*2.28E-10*	**9191701.25**	9.1
15	27	12	21	**294**	9.81	0.003401	0.008	0.713	*2.3E-10*	**9950781.14**	9.9
14	25	11	19.5	**292.5**	9.81	0.003419	0.008	0.713375	*2.26E-10*	**9334178.86**	9.3
13	24	11	18.5	**291.5**	9.81	0.003431	0.008	0.713625	*2.23E-10*	**9479618.12**	9.4
12	23	11	17.5	**290.5**	9.81	0.003442	0.008	0.713875	*2.2E-10*	**9628096.92**	9.6
11	22	11	16.5	**289.5**	9.81	0.003454	0.008	0.71415	*2.18E-10*	**9775069.12**	9.7
10	20	10	15	**288**	9.81	0.0035	0.008	0.7146	*2E-10*	**9085469.3**	9
10	21	11	15.5	**288.5**	9.81	0.0035	0.008	0.7145	*2E-10*	**9920317.94**	9.9

Rayleigh no' from $10x10^6$ (10'000'000) to $11.0x10^6$ (11'000'000)

Cc temp	Room temp	rm-cc	av-room temp	kelvin	*g*	β	L	*Pr*	V^2	*Ra*	Ra
15	28	13	21.5	**294.5**	9.81	0.003396	0.008	0.712875	*2.31E-10*	**10697947.9**	10.6
14	26	12	20	**293**	9.81	0.003413	0.008	0.71325	*2.27E-10*	**10104626.9**	10
14	27	13	20.5	**293.5**	9.81	0.003407	0.008	0.713125	*2.28E-10*	**10862919.7**	10.8
13	25	12	19	**292**	9.81	0.003425	0.008	0.7135	*2.24E-10*	**10261662**	10.2
12	24	12	18	**291**	9.81	0.003436	0.008	0.71375	*2.22E-10*	**10407983.2**	10.4
11	23	12	17	**290**	9.81	0.003448	0.008	0.714	2.19E-10	**10585637.6**	10.5
10	22	12	16	**289**	9.81	0.0035	0.008	0.7143	*2E-10*	**10742551.1**	10.7

Rayleigh no' from $11x10^6$ (11'000'000) to $12.0x10^6$ (12'000'000)

Cc temp	Room temp	rm-cc	av-room temp	kelvin	*g*	β	L	*Pr*	V^2	*Ra*	Ra
14	28	14	21	294	9.81	0.003401	0.008	0.713	*2.3E-10*	11609244.7	11.6
13	26	13	19.5	292.5	9.81	0.003419	0.008	0.713375	*2.26E-10*	11031302.3	11
13	27	14	20	293	9.81	0.003413	0.008	0.71325	*2.27E-10*	11788731.3	11.7
12	25	13	18.5	291.5	9.81	0.003431	0.008	0.713625	*2.23E-10*	11203185	11.2
12	26	14	19	292	9.81	0.003425	0.008	0.7135	*2.24E-10*	11971939	11.9
11	24	13	17.5	290.5	9.81	0.003442	0.008	0.713875	*2.2E-10*	11378660	11.3
10	23	13	16.5	289.5	9.81	0.0035	0.008	0.7142	*2E-10*	11552354.4	11.5

Rayleigh no' from $12x10^6$ (12'000'000) to $13.0x10^6$ (13'000'000)

Cc temp	Room temp	rm-cc	av-room temp	kelvin	*g*	β	L	*Pr*	V^2	*Ra*	Ra
13	28	15	20.5	293.5	9.81	0.003407	0.008	0.713125	*2.28E-10*	12534138.1	12.5
12	27	15	19.5	292.5	9.81	0.003419	0.008	0.713375	*2.26E-10*	12728425.7	12.7
11	25	14	18	291	9.81	0.003436	0.008	0.71375	*2.22E-10*	12142647.1	12
11	26	15	18.5	291.5	9.81	0.003431	0.008	0.713625	*2.23E-10*	12926752	12.9
10	24	14	17	290	9.81	0.0034	0.008	0.714	2E-10	12349910.6	12.3

Rayleigh no' from $13x10^6$ (13'000'000) to $14.0x10^6$ (14'000'000)

Cc temp	Room temp	rm-cc	av-room temp	kelvin	*g*	β	L	*Pr*	V^2	*Ra*	Ra
12	28	16	20	293	9.81	0.003413	0.008	0.71325	*2.27E-10*	13472835.8	13.4
11	27	16	19	292	9.81	0.003425	0.008	0.7135	*2.24E-10*	13682216	13.6
10	25	15	17.5	290.5	9.81	0.0034	0.008	0.7139	*2E-10*	13129223.1	13
10	26	16	18	291	9.81	0.0034	0.008	0.7138	*2E-10*	13877311	13.8

Rayleigh no' from $14x10^6$ (14'000'000) to $15.0x10^6$ (15'000'000)

Cc temp	Room temp	rm-cc	av-room temp	kelvin	*g*	β	L	*Pr*	V^2	*Ra*	Ra
11	28	17	19.5	292.5	9.81	0.003419	0.008	0.713375	*2.26E-10*	**14425549.1**	14.4
10	27	17	18.5	291.5	9.81	0.0034	0.008	0.7136	*2E-10*	**14650318.9**	1.46

Rayleigh no' from $15x10^6$ (15'000'000) to $16.0x10^6$ (16'000'000)

Cc temp	Room temp	Rm-cc	av-room temp	kelvin	*g*	β	L	*Pr*	V^2	*Ra*	Ra
10	28	18	19	292	9.81	0.0034	0.008	0.7135	*2E-10*	**15392493**	15.3

Appendix B

Publication literatures form this Thesis.

Taki AH, Jalil L and Loveday DL, Stabilising Airflows in Chilled Ceiling / Displacement Ventilation Environments. 22nd International Conference on Passive Low Energy Architecture(PLEA), Beirut, Lebanon, November 2005

Jalil L, Taki AH, Loveday, DL, Computation of Airflow in a Displacement Ventilation / Chilled Ceiling Environmental, IndoorAir 2002, 9th Int' Conference on Indoor Air Quality and Climate, June 30th-July-5th 2002, Monterey, California, USA.

Taki AH, Jalil L and Loveday DL Use of Computational FluidDynamics for Modelling Displacement Ventilation Environments. The International Conference on Research Trends in Science and Technology, Beirut, Lebanon March 4th to march 8th 2002.

Stabilising Airflows in Chilled Ceiling/Displacement Ventilation Environments

Ahmad H Taki[1], Latifimran Jalil[1], and Dennis L Loveday[2]

[1]Department of Product & Spatial Design (Incorporating Leicester School of Architecture), De Montfort University, Leicester LE1 9BH, UK

[2]Department of Civil & Building Engineering, Loughborough University, Loughborough, LE11 3TU, UK

ABSTRACT: A significant amount of work has taken place to investigate the performance of chilled ceilings and displacement ventilation systems operated together so as to achieve the appropriate cooling capacities while at the same time enhancing the sensation of thermal comfort. However, Taki etal (1996) have shown that combination of a chilled ceiling with a displacement ventilation system can cause destruction of the displacement flow pattern. This is caused by inversion, due to the downward cool air currents, which leads to a poorer environment and a failure to realise the enhanced comfort and air quality that these systems are individually claimed to bring. This paper has investigated a new technique for achieving stable conditions for displacement airflow. The technique used here was the attachment of a honeycomb slat system to the chilled ceiling, thereby suppressing downward cool natural convection. The vertical temperature profiles of the room air were compared with those from the conventional arrangement to confirm that such technique could minimise the downward cool air currents and the displacement flow pattern could be preserved in the presence of chilled ceiling. The outcome of the study is the provision of general advice for designers as regards the combination of radiant cooling/displacement ventilation systems. Further, the work will enhance the knowledge of continuing the international trend towards low energy cooling technologies.

Conference Topics: Low energy architecture; Innovative low energy technologies
Keywords: energy, chilled ceiling, displacement ventilation, honeycomb slats, air quality, comfort

1. INTRODUCTION

In commercial premises and deep-plan designs with significant internal heat gains, air conditioning has often been specified in order to achieve the required internal space conditions. Air conditioning is widely recognised as an energy-intensive solution. Interest has grown, therefore, in the development of low energy techniques for space cooling, and among these is the use of displacement ventilation and chilled ceiling systems.

1.1 Displacement Ventilation

In displacement ventilation system low velocity full fresh air is introduced gently into the occupied zone at low level and at a temperature slightly lower than that of the desired zone air temperature. As a result of density differences, the fresh air forms a cool layer over the floor. The air then rises as it is warmed by heat sources in the zone, and the convective plumes generated by these sources remove heat and contaminants that are extracted at ceiling level. In this way the system is able to provide an environment of improved air quality as compared with mixing of air which occurs in conventional HVAC systems for the same airflow rate conditions. Further, the same heat load loads can be removed for a supply temperature of typically 19°C as compared with a supply temperature of 13°C in an HVAC system. The system offers enhanced thermal comfort, improved air quality and reduced energy consumption, for removal of the same loads as those removed by a conventional HVAC system.

In order to remain within the guidelines presented in International Standard ISO 7730 (1994), on thermal comfort (that is, the vertical temperature gradient should be less than 3°C per metre) a displacement ventilation system is limited to removing a convective heat load of up to 25 W/m^2 of floor area (Sandberg and Blomqvist, 1989). However, the typical heating load in offices frequently exceeds this figure, necessitating the provision of an additional cooling mechanism such as a chilled ceiling.

1.2 Chilled Ceilings

In a chilled ceiling system, cool water passes through pipe work which is bonded to ceiling tiles and is insulated at the rear. This produces a typical ceiling tile surface temperature in the range of 14-19°C. Chilled ceiling system can remove up to 100W/m^2 of floor area by the combined processes of radiation and convection and are considered to

enhance the thermal comfort sensation of occupants in a manner analogous to the outdoors and beneath the open sky. When combined with displacement ventilation, the advantages offered by each system separately (improved air quality, enhanced thermal comfort) are not retained for the combined arrangement.

1.3 Combined Displacement Ventilation and Chilled Ceiling system

When chilled ceilings are used in combination with displacement ventilation systems, it has been reported that the height of the stratification boundary layer above the floor decreases gradually as the relative cooling load of the chilled increases. Characterisation tests in such a combination system revealed that the use of a chilled ceiling with displacement ventilation could have a detrimental effect upon the displacement flow pattern. This is caused by inversion, which leads to a poorer environment and a failure to realise the enhanced comfort and air quality that these systems are individually claimed to bring. Fitzner (1996) suggested that the airflow pattern turned into mixed flow when 50% of the cooling load was removed by the chilled ceiling. He concluded that the vertical profiles of contamination were severely affected by a chilled ceiling. Alamdari and Eagle (1996), Loveday et al (1998) and Riffat etal (2004) showed that combination of a chilled ceiling with a displacement ventilation system had a detrimental effect upon displacement flow. Figures 1 and 2 confirm the inversion phenomena as reported by Jalil etal (2002) using computational fluid dynamics simulation and Taki etal (1996) using experimental investigations, where it can be seen that at ceiling temperature of 12-14°C, there is complete mixing of air throughout the room as shown by the vertical air temperature profiles from floor to ceiling.

1.4 The Aim

The aim of our work was to experimentally investigate a new technique for achieving stable conditions for displacement airflow, thereby ensuring that the combined arrangement can work together effectively.

The technique used here was the attachment of a honeycomb slat system to the chilled ceiling, thereby suppressing downward cool natural convection. A full-scale office zone has been used to characterise the new arrangement consisting of displacement ventilation and honeycomb slat-clad chilled ceiling environment.

2. THE EXPERIMENTAL FACILITY

Figure 3 shows a schematic diagram of the test room that acts as an office environment. It is light weight room 5.4m long, 3m wide and 2.8m high, employing a chilled ceiling and displacement ventilation system.

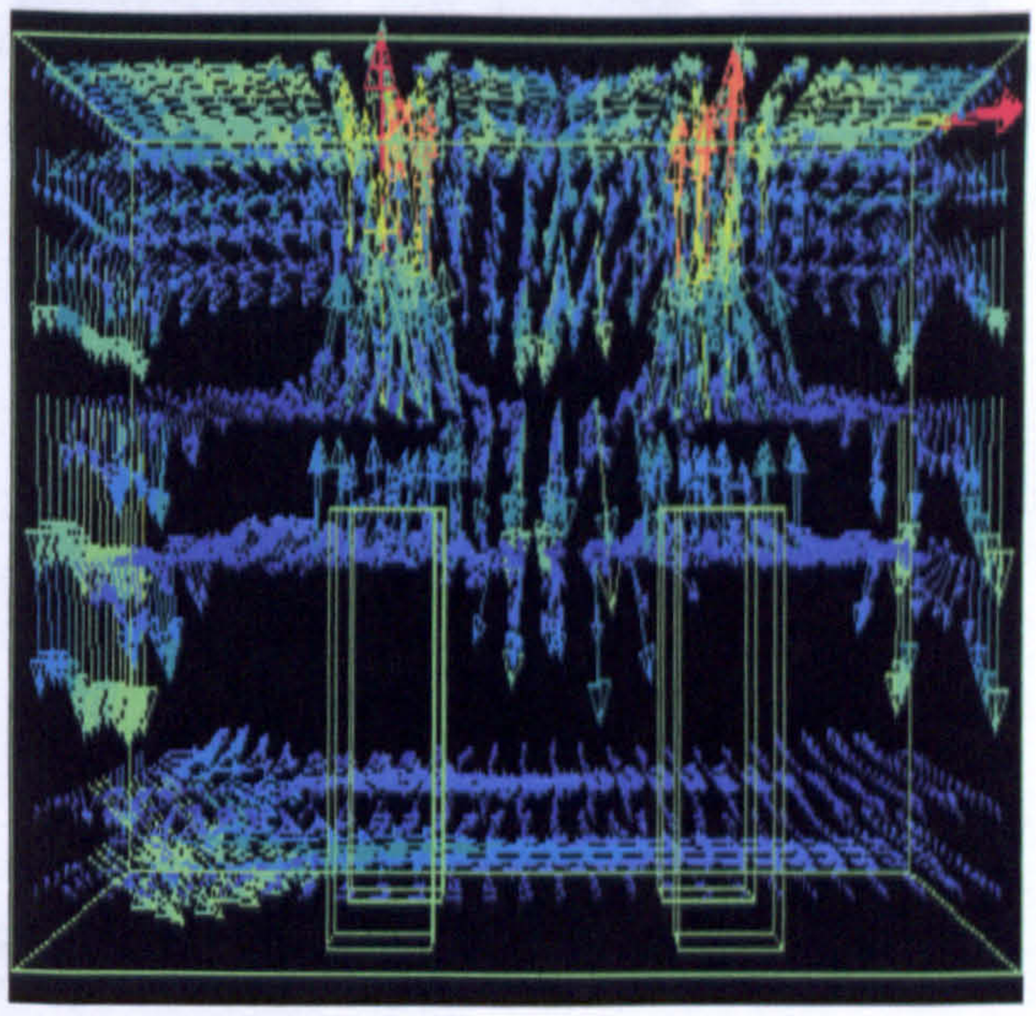

Figure 1: Cool air being pushed down into the fresh air occupied zone (Jalil etal 2002)

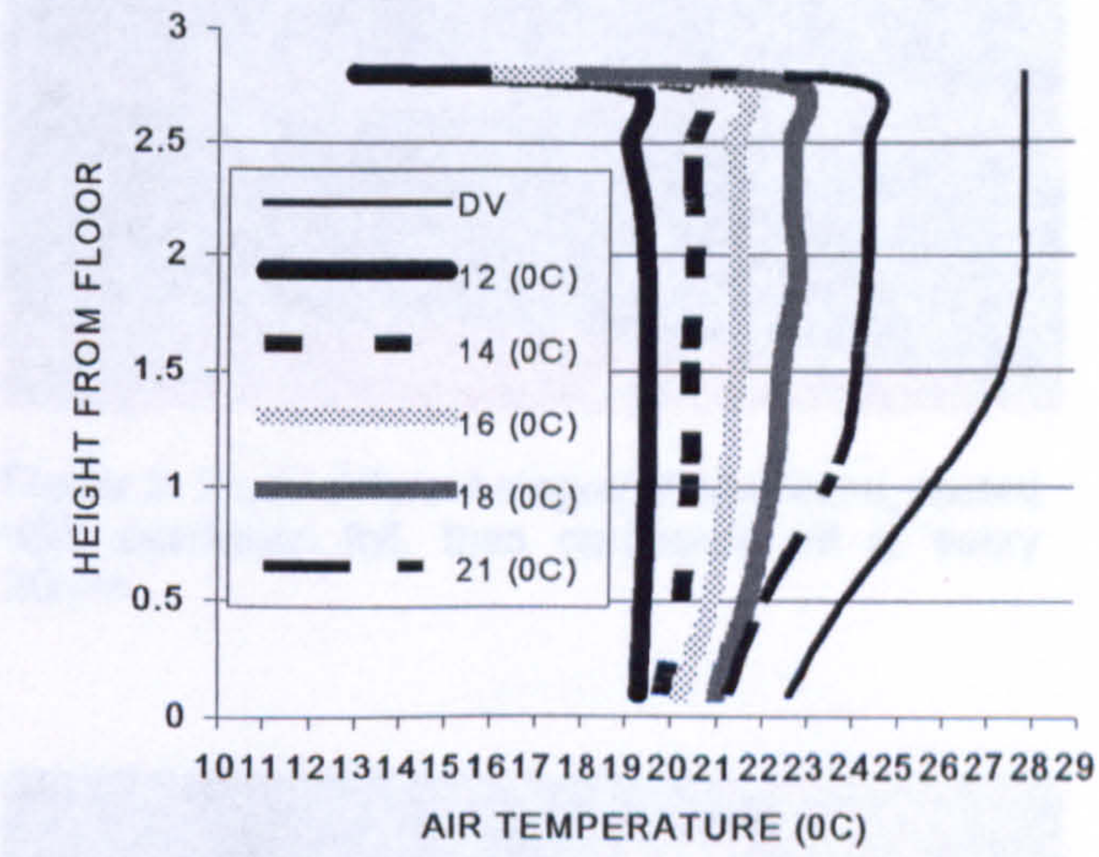

Figure 2: Air temperature versus height for a range of ceiling temperature at a heat load of 62 W/m^2

All environmental parameters within the room are controllable; these include supply airflow rate, air temperature, relative humidity, ceiling and walls surfaces temperatures. The test room is carpeted and furnished to a normal office standard, and is equipped with thermal dummies to simulate human heat sources. Temperatures and the mean air velocity were measured at different heights and locations. All environmental parameters were logged every 5 seconds and average values were calculated every 5 minutes.

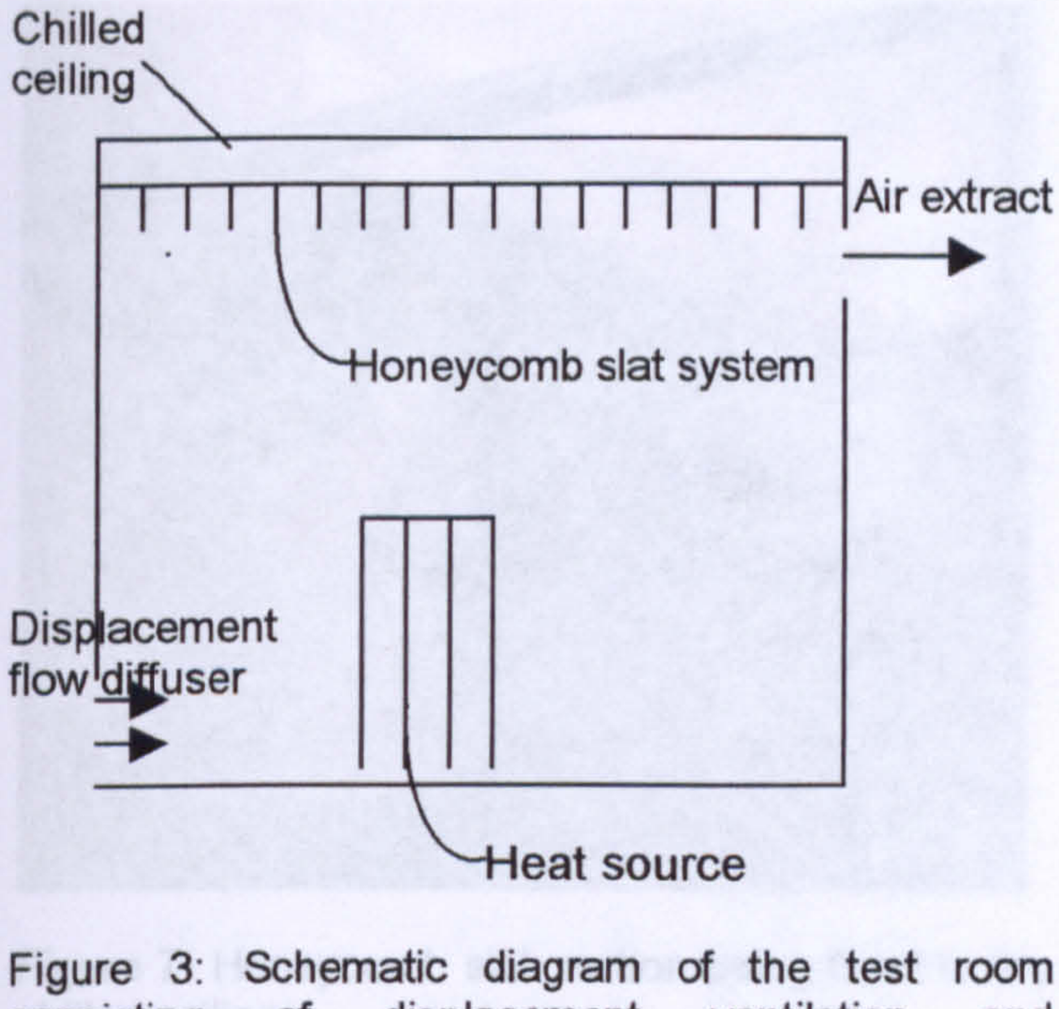

Figure 3: Schematic diagram of the test room consisting of displacement ventilation and honeycomb slat-clad chilled ceiling environment.

3. EXPERIMENTAL PROCEDURE

Prior to any experimental investigation into the attachment of honeycomb slats to the chilled, it was necessary to apply CFD simulation to predict as to which conditions and configuration of the honeycomb slat system could suppress natural convection, which would lead to better control of the stratified boundary layer. The CFD investigation is beyond the scope of this paper as such results will be published elsewhere. However, the optimised depth to width ratio of the honeycomb system was found to be 10 as shown in Figure 4 where convection currents between the honeycomb slats have been almost suppressed. Their implications on displacement flow pattern will be experimentally investigated.

The honeycomb slats were made of corrugated cardboards. The slats of dimensions 1000mm wide x 200mm high x 2mm thick were slit at every 20mm. Both sides of the slats were coated with aluminium foil tape. The emissivity of aluminium foil tape was experimentally determined to be 0.03. The honeycomb slat was made into sections of 1000mm x 1000mm x 200mm, with 20mm gap between each slat giving a depth width ratio of 10:1. Each section was then attached to the chilled ceiling forming a honeycomb slat system. Figures 5, 6, 7 and 8 show the different stages of design, fabrication and installation of the honeycomb slat system.

The experimental procedure adopted was to measure the vertical air temperature profile in the room for the following conditions. The displacement ventilation system was set into operation at a supply air temperature of 19°C, for four values of displacement air supply flow rate (2, 4, 6 and 8 air changes per hour). The heat load in the space was fixed to 62 W/m^2 of floor area; this was achieved by placing seven thermal dummies within the room to simulate heat sources such occupants and office equipment. The ceiling temperatures were set up to the following values 12, 14, 16, 18 and 21°C. The above conditions were carried out in a conventional

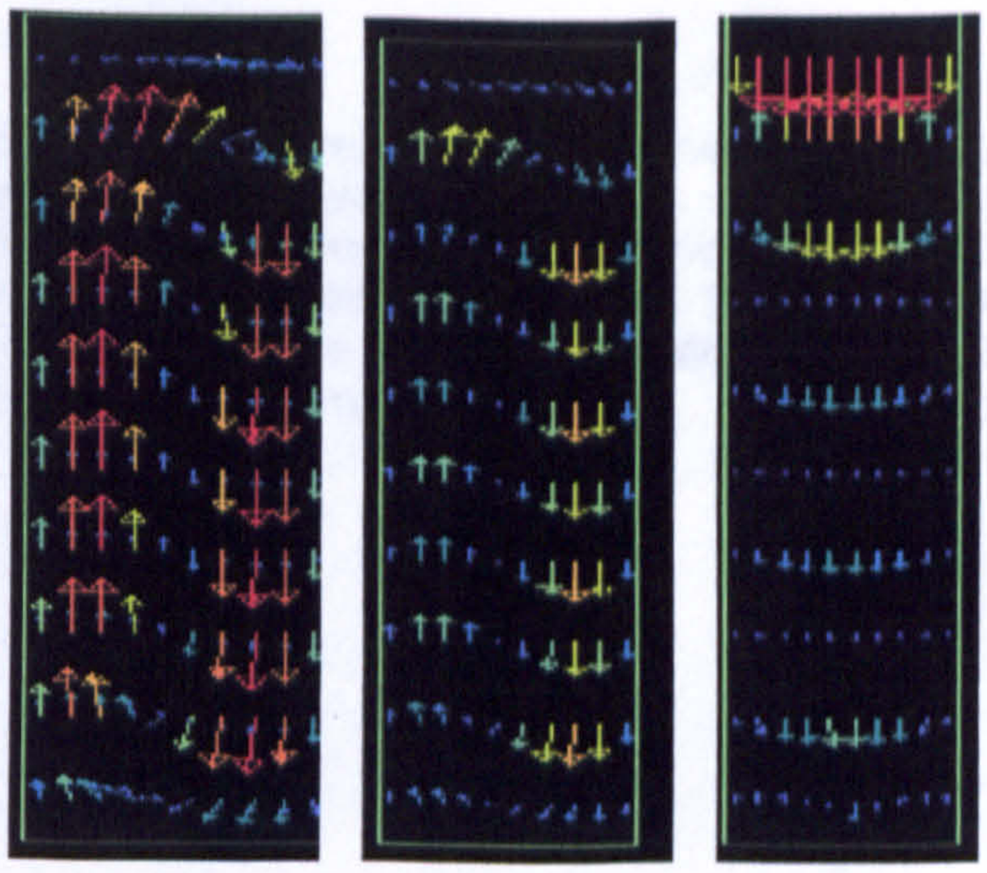

Figure 4: CFD simulations showing the process of convection current being suppressed for different depth to width ratio

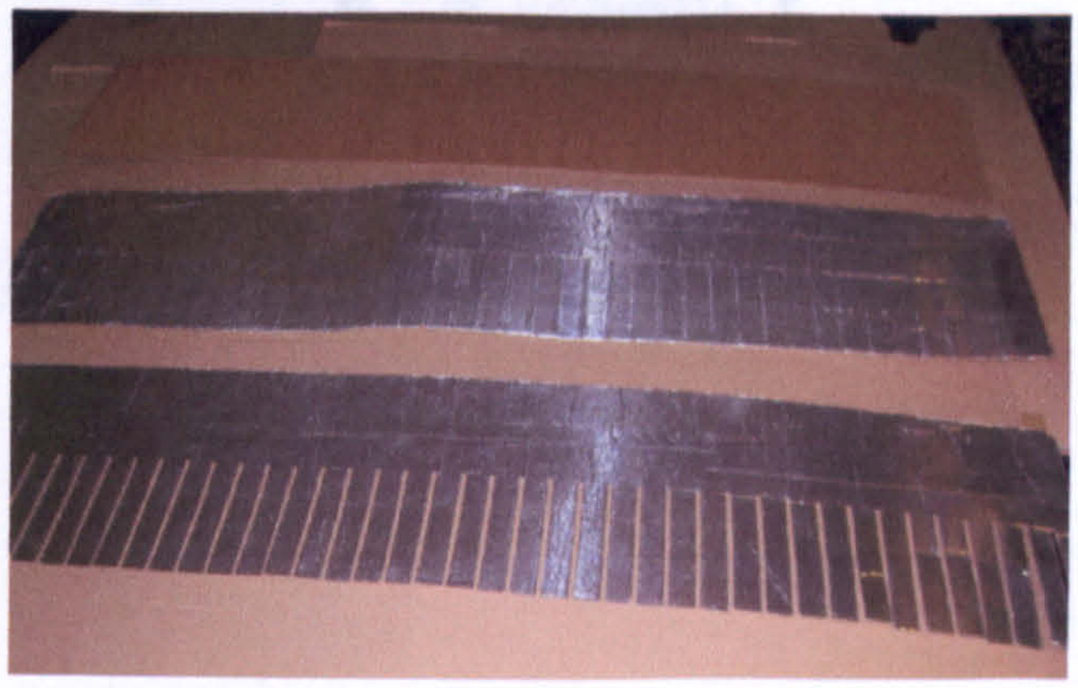

Figure 5: Three different stages of cardboard, coated with aluminium foil, then cardboard slit at every 20mm

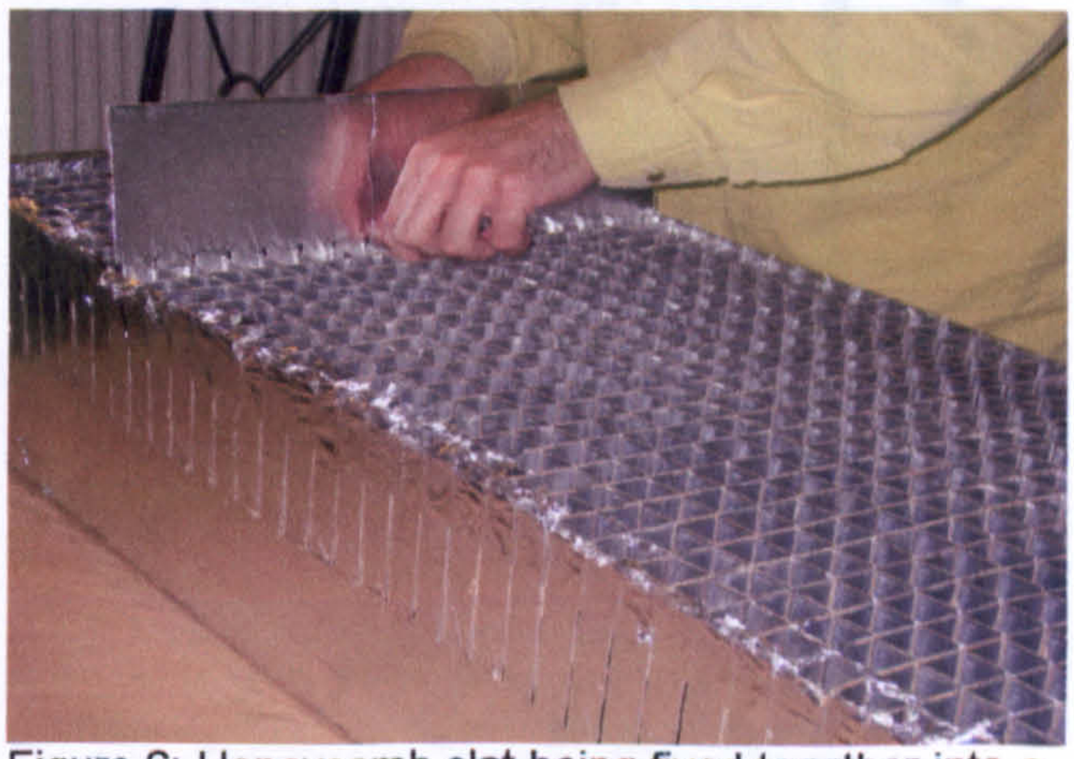

Figure 6: Honeycomb slat being fixed together into a section.

combined arrangement environment, and in the presence of a honeycomb slat system attached to ceiling.

Figure 7: Honeycomb slat section being fixed to the chilled ceiling

Figure 8: The test room with honeycomb slats attached to the chilled ceiling.

4. RESULTS

A series of measurements was carried out to determine the effect of the honeycomb system on displacement flow pattern in the presence of chilled ceiling system. Figures 9, 10 and 11 show the vertical temperature profiles in the room for ceiling temperatures of 12, 14 and 16°C respectively, at a fixed heat load of 62 W/m^2, and at airflow rate of 4 air changes per hour. The corresponding profiles for the case of conventional combined arrangement (i.e. with no honeycomb slats) are also shown for comparison. It can be seen that there is almost vertical air temperature profiles for the case of environment without the honeycomb slat system attached. The vertical temperature profiles are indicative of complete mixing of air in the room. This is caused by downward movement of cool air destroying the displacement flow pattern, resulting in almost all heat loads being removed by the chilled ceiling. However, when the honeycomb slats are attached to the ceiling the results show that the displacement airflow pattern is allowed to take place as shown by the presence of an inclined temperature gradient in the vertical direction. This can be explained by the suppression of the cool downward air currents permitting displacement flow pattern to be preserved in the presence of chilled ceiling even at lower surface temperatures.

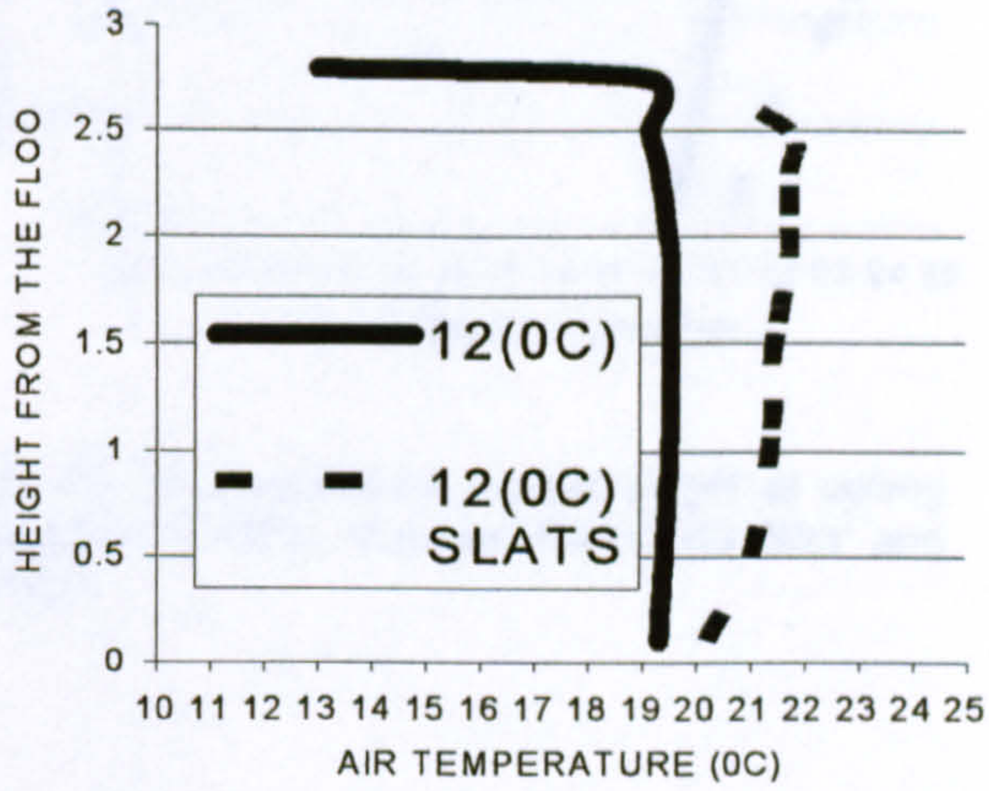

Figure 9: Air temperature versus height at ceiling temperature of 12°C, at a heat load of 62 W/m^2 and at 4 ACH

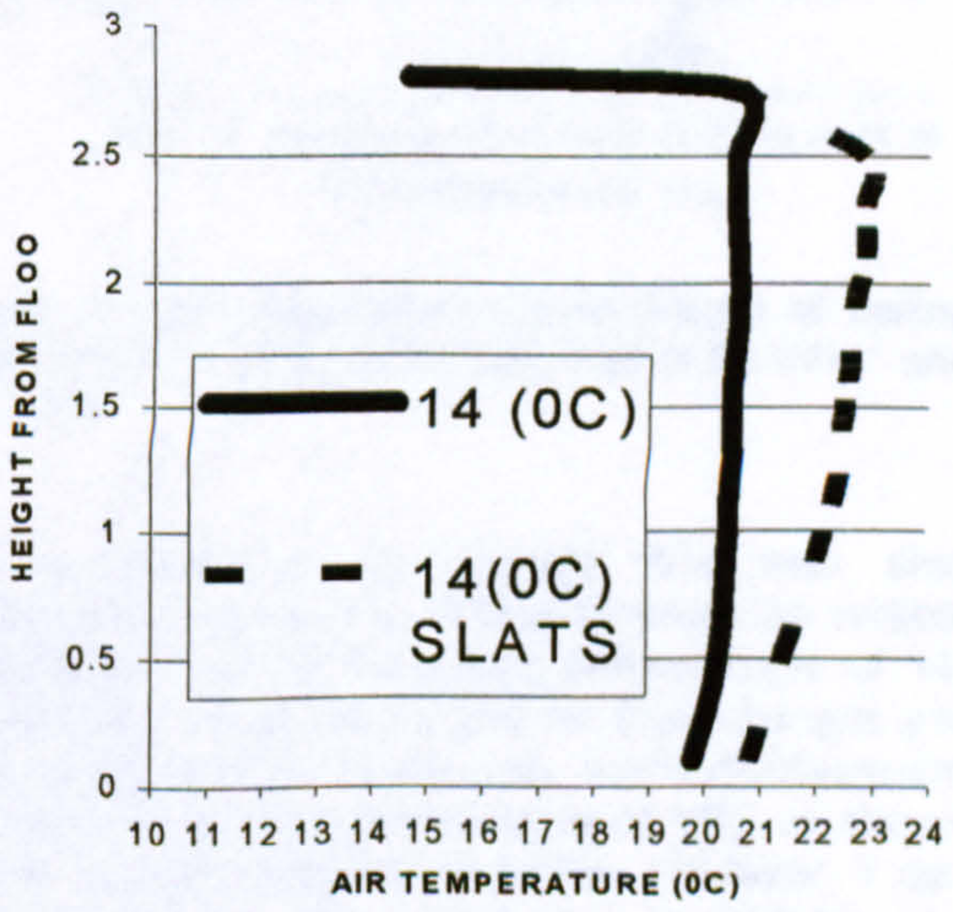

Figure 10: Air temperature versus height at ceiling temperature of 14°C, at a heat load of 62 W/m^2 and at 4 ACH

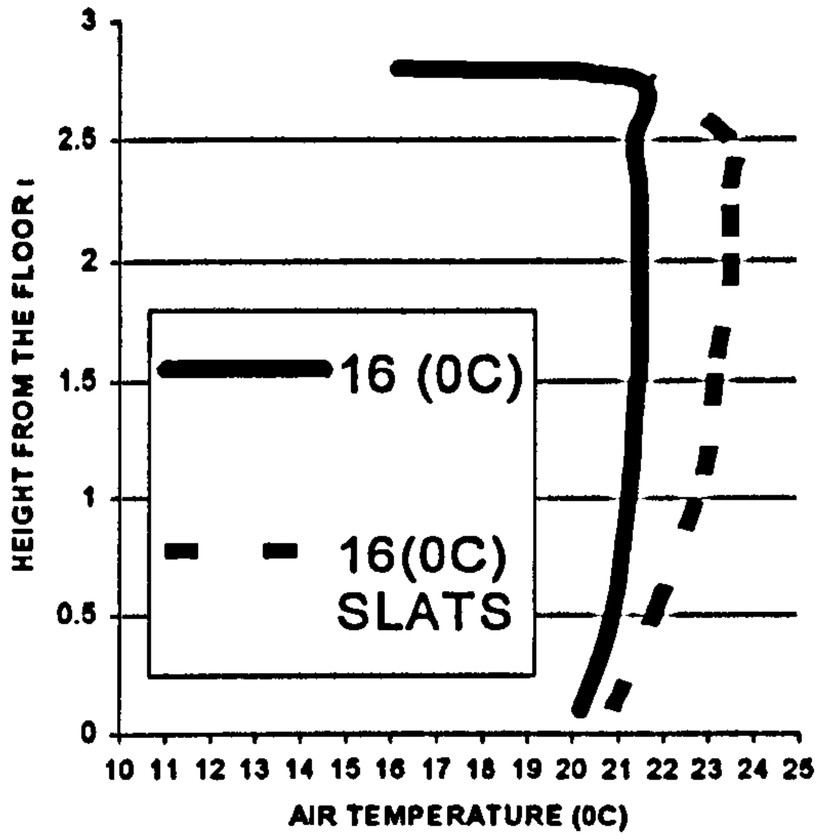

Figure 11: Air temperature versus height at ceiling temperature of 16°C, at a heat load of 62 W/m^2 and at 4 ACH

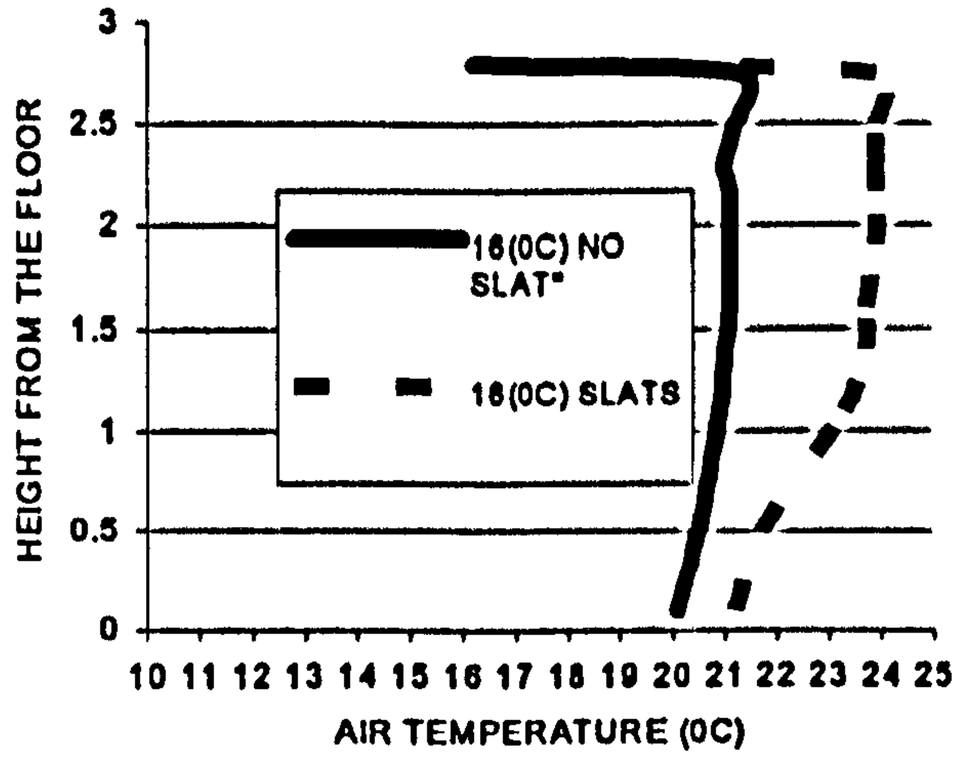

Figure 13: Air temperature versus height at ceiling temperature of 16°C, at a heat load of 62 W/m^2 and at 6 ACH

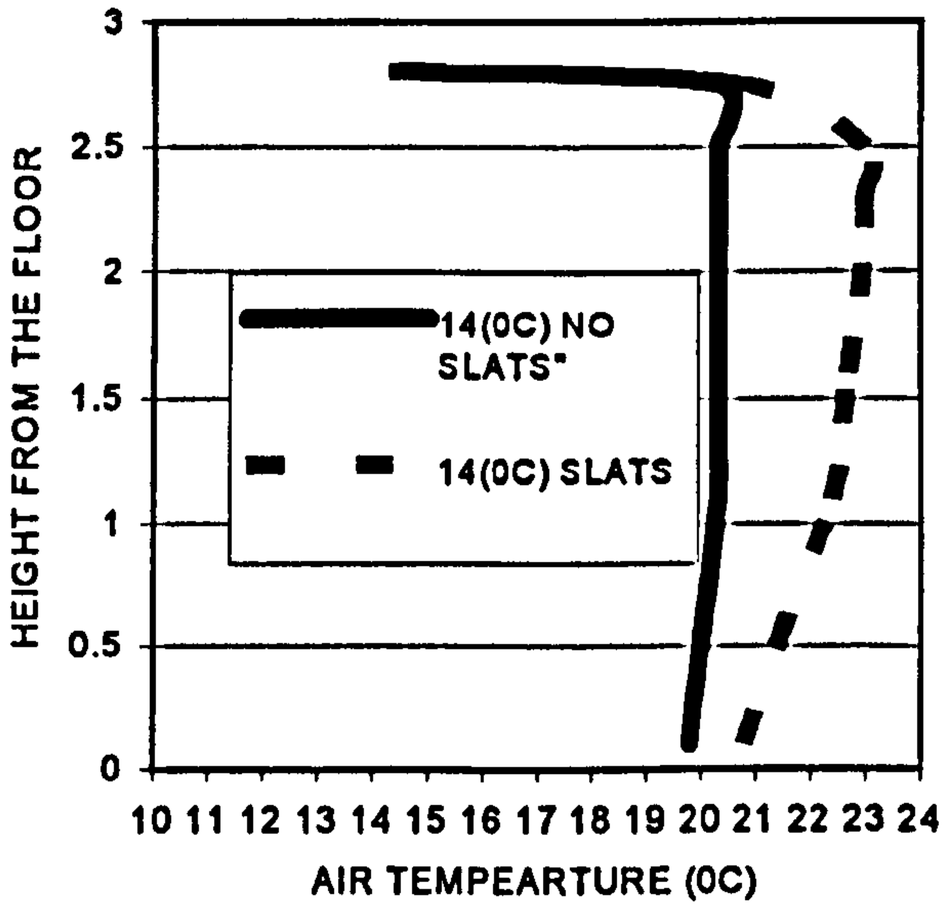

Figure 12: Air temperature versus height at ceiling temperature of 14°C, at a heat load of 62 W/m^2 and at 6 ACH

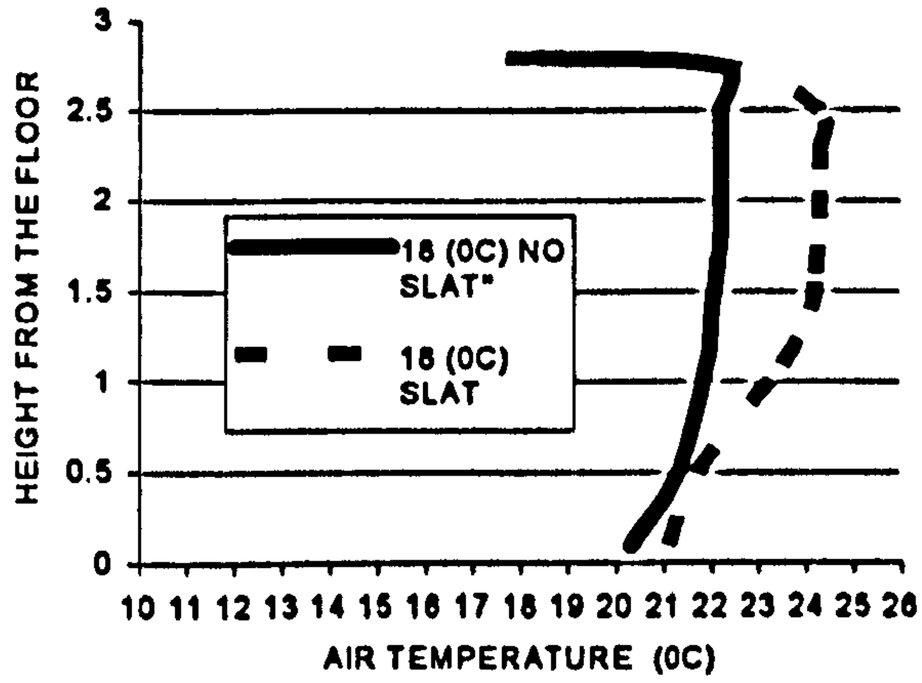

Figure 14: Air temperature versus height at ceiling temperature of 18°C, at a heat load of 62 W/m^2 and at 6 ACH

The effect of air change rate was also investigated. Figures 12, 13 and 14 show the vertical temperature profiles for ceiling temperatures of 14, 16 and 18°C respectively, and for 6 air changes per hour. In the absence of the slats, some displacement is present at a ceiling temperature of 18°C as shown by the inclined temperature profile. However, it can be seen that the attachment of a honeycomb slat system can raise the air temperature in the space allowing more heat load being removed by displacement ventilation permitting true displacement flow pattern to occur in the presence of chilled ceiling. This also applies when supply air flow rate was

reduced to 2 air changes per hour as shown in Figure 15.

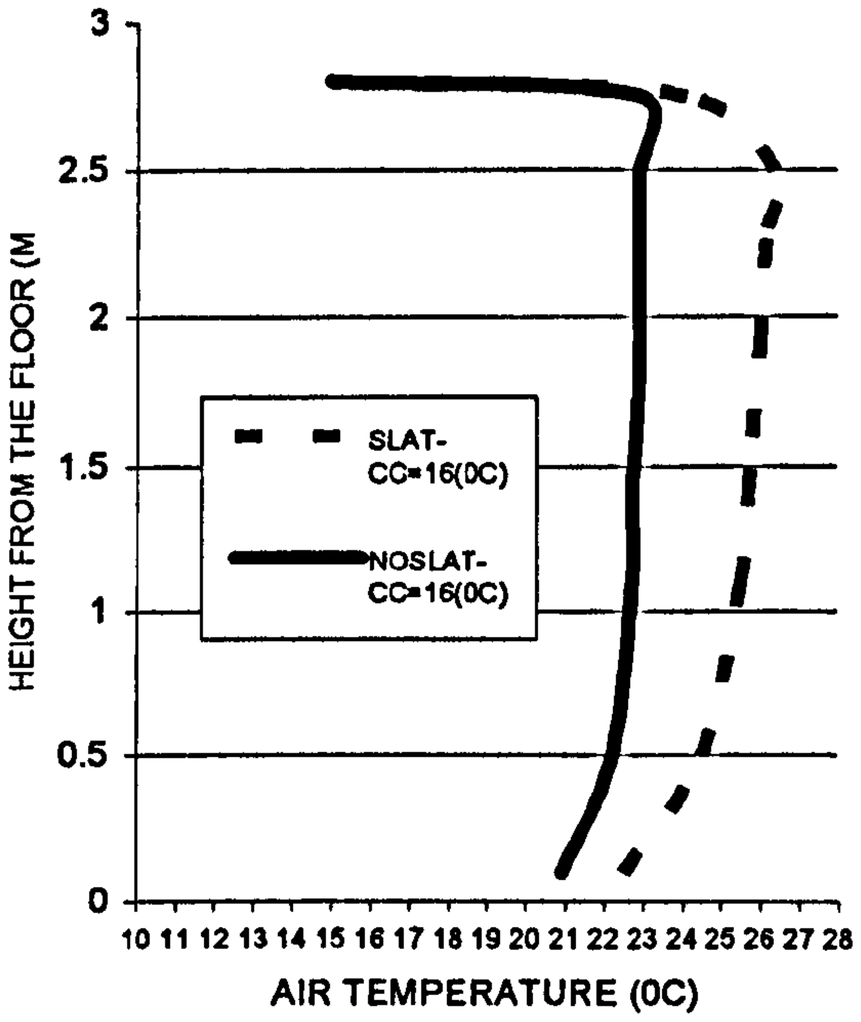

Figure 15: Air temperature versus height at ceiling temperature of 16°C, at a heat load of 62 W/m^2 and at 2 ACH

5. CONCLUSIONS

Experiments have been carried out to test the use of a honeycomb slat system for suppressing downward cool air currents in a combined chilled ceiling/displacement ventilation environment. The following conclusions may be drawn from this study:

- In the absence of slats, the combination of a chilled ceiling with a displacement ventilation system can potentially destroy the displacement flow pattern. This is particularly the case at ceiling temperatures less than 16°C, and is caused by downward currents of cool air producing mixing of the room airflow. At a ceiling temperature of 18°C, displacement flow is evident. Such a combination therefore requires careful design to work effectively (see also Loveday et al, 1998).

- The attachment of a honeycomb slat system can raise the general air temperature in the space and permit some displacement ventilation to occur (as shown by the presence of an inclined temperature gradient in the vertical direction) in situations where, without the slats, it would have been completely destroyed. This can be explained by the suppression of the cool downward air currents as a result of the honeycomb slat-clad ceiling system.

The work presented here has confirmed the feasibility of the slat system approach as a means for preserving displacement flow in the presence of a chilled ceiling. Further analysis is currently taking place to develop guidance that can be used by designers in this context. Such analysis will take into account required heat removal rates from the space, maintenance of a suitable vertical temperature gradient commensurate with satisfactory thermal comfort sensations, and dimensioning of the slat system itself for practical application.

REFERENCES

1. Alamdari, F and Eagles, N, (1996) Displacement Ventilation and Chilled Ceilings', BSRIA, Technical Note TN2/96.
2. Fitzner, K (1996), 'Displacement Ventilation and Cooled Ceilings, Results of Laboratory Tests and Practical Installation', The Seventh International Conference on Indoor Air Quality and Climate, Indoor Air '96, Nagoya, Japan, pp 41-50, July 1996.
3. ISO 7730 (1994) Moderate Thermal Environments - Determination of the PMV and PPD indices and specification of the conditions for thermal comfort, Geneva: International Standards Organisation, 1994.
4. Jalil, L, Taki, AH and Loveday DL (2002) Computation of Airflow in a Displacement Ventilation/Chilled Ceiling Environment. Indoor Air 2002, the 9th International Conference on Indoor Air Quality and Climate, vol.1, pp 272-277, ISBN 0-9721832-0-5, Monterey, California, USA.
5. Loveday, DL, Parsons, KC, Taki, AH, Hodder, SG and Jeal, L (1998), Designing for Thermal Comfort in Combined Chilled Ceiling/Displacement Ventilation Environments, *ASHRAE Transactions,* vol. 104, Pt 1B, pp901-911, SF-98-4-4, ISSN 0001-2505.
6. Riffat, S B, Zhao, X and Doherty, P. S. (2004) Review of Research into and application of chilled ceilings and displacement ventilation systems in Europe, International Journal of Energy Research, 2004 no28, pp 257-286.
7. Taki, AH, Loveday, DL and Parsons, KC (1996), The Effect of Chilled Ceiling Temperatures on Displacement Flow and Thermal Comfort- experimental and simulation studies, The Fifth International Conference on Air Distribution in Rooms-Room Vent '96, Yokohama -Japan, vol. 3, pp307-314, 1996, ISBN 492455701 3.

COMPUTATION OF AIRFLOW IN DISPLACEMENT VENTILATION ENVIRONMENT.

L. Jalil*, A.H.Taki* and D.L. Loveday +

*** School of Architecture, De Montfort University, Leicester LE1 9BH UK**
+Department of Civil and Building Engineering, Loughborough University, Loughborough, LE11 3TU UK

ABSTRACT

To meet the demands for better air quality, enhanced thermal comfort and reduced energy consumption in commercial offices, the use of displacement ventilation systems has increased rapidly over the last ten years.
Displacement ventilation can provide an efficient and effective system for an enclosure that helps in achieving the demands stated above (Alamdari 98).

This paper presents an assessment of the ability to model airflow and temperature distributions in such environments that employ Natural Ventilation and Displacement Ventilation system, with a standard Computational Fluid Dynamics (CFD) code. Modelling is carried out over a range of typical office conditions for a range of heat loads

It was found that the CFD code could be used to successfully predict the airflow in these environments by showing good agreement with those of earlier studies. It is concluded that CFD is an effective tool that can be used for accurately predicting airflow and air temperature at the design stage for such environments.

INTRODUCTION

Over the last few decades the office environment has changed rapidly and is continuing changing. One such change is the office space has expanded and we are now in the trend of open office environment in place of the traditional segregated office units. With the large open office space came the problem of providing adequate air ventilation to the office, one method used is displacement ventilation. Which is to introduce a supply of air at one part of the room and allow it to sweep in one direction across the space taking the pollutants with it for exhaust at the opposite part of the room. Displacement ventilation is mainly characterized by buoyancy-driven airflow. In this system low velocity air is supplied from a low level supply device in the occupied zone at a temperature slightly cooler then the design room temperature, in order to obtain the displacement effects. Natural convection from internal heat sources, such as occupants and equipment, cause upward air movement in the room. The warm, contaminated air forms a stratified region above the occupied zone, which is then exhausted at higher level. The airflow in displacement ventilation has both horizontal and vertical air movement characteristics. The horizontal air movement occurs in the thermally stratified layers, which are formed between the upper and lower part of the room and have a vertical air movement in displacement ventilation; The vertical air movement is caused by cold and warm objects in the space. The warm objects such as occupants, small power loads create upward convection currents. The

cold objects such as windows and walls cause downward current. The use of displacement ventilation has the potentent to provide thermal comfort and good air quality to limit of 30W/m^2 Alamdari (1998), Rees (1998). The objective is to use the CFD code to predict airflow in an environment, which employs displacement ventilation over a range of heat loads; and also to predict airflow in an environment that employs both natural and displacement ventilation system.

COMPUTATIONAL FLUID DYNAMICS (CFD) MODELING.

CFD modeling is the process of representing a fluid flow problem by mathematical equations based on the fundamental laws of physics, and solving those equations to predict the variation of the relevant parameters within the flow field. Usually these could be velocity, pressure and temperature, and also concentrations of chemical species. These conservation laws can be expressed in terms of non-linear " elliptic" partial differential equations, the solutions of which provide the basis for the CFD model. The CFD models solve, numerical the equations and produces field values for the temperature, velocity and the chemical species. The CFD code used, Sabre-One has the ability to simulate advanced computational of three-dimensional airflow and temperature in and around enclosures.

THE PROBLEM BEING MODELED.

A cuboidel room which is based in Loughborough University, consists of 5.4m long 3m wide and 2.8m height, was modelled with adiabatic walls. The room employed a displacement ventilation system. The displacement ventilation system was set into operate at a supply temperature of 19 ^{0}C and 3.9 air change per hour. The heat load was varied from 15-25-35-50 and 60 W/m^2 of floor area was achieved by placing within the room four thermal dummies to represent human occupants and office appliance. A Cartesian mesh consisting of 22680 cells was used to model the room, 27 cells in length (x) direction, 56 cells in height (y) direction and 15 cells in width (z) directions.

For the second bench mark the same room size, ACH and air supply temperature was used. A heat load of 25W/m^2 was imposed on the top surface of the four dummies at heights of 0.6m, 1.0m above the floor and at floor height. The Cartesian mesh consisted of 27 cells in length, 28 cells in height and 15 cells in width total cells used were 11340, a K-E turbulence model was adopted for the simulation. This will allow for comparison between CFD code results and the measured results at the laboratory at a later date.

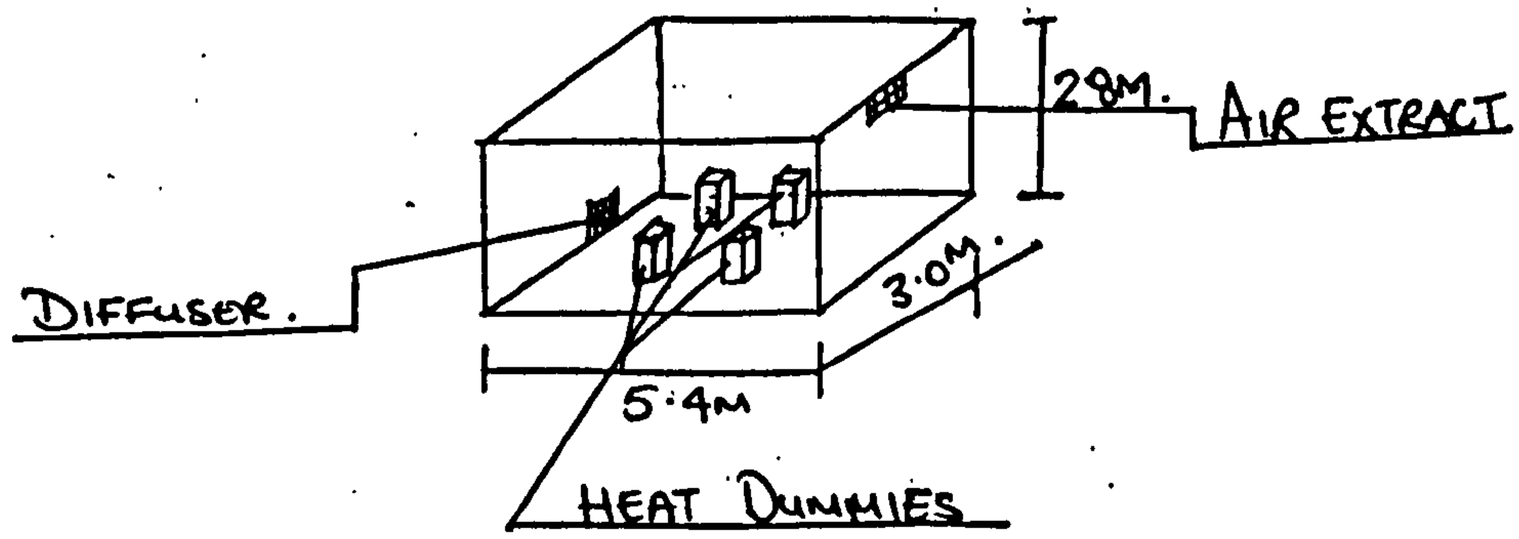

Figure 1 Schematic diagram of the test room.

RESULTS AND DISCUSSION.

The results show a good agreement with others (Taki et al 1996, Alamdari, 1998) that Displacement Ventilation is not capable of removing the heat loads greater than 35 W/m^2 (figure). The result show that the room is divided into two layers one the clean layer of air and the second layer, which is the mixed air, layer (contaminated air). The two layers are divided by the Stratified boundary layer. The height of the stratified boundary layer plays an important part in determining the cleanness of the air in the room.

Figures 1 and 2 show the effects of the heat load of $25W/m^2$ imposed on the top surface of the dummies at 1.4m, 1.0m and 0.6m above the floor height and at floor level. It can be clearly seen that the when the heat load is imposed at 1.4m above the floor the temperature profile gradient is the most steepest, then when the heat loads are imposed at 0.6m or at floor level. The results show that the temperature in the fresh zone is lower when the heat load is imposed at 1.4m height above the floor and the temperature is higher when heat is located neat the floor. When the heat load is located at 1.4m height the temperature difference between the supply temperature and temperature at ankle height was found to be in the region of 26% of total temperature difference. Where in the case of heat load located at the floor surface the figure was in the region of 78% of total temperature difference this can be clearly seen in figure 6 and figure 7. Therefore it can be concluded that height of the heat load can influence the temperature profile gradient. The results have raised a question on the findings of researches and the ISO standard 7730 (1994). The ISO standards 7730 states that for occupants to have clean air and experience thermal comfort the temperature gradient at ankle and noise height (1.1m) should not exceed 3 $^0C/m^2$. The results (figure) clearly show that when heat load is imposed at 1.4m above the floor the temperature gradient is within the requirements but when the heat load is imposed on 1.0m and at 0.6m above the floor, the temperature gradient exceed the requirements. Suggesting that displacement ventilation is not able to remove heat loads of $25W/m^2$. Where we know this is not true, as figure 8 show that displacement ventilation can remove heat loads of up to $35W/m^2$. Therefore it is important to note that when determining the temperature gradient it is very important to take in mind the height of the heat loads.

Using the same boundary conditions as above, the velocity along the floor was investigated. The CFD simulations showed that velocity along the floor increases as it moves in the opposite direction to the diffuser until it reaches it maximum and then it reduces back down (figure); these results also agree with Skistad (1994).

For the conditions used the velocity for the heat load imposed on the floor gave the highest increase in velocity and at the height of load at 1.4m gave the lowest increase in velocity, thus suggesting that the displacement ventilation can only influence the airflow pattern at low heights.

The results from benchmark 1 suggest that not only height of the heat loads effect the temperature profile but the increase in heat loads can also have an effect on the temperature profile, this is clearly visible in figure 8. Where It can be seen that the height of the stratified boundary layer for heat load of $15W/m^2$ is to $60W/m^2$ are at very similar heights. Figure 9 and 10 shows the difference between theat loads of 15W/m2 and $60W/m^2$. It is interesting to note the strength of the plume is greater for higher heat loads.

The results of the CFD simulation showed a pattern that the supply temperature and the extract temperature added together divided by two should provide the temperature

at ankle height. This should be regarded as an estimate only and for some cases this may not be true.
(Extract temperature + Supply temperature) / 2 = Ankle temperature.

VERIFICATION OF THE MODEL.

To assess the accuracy of the CFD code used it was compared with other CFD codes available, CFX, FLOVENT and Taki et al 1996 laboratory results.

The codes were compared with CFX.
Cook has used this code for his finding in natural ventilation work, similar boundary conditions were set, where a room 5.1m in length, 1.0m in width and 2.55 in height. Having two opening, one in the floor and the other in the ceiling to allow the air in and out by natural ventilation with a line heat source of 200 watts distributed in the centre of the room having an area of 0.1m width x 1.0m length.
The results showed similar flow pattern and temperature in the room.
The temperature at and above the stratification boundary layer is the same, the only difference is in the displacement flow curve leading to the stratification boundary layer, this could have been caused by inaccurate simulation of the correct size of the openings inlet and outlet (see figure 11).

The code was further compared with FLOVENT CFD code that was used by Alamdari and Eagels (1996) in his investigation with displacement ventilation and chilled ceiling. Similar boundary conditions were simulated to that of Alamdari work. Room size 4.5m in length, 2.7m in height and 4.5m in width, having two dummies with 20W/m^2 heat load imposed on them, with 19 ^{0}C supply air temperature with 3.5 ACH. The results showed very good agreement with the Flovent CFD code, both having similar airflow pattern, and temperature (see figure 12)

The code was compared to Taki et al (1996) laboratory results. The same boundary conditions were simulated using the CFD code, room size 5.4m length, 3.m width and 2.8m height, with four work dummies each having various heat loads imposed on them ranging from 15-25-35-50 and 60 W/m^2. The supply temperature was 19 ^{0}C with 3.9 ACH. The results at first showed large differences in temperature, and airflow patterns, this was due heat transmission and heat accumulation in the building and only a part of the heat gain inside the room was removed by ventilation. Theses heat losses were calculated as being in the region of 40% of the heat loads. These heat losses were incorporated into the CFD simulation to represent correct heat loads in the lab. The results from this simulation showed very good agreement both in temperature and airflow pattern (see figure 13)

The identical temperature was not obtained to Taki et al (1996) work, could have been due to that fact that inaccurate calculation of heat loss via the room was estimated as 40% where it could be otherwise.

From the results obtained from Sabre-One simulation and other codes it can be concluded that the Sabre-One CFD code is as accurate as any other CFD code currently available.

CONCLUSION

The results of the CFD simulations prove that, CFD can be regarded as an effective tool for predicting temperatures, velocity and airflow in an environment that use natural ventilation and displacement ventilation.

In order to remain in the guidelines of the International Standards (ISO 7730) 1994, on thermal comfort, the vertical temperature gradient should be less than 3 ^{0}C per meter. The use of displacement ventilation at times will not be able to remain with in the guidelines, as it is only able to remove heats loads in the regions between 30 W/m^2. Where general office heat loads are in excess of 60W/m^2, therefore alternative methods are required to remove these heat loads, the use of chilled ceiling and displacement ventilation as one system can remove heat loads in the region of 80-100W/m^2 (Taki 96). The author has published work relating to the effects on the airflow using Computational Fluid Dynamics in an environment the employ displacement ventilation and chilled ceiling.

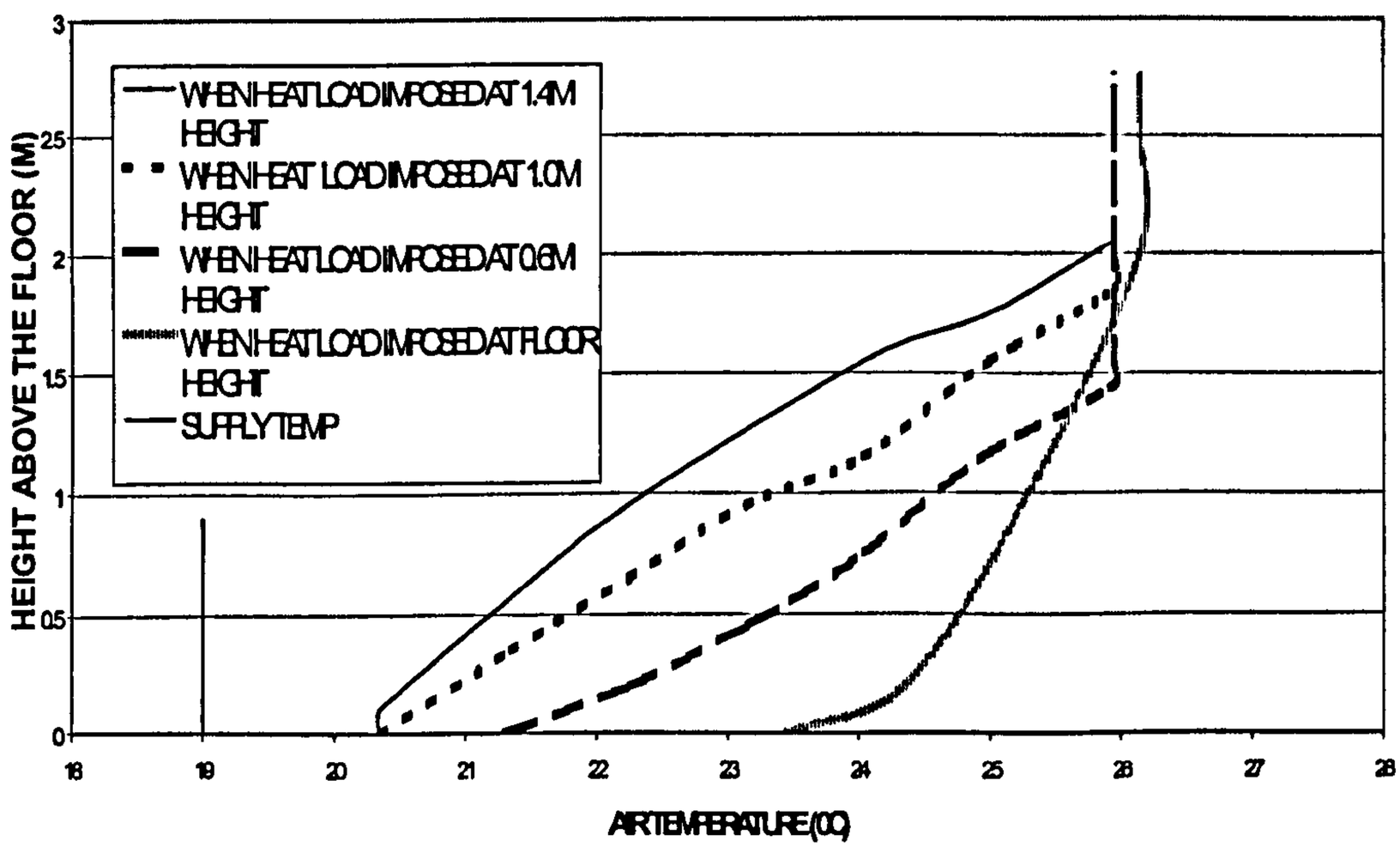

CFD PRESENTATION OF TEMPERATURE PROFILE FOR A FIXED HEAT LOAD OF 25W/M2 IMPOSED ON THE TOP SURFACE OF THE 4 DUMMIES AT 1.4M, 1.0M AND 0.6M ABOVE THE FLOOR AND ALSO AT FLOOR HEIGHT.

Figure 2 Graph showing the height of the stratified boundary layer, when heat load of 25W/m2

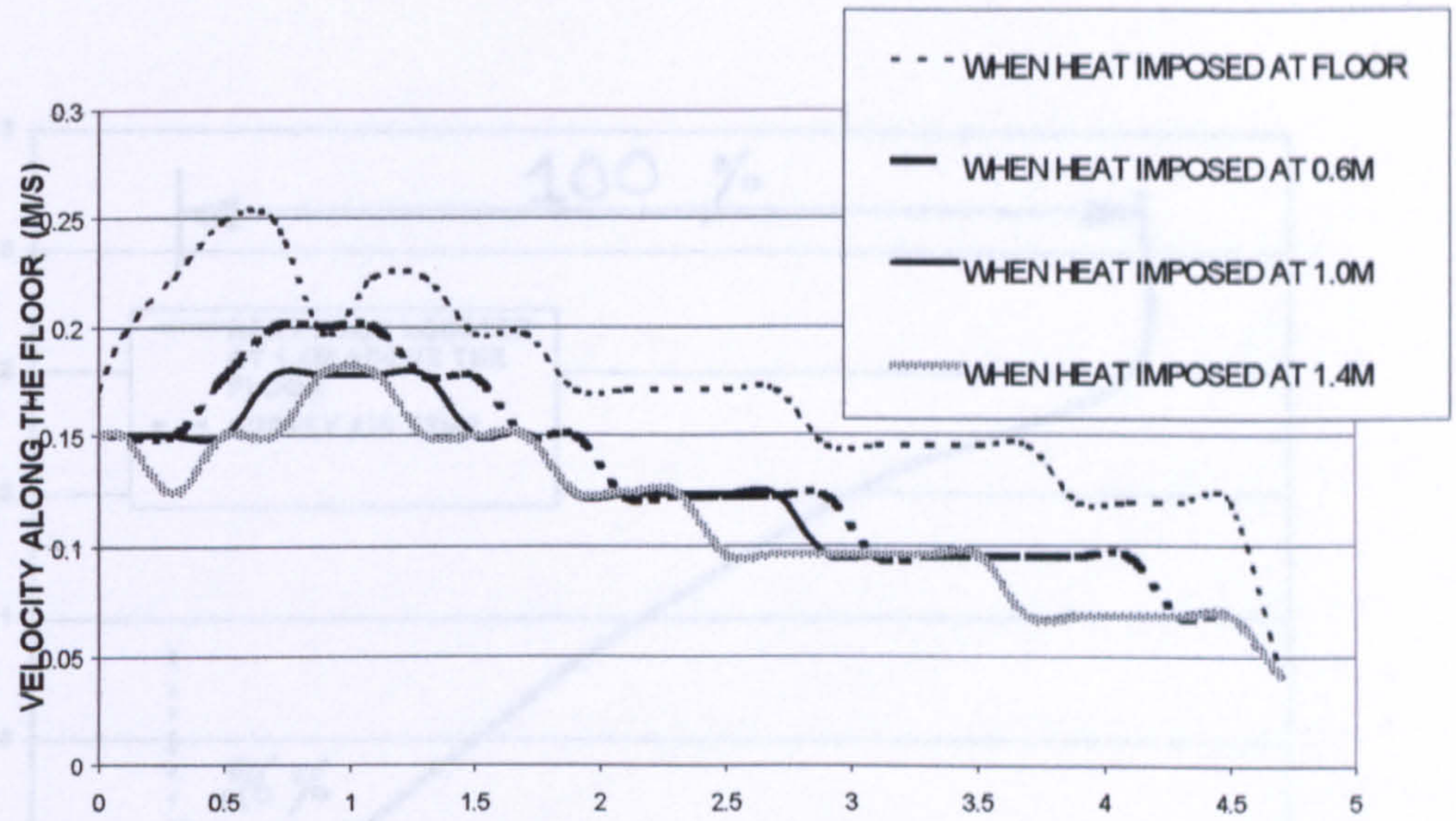

VELOCITY PROFILE FOR HEAT LOAD OF 25W/M2 IMPOSED AT VARIOUS HEIGHTS. THE VELOCITY RECORDED AT ANKLE HEIGHT (SUPPLY VELOCITY 0.182 M/S)

Figure 3 the graph represents the velocity at floor level for the bench mark 2 conditions. It can be clearly seen that the when heat load of 25W/m^2 is imposed at floor height the increase in velocity is the greatest and the lease for when heat load is imposed at 1.4m above the floor.

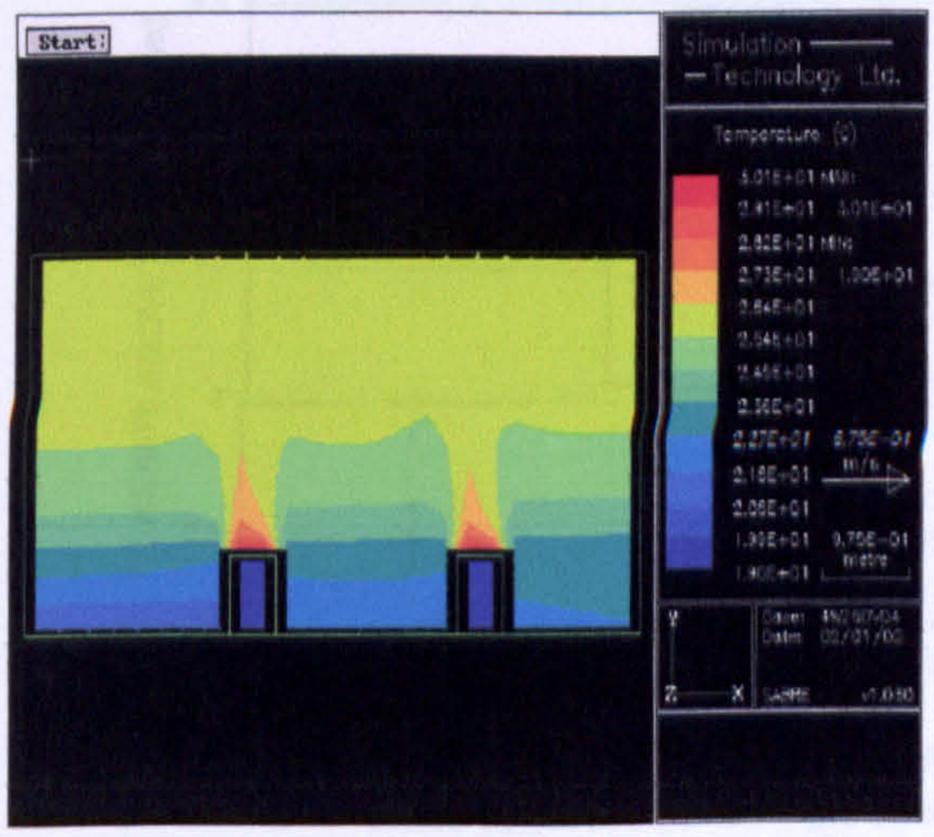

Figure 4

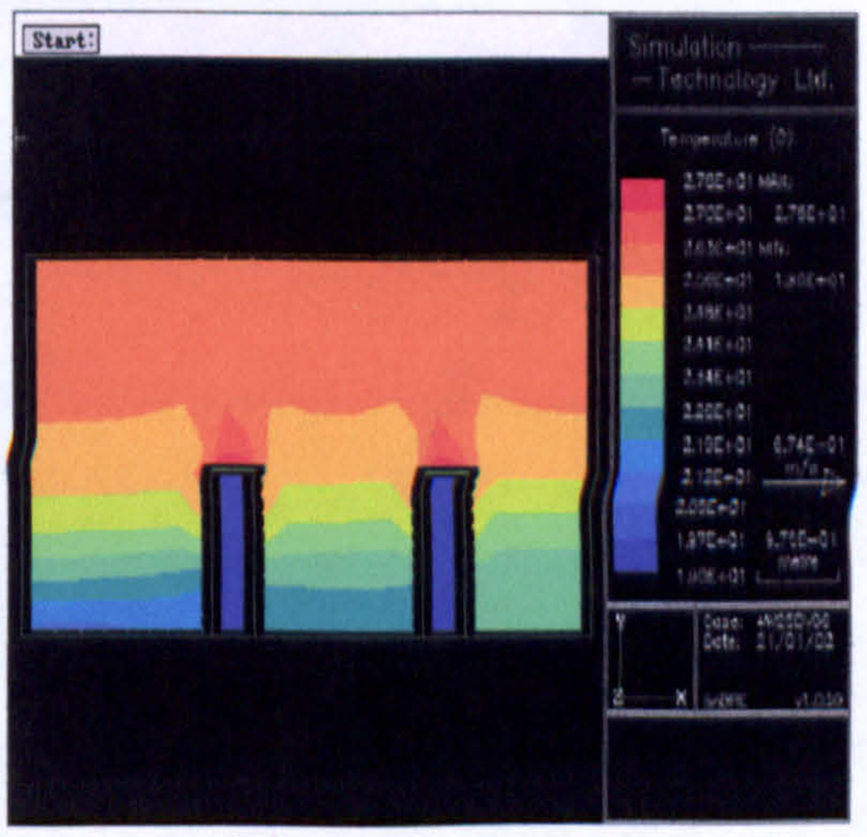

Figure 5

Figure: 4 Heat load of 25W/m^2 at 0.6m above the floor, clearly showing that the stratified boundary layer is at a lower point, then when heat load is imposed at 1.0m above the floor.

Figure: 5 Temperature contours for heat loads of 25W/m^2 at 1.0m form the floor.

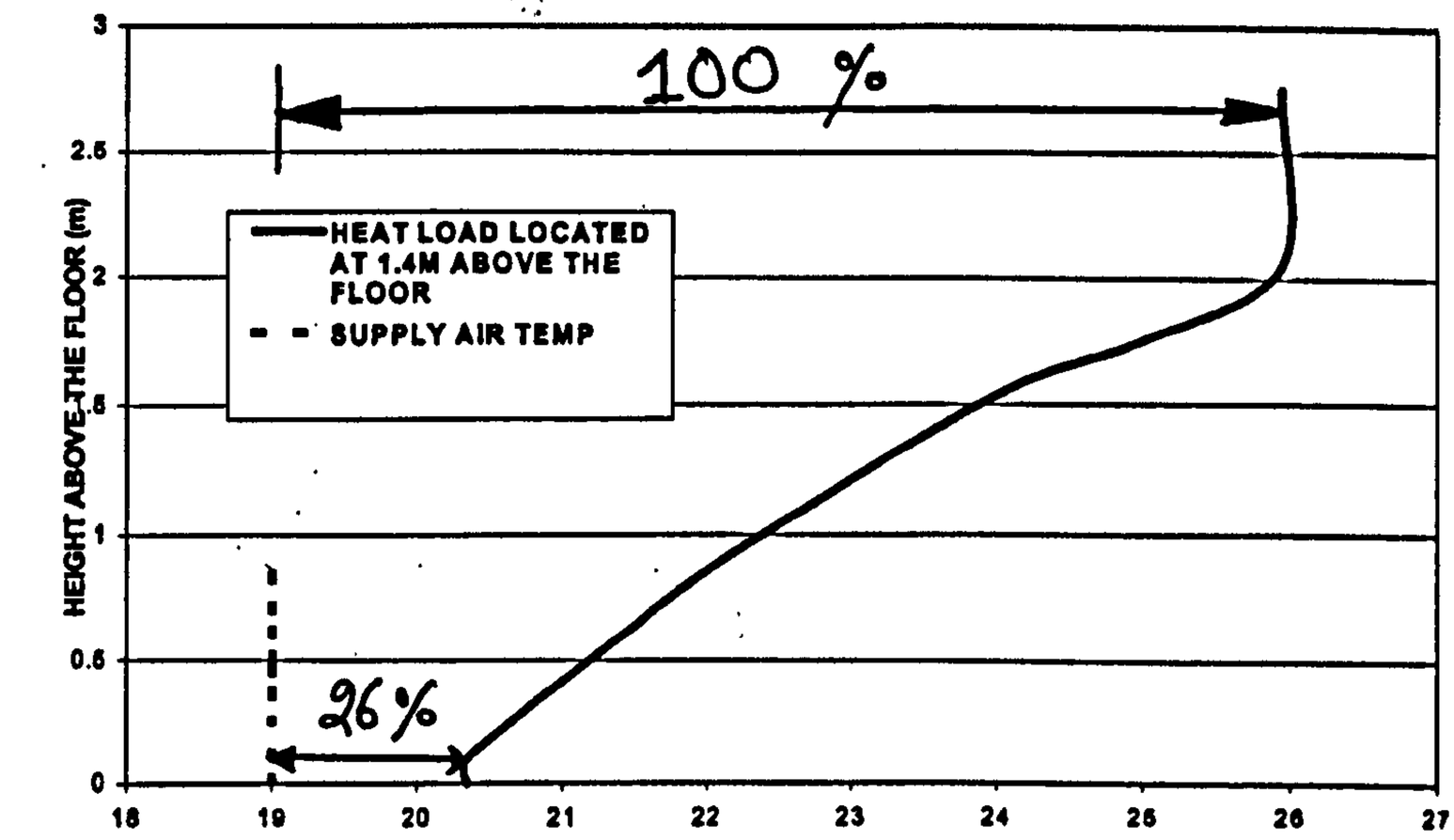

TEMPEARTURE DISTRIBUTION WITH A HEAT LOAD OF 25W/M2 AT 1.4M ABOVE THE FLOOR

Figure 6 showing the temperature profile when heat load of 25w/m2 is imposed at height of 1.4m above the flow. The results the temperature difference between the supply temperature and the ankle height is 26% of the total temperature difference.

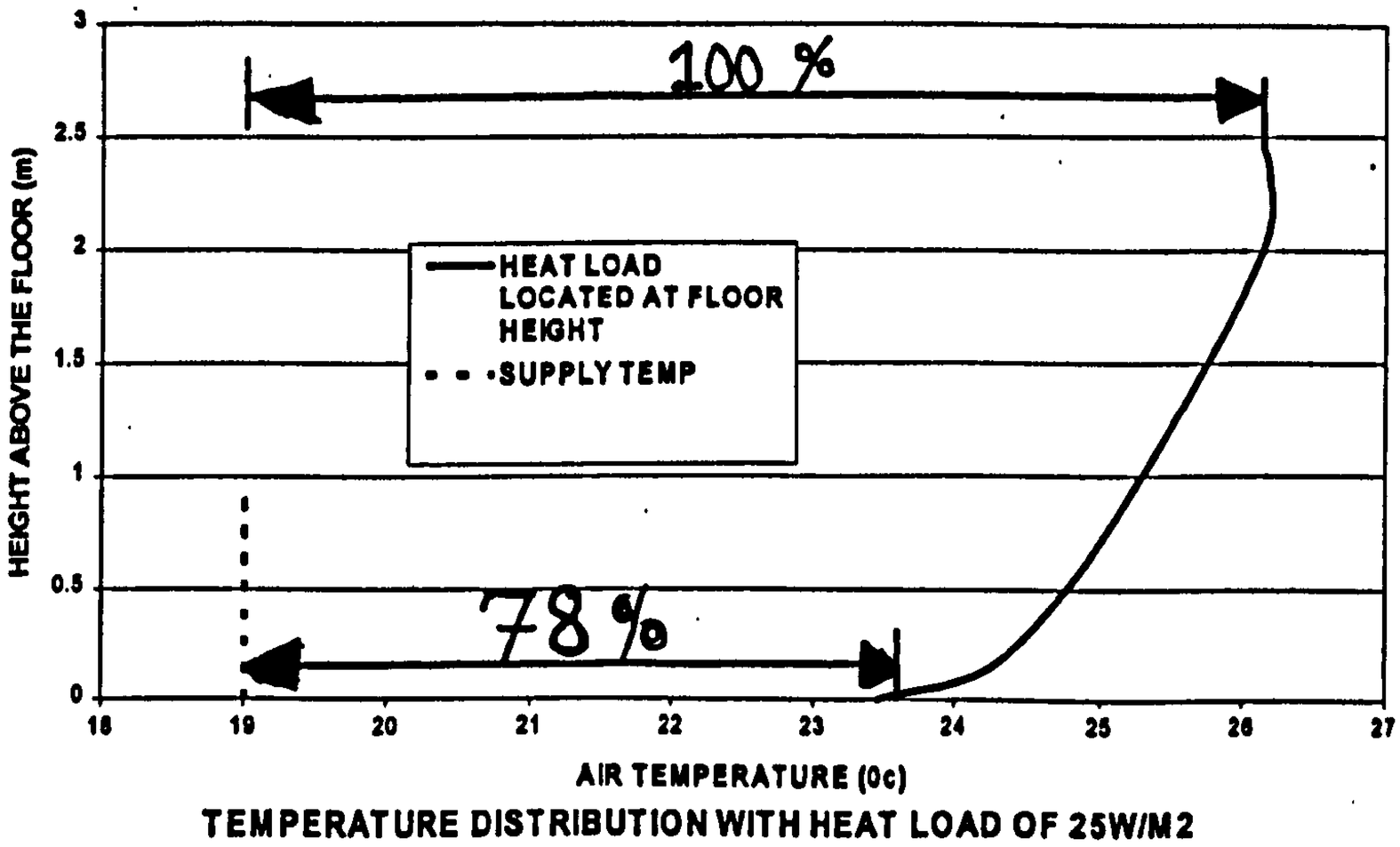

TEMPERATURE DISTRIBUTION WITH HEAT LOAD OF 25W/M2 LOCATED AT FLOOR HEIGHT

Figure 7 shows the temperature profile for a heated load of 25w/m2 located at the floor. The result shows that the temperature difference between the supply temperature and at ankle height is in the region of 78% of the total temperature difference.

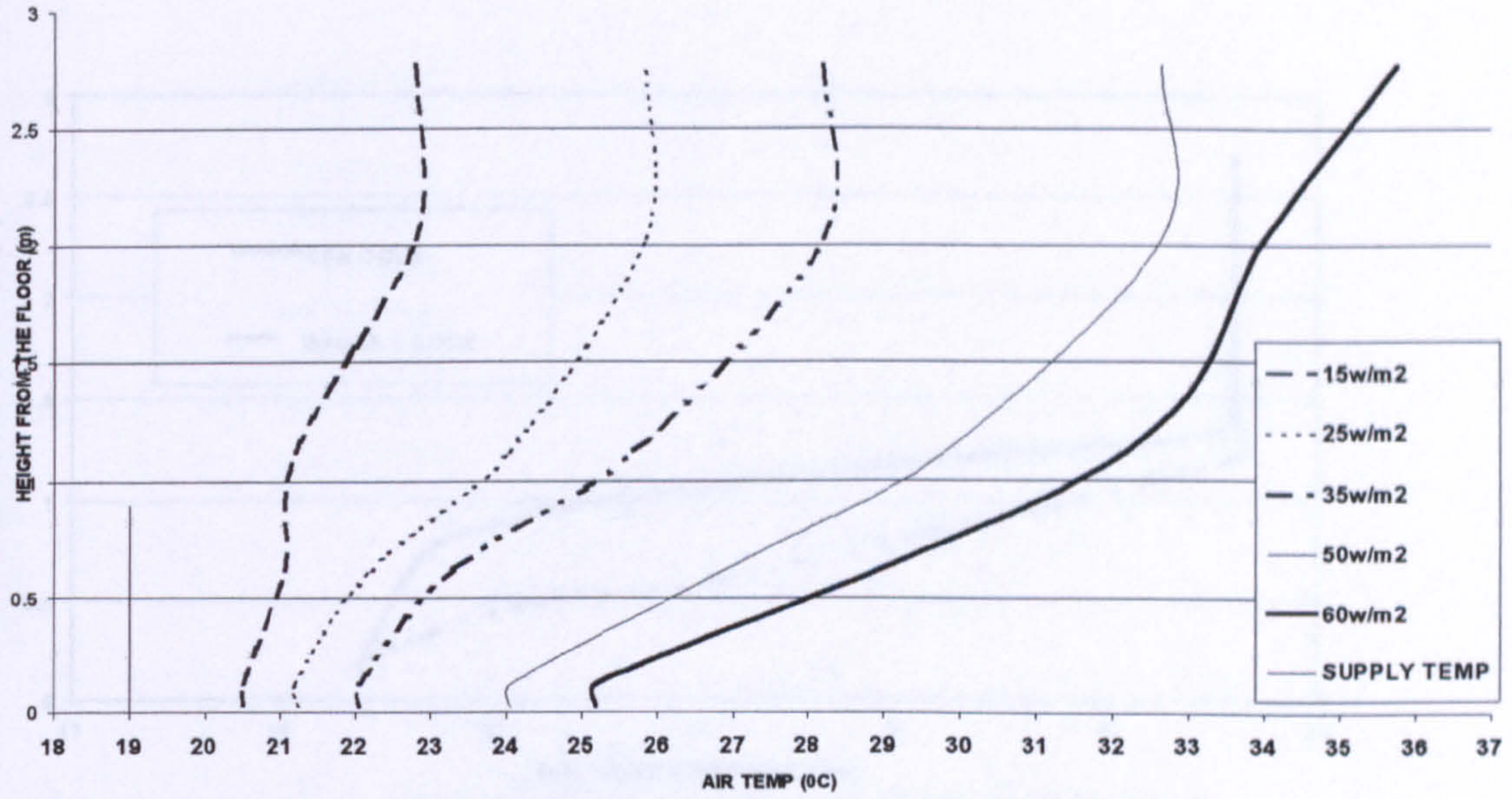

CFD SIMULATION OF AIR TEMPERATURE VERSUS HEIGHT FOR A RANGE OF HEAT SOURCE

Figure: 8 CFD Simulations representing various heats loads versus height in the room. It can be clearly seen that the displacement ventilation system can not remove heat loads greater than 35W/m^2.

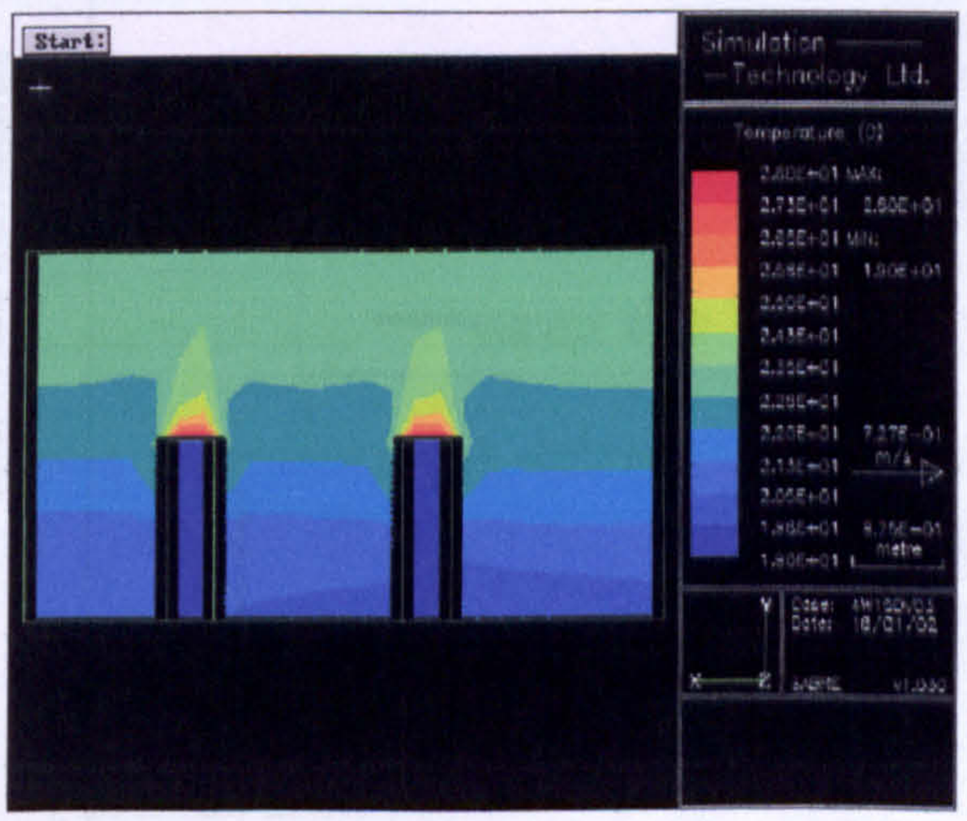

Figure 9

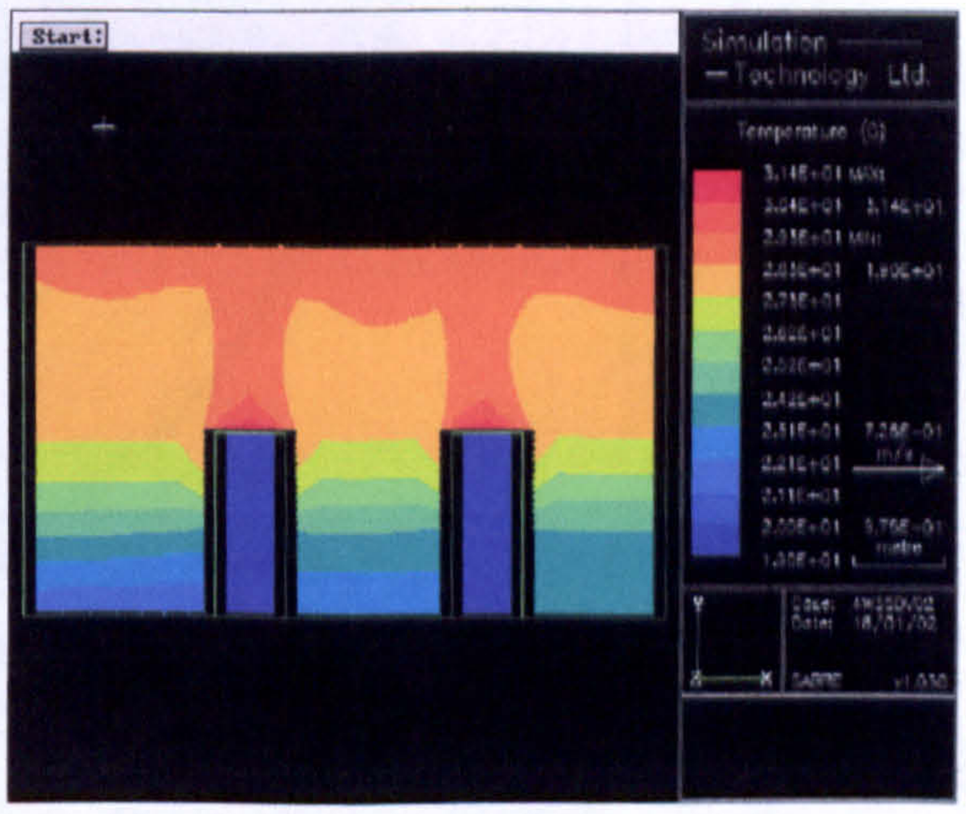

Figure 10

Figure: 9 showing the heat profile for 15W/m^2. It can be clearly seen that the stratified boundary layer is at a higher height than the stratified boundary layer for 60W/m^2 shown in figure 10. The two figures also show that the strength of the heat plumes, it can be seen that the plume for 60W/m^2 has a greater strength than for 15W/m^2.

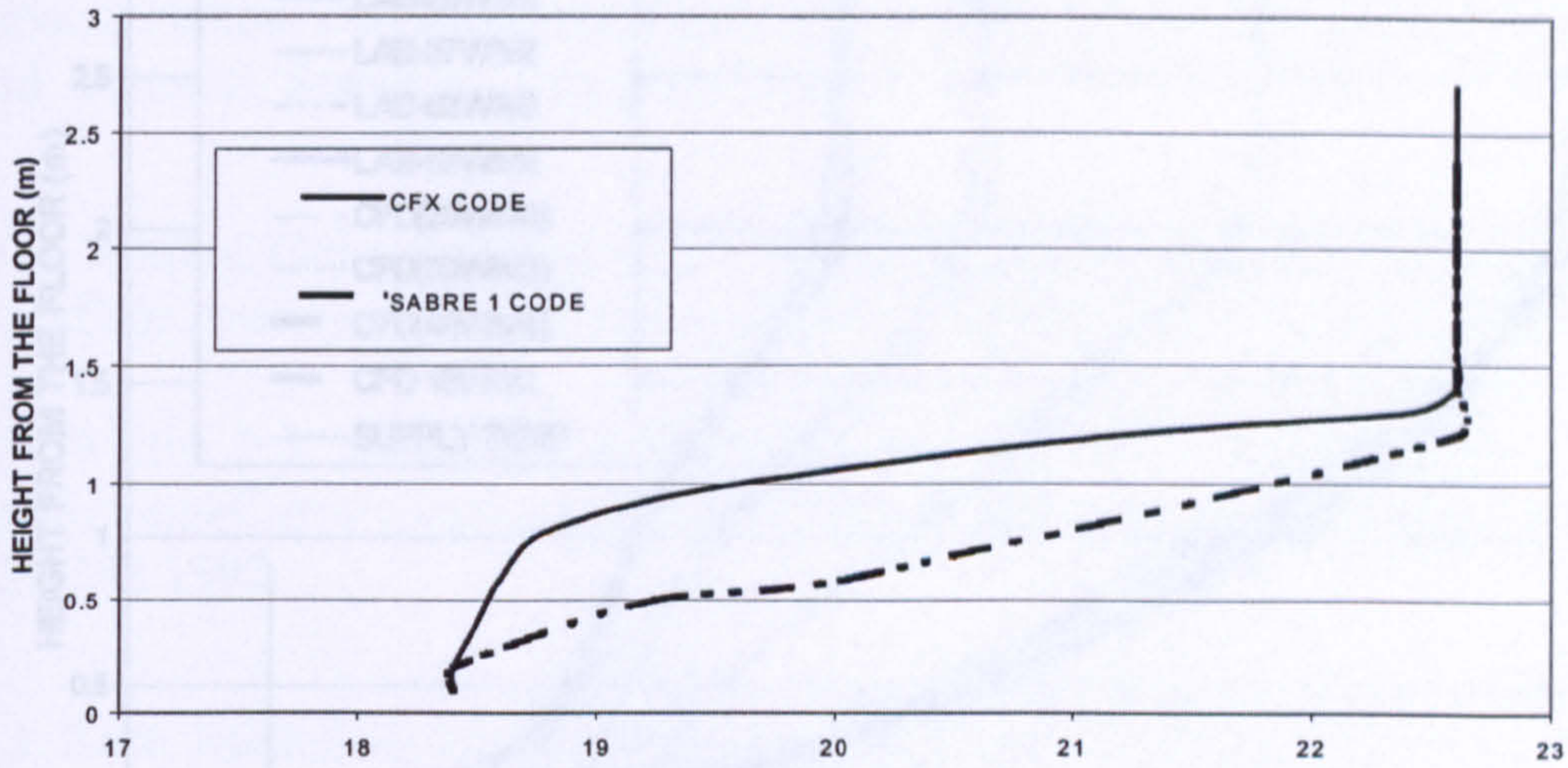

COMPARISON OF RESULTS BETWEEN CFX AND SABRE1 CFD CODE TO REPRESENT NATURAL VENTILATION

Figure 11 showing the comparison of results between CFX sued by Cook (1997) and Sabre-One CFD code. We can be seen that the code has predicted the same height of the stratified boundary layer and similar temperature.

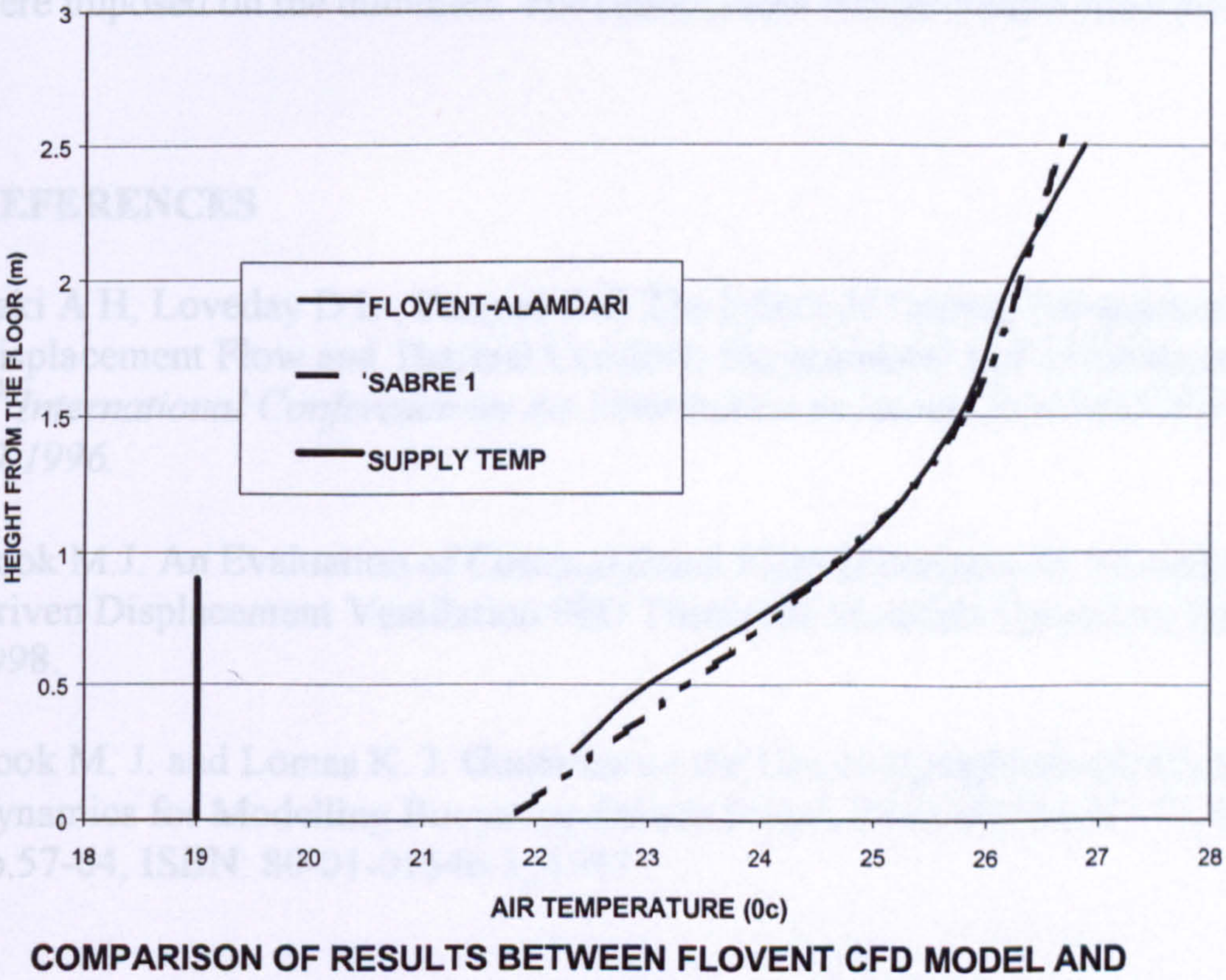

COMPARISON OF RESULTS BETWEEN FLOVENT CFD MODEL AND SABRE 1 CFD MODEL FOR 20W/M2 HEAT LOAD IN THE ROOM AGAINST HEIGHT

Figure 12 showing the results between the Flovent Code used by Alamdari (1998), and the Sabre-One CFd code. The results show the same temperature profile.

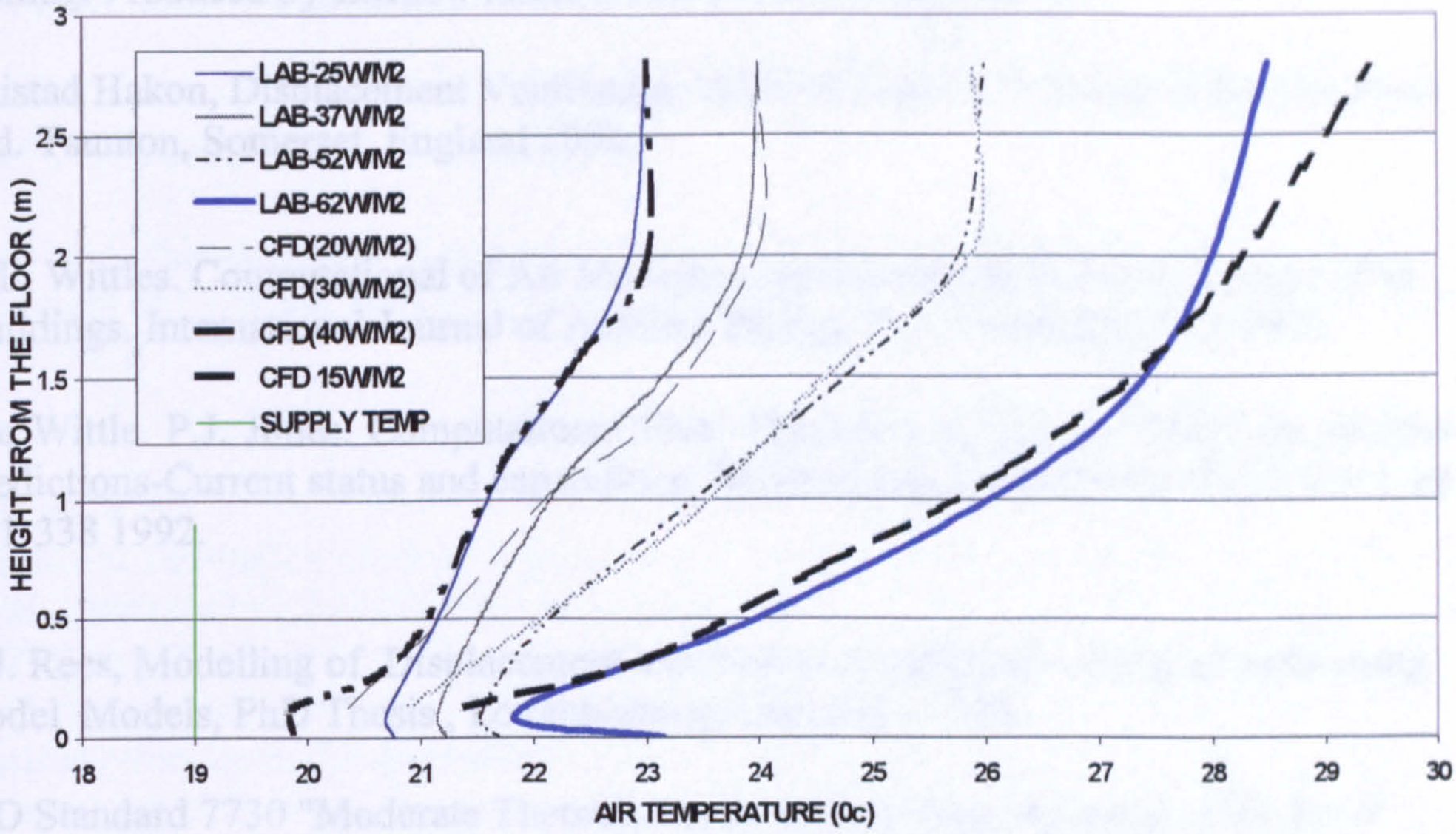

Figure 12 Graph showing the comparison between the results of Taki et al (1996) and the predictions of the CFD code. When various heat loads of 25-37-52-and 62W/m^2 were imposed on the dummies. The results show similar temperature profiles.

REFERENCES

Taki A H, Loveday D L , Parsons K C The Effect of Ceiling Temperature on Displacement Flow and Thermal Comfort- Experimental and Simulation Studies. *5th International Conference on Air Distribution in Rooms ROOMVENT 96, July 17-19,1996.*

Cook M.J. An Evaluation of Computational Fluid Dynamics for Modelling Buoyancy Driven Displacement Ventilation PhD Thesis De Montfort University England August 1998.

Cook M. J. and Lomas K. J. Guidance on the Use of Computational Fluid Dynamics for Modelling Buoyancy-Driven Flows. Proc. IBPSA '97, Volume 3, pp.57-64, ISBN: 80-01-01646-3, 1997

Alamdari F. Displacement Ventilation and Cooled Ceilings. Environmental Dynamics Centre, Building Research Establishment Ltd, United Kingdom. *6th International Conference on Air Distribution in Rooms, Stockhom, Sweden June 14-17 1998 pp197-205.* Room Vent 98,

Alamdari F. Eagles. N Technical Notes 2/96 Displacement Ventilation and Chilled Ceiling. Produced by BSRIA. ISBN 0 860224 333. March 1996.

Skistad Hakon, Displacement Ventilation, ISBN 086380 1471 Research Studies Press Ltd. Taunton, Somerset, England 1994.

G.E. Wittles. Computational of Air Movement and Convective Heat Transfer within Buildings. International Journal of Ambient Energy. Vol 7 number 3 July 1986.

G.e Wittle. P.J. Jones. Computational Fluid Dynamics (CFD) for Buildings Airflow Predictions-Current status and capabilities. Building and Environment Vol 27 no 3, pp 321-338 1992.

S.J. Rees, Modelling of Displacement Ventilation and Chilled Ceiling systems using Nodel Models, PhD Thesis , Loughborough University, 1998.

ISO Standard 7730 "Moderate Thermal Environments- Determination of the PMV and PPD Indices and Specification of the Conditions for Thermal Comfort", 1994.

COMPUTATION OF AIRFLOW IN A DISPLACEMENT VENTILATION/CHILLED CEILING ENVIRONMENT

L. Jalil [1*], A.H.Taki [1] and D.L. Loveday [2]

[1] School of Architecture, De Montfort University, Leicester LE1 9BH UK
[2] Department of Civil and Building Engineering, Loughborough University, Loughborough, LE11 3TU UK

ABSTRACT

Displacement ventilation combined with a chilled ceiling system have been investigated by (Kofoed, 1994), (Almadari and Eagles, 1996), (Fitzner, 1996), (Taki et al., 1996), (Loveday, et al 1998) and (Rees, 2001). However, characterisation tests in such a combination system revealed that the use of a chilled ceiling with displacement ventilation could have a detrimental effect upon the displacement flow. This paper presents an assessment of the ability to model airflow and temperature distributions in such combination environments with a standard Computational Fluid Dynamics (CFD) code. Modelling is carried out over a range of typical office conditions for a range of heat loads and ceiling surface temperatures. It was found that the CFD code could be used to successfully predict the airflow in these environments by showing good agreement with those of earlier studies. The implications for the future design of displacement ventilation and chilled ceiling environment are discussed.

INDEX TERMS

Computation Fluid Dynamics, Displacement Ventilation, Chilled Ceiling, Airflow.

INTRODUCTION

Over the last few decades the office environment has changed rapidly and is continuing to do so. One such change is the fact that office space has expanded with open-plan office environments taking the place of the traditional segregated office units. With the large open-open office space came the problem of providing adequate air ventilation to the whole office. One method used was displacement ventilation, where air is introduced at one part of the room and is allowed to sweep in one direction across the space taking the pollutants and exhausting them at the opposite part of the room. Displacement ventilation is mainly characterized by buoyancy-driven airflow. In this system, low velocity air is supplied from a low level supply device in the occupied zone at a temperature slightly cooler than the design room temperature, in order to obtain the displacement effects. As a result of thermal comfort limitations given in BS EN ISO Standard 7730 (ISO 1995) (namely that the vertical air temperature gradient should be less than 3°C/m), a displacement ventilation system is limited to removing a convective load of up to 25W/m^2 of floor area. A typical office might exceed 60W/m^2 of heating load. Therefore, an additional cooling mechanism was required to meet this load, frequently a chilled ceiling. The chilled ceiling system provides an additional heat removal mechanism from the space. In this system the ceiling temperature is maintained by circulating cool water through pipes. In principle, the combined system of displacement ventilation and chilled ceiling has the potential to remove the convective heat gains generated

* Contact author email: ljalil@dmu.ac.uk

by peoples and equipment with chilled ceiling providing radiant cooling and reducing the overall temperature gradient by cooling air in the upper part of the room.

It is understood that chilled ceilings can remove heat loads of up to 100W/m^2 mainly by radiation, and can also enhance the thermal comfort sensation of the occupants (Loveday et al., 1998). This paper aims to assess the use of CFD code for predicting airflow and temperature distributions in such combination environments and to highlight the implications on air quality.

COMPUTATIONAL FLUID DYNAMICS (CFD) MODELLING

CFD modeling is the process of representing a fluid flow problem by mathematical equations based on the fundamental conservation laws of physics, and solving those equations to predict the variation of the relevant parameters within the flow field. Usually these could be velocity, pressure and temperature, and also concentrations of chemical species. These conservation laws can be expressed in terms of non-linear "elliptic" partial differential equations, the solutions of which provide the basis for the CFD model. The CFD model solves numerically the equations and produces field values for the temperature, velocity and the chemical species. The CFD code used in this study, has the ability to simulate advanced computation of three-dimensional airflow and temperature in and around enclosures (Wittles, 1986, 1992). The accuracy of the CFD code used has been compared with other CFD codes, and also with laboratory results for environments that employs displacement ventilation systems. The results showed good agreement with these codes (Taki et al. 2002).

THE SITUATION BEING MODELLED

The Environmental Test Room facility based at the Department of Civil and Building Engineering, Loughborough University is 5.4m long 3m wide and 2.8m high, was used in this study and was modeled with adiabatic walls.

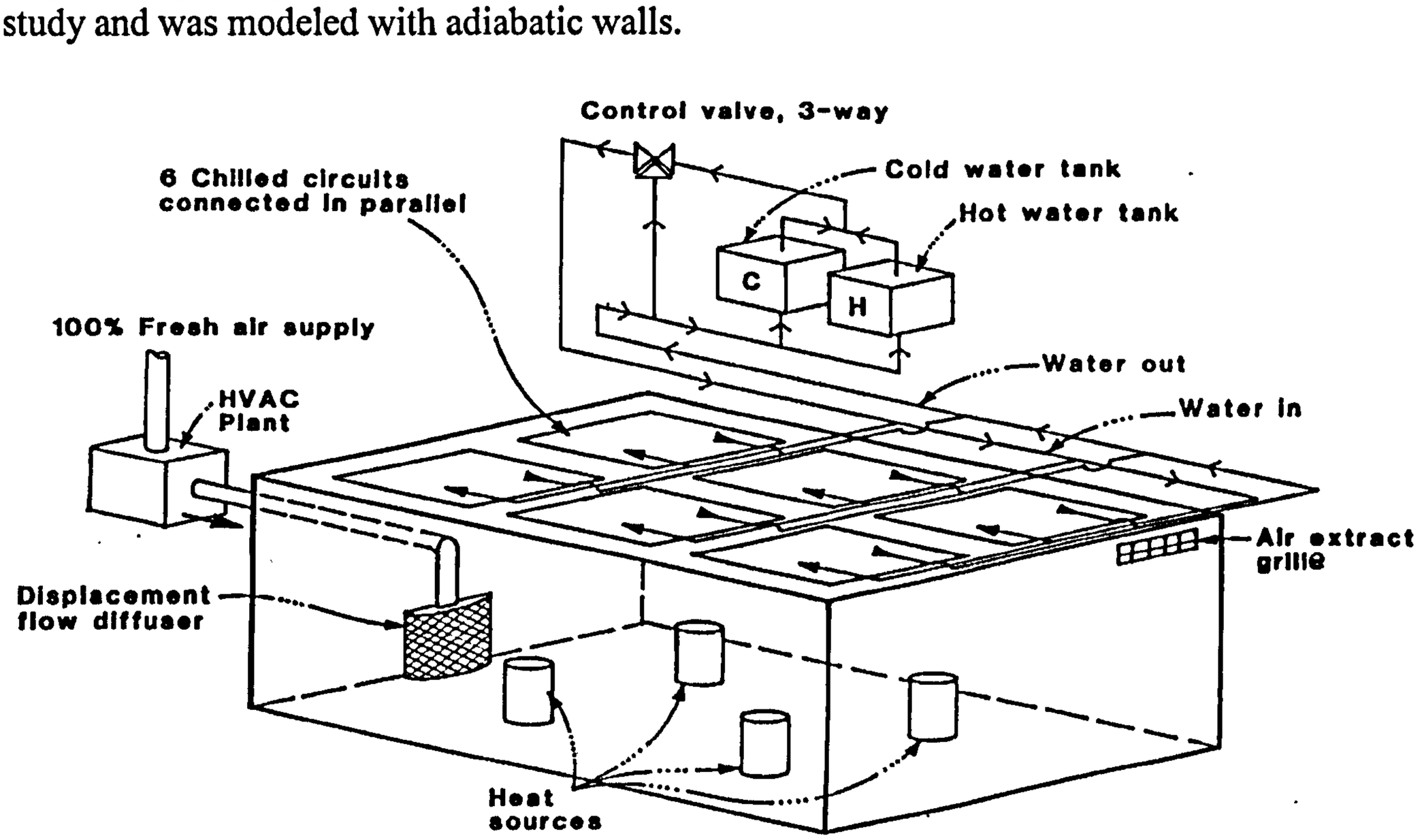

Figure 1. Schematic diagram of the room being modelled

The room employed a chilled ceiling and displacement ventilation system. The displacement ventilation system was set to operate at a supply temperature of 19°C and 3.9 air changes per hour. A heat load of 60W/m^2 of floor area was achieved by placing within the room four thermal dummies to represent human occupants and office equipment. The ceiling surface temperatures were set to the following values 14, 16, 18 and 21°C (Figure 1). A Cartesian mesh consisting of 22680 cells was used to model the room, 27 cells in length (x) direction, 56 cells in height (y) direction and 15 cells in width (z) directions, κ-ε turbulence model was adopted for the simulation.

RESULTS AND DISCUSSIONS

Using the CFD simulation, Figure 2 shows vertical temperature profiles in the room, (that is, plots of room air temperature versus height) for a range of ceiling temperatures (14, 16, 18 and 21°C) at a fixed heat load of 60W/m^2. Figure 2 also shows the predictions of temperature profile for the case of displacement ventilation only (where there was no chilled ceiling). The results show that at low ceiling temperatures of 14°C the stratified boundary layer is strongly suppressed, and that there is some destruction of displacement flow pattern. At higher ceiling temperatures of 16 -21°C, some displacement flow is present. This agrees with work carried out by (Taki et al., 1996).

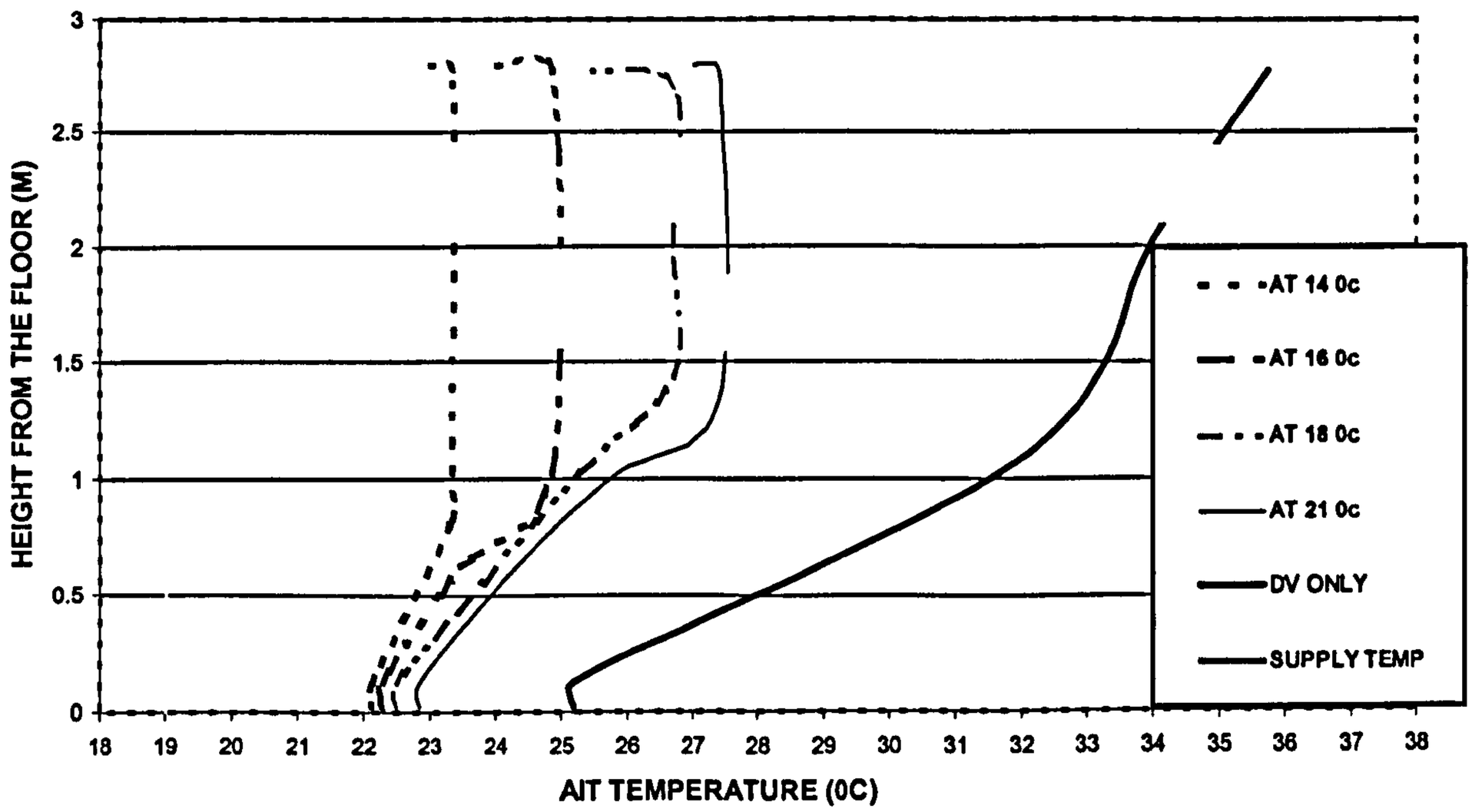

Figure 2. Air temperature versus height for a range of ceiling surface temperature at a heat load of 60W/m^2.

The CFD simulation also showed that the wall temperatures were lower than the room temperatures. This could have been caused mainly through the radiative heat exchange between the room walls and cooled ceiling, where the air is then driven downwards by the negative buoyancy thus, the walls tend to have a lower temperature than room air temperature. This agrees with the findings of (Kruhne, 1996), (Alamdari, 1996), (Brohus, 1998) and (Fitzner, 1996). Because the air begins to flow downward and out of the mixing zone below the ceiling, the contaminated air reaches the zone of fresh air and increases contamination near the floor and at the breathing level. Therefore it can be concluded that the use of a chilled ceiling with displacement ventilation can have an adverse effect on the air quality in the zone of fresh air.

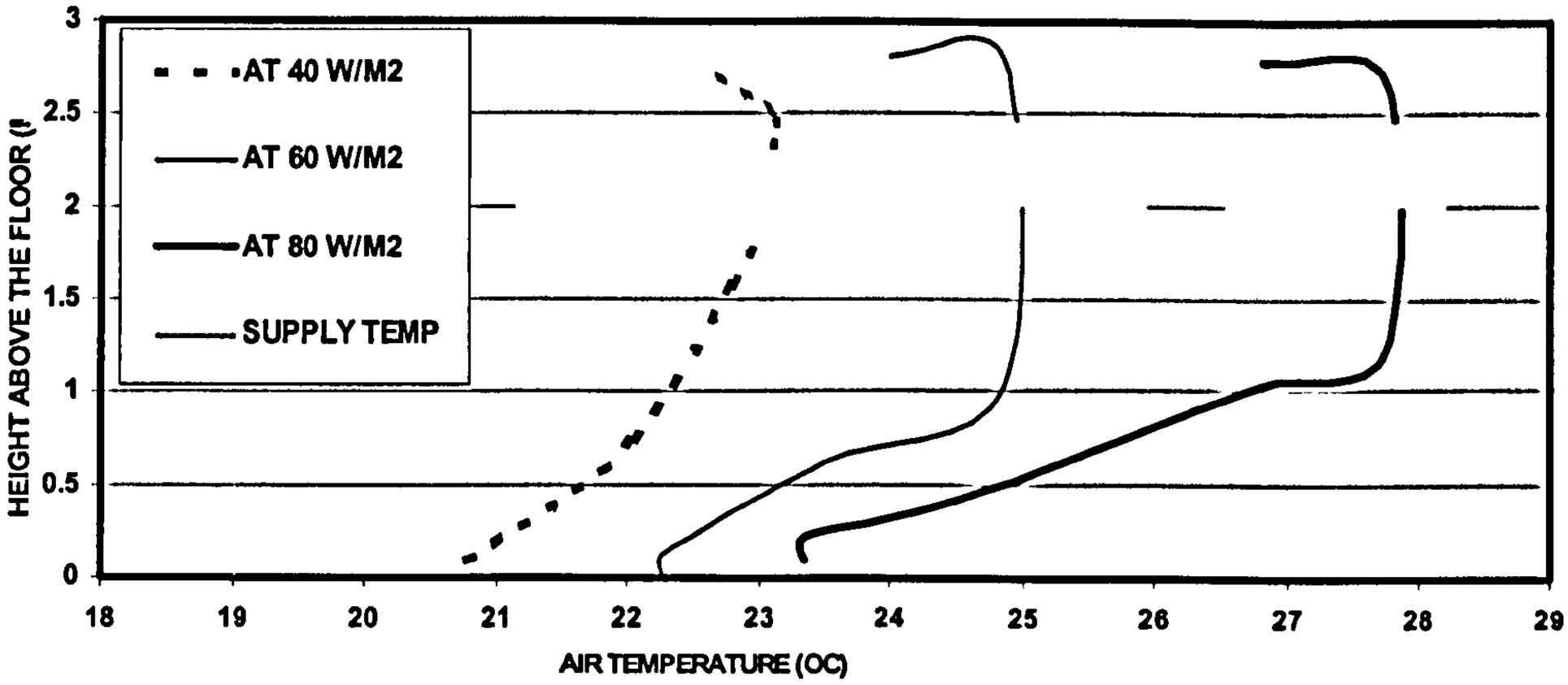

Figure 3. Air temperature versus height for a range of heat loads at a ceiling temperature of 16 °C

Figure 3 shows the air temperature profiles for a range of heat loads, 40, 60 and 80 W/m^2 at ceiling temperature of 16°C. It shows that air temperatures are almost constant above the height of 1.1m from the floor. The results also show that the vertical temperature gradient increases with the heat load and it exceeds 3°C/m for the heat load of 80W/m^2. To meet the criteria given in the ISO 7730, the ceiling temperature should be lowered to remove such heat loads. Figure 4 shows the results of (Alamdari and Eagles, 1996) who also used a CFD code to investigate the effects that a chilled ceiling has on the temperature profile. The results show good agreement with regards to the temperature profile and agree as regards the height of the stratified boundary layer.

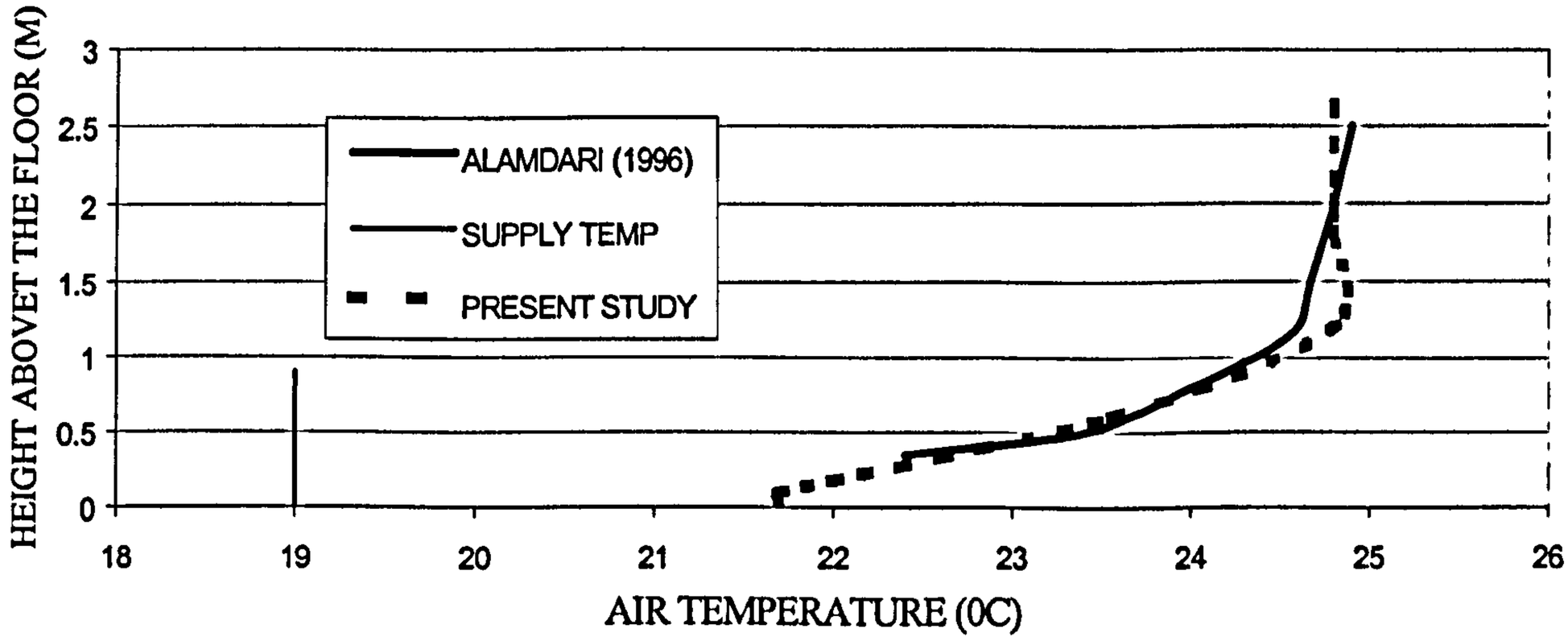

Figure 4. Air temperature versus height above the floor, for ceiling temperature 16°C, 3.5ACH and 60W/m^2: comparison of this with (Alamdari and Eagles, 1997)

The results presented by (Taki et al., 1996) did not satisfy the room heat balance equation due to heat losses through the room surfaces. These heat losses were estimated from the knowledge of surfaces U-values, internal and external air temperatures, and were found to be approximately 40% of the total heat load within the room. For the aim of comparison, the room was modelled with a heat load of 40 W/m^2 of floor area and the results are presented in Figure 5; the predictions are in agreement with the experimental data for ceiling temperatures of 14,16 and 18 °C. The CFD findings prove that the combined operation of displacement ventilation and chilled ceiling systems could cause deterioration in air quality as a result of flow pattern.

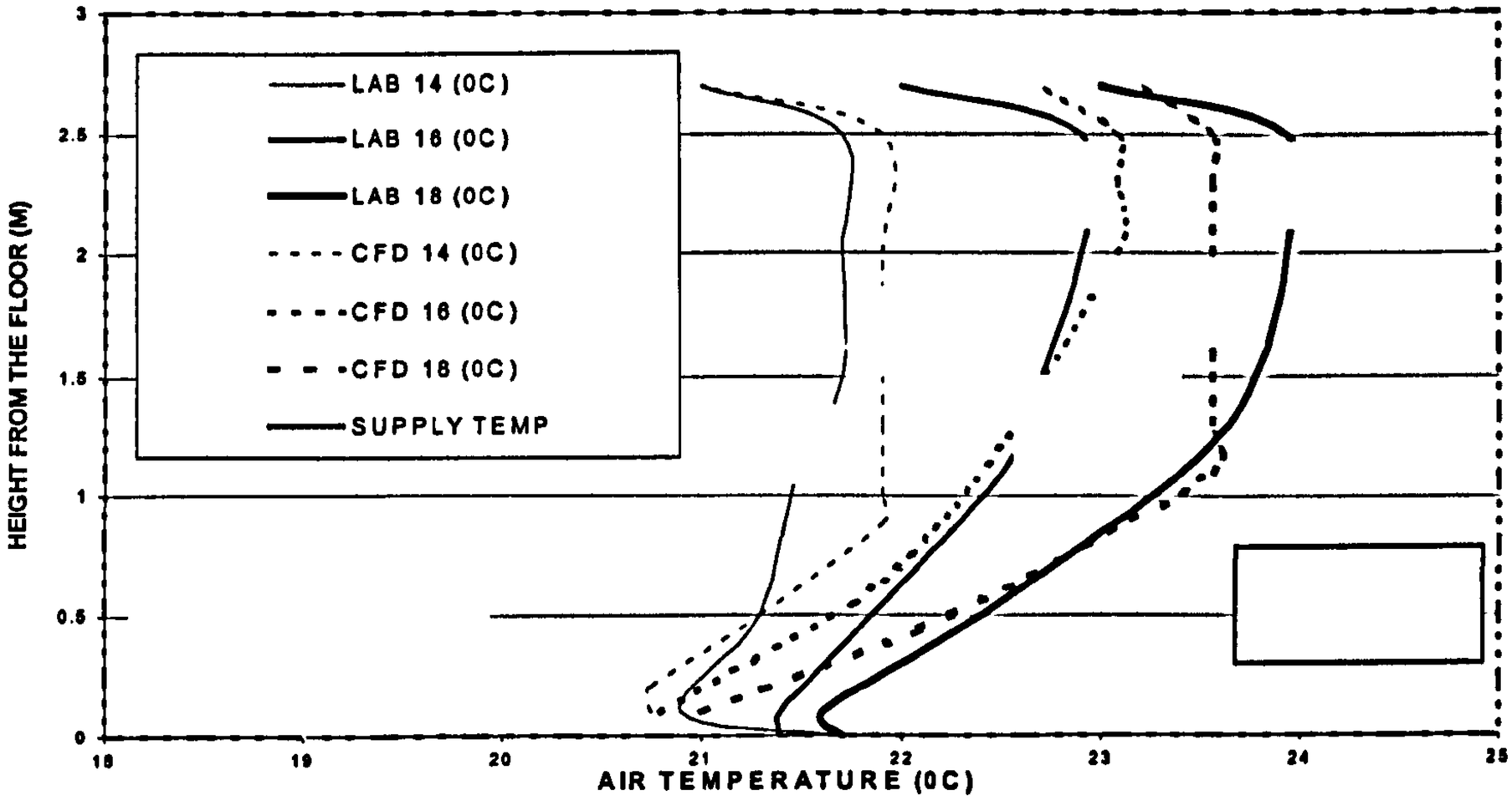

Figure 5. Air temperature versus height above the floor for a range of ceiling temperatures, and at fixed heat load of 40W/m^2 and 3.9 ACH.

CONCLUSIONS

Using CFD, computational predictions have been produced for a chilled ceiling and displacement ventilation environment. The CFD predictions agreed with those reported by (Taki et al, 1996), (Kruhne, 1993), (Alamdari and Eagles, 1996), and (Fitzner, 1996). This proves that the CFD code can be regarded as an effective tool for accurately predicting airflow and temperature distributions, and for assessing the adverse effect on the air quality in such combination environments.

It is now our intention to investigate techniques that can be used to suppress the downward cold convection currents from a chilled ceiling, thereby helping that the combined arrangement to work together more effectively. The authors are currently researching possible solutions. The study will be based on findings predicted by CFD and validated using laboratory measurements.

REFERENCES

Alamdari F, Eagles N (1996), Technical Notes 2/96 Displacement Ventilation and Chilled Ceiling. Produced by BSRIA, ISBN 0 860224 333.

Brohus H (1998), Influence of Cooled Ceiling on Indoor Air Quality in a Displacement Ventilation room Examined by means of Computational Fluid Dynamics, *The 6th International Conference on Air Distribution in Rooms, RoomVent'98, pp53-60*, Sweden.

Cook MJ (1998), An Evaluation of Computational Fluid Dynamics for Modelling Buoyancy Driven Displacement Ventilation Ph.D. Thesis De Montfort University England.

Fitzner K (1996), Displacement Ventilation and Cooled Ceiling, Results of Laboratory Tests and Practical Installations. *The 7th International Conference on Indoor Air Quality and Climate Indoor Air'96*, Vol. 1, pp 41-50, Nagoya, Japan.

ISO Standard 7730 (1994) "Moderate Thermal Environments- Determination of the PMV and PPD Indices and Specification of the Condition for Thermal Comfort".

Kruhne Holger (1993), Effects of Cooled Ceilings in Rooms with Displacement Ventilation on the Air Quality. *6th International Conference on Indoor Air Quality and climate Proceedings of Indoor Air 93 Vol 5, pp 395-400.*

Loveday DL, Parsons KC, Taki AH (1998), Designing for Thermal Comfort in Combined Chilled Ceiling/Displacement Ventilation Environments. ASHRAE Transactions: Symposia Vol 104, pp 901-911, ISSN 0001-2505.

Rees SJ, Haves PA (2001), Nodal model for Displacement Ventilation and Chilled Ceiling Systems in Office Spaces. Building and Environment 36, pp 753-762.

Skistad Hakon (1994), Displacement Ventilation, ISBN 086380 1471 Research Studies Press Ltd. Taunton, Somerset, England 1994.

Taki AH, Loveday DL, Parsons KC (1996), The Effect of Ceiling Temperature on Displacement Flow and Thermal Comfort- Experimental and Simulation Studies. *5th International Conference on Air Distribution in Rooms ROOMVENT 96, July 17-19, pp307-314* Japan.

Taki AH, Jalil L and Loveday DL (2002) Use of Computational Fluid Dynamics for Modelling Displacement Ventilation Environments. *To be published in the International Conference on Research Trends in Science and Technology,* Lebanon.

Wittles, GE (1986), Computational of Air Movement and Convective Heat Transfer within Buildings International Journal of Ambient Energy. Vol.7, No.3, pp 151-164.

Wittles, GE and Jones, PJ (1992), Computational Fluid Dynamics (CFD) for Buildings Airflow Predictions-Current status and capabilities. Building and Environment Vol. 27 no 3, pp 321-338.